UCLA
UCLA Electronic Theses and Dissertations

Title

Harnessing Strain-Driven Reactivity for Complex Molecule Synthesis and Advances in Chemical Education

Permalink

https://escholarship.org/uc/item/45t962s6

Author

Chari, Jason

Publication Date

2022

Peer reviewed|Thesis/dissertation

eScholarship.org Powered by the California Digital Library
University of California

UNIVERSITY OF CALIFORNIA

Los Angeles

Harnessing Strain-Driven Reactivity for Complex Molecule Synthesis and Advances in Chemical Education

A dissertation submitted in partial satisfaction of the

requirements for the degree Doctor of Philosophy

in Chemistry

by

Jason Chari

2022

© Copyright by

Jason Chari

2022

ABSTRACT OF THE DISSERTATION

Harnessing Strain-Driven Reactivity for Complex Molecule Synthesis

and Advances in Chemical Education

by

Jason Chari

Doctor of Philosophy in Chemistry

University of California, Los Angeles, 2022

Professor Neil Kamal Garg, Chair

This dissertation describes the development of synthetic methodologies and approaches that leverage strain-driven reactivity to access complex molecules, as well as enzymatic studies and advances in the field of chemical education. The high potential energy stored within strained bonds offers a powerful tool in organic synthesis for the construction of new covalent bonds. Controlling the reactivity of strained molecules, while challenging in many cases, offers a means to form multiple bonds in a single step, under mild reaction conditions, and generate products that may be inaccessible by other means. Herein, several synthetic endeavors are described that seek to leverage strain release to push our understanding of chemical reactivity and gain new entryways

into important classes of organic and organometallic compounds. Moreover, two studies in the area of biosynthesis and are described, which take advantage of synergy between chemical synthesis and enzymatic chemistry to access bioactive compounds with high selectivity. Finally, studies in the area of chemical education are described. These efforts seek to make organic chemistry accessible to wider audiences through the development of interactive, globally available educational tools and the creation of a new undergraduate lecture course that highlights the role of organic chemistry in the world around us.

Chapter one describes a perspective on the field of complex molecule synthesis (i.e., total synthesis), with a focus on the power of collaborations across research groups. Although historically competitive, there is a growing spirit of teamwork and collaboration in the field of total synthesis. This chapter discusses recent breakthroughs in both academic and industrial laboratories that have succeeded as a direct result of alliances between research groups.

Chapter two describes progress toward the total synthesis of dodecahedrane, a complex and highly symmetrical hydrocarbon that bears twelve fused rings arranged in a cage-like architecture. Central to our approach is an ambitious [2+2+2+2+2] poly-ene cyclization cascade which would serve to provide new insights into chemical reactivity. Current efforts center around constructing key linkages found in the target by harnessing the strain release of norbornene ring systems to form new carbon–carbon bonds.

Chapter three describes a concise and scalable synthetic approach to precursors to strained intermediates. Although historically avoided due to their high reactivity, strained cyclic alkynes and allenes have demonstrated value in the synthesis of medicinally privileged, polycyclic compounds. These efforts, which provide efficient access to silyl triflate precursors to cyclohexyne and 1,2-cyclohexadiene, serve to enable further studies involving strained alkynes and allenes.

Chapters four and five describe the development of new methodologies that exploit strained aryne intermediates in the synthesis of complex organic and organometallic materials. Both chapters investigate the controlled generation and reactivity of aryne intermediates, as well as engagement of these intermediates in Pd-catalysis to build new ring systems. Chapter four specifically details the development of aryne chemistry "on-the-complex," wherein fleeting aryne intermediates are reacted with pre-coordinated metal–ligand complexes to form new carbon–carbon bonds. These studies, performed in the context of privileged, photoactive polypyridyl metal complexes, provide an effective strategy to annulate organometallic complexes and access complex metal–ligand scaffolds, while furthering the synthetic utility of strained intermediates in chemical synthesis. Chapter five details the development of Pd-catalyzed reactions of indole and carbazole-based arynes (i.e., hetarynes) to access π-extended heterocyclic materials. The products obtained were applied as ligands in two-coordinate metal complexes to access new OLED emitters.

Chapters six and seven are concerned with uncovering and investigating highly selective reactions catalyzed by fungal enzymes. In particular, chapter six describes the discovery of two groups of enzymes that catalyze distinct reactions, an Alder-ene reaction (previously unknown in biology) and a stereoselective hetero-Diels–Alder reaction. Chapter seven presents studies pertaining to the aminoacylation and thiolation of polyketides in fungi, with a focus on elucidating mechanistic pathways. Both chapters showcase important synergy between chemical synthesis and enzymatic chemistry, and elucidate new enzymatic pathways that ultimately give rise to molecular complexity.

Chapters eight and nine illustrate advances in chemical education. Chapter eight specifically details the development and execution of a new undergraduate course taught by graduate students. The course, entitled Catalysis in Modern Drug Discovery, served to highlight the central role of

organic chemistry in drug discovery, while also conveying key concepts in catalysis. Moreover, the course spotlighted the various careers that organic chemists play in the development of new medicines. Chapter nine presents a perspective that highlights our recent efforts to develop interactive resources in chemical education for worldwide usage. In particular, these efforts seek to promote a spirit of innovation in chemical education and spur the development of widely accessible resources that improve learning outcomes and promote positive perception of chemistry in the broader community.

The dissertation of Jason Chari is approved.

Kendall N. Houk

Abigail Gutmann Doyle

Yi Tang

Neil Kamal Garg, Committee Chair

University of California, Los Angeles

2022

"The difference between science and the arts is not that they are different sides of the same coin, or even different parts of the same continuum, but rather, they are manifestations of the same thing. The arts and sciences are avatars of human creativity."

– Mae Jemison

For my family.

TABLE OF CONTENTS

LIST OF FIGURES AND SCHEMES

CHAPTER ONE

CHAPTER TWO

CHAPTER THREE

CHAPTER FOUR

CHAPTER FIVE

CHAPTER SIX

CHAPTER SEVEN

CHAPTER EIGHT

CHAPTER NINE

LIST OF TABLES

CHAPTER FOUR

CHAPTER FIVE

LIST OF ABBREVIATIONS

α	alpha
β	beta
γ	gamma
λ	wavelength
μ	micro
π	pi
δ	chemical shift
Δ	heat
(Het)	hetero
[H]	reduction
[O]	oxidation
$[\alpha]_D$	specific rotation at wavelength of sodium D line
°C	degrees Celsius
Å	angstrom
AcOH	acetic acid
$AlCl_3$	aluminum trichloride
Alk	alkyl
APCI	atmospheric-pressure chemical ionization
app.	apparent
aq.	aqueous
Ar	aryl
Au	gold
B(pin)	pinacol borane
Benz-ICy•HCl	1,3-dicyclohexylbenzimidazolium chloride
BF_3•Et_2O	boron trifluoride diethyl etherate
Bn	benzyl
$BnNH_2$	benzylamine
Boc	*tert*-butoxycarbonyl
Boc_2O	di-*tert*-butyl dicarbonate
Bu	butyl
Bz	benzoyl
c	centi
c	concentration for specific rotation measurements

C	carbon
C_6D_6	deuterated benzene
C_6H_6	benzene
CaH_2	calcium hydride
cal	calorie
calcd	calculated
cat.	catalytic or catalyst
CD_3CN	deuterated acetonitrile
$CDCl_3$	deuterated chloroform
CF_3	trifluoromethyl
CH_2Cl_2	dichloromethane
CH_3	methyl
CH_3CN	acetonitrile
$CHCl_3$	chloroform
CO_2	carbon dioxide
cod	1,5-cyclooctadiene
d	doublet
DART	direct analysis in real time
DMAP	4-dimethylaminopyridine
DMF	*N*,*N*-dimethylformamide
DMSO	dimethyl sulfoxide
dppf	1,1′-bis(diphenylphosphino)ferrocene
EDC	1-ethyl-3-(3-dimethylaminopropyl)carbodiimide
EDC•HCl	1-ethyl-3-(3-dimethylaminopropyl)carbodiimide hydrochloride
eds.	editors
EDTA	ethylenediaminetetraacetic acid
ee	enantiomeric excess
equiv	equivalent
ESI	electrospray ionization
Et	ethyl
Et_2O	diethyl ether
Et_3N	triethylamine
EtOAc	ethyl acetate
FAQ	frequently asked questions

FT	Fourier transform
g	gram(s)
GC-MS	gas chromatography mass spectrometry(er)
h	hour(s)
H	proton
$h\nu$	light
HCl	hydrochloric acid
Hf	hafnium
HMB	hexamethylbenzene
HOBt	hydroxybenzatriazole
HPLC	high-performance liquid chromatography
HRMS	high resolution mass spectroscopy
Hz	hertz
i-Bu	isobutyl
i-Pr	*iso*-propyl
i-$PrNH_2$	*iso*-propyl amine
i-PrOAc	*iso*-propyl acetate
i-PrOH	*iso*-propyl alcohol
I_2	iodine
ICy•HCl	1,3-dicyclohexylimidazolium chloride
IPr	1,3-Bis(2,6-diisopropylphenyl)-imidazol-2-ylidene
IR	infrared (spectroscopy)
J	coupling constant
K_3PO_4	potassium phosphate tribasic
KO*t*-Bu	potassium *tert*-butoxide
KRED	ketoreductase
L	liter
LDA	lithium diisopropylamide
$LiAlH_4$	lithium aluminum hydride
LiCl	lithium chloride
LiHMDS	lithium bis(trimethylsilyl)amide
m	multiplet or milli or meter
M	molecular mass, molar, or metal
m-	meta
m/z	mass to charge ratio

Me	methyl
$MgSO_4$	magnesium sulfate
MHz	megahertz
min	minute(s)
Mo	molybdenum
mol	mole(s)
mp	melting point
MS	molecular sieves
N	normal
n-Bu	butyl (linear)
n-BuLi	butyl (linear) lithium
N_2	nitrogen gas
Na^0	sodium metal
$Na_2S_2O_3$	sodium thiosulfate
Na_2SO_4	sodium sulfate
NADP	nicotinamide adenine dinucleotide phosphate
NaH	sodium hydride
$NaHCO_3$	sodium bicarbonate
NaOH	sodium hydroxide
NaO*t*-Bu	sodium *tert*-butoxide
NH_4Cl	ammonium chloride
NHC	*N*-heterocyclic carbene
Ni	nickel
nM	nanomolar
NMR	nuclear magnetic resonance
NOESY	nuclear overhauser effect spectroscopy
o-	ortho
OMe	methoxy
p-	para
Pd	palladium
PDB	protein data bank
Ph	phenyl
$PhCOCF_3$	2,2,2-trifluoroacetophenone
PhH	benzene
PhMe	toluene

Piv	pivaloyl
PPh_3	triphenylphosphine
ppm	parts per million
Pr	Propyl
Pt	platinum
PTFE	polytetrafluoroethylene
q	quartet
quint.	quintet
rac	racemic
R_f	retention factor
rpm/RPM	revolutions per minute
Ru	ruthenium
s	singlet or second
sat.	saturated
sext.	sextet
SFC	supercritical fluid chromatography
SiPr	1,3-Bis(2,6-diisopropylphenyl)-1,3-dihydro-2*H*-imidazol-2-ylidene
SiPr•HCl	1,3-Bis(2,6-diisopropylphenyl)-1,3-dihydro-2*H*-imidazol-2-ylidene hydrochloride
SmI_2	samarium diiodide
t	triplet
t-Bu	*tert*-butyl
t-$BuNH_2$	*tert*-butyl amine
t-BuOH	*tert*-butyl alcohol
TA	teaching assistant
TBDPS	*tert*-butyldiphenylsilyl
TBDPSCl	*tert*-butyldiphenylchlorosilane
TCI	Tokyo Chemical Industry Co.
temp	temperature
THF	tetrahydrofuran
Ti	titanium
TLC	thin layer chromatography
TMB	1,3,5-trimethoxybenzene
TMSCl	chlorotrimethylsilane

t_R	retention time
Trit	trityl
Ts	tosyl
UATR	universal attenuated total reflectance
UHP	ultra-high purity
UV	ultraviolet
WT	wild-type
$ZnEt_2$	diethyl zinc
Zr	zirconium

ACKNOWLEDGEMENTS

They say it takes a village and, in my case, it feels like I had much more than that. Throughout this journey, I've been supported, guided, and inspired by so many amazing individuals, and needless to say, I wouldn't be writing this without them. My path to chemistry began in the halls of Baker Lab in Ithaca, New York, where I took my first organic chemistry course with Professors Will Dichtel and Bruce Ganem. At the time, it was fairly late in my undergraduate studies and I had little intention of pursuing chemistry. But Profs. Dichtel and Ganem completely reshaped my perceptions and showed me that organic chemistry is not only all around us, but is an art form, brimming with opportunities for creativity, visual expression, and human ingenuity. Prof. Ganem also taught me that in life it is never too late to change course, and illuminated career paths in chemistry that until that point had been invisible to me. This led me to Prof. Song Lin, who took me under his wing and became my undergraduate research advisor. With no laboratory experience, I had everything to learn from Song, and he helped me draw the connection between pen-and-paper ideas and experimentation. Looking back, I didn't have much of a clue what I was doing as I started in Song's lab, which makes it all the more meaningful to me that Song took the time and had the patience to help guide me through these formative experiences.

This brings me to my doctoral advisor and one of my biggest role models, Professor Neil Garg. I came to graduate school hoping to become a capable chemist, but Neil has showed me that this experience is about much, much more than that. I've grown in ways I never thought I could, and have moved past personal fears and encumbrances that had held me back for years. Before coming to graduate school, I feared public speaking, I rarely thought of myself as a leader, and I also arrived with an immense amount of imposter syndrome. From Neil, I've learned how to move

past these limits. I've learned to believe in my own abilities, and along the way, Neil has helped me to become a better scientist, leader, teacher, and communicator. Perhaps the most impactful advice I've received from Neil is to *know your audience*. Such a simple mantra, but Neil's message of always being aware of who you are interacting with became invaluable to me across everything I did in graduate school, and I will keep it with me everywhere I go. Working with Neil on education projects has also been one of my favorite parts of graduate school, and I've gotten to learn so much from Neil on how to be an effective teacher while making chemistry fun and accessible to others. Neil happens to also be an exceptional scientist, and has an amazing ability to break down *any* problem down into simple, solvable pieces. I could always count on Neil to be there to help guide the ship and encourage me through the most difficult challenges I was faced with. I should also mention that Neil has done all of this for me while also serving as the department chair and raising a family that includes two twin boys. Neil's resilience and leadership in guiding our department through the COVID-19 pandemic further illustrates his care for others and his willingness to go the extra mile to make sure everyone is taken care of. I could continue singing Neil's praises for days, but alas, he has also taught me the importance of being concise. In short, I'm forever grateful for Neil as a mentor, teacher, advocate, and friend.

I would also like to acknowledge the rest of my doctoral committee: Professors Ken Houk, Abigail Doyle, and Yi Tang. Their support, advice, and mentorship throughout my time at UCLA has been critical, and I thank each of them for serving on my committee.

Since coming to UCLA, I have been asked on several occasions, "what is the best part of the Garg lab?" And my answer is always the people. I have been incredibly lucky to be surrounded by the most supportive and kind-hearted individuals I could have hoped for. They have supported me over each and every hurdle, and have served as role models for me throughout my time in

graduate school. Being able to say that your co-workers are also some of your closest friends really is something special, and I couldn't have made it to this point without them.

Post-doctoral scholars play a rather unique role in the Garg lab, providing seasoned perspectives and deep knowledge from their previous academic experiences. When I joined the lab, Swiss post-doctoral scholars Maude Giroud and Sophie Racine, as well as the (very) proud Arizona native Evan Darzi, represented excellent role models. Sophie's quirky and boisterous energy was nicely complemented by Maude's warm, humble charm. Both were excellent role models and happily helped answer the many questions I entered the lab with. And it didn't take long for me to recognize Evan Darzi as an exceptionally talented, resourceful, and creative chemist, and one who helped shape me as a scientist. His enthusiasm and love for chemistry is infectious, and his constant stream of clever ideas not only inspired me to reach his level, but also led me toward some of my biggest successes in graduate school. Darzi also challenged me and pushed me throughout my first two years, and although he came across quite harsh at times ("Chari, this is just not well written!"), it led me to try even harder and set a high bar for myself.

Post-doctoral scholars Veronica Tona and Logan Bachmann joined later on during my time in the lab, and I quickly gravitated toward both of them. Veronica's big personality, Italian upbringing, hot takes on America, and quotable moments provided for endless entertainment, but were uniquely melded with her caring and ever-supportive nature. Veronica inspired me to be more adventurous and not over-think things, and I enjoyed constantly exchanging chemistry ideas with her. I can't wait to make the long-promised trip to Belgium to visit her this summer. And Logan is a quirky and kind-hearted person with an incredible work ethic (as well as tremendous Texas pride), and never hesitated to help me or provide reassurance whenever I needed it. Logan shepherded me through the job-hunting process, and provided much-needed advice and

encouragement every step of the way. And finally, I am grateful for our current post-doctoral scholars, Dan Nasrallah and Nathan Adamson. Dan has an unshakable and infectious passion for teaching, even taking advantage of opportunities to quiz Neil on physical organic chemistry concepts in front of the entire group. Dan's love for turning everything into a teachable moment has greatly contributed to our lab's culture of education and of viewing ourselves as more than just researchers. I've also especially enjoyed our weekly Friday evening bike commutes and getting to learn about his new life as a father. And Nathan is one of the most efficient problem-solvers I have known, quickly devising clever solutions to any challenge he faces. I have strived to think about chemistry to the level of depth that Nathan does, and I've learned a lot just from hearing him break down his way of thinking. I also use every opportunity I can to roast Nathan for being on so many high-priority projects at once ("no, Nathan can't do that right now, he's busy with his three other projects at the moment…") which I think speaks to his high level of ambition and passion for chemistry.

The graduate students I have met throughout my time in the Garg lab have shaped my development both personally and professionally. In my first year in the Garg Lab, the graduating class of Elias Picazo, Emma Baker-Tripp, and Junyong Kim each set a high bar for professionalism, productivity, and classiness. Whereas Emma and Junyong were excellent experimentalists with deep knowledge, Elias was a legend in his own right in the laboratory, which is no doubt a product of his unwavering positivity and optimism. Elias served as an inspiring role model for me in my first year and showed me early on that challenges in graduate school can be surmounted with an unrelenting work ethic and a positive outlook on life.

The next class, which featured Bryan Simmons, Joyann Donaldson, and Lucas Morrill, brought an eclectic range of personalities. Bryan had worked in every single research area our lab

offered, which made him a go-to person for chemistry questions of all sorts. His two-sided personality brought both lively insight and unfiltered, dark sarcasm. Joyann, a lover of all things Disney, brought with her an upbeat, bright energy and showed me that a failure in the lab is never the end of the world (which sometimes I needed to hear). As a competitive roller skater, she also demonstrated that you can be super-productive in the lab while also cultivating hobbies and passions outside of it. And finally, Lucas is an extremely accomplished chemist, an excellent teacher and scientific communicator, and also provided a witty, sarcastic sense of humor. We immediately bonded over our love for Boston, which provided me with a sense of home despite being in a completely new and foreign part of the country to start graduate school. One of the best pieces of advice I received through graduate school was from Lucas, who told me to "always be unapologetically yourself." I still strive to fulfill that life lesson every day.

The class of 2020, fondly referred to as "the Fellas," was a tight-knit crew of four individuals teeming with personality: Robert Susick, Jordan Dotson, Michael Yamano, and Jacob Dander. Rob served as my mentor when I joined the lab, and was an incredibly patient and perceptive teacher. I made innumerable mistakes in my first year, and Rob never once shamed me for it, but instead kindly helped guide me in learning from them and looking forward to the next goal. In Rob's eyes, no question was a dumb question, which freed me up to ask anything without fear of being judged. I can't emphasize enough how important this ended up being for my growth as a chemist in my first year. Rob and I were also partners on two long-term projects in the lab, and I'm grateful for his optimism and resilience on these journeys as well. Jordan is a walking encyclopedia with impeccable teaching skills, and who also happens to be the most humble, down-to-earth person you could meet. It's pretty rare to encounter a person with such deep intellect and abilities as a scientist while also being entirely selfless, kind-hearted and non-judgmental. I

constantly relied on Jordan for support and guidance as I prepared for my candidacy exam, and he was always happy to provide it. Jacob Dander cultivated one of the most unique, multi-faceted personalities I have encountered, and has played a major role in my professional growth in graduate school. Among many things, Jacob is a natural communicator. This can be seen across many areas, from his impassioned story-telling ("and then *of course* Neil finds me searching through the custodial closet!") to his love for scientific writing and presenting. Jacob taught me so much of what I know about how to be a good writer and presenter, and the communication skills he helped me grow during my first three years in the lab have left an indelible impact on my career as a scientist. I also appreciated the sense of perspective that Jacob brought to the lab, as he was always good at putting things into a broader context and led me to think more holistically about my goals in graduate school. And finally, Michael Yamano rounded out the 2020 crew. Michael is a remarkably talented scientist who is also a quick-witted critic. Michael is an expert at spotting holes in logic—even as it pertains to such questions of whether a taco is a sandwich and whether an egg is a ball—and he pushed me to think critically and challenge my assumptions. He is also an excellent problem-solver and I frequently relied on him for chemistry advice and insight.

The class above me, which comprised Melissa Ramirez, Sarah Anthony, and Tim Boit, was with me through my first four years of graduate school, and played central roles in shaping my development long-term. Melissa is the sweetest, most caring labmate I could have asked for, and her inspiring story and journey motivated me to work hard and never take anything for granted. As a joint member of both the Garg and Houk groups, Melissa demonstrated an incredible work ethic and brought a diverse set of skills that we all benefitted directly from. She is also an amazing friend, and supported me through some of the most challenging phases of graduate school. As my first hoodmate in the lab, Sarah is someone I quickly connected with and looked up to since day

one, and made me feel welcomed and appreciated from the moment I set foot in the lab. Also, her powerhouse vocals—although many times off-key—helped to create an atmosphere where work and fun could both thrive. Nonetheless, Sarah not only inspired me as an incredibly productive and talented scientist, but was also someone I connected with on a deeper level and turned to for life advice and encouragement through graduate school, especially as I tackled second-year milestones and later decided on what I wanted to do with my life post-graduation. Sarah represented a wonderful hoodmate, *Org. Synth.* checking mate, project partner, teacher, and friend who helped guide me through everything, and I can't wait to see where the future takes her. And finally, fellow northeasterner Tim is a remarkably intelligent leader in the lab who is as talented a researcher as he is a teacher. As a supreme perfectionist, Tim did not miss a single detail in anything he did, and this led him to create an incredibly high bar in the lab and leave minimal room for error. Teaming up with Tim to create an undergraduate course at UCLA is one of the things I'm most proud of, and it couldn't have happened without him on board.

That brings me to two of my closest friends and fellow fifth years, Rachel Knapp and Francesca Ippoliti. I still don't know how I got so lucky as to have had both of them alongside me throughout these five years, and I might never get over that. Rachel and Francesca are both truly incredible humans and I couldn't have made it to the finish line without them both there with me through it all. Rachel is one of the most kind, honest, and perceptive people I have met, and was always able to understand and empathize with any challenge I faced. I'll never forget being at my wits' end during the COVID-19 lockdown, completely buried in work as I prepared for our summer course, and Rachel was there to calm me down and reassure me that it'd be okay (despite being in the middle of an apocalyptic COVID-19 test line at Dodger Stadium). I also look up to Rachel so much as a scientist. I've been constantly blown away by the way Rachel is able to, time and time

again, set an ambitious goal and achieve it with great efficiency and apparent ease, no matter how difficult the challenge is nor how new the subject area. She has also set such a great example for the lab of having a vibrant social life outside of work, and I think we've all benefitted greatly from seeing that model of living. Francesca has also become one of my closest friends and is one of the sweetest, most caring people I've ever met. We also go way back, as I got to meet her during recruitment weekends even before we even decided to both come to UCLA. I'm so glad we both did. Francesca really gets me, and because of that I found myself looking to her for support at every turn. We've always been on the same wavelength and have relied on each other for help on almost everything. I get really sad thinking about Francesca moving away to the Midwest, but I know she will be just a phone call away and will continue to be an amazing friend. She is also an excellent scientist in her own right, and it has been inspiring to see her vanquish the many challenges she faced en route to lissodendoric acid A.

The class below me brought much energy and personality to the Garg lab. This started with Katie Spence, who I had the honor of mentoring when she first joined the lab. Katie and I were partners-in-crime on two of my most significant projects in graduate school, and I am so glad to have had her by my side through all of the challenges we encountered en route to finishing those projects. She has an amazing sense of humor but is also an amazing listener and has provided much support and encouragement for me from the beginning. Katie also turned just about every experience in graduate school into a fun and enjoyable experience and made sure that every big moment in graduate school got the celebration it deserved, which I appreciated every time. I didn't get to know Milauni as well until we were moved into the same room my fourth year, where I got to know a lot of her endearing (and very loud!) quirks. An outspoken force in the lab—and our *Youth Culture Embassador*—Milauni always creates an energy-filled environment. We bonded

over the great overlap in our music taste, and she also helped me connect with and appreciate my own Indian heritage through celebrating Indian music, food, and holidays. Her openness as a person also really helped me let my guard down and be my most authentic self (especially as we discussed "woke" topics), which I think really helped me grow through my last couple of years in graduate school. Finally, Andrew brought an immense amount of chemistry knowledge and intuition to the lab, and it's been great to see him flourish as a scientist (which I have no doubt he will always continue to do). I've come to Andrew with my most difficult of problems—both chemistry-related and professional—and he has consistently helped me break them down. He is also remarkably quick-witted and has a great sense of humor, which made him an awesome hoodmate.

The COVID-19 pandemic tested the resilience of everyone in the lab, but especially the younger students, who went through many of their milestones in graduate school virtually. I've been so proud to see Laura Wonilowicz, Matt McVeigh, and Ana Bulger conquer everything that has been thrown their way and grow throughout their first three years in the lab. Laura and I share a passion for unifying science and art (which is what drew me to organic chemistry in the first place), and she was the first person I met who I could truly relate to on that front. Laura is one of the kindest and least judgmental people I've met, and I always felt comfortable coming to her with even my silliest qualms and questions. It has been great collaborating with her on education projects and I take great satisfaction in being one of her biggest cheerleaders when it comes to her research. Matt McVeigh immediately created a genuine sense of warmth and approachability when he entered the lab. Matt is an ideal labmate: humble, down-to-earth, and supportive, without any hint of an ego. I was pretty heartbroken when Matt was moved to a different room and I no longer got to sit next to him (yes, I can actually be rather dramatic sometimes), but we've nonetheless

been able to continue sharing chemistry ideas with each other and he's been able to support me through the many practice talks I've put him through. Matt's creative mind and resilience will take him far in science and in life, and I can't wait to see all that he accomplishes in graduate school and beyond. And finally, since becoming hoodmates, Ana and I have grown close (and I now know more about Harry Styles and the Kardashians than I ever thought I would), and I really feel like I can be myself around her, which is such a wonderful feeling. Everyone deserves a labmate and friend like Ana—someone who brings the best out of you and makes you feel valued and heard. I have also really admired her ability to approach every problem with careful logic, and it has been impressive to see her grow into her role as a leader in the lab so incredibly quickly. Also, her amazing singing voice, coupled with her excellent taste in music, have created a wonderful atmosphere in the lab.

The rising third years in the lab, Arismel Tena-Meza, Dominick Witkowski, and Luca McDermott Catena, were also significantly impacted by the COVID-19 pandemic, but handled it with enthusiasm and resilience. Ari is a kind-hearted soul who also has a sassiness about her that you never see coming. It was a joy to see her grow through her first two years and I have shared so many great laughs with Ari throughout her time in the lab (which has included sending each other messages via AirDrop from adjoining rooms). It has been impressive to see Dominick take control of a new project in the lab and steer it to success, and he will no doubt be met with many future successes through his time in graduate school. Dominick is one of the coolest people I know, and it's been great to work alongside him on the education team and see him come into his own in the lab, and even mentor a new student. And finally, I had the privilege of getting to mentor and befriend Luca McDermott Catena. Luca is truly unlike anyone I have every interacted with. He is one of the most dedicated, enthusiastic, resilient, hardworking, and positive forces I can imagine,

and he represents the labmate that I never knew I needed. We have worked together on a mentally challenging project, the total synthesis of dodecahedrane, and being able to constantly exchange ideas (however outrageous they were) with Luca has allowed us to learn and grow together on this project, even though I was technically the older student. Luca's deep knowledge of chemistry—including knowing basically every named reaction—is equally impressive. Luca is also extremely cognizant of the experiences of those around him, which will make him the ideal mentor for younger students over the next few years. He will no doubt find lots of success as a professor in the future.

Rounding out the graduate students in the Garg lab are Georgia Scherer and Jordan Gonzalez. In spite of only overlapping for one year, it feels like I have known both for longer than that. I take at least some responsibility for helping recruit Georgia to UCLA, and she has been a beacon of positive energy in the lab. As a fellow runner, Georgia and I bonded over training for races and it was so awesome to get to introduce her (as well as Melissa and Rachel!) to November Project, my favorite workout group. She has already made great strides in research, and I can't wait to see all that she accomplishes in the future. And Jordan is an incredibly sweet and thoughtful soul. We've been lab roomies for a year now, and Jordan always goes out of his way to make people feel appreciated, whether it is by quickly finding a get-well-soon card for an injured labmate or buying me lunch on my birthday. I'll really miss having Jordan around and can't wait to see how much he evolves as a scientist over the next few years.

Throughout my time in the Garg lab, I have only worked with one undergraduate student, but she was a great one: Melinda Nguyen. Melinda's love for teaching was immutable, and she became a fixture in the education team before I even knew of its existence. Melinda was such a fun labmate to be around—I especially enjoyed her dramatic recountings of laboratory mishaps in

subgroup—and was incredibly humble despite all of her accomplishments. I know that countless students will benefit from Melinda's great teaching skills and care for others.

I really wouldn't have gotten to where I am today if it weren't for my closest friends outside of the lab who helped support me and encourage me through everything, even if they had minimal idea of what I was actually doing these past five years. This is especially true of Max, Natsuko, Justin, Connor, and Karen. Thank you for always being there for me throughout this long journey. And to Max and Natsuko: despite moving across the country from each other after graduating at Cornell, I always felt that you two had never left my side, and that has meant the world to me. Natsuko, you've always been there to pick up the phone any time I needed to talk, and as an incredible listener, you always made sure I made it through whatever challenge I was facing. Max, you've helped keep me grounded me in times when I was the most frazzled, and you've been such a consistent pillar of support for me from the beginning. I truly couldn't have done it without you two.

And of course, my partner through it all, Lauren. Lauren, you've become such a fixture in my life! You've been such an encouraging, patient, generous, and unconditional supporter of everything I've worked through in graduate school and I struggle to imagine what the past few years would have been like without you in it. To me, the impact you've had in my life has been a summation of all of the little things. It's the early morning texts of encouragement, the spontaneous 'donut money' Venmo gifts to ensure that I take breaks, the little evening phone calls where you patiently listen to me ramble on about whatever happened that day, and the way you've seldom complained about my demanding schedule but, rather, appreciated each moment we've had together. I'm so lucky and grateful for all of the little things you do to make me feel appreciated, and for all of the encouragement you've given me over the past few years to make me feel I can

do anything. You've shown me that together, we can conquer everything we set our minds to. I love you, and I cannot wait for our next chapter together in Colorado!

And finally, my family. I'm so grateful for my sister, Sara, and for my parents for being the best role models I could ask for, and for supporting me from the very beginning. Sara, I had the fortune of being able to watch you work toward and earn your own Ph.D. three years ago, and the resilience and grit you showed in pursuit of your own goals inspired me to stay focused and never give up. I'll never forget the feeling of awe and pride I felt in seeing you walk across the stage to be hooded as Dr. Chari, knowing all that you had worked through to make it to that stage. The many students you've taught and inspired since then don't know how lucky they are to be able to call you their instructor. And Mom, you've always taught me to follow my dreams and to always pursue what makes me happy. That's been the most important advice I could have received and I'm so glad to have gotten to fulfill that message in graduate school. Your consistent optimism continues to inspire me, as well as your unwavering selflessness and generosity, and I strive to follow your example every day. And Dad, I am thankful for the way you've always taught me to be humble and never take anything for granted. Regardless of all of your accomplishments and career feats, you've never once flaunted your own abilities, and instead remained intent on helping others succeed. Your humbleness and constant support of my education and my interests has motivated me to always give everything my absolute best. I'm so lucky to have such gracious and selfless parents to guide me and inspire me today, tomorrow, and forever.

Chapter 1 is a version of Morrill, L. A.; Susick, R. B.; Chari, J. V.; Garg, N. K. *J. Am. Chem. Soc.* **2019**, *141*, 12423–12443. Morrill, Susick, Chari, and Garg were responsible for the manuscript.

Chapter 2 is unpublished material.

Chapter 3 is a version of Chari, J. V.; Ippoliti, F. M.; Garg, N. K. *J. Org. Chem.* **2019**, *84*, 3652–3655. Chari and Ippoliti were responsible for experimental studies.

Chapter 4 is a version of Chari, J. V.; Spence, K. A.; Susick, R. B.; Garg, N. K. *Nat. Commun.* **2021**, *12*, 3706. Chari, Spence, and Susick were responsible for experimental studies.

Chapter 5 is a version of Spence, K. A.; Chari, J. V.; Di Niro, M.; Susick, R. B.; Ukwitegetse, N.; Djurovich, P. I.; Thompson, M. E.; Garg, N. K. *Chem. Sci.* **2022**, *13*, 5884–5892. Spence, Chari, Di Niro, Susick, and Ukwitegetse were responsible for experimental studies.

Chapter 6 is a version of Ohashi, M.; Jamieson, C. S.; Cai, Y.; Tan, D.; Kanayama, D.; Tang, M.-C.; Anthony, S. M.; Chari, J. V.; Barber, J. S.; Picazo, E.; Kakule, T. B.; Cao, S.; Garg, N. K.; Zhou, J.; Houk, K. N.; Tang, Y. *Nature* **2020**, *586*, 64–69. Anthony, Chari, and Picazo were responsible for the experimental synthetic chemistry. Cai was responsible for all structural biology. Jamieson was responsible for all computational experiments. Ohashi performed in vivo and in vitro experiments, as well as compound isolation and characterization. Tan, Kanayama, Cao, and Tang performed compound isolation and characterization. Ohashi and Kakule performed bioinformatic analysis to identify the biosynthetic gene cluster. Ohashi and Cai performed protein purification.

Chapter 7 is a version of Tang, M.-C.; Fischer, C. R.; Chari, J. V.; Tan, D.; Suresh, S.; Chu, A.; Miranda, M.; Smith, J.; Zhang, Z.; Garg, N. K.; St. Onge, R. P.; Tang, Y. *J. Am. Chem. Soc.*

2019, *141*, 8198−8206. Tang, Fischer, Chari, Tan, Suresh, Chu, Miranda, Smith, and Zhang were responsible for experimental studies.

Chapter 8 is a version of Chari, J. V.; Knapp, R. R.; Boit, T. B.; Garg, N. K. *J. Chem. Educ.* **2022**, *99*, 1296–1303. Chari, Knapp, Boit, and Garg were responsible for the manuscript.

Chapter 9 is a version of Ippoliti, F. M.; Chari, J. V.; Garg, N. K. *Chem. Sci.* **2022**, *13*, 5790–5796. Ippoliti, Chari, and Garg were responsible for the manuscript.

BIOGRAPHICAL SKETCH

Education:

University of California, Los Angeles, CA

- Ph.D. in Organic Chemistry, anticipated Spring 2022
- Current GPA: 3.80/4.00

Cornell University, Ithaca, NY

- B.S. in Biometry and Statistics, May 2017
- Cumulative GPA: 3.60/4.00

Professional and Academic Experience:

Graduate Research Assistant: University of California, Los Angeles, CA

- August 2017 – present; Advisor: Prof. Neil K. Garg.
- Developed a modular platform for the Pd-catalyzed annulation of photoactive organometallic complexes using transient aryne intermediates and performed late-stage cyclization reactions of elaborated organometallic complexes.
- Devised a photochemical [2+2] cyclization reaction and tethering strategy to facilitate the synthesis of advanced intermediates toward the synthesis of the highly symmetrical hydrocarbon dodecahedrane.
- Designed and executed a methodology for the π-extension of heterocycles using heterocyclic strained aryne intermediates, and engaged in an interdisciplinary collaboration to evaluate the utility of the π-expanded products in Au-centered metal complexes for use as OLED dopants and emitters.
- Realized a concise, scalable route to silyl triflate precursors to strained intermediates cyclohexyne and 1,2-cyclohexadiene from a common synthetic intermediate.
- Executed the multistep synthesis of a key substrate for studies pertaining to the first reported enzymatic Alder-ene reaction, and designed and executed a concise second-generation route to the desired scaffold.
- Synthesized a postulated biosynthetic intermediate of polyketide synthase enzymes, helping to elucidate the novel programming rules by which they operate.
- Contributed to a perspective article in the area of total synthesis, highlighting the constructive power of collaborations to yield new scientific discoveries.
- Organized and managed biweekly literature club meetings for lab members to share and discuss recently published scientific works.

Course Instructor: University of California, Los Angeles, CA.

- Catalysis in Modern Drug Discovery (Chem 101; Summer 2020 and Summer 2021)
  - Designed, developed, and co-taught a new upper division, 4-credit online elective course, which provided an overview of the drug discovery process with a focus on transition metal catalysis in the synthesis of medicines.
  - Taught 90+ undergraduate students about how organic chemistry can impact the world around us, particularly in the development of pharmaceuticals, and recruited industry experts to provide insight on career opportunities in the field. Received the 2020 Education Innovation Award for the success of the course and positive response from students.

Graduate Teaching Assistant: University of California, Los Angeles, CA.

- Undergraduate organic chemistry laboratory (Chem 30BL; Fall 2017 — Summer 2018)
  - Facilitated student learning and mastery of experimental technique through hands-on interaction with students and design of problem sets.
- Undergraduate organic chemistry lecture (Chem 30B; Winter 2019)
  - Designed and presented lesson plans for discussion sections to support students' mastery of course content.

Undergraduate Research Assistant: Cornell University, Ithaca, NY.

- Summer 2016 – Spring 2017; Advisor: Prof. Song Lin.
- Investigated electrochemical methods to synthesize amino acids via nucleophilic capture of CO_2.

Honors and Awards:

- Pfizer-UCLA Dissertation Award for Outstanding Contributions to Organic Synthesis, 2022
- Horizon Prize in Education, Royal Society of Chemistry, 2021
- Summer Mentored Research Fellowship (SMRF), UCLA, 2021
- Dissertation Year Fellowship, UCLA, 2021
- Horizon Prize in Bioorganic Chemistry, Royal Society of Chemistry, 2021
- Ralph and Charlene Bauer Award, UCLA, 2021
- Education Innovation Award, UCLA, 2020
- Jim and Barbara Tsay Excellence in Second Year Research and Academics Award, UCLA, 2020
- UCLA Department of Chemistry and Biochemistry Travel Fellowship, 2020
- Senior Christopher S. Foote Fellowship, UCLA, 2020–2022
- Poster Prize Winner, 33rd Annual Glenn T. Seaborg Symposium, 2019
- Saul Winstein Fellowship, UCLA, 2019
- Hanson-Dow Excellence in Teaching Award, UCLA, 2019
- Graduate Research Fellowship Program Honorable Mention, National Science Foundation, 2019
- Finalist, Berkeley-Haas Patagonia Case Competition, 2019
- Junior Christopher S. Foote Fellowship, UCLA, 2017–2019

Publications:

1. **Advancing Global Chemical Education Through Interactive Teaching Tools.** Francesca M. Ippoliti,[†] Jason V. Chari,[†] and Neil K. Garg. *Chem. Sci.* **2022**, *13*, 5790–5796.
2. **π-Extension of Heterocycles via a Pd-Catalyzed Heterocyclic Aryne Annulation: π-Extended Donors for TADF Emitters.** Katie A. Spence,[†] Jason V. Chari,[†] Mattia Di Niro, Robert B. Susick, Narcisse Ukwitegetse, Peter I. Djurovich, Mark E. Thompson, and Neil K. Garg. *Chem. Sci.* **2022**, *13*, 5884–5892.
3. **Catalysis in Modern Drug Discovery: Insights from a Graduate Student-Taught Undergraduate Course.** Jason V. Chari,[†] Rachel R. Knapp,[†] Timothy B. Boit, and Neil K. Garg. *J. Chem. Educ.* **2022**, *99*, 1296–1303.
4. **A Platform for On-the-Complex Annulation Reactions with Transient Aryne Intermediates.** Jason V. Chari,[†] Katie A. Spence,[†] Robert B. Susick, and Neil K. Garg. *Nat. Commun.* **2021**, *12*, 3706.
5. **An Enzymatic Alder-Ene Reaction.** Masao Ohashi, Cooper S. Jamieson, Yujuan Cai, Dan Tan, Daiki Kanayama, Man-Cheng Tang, Sarah M. Anthony, Jason V. Chari, Joyann S. Barber, Elias Picazo, Thomas B. Kakule, Shugeng Cao, Neil K. Garg, Jiahai Zhou, K. N. Houk, and Yi Tang. *Nature* **2020**, *586*, 64–69.
6. **Total Synthesis as a Vehicle for Collaboration.** Lucas A. Morrill, Robert B. Susick, Jason V. Chari, and Neil K. Garg. *J. Am. Chem. Soc.* **2019**, *141*, 12423–12443.
7. **Thioesterase-Catalyzed Aminoacylation and Thiolation of Polypeptides in Fungi.** Man-Cheng Tang, Curt R. Fischer, Jason V. Chari, Dan Tan, Sundari Suresh, Angela Chu, Molly Miranda, Justin Smith, Zhuan Zhang, Neil K. Garg, Robert St. Onge, and Yi Tang. Thioesterase-Catalyzed Aminoacylation and Thiolation of Polyketides in Fungi. *J. Am. Chem. Soc.* **2019**, *141*, 8198–8206.
8. **Concise Approach to Cyclohexyne and 1,2-Cyclohexadiene Precursors.** Jason V. Chari,[†] Francesca M. Ippoliti,[†] and Neil K. Garg. *J. Org. Chem.* **2019**, *84*, 3652–3655.
9. **Cryptic Species Account for the Seemingly Idiosyncratic Secondary Metabolism of *Sarcophyton glaucum* Specimens Collected in Palau.** Katherine N. Maloney, Ryan T. Botts, Taylor S. Davis, Bethany K. Okada, Elizabeth M. Maloney, Christopher A. Leber, Oscar Alvarado, Charlie Brayton, Andrés Mauricio Caraballo-Rodríguez, Jason V. Chari, Brent Chicoine, J. Chance Crompton, Sydney R. Davis, Samantha M. Gromek, Viqqi Kurnianda, Kim Quach, Robert M. Samples, Vincent Shieh, Camille M. Sultana, Junichi Tanaka, Pieter C. Dorrestein, Marcy J. Balunas, and Catherine S. McFadden. *J. Nat. Prod.* **2020**, *83*, 693–705.

[†]Authors Contributed Equally.

CHAPTER ONE

Total Synthesis as a Vehicle for Collaboration

Lucas A. Morrill, Robert B. Susick, Jason V. Chari, and Neil K. Garg.

J. Am. Chem. Soc. **2019**, *141*, 12423–12443.

1.1 Abstract

"Collaboration" is not the first word most would associate with the field of total synthesis. In fact, the spirit of total synthesis is all-too-often reputed as being more competitive, rather than collaborative, sometimes even within individual laboratories. However, recent studies in total synthesis have inspired a number of collaborative efforts that strategically blend synthetic methodology, biocatalysis, biosynthesis, computational chemistry, and drug discovery with complex molecule synthesis. This chapter highlights select recent advances in these areas, including collaborative syntheses of chlorolissoclimide, nigelladine A, artemisinin, ingenol, hippolachnin A, communesin A, and citrinalin B. The legendary Woodward–Eschenmoser collaboration that led to the total synthesis of vitamin B_{12} is also discussed.

1.2 Introduction

One of the most stunning scientific achievements of the 20th century is the landmark total synthesis[1] of vitamin B_{12} (**1.1**, Figure 1.1).[2,3] Vitamin B_{12} (**1.1**) is the largest and most structurally complex vitamin known and is comprised of a number of structural challenges, including 63 carbons, 14 nitrogens, a cobalt center, and 14 stereocenters. The vitamin, which plays a critical

role in metabolism, was first isolated in pure form in 1948.[4] Subsequently, Nobel Laureate Dorothy Hodgkin determined the structure of **1.1** using X-ray crystallography in 1956.[5] In turn, the remarkable structure of the natural product captivated the minds of the legendary synthetic chemists R. B. Woodward (Harvard, USA) and Albert Eschenmoser (ETH Zurich, Switzerland). The two would initially pursue the synthesis of **1.1** independently, but ultimately realized the difficulty was too great for either group to bear independently. Thus, an international collaboration was formed between the two laboratories in 1965.[2]

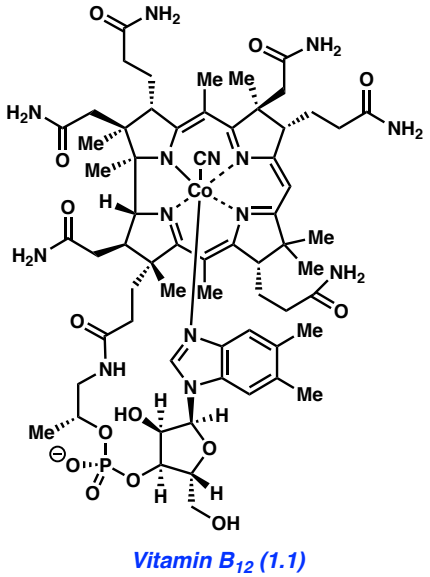

Figure 1.1. The remarkable structure of vitamin B_{12} (**1.1**).

Two of the most memorable moments of the epic vitamin B_{12} collaboration are summarized in Figure 1.2. The groups had decided to each prepare one half of the molecule. Woodward's group arrived at cyanobromide **1.2**, whereas Eschenmoser's team prepared thiodextrolin **1.3**. The two units were then successfully joined using Eschenmoser's sulfide contraction methodology.[6] This transformation delivered product **1.4** bearing the necessary A–D

rings, which, in turn, was elaborated to cobalt derivative **1.5**. The synthesis of **1.5**, bearing much of the natural product's core, constituted an amazing achievement toward the natural product. The second aspect of the highlighted chemistry reflects a somewhat tragic incident. Eschenmoser's group had developed a new, high yielding set of conditions for adding a carbon to each of the one-carbon linkers between the A–B and C–D ring systems. This information was given to Woodward's group, as they had significant quantities of **1.5** on hand, while the Eschenmoser group completed the characterization. Using IR spectroscopy, it was regrettably realized that the nitrile unit stemming off of the D ring had been unintentionally converted to a methyl ester, giving rise to **1.6**. This marked a dead-end, as moving forward it would be impossible to differentiate the newly formed methyl ester from the other esters in **1.6**. Eschenmoser tried to call Woodward immediately, but it was too late. One of Woodward's postdoctoral scholars had come to the laboratory early (ca. 3:30 A.M.) to start the alkylation sequence. Almost all of the material was lost in the incident commonly referred to by the groups as "Black Friday" (July 9, 1971).[3b]

Despite the "Black Friday" setback, the team ultimately persevered and developed an alternate protocol to give the desired alkylated product **1.7** by simply using $ClCH_2OBn$ in place of $ClCH_2OCH_3$.[3b] They would go on to complete the total synthesis of **1.1** in 1972, which remains the only total synthesis of vitamin B_{12} (**1.1**) to date.[7] The total synthesis is said to have involved a remarkable team of 103 co-workers over the course of 12 years, representing 19 countries. Overall, the Woodward–Eschenmoser collaborative synthesis of **1.1** would be an incredible feat, even if accomplished today.

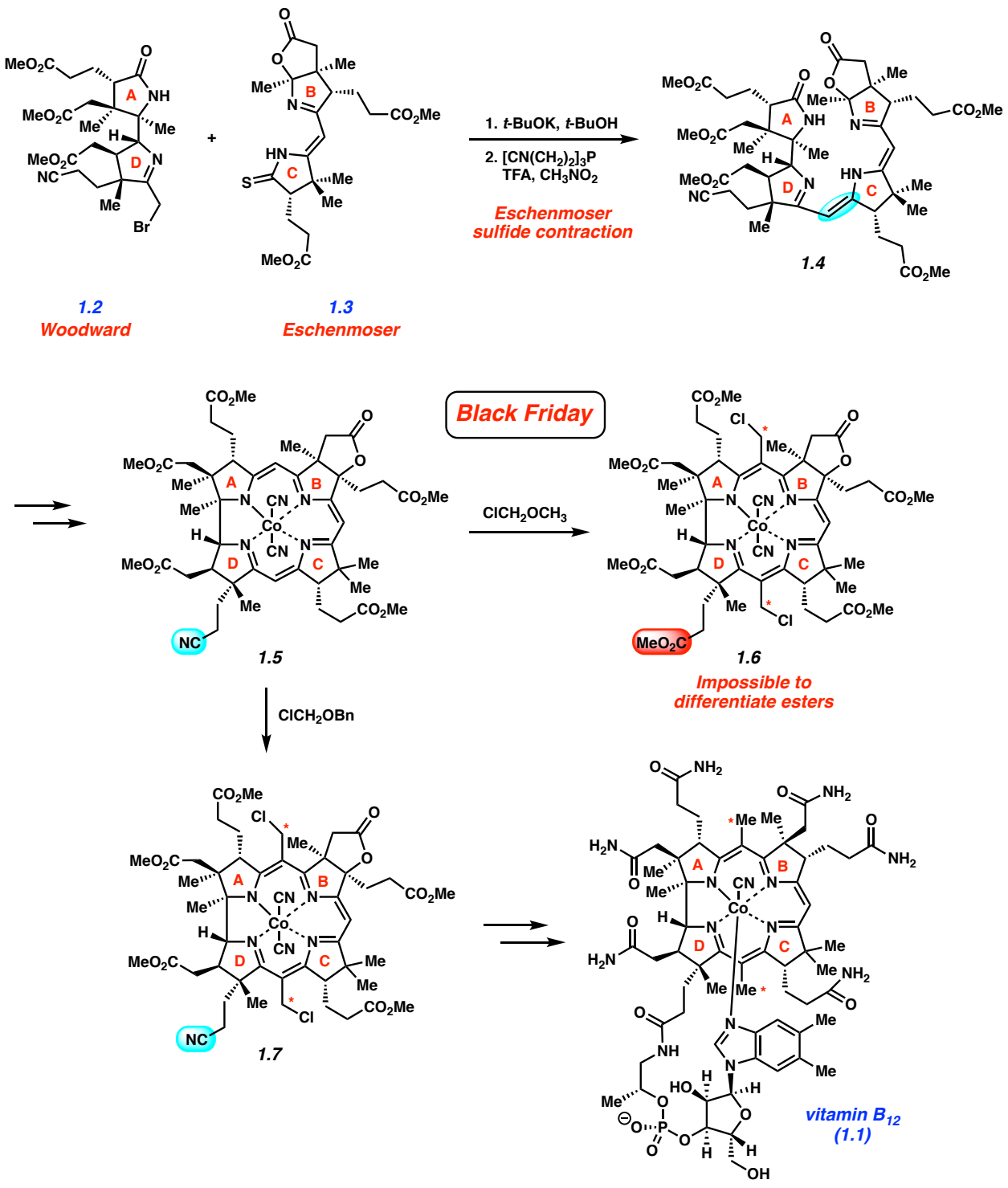

Figure 1.2. Woodward–Eschenmoser approach to vitamin B_{12} (**1.1**)

and the infamous "Black Friday" loss of material.

In the modern era, "collaboration" is perhaps not the first word one would associate with the field of total synthesis. Even practioners like us might think of the field as being more competitive, rather than collaborative, in general. *Who will make the molecule first? Whose synthesis is more elegant? Which synthesis is shorter or more efficient?* Such questions are commonplace amongst total synthesis chemists, and the resulting discussions do ultimately prompt innovations and achievements. That being said, we admire the glory days of collaboration in total synthesis pioneered by Woodward and Eschenmoser. Although we may never see a collaboration of such magnitude within the field of total synthesis again, a number of striking collaborations surrounding total synthesis have been reported in recent years. We describe some of our favorite examples in this chapter that tie together synthetic methodology, biocatalysis, biosynthesis, computations, and pharmaceutical science with total synthesis. The specific targets described are chlorolissoclimide (**1.8**),[8] nigelladine A (**1.9**),[9] artemisinin (**1.10**),[10] ingenol (**1.11**),[11] hippolachnin A (**1.12**),[12] communesin A (**1.13**),[13] and citrinalin B (**1.14**),[14] as highlighted in Figure 1.3.

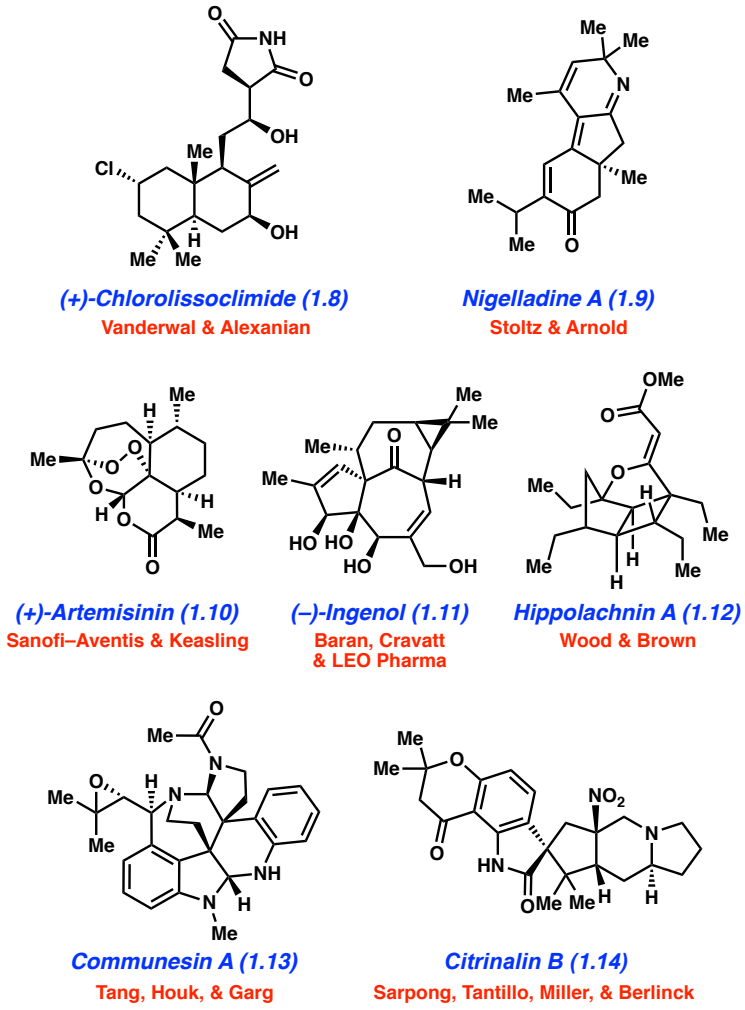

Figure 1.3. Natural products **1.8**–**1.14** synthesized via collaborations.

1.3 Collaborative Synthesis of (+)-Chlorolissoclimide

An elegant collaboration between the Alexanian and Vanderwal laboratories[8] nicely showcases the modern synergy between methodology and total synthesis. (+)-Chlorolissoclimide (**1.8**) (Figure 1.4) was first isolated in the early 1990s from *Lissoclinum voeltzkowi* Michaelson, a coral reef ascidian found in New Caledonia.[15] It displays potent activity against the P388 murine leukemia and KB human oral carcinoma cell lines.[15d,16] The natural product, bearing three rings and 7 stereogenic centers, poses a formidable challenge for total synthesis.[17] One of the

stereocenters is quaternary, whereas another is a secondary stereocenter bearing an alkyl chloride. The latter challenge provided an opportunity for the Alexanian and Vanderwal groups to join forces. Vanderwal's group had already displayed an affinity for chlorinated natural products, which led to several completed total syntheses.[18] Fortuitously, Alexanian's team had established an innovative means to carry out site- and stereoselective halogenation of aliphatic carbons.[19] A compelling example of Alexanian's methodology is shown in Figure 1.4, where (+)-sclareolide (**1.15**) was treated with *N*-bromoamide **1.16** in the presence of visible light to yield bromide **1.17** in 67% yield.[19] A chlorinative counterpart to this methodology did not exist at the time, but if available, could enable the synthesis of (+)-chlorolissoclimide (**1.8**).

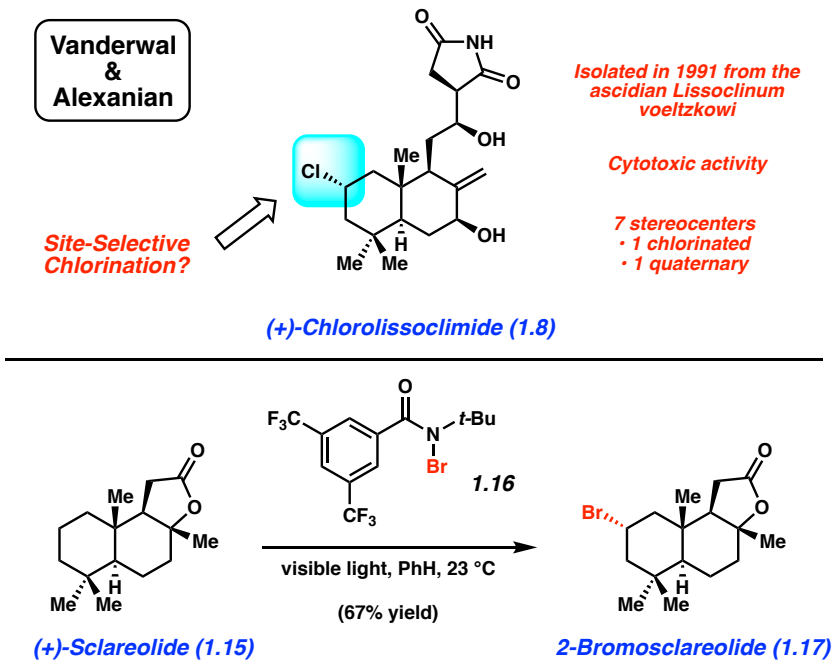

Figure 1.4. (+)-Chlorolissoclimide (**1.8**) and site-selective halogenation methodology.

The success of the Vanderwal–Alexanian collaboration would hinge upon the development of a site-selective, stereocontrolled C–H chlorination reaction. Although highly predictable and chemoselective aliphatic C–H bromination reactions had been developed,[19] aliphatic C–H chlorination reactions remained challenging. Existing methods required the use of strongly acidic conditions or the presence of highly reactive reagents to enable such transformations.[20]

Ultimately, the Alexanian group was able to identify suitable conditions using *N*-chloroamide **1.18** to enable efficient C–H chlorination, which was evaluated on a range of substrates (Figure 1.5). Several products are shown (**1.19**–**1.22**), which reflect that the reaction primarily leads to monochlorination and is sensitive to sterics. It was envisioned that this strategy could be applied to (+)-sclareolide (**1.15**), which has become a popular testing ground as a substrate for C–H functionalization protocols that rely on radical intermediates.[21] Impressively, applying their optimal chlorination reaction conditions to (+)-sclareolide (**1.15**) furnished chloride **1.23** in 82% yield. For gram-scale reactions, an alternate procedure was developed wherein benzoyl peroxide was used in place of visible light for radical initiation. This flexibility underscores the robustness of the Alexanian C–H functionalization protocol.

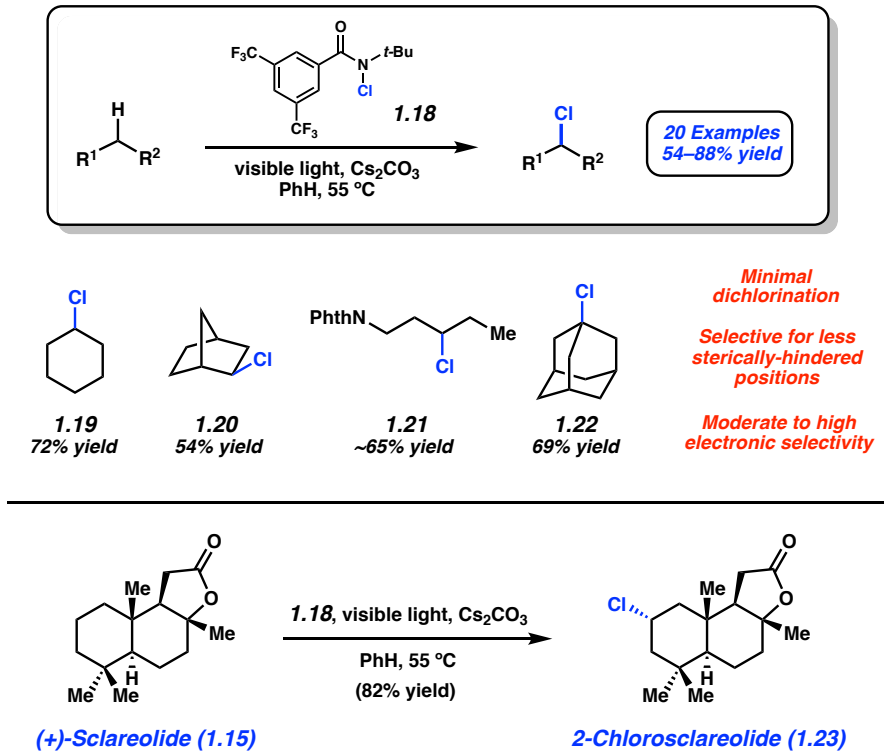

Figure 1.5. C–H chlorination methodology and gram-scale synthesis of (+)-2-chlorosclareolide (**1.23**).

Following the development of the successful C–H chlorination step as the first step of the total synthesis, Vanderwal's team was well poised to develop the necessary synthetic steps to access (+)-chlorolissoclimide (**1.8**) (Figure 1.6). 2-Chlorosclareolide (**1.23**) was elaborated to Weinreb amide **1.24** using a two-step sequence. This set the stage for a site-selective C–H oxidation,[22] followed by Swern oxidation, to deliver enone **1.25**. Further modification gave rise to aldehyde **1.26**, which underwent an Evans aldol reaction with **1.27**.[23] This allowed for the introduction of two new stereocenters and generated alcohol **1.28**. The final steps, involving ammonolysis of the chiral auxillary and ring closure, provided (+)-chlorolissoclimide (**1.8**).

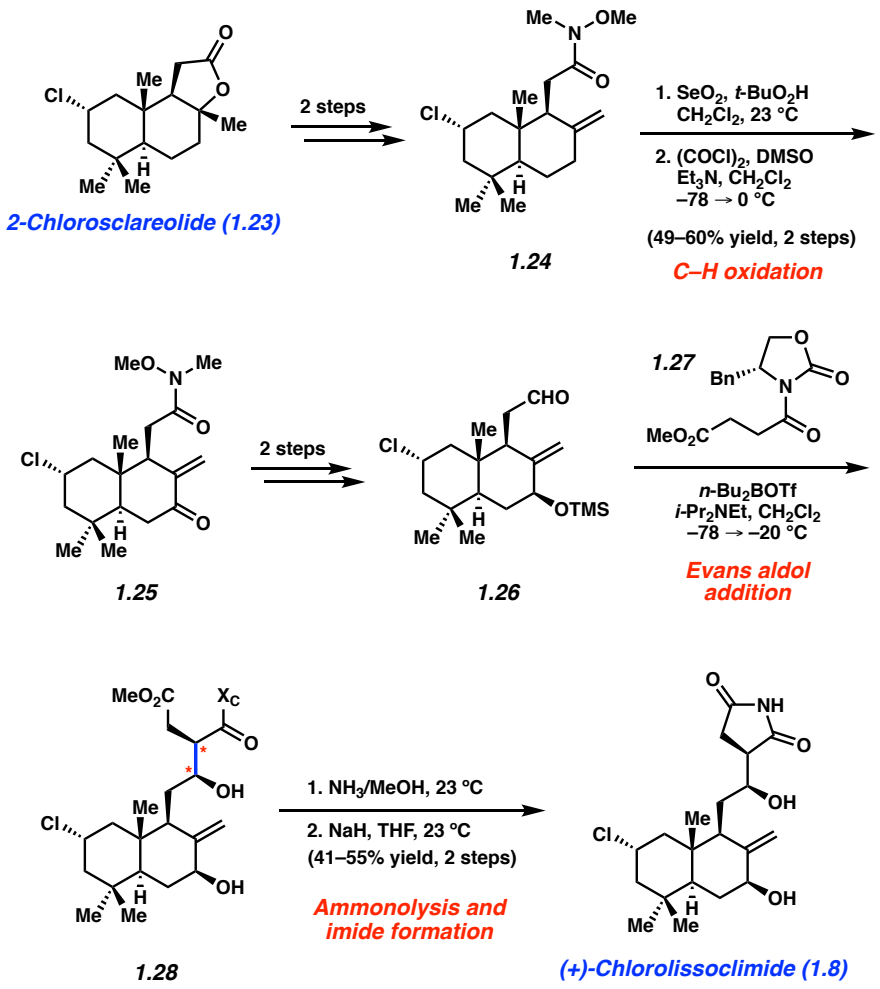

Figure 1.6. A robust route to (+)-chlorolissoclimide (**1.8**).

The Alexanian–Vanderwal collaboration provides a striking example of the synergy between methods development and total synthesis between two different research groups. The effort led to a powerful new methodology for achieving site-selective and stereoselective chlorination, while also facilitating a concise total synthesis of (+)-chlorolissoclimide (**1.8**). The authors were also able to prepare unnatural analogs that show promise as cytotoxic agents toward melanoma and prostate cancer cell lines.[8,24]

1.4 Collaborative Total Synthesis of Nigelladine A

The collaborative synthesis of nigelladine A (**1.9**) (Figure 1.7) by the Stoltz and Arnold laboratories presents a compelling example of synergy between biocatalysis and total synthesis.[9] The natural product, **1.9**, a norditerpenoid alkaloid, was first isolated in 2014 from *Nigella glandulifera* and exhibits potent protein tyrosine phosphatase 1B (PTP1B) inhibitory activity.[25] Nigelladine A (**1.9**) bears a highly conjugated tricyclic skeleton and a quaternary stereocenter, thus offering an intriguing synthetic challenge. Moreover, the natural product possesses oxidation at C7, which the Stoltz group viewed as a potential testing ground for late-stage C–H oxidation protocols. Ultimately, this challenge proved to be a formidable one and could not be easily resolved using conventional synthetic chemistry. This difficulty was eventually resolved using a biocatalytic oxidation.

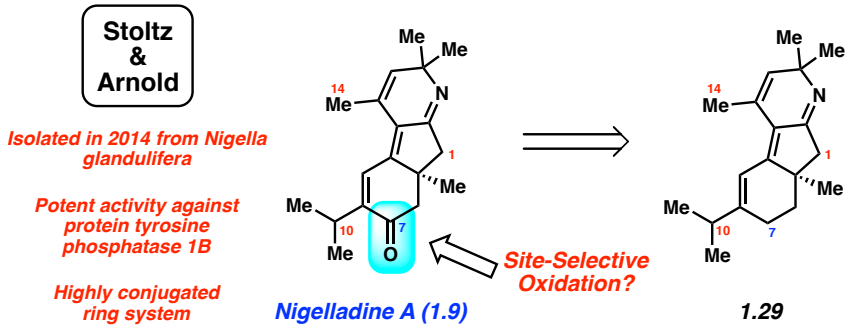

Figure 1.7. Collaborative total synthesis of nigelladine A (**1.9**) by the Stoltz and Arnold laboratories.

With the aim of testing late-stage oxidation chemistry, the Stoltz laboratory first developed the synthetic sequence shown in Figure 1.8. Beginning with known enone **1.30**,[26] a four-step sequence provided multigram quantities of β-ketoester **1.31**. Next, to establish a key

quaternary stereocenter, an asymmetric allylic alkylation was performed.[27] This furnished allylated product **1.32** in 96% yield and 87% ee. Enone **1.32** was further elaborated to vinyl bromide **1.33**, which set the stage for a Suzuki–Miyaura cross-coupling. In the event, treatment of **1.33** with vinyl boronate **1.34** using palladium catalysis delivered triene **1.35**.[28] Lastly, the Boc group was removed using TFA (trifluoroacetic acid). Upon neutralization and exposure to SiO_2, the amine underwent cyclization with subsequent olefin isomerization to provide iminium salt **1.29**.

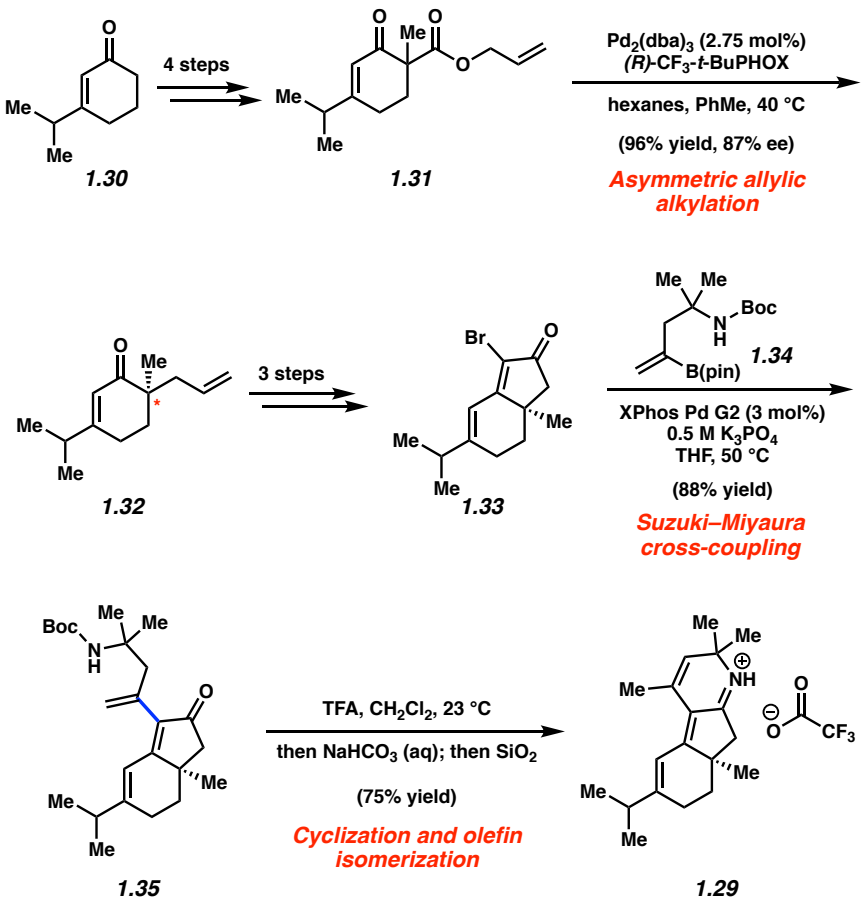

Figure 1.8. Stoltz's synthesis of tricycle **1.29**.

With **1.29** in hand, the Stoltz group was just an oxidation step away from completing the total synthesis of **1.9** (Figure 1.9). The group examined a number of conditions to effect the desired oxidation of neutral imine **1.29** to deliver the natural product nigelladine A (**1.9**).[29] Unfortunately, these efforts were hampered by low yields and poor site-selectivity. At best, nigelladine A (**1.9**) could be obtained in 10% yield using a Rh-catalyzed oxidation protocol. Faced with near defeat, the graduate student lead, Steven Loskot, approached the Arnold laboratory and connected with Dr. David Romney, who coincidentally performed research with Stoltz as an undergraduate student. Together, they envisioned carrying out the key oxidation step enzymatically.[30] A select library of mutated cytochrome P450 enzymes was evaluated and, fortunately, several delivered the desired secondary alcohol. P450 8C7 was identified as the enzyme of choice. In their optimal sequence, the enzymatic oxidation was followed directly by a Dess–Martin oxidation to give nigelladine A (**1.9**) in 21% yield (43% based on recovered starting material **1.29**). This result not only allowed for the completed total synthesis, but also provides a persuasive example of how biocatalysis can be used to effect a challenging late-stage transformation in target-oriented synthesis.

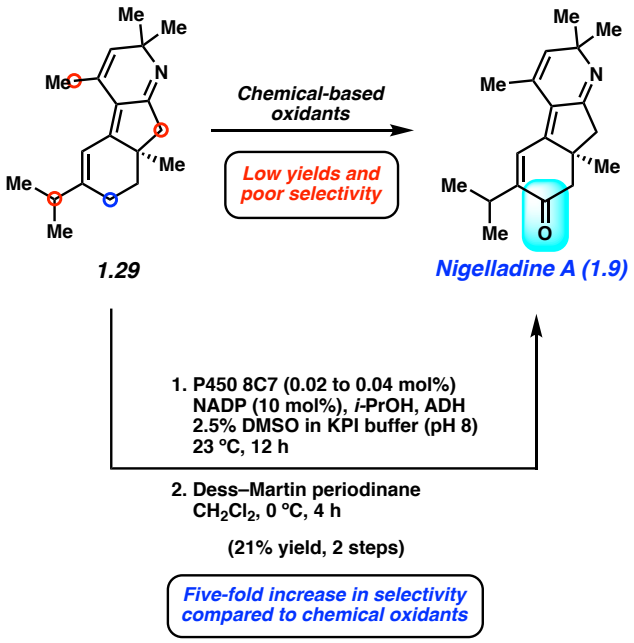

Figure 1.9. The crucial site-selective, late-stage oxidation of tricycle **1.29** was achieved using an enzymatic oxidation and allowed for the total synthesis of nigelladine A (**1.9**).

The alliance between the Stoltz and Arnold laboratories proved instrumental in enabling the first total synthesis of nigelladine A (**1.9**). More specifically, the synthetic expertise of the Stoltz group, including their enantioselective allylation methodology, was leveraged in combination with the Arnold laboratory's proficiency in biocatalysis using mutated enzymes to concisely deliver the natural product. Stoltz notes, "I hope this effort will influence the synthetic community to not only use biocatalysis when faced with a synthetic obstacle, but also to more frequently consider the use of biocatalysis and particularly engineered enzymes during strategic planning."[31]

1.5 Collaborative Total Synthesis of Artemisinin

One of the most exciting collaborations reported in recent years involves the Keasling laboratory and the pharmaceutical giant Sanofi, who came together to develop a semisynthetic route to artemisinin (**1.10**) (Figure 1.10).[10] Artemisinin (**1.10**) is a naturally occurring small molecule first isolated in 1971 in an effort to boost anti-malarial medicinal abilities during the Vietnam War.[32] Artemisinin (**1.10**) and its derivatives display exceptional potency, showing low nanomolar EC_{50} values with regard to their inhibition of the parasitic cause of malaria *Plasmodium falciparum*.[33] Although the development of resistance has historically made malaria difficult to treat, the discovery of artemisinin (**1.10**) and derivatives, such as artesunate (**1.36**) and artemether (**1.37**), has been a tremendous breakthrough for humanity. These compounds function through a novel mode of action relative to previously used anti-malarial drugs.[34] Thus, therapies involving the combination of **1.36** or **1.37** alongside drugs with separate modes of action, termed artemisinin-based combination therapy (ACT), have revolutionized modern malarial treatments. ACTs have led to reduced treatment times, diminished parasite recurrence, and lower resistance development. The impact of these therapies cannot be understated, and was recognized by the awarding of the 2015 Nobel Prize in Physiology or Medicine to Youyou Tu "for her discoveries concerning a novel therapy against malaria."[35] Despite these remarkable advances, malaria continues to be a deadly threat to people, especially children, in the developing world.

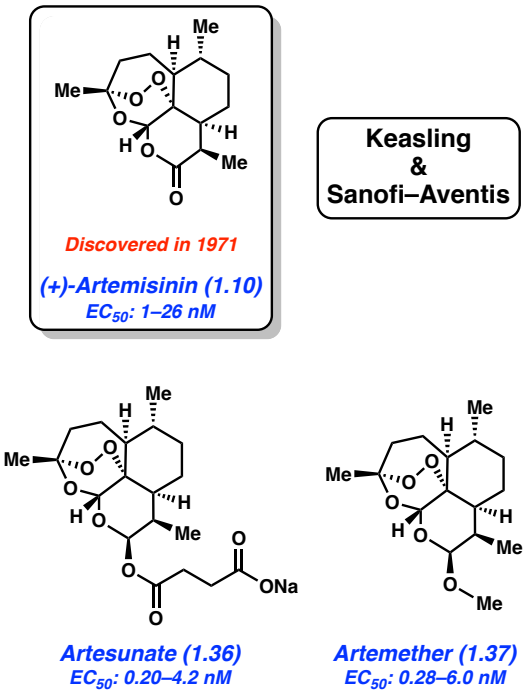

Figure 1.10. Artemisinin (**1.10**) accessed through a collaboration between the Keasling laboratory and Sanofi–Aventis, in addition to unnatural derivatives **1.36** and **1.37**.

ACTs have proven difficult to access for the developing world due to challenges in obtaining reliable supplies of artemisinin (**1.10**).[36] The industrial production of artemisinin (**1.10**) has long relied on isolation from *Artemisia annua*, which gives low and inconsistent yields. This has led to fluctuations in price and availability, which, in turn, has prompted research efforts towards alternative sources of the compound. One such approach involves chemical synthesis, an avenue which has been explored for many years due in part to the provocative structure of artemisinin (**1.10**). The natural product contains four rings and seven stereocenters, as well as a unique endoperoxide bridge. To date, more than 10 completed syntheses have been reported,[37] including those by the laboratories of Schmid and Hofheinz,[38] Yadav,[39] and Cook.[40] Despite these breakthroughs, an approach based solely on synthetic chemistry has yet to meet the high global demand for artemisinin (**1.10**). In addition, synthetic biology on its own has not provided a cost-

efficient synthesis of **1.10**. However, an approach that utilizes both synthetic chemistry and synthetic biology in a synergistic fashion had tremendous potential to unlock a low-cost production route.

The tag-team approach taken by Keasling and Sanofi involved a strategic blend of engineered biosynthesis and organic synthesis. First, the Keasling laboratory and Amyris[41] developed the conversion of glucose (**1.38**) to artemisinic acid (**1.42**) (Figure 1.11). After initial optimization studies performed in *E. Coli* yielded high titres of key intermediate amorphadiene (**1.41**, 25 g/L), the Keasling lab made a pivotal discovery in performing the engineered biosynthesis in a less common strain (CEN.PK2) of *S. cerevisiae*. This switch, driven by the need to express downstream enzymes, allowed for the entire engineered biosynthesis to take place in a single organism. In the final process, glucose (**1.38**) was used as a precursor to acetyl-CoA (**1.39**), which provided an entryway into terpene biosynthesis. A variety of different enzymes then transform acetyl-CoA into amorphadiene (**1.41**) via intermediate farnesyl pyrophosphate (**1.40**). After extensive optimization, the Keasling lab was able to obtain amorphadiene (**1.41**) in a remarkable 40 g/L titre. Further downstream enzymatic oxidations, performed by enzymes characterized in *A. annua* and expressed in yeast, provided artemisinic acid (**1.42**) in an overall isolation of 25 g/L.

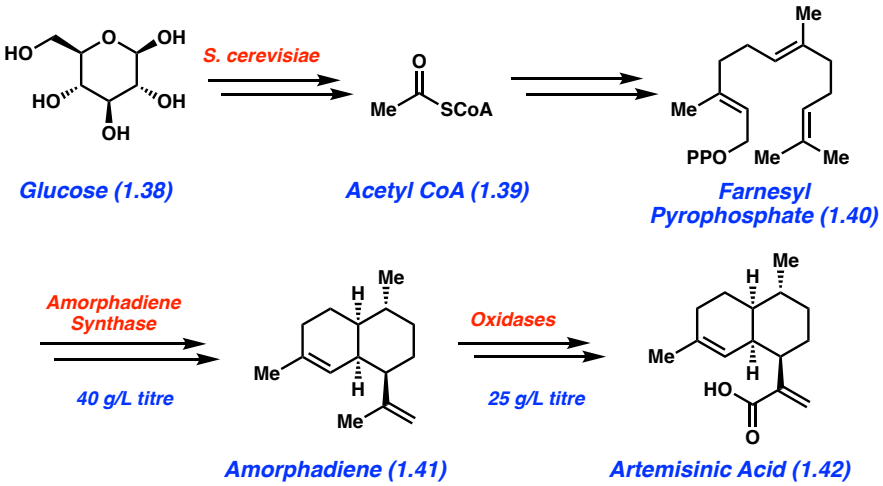

Figure 1.11. Keasling's contribution: an efficient biosynthetic route to artemisinic acid (**1.42**).

With Keasling's biosynthetic efforts providing artemisinic acid (**1.42**), Sanofi took to the task of developing the chemical conversion of **1.42** to artemisinin (**1.10**). Original efforts by Acton and Roth[42] had established the viability of this route, but were not commercially feasible. Thus, over several years, Sanofi optimized the sequence shown in Figure 1.12.[10] First, reduction of **1.42** with a Ru-Segphos catalytic system proceeds in nearly quantitative yield to give acid **1.43** with excellent diastereoselectivity. Activation of **1.43** provides the corresponding mixed anhydride, **1.44**, thus setting the stage for a key photocyclization. Such a photocyclization is thought to occur naturally when **1.44** is exposed to sunlight[43] and has been shown to be viable in a flow process.[44] In the Sanofi procedure, **1.44** is exposed to a sensitizer and light in a semi-batch reactor, with exposure to oxygen. The resulting hydroperoxide intermediate **1.45** then reacts with another equivalent of oxygen to ultimately provide artemisinin (**1.10**). This three-step sequence is remarkably efficient, furnishing the desired natural product in 55% yield. Notably, single batches of 600 kg of artemisinic acid (**1.42**) have delivered 370 kg of artemisinin (**1.10**) using this approach.

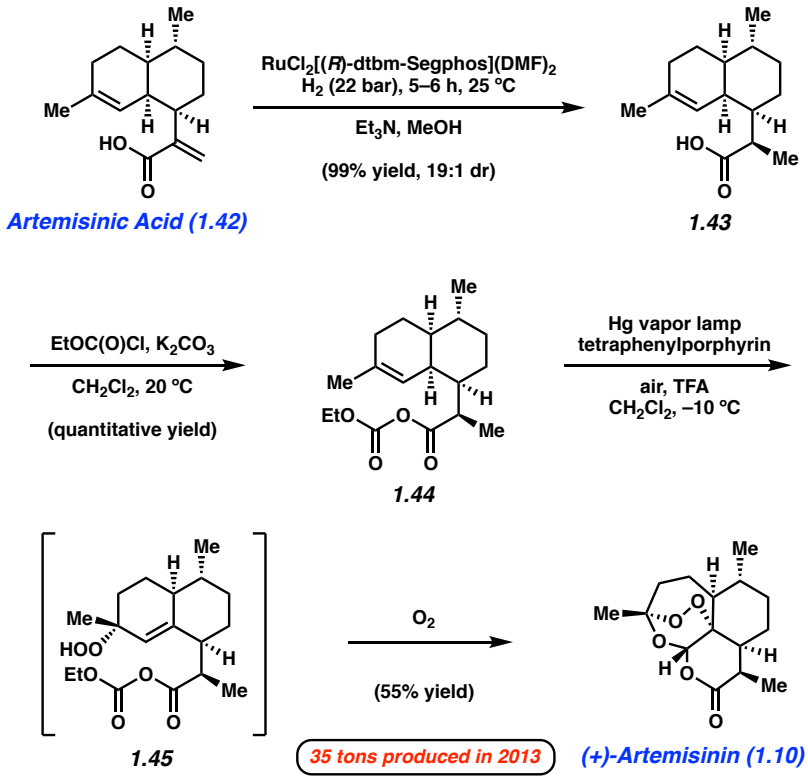

Figure 1.12. The finishing touches by Sanofi: industrial scale conversion of artemisinic acid (**1.42**) to artemisinin (**1.10**).

There have been relatively few collaborations between academic laboratories and industrial laboratories that blend biosynthesis and chemical synthesis to solve a production problem in the pharmaceutical field. Perhaps the most classic example of such a collaboration is the production route to Taxol devised by Holten[45] and licensed by Bristol-Myers Squibb in the 1990s. The collaboration described herein that addresses the artemisinin production problem sets another gold standard for this type of blended approach. The Keasling/Sanofi collaboration delivered 35 tons of artemisinin (**1.10**) in 2013, with the potential to produce up to 60 tons annually. Although the amounts of synthetic artemisinin needed to complement natural material

will vary annually and may even be negligible at times,[46] having a scalable route offers long-term stability to the artemisinin supply problem.

1.6 Total Synthesis of Ingenol

Another exciting collaboration between the pharmaceutical industry and academia is presented in the efficient total synthesis of (+)-ingenol (**1.11**) in 2013 via a partnership between the Baran and Cravatt laboratories and LEO Pharma (Figure 1.13).[11] (+)-Ingenol (**1.11**) was first isolated from *Euphorbia ingens* in 1968,[47] and its derivatives have since been employed as effective treatments for the precancerous skin condition actinic keratosis. The potent analog, ingenol mebutate (**1.46**), marketed as Picato® by LEO Pharma, is an FDA-approved topical treatment for the disease, whereas isoxazole derivative ingenol disoxate (**1.47**) is currently undergoing clinical trials for the same ailment.[48] The preparation of these therapeutic agents presented a major obstacle for LEO Pharma, as only 275 milligrams of ingenol (**1.11**) can be isolated per kilogram of plant material.[11] Artemisinin, in comparison, can be accessed in recovery yields of about 5 grams per kilogram.[49] In addition to this crucial isolation problem, previous synthetic approaches[50] were lengthy due to the complex architecture of the molecule that contains four interconnected rings including an *in/out*-[4.4.1]bicycloundecane core and eight stereocenters, one of which is quaternary and five of which are contiguous. Further, structure–activity relationships were not fully understood, and structural analogs could only be accessed through derivatization of (+)-ingenol (**1.11**) itself.[11] To address these challenges, LEO Pharma partnered with the Baran laboratory to devise a concise, enantioselective total synthesis of (+)-ingenol (**1.11**).

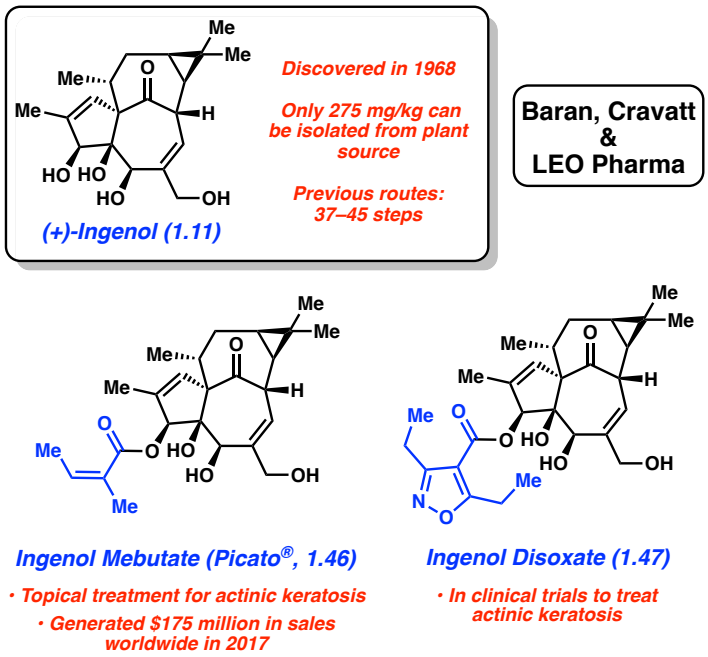

Figure 1.13. (–)-Ingenol (**1.11**) and medicinally important derivatives.

(+)-3-Carene (**1.48**) was identified as a cost-effective starting material for the synthesis of (+)-ingenol (**1.11**) (Figure 1.14).[11] From **1.48**, elaboration to allene **1.49** was achieved through a five-step alkylation sequence, which established four contiguous stereocenters and set the stage for a key allenic Pauson–Khand cyclization.[51] Treatment of **1.49** with an appropriate rhodium catalyst under an atmosphere of CO furnished the 5/7-fused ring system of the natural product to deliver dienone **1.50** in 72% yield. After elaboration to **1.51**, a semi-pinacol rearrangement was employed to furnish **1.52**. Of note, this crucial step assembles the necessary 7-membered ring and the notorious *in/out*-[4.4.1]bicycloundecane. Selective allylic oxidations and protecting group removal ultimately gave rise to (+)-ingenol (**1.11**) in a total of 14 steps from (+)-3-carene (**1.48**).

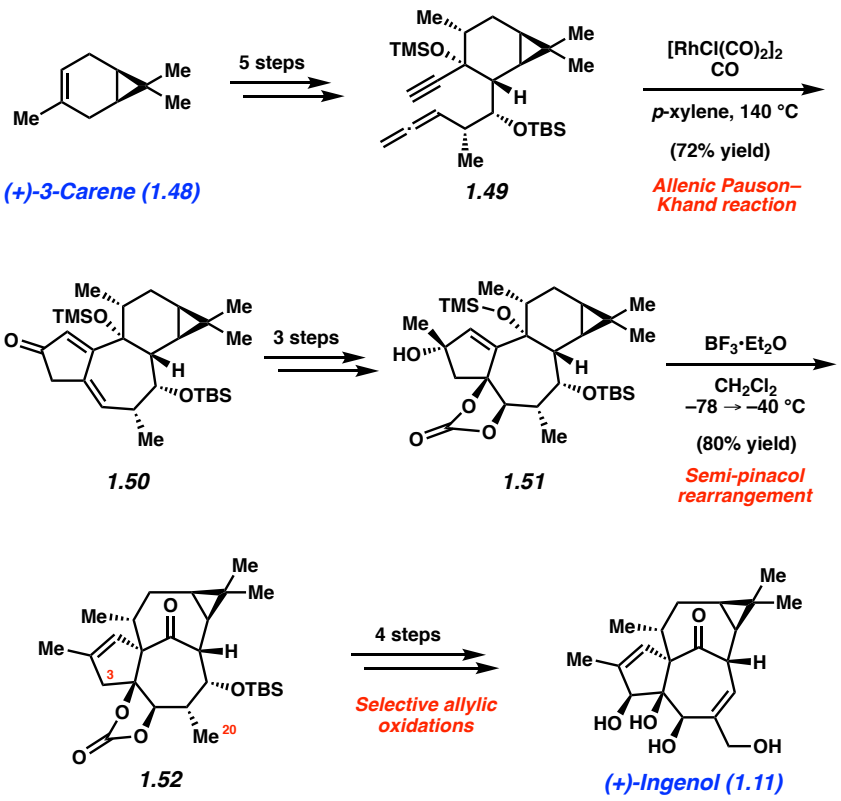

Figure 1.14. Expedient total synthesis of (+)-ingenol (**1.11**).

The newly developed synthetic route to (+)-ingenol (**1.11**) enabled the synthesis of unnatural derivatives for biological investigations. One prominent example is related to the aforementioned analog ingenol mebutate (**1.46**) (Figure 1.15), which is an effective treatment for actinic keratosis commercialized by LEO Pharma. Whereas the general mode of action for **1.46** had been well characterized,[52] the specific proteins it targets within cancer cells had not been identified. In collaboration with the Cravatt laboratory, a suitable substrate for chemical proteomic discovery was synthesized to enable the identification of ingenol mebutate (**1.46**) binding proteins. A "fully functionalized" probe was realized in the ingenol mebutate derivative **1.53**, which harbors a photoreactive dialkyl diazirine and clickable alkyne for visualization of the binding proteins.[53] This derivative was accessed from allylic alcohol **1.54**, available from the

route described above,[11] by treatment with MsCl, followed by TBACl and LiN_3, to provide azide **1.55** in 60% yield over two steps. Further elaboration generated "azido-ingenol" (**1.56**), which, in turn, underwent a copper-catalyzed click reaction[54] with bis(alkyne) **1.57** to furnish clickable probe **1.53** in 37% yield. Empowered with the ingenol-based probe, Cravatt and co-workers employed quantitative mass spectrometry-based proteomics to discover a new protein target for ingenol mebutate (**1.46**).[55] Specifically, the mitochondrial carnitine/acylcarnitine carrier protein SLC25A20 was identified as a highly ligandable site for **1.46** and **1.53**. Further studies revealed that ingenol mebutate (**1.46**) inhibits SLC25A20, thereby perturbing mitochondrial function and leading to necrotic cell death in a pathway independent of that known via protein kinase C agonism.

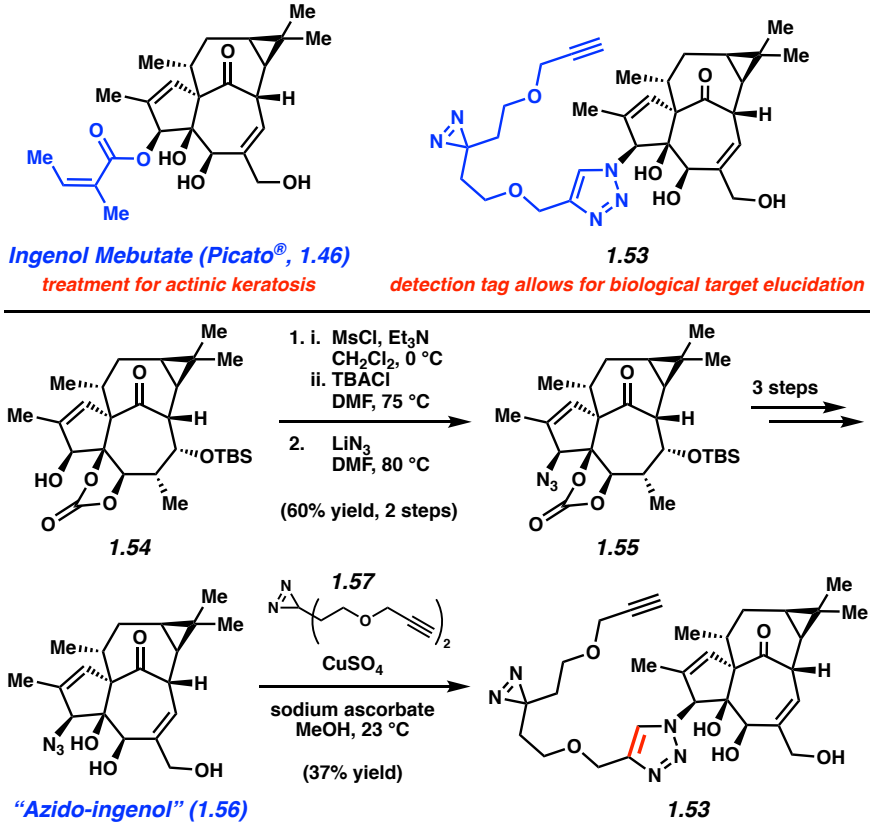

Figure 1.15. Synthesis of ingenol derivative **1.53** bearing a photoaffinity probe.

The partnership between the Baran laboratory, the Cravatt laboratory, and LEO Pharma illustrates the effectiveness of leveraging academic resources to solve critical problems in the pharmaceutical industry. The concise total synthesis of (+)-ingenol (**1.11**) delivered an attractive solution to access valuable material.[11] Additionally, the synthetic route enabled further biological studies by the Cravatt laboratory to elucidate the molecular targets of ingenol derivatives, including that of the FDA-approved drug ingenol mebutate (**1.46**). In turn, this effort led to the elucidation of a novel mechanism of action. The Baran–LEO Pharma team subsequently synthesized the classic target (+)-phorbol, where LEO Pharma provided large quantities of **1.50**, a common intermediate from their synthesis of (+)-ingenol (**1.11**).[56] The total syntheses of several other terpene targets have also been achieved as a result of this collaboration.[57]

1.7 Total Synthesis of Hippolachnin A

Collaboration between two total synthesis groups is rare today, despite the precedent set by Eschenmoser and Woodward decades earlier. Nonetheless, the Wood and Brown laboratories reported a particularly successful example with their total synthesis of hippolachnin A (**1.12**) described in 2016 (Figure 1.16).[12,58] The natural product was first isolated in 2013 from *Hippospongia lachne*. Hippolachnin A (**1.12**) bears a densely functionalized polycyclic core, which presents a challenge for chemical synthesis. Notably, **1.12** possesses six contiguous stereocenters, one of which is quaternary, and a structurally unique, highly congested tricyclic skeleton. In addition to its unique structure, **1.12** was initially reported to display potent antifungal activity against several pathogenic fungi, in particular *Cryptococcus neoformans*.[59] Thus, developing a synthetic strategy to access the scaffold of **1.12** was highly desirable.

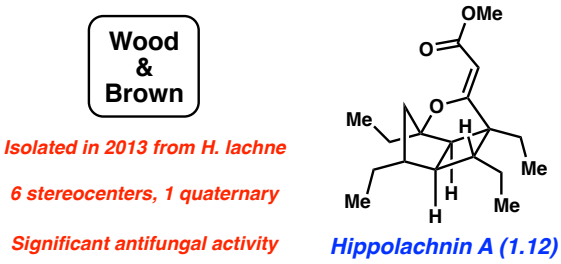

Figure 1.16. Collaborative total synthesis of hippolachnin A (**1.12**).

The collaboration between the Wood and Brown groups was spurred by a serendipitous meeting during a poster session at the 2015 National Organic Symposium.[12,60] The lead graduate students on the project realized their synthetic designs toward hippolachnin A (**1.12**) were nearly identical, including the non-obvious use of quadricyclane (**1.60**) as the starting material (Figure 1.17). Although one could imagine each group trying to reach the finish line first, the researchers took the opportunity to work together. Ultimately, they were able to combine the strengths of each independent synthesis to formulate an improved and elegant route to hippolachnin A (**1.12**). The natural product, **1.12**, was envisioned to arise from fused-[3.2.0]-bicyclic intermediate **1.58** through a late-stage C–H oxidation. Fused bicycle **1.58** could be traced back to bridged-[2.2.1]-bicycle **1.59**. In the forward sense, ring-opening metathesis of the bridged bicycle present in **1.59** would yield **1.58**. Lastly, the cyclobutane found in **1.59** would arise from quadricyclane (**1.60**). In the Brown laboratory's route, quadricyclane (**1.60**) would undergo a [2+2+2] cycloaddition with acid chloride **1.61** to generate the desired cyclobutane intermediate. Separately, the Wood laboratory envisioned a [2+2+2] cycloaddition between quadricyclane (**1.60**) and diester **1.62**, with further manipulations, would deliver the key cyclobutane intermediate **1.59**.

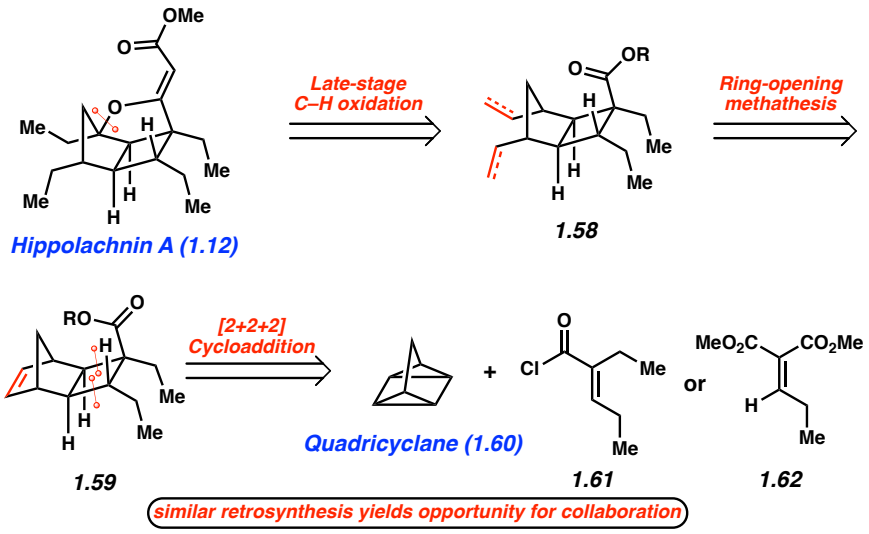

Figure 1.17. Shared retrosynthetic analysis of hippolachnin A (**1.12**).

Figure 1.18 provides a summary of the collaborative route to hippolachnin A (**1.12**) devised by the Brown and Wood laboratories. Using Brown's initial step, quadricyclane (**1.60**) underwent a [2+2+2] cycloaddition[61] with acid chloride **1.61**, thus forming carboxylic acid **1.59** in 50% yield after hydrolysis of the acid chloride. This remarkable key reaction installed all six stereocenters of the natural product in a single transformation. From **1.59**, ring-opening metathesis of the bridged bicycle in the presence of ethylene delivered fused-[3.2.0]-bicycle **1.58** with high efficiency.[62] This set the stage for a key C–H oxidation developed by the Wood laboratory. In the event, **1.58** was treated with a modification of White's conditions using catalyst **1.63** to generate lactone **1.64** in 70% yield.[63] With lactone **1.64** in hand, a three-step sequence involving a condensation, reduction, and transesterification produced hippolachnin A (**1.12**). Interestingly, the reported antifungal activity of hippolachnin A (**1.12**) could not be reproduced using synthetic material.[64] This same observation was verified independently by Trauner's laboratory during bioactivity studies of synthetic analogs of **1.12**.[65] In fact, none of the analogs displayed antifungal activity, and only weakly potent growth inhibition of the nematode

Caenorhabditis elegans was observed. This clarification of the biological activity of hippolachnin A (**1.12**) and derivatives underscores the utility of total synthesis in enabling bioactivity studies.

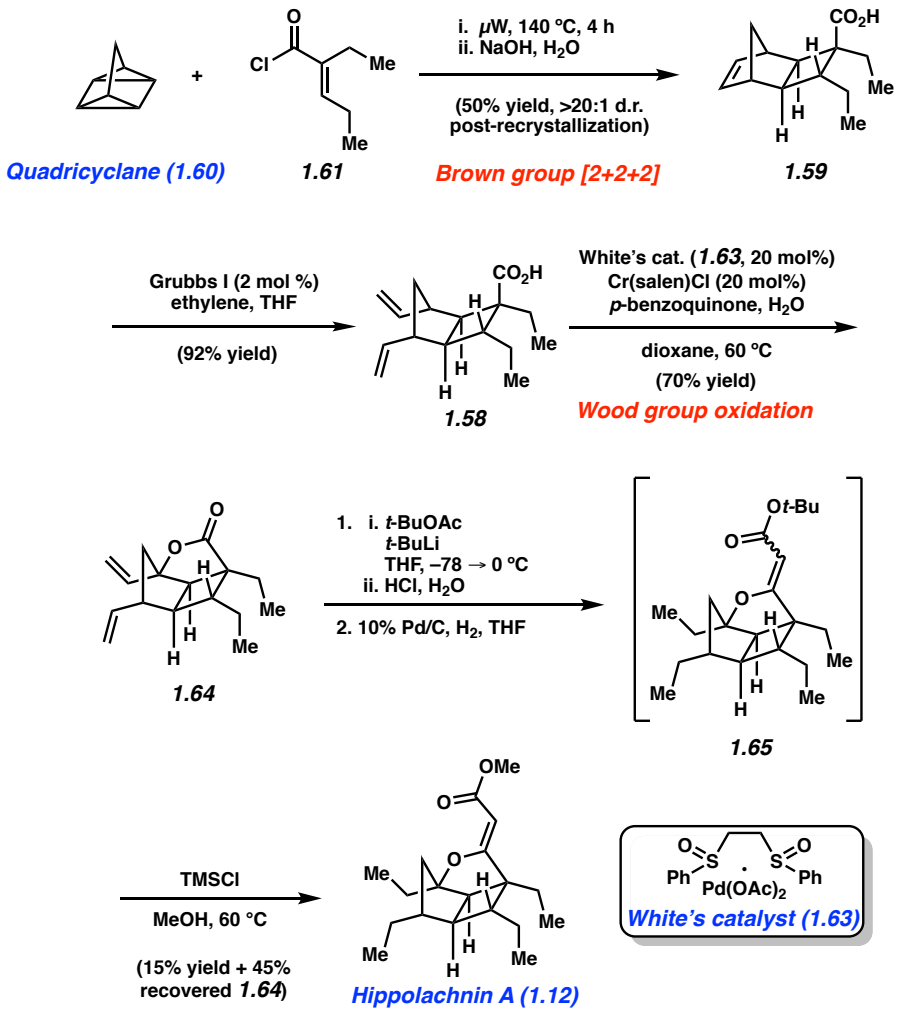

Figure 1.18. Collaborative route to achieve the total synthesis of hippolachnin A (**1.12**).

Overall, the joint synthetic route developed by the Brown and Wood laboratories represents an uncommon synergetic relationship between two synthetic research groups. The individual laboratories' total syntheses of hippolachnin A (**1.12**) each totaled nine steps. Upon collaborating and finding advantageous portions of each route, the team was able to establish a

six-step route to **1.12**. The final synthesis featured impressive [2+2+2] cycloaddition chemistry using quadricyclane (Brown laboratory) in combination with an elegant C–H oxidation and subsequent elaboration (Wood laboratory). Moreover, the joint effort provided students with many opportunities to exchange ideas beyond the confines of their individual institutions. Although collaborations of this nature between total synthesis groups remain rare, the elegant Brown and Wood synthesis of **1.12** underscores the value of such partnerships.

1.8 Biosynthesis of Natural and Unnatural Communesin Scaffolds

Understanding the biosynthetic origins of highly intricate natural product scaffolds can require collaboration across synthetic, computational, and enzymatic chemists. A compelling example of this cooperation that was borne out of a total synthesis endeavour is exemplified by the investigation of the communesin alkaloid biosynthesis recently reported by the Houk and Tang laboratories, together with our laboratory.[13] The communesins possess daunting chemical structures and promising biological activities, and have therefore been popular targets for synthetic chemists.[66] With regard to their structural features, the communesin scaffold **1.68** (Figure 1.19) bears four nitrogen atoms and a multitude of stereocenters embedded in a heptacyclic framework. The vicinal quaternary centers at C3 and C3' are particularly challenging to install.

The nature of how this particular collaboration arose deserves special mention. Garg had studied in two laboratories where the communesin alkaloids were being pursued.[67] In addition, his own laboratory had devised a synthetic route to the communesin scaffold using the so-called interrupted Fischer indolization methodology.[68] When this synthetic methodology failed to generate scaffolds containing vicinal quaternary stereocenters, over a casual lunch meeting,

Professors Tang and Garg decided the problem should be investigated biosynthetically. Tang procured the necessary fungus and a joint student was able to isolate communesin alkaloids in a matter of weeks. Both research groups became fascinated by the remarkable ability of Nature to generate vicinal quaternary stereocenters and the challenging communesin framework.

The Tang group went on to identify the biosynthetic gene cluster for quaternary stereocenter formation.[69] However, the exact mechanism of formation of these quaternary centers remained elusive (**1.66** + **1.67** → **1.68**, R=H, Figure 1.19). Thus, the Houk laboratory was also recruited and together, the team performed a combination of feeding studies, computations, and mechanism of action studies that ultimately led to new insights and access to a novel communesin scaffold (i.e., **1.69**).

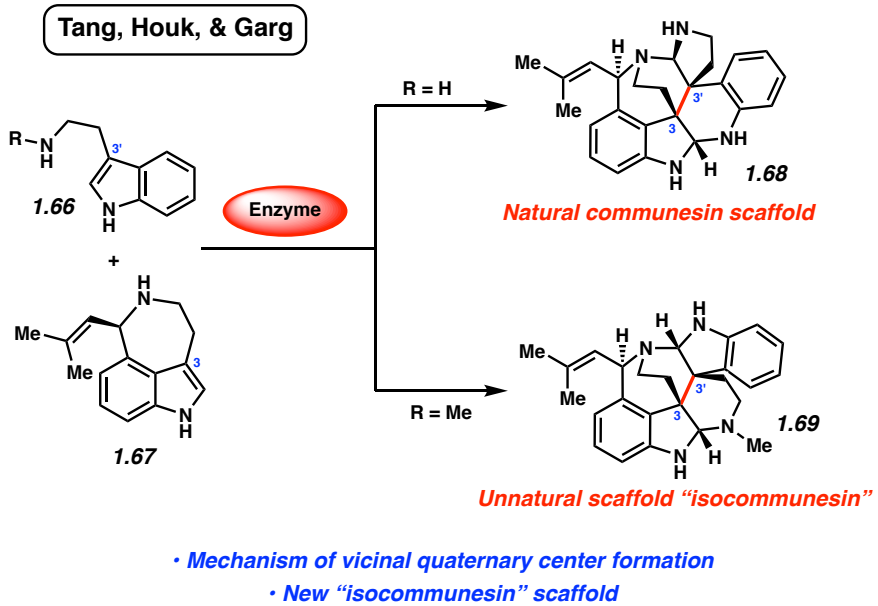

Figure 1.19. Biosynthetic studies of the heterodimeric scaffolds of communesin indole alkaloids.

To determine the order of bond forming steps, the Tang laboratory engineered yeast to express the cytochrome P450 oxidoreductase. Concurrently, the Garg laboratory synthesized

substrate analogs for feeding studies. Several key results are depicted in Figure 1.20. For example, when N10' methylated tryptamine derivative **1.70** was employed in the enzymatic coupling with aurantioclavine (**1.67**), a new oxidatively coupled product was obtained. This compound, **1.69**, bears a new scaffold that was termed "isocommunesin". An analogous outcome was seen when tryptophol (**1.71**) was utilized, which gave rise to "isocommunesin" **1.72**. Interestingly, isocommunesins were obtained when ω-*N*-dimethyl-tryptamine (**1.73**) and 3-(2-azidoethyl)-indole (**1.74**) were used, whereas no product was seen if N1 and N1' methylated derivatives of tryptamine or aurantioclavine were employed (**1.75** or **1.76**, respectively). The latter results indicate that the indole hydrogens are essential for coupling and supports previous hypotheses.[70,71] Overall, the fact that a new communesin-type framework could be accessed through the use of natural enzymes showcases the power of this strategy for accessing new chemical space.

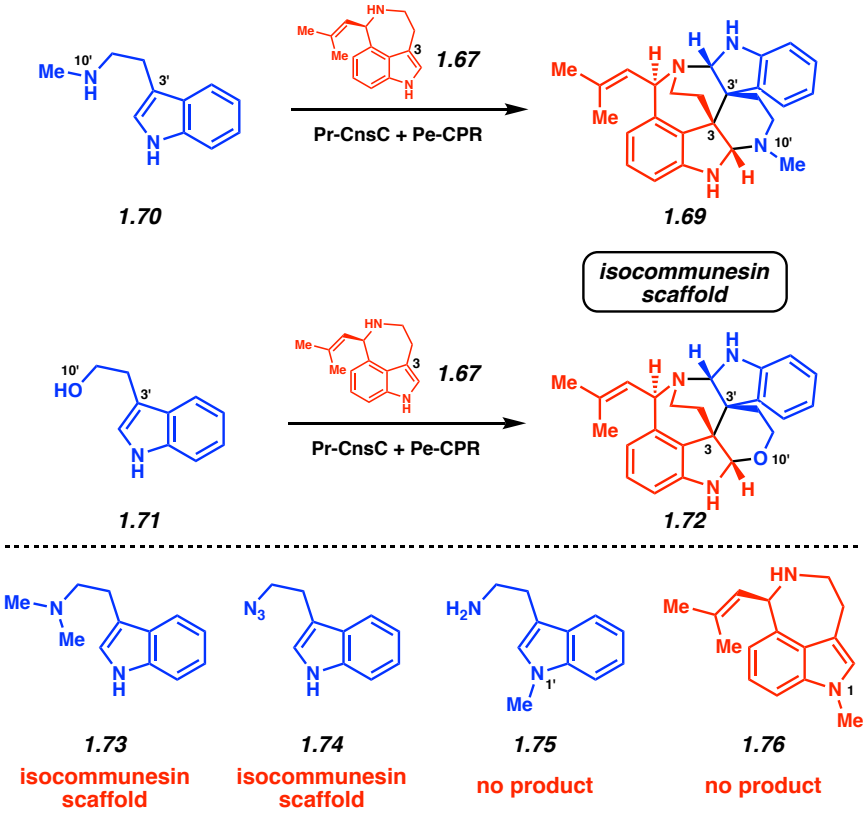

Figure 1.20. Feeding studies of P450 oxidoreductase with analogs.

With access to both communesin and "isocommunesin" scaffolds, the researchers questioned what factors govern the formation of one scaffold over the other as a function of substituents. As such, the Houk laboratory performed computations to determine the energetics of the two competing pathways in the absence of enzymes (Figure 1.21). Although no transition states were identified, it was assumed that the activation energy of each step was proportional to the energy of formation for each intermediate in the proposed reaction pathway. Given the commonality of the C3–C3' linkage in both scaffolds, the indole coupling step is proposed to occur first in the active site of CnsC. Beginning from **1.66** and **1.67**, two sequential one-electron transfer processes lead to aza-allyl radicals **1.77** and **1.78** (with net two-electron reduction of Fe), which combine to generate the vicinal quaternary stereocenters in **1.79**. From heterodimer **1.79**,

two possible intramolecular aminal formations can occur that lead to either the communesin or isocommunesin scaffold. It was found that aminal formation between N10' and C2 is more energetically favored, leading to the unnatural isocommunesin scaffold **1.80**. The competing process involving aminal formation between N10' and C2' (leading to the natural communesin scaffold **1.81**) is actually less energetically favorable. Thus, it is thought that elaboration to the communesin scaffold **1.82** requires the CnsC enzyme to override the inherent thermodynamic preference of the system. As observed in the feeding studies, the enzyme's substrate specificity about N10' is limited to R=H.

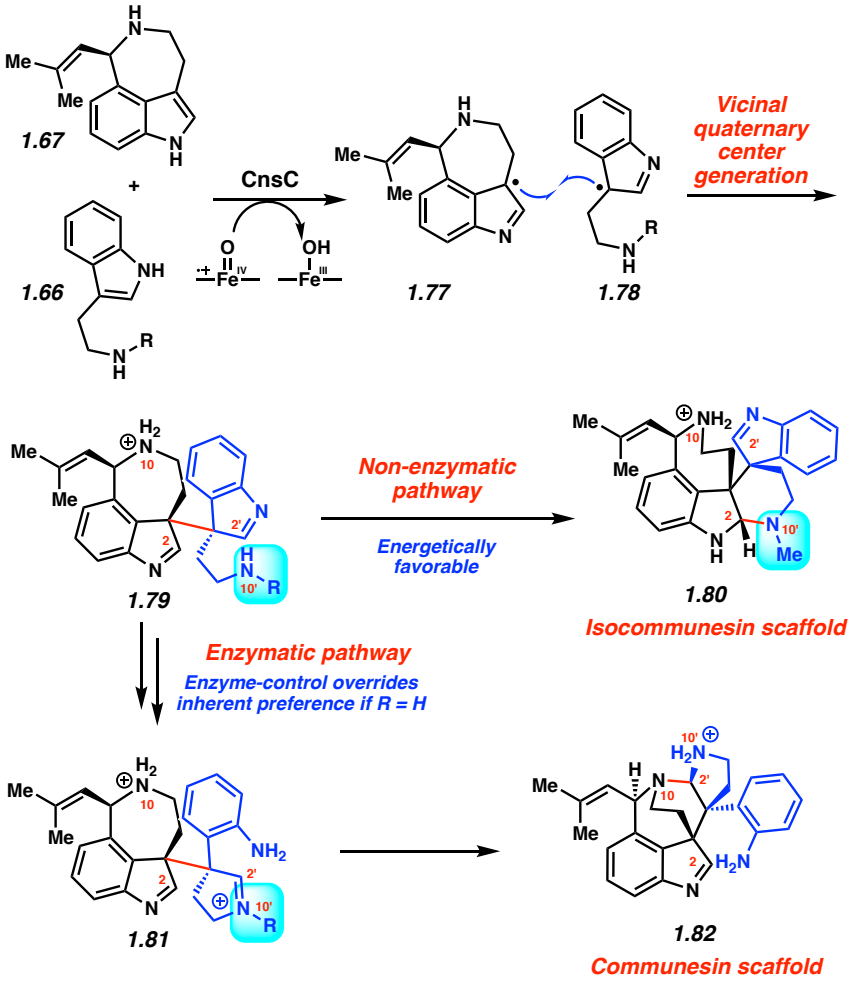

Figure 1.21. Mechanistic studies on communesin scaffold formation by the Houk laboratory.

The collaboration between the Tang, Garg, and Houk laboratories does not necessarily fall under the general category of total synthesis. However, the study is an important one in the area of natural products, as it strategically leverages the collective powers of synthetic chemistry, biosynthetic chemistry, and computational chemistry to furnish access to natural products, new and highly complex natural product analogs, and mechanistic insights. Moreover, the enzymatic coupling of two indole units to generate vicinal quaternary stereocenters sets a high bar for synthetic chemists in pursuit of such alkaloids.

1.9 Total Synthesis of Cyclopiamine B and Biogenetic Studies

The final collaboration we discuss involves research performed by four teams pertaining to the citrinalin and cyclopiamine natural products. Here, Sarpong, Tantillo, Miller, and Berlinck[14] demonstrated the interplay between total synthesis, computational tools, peptide catalysis, and natural product biosynthesis. Ultimately, these efforts led to a natural product structural revision, seminal total syntheses, discoveries in peptide-based catalysis, and insights into natural product biosynthesis.

The specific targets accessed in this endeavour using total synthesis are the indole alkaloids citrinalin B (**1.14**) and cyclopiamine B (**1.85**) (Figure 1.22).[72] Both the originally assigned structure **1.83** and the revised structure for citrinalin B (**1.14**) are depicted. Citrinalin B (**1.14**) was first isolated in 2010 from *Penicillium citrinum*[73] and cyclopiamine B (**1.85**) was isolated from a toxinogenic strain of *Penicillium cyclopium* in 1979.[74] The natural products have six rings, and each bears four stereocenters, including one quaternary stereocenter as part of the spirooxindole framework. In addition, citrinalin B (**1.14**) and cyclopiamine B (**1.85**) each possess three distinct nitrogen substituents. One of the substituents is an alkyl nitro group, which is rarely seen in natural products.[75] From a biosynthetic perspective, **1.14** and **1.85** are curiosities because they lack the typical bicyclo[2.2.2]diazaoctane moiety present in many congeners,[76] such as citrinalin C (**1.84**).

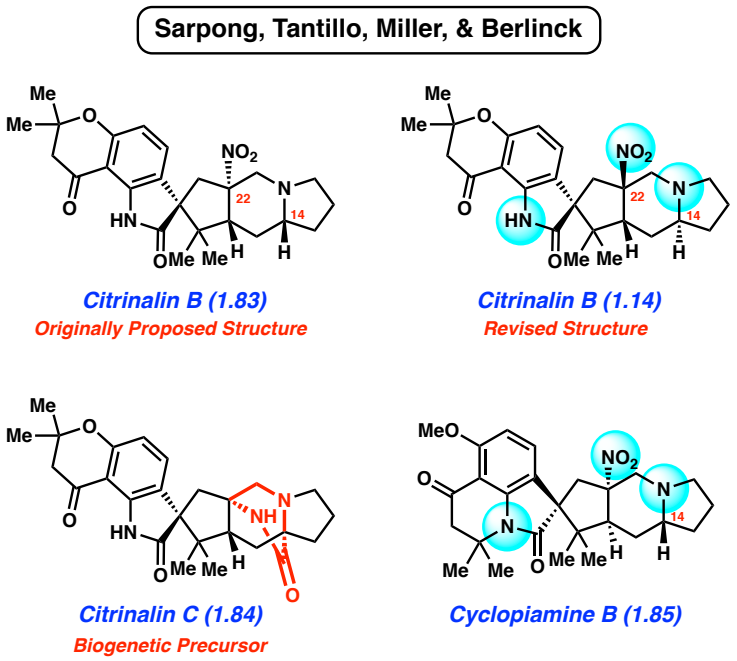

Figure 1.22. Reported structures of natural products **1.83**–**1.85** and revised structure of citrinalin B (**1.14**).

With the aim of completing the total syntheses and exploring various biosynthetic considerations, the Sarpong laboratory devised a synthetic strategy wherein *ent*-citrinalin B (*ent*-**1.14**) would first be synthesized and then converted to cyclopiamine B (**1.85**) using a chromanone rearrangement. However, based on biosynthetic hypotheses and known transformations across the cyclopiamine family,[74] the group suspected that the stereocenters at C22 and C14 in the originally proposed structure of citrinalin B (**1.83**) were incorrect. Instead, they proposed **1.14** as the revised natural product structure. To validate this hypothesis, the Tantillo laboratory performed computations to predict the ^{1}H and ^{13}C NMR spectra for both **1.83** and **1.14**, which were then compared to experimentally reported NMR data. Tantillo's findings supported the revised structural assignment of **1.14** and enabled the Sarpong laboratory to aggressively launch their

synthetic campaign targeting *ent*-**1.14**.[77] Moreover, these results underscore the value of computations in the determination and revision of natural product structures.[78]

The early stages of Sarpong's synthetic sequence are shown in Figure 1.23. D-Proline (**1.86**) was first elaborated to vinyl iodide **1.87** over a series of transformations. Next, vinyl iodide **1.87** underwent Suzuki–Miyaura cross-coupling with known boronic ester **1.88**[79] to give adduct **1.89** in 95% yield. **1.89** was converted to the fused indole **1.90** using two sequential reductions, setting the stage for spirooxindole formation. Face-selective oxygenation of a C2–C3-fused indole to the hydroxyindolenine, followed by spirooxindole formation is well established.[80] It was envisioned that the carbamate would direct oxidation to the alpha face of the indole. However, attempts to employ typical heteroatom-directed oxygenation using Davis' oxaziridines[81] did not provide the desired stereoselectivity. Instead, hydroxyindolenine **1.91** was typically observed as the major product, with only trace amounts of the desired hydroxyindolenine **1.92**, as well as undesired spirooxindole **1.93**.

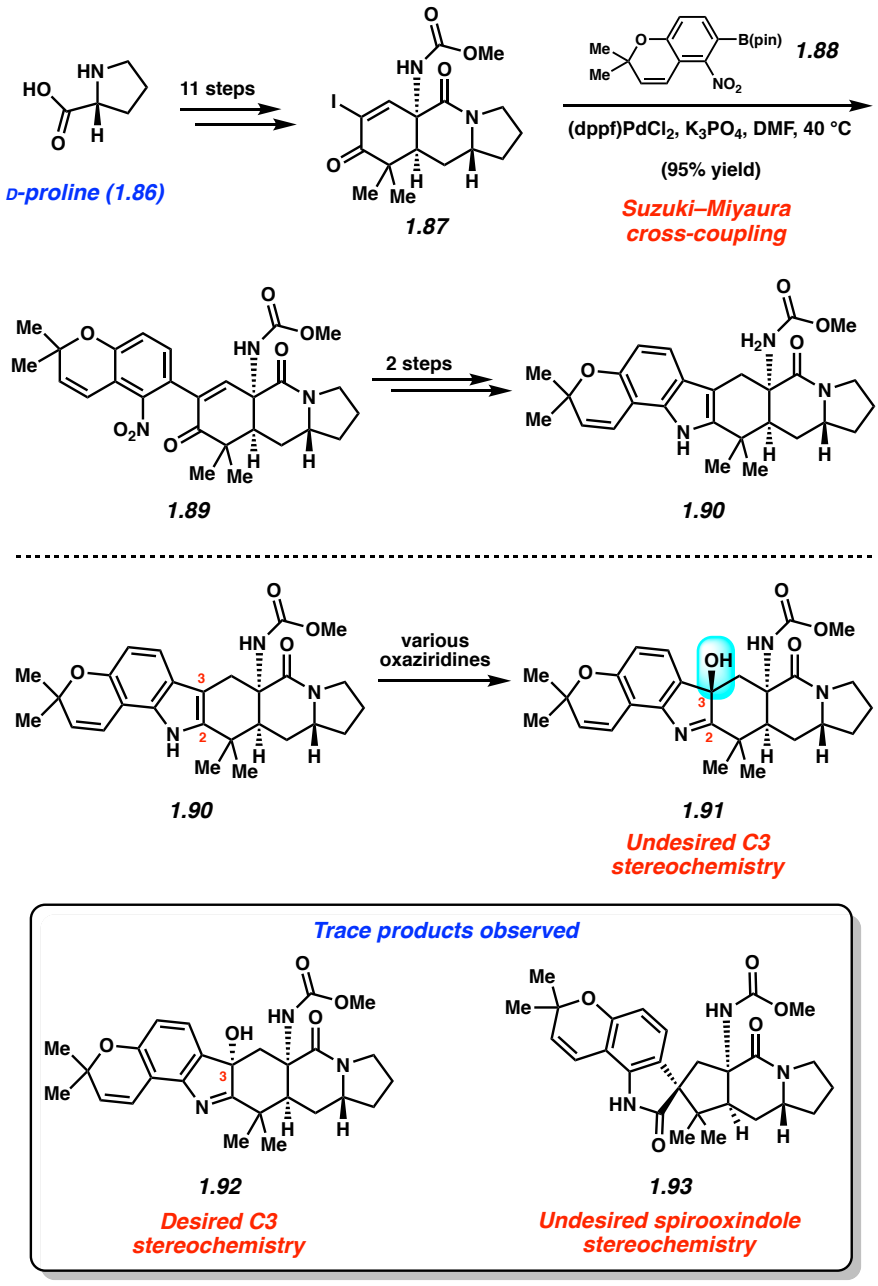

Figure 1.23. Overview of Sarpong's synthesis of spirooxindole precursor **1.90** and unsuccessful oxidation attempts.

Following a fruitful conversation at a Gordon Research Conference between Professors Richmond Sarpong and Scott Miller, the Sarpong laboratory bridged a collaboration with Miller's laboratory at Yale University.[82] The groups hoped to employ Miller's peptide catalysts to achieve

the stereoselective oxidation of substrate **1.90** (Figure 1.24).[83] Ironically, the experimental effort was carried out by graduate student David Romney, who was mentioned earlier as a key player in the nigelladine A collaboration. After screening a library of peptide catalysts, it was found that desired hydroxyindolenine **1.92** could be obtained in 83% yield upon oxidation of fused indole **1.90** in the presence of peptide catalyst **1.94** and H_2O_2. With desired stereoisomer **1.92** in hand, attempted formation of the spirooxindole was pursued. However, attempts to perform the rearrangement led only to intermediate pseudoindoxyl **1.95**, which did not undergo further rearrangement to oxindole **1.96**.[84] The failure of **1.95** to rearrange was posited to be the result of a stabilizing hydrogen bond between the carbonyl of the pseudoindoxyl and carbamate N–H (calculated to be 2.24 Å apart). Although the peptide-based catalysis would ultimately not be used to achieve the total syntheses at hand, the collaboration with the Miller laboratory demonstrated the high selectivity of peptide catalysts in an extraordinarily complex environment. Moreover, the failed conversion of **1.95** to **1.96** informed the Sarpong laboratory's efforts and prompted them to design a more viable substrate for attempted spirooxindole formation.

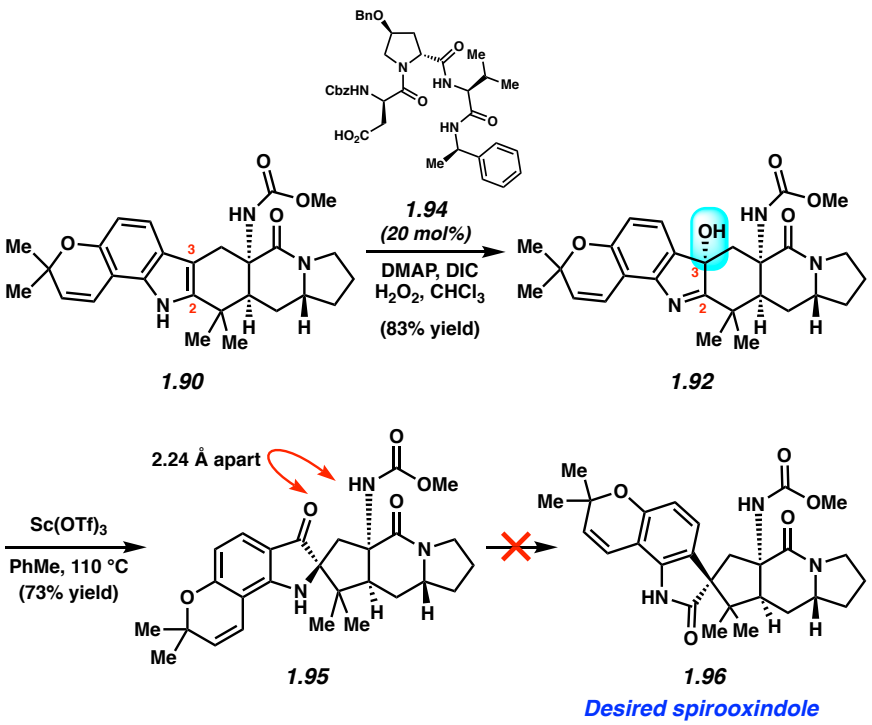

Figure 1.24. Successful oxidation to give **1.92** using Miller's peptide catalyst and challenges encountered in attempted rearrangement toward **1.96**.

The Sarpong laboratory identified indole **1.97** as a revised precursor to construct the desired spirooxindole and set out to complete the syntheses (Figure 1.25). It was believed that the free amine of **1.97** could still serve as a hydrogen-bond donor to effect stereoselective oxidation of the C2–C3 face of the indole. However, it could also be oxidized to the nitro group present in the natural product in situ. Importantly, the presence of the nitro group would subvert the hypothesized hydrogen bond stabilization effect mentioned earlier, which was thought to prevent pseudoindoxyl rearrangement to the spirooxindole. Indole **1.97** was prepared in two steps from **1.90** via Wacker oxidation[85] and carbamate cleavage. Remarkably, **1.97** was transformed to spirooxindole **1.98** with simultaneous introduction of the nitro group in a single step. Using excess dimethyldioxirane (DMDO) generated in situ,[86] the rearrangement proceeded in 56% yield

to give **1.98** as a mixture of diastereomers in a 4:1 ratio favoring the desired compound. To complete the synthesis of *ent*-citrinalin B (*ent*-**1.14**), the group performed a selective two-step reduction of the tertiary amide.[87] Spectral data for *ent*-**1.14** matched those of the isolated material,[73] but with the opposite sign of optical rotation. Moreover, *ent*-**1.14** was unambiguously characterized by X-ray crystallographic analysis. *ent*-Citrinalin B (*ent*-**1.14**) was then converted to cyclopiamine B (**1.85**) in 78% yield over two additional steps involving chromanone rearrangement. The completed syntheses of *ent*-citrinalin B (*ent*-**1.14**) and cyclopiamine B (**1.85**) provided unambiguous structural confirmation of these natural products, while also lending support to the notion that the cyclopiamines may arise from the citrinalin family of alkaloids.

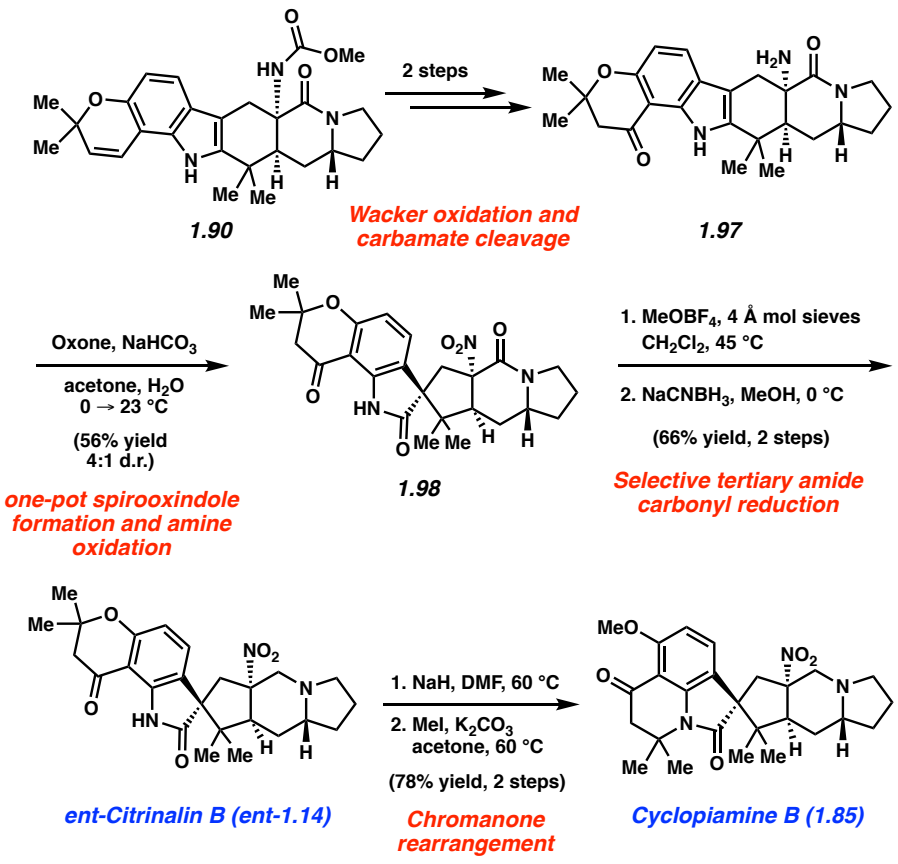

Figure 1.25. Successful spirooxindole formation and total syntheses of *ent*-citrinalin B (*ent*-**1.14**) and cyclopiamine B (**1.85**).

The final part of the collaboration was spearheaded by the Berlinck laboratory and focused on establishing the biosynthetic origins of the natural products in question (Figure 1.26). In a key finding, employing ^{13}C labeled glucose (**1.99**), anthranilic acid (**1.100**), and ornithine (**1.101**), in feeding studies gave rise to citrinalin A (**1.102**), citrinalin B (**1.14**), and two new metabolites that were determined to be citrinalin C (**1.84**) and **1.103**. Upon refractionation and re-analysis of secondary metabolites from *P. citrinum* F53, both **1.84** and **1.103** were found. Interestingly, although ^{13}C labeled ornithine (**1.101**) was incorporated, the use of ^{13}C labeled proline in feeding studies was unsuccessful. This suggests that ornithine is not converted to proline in the biosynthesis of the citrinalins, despite proline being a known biosynthetic derivative of ornithine. Lastly, and perhaps most importantly, the isolation of citrinalin C (**1.84**) among congeners like 17-hydroxycitrinalin B (**1.103**)[88] provides support for the notion that **1.102** and other family members may arise from biosynthetic precursors that contain bicyclo[2.2.2]diazaoctane units.[89]

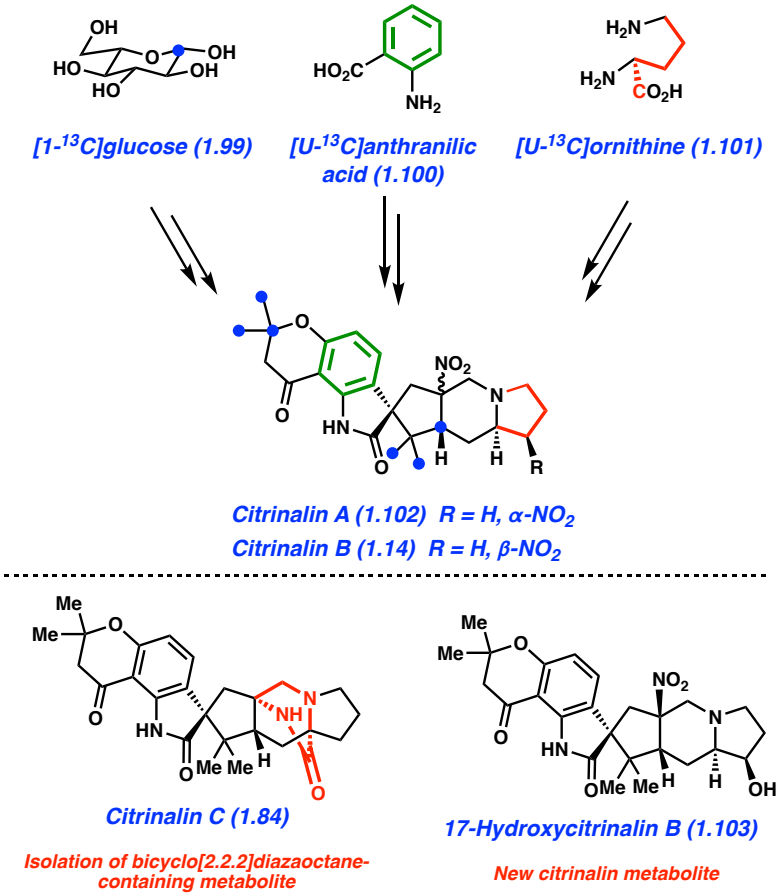

Figure 1.26. Results of feeding studies of *P. citrinum* F53 with ^{13}C labeled precursors.

The combined efforts of the Sarpong, Tantillo, Miller, and Berlinck laboratories led to many advances. These include a computationally-supported structural revision of a natural product (Tantillo), a peptide-mediated oxidation reaction of a complex substrate (Miller), the completed total syntheses of two indole alkaloids using a late-stage stereoselective spirooxindole-forming reaction (Sarpong), and insight into the biosynthetic origins of the targeted natural products (Berlinck). Overall, these collective studies beautifully intertwine the expertise of four laboratories, leading to new knowledge and achievements, in addition to the interdisciplinary training of many talented coworkers.

1.10 Conclusion

We have described a collection of recent total synthesis-related efforts that were performed in highly collaborative manners. These efforts showcase how collaborations in areas such as synthetic methodology, biocatalysis, biosynthesis, computations, and pharmaceutical research can lead to new insights and ultimately facilitate our ability to access intricate chemical structures. Moreover, such collaborations allow for students and postdoctoral scholars to be exposed to new areas of science, while benefiting from interactions with scientists from other groups and institutions. We hope this perspective will help to prompt synthetic chemists to further build a growing spirit of collaboration in the future.

1.11 Notes and References

(1) For recent reviews, views, and perspectives on total synthesis, see: a) Seebach, D. *Angew. Chem., Int. Ed.* **1990**, *29*, 1320–1367. b) Nicolaou, K. C.; Vourloumis, D.; Winssinger, N.; Baran, P. S. *Angew. Chem., Int. Ed.* **2000**, *39*, 44–122. c) Nicolaou, K. C.; Snyder, S. A. *Angew. Chem., Int. Ed.* **2005**, *44*, 1012–1044. d) Roush, W. R. *J. Am. Chem. Soc.* **2008**, *130*, 6654–6656. e) Hale, K. J. *Org. Lett.* **2013**, *15*, 3181–3198. f) Molinski, T. F. O*rg. Lett.* **2014**, *16*, 3849–3855. g) Notman, N. https://www.chemistryworld.com/features/unpicking-natural-product-synthesis/7663.article. (accessed April 22, 2019). h) Ball, P. *Nature* **2015**, *528*, 327–329. i) Denmark, S. E. *Isr. J. Chem.* **2018**, *58*, 61–72. j) Baran, P. S. *J. Am. Chem. Soc.* **2018**, *140*, 4751–4755.

(2) a) Woodward, R. B. *Pure Appl. Chem.* **1968**, *17*, 519–547. b) Eschenmoser, A. *Quart. Rev.* **1970**, *24*, 366–415. c) Woodward, R. B. *Pure Appl. Chem.* **1971**, *25*, 283–304. d)

Eschenmoser, A. Studies on Organic Synthesis. *XXIIIrd International Congress of Pure and Applied Chemistry: special lectures presented at Boston, USA, 26-30 July 1971, Vol 2*. **1971**, *2*, 69–106. e) Woodward, R. B. *Pure. Appl. Chem.* **1973**, *33*, 145–178. f) Eschenmoser, A. *Naturwissenschaften* **1974**, *61*, 513–525. g) Eschenmoser, A.; Wintner, C. E. *Science* **1977**, *196*, 1410–1420.

(3) For book chapters regarding the total synthesis of vitamin B_{12} (**1.1**), see: a) Nicolaou, K. C.; Sorensen, E. J. Vitamin B_{12}. In *Classics in Total Synthesis: Targets, Strategies, Methods*, 1st edn. VCH Publishers: New York, NY. b) Benfey, O. T.; Morris, P. J. T. eds Vitamin B_{12}. In *Robert Burns Woodward: Architect and Artist in the World of Molecules*, 1st edn. Chemical Heritage Foundation: Philadelphia, PA.

(4) Rickes, E. L.; Brink, N. G.; Koniuszy, F. R.; Wood, T. R.; Folkers, K. *Science* **1948**, *107*, 396–397.

(5) Hodgkin, D. C.; Kamper, J.; Mackay, M.; Pickworth, J.; Trueblood, K. N.; White, J. G. *Nature* **1956**, *178*, 64–66.

(6) Yamada, Y.; Miljkovic, D.; Wehrli, P.; Golding, B.; Löliger, P.; Keese, R.; Müller, K.; Eschenmoser, A. *Angew. Chem., Int. Ed.* **1969**, *8*, 343–348.

(7) The total synthesis of vitamin B_{12} (**1.1**) actually represents a formal synthesis through cobyric acid. The conversion of cobyric acid to vitamin B_{12} (**1.1**) had been reported previously, see: Friedrich, W.; Gross, G.; Bernhauer, K.; Zeller, P. *Helv. Chim. Acta* **1960**, *43*, 704.

(8) Quinn, R. K.; Könst, Z. A.; Michalak, S. E.; Schmidt, Y.; Szklarski, A. R.; Flores, A. R.; Nam, S.; Horne, D. A.; Vanderwal, C. D.; Alexanian, E. J. *J. Am. Chem. Soc.* **2016**, *138*, 696–702.

(9) Loskot, S. A.; Romney, D. A.; Arnold, F. H.; Stoltz, B. M. *J. Am. Chem. Soc.* **2017**, *139*, 10196–10199.

(10) Turconi, J.; Griolet, F.; Guevel, R.; Oddon, G.; Villa, R.; Geatti, A.; Hvala, M.; Rossen, K.; Göller, R.; Burgard, A. *Org. Process Res. Dev.* **2014**, *18*, 417–422.

(11) a) Jorgensen, L.; McKerrall, S. J.; Kuttruff, C. A.; Ungeheuer, F.; Felding, J.; Baran, P. S. *Science* **2013**, *341*, 878–882. b) McKerral, S. J.; Jorgensen, L.; Kuttruff, C. A.; Ungeheuer, F.; Baran, P. S. *J. Am. Chem. Soc.* **2014**, *136*, 5799–5810.

(12) McCallum, M. E.; Rasik, C. M.; Wood, J. L.; Brown, M. K. *J. Am. Chem. Soc.* **2016**, *138*, 2437–2442.

(13) Lin, H.-C.; McMahon, T. C.; Patel, A.; Corsello, M.; Simon, A.; Xu, W.; Zhao, M.; Houk, K. N.; Garg, N. K.; Tang, Y. *J. Am. Chem. Soc.* **2016**, *138*, 4002–4005.

(14) Mercado-Marin, E. V.; Garcia-Reynaga, P.; Romminger, S.; Pimenta, E. F.; Romney, D. K.; Lodewyk, M. W.; Williams, D. E.; Andersen, R. J.; Miller, S. J.; Tantillo, D. J.; Berlinck, R. G. S.; Sarpong, R. *Nature* **2014**, *509*, 318–324.

(15) a) Malochet-Grivois, C.; Cotelle, P.; Biard, J. F.; Henichart, J. P.; Debitus, C.; Roussakis, C.; Verbist, J.-F. *Tetrahedron Lett.* **1991**, *32*, 6701–6702. b) Malochet-Grivois, C.; Roussakis, C.; Robillard, N.; Biard, J. F.; Riou, D.; Debitus, C.; Verbist, J.-F. *Anti-Cancer Drug Des.* **1992**, *7*, 493–502. c) Roussakis, C.; Charrier, J.; Riou, D.; Biard, J. F.; Malochet, C.; Meflah, K.; Verbist, J. F. *Anti-Cancer Drug Des.* **1994**, *9*, 119–128. d) Biard, J.-F.; Malochet-Grivois, C.; Roussakis, C.; Cotelle, P.; Hénichart, J.-P.; Débitus, C.; Verbist, J.-F. *Nat. Prod. Lett.* **1994**, *4*, 43–50.

(16) Uddin, J.; Ueda, K.; Siwu, E. R. O.; Kita, M.; Uemura, D. *Bioorg. Med. Chem.* **2006**, *14*, 6954–6961.

(17) For relevant synthetic studies, see: a) Jung, M. E.; Gomez, A. V. *Tetrahedron Lett.* **1993**, *34*, 2891–2894. b) González, M. A.; Romero, D.; Zapata, B.; Bentancur-Galvis, L. *Lett. Org. Chem.* **2009**, *6*, 289–292.

(18) a) Bedke, D. K.; Shibuya, G. M.; Pereira, A.; Gerwick, W. H.; Haines, T. H.; Vanderwal, C. D. *J. Am. Chem. Soc.* **2009**, *131*, 7570–7572. b) Bedke, D. K.; Shibuya, G. M.; Pereira, A. R.; Gerwick, W. H.; Vanderwal, C. D. *J. Am. Chem. Soc.* **2010**, *132*, 2542–2543. c) Chung, W.-J.; Carlson, J. S.; Bedke, D. K.; Vanderwal, C. D. *Angew. Chem., Int. Ed.* **2013**, *52*, 10052–10055. d) Chung, W.-J.; Vanderwal, C. D. *Acc. Chem. Res.* **2014**, *47*, 718–728. e) Chung, W.-J.; Carlson, J. S.; Vanderwal, C. D. *J. Org. Chem.* **2014**, *79*, 2226–2241. f) Vogel, C. V.; Pietraszkiewicz, H.; Sabry, O. M.; Gerwick, W. H.; Valeriote, F. A.; Vanderwal, C. D. *Angew. Chem., Int. Ed.* **2014**, *53*, 12205–12209. g) Daub, M. E.; Prudhomme, J.; Le Roch, K.; Vanderwal, C. D. *J. Am. Chem. Soc.* **2015**, *137*, 4912–4915.

(19) Schmidt, V. A.; Quinn, R. K.; Bruscoe, A. T.; Alexanian, E. J. *J. Am. Chem. Soc.* **2014**, *136*, 14389–14392.

(20) a) Minisci, F.; Galli, R.; Galli, A.; Bernardi, R. *Tetrahedron Lett.* **1967**, *8*, 2207–2209. b) Deno, N. C.; Fishbein, R.; Wyckoff, J. C. *J. Am. Chem. Soc.* **1971**, *93*, 2065–2066.

(21) For select examples of 2-functionalization of sclareolide, see the following. Oxygenation: a) Chen, M. S.; White, M. C. *Science* **2010**, *327*, 566–571. Fluorination: b) Liu, W.; Huang, X.; Cheng, M.-J.; Nielsen, R. J.; Goddard, W. A., III; Groves, J. T. *Science* **2012**, *337*, 1322–1325. c) Halperin, S. D.; Fan, H.; Chang, S.; Martin, R. E.; Britton, R. *Angew. Chem., Int. Ed.* **2014**, *53*, 4790–4693. d) Bloom, S.; Knippel, J. L.; Lectka, T. *Chem. Sci.* **2014**, *5*, 1175–1178. e) Xia, J.-B.; Ma, Y.; Chen, C. *Org. Chem. Front.* **2014**, *2*, 806–810.

Chlorination: f) Liu, W.; Groves, J. T. *J. Am. Chem. Soc.* **2010**, *132*, 12847–12849. Bromination: g) Kee, C. W.; Chan, K. M.; Wong, M. W.; Tan, C.-H. *Asian J. Org. Chem.* **2014**, *3*, 536–544. Azidation: h) Huang, X.; Bergsten, T. M.; Groves, J. T. *Org. Lett.* **2015**, *17*, 5828–5831.

(22) Umbreit, M. A.; Sharpless, K. B. *J. Am. Chem. Soc.* **1977**, *99*, 5526–5528.

(23) a) Nguyen, T. M.; Vu, N. Q.; Youte, J.-J.; Lau, J.; Cheong, A.; Ho, Y. S.; Tan, B. S. W.; Yogonathan, K.; Butler, M. S.; Chai, C. L. L. *Tetrahedron* **2010**, *66*, 9270–9276. b) Hajra, S.; Giri, A. K.; Karmakar, A.; Khatua, S. *Chem. Commun.* **2007**, *23*, 2408–2410.

(24) Konst, Z. A.; Szklarski, A. R.; Michalak, S. E.; Pellegrino, S.; Meyer, M.; Zanette, C.; Cencil, R.; Nam, S.; Voora, V.; Horne, D. A.; Pelletier, J.; Mobley, D. L.; Yusupov, M.; Vanderwal, C. D. *Nat. Chem.* **2017**, *9*, 1140–1149.

(25) Chen, Q.-B.; Xin, X.-L.; Yang, Y.; Lee, S.-S.; Aisa, H. A. *J. Nat. Prod.* **2014**, *77*, 807–812.

(26) Stork, G.; Danheiser, R. L. *J. Org. Chem.* **1973**, *38*, 1775–1776.

(27) McDougal N. T.; Streuff, J.; Mukherjee, H.; Virgil, S. C.; Stoltz, B. M. *Tetrahedron Lett.* **2010**, *51*, 5550–5554.

(28) Bruno, N. C.; Tudge, M. T.; Buchwald, S. L. *Chem. Sci.* **2013**, *4*, 916–920.

(29) Oxidation of imine **1.29** was attempted using a variety of chemical methods, including the use of SeO_2, Pd/C and TPHP, Cr(V), $Rh_2(esp)_2$ and T-HYDRO, and CrO_3-based reaction conditions. The rhodium-catalyzed oxidation protocol gave the desired product in 10% isolated yield.

(30) a) Roiban, G.-D.; Reetz, M. T. *Chem. Commun*. **2015**, *51*, 2208–2224. b) Lewis, J. C.; Mantovani, S. M.; Fu, Y.; Snow, C. D.; Komor, R. S.; Wong, C.-H.; Arnold, F. H.

ChemBioChem **2010**, *11*, 2502–2505. c) Rentmeister, A.; Arnold, F. H.; Fasan, R. *Nat. Chem. Biol.* **2009**, *5*, 26–28. d) Lewis, J. C.; Bastian, S.; Bennett, C. S.; Fu, Y.; Mitsuda, Y.; Chen, M. M.; Greenberg, W. A.; Wong, C.-H.; Arnold, F. H. *Proc. Natl. Acad. Sci. U.S.A.* **2009**, *106*, 16550–16555. e) Kille, S.; Zilly, F. E.; Acevedo, J. P.; Reetz, M. T. *Nat. Chem.* **2011**, *3*, 738–743.

(31) Stoltz, B. M. California Institute of Technology, Pasadena CA. Personal communication, 2019.

(32) a) Qinghaosu Antimalaria Coordinating Research Group, Antimalaria Studies on Qinghaosu. *Chin. Med. J.* **1979**, *92*, 811–816. b) White, N. J. *Science* **2008**, *320*, 330–334. c) Tu, Y. *Nat. Med.* **2011**, *17*, 1217–1220.

(33) Guidelines for the Treatment of Malaria, World Health Organization, Geneva, 2nd ed, 2010.

(34) a) Meshnick, S. R. *Int. J. Parasitol.* **2002**, *32*, 1655–1660. b) Cui, L.; Su, X.-Z. *Expert Rev. Anti Infect. Ther.* **2009**, *7*, 999–1013. c) Edikpo, N.; Ghasi, S.; Elias, A.; Oguanobi, N. *Mol. Cell. Pharmacol.* **2013**, *5*, 75–89.

(35) Nobel Prize Press Release https://www.nobelprize.org/nobel_prizes/medicine/laureates/2015/press.pdf, accessed March 2018.

(36) Enserink, M. *Science* **2005**, *307*, 33.

(37) a) Xu, X.-X.; Zhu, J.; Huang, D.-Z.; Zhou, W.-S. *Tetrahedron* **1986**, *42*, 819–828. b) Avery, M. A.; Jennings-White, C.; Chong, W. K. M. *Tetrahedron Lett.* **1987**, *28*, 4629–4632. c) Ravindranathan, T.; Kumar, M. A.; Menon, R. B.; Hiremath, S. V. *Tetrahedron Lett.* **1990**, *31*, 755–758. d) Avery, M. A.; Chong, W. K. M.; Jennings-White, C. *J. Am. Chem. Soc.* **1992**, *114*, 974–979. e) Liu, H. J.; Yeh, W. L.; Chew, S. Y. *Tetrahedron Lett.*

1993, *34*, 4435–4438. f) Constantino, M. G.; Beltrame, M.; da Silva, G. V. J.; Zukerman-Schepector, J. *Synth. Commun.* **1996**, *26*, 321–329.

(38) Schmid, G.; Hofheinz, W. *J. Am. Chem. Soc.* **1983**, *105*, 624–625.

(39) a) Yadav, J. S.; Babu, R. S.; Sabitha, G. *Tetrahedron Lett.* **2003**, *44*, 387–389. b) Yadav, J. S.; Thirupathaiah, B.; Srihari, P. *Tetrahedron* **2010**, *66*, 2005–2009.

(40) Zhu, C.; Cook, S. P. *J. Am. Chem. Soc.* **2012**, *134*, 13577–13579.

(41) Paddon, C. J.; Westfall, P. J.; Pitera, D. J.; Benjamin, K.; Fisher, K.; McPhee, D.; Leavell, M. D.; Tai, A.; Main, A.; Eng, D.; Polichuk, D. R.; Teoh, K. H.; Reed, D. W.; Treynor, T.; Lenihan, J.; Fleck, M.; Bajad, S.; Dang, G.; Dengrove, D.; Diola, D.; Dorin, G.; Ellens, K. W.; Fickes, S.; Galazzo, J.; Gaucher, S. P.; Geistlinger, T.; Henry, R.; Hepp, M.; Horning, T.; Iqbal, T.; Jiang, H.; Kizer, L.; Lieu, B.; Melis, D.; Moss, N.; Regentin, R.; Secrest, S.; Tsuruta, H.; Vazquez, R.; Westblade, L. F.; Xu, L.; Yu, M.; Zhang, Y.; Zhao, L.; Lievense, J.; Covello, P. S.; Keasling, J. D.; Reiling, K. K.; Renninger, N. S.; Newman, J. D. *Nature* **2013**, *496*, 528–532.

(42) a) Acton, N.; Roth, R. J. *J. Nat. Prod.* **1989**, *52*, 1183–1185. b) Acton, N.; Roth, R. J. *J. Org. Chem.* **1992**, *57*, 3610–3614.

(43) a) Bertea, C. M.; Freije, J. R.; van der Woude, H.; Verstappen, F. W.; Perk, L.; Marqeuz, V.; De Kraker, J. W.; Posthumus, M. A.; Jansen, B. J.; de Groot, A.; Franssen, M. C.; Bouwmeester, H. J. *Planta Med*. **2005**, *71*, 40–47. b) Brown, G. D. *Molecules* **2010**, *15*, 7603–7698.

(44) a) Lévesque, F.; Seeberger, P. H. *Angew. Chem., Int. Ed.* **2012**, *51*, 1706–1709. b) Kopetzki, D.; Lévesque, F.; Seeberger, P. H. *Chem. Eur. J.* **2013**, *19*, 5450–5456. c)

Lévesque, F.; Seeberger, P. H. *Org. Lett.* **2011**, *13*, 5008–5011. d) McQuade, D. T.; Seeberger, P. H. *J. Org. Chem.* **2013**, *78*, 6384–6389.

(45) Holton, R. A. Patent US005254703A, (Oct. 19, 1993).

(46) At the present time, the yield of natural artemisin is such that the synthetic route is not essential to meet the current demand. For a pertinent discussion, see: Peplow, M. *Chem. Eng. News* **2018**, *96*, 29–31.

(47) Hecker, E. *Cancer Res*. **1968**, *28*, 2338–2348.

(48) Bertelsen, M.; Stahlhut, M.; Grue-Sorensen, G.; Liang, X.; Christensen, G. B.; Skak, K.; Engell, K. M.; Högberg, T. *Dermatol. Ther.* **2016**, *6*, 599–626.

(49) Hale, V.; Keasling, J. D.; Renninger, N.; Diagana, T. T. *Am. J. Trop. Med. Hyg.* **2007**, *77 (suppl. 6)*, 198–202.

(50) a) Winkler, J. D.; Rouse, M. B.; Greaney, M. F.; Harrison, S. J.; Jeon, Y. T. *J. Am. Chem. Soc.* **2002**, *124*, 9726–9728. b) Tanino, K.; Onuki, K; Asano, K.; Miyashita, M.; Nakamura, T.; Takahashi, Y.; Kuwajima, I. *J. Am. Chem. Soc.* **2003**, *125*, 1498–1500. c) Nickel, A.; Maruyama, T.; Tang, H.; Murphy, P. D.; Greene, B.; Yusuff, N.; Wood, J. L. *J. Am. Chem. Soc.* **2004**, *126*, 16300–16301. d) Watanabe, K.; Suzuki, Y.; Aoki, K.; Sakakura, A.; Suenaga, K.; Kigoshi, H. *J. Org. Chem.* **2004**, *69*, 7802–7808.

(51) a) Mukai, C.; Nomura, I.; Yamanishi, K.; Hanaoka, M. *Org. Lett.* **2002**, *4*, 1755–1758. b) Brummond, K. M.; Chen, H.; Fisher, K. D.; Kerekes, A. D.; Rickards, B.; Sill, P. C.; Geib, S. J. *Org. Lett.* **2002**, *4*, 1931–1934. c) Mukai, C.; Nomura, I.; Kitagaki, S. *J. Org. Chem.* **2003**, *68*, 1376–1385. d) Brummond, K. M.; Chen, D.; Davis, M. M. *J. Org. Chem.* **2008**, *73*, 5064–5068.

(52) a) Gillespie, S. K.; Zhang, X. D.; Hersey, P. *Mol. Cancer Ther.* **2004**, *3*, 1651−1658. b) Rosen, R. H.; Gupta, A. K.; Tyring, S. K. *J. Am. Acad. Dermatol.* **2012**, *66*, 486−493. c) Ogbourne, S. M.; Suhrbier, A.; Jones, B.; Cozzi, S.-J.; Boyle, G. M.; Morris, M.; McAlpine, D.; Johns, J.; Scott, T. M.; Sutherland, K. P., Gardner, J. M.; Le, T. T. T.; Lenarczyk, A.; Aylward, J. H.; Parsons, P. G. *Cancer Res.* **2004**, *64*, 2833−2839.

(53) a) Parker, C. G.; Galmozzi, A.; Wang, Y.; Correia, B. E.; Sasaki, K.; Joslyn, C. M.; Kim, A. S.; Cavallaro, C. L.; Lawrence, R. M.; Johnson, S. R.; Narvaiza, I.; Saez, E.; Cravatt, B. F. *Cell* **2017**, *168*, 527−541. b) Horning, B. D.; Suciu, R. M.; Ghadiri, D. A.; Ulanovskaya, O. A.; Matthews, M. L.; Lum, K. M.; Backus, K. M.; Brown, S. J.; Rosen, H.; Cravatt, B. F. *J. Am. Chem. Soc.* **2016**, *138*, 13335−13343. c) Hulce, J. J.; Cognetta, A. B.; Niphakis, M. J.; Tully, S. E.; Cravatt, B. F. *Nat. Methods* **2013**, *10*, 259−264. d) Li, Z.; Hao, P.; Li, L.; Tan, C. Y. J.; Cheng, X. M.; Chen, G. Y. J.; Sze, S. K.; Shen, H. M.; Yao, S. Q. *Angew. Chem., Int. Ed.* **2013**, *52*, 8551−8556. e) Li, Z.; Wang, D.; Li, L.; Pan, S.; Na, Z.; Tan, C. Y. J.; Yao, S. Q. *J. Am. Chem. Soc.* **2014**, *136*, 9990−9998. f) Niphakis, M. J.; Lum, K. M.; Cognetta, A. B.; Correia, B. E.; Ichu, T. A.; Olucha, J.; Brown, S. J.; Kundu, S.; Piscitelli, F.; Rosen, H.; Cravatt, B. F. *Cell* **2015**, *161*, 1668−1680. g) Shi, H.; Zhang, C.-J.; Chen, G. Y. J.; Yao, S. Q. *J. Am. Chem. Soc.* **2012**, *134*, 3001−3014.

(54) Rostovtsev, V. V.; Green, L. G.; Fokin, V. V.; Sharpless, K. B. *Angew. Chem., Int. Ed.* **2002**, *41*, 2596−2599.

(55) Parker, C. G.; Kuttruff, C. A.; Galmozzi, A.; Jorgensen, L.; Yeh, C.-H.; Hermanson, D. J.; Wang, Y.; Artola, M.; McKerrall, S. J.; Josyln, C. M.; Norremark, B.; Dunstl, G.; Felding, J.; Saez, E.; Baran, P. S.; Cravatt, B. F. *ACS Cent. Sci.* **2017**, *3*, 1276–1285.

(56) Kawamura, S.; Chu, H.; Felding, J.; Baran, P. S. *Nature* **2016**, *532*, 90–93.

(57) a) Foo, K.; Usui, I.; Götz, D. C. G.; Werner, E. W.; Holte, D.; Baran, P. S.; *Angew. Chem., Int. Ed.* **2012**, *51*, 11491–11495. b) Dixon, D. D.; Lockner, J. W.; Zhou, Q.; Baran, P. S. *J. Am. Chem. Soc.* **2012**, *134*, 8432–8435. c) Rosen, B. R.; Simke, L. R.; Thuy-Boun, P. S.; Dixon, D. D.; Yu, J.-Q.; Baran, P. S. *Angew. Chem., Int. Ed.* **2013**, *52*, 7317–7310. d) Renata, H.; Zhou, Q.; Baran, P. S. *Science* **2013**, *339*, 59–63. e) Michaudel, Q.; Ishihara, Y.; Baran, P. S. *Acc. Chem. Res.* **2015**, *48*, 712–721.

(58) Piao, S.-J.; Song, Y-L.; Jiao, W.-H.; Yang, F.; Liu, X.-F.; Chen, W.-S.; Han, B.-N. Lin, H.-W. *Org. Lett.* **2013**, *15*, 3526–3529.

(59) Piao, S.-J.; Song, Y.-L.; Jiao, W.-H.; Yang, F.; Liu, X.-F.; Chen, W.-S.; Han, B.-N.; Lin, H. W. *Org. Lett.* **2013**, *15*, 3526–3529.

(60) a) Rasik, C. M.; Brown, M. K. Total Synthesis of Gracilioether F and (±)-Hippolachnin A. Poster presentation at the 44th National Organic Chemistry Symposium, University of Maryland, College Park, MD, USA, June 28th, 2015. b) McCallum, M. E.; Wood, J. L. Total Synthesis of Hippolachnin A. Poster presentation at the 44th National Organic Chemistry Symposium, University of Maryland, College Park, MD, USA, June 28th, 2015.

(61) For seminal reports regarding cycloadditions with quadricyclane, see: (a) Smith, C. D. *J. Am. Chem. Soc.* **1966**, *88*, 4273−4274. (b) Tabushi, I.; Yamamura, K.; Yoshida, Z. *J. Am. Chem. Soc*. **1972**, *94*, 787−792. For a review, see: (c) Petrov, V. A.; Vasil'ev, N. V. *Curr. Org. Synth.* **2006**, *3*, 215–259.

(62) Schwab, P. E.; Grubbs, R. H.; Ziller, J. W. *J. Am. Chem. Soc.* **1996**, *118*, 100–110.

(63) a) Gormisky, P. E.; White, M. C. *J. Am. Chem. Soc.* **2013**, *135*, 14052–14055. b) Osberger, T. J.; White, M. C. *J. Am. Chem. Soc.* **2014**, *136*, 11176–11181. c) Ammann, S.

E.; Rice, G. T.; White, M. C. *J. Am. Chem. Soc.* **2014**, *136*, 10834–10837. d) Malik, M.; Witkowski, G.; Jarosz, S. *Org. Lett.* **2014**, *16*, 3816–3819.

(64) Timmerman, J. C.; Wood, J. L. *Org. Lett.* **2018**, *20*, 3788–3792.

(65) Winter, N.; Rupcic, Z.; Stadler, M.; Trauner, D. *J. Antibiot.* **2019**, *72*, 375–383.

(66) For synthetic studies and completed syntheses of communesins, see: a) Zuo, Z.; Ma, D. *Isr. J. Chem.* **2011**, *51*, 434–441. b) Suetsugu, S.; Tsukano, C.; Takemoto, Y. *Eur. J. Org. Chem.* **2016**, *1*, 108–115.

(67) a) May, J. A.; Zeidan, R. K.; Stoltz, B. M. *Tetrahedron Lett.* **2003**, *44*, 1203–1205. b) Peterson, E. A. Formation of Contiguous Stereogenic Quaternary Carbon Centers in Natural Products Synthesis: the Enantioselective Total Synthesis of (–)-Idiospermuline and Approaches Toward the Total synthesis of Communesins A and B. Ph.D. Thesis, University of California, Irvine, 2005. c) May, J. A.; Stoltz, B. M. *Tetrahedron* **2006**, *62*, 5262–5271. d) Han, S.-J.; Vogt, F.; Krishnan, S.; May, J. A.; Gatti, M.; Virgil, S. C.; Stoltz, B. M. *Org. Lett.* **2014**, *16*, 3316–3319. e) Han, S.-J.; Vogt, F.; May, J. A.; Krishnan, S.; Gatti, M.; Virgil, S. C.; Stoltz, B. M. *J. Org. Chem.* **2015**, *80*, 528–547.

(68) a) Boal, B. W.; Schammel, A. W.; Garg, N. K. *Org. Lett.* **2009**, *11*, 3458–3461. b) Schammel, A. W.; Boal, B. W.; Zu, L.; Mesganaw, T.; Garg, N. K. *Tetrahedron* **2010**, *66*, 4687–4695. c) Schammel, A. W.; Chiou, G.; Garg, N. K. *Org. Lett.* **2012**, *14*, 4556–4559. d) Susick, R. B.; Morrill, L. A.; Picazo, E.; Garg, N. K. *Synlett* **2017**, *28*, 1–11.

(69) Lin, H.-C.; Chiou, G.; Chooi, Y.-H.; McMahon, T. C.; Xu, W.; Garg, N. K.; Tang, Y. *Angew. Chem., Int. Ed.* **2015**, *54*, 3004–3007.

(70) Gerken, T.; Walsh, C. T. *ChemBioChem*, **2013**, *14*, 2256–2258.

(71) Walsh, C. T. *ACS Chem. Biol.* **2014**, *9*, 2718–2728.

(72) For a pertinent review, see: Miller, K. A.; Williams, R. M. *Chem. Soc. Rev.* **2009**, *38*, 3160–3174.

(73) Pimenta, E. F.; Vita-Marques, A. M.; Tininis, A.; Seleghim, M. H. R.; Sette L. D.; Veloso, K.; Ferreira, A. G.; Williams, D. E.; Patrick, B. O.; Dalisay, D. S.; Andersen, R. J.; Berlinck, R. G. S. *J. Nat. Prod.* **2010**, *73*, 1821–1832.

(74) Bond, R. F.; Boeyens, J. C. A.; Holzapfel, C. W.; Steyn, P. S. *J. Chem. Soc. Perkin Trans. I* **1979**, *0,* 1751–1761.

(75) Parry, R.; Nishino, S.; Spain, J. *Nat. Prod. Rep.* **2011**, *28*, 152–167.

(76) Finefield, J. M.; Frisvad, J. C.; Sherman, D. H.; Williams, R. M. *J. Nat. Prod.* **2012**, *75*, 812–833.

(77) Though *ent*-citrinalin B (*ent*-**1.14**) is not the natural configuration of the natural product, it bears the correct stereochemistry as cyclopiamine B (**1.85**), thus *ent*-**1.14** was targeted for total synthesis.

(78) Lodwyk, M. W.; Siebert, M. R.; Tantillo, D. J. *Chem. Rev.* **2012**, *112*, 1839–1862.

(79) Herzon, S. B.; Myers, A. G. *J. Am. Chem. Soc.* **2005**, *127*, 5342–5344.

(80) Marti, C.; Carreira, E. *Eur. J. Org. Chem.* **2003**, *12,* 2209–2219.

(81) Davis, F. A.; Stringer, O. D. *J. Org. Chem.* **1982**, *47*, 1774–1775.

(82) Sarpong, R. University of California, Berkeley, Berkeley CA. Personal communication, 2019.

(83) Kolundzic, F.; Noshi, M. N.; Meiliana, T.; Movassaghi, M.; Miller, S. J. *J. Am. Chem. Soc.* **2011**, *133*, 9104–9111.

(84) a) Guller, R.; Borschberg, H.-J. *Tetrahedron Lett.* **1994**, *35*, 865–868. b) Movassaghi, M.; Schmidt, M. A.; Ashenhurst, J. A. *Org. Lett.* **2008**, *10*, 4009–4012.

(85) Miller, D. G.; Wayner, D. D. M. *J. Org. Chem.* **1990**, *55*, 2924–2927.

(86) Zhang, X.; Foote, C. S. *J. Am. Chem. Soc.* **1993**, *115*, 8867–8868.

(87) Borch, R. F. *Tetrahedron Lett.* **1968**, *9*, 61–65.

(88) For subsequent total synthesis, see: Mercado-Marin, E. V.; Sarpong, R. *Chem. Sci.* **2015**, *6*, 5048–5052.

(89) Ding, Y.; de Wet, J. R.; Cavalcoli, J.; Li, S.; Greshock, T. J.; Miller, K. A.; Finefield, J. M.; Sunderhaus, J. D.; McAfoos, T. J.; Tsukamoto S.; Williams, R. M.; Sherman, D. H. *J. Am. Chem. Soc.* **2010**, *132*, 12733–12740.

CHAPTER TWO

Progress Toward the Total Synthesis of Dodecahedrane

2.1 Abstract

The total synthesis of complex, sp^3-rich molecules provides an important testing ground for the development and evaluation of new synthetic strategies. Herein, we describe our progress toward the total synthesis of dodecahedrane, a complex and highly symmetrical hydrocarbon that bears twelve fused rings arranged in a cage-like architecture. Central to our approach is a [2+2+2+2+2] poly-ene cyclization cascade, which is expected to construct five new bonds and ten new rings in a single transformation. Toward this end, we describe efforts to construct key linkages found in the target, which hinge on the application of modern C–C bond-forming metathesis reactions, as well as outline future steps. The success of these studies would represent a milestone in total synthesis and serve to provide new insights into chemical reactivity.

2.2 Introduction

Achieving access to complex, sp^3-rich molecules has grown increasingly desirable in the discovery of new drug molecules.[1] Indeed, the escalating complexity of targets in the pharmaceutical and agrochemical industries has highlighted the need for new synthetic approaches that rapidly build molecular complexity.[2] Toward this end, the total synthesis of molecules with high three-dimensional character can serve to inform the development of new synthetic strategies and inspire new approaches. Dodecahedrane (**2.1**, Figure 2.1) represents a particularly compelling target, bearing a highly symmetrical and sp^3-rich carbon skeleton that harbors twelve fused rings

arranged in a cage-like structure.[3] Indeed, dodecahedrane (**2.1**) has long fascinated scientists and was even regarded as the "Mount Everest of Alicyclic Chemistry" due to its extraordinary architecture.[3d,4] From a synthetic standpoint, dodecahedrane (**2.1**) poses notable synthetic challenges. Although **2.1** is not chiral, its synthesis requires that the relative stereochemistry at each sp^3 center is carefully orchestrated, such that all twenty hydrogen atoms are arranged *syn* to one another. In addition to its twelve fused rings and unique symmetry, the lack of polarizable functional groups in the molecule complicates retrosynthetic logic, which traditionally relies on identifying combinations of positively and negatively charged synthons.[5] With these challenges in mind, dodecahedrane (**2.1**) offers exciting opportunities for the development of new synthetic methodologies and strategies. Moreover, despite the limited quantities of dodecahedrane (**2.1**) accessed to date, experimental[6]—as well as theoretical[7]—studies of **2.1** and its derivatives demonstrate that it may hold promise in the fields of polymer chemistry and materials science.

The compelling structure of dodecahedrane (**2.1**) has prompted several research groups to engage in efforts to achieve its synthesis. Beginning in 1964, the Woodward group attempted a dimerization of triquinacene as a means to synthesize **2.1**.[8] Nearly two decades later, in 1982, the first total synthesis of dodecahedrane (**2.1**) was accomplished by Paquette and co-workers in 23 synthetic operations.[4b,9] In 1987, Prinzbach disclosed a route to **2.1** from its constitutional isomer pagodane that was subsequently optimized to give dodecahedrane (**2.1**) in a total of 20 steps.[10] Although no synthetic reports of dodecahedrane (**2.1**) have been described over the past two decades, these early efforts highlight the value of pursuing unnatural hydrocarbons as a means to push our understanding of bonding and molecular reactivity.[11]

Intrigued by the extraordinary structure of dodecahedrane (**2.1**), we are pursuing a concise synthesis of **2.1** that relies on a symmetry-based disconnection. Our proposed strategy hinges on

an ambitious [2+2+2+2+2] polyene cyclization (**2.2** → **2.1**) that should provide valuable insights into molecular reactivity. Moreover, our approach serves to validate and extend the capabilities of modern synthetic methods for C–C bond formation, including alkyne metathesis and olefin metathesis. The success of these studies would signify a milestone in the field of total synthesis and should provide efficient access to dodecahedrane (**2.1**), which is expected to facilitate investigations of its material properties and applications.

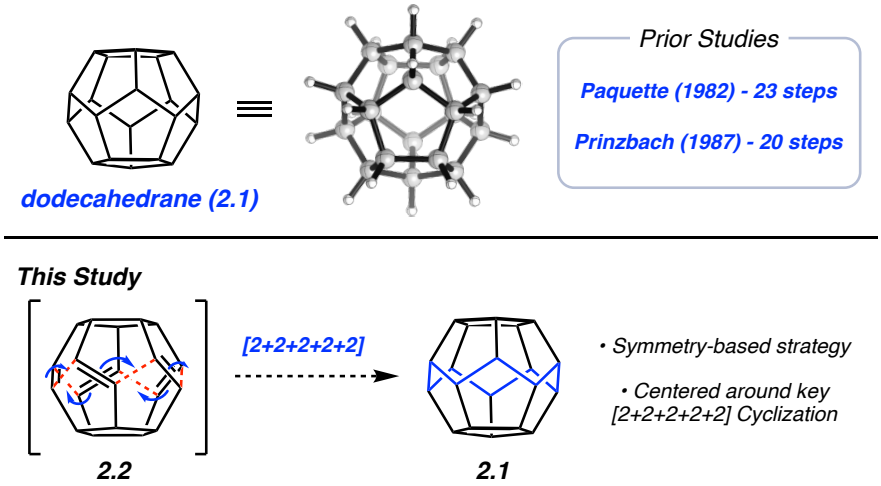

Figure 2.1. The structure of dodecahedrane (**2.1**) and overview of current approach.

2.3 Retrosynthetic Analysis

A brief retrosynthetic analysis for dodecahedrane (**2.1**) is depicted in Figure 2.2. Conceptually, we view the molecule as having all-*cis* cyclopentyl rings at the northern and the southern faces, with these rings connected via ten central sp^3 carbons that are attached to one another. We envision the central ten-membered ring (highlighted in blue) could be derived from a penta-ene precursor, such as **2.3**. In the forward sense, **2.3** would undergo a thermodynamically driven [2+2+2+2+2] polyene cyclization reaction, via a transition structure such as **2.2**.

Interestingly, in this proposed transformation, one of the five olefins in **2.3** would serve as both the initiation point and terminus of cyclization. Although this parent transformation is unknown, a variety of polyene cyclizations[12] and [2+2+2] reactions have been reported, including the hexadehydro-Diels–Alder reaction, which is similarly driven by favorable thermodynamics.[13]

We envision that **2.3** could be accessed through the phased construction of its five alkenes. In particular, it is envisioned that penta-ene **2.3** could be derived from tetracycle **2.4** through ring-closing metathesis. **2.4** would in turn be constructed from **2.5** through olefin insertion, and the latter could be traced back to bis(norbornene) **2.6** by means of metathesis isomerization and functional group manipulations. Importantly, the two norbornene fragments of **2.6** would be covalently linked to one another to enable intramolecular reactivity. It is expected that **2.6** could be derived from generalized cyclopentyl monomers **2.7** via dimer formation.

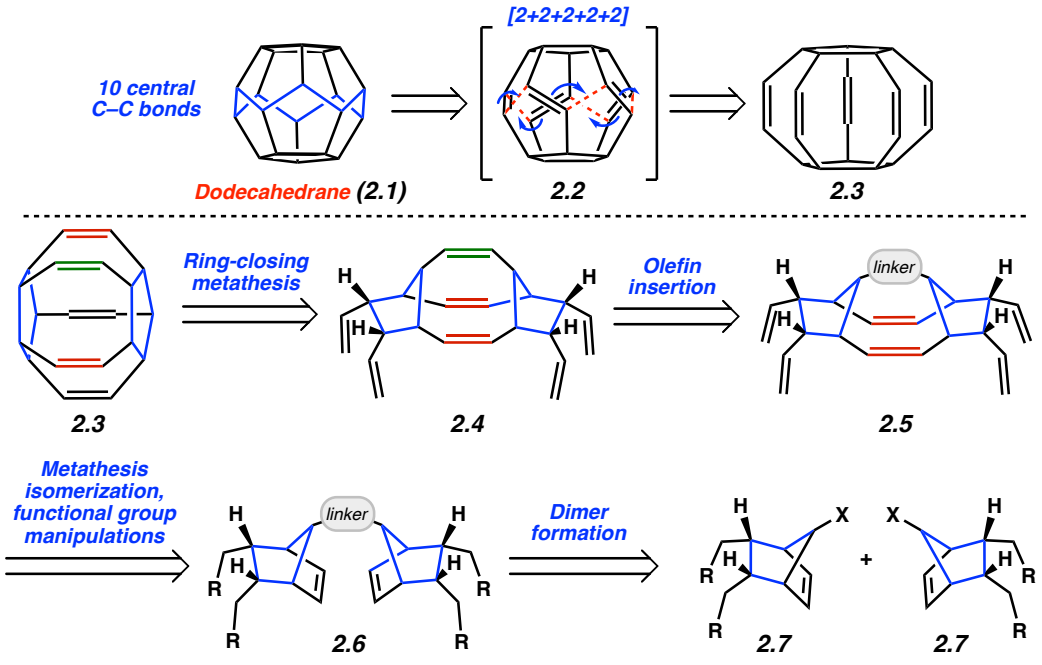

Figure 2.2. Retrosynthetic analysis of dodecahedrane (**2.1**).

2.4 Key Pinacol Coupling and Metathesis Cascade Studies

Studies toward the total synthesis of dodecahedrane (**2.1**) commenced by preparing known norbornene derivative **2.8**, which is available from cyclopentanone in three synthetic steps (Figure 2.3).[14] Elaboration of ketal **2.8** to norbornyl ketone **2.9** was achieved through an additional 3-step sequence. Specifically, ketal **2.8** was reduced to yield the corresponding diol, which was then silylated. Subsequent BF_3•Et_2O-mediated deketalization[14] afforded **2.9** in 22% yield over three steps. To date, over 25 grams of ketone **2.9** have been prepared. With ketone **2.9** in hand, efforts were undertaken to achieve the desired homocoupling to generate dimer **2.10**. Following extensive optimization, a SmI_2-mediated pinacol coupling was found to reliably generate dimer **2.10** in 43% yield, thus forming a highly congested C–C bond with complete facial selectivity. Moreover, this step could be executed on gram scale. Strategically, the direct C–C linkage (highlighted in red) of **2.10** joining the two norbornene fragments was anticipated to bring the two olefins into optimal proximity for the later C–C bond-forming steps.

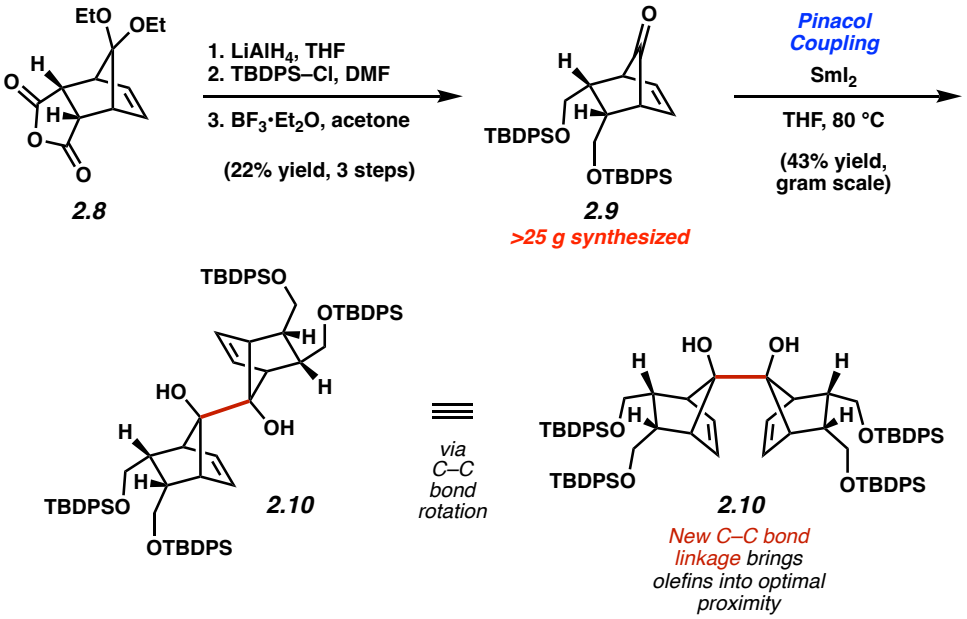

Figure 2.3. Forward synthesis of **2.10** enabled by a key SmI_2-mediated pinacol coupling.

With access to gram quantities of **2.10**, we were poised to engage in late-stage efforts to form two of the key remaining C–C bonds of dodecahedrane (**2.1**). In particular, we sought to leverage olefin metathesis to construct two key olefins. First, the vicinal alcohols in diol **2.10** were protected as methyl ethers using MeI and NaH to generate protected bis(alkene) **2.11** in 89% yield (Figure 2.4). With **2.11** in hand, we evaluated a variety of metathesis catalysts and reaction conditions to achieve the desired metathesis isomerization, including Mo-based Schrock-type alkylidene catalysts, Ru-based Grubbs-type alkylidene catalysts, as well as various solvents and temperatures. However, these exhaustive efforts to **2.12** ultimately proved fruitless, and recovered starting material was observed in nearly all cases. Removal of the TBDPS groups was also performed to alleviate steric congestion, but proved ineffective in enabling the metathesis rearrangement.

We surmised that difficulties in the latter transformation (**2.11** $\rightarrow$ **2.12**) could be ascribed to the freely rotating nature of the two norbornyl fragments about the central C–C σ-bond, leading to the two olefins residing distant from one another. To evaluate this hypothesis, we sought to lock the vicinal diol moiety into a rigid conformation and bring the two olefins into closer proximity. In particular, diol **2.10** was treated with tosic acid in acetone to give conformationally rigid acetonide **2.13** in 22% yield. Unfortunately, metathesis isomerization of this substrate also proved untenable. It was concluded from these results that the high level of steric congestion in these systems, specifically surrounding the alkene of each norbornene, prevents the large metathesis catalysts from engaging with the substrate.

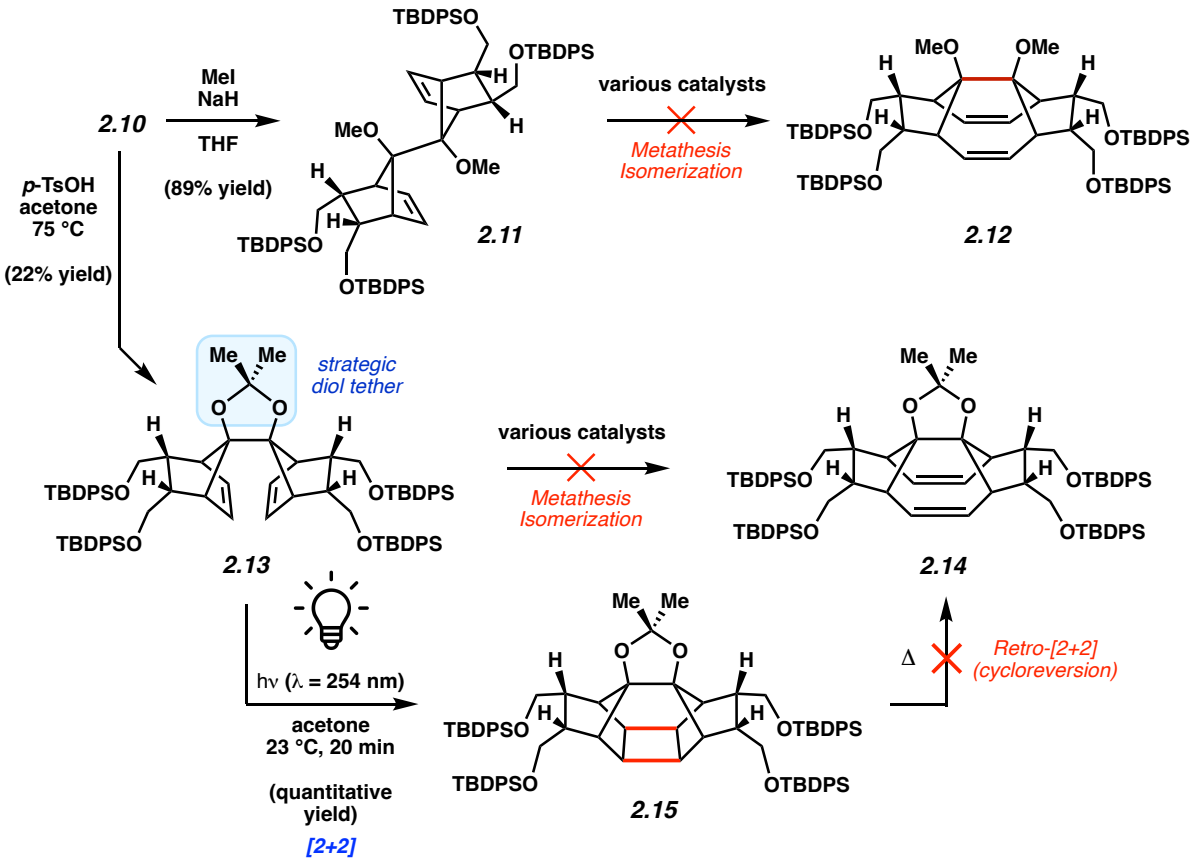

Figure 2.4. Metathesis studies and an intermolecular [2+2] photocyclization approach.

With these results in mind, and considering the close proximity of the two olefins in the locked conformation found in **2.13**, we pursued an alternative [2+2] / retro-[2+2] cascade approach from **2.13** (Figure 2.4). The first step, photochemical [2+2] cyclization of **2.13**, was successfully achieved via irradiation with 254 nm light, delivering cyclobutane product **2.15**. Acetone was identified as an ideal solvent for this transformation, which is attributed to its well-documented role as a triplet sensitizer.[15] Notably, this transformation reliably occurs in quantitative yield in only 20 minutes, allowing for efficient construction of the two desired C–C bonds. Moreover, this result suggests the spatial proximity of the two olefins and demonstrates that two C–C bonds can indeed be formed in this system to link the two norbornyl fragments. It should also be noted that

the [2+2] reaction does not proceed when free rotation about the central C–C bond is allowed (e.g., using **2.11**). With **2.15** in hand, we then pursued a retro-[2+2] cycloreversion reaction, which would serve to rupture the cyclobutane ring and generate diene **2.14**. However, despite evaluation of a variety of thermal and catalyst-mediated conditions, the cyclobutane ring remained unreactive and only off-target side reactivity was observed.

2.5 Strategy Revision: Introduction of an Alkyne Linkage

Given the challenges encountered in both catalytic metathesis isomerization and [2+2] / retro-[2+2] approaches, we turned our attention to evaluation of alternative synthetic strategies toward key intermediate **2.4** (Figure 2.5). In particular, rather than linking the two norbornyl fragments directly via a C–C σ-bond (as in **2.16**), we posited that a two-carbon alkyne linker could instead be leveraged, as exemplified by **2.17**. This would not only create a less sterically demanding environment for alkene manipulation, but would also obviate the need for late-stage installation of the olefin shown in **2.4** (depicted in green), which was required in the previous route.

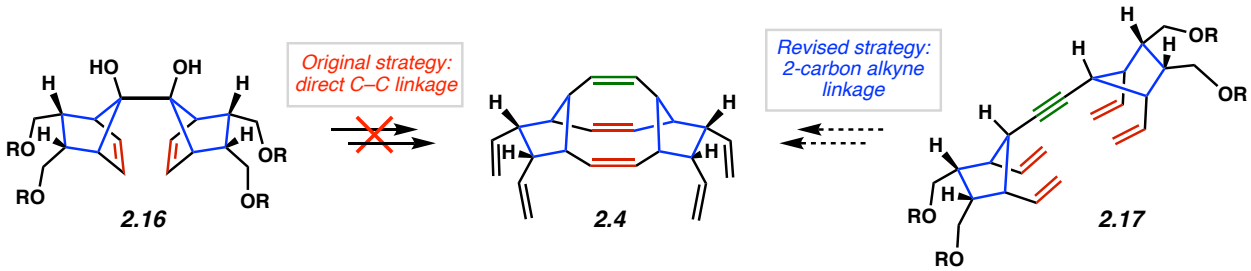

Figure 2.5. Reassessment of route to intermediate **2.4**: strategy shift from a direct C–C bond linkage to a two-carbon alkyne linker approach.

2.6 Revised Approach: Forward Synthesis

As delineated in Figure 2.6, we commenced our revised synthesis starting from ketone **2.9**, as obtained previously. Wittig olefination of **2.9** using (methoxymethyl)triphenylphosphonium chloride, followed by acid-mediated hydrolysis of the resulting enol ether, provided aldehyde **2.18** as the major diastereomer in 26% yield over two steps.[16] Subsequent alkynylation using Bestmann–Ohira Reagent (**2.19**) generated **2.20** in 85% yield. With **2.20** in hand, we were delighted to find that alkyne metathesis dimerization could be achieved using tungsten alkylidyne catalyst **2.21** to deliver **2.22** in 46% yield (62% based on recovery of **2.20**). This transformation represents a rare example of an alkyne metathesis dimerization using a sterically demanding α-tertiary alkyne,[17] and also demonstrates that alkyne metathesis can be performed with conformationally rigid substrates. Moreover, the product obtained bears all 20 carbon atoms found in dodecahedrane, as well as the desired *syn*-relationship among the five H atoms on each of the two cyclopentyl rings. With access to **2.22**, we were then tasked with executing a ring-opening protocol to give tetra-ene **2.23**. Ethenolysis, or cross-metathesis with ethylene gas, has proven useful in ring-opening cyclic olefins to produce dienes,[18] and thus offered a compelling option for achieving direct conversion to **2.23**.

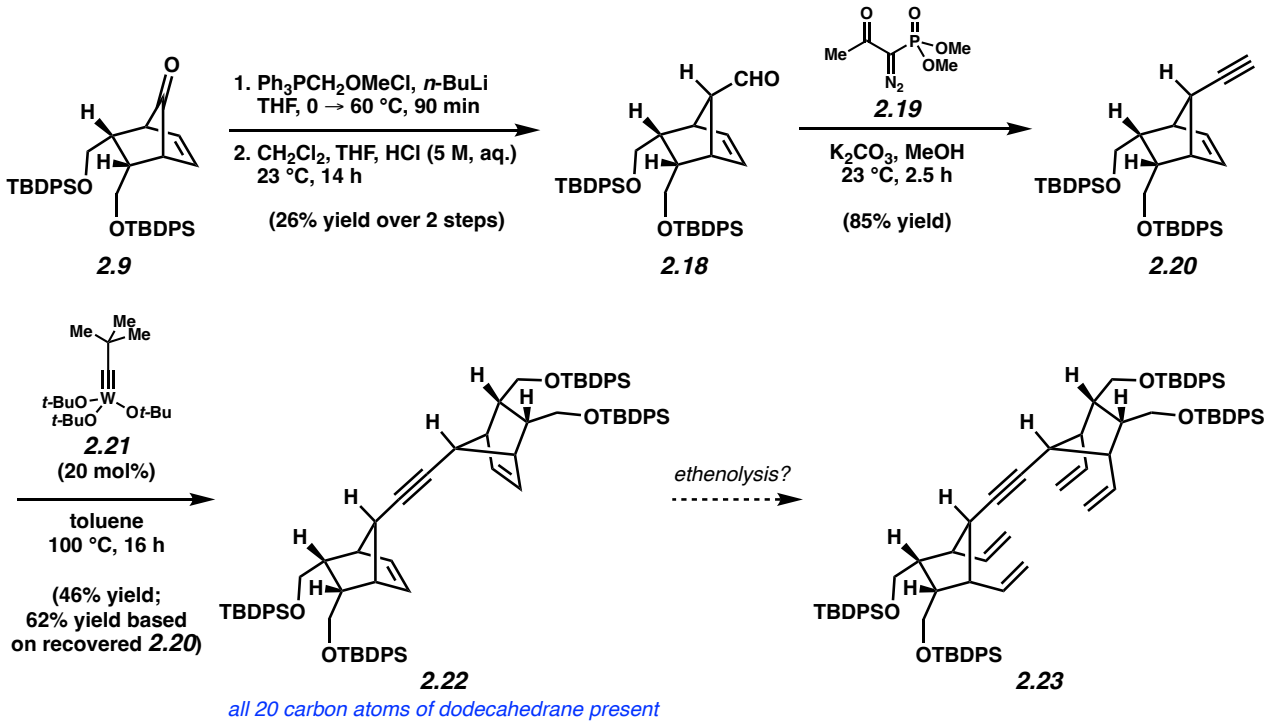

Figure 2.6. Synthesis of alkyne linked dimers.

To evaluate the feasibility of ethenolysis, we conducted model system studies (Figure 2.7). In particular, we sought to evaluate the compatibility of various norbornene substrates with ethenolysis conditions. We were initially gratified to find that substrates such as **2.26** and **2.27**, bearing aldehyde and alcohol substituents, respectively, could be converted to the corresponding ring-opened diene products in good yields using Grubbs 2nd Generation Catalyst in an atmosphere of ethylene. However, substrates bearing bridgehead substituents that extend over the olefin of the norbornene proved problematic. Namely, dienes **2.28**, **2.29**, and **2.30** could not be formed, even with heating, and starting material was recovered in all cases. From these results, it is concluded that ethenolysis of norbornene systems is highly sensitive to sterics at the bridgehead and would likely prove challenging in the desired system.

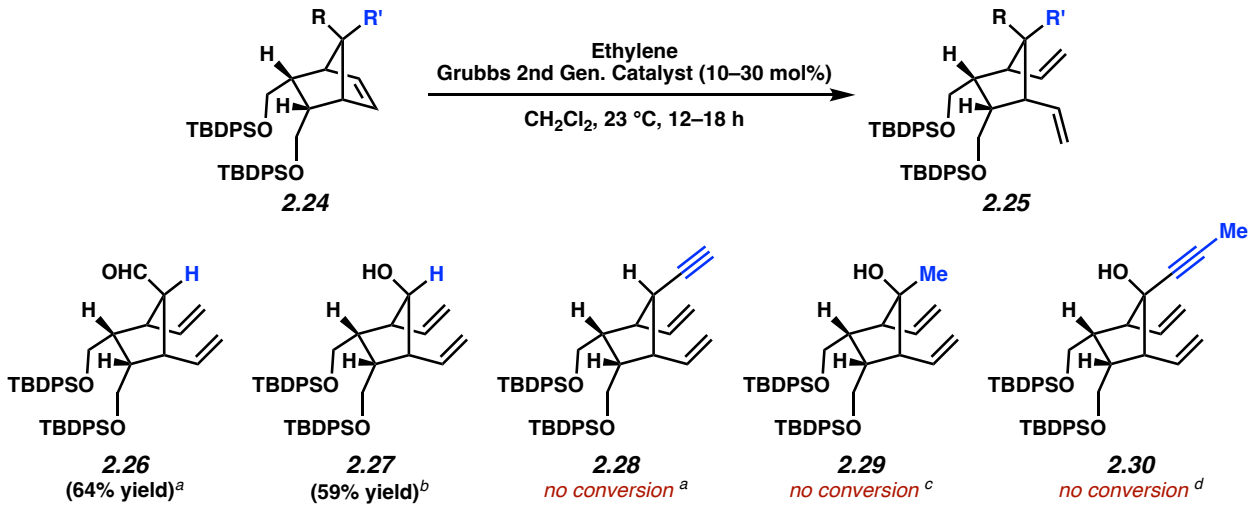

See Section 2.9.2.2 for substrate syntheses. [a] 30 mol% catalyst was added (see Section 2.9.2.3) [b] 30 mol% catalyst was added over three 10 mol% portions to maximize catalytic activity (see Section 2.9.2.3); [c] 10 mol% catalyst was added; [d] 10 mol% catalyst was added and ethenolysis was run at both 23 °C and elevated temperatures, with alternative catalysts attempted as well, and in all cases no conversion to **2.30** was observed.

Ethenolysis of norbornenes is highly sensitive to sterics at bridgehead

Figure 2.7. Analysis of substrate compatibility in the ethenolysis of norbornene substrates.

2.7 Future Directions

Given the aforementioned challenges associated with ethenolysis, we aim to pursue an alternative two-step sequence to produce tetra-ene **2.23** (Figure 2.8). Namely, future directions will involve ozonolysis of **2.22** to produce a tetra-aldehyde intermediate, followed immediately by Wittig olefination to give **2.23**. Preliminary results have validated the feasibility of this approach, and further optimization will be conducted to obtain appreciable quantities of **2.23**. The next key step will involve ring-closing metathesis to form two new rings. It is expected, however, that the alkyne linker of **2.23** would likely give rise to considerable build-up of strain in the ring-closing metathesis, as such a transformation would involve formation of an eight-membered ring bearing both an alkyne and an alkene. Complexation of alkynes to $Co_2(CO)_8$ has, encouragingly, been demonstrated to give rise to "bent" alkynes, resulting in a reduced alkyne bond angle from 180° to roughly 140°.[19] This has been leveraged strategically to form strained cyclic alkynes,[19] and

alkyne–$Co_2(CO)_6$ complexes have been utilized in ring-closing metathesis to form medium-sized cycloheptyne and cyclooctyne products.[20] With these geometric advantages in mind, future steps will involve treatment of alkyne **2.23** with $Co_2(CO)_8$ to give "bent" alkyne–$Co_2(CO)_6$ complex **2.24**, and this step has been validated experimentally. Subsequent ring-closing metathesis should furnish caged intermediate **2.32**. Reductive removal of $Co_2(CO)_6$ to provide a *Z*-olefin,[21] followed by protecting group manipulations and installation of four terminal olefins, should give rise to poly-ene **2.4**. Finally, ring-closing metathesis should afford penta-ene **2.3**.

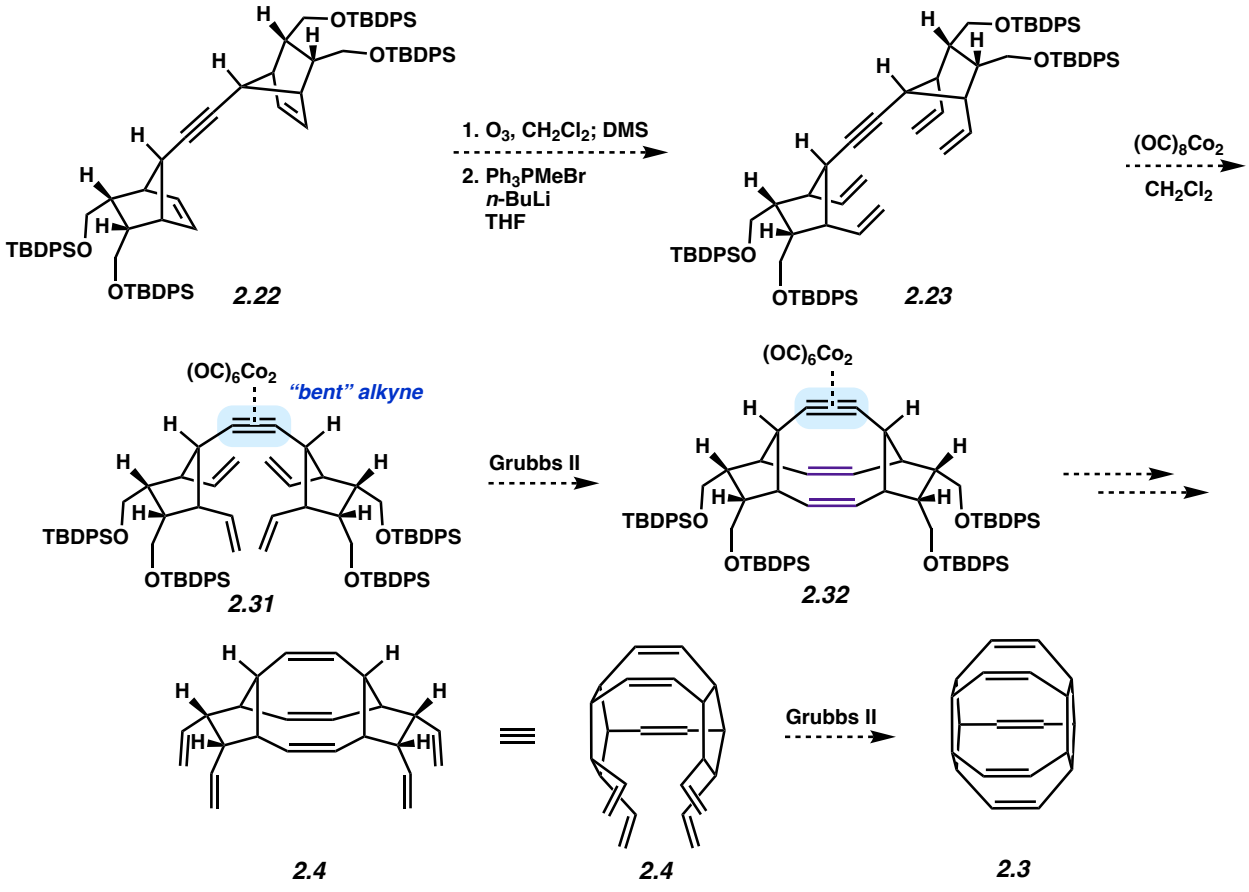

Figure 2.8. Future directions toward penta-ene **2.3**.

Access to **2.3** would set the stage for the key [2+2+2+2+2] polyene cyclization (Figure 2.9). Although such a transformation has not been reported previously, carbon–carbon bond-forming cascades of poly-enes have been explored extensively in other settings. Key examples include cationic cascades, as achieved in the synthesis of steroid natural products, radical initiated cascades for the synthesis of polycyclic natural products, and [2+2+2] cyclizations to assemble aromatic systems within natural products.[22]

With these prior examples in mind, a variety of conditions to effect the desired [2+2+2+2+2] cyclization will be evaluated. For example, heating of **2.3** could lead to sufficient orbital overlap to initiate the cyclization event. As this may be kinetically challenging, an alternative plan involving excitation with light could be examined. Such conditions could lead to olefin equilibration and cyclization, based on the well-known ability of light to cause alkene activation via electronic excitation.[23] Alternatively, we surmise that π-Lewis acids, such as Au(I)[24] or Pt(II),[25] could initiate the cyclization event. Although polyene cyclizations wherein a single olefin serves as both the initiation and termination points are currently unknown, the intramolecular [2+2+2] reaction is now well established and has been achieved photochemically or using metal promoters.[13] Similarly, polyene cyclizations are well precedented[12] and may occur under radical-based conditions.[26] The feasibility of this latter approach is supported by computational studies on stepwise radical polycyclizations in the construction of dodecahedrane (**2.1**).[27]

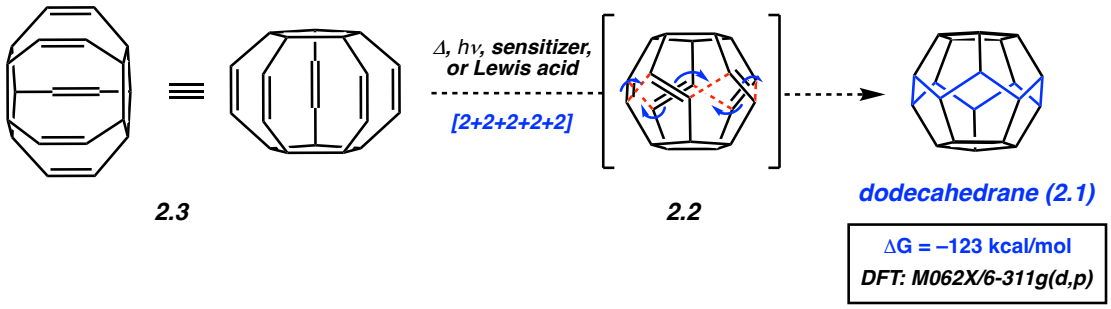

Figure 2.9. Proposed [2+2+2+2+2] polyene cyclization to complete the total synthesis of dodecahedrane (**2.1**).

To complement our experimental efforts, theoretical calculations will be performed in collaboration with the Houk laboratory. Earlier DFT studies have already established the favorable thermodynamics of the desired [2+2+2+2+2] polyene cyclization (~123 kcal/mol downhill using M062X/6-311g(d,p)). In addition, calculations will be used to assess the kinetic barrier for cyclization using non-activated conditions, or those with additives. If the proposed cyclization proves challenging, computations will be used to guide substrate modifications that may be more likely to promote the [2+2+2+2+2] polyene cyclization, assuming that the modifying group could be removed.

2.8 Conclusions

In summary, we have detailed an ambitious plan to synthesize dodecahedrane (**2.1**), as well as reported ongoing experimental efforts toward this end. Central to our symmetry-driven approach is a polyene cyclization cascade that is expected to form five new bonds and ten new rings, wherein one of the olefins serves as both the initiation point and terminus of the cyclization. Thus far, we have evaluated multiple strategies toward the key penta-ene precursor to dodecahedrane (**2.1**) and have gleaned insight into the opportunities and limitations of catalytic

ring-opening of norbornene ring systems. Moreover, we accomplished a key alkyne metathesis reaction to form a complex alkyne-linked dimer intermediate that will prove crucial in late-stage investigations. In addition to providing insight into a new polyene cyclization, these studies are expected to provide access to dodecahedrane in a concise manner, and would therefore represent a milestone in chemical synthesis. The findings from these studies should provide new synthetic tools and strategic insights that can serve to motivate and inform future studies in the area of complex molecule synthesis.

2.9 Experimental Section

2.9.1 Materials and Methods

Unless stated otherwise, reactions were conducted in flame-dried glassware under an atmosphere of nitrogen and commercially obtained reagents were used as received. Anhydrous solvents were either freshly distilled or passed through activated alumina columns, unless otherwise stated. Acetone and THF were further dried over activated 3 Å Mol Sieves for >24 h before use. Prior to use, toluene was purified by distillation over CaH_2 and taken through five freeze-pump-thaw cycles. $LiAlH_4$ (2.0 M in THF), boron trifluoride diethyl etherate (BF_3•Et_2O), 1,2-diiodoethane, sodium hydride (NaH), Grubbs 2nd Generation Catalyst, sodium borohydride ($NaBH_4$), methylmagnesium bromide (3.0 M in Et_2O), 1-propynylmagnesium bromide (**2.36**, 0.5 M in THF), Bestmann–Ohira reagent (**2.19**, 10 wt% solution in MeCN), and ethylene were obtained from Sigma-Aldrich. *tert*-Butyldiphenylchlorosilane (TBDPSCl) and *p*-toluenesulfonic acid monohydrate (*p*-TsOH) were obtained from Oakwood Chemical, Inc. Imidazole was obtained from Acros Organics. Samarium metal (powder, 40 mesh) and tungsten catalyst **2.21** were obtained from Strem Chemicals, Inc. Iodomethane (stabilized) was obtained from Spectrum

Chemical Mfg. Corp. (Methoxymethyl)triphenylphosphonium chloride was obtained from TCI and dried under high vacuum at 60 °C for 1.5 h prior to use. Reaction temperatures were controlled using an IKAmag temperature modulator, and unless stated otherwise, performed at room temperature (approximately 23 °C). [2+2]-Photocyclization reactions were conducted in a Rayonet RPR-100 photoreactor equipped with eight 14-watt lamps (λ = 254 nm). Thin-layer chromatography (TLC) was conducted with EMD gel 60 F_{254} pre-coated plates (0.25 mm for analytical chromatography and 0.50 mm for preparative chromatography) and visualized using a combination of UV and potassium permanganate staining techniques. Silicycle Siliaflash P60 (particle size 40–63 μm) was used for flash column chromatography. ^{1}H NMR and 2-D NOESY spectra were recorded on Bruker spectrometers (at 400 and 500 MHz) and are reported relative to residual solvent signals. Data for ^{1}H NMR spectra are reported as follows: chemical shift (δ ppm), multiplicity, coupling constant (Hz), integration. Data for ^{13}C NMR are reported in terms of chemical shift (125 MHz). DART-MS spectra were collected on a Thermo Exactive Plus MSD (Thermo Scientific) equipped with an ID-CUBE ion source and a Vapur Interface (IonSense Inc.). Both the source and MSD were controlled by Excalibur software version 3.0. The analyte was spotted onto OpenSpot sampling cards (IonSense Inc.) using $CHCl_3$ as the solvent. Ionization was accomplished using UHP He plasma with no additional ionization agents. The mass calibration was carried out using Pierce LTQ Velos ESI (+) and (–) Ion calibration solutions (Thermo Fisher Scientific).

2.9.2 Experimental Procedures

2.9.2.1 Synthesis of Elaborated Dimeric Intermediates

*Note: An experimental procedure for the synthesis of ketal **2.8** has been published and spectral data match those previously reported.*[14]

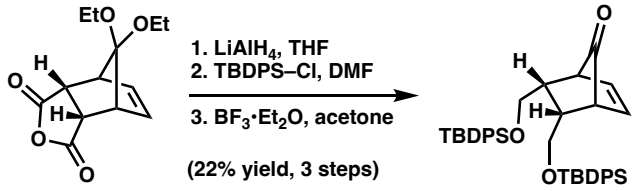

2.8 ***2.9***

Ketone 2.9. A 500 mL round bottom flask equipped with a magnetic stir bar was charged with **2.8** (7.84 g, 31.1 mmol, 1.0 equiv) and then purged with N_2 for 5 min. Next, THF (100 mL, 0.3 M) was added, and stirring began at 23 °C. The mixture was then cooled to 0 °C. At 0 °C, $LiAlH_4$ (2.0 M in THF, 42.2 mL, 84.4 mmol, 2.72 equiv) was added slowly (5 drops/sec) to the vigorously stirring reaction mixture. Following complete addition, the ice bath was removed and the reaction was left to stir and warm to 23 °C. Next, the flask was fitted with a flame-dried air condenser and the reaction mixture was heated to 70 °C.

After stirring at 70 °C for 2 h, the reaction was removed from heat, and subsequently cooled to 0 °C. At 0 °C, EtOAc (15 mL) was added dropwise across 5 min to quench any unreacted $LiAlH_4$. Following complete addition, the ice bath was removed and the reaction mixture was warmed to 23 °C. Sat. aq. EDTA (150 mL) was added and the resultant mixture was left to stir vigorously for 1 h at 23 °C. This mixture was then transferred to a separatory funnel with EtOAc (100 mL), brine (100 mL), and deionized H_2O (100 mL). The layers were separated and the aqueous layer was extracted with EtOAc (3 x 100 mL). The organic layers were combined, washed with brine (150 mL, sat. aq.), dried over Na_2SO_4, and filtered before the volatiles were removed

under reduced pressure. The crude material was then dissolved in EtOAc (10 mL), loaded onto a silica gel plug (3 x 4 cm contained in a fritted funnel), and eluted with EtOAc (1.5 L). The volatiles were again removed under reduced pressure. The resulting crude material was used in the subsequent step without further purification.

To a flask containing a magnetic stir bar and the crude material from the prior step was added DMF (89 mL, 0.2 M). Stirring was started and the resultant solution was subsequently cooled to 0 °C. Next, imidazole (6.1 g, 89 mmol, 5.0 equiv) and TBDPSCl (12.3 g, 44.7 mmol, 2.0 equiv) were added, the ice bath was removed, and the reaction mixture was allowed to warm to 23 °C while stirring.

After stirring at 23 °C for 42 h, HCl (30 mL, 1.0 M in H_2O) was added to the reaction mixture and the resulting slurry was transferred to a separatory funnel with EtOAc (50 mL). The layers were separated and the aqueous layer was extracted with EtOAc (3 x 75 mL). The combined organic layers were washed sequentially with $NaHCO_3$ (sat. aq., 50 mL), brine (50 mL), and deionized H_2O (3 x 50 mL), before being dried over Na_2SO_4, and filtered. The volatiles were removed under reduced pressure and the resulting crude residue was purified by flash chromatography (49:1 hexanes:EtOAc) to yield the silylated product (7.91 g, 11.0 mmol) as a colorless oil.

To a flame-dried flask containing a magnetic stir bar and the purified product from the prior step was added acetone (16 mL) and stirring began at 23 °C. The solution was then further diluted by the addition of acetone (76 mL, 0.12 M final concentration). BF_3•Et_2O (1.4 mL, 11 mmol, 1.0 equiv) was then added dropwise to the stirring reaction mixture. Next, the flask was fitted with a flame-dried air condenser and the reaction mixture was heated to 60 °C and allowed to stir at 60 °C for 1.5 h.

After 1.5 h, the reaction was removed from heat, cooled to 23 °C, and the volatiles were removed under reduced pressure. The resulting crude residue was purified by flash chromatography (49:1 hexanes:EtOAc). Subsequently, the purified material was recrystallized from *n*-heptane to yield ketone **2.9** (4.48 g, 22% yield, over two steps) as a white solid. Ketone **2.9**: mp 108.3–110.2 °C; R_f 0.27 (18:1:1 hexanes:benzene:EtOAc); ^{1}H NMR (500 MHz, $CDCl_3$): δ 7.58–7.50 (m, 8H), 7.40–7.30 (m, 12H), 6.19 (t, *J* = 2.2, 2H), 3.61 (dd, *J* = 10.4, 5.7, 2H), 3.35–3.26 (m, 2H), 3.06 (br s, 2H), 2.73–2.64 (br m, 2H), 0.98 (s, 18H); ^{13}C NMR (125 MHz, $CDCl_3$): δ 204.8, 135.7, 135.6, 133.58, 133.55, 131.7, 129.9, 129.8, 127.9, 127.8, 61.9, 50.9, 40.4, 26.9, 19.2 *(note: the additional aryl ^{13}C signals observed are attributed to conformational effects*); IR (film): 3070, 2933, 2858, 1787, 1428, 1112 cm^{-1}; HRMS–APCI (*m/z*) $[M + H]^+$ calcd for $C_{41}H_{49}O_3Si_2^+$, 645.32147; found, 645.32122.

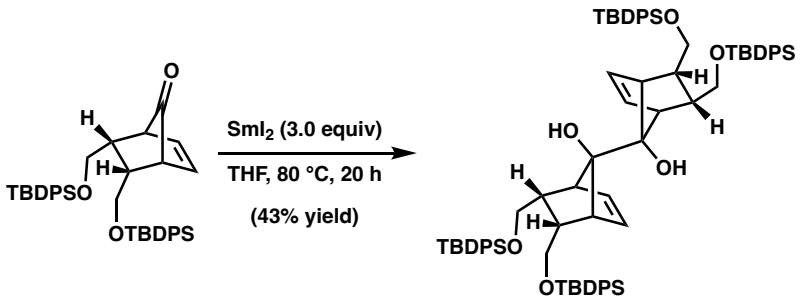

2.9 ***2.10***

Dimer 2.10. A flame-dried Schlenk flask equipped with a magnetic stir bar was purged with N_2 for 10 min and then taken into a nitrogen-filled glovebox. In the glovebox, the flask was charged with samarium metal (1.17 g, 7.81 mmol, 1.1 equiv). The flask was then removed from the glovebox and placed under N_2.

Next, a scintillation vial equipped with a magnetic stir bar was flame-dried under reduced pressure and cooled to 23 °C under N_2. To this vial was added 1,2-diiodoethane (2.0 g, 7.1 mmol,

1.0 equiv) and the vial was purged with N_2 for 2 min. Next, THF (8.35 mL, 0.85 M) was added and the resulting mixture was stirred for 2 min at 23 °C. This solution was then added dropwise (1 drop/sec) to the Schlenk flask containing the samarium. Following complete addition, the resultant suspension was stirred for 1 h at 23 °C, generating a dark blue solution of SmI_2 (assumed 0.85 M).

To a separate Schlenk flask equipped with a magnetic stir bar was added ketone **2.9** (0.84 g, 1.3 mmol, 1.0 equiv) and the system was flushed with N_2 for 5 min. Next, the freshly prepared solution of SmI_2 (0.85 M in THF, 4.6 mL, 3.9 mmol, 3.0 equiv) was added. The reaction was then heated to 80 °C and left to stir vigorously at 80 °C overnight.

After 20 h, the reaction mixture was removed from heat and cooled to 23 °C. Next, the reaction was quenched by the addition of $Na_2S_2O_3$ (sat. aq., 2 mL) and diluted with EtOAc (2 mL). The resultant heterogeneous mixture was stirred vigorously at 23 °C for 10 min. The layers were then separated and the aqueous layer was extracted with EtOAc (3 x 2 mL). The organics layers were then combined, washed with brine (3 mL), and dried over Na_2SO_4. The volatiles were removed under reduced pressure and the resulting crude residue was purified by flash chromatography (45:4:1 → 18:1:1 hexanes:benzene:EtOAc) to yield dimer **2.10** (0.36 g, 43% yield) as a white foam. Dimer **2.10**: R_f 0.11 (18:1:1 hexanes:benzene:EtOAc); ^{1}H NMR (400 MHz, $CDCl_3$): δ 7.60–7.53 (m, 16H), 7.40–7.28 (m, 24H), 5.52 (br t, J = 1.9, 4H), 3.56 (dd, J = 9.7, 6.1, 4H), 3.25 (m, 4H), 2.82 (br m, 4H), 2.62 (br s, 4H), 2.33 (s, 2H), 0.97 (s, 36H); ^{13}C NMR (125 MHz, $CDCl_3$): δ 135.6, 135.5, 133.98, 133.95, 132.6, 129.5, 129.4, 127.6, 93.9, 62.7, 52.5, 43.4, 26.9, 19.2 *(note: the additional aryl ^{13}C signals observed are attributed to conformational effects)*; HRMS-APCI (*m/z*) $[M + H]^+$ calcd for $C_{82}H_{99}O_6Si_4^+$, 1291.65132; found 1291.65244.

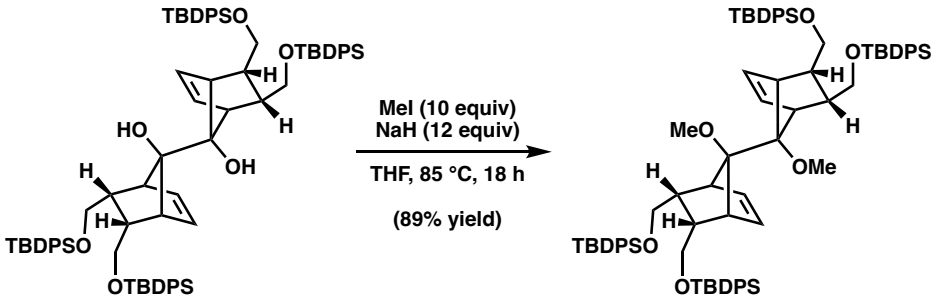

2.10 ***2.11***

Methylated Dimer 2.11. To a 20 mL scintillation vial equipped with a magnetic stir bar were added NaH (60% dispersion in mineral oil, 157 mg, 3.93 mmol, 12.0 equiv) and **2.10** (423 mg, 0.33 mmol, 1.0 equiv), and the system was flushed with N_2 for 5 min. Next, THF (6.5 mL, 0.05 M) and MeI (205 µL, 3.28 mmol, 10.0 equiv) were added sequentially in single portions. The septa cap was then replaced under a stream of N_2 with a Teflon-lined screw cap and the reaction mixture was transferred to an Al-block preheated to 85 °C, where it was stirred for 18 h. After 18 h, the reaction was removed from heat and cooled to 23 °C. The reaction was then diluted with EtOAc (2 mL) and quenched with sat. aq. NH_4Cl (3 mL). This heterogeneous mixture was stirred vigorously at 23 °C for 3 min. Next, the mixture was diluted with deionized H_2O (20 mL) and EtOAc (20 mL), the layers were separated, and the aqueous layer was extracted with EtOAc (4 x 20 mL). The organic layers were combined, dried over Na_2SO_4, and filtered. The volatiles were removed under reduced pressure and the resulting crude residue was purified by flash chromatography (95:4:1 hexanes:benzene:EtOAc → 45:4:1 hexanes:benzene:EtOAc) to afford methylated dimer **2.11** (386 mg, 89% yield) as a white foam. Methylated dimer **2.11**: R_f 0.32 (18:1:1 hexanes:benzene:EtOAc); ^{1}H NMR (500 MHz, C_6D_6, 70 °C): δ 7.77–7.70 (m, 16H), 7.23–7.17 (m, 24H), 5.74–5.63 (m, 4H), 3.88–3.76 (m, 4H), 3.58–3.50 (m, 4H), 3.33 (br s, 6H), 3.17 (br s, 4H), 2.99–2.90 (m, 4H), 1.39 (s, 36H); ^{13}C NMR (125 MHz, C_6D_6): δ 135.7, 135.6, 134.1. 132.8, 129.54, 129.53, 101.1, 77.3, 63.4, 53.2, 26.8, 19.1 *(note: the additional aryl ^{13}C signals observed*

are attributed to conformational effects); IR (film): 3070, 2931, 2857, 1428, 1112 cm^{-1}; HRMS–APCI (*m/z*) $[M + H]^+$ calcd for $C_{84}H_{103}O_6Si_4^+$, 1319.68262; found, 1319.69068.

The structure of **2.11** was verified by 2D-NOESY, as the following interaction was observed:

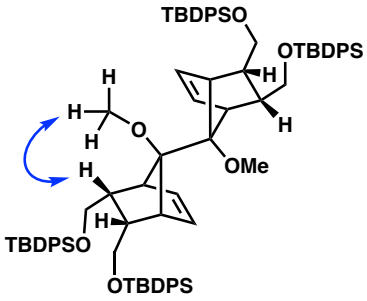

2.11

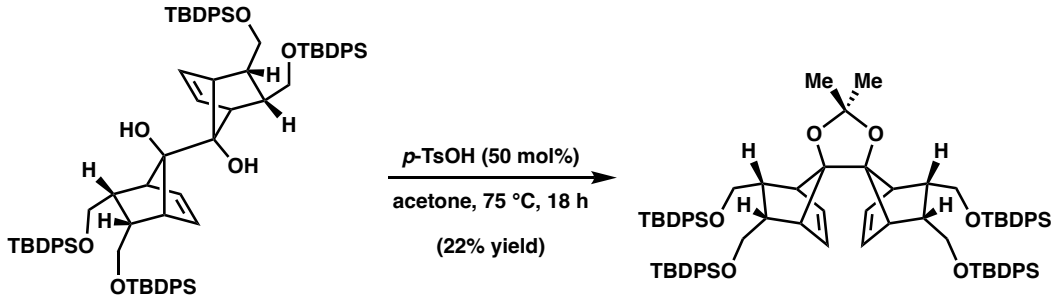

2.10 ***2.13***

Acetonide 2.13. To a 250 mL round bottom flask equipped with a magnetic stirbar was added *p*-toluenesulfonic acid monohydrate (74 mg, 0.39 mmol, 50 mol%) and dissolved in acetone (30 mL mL). **2.10** (1.0 g, 0.77 mmol, 1.0 equiv) was then added as a solution in acetone (6.7 mL), and the flask was topped with a reflux condenser and placed under N_2. The reaction was then warmed to 75 °C and stirred for 18 h. After 18 h, the reaction was removed from heat and allowed to cool to 23 °C. The volatiles were removed under reduced pressure and the resulting crude residue was purified by flash chromatography (hexanes → 50:1 hexanes:EtOAc → 20:1 hexanes:EtOAc) to afford acetonide **2.13** (226 mg, 22% yield) as an off-white foam. Acetonide **2.13**: R_f 0.53 (9:1

hexanes:EtOAc); ^{1}H NMR (500 MHz, $CDCl_3$): δ 7.58 (dd, *J* = 15.1, 6.9, 16H), 7.43–7.35 (m, 8H), 7.35–7.27 (m, 16H), 5.46 (s, 4H), 3.56 (dd, *J* = 9.8, 5.1, 4H), 3.25 (dd, *J* = 10.7, 8.9, 4H), 2.85 (br s, 4H), 2.57 (s, 4H), 1.45 (s, 6H), 0.98 (s, 36H); ^{13}C NMR (125 MHz, $CDCl_3$): δ 135.73, 135.65, 134.2, 134.1, 131.9, 129.6, 129.5, 127.7, 105.1, 98.4, 63.0, 49.9, 43.4, 28.7, 27.0, 19.3 *(note: the additional aryl ^{13}C signals observed are attributed to conformational effects)*; IR (film): 3070, 2931, 2857, 1428, 1111, 1068, 700 cm^{-1}; HRMS–APCI (*m/z*) $[M + H]^+$ calcd for $C_{85}H_{103}O_6Si_4^+$, 1331.68262; found, 1331.69446.

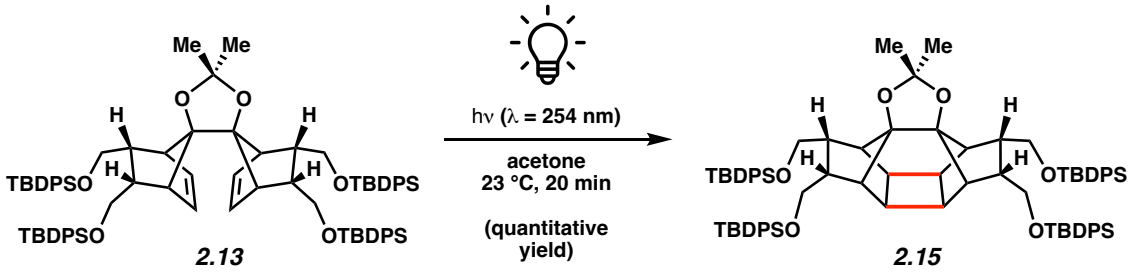

Cyclobutane 2.15. A solution of **2.13** (19.7 mg, 14.8 μmol, 1.0 equiv) in acetone (2.0 mL, 7.4 mM) was transferred to a 2 mL quartz tube equipped with a magnetic stirbar. The solution was sparged with N_2 for 10 min. The vial was then sealed and transferred into a Rayonet RPR-100 photoreactor, where it was irradiated with 254 nm light at 23 °C for 20 min. After 20 min, the reaction was removed from the photobox and the volatiles were removed under reduced pressure to afford cyclobutane **2.15** (19.8 mg, quantitative yield) as a clear oil. Cyclobutane **2.15**: R_f 0.48 (9:1 hexanes:EtOAc); ^{1}H NMR (500 MHz, $CDCl_3$): δ 7.55 (dd, *J* = 15.3, 7.1, 16H), 7.40–7.27 (m, 24H), 3.75 (dd, *J* = 9.7, 6.1, 4H), 3.41 (t, *J* = 8.7, 4H), 2.70 (s, 4H), 2.19 (s, 4H), 1.94 (s, 4H), 1.58 (s, 6H), 0.92 (s, 36H); ^{13}C NMR (125 MHz, $CDCl_3$): δ 135.7, 135.6, 134.01, 133.97, 129.61, 129.57, 127.7, 107.7, 90.8, 61.5, 42.4, 39.8, 32.9, 27.8, 26.9, 19.2 *(note: the additional aryl ^{13}C signals observed are attributed to conformational effects)*; IR (film): 3072, 2929, 2856, 1428, 1112

cm^{-1}; HRMS–APCI (*m/z*) $[M + H]^+$ calcd for $C_{85}H_{103}O_6Si_4^+$, 1331.68262; found, 1331.69389.

Note: acetone does not need to be anhydrous for this reaction, but degassing is important.

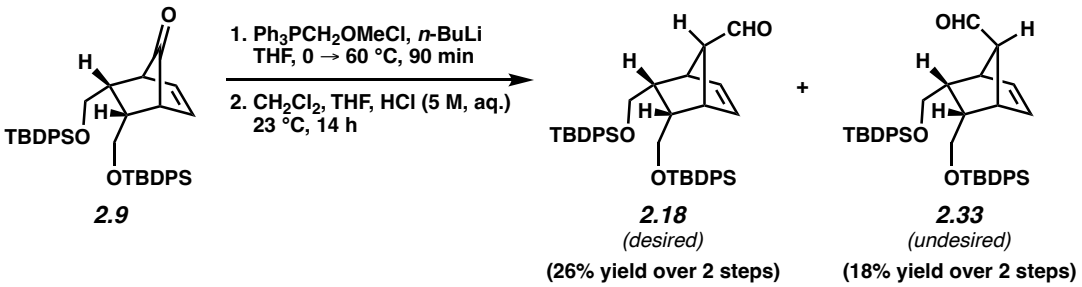

Aldehydes 2.18 and 2.33. To a stirred solution of (methoxymethyl)triphenylphosphonium chloride (2.02 g, 5.90 mmol, 1.6 equiv) in THF (30 mL) at 0 °C was added *n*-BuLi (1.9 mL, 2.33 M in hexanes, 1.2 equiv) dropwise over 2 min. The solution was stirred at 0 °C for 10 min, followed by dropwise addition of **2.9** (2.38 g, 3.69 mmol, 1.0 equiv) in THF (5 mL) over 3 min. The reaction was then allowed to warm to 23 °C and the flask was topped with an air condenser and the system was placed under N_2. The reaction was then heated to 60 °C and stirred for 90 min before being removed from heat and allowed to cool to 23 °C. The reaction was quenched with deionized H_2O (10 mL) and brine (5 mL). Next, the mixture was diluted with EtOAc (50 mL) and deionized H_2O (10 mL). The layers were separated and the aqueous layer was extracted with EtOAc (3 x 50 mL). The organic layers were combined, dried over Na_2SO_4, and filtered. The volatiles were removed under reduced pressure and the resulting crude residue was adsorbed onto silica gel (7.0 g) under reduced pressure and purified by flash chromatography (4:1 hexanes:EtOAc → 1:1 hexanes:EtOAc) to afford the intermediate enol ether.

To a stirred solution of the intermediate enol ether in CH_2Cl_2 (40 mL) and THF (10 mL) was added 5 M HCl (5 mL, aq.) over 1 min at 23 °C and the solution was stirred vigorously at 23 °C for 14 h. After 14 h, the mixture was diluted with sat. aq. $NaHCO_3$ (20 ml), deionized H_2O (10

mL) and EtOAc (100 mL). The layers were separated and the aqueous layer was extracted with EtOAc (2 x 100 mL). The organic layers were combined, dried over Na_2SO_4, and filtered. The volatiles were removed under reduced pressure and the resulting crude residue was adsorbed onto silica gel (5.0 g) under reduced pressure and purified by flash chromatography (99:1 hexanes:EtOAc → 49:1 hexanes:EtOAc → 9:1 hexanes:EtOAc) to afford desired aldehyde **2.18** (631 mg, 26% yield over two steps) as a white foam and undesired aldehyde **2.33** (438 mg, 18% yield over two steps) as a white solid. Aldehyde **2.18** (desired diastereomer): R_f 0.43 (9:1 hexanes:EtOAc); ^{1}H NMR (500 MHz, $CDCl_3$): δ 9.64 (d, *J* = 2.6, 1H), 7.60–7.53 (m, 8H), 7.43–7.37 (m, 4H), 7.36–7.29 (m, 8H), 5.89 (s, 2H), 3.51 (dd, *J* = 10.1, 5.7, 2H), 3.30 (s, 2H), 3.21 (dd, *J* = 9.4, 9.4, 2H), 2.57–2.49 (br m, 2H), 2.37 (s, 1H), 0.98 (s, 18H); ^{13}C NMR (125 MHz, $CDCl_3$): δ 206.0, 135.7, 135.6, 133.81, 133.79, 133.5, 129.8, 129.7, 127.79, 127.78, 71.1, 62.5, 47.5, 44.6, 27.0, 19.3 *(note: the additional aryl ^{13}C signals observed are attributed to conformational effects)*; IR (film): 3068, 2929, 1724, 1112, 701 cm^{-1}; HRMS-APCI (*m/z*) $[M + H]^+$ calcd for $C_{42}H_{51}O_3Si_2^+$, 659.3371; found 659.3417. Aldehyde **2.33** (undesired diastereomer): mp 99.4–101.1 °C; R_f 0.47 (9:1 hexanes:EtOAc); ^{1}H NMR (500 MHz, $CDCl_3$): δ 9.63 (s, 1H), 7.58 (dd, *J* = 15.6, 7.1, 8H), 7.44–7.28 (m, 12H), 5.91 (s, 2H), 3.58 (dd, *J* = 9.9, 5.3, 2H), 3.32–3.19 (m, 4H), 2.50–2.39 (m, 2H), 2.36 (s, 1H), 0.98 (s, 18H); ^{13}C NMR (125 MHz, $CDCl_3$): δ 202.0, 135.7, 135.6, 135.5, 133.8, 129.73, 129.69, 127.78, 127.76, 69.0, 63.2, 45.6, 42.0, 27.0, 19.3 *(note: the additional aryl ^{13}C signals observed are attributed to conformational effects)*; IR (film): 3070, 2930, 2857, 1720, 1427, 1111, 1075 cm^{-1}; HRMS–APCI (*m/z*) $[M + H]^+$ calcd for $C_{42}H_{51}O_3Si_2^+$, 659.33712; found, 659.33600.

The structure of **2.18** was verified by 2D-NOESY, as the following interaction was observed:

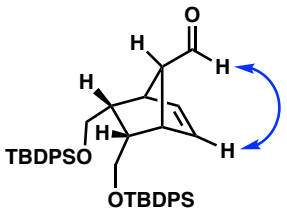

2.18
(desired)

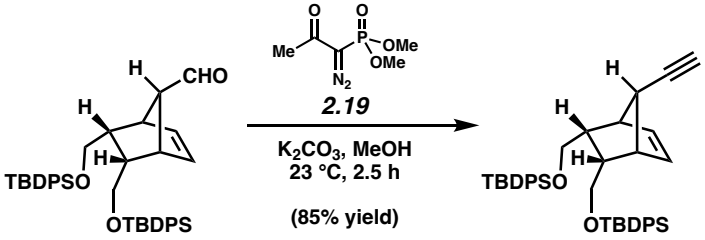

2.18 ***2.20***

Alkyne 2.20. To a stirred solution of aldehyde **2.18** (627 mg, 0.95 mmol, 1.0 equiv) in methanol (9.5 mL, 0.1 M) at 23 °C was added potassium carbonate (263 mg, 1.90 mmol, 2.0 equiv) in one portion, followed by dropwise addition of Bestmann–Ohira Reagent (**2.19**, 2.9 mL, 10 wt% solution in MeCN, 1.5 equiv) over 1 min. The solution was stirred at 23 °C for 2 h. After stirring for 2 h, the reaction was diluted with EtOAc (50 mL), brine (30 mL), and deionized H_2O (10 mL). The layers were separated and the aqueous layer was extracted with EtOAc (2 x 50 mL). The organic layers were combined, dried over Na_2SO_4, and filtered. The volatiles were removed under reduced pressure and the resulting crude residue was purified by flash chromatography (49:1 hexanes:EtOAc) to afford alkyne **2.20** (531 mg, 85% yield) as a colorless foam. Alkyne **2.20**: R_f 0.54 (9:1 hexanes:EtOAc); ^{1}H NMR (500 MHz, $CDCl_3$): δ 7.60–7.53 (m, 8H), 7.43–7.36 (m, 4H), 7.36–7.28 (m, 8H), 5.94 (s, 2H), 3.50 (dd, J = 10.0, 5.7, 2H), 3.18 (dd, J = 9.3, 9.3, 2H), 3.14 (s, 2H), 2.50 (s, 1H), 2.47 (br s, 2H), 1.89 (d, J = 2.1, 1H), 0.97 (s, 18H); ^{13}C NMR (125 MHz, $CDCl_3$): δ 135.7, 135.6, 133.9, 133.6, 129.72, 129.67, 127.76, 127.75, 85.7, 67.9, 63.0, 51.2, 50.3, 44.0, 27.0, 19.3 *(note: the additional aryl ^{13}C signals observed are attributed to conformational effects)*;

IR (film): 3311, 3069, 2930, 1428, 1112, 701 cm^{-1}; HRMS-APCI (*m/z*) $[M + H]^+$ calcd for $C_{43}H_{51}O_2Si_2^+$, 655.3422; found 655.3468.

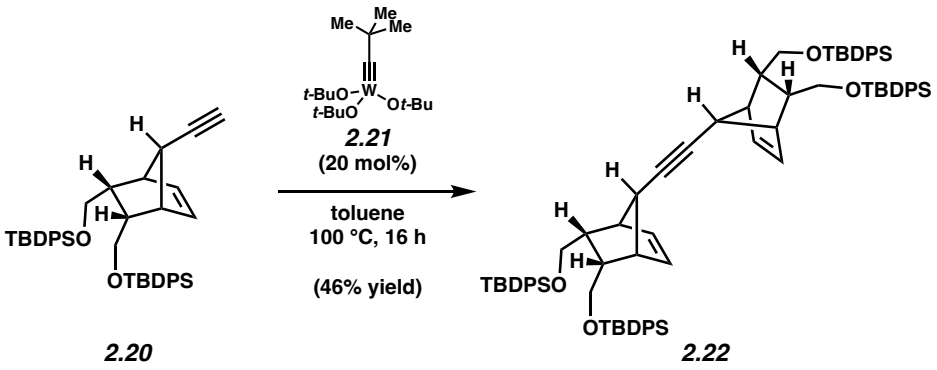

Alkyne Dimer 2.22: To a 1-dram vial equipped with a magnetic stir bar was added **2.20** (45 mg, 69 μmol, 1.0 equiv) and the vial was brought into a nitrogen-filled glovebox. In the glovebox, tungsten catalyst **2.21** (4.0 mg, 14 μmol, 20 mol%) was added followed by toluene (1.0 mL, 0.07 M). The vial was then sealed with a Teflon-lined cap and removed from the glovebox. Outside of the glovebox, the reaction was placed in a preheated, 100 °C aluminum heating block and stirred for 12 h. After 12 h, the reaction was removed from heat and cooled to 23 °C. The reaction was then diluted with hexanes (2 mL) and filtered through a plug of silica gel (9:1 hexanes:EtOAc eluent). The volatiles were removed under reduced pressure and the resulting crude residue was purified by preparative thin layer chromatography (18:1:1 hexanes:Et_2O:CH_2Cl_2) to afford alkyne dimer **2.22** (20 mg, 46% yield) as a white foam. Starting material **2.20** was also isolated (12 mg, 27% recovery). Dimer **2.22**: R_f 0.48 (9:1 hexanes:EtOAc); ^{1}H NMR (500 MHz, $CDCl_3$): δ 7.63–7.54 (m, 16H), 7.45–7.37 (m, 8H), 7.37–7.29 (m, 16H), 5.94 (s, 4H), 3.50 (dd, *J* = 9.6, 4.8, 4H), 3.20 (dd, *J* = 8.6, 8.6, 4H), 3.08 (s, 4H), 2.49 (s, 2H), 2.44 (s, 4H), 0.99 (s, 36H); ^{13}C NMR (125 MHz, $CDCl_3$): δ 135.7, 135.6, 134.0, 133.9, 133.5, 129.7, 129.6, 127.7, 80.6, 63.2, 51.4, 50.9, 44.0, 27.0, 19.3 *(note: the additional aryl ^{13}C signals observed are attributed to conformational*

effects); IR (film): 3070, 2929, 2856, 1427, 1111, 700 cm^{-1}; HRMS-APCI (*m/z*) $[M + H]^+$ calcd for $C_{84}H_{99}O_4Si_4^+$, 1283.6615; found 1283.6634.

2.9.2.2 Synthesis of Substrates for Ethenolysis Studies

*Note: Aldehyde substrate **2.33** for ethenolysis studies was prepared as described above.*

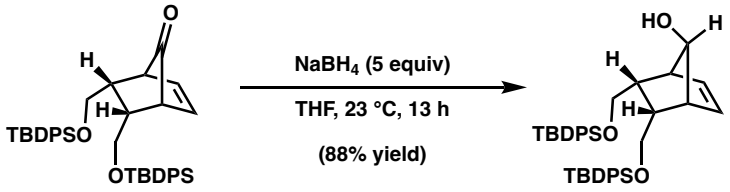

2.9 ***2.34***

Alcohol 2.34. To a stirred solution of **2.9** (600 mg, 0.93 mmol, 1.0 equiv) in THF (20.0 mL, 0.05 M) at 23 °C was added $NaBH_4$ (176 mg, 4.65 mmol, 5.0 equiv) in one portion and the reaction was stirred at 23 °C for 13 h. After 13 h, the reaction was cooled to 0 °C and deionized H_2O (20 mL) was added over 15 seconds. The reaction was then diluted with EtOAc (50 mL) and H_2O (5 mL) and the layers were separated. The aqueous layer was then extracted with EtOAc (3 x 50 mL). The organic layers were combined, dried over Na_2SO_4, and filtered. The volatiles were removed under reduced pressure and the resulting crude residue was purified by flash chromatography (10:1 hexanes:EtOAc) to afford alcohol **2.34** (532 mg, 88% yield) as a white foam. Alcohol **2.34**: R_f 0.24 (4:1 Hexanes:EtOAc); ^1H NMR (500 MHz, $CDCl_3$): δ 7.59 (dd, J = 14.2, 6.9, 8H), 7.43–7.36 (m, 4H), 7.36–7.27 (m, 8H), 5.80 (br s, 2H), 3.67 (dd, J = 9.9, 5.3, 2H), 3.63 (s, 1H), 3.36 (t, J = 8.5, 2H), 2.81–2.69 (m, 4H), 0.98 (s, 18H); ^{13}C NMR (125 MHz, $CDCl_3$): δ 135.7, 135.6, 134.0, 129.62, 129.59, 127.7, 82.9, 63.1, 49.8, 41.3, 27.0, 19.3 *(note: the additional aryl ^{13}C signals observed are attributed to conformational effects)*; IR (film): 3376, 2930, 2857, 1427, 1111, 1072 cm^{-1}; HRMS–APCI (*m/z*) $[M + H]^+$ calcd for $C_{41}H_{51}O_3Si_2^+$, 647.33712; found, 647.33591.

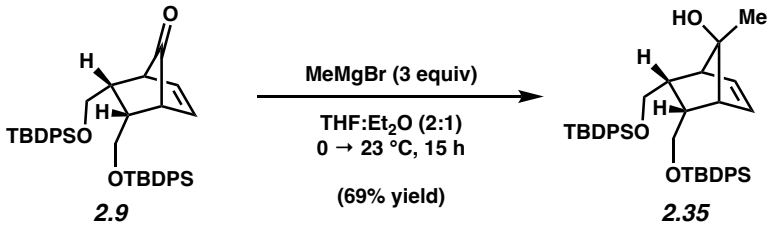

Alcohol 2.35. To a stirred solution of **2.9** (100 mg, 0.16 mmol, 1.0 equiv) in THF (1.0 mL) and Et_2O (0.5 mL) at 0 °C was added MeMgBr (155 µL, 0.47 mmol, 3.0 equiv, 3.0 M solution in Et_2O) dropwise over 30 sec. The reaction was then allowed to warm to 23 °C and stirred for 15 h. After stirring at 23 °C for 15 h, the reaction was cooled to 0 °C and quenched by dropwise addition of sat. aq. NH_4Cl (1 mL) over 30 sec. The reaction was then allowed to warm to room temperature before being diluted with EtOAc (25 mL) and sat. aq. NH_4Cl (20 mL). The layers were separated and the aqueous layer was extracted with EtOAc (3 x 20 mL). The organic layers were combined, dried over Na_2SO_4, and filtered. The volatiles were removed under reduced pressure and the resulting crude residue was purified by flash chromatography (20:1 hexanes:EtOAc) to afford alcohol **2.35** (70.7 mg, 69% yield) as a white foam. Alcohol **2.35**: R_f 0.34 (9:1 Hexanes:EtOAc); ^{1}H NMR (500 MHz, $CDCl_3$): δ 7.59 (dd, *J* = 14.4, 7.2, 8H), 7.43–7.27 (m, 12H), 5.86 (br s, 2H), 3.59 (dd, *J* = 9.7, 5.6, 2H), 3.30 (app dd, *J* = 9.8, 8.8, 2H), 2.99–2.87 (m, 2H), 2.59 (s, 2H), 1.33 (s, 3H), 0.97 (s, 18H); ^{13}C NMR (125 MHz, $CDCl_3$): δ 135.7, 135.6, 135.0, 134.11, 134.07, 129.59, 129.56, 127.7, 90.3, 63.2, 54.2, 42.8, 26.7, 21.4, 19.3 *(note: the additional aryl ^{13}C signals observed are attributed to conformational effects)*; IR (film): 3331, 2957, 2931, 2857, 1428, 1111 cm^{-1}; HRMS–APCI (*m/z*) $[M + H]^+$ calcd for $C_{42}H_{53}O_3Si_2^+$, 661.35278; found, 661.35154.

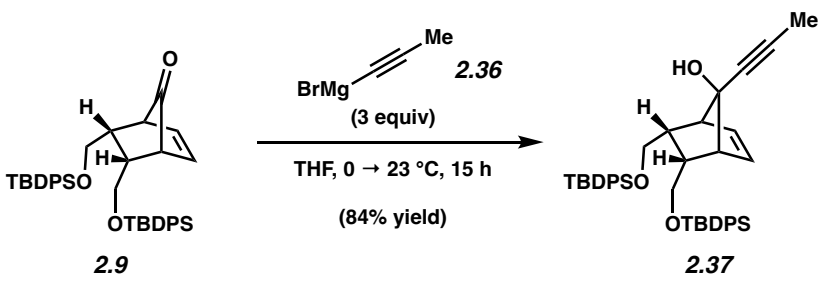

Alkyne 2.37. To a stirred solution of **2.9** (100 mg, 0.16 mmol, 1.0 equiv) in THF (0.5 mL) and at 0 °C was added **2.36** (930 μL, 0.47 mmol, 3.0 equiv, 0.5 M solution in THF) dropwise over 30 seconds. The reaction was then allowed to warm to 23 °C and stirred for 15 h. After stirring at 23 °C for 15 h, the reaction was cooled to 0 °C and quenched by dropwise addition of sat. aq. NH_4Cl (1 mL) over 30 sec. The reaction was then allowed to warm to room temperature before being diluted with EtOAc (25 mL) and sat. aq. NH_4Cl (20 mL). The layers were separated and the aqueous layer was extracted with EtOAc (3 x 20 mL). The organic layers were combined, dried over Na_2SO_4, and filtered. The volatiles were removed under reduced pressure and the resulting crude residue was purified by flash chromatography (20:1 hexanes:EtOAc → 10:1 hexanes:EtOAc) to afford alkyne **2.37** (89.1 mg, 84% yield) as a clear oil. Alkyne **2.37**: R_f 0.31 (9:1 Hexanes:EtOAc); ^{1}H NMR (500 MHz, $CDCl_3$): δ 7.57 (dd, *J* = 14.2, 7.4, 8H), 7.42–7.27 (m, 12H), 5.94 (br t, *J* = 1.9, 2H), 3.57 (dd, *J* = 9.8, 5.9, 2H), 3.28 (app t, *J* = 9.1, 2H), 2.89 (s, 2H), 2.87–2.78 (m, 2H), 1.80 (s, 3H), 0.96 (s, 18H); ^{13}C NMR (125 MHz, $CDCl_3$): δ 135.7, 135.6, 134.9, 134.0, 133.9, 129.64, 129.60, 127.7, 84.6, 81.8, 78.4, 62.7, 55.1, 41.8, 26.9, 19.3, 3.8 *(note: the additional aryl ^{13}C signals observed are attributed to conformational effects)*; IR (film): 3072, 2962, 2931, 2857, 1428, 1112, 1075 cm^{-1}; HRMS–APCI (*m/z*) $[M + H]^+$ calcd for $C_{44}H_{53}O_3Si_2^+$, 685.35278; found, 685.35151.

2.9.2.3 Ethenolysis of Norbornene Substrates

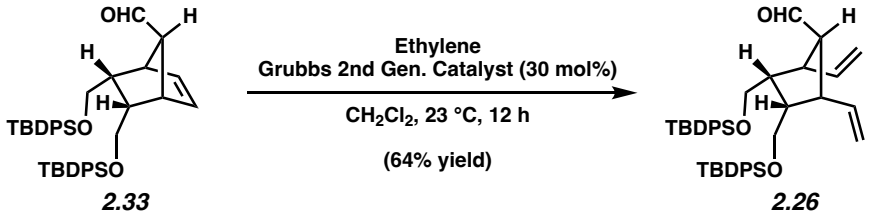

2.33 *2.26*

Diene 2.26. A stirred solution of **2.33** (20.0 mg, 30.3 μmol, 1.0 equiv) and Grubbs 2nd Generation Catalyst (7.7 mg, 9.1 μmol, 30 mol%) in CH_2Cl_2 (2.0 mL, 0.015 M) was sparged with an ethylene balloon for 10 min before being stirred for 12 h at 23 °C under an ethylene atmosphere (1 atm, using balloon). After 12 h, the reaction was filtered through a plug of silica gel, eluting with 2:1 EtOAc:hexanes (10 mL). The volatiles were removed under reduced pressure and the resulting crude residue was purified by preparative thin layer chromatography (9:1 hexanes:EtOAc) to afford diene **2.26** (13.3 mg, 64% yield) as a white solid. Diene **2.26**: mp 107.2–110.5 °C; R_f 0.47 (9:1 Hexanes:EtOAc); ^{1}H NMR (400 MHz, $CDCl_3$): δ 9.57 (d, *J* = 2.9, 1H), 7.59 (dt, *J* = 8.0, 1.4, 8H), 7.42–7.29 (m, 12H), 5.80 (ddd, *J* = 17.2, 10.2, 8.2, 2H), 5.00 (ddd, *J* = 17.1, 1.1, 1.1, 2H), 4.94 (ddd, *J* = 10.2, 1.1, 1.1, 2H), 3.72 (qd, *J* = 11.3, 6.7, 4H), 2.96 (q, *J* = 8.4, 2H), 2.76 (td, *J* = 9.2, 2.8, 1H), 2.48–2.34 (m, 2H), 0.98 (s, 18H); ^{13}C NMR (100 MHz, $CDCl_3$): δ 202.5, 137.8, 135.78, 135.75, 133.7, 133.6, 129.7, 127.8, 127.7, 116.4, 62.0, 60.4, 48.7, 46.2, 27.0, 19.2 *(note: the additional aryl ^{13}C signals observed are attributed to conformational effects)*; IR (film): 3072, 2930, 2857, 1724, 1428, 1111, 701 cm^{-1}; HRMS–APCI (*m/z*) $[M + H]^+$ calcd for $C_{44}H_{55}O_3Si_2^+$, 687.36843; found, 687.36732.

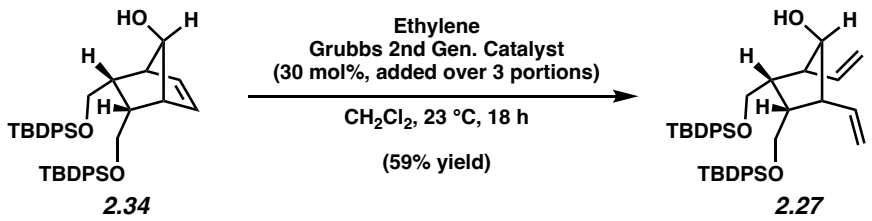

Diene 2.27. To a stirred solution of **2.34** (144 mg, 0.22 mmol, 1.0 equiv) in CH_2Cl_2 (10 mL) was added a solution of Grubbs 2nd Generation Catalyst (18.9 mg, 0.022 mmol, 10 mol%) in CH_2Cl_2 (0.6 mL) in one portion at 23 °C. While stirring at 23 °C, the reaction was sparged with an ethylene balloon for 20 min before being stirred for 2 h at 23 °C under an ethylene atmosphere (1 atm, using balloon). After 2 h, a second aliquot of Grubbs 2nd Generation Catalyst (18.9 mg, 0.022 mmol, 10 mol%) was added as a solution in CH_2Cl_2 (0.6 mL) in one portion at 23 °C. While stirring at 23 °C, the reaction was sparged again with ethylene for 20 min before being stirred for an additional 2 h at 23 °C under ethylene. After 2 h, a third aliquot of Grubbs 2nd Generation Catalyst (18.9 mg, 0.022 mmol, 10 mol%) was added as a solution in CH_2Cl_2 (0.6 mL) in one portion at 23 °C. While stirring at 23 °C, the reaction was sparged with ethylene again for 20 min before being stirred for an additional 14 h at 23 °C under ethylene. After 14 h, the volatiles were removed under reduced pressure and the resulting crude residue was purified by flash chromatography (20:1 hexanes:EtOAc → 10:1 hexanes:EtOAc → 5:1 hexanes:EtOAc) to afford diene **2.27** (88.9 mg, 59% yield) as a clear oil. Diene **2.27**: R_f 0.50 (4:1 Hexanes:EtOAc); ^{1}H NMR (500 MHz, $CDCl_3$): δ 7.60 (t, *J* = 6.5, 8H), 7.43–7.36 (m, 4H), 7.36–7.28 (m, 8H), 5.81 (dt, *J* = 17.1, 9.7, 2H), 5.07 (d, *J* = 17.3, 2H), 4.98 (d, *J* = 10.1, 2H), 4.04 (t, *J* = 8.0, 1H), 3.77 (dd, *J* = 10.7, 4.9, 2H), 3.70 (dd, *J* = 10.7, 5.0, 2H), 2.56 (q, *J* = 8.5, 2H), 2.51–2.41 (m, 2H), 0.99 (s, 18H); ^{13}C NMR (125 MHz, $CDCl_3$): δ 138.0, 135.9, 135.8, 133.74, 133.72, 129.71, 129.70, 127.72, 127.71, 116.7, 80.7, 62.1, 53.9, 46.2, 27.1, 19.2 *(note: the additional aryl ^{13}C signals observed are attributed to*

conformational effects); IR (film): 3371, 3071, 2930, 2857, 1472, 1428, 1112, 1072 cm^{-1}; HRMS–APCI (*m/z*) $[M + H]^+$ calcd for $C_{43}H_{55}O_3Si_2^+$, 675.36843; found, 675.36702.

2.10 Spectra Relevant to Chapter Two:

Progress Toward the Total Synthesis of Dodecahedrane

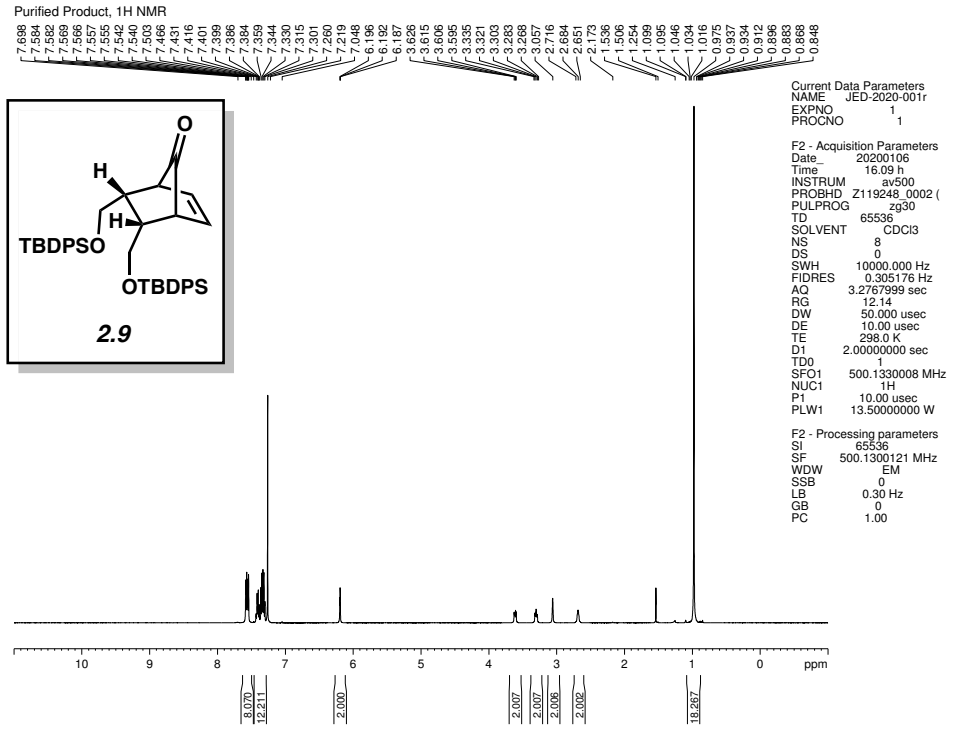

Figure 2.10 ^{1}H NMR (500 MHz, $CDCl_3$) of compound **2.9**.

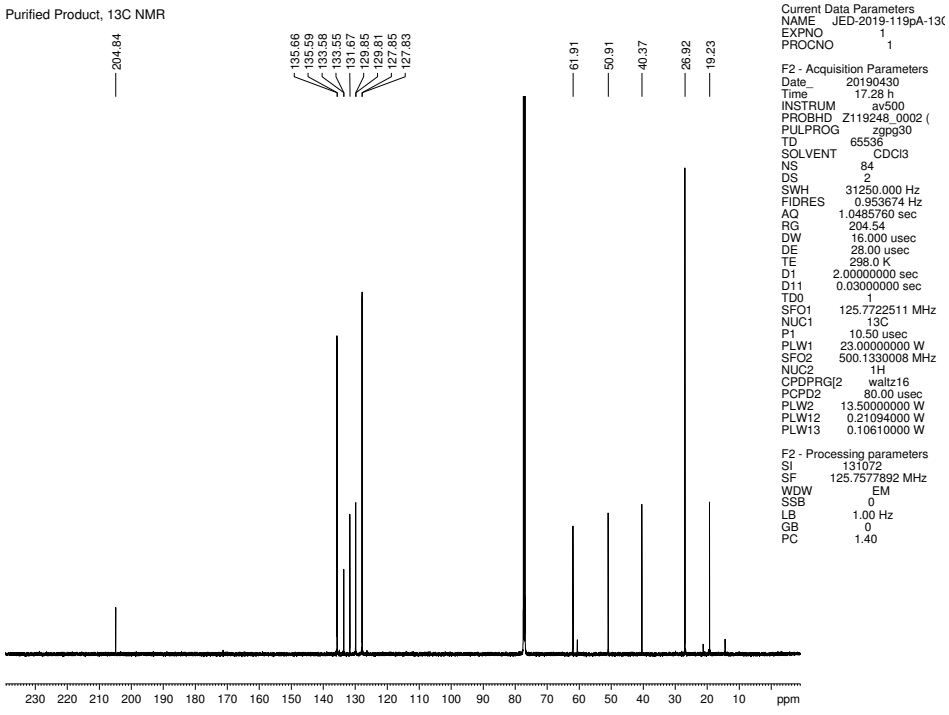

Figure 2.11 ^{13}C NMR (125 MHz, $CDCl_3$) of compound **2.9**.

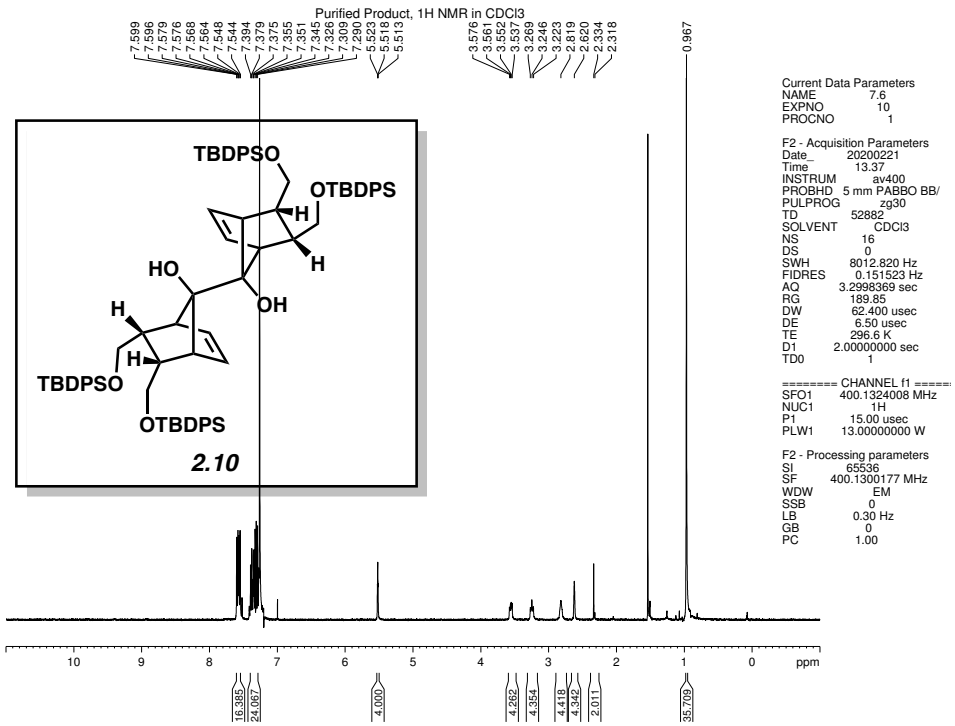

Figure 2.12 ^{1}H NMR (400 MHz, $CDCl_3$) of compound **2.10**.

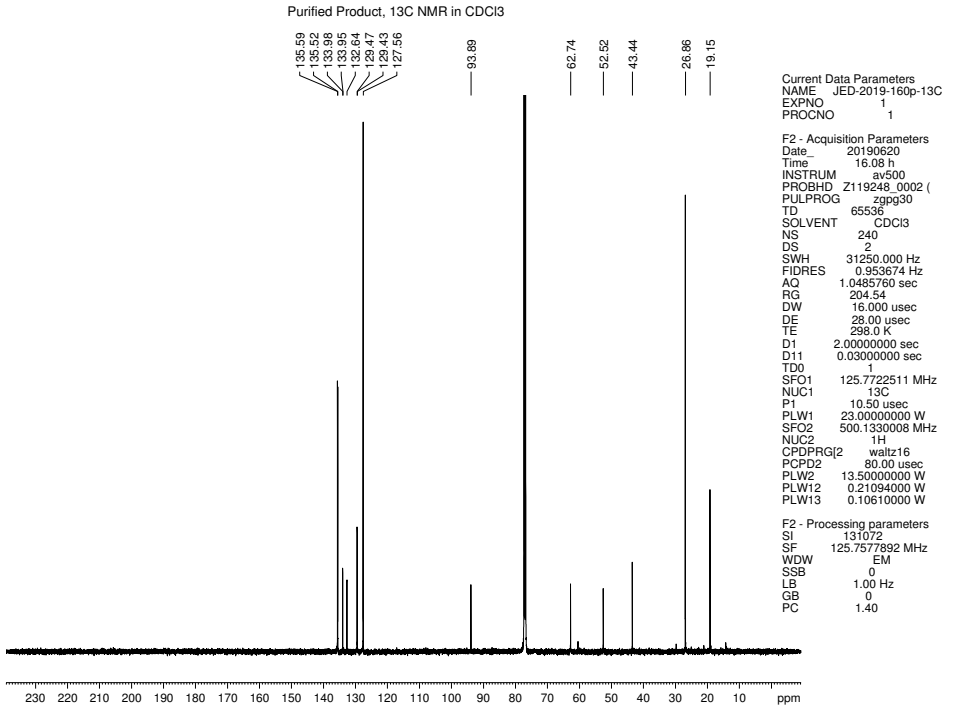

Figure 2.13 ^{13}C NMR (125 MHz, $CDCl_3$) of compound **2.10**.

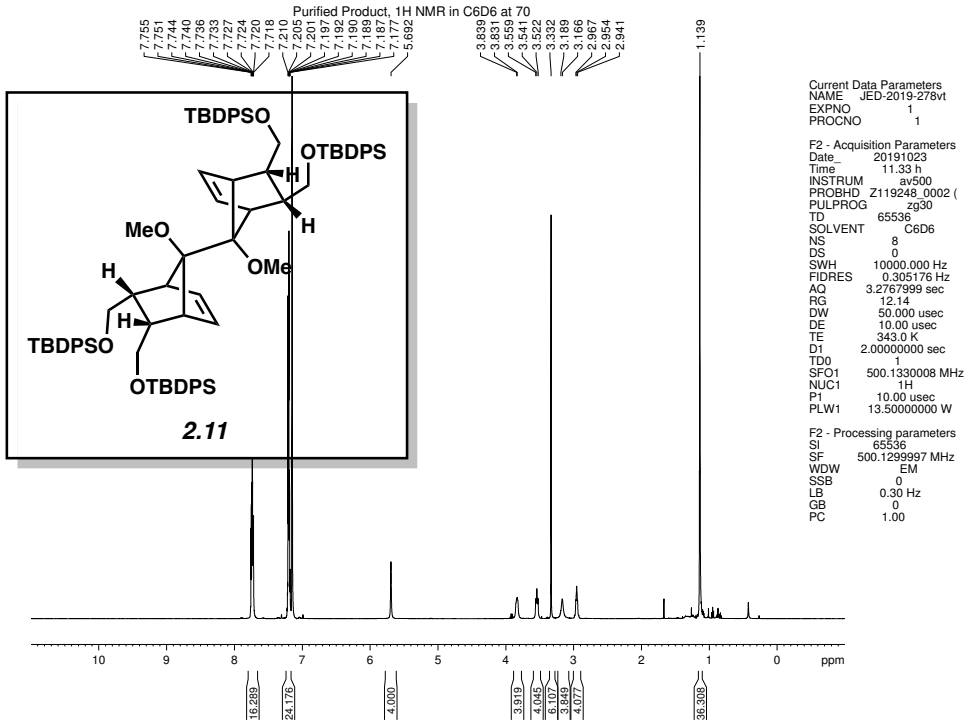

Figure 2.14 ^{1}H NMR (500 MHz, C_6D_6) of compound **2.11**.

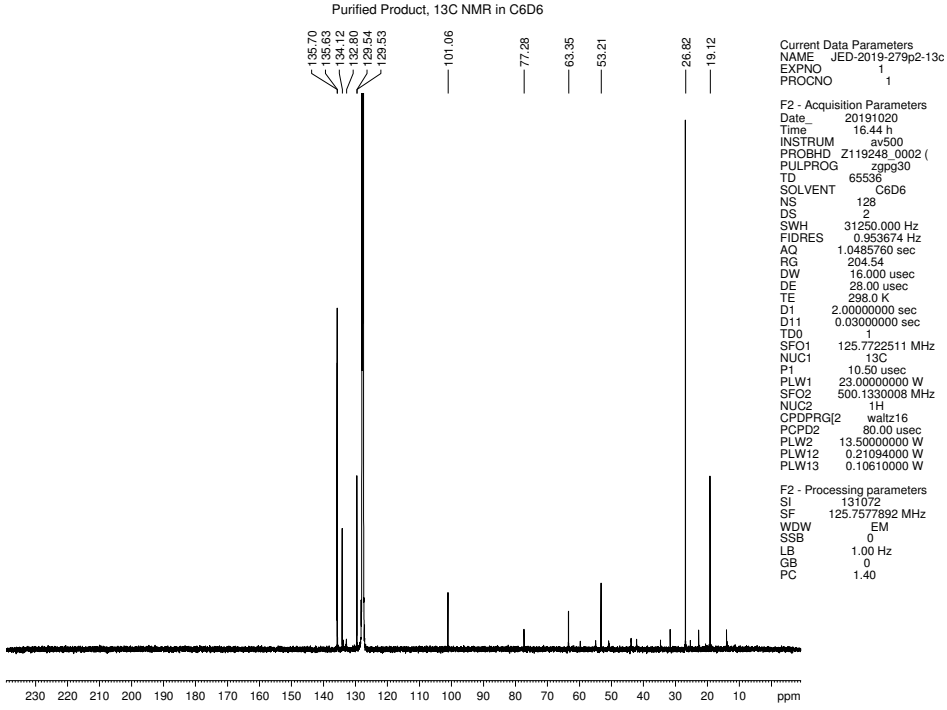

Figure 2.15 ^{13}C NMR (125 MHz, C_6D_6) of compound **2.11**.

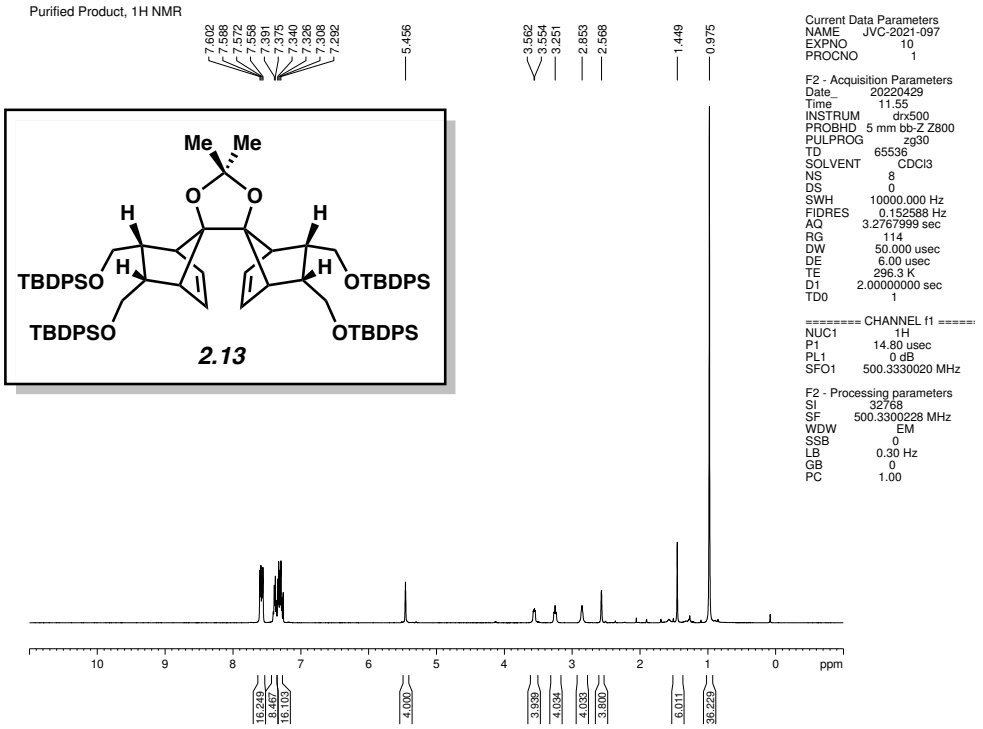

Figure 2.16 ^{1}H NMR (500 MHz, $CDCl_3$) of compound **2.13**.

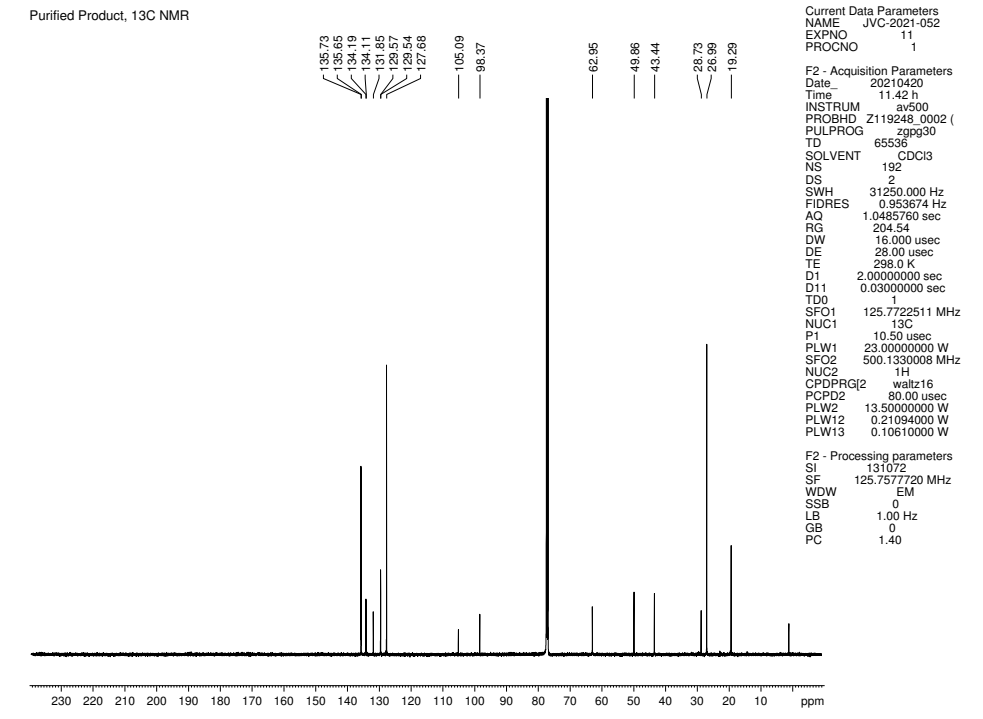

Figure 2.17 ^{13}C NMR (125 MHz, $CDCl_3$) of compound **2.13**.

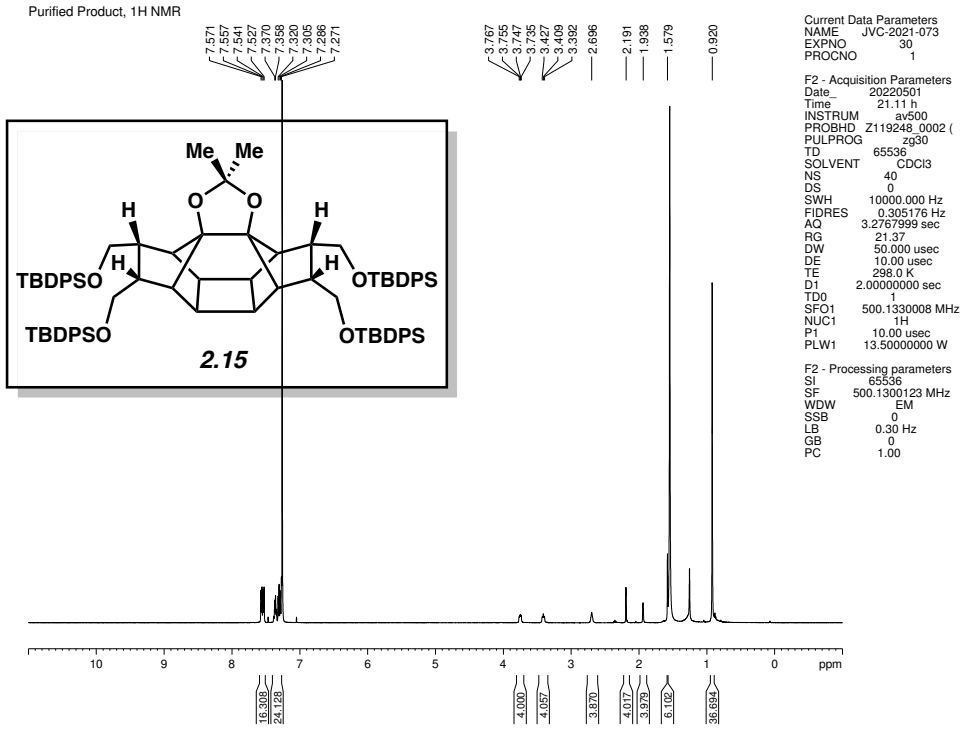

Figure 2.18 ^{1}H NMR (500 MHz, $CDCl_3$) of compound **2.15**.

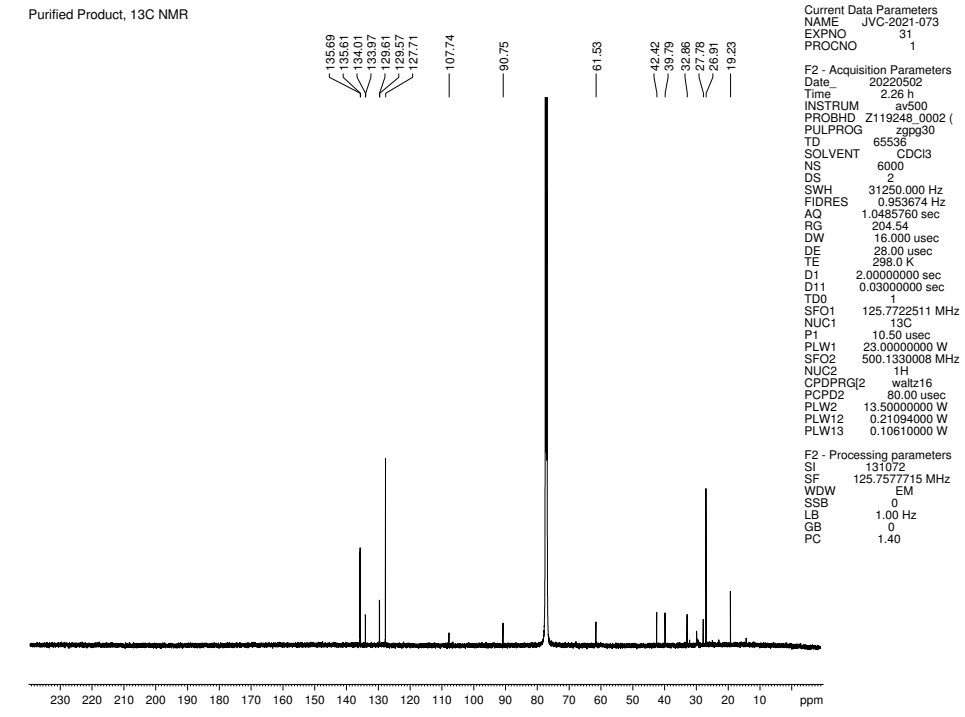

Figure 2.19 ^{13}C NMR (125 MHz, $CDCl_3$) of compound **2.15**.

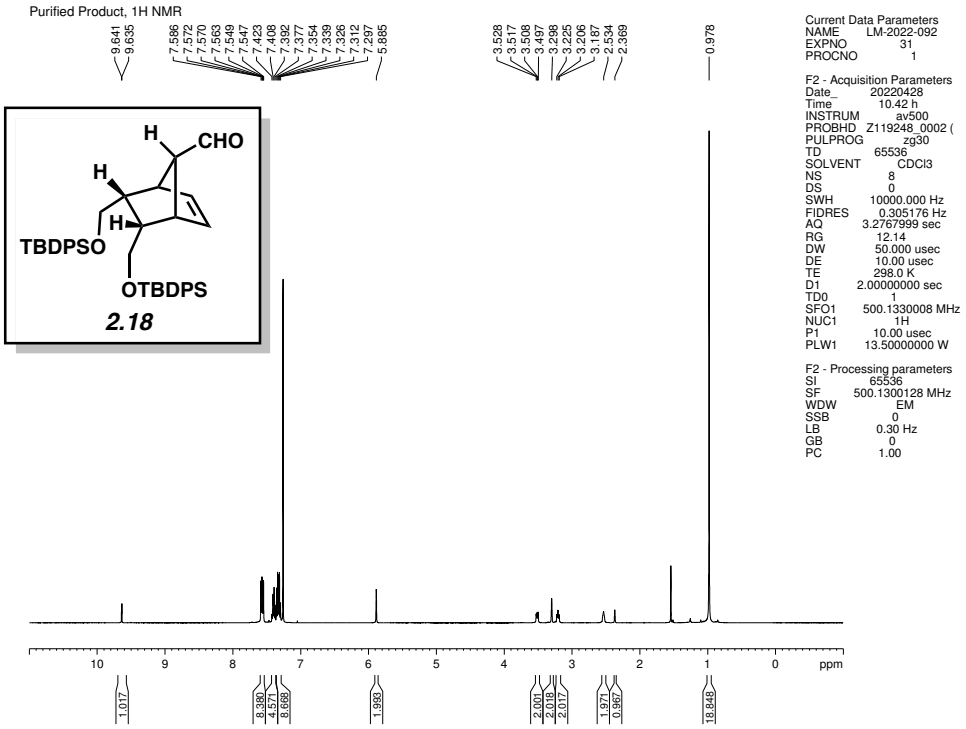

Figure 2.20 ^{1}H NMR (500 MHz, $CDCl_3$) of compound **2.18**.

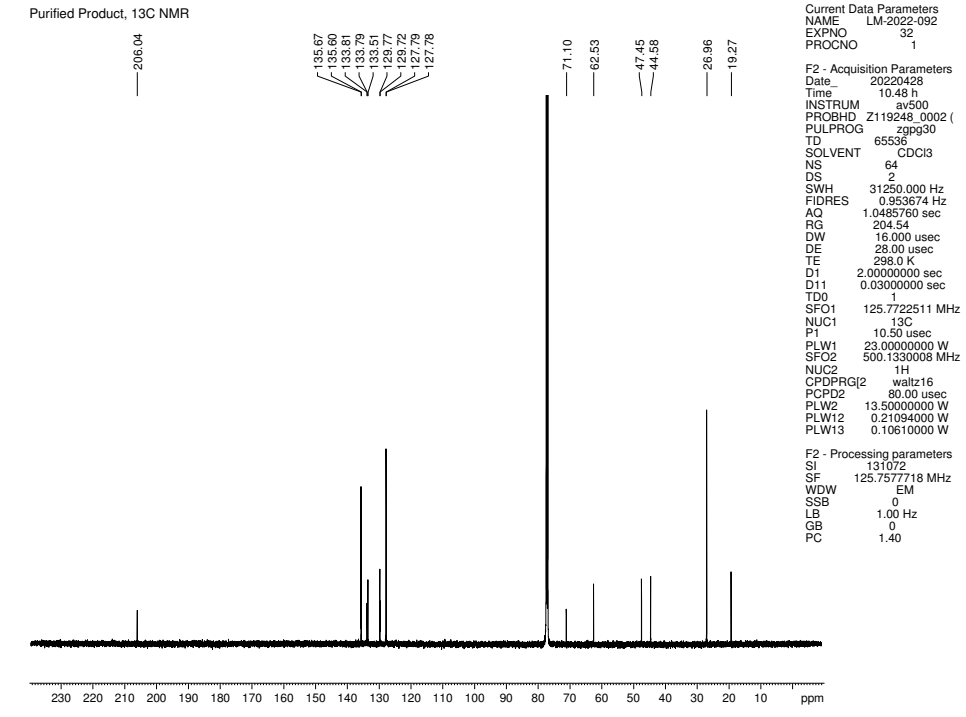

Figure 2.21 ^{13}C NMR (125 MHz, $CDCl_3$) of compound **2.18**.

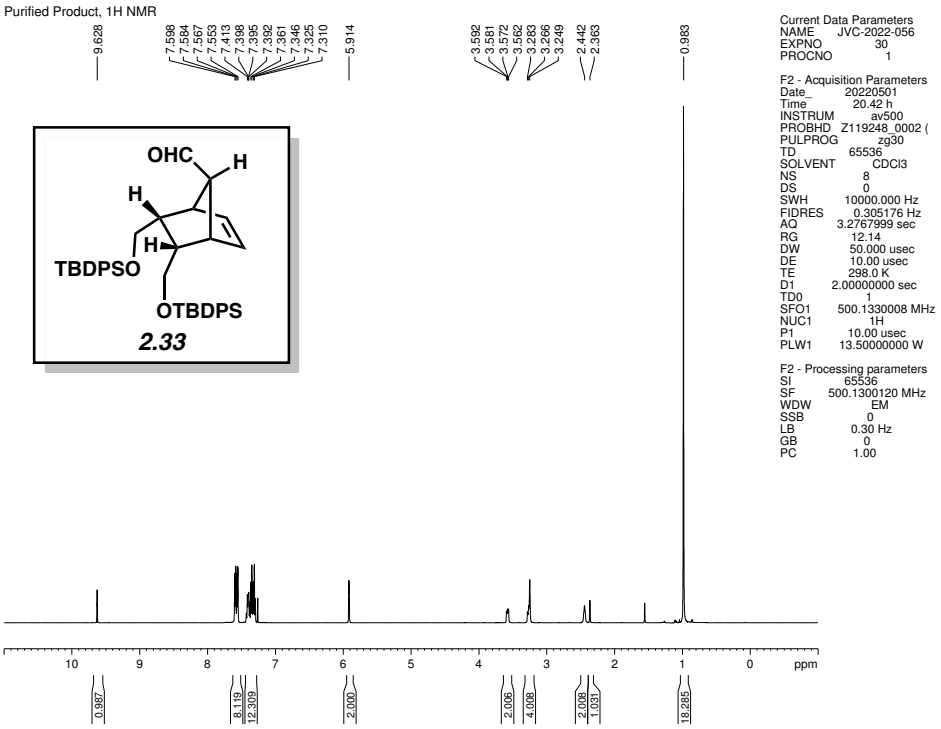

Figure 2.22 ^{1}H NMR (500 MHz, $CDCl_3$) of compound **2.33**.

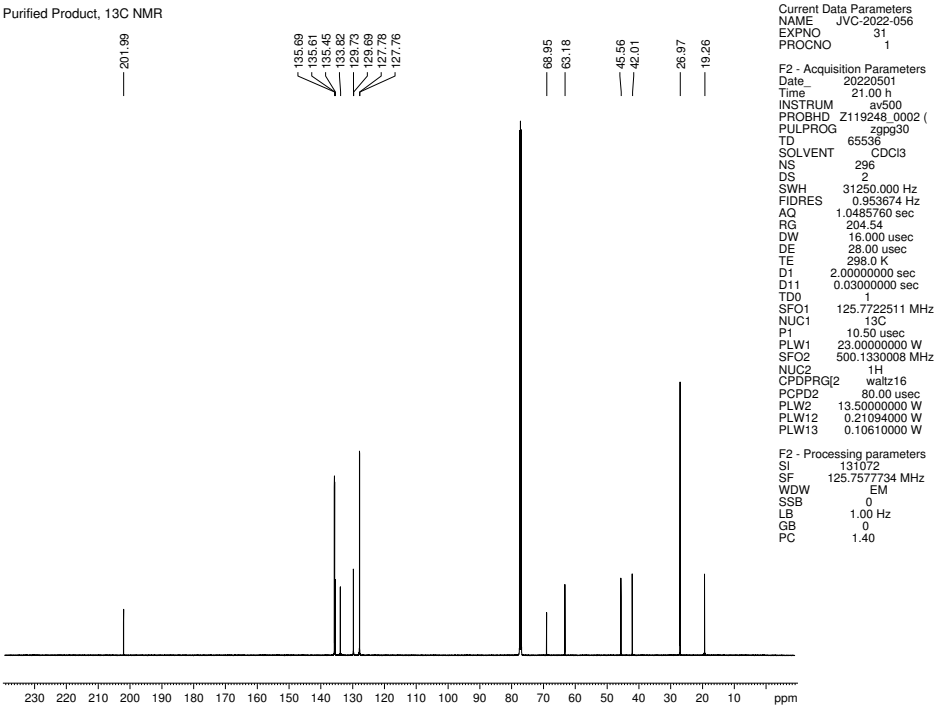

Figure 2.23 ^{13}C NMR (125 MHz, $CDCl_3$) of compound **2.33**.

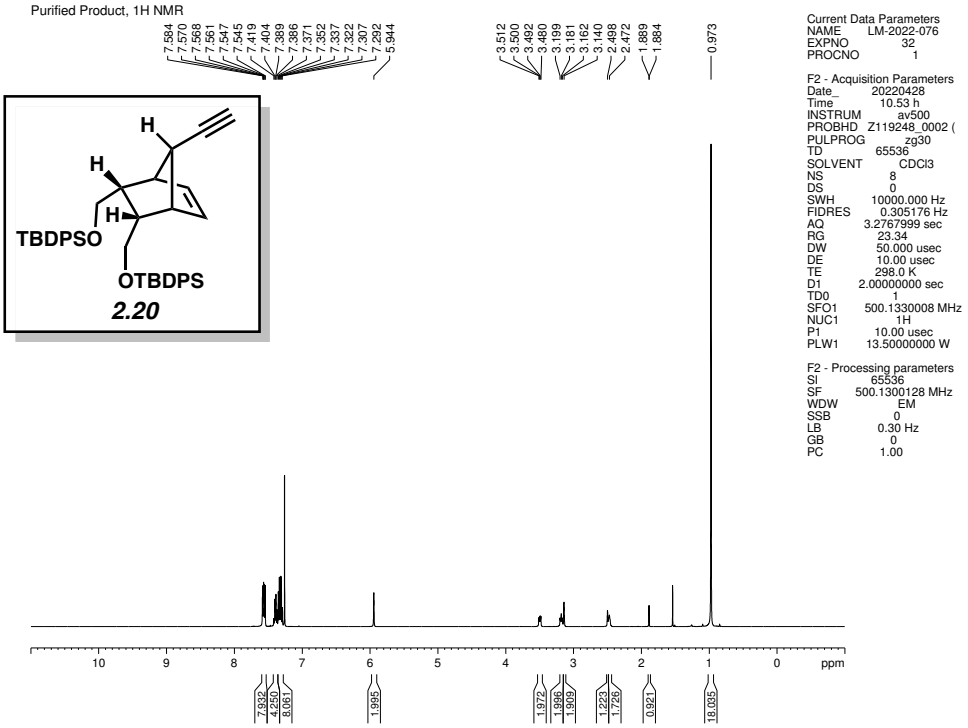

Figure 2.24 ^{1}H NMR (500 MHz, $CDCl_3$) of compound **2.20**.

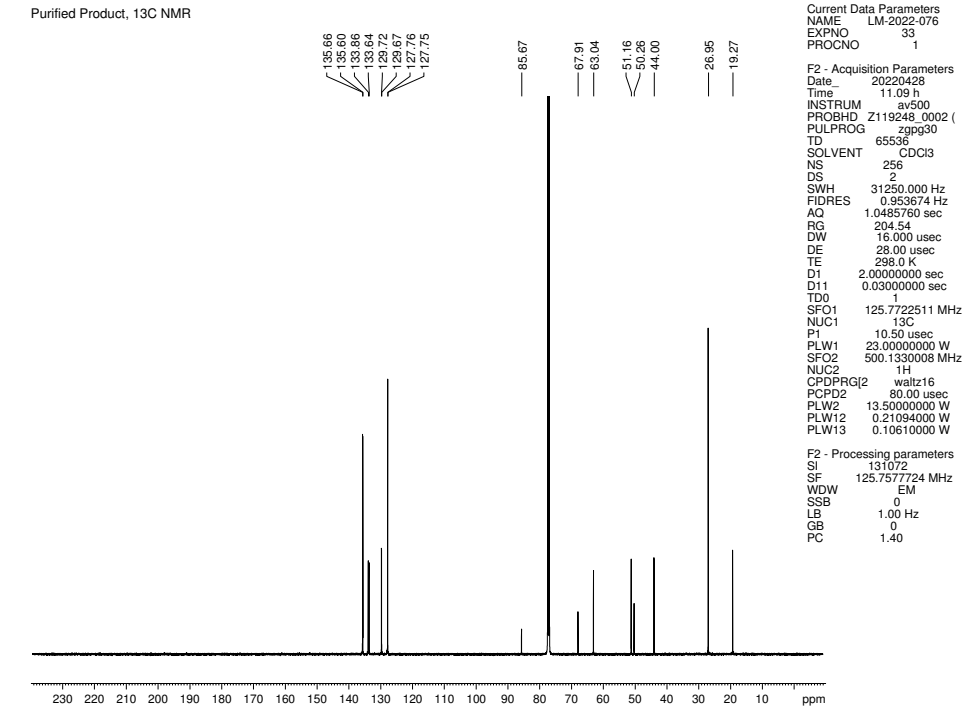

Figure 2.25 ^{13}C NMR (125 MHz, $CDCl_3$) of compound **2.20**.

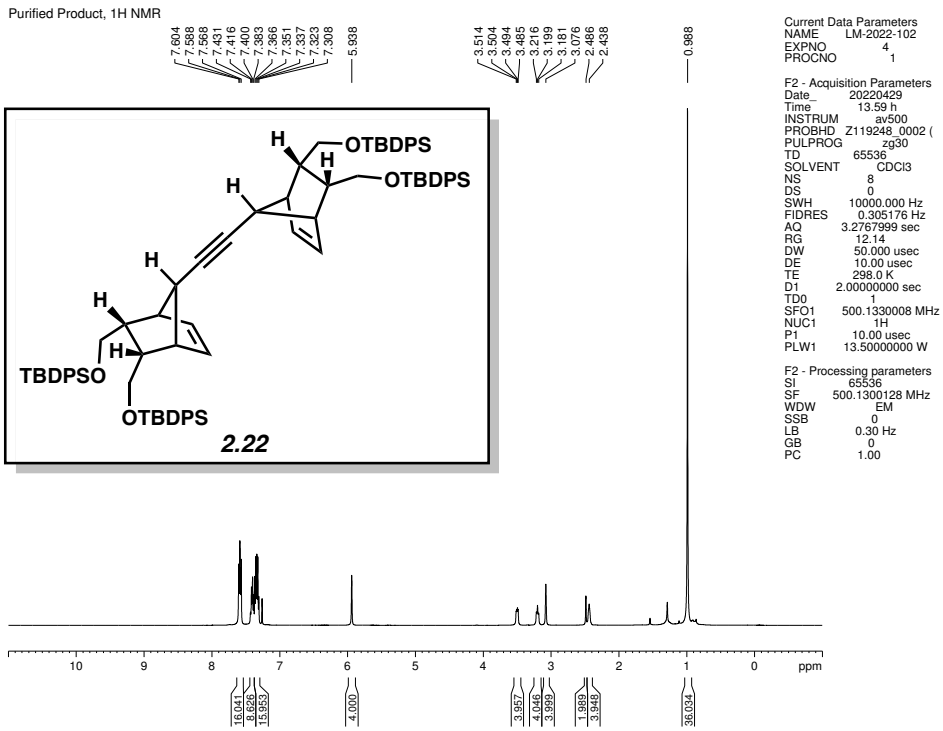

Figure 2.26 ^{1}H NMR (500 MHz, $CDCl_3$) of compound **2.22**.

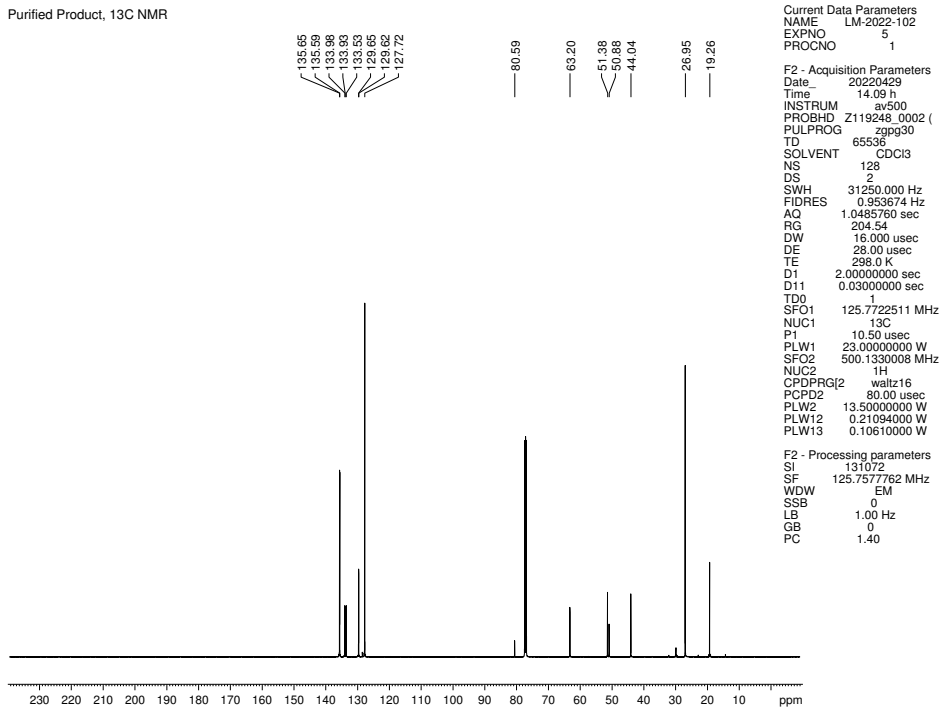

Figure 2.27 ^{13}C NMR (125 MHz, $CDCl_3$) of compound **2.22**.

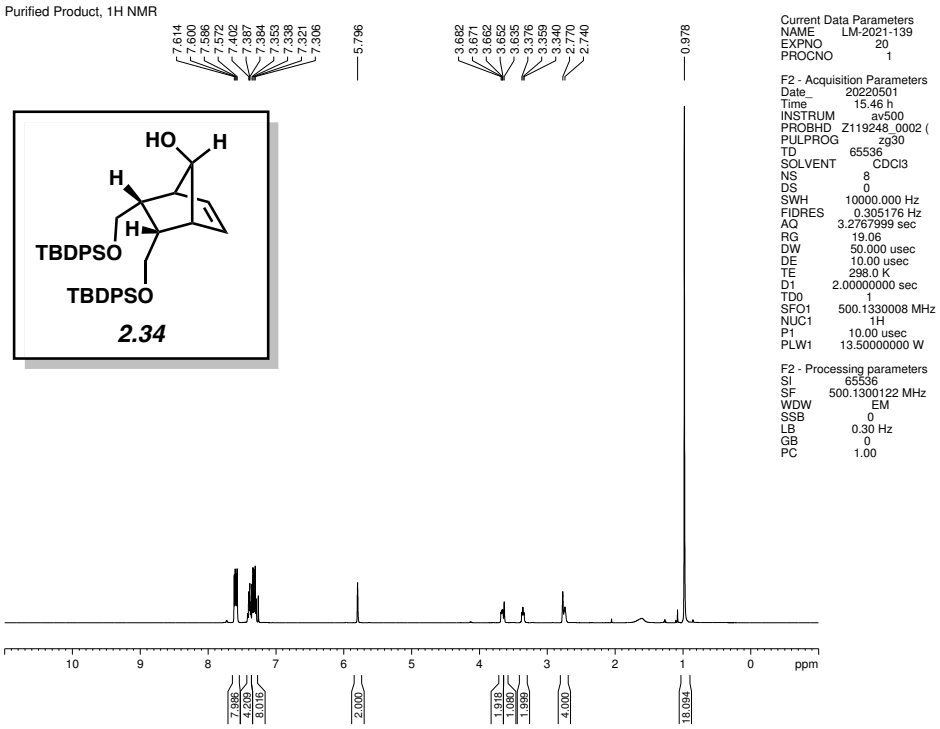

Figure 2.28 ^{1}H NMR (500 MHz, $CDCl_3$) of compound **2.34**.

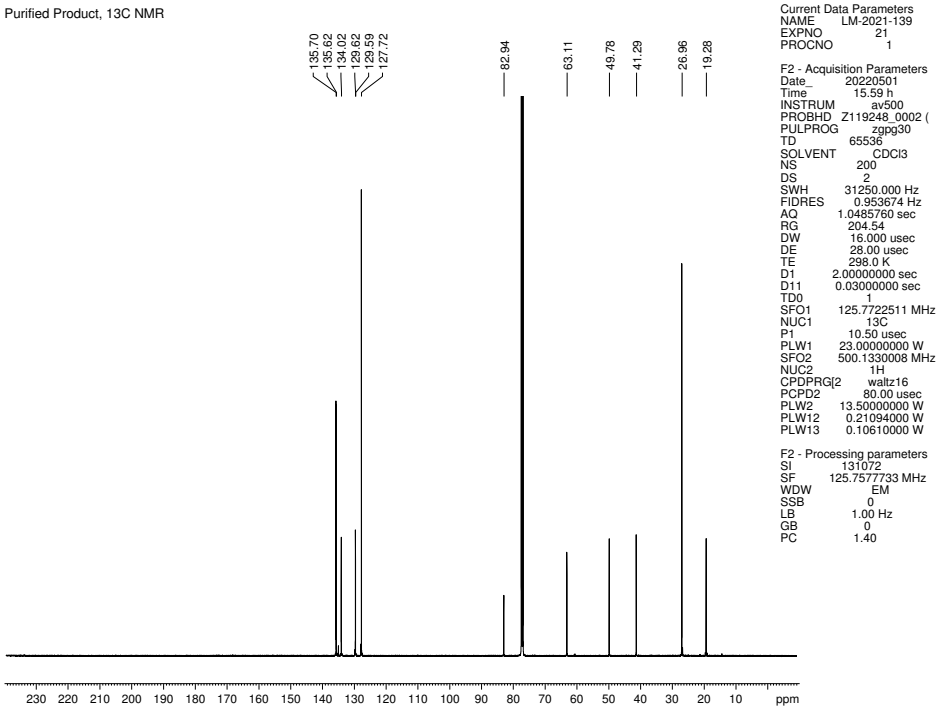

Figure 2.29 ^{13}C NMR (125 MHz, $CDCl_3$) of compound **2.34**.

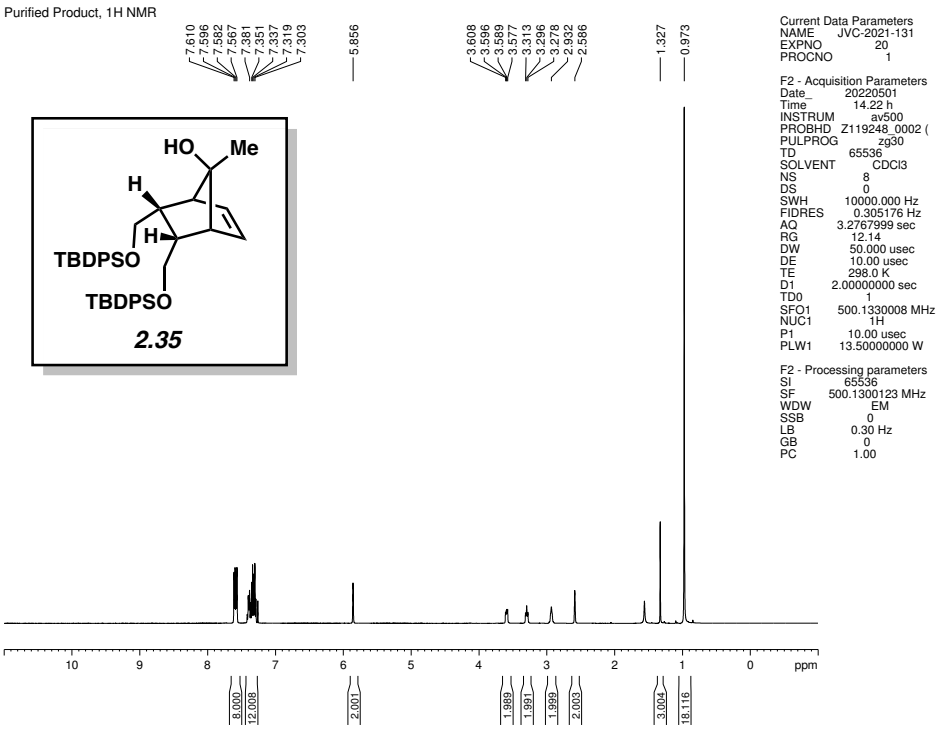

Figure 2.30 ^{1}H NMR (500 MHz, $CDCl_3$) of compound **2.35**.

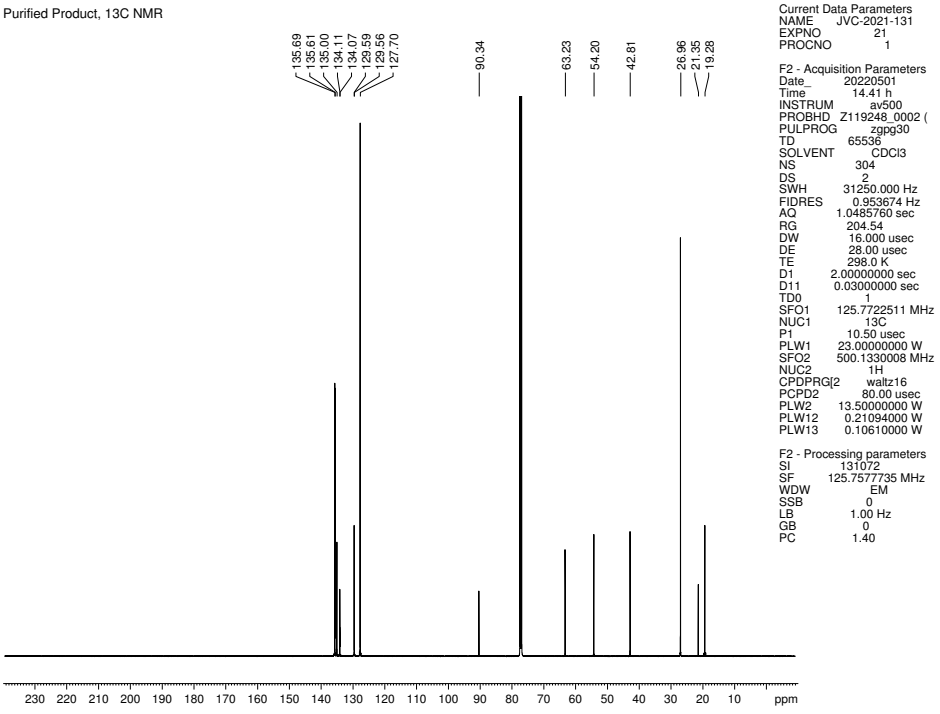

Figure 2.31 ^{13}C NMR (125 MHz, $CDCl_3$) of compound **2.35**.

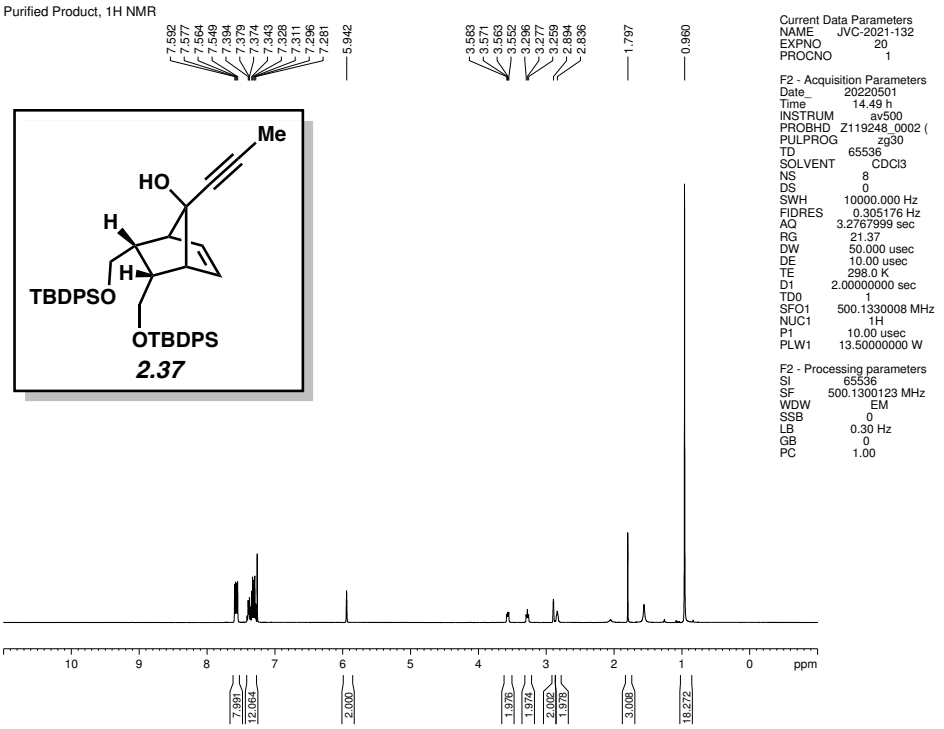

Figure 2.32 ^{1}H NMR (500 MHz, $CDCl_3$) of compound **2.37**.

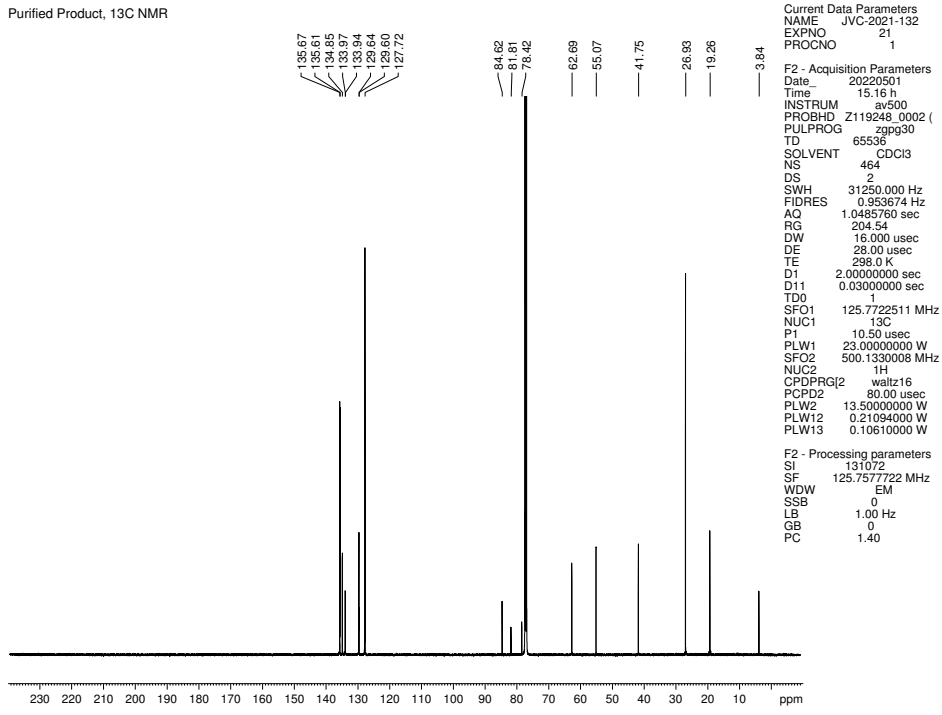

Figure 2.33 ^{13}C NMR (125 MHz, $CDCl_3$) of compound **2.37**.

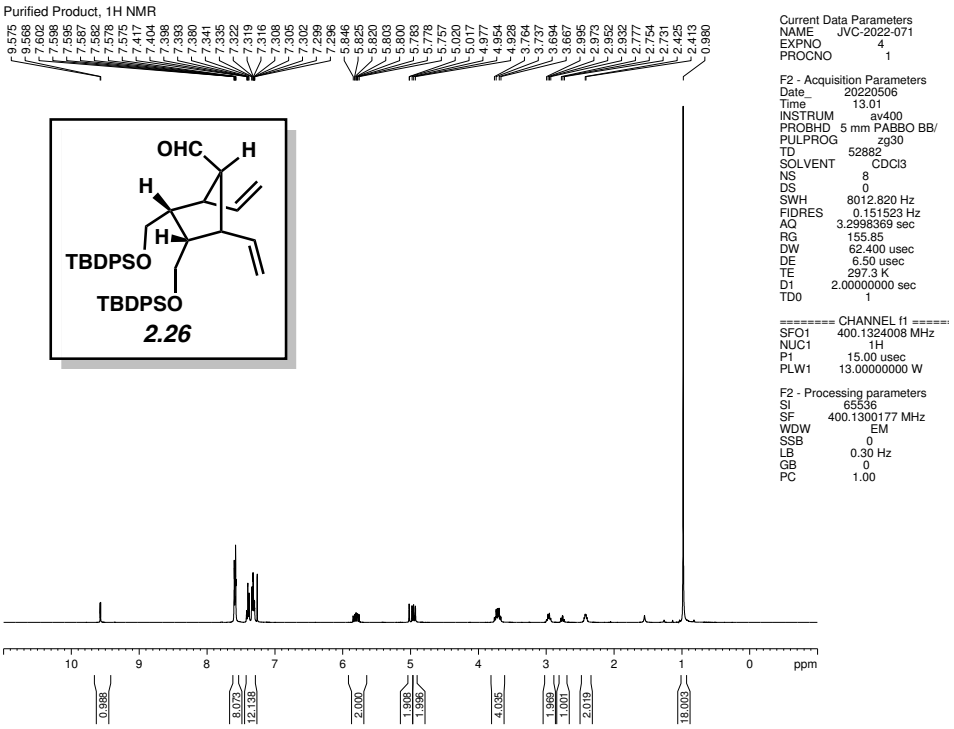

Figure 2.34 ^{1}H NMR (400 MHz, $CDCl_3$) of compound **2.26**.

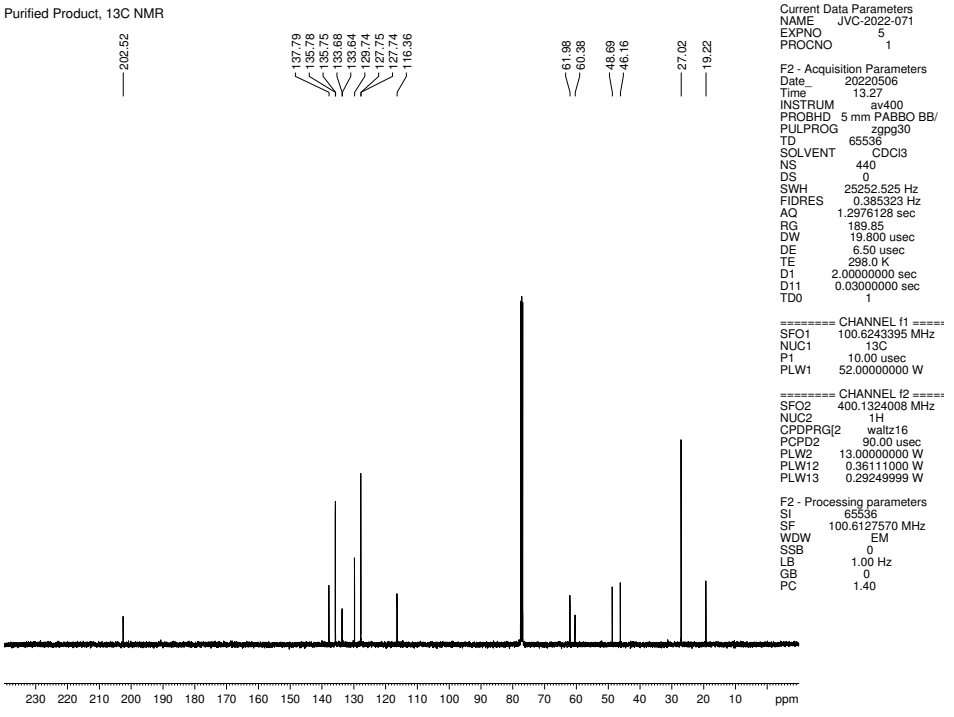

Figure 2.35 ^{13}C NMR (100 MHz, $CDCl_3$) of compound **2.26**.

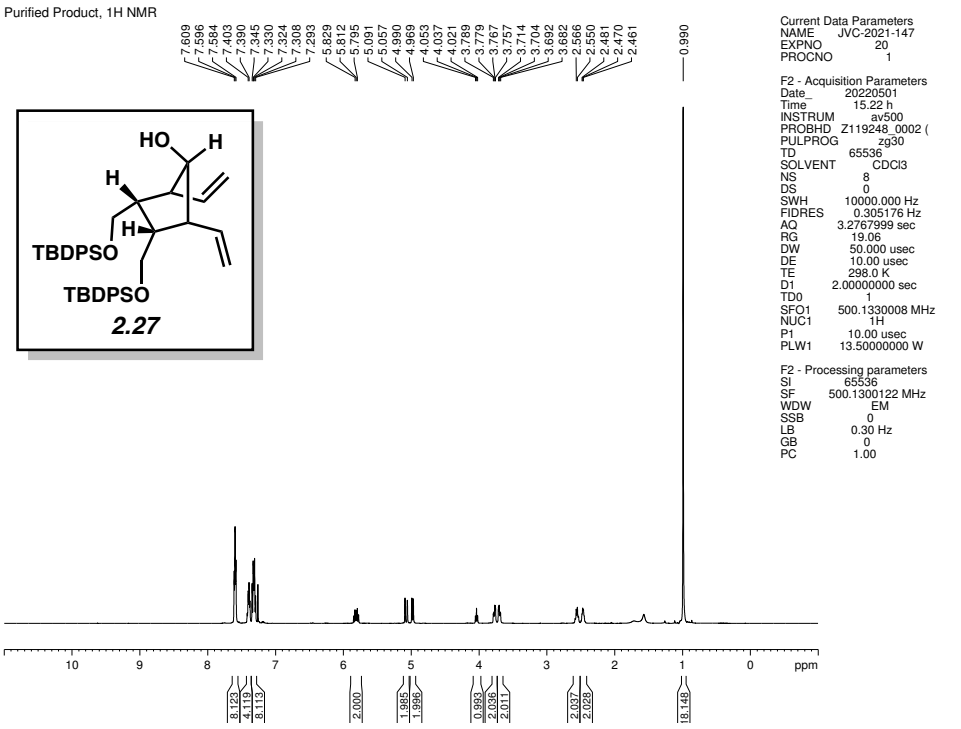

Figure 2.36 ^{1}H NMR (500 MHz, $CDCl_3$) of compound **2.27**.

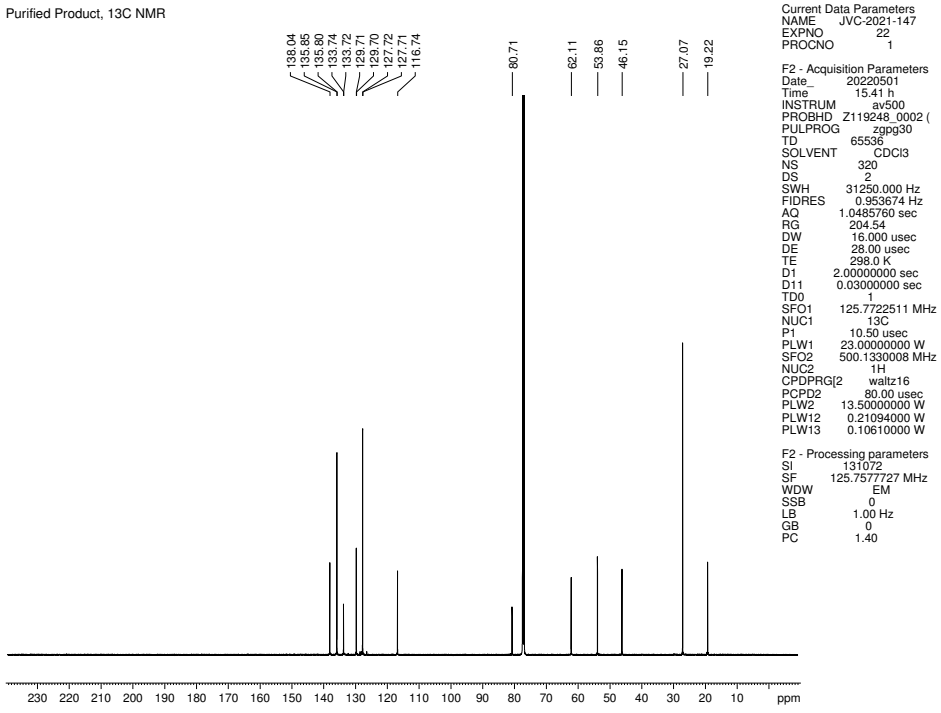

Figure 2.37 ^{13}C NMR (125 MHz, $CDCl_3$) of compound **2.27**.

2.11 Notes and References

(1) Lovering, F.; Bikker, J.; Humblet, C. Escape from Flatland: Increasing Saturation as an Approach to Improving Clinical Success. *J. Med. Chem.* **2009**, *52*, 6752–6756.

(2) Lovering, F. Escape from Flatland 2: Complexity and Promiscuity. *MedChemComm* **2013**, *4*, 515−519.

(3) (a) Eaton, P. E. Towards Dodecahedrane. *Tetrahedron* **1979**, *35*, 2189–2223. (b) Paquette, L. A. Dodecahedrane—The Chemical Transliteration of Plato's Universe (A Review). *Proc. Natl. Acad. Sci. U.S.A.* **1982**, *79*, 4495–4500. (c) Olah, G. A.; Schleyer, P. v. R., Eds. *Cage Compounds.* Wiley: New York, 1990. (d) Grubmüller, P. PhD Dissertation, Friedrich-Alexander-Universität, Erlangen-Nürnberg, West Germany, 1979.

(4) Paquette, L. A.; Ternansky, R. J.; Balogh, D. W.; Kentgen, G. Total Synthesis of Dodecahedrane. *J. Am. Chem. Soc.* **1983**, *105*, 5446–5450.

(5) Corey, E. J.; Cheng, X.-M. *The Logic of Chemical Synthesis*; John Wiley, 1995.

(6) (a) Cross, R. J.; Saunders, M.; Prinzbach, H. Putting Helium Inside Dodecahedrane. *Org. Lett*. **1999**, *1*, 1479–1481. (b) Wahl, F.; Weiler, A.; Landenberger, P.; Sackers, E.; Voss, T.; Haas, A.; Lieb, M.; Hunkler, D.; Wörth, J.; Knothe, L.; Prinzbach, H. Towards Perfunctionalized Dodecahedranes—En Route to C_{20} Fullerene. *Chem. Eur. J.* **2006**, *12*, 6255–6267.

(7) (a) Banfalvi, G. Dodecahedrane Minibead Polymers. *RSC Adv.* **2014**, *4*, 3003–3008. (b) Ariyarathna, I. R. Superatomic Nature of Metal Encapsulated Dodecahedrane: The Case of $M@C_{20}H_{20}$ (M = Li, Na, Mg^+). *Int. J. Quantum Chem.* **2021**, *121*, e26774.

(8) Woodward, R. B.; Fukunaga, T.; Kelly, R. C. Triquinacene. *J. Am. Chem. Soc.* **1964**, *86*, 3162–3164.

(9) Ternansky, R. J.; Balogh, D. W.; Paquette, L. A. Dodecahedrane. *J. Am. Chem. Soc.* **1982**, *104*, 4503–4504.

(10) (a) Fessner, W.-D.; Murty, B. A. R. C.; Prinzbach, H. The Pagodane Route to Dodecahedranes—Thermal, Reductive, and Oxidative Transformations of Pagodanes. *Angew. Chem., Int. Ed.* **1987**, *26*, 451–452. (b) Fessner, W.-D.; Murty, B. A. R. C.; Wörth, J.; Hunkler, D.; Fritz, H.; Prinzbach, H.; Roth, W. D.; Schleyer, P. v. R.; McEwen, A. B.; Maier, W. F. Dodecahedranes from [1.1.1.1]Pagodanes. *Angew. Chem., Int. Ed.* **1987**, *26*, 452–454. (c) Bertau, M.; Wahl, F.; Weiler, A.; Scheumann, K.; Wörth, J.; Keller, M.; Prinzbach, H. From Pagodanes to Dodecahedranes - Search for a Serviceable Access to the Parent ($C_{20}H_{20}$) Hydrocarbon. *Tetrahedron* **1997**, *53*, 10029–10040.

(11) Hoffmann, R.; Hopf, H. Learning from Molecules in Distress. *Angew. Chem., Int. Ed.* **2008**, *47*, 4474–4481.

(12) Ungarean, C. N.; Southgate, E.; Sarlah, D. Enantioselective Polyene Cyclizations. *Org. Biomol. Chem.* **2016**, *14*, 5454–5467.

(13) (a) Domínguez, G.; Pérez-Castells, J. Recent Advances in [2+2+2] Cycloaddition Reactions. *Chem. Soc. Rev.* **2011**, *40*, 3430–3444. (b) Xu, F.; Xiao, X.; Hoye, T. R. Photochemical Hexadehydro-Diels–Alder Reaction. *J. Am. Chem. Soc.* **2017**, *139*, 8400–8403. (c) Diamond, O. J.; Marder, T. B. *Org. Chem. Front.* **2017**, *4*, 891−910.

(14) Meador, M. A. B.; Johnston, J. C. 7-Hydroxynadic Acid: A New End Cap for Improved Oxidation Resistance in Addition Polyimides. *Chem. Mater.* **2001**, *13*, 2649–2655.

(15) Borkman, R. F.; Kearns, D. R. Triplet-State Energy Transfer in Liquid Solutions. Acetone-Photosensitized *cis-trans* Isomerization of Pentene-2. *J. Am. Chem. Soc.* **1966**, *88*, 3467–3475.

(16) Modest preference for the desired aldehyde diastereomer over the undesired aldehyde diastereomer was observed (see Section 2.9.2.1 for details). Preliminary results demonstrate that the undesired aldehyde diastereomer **2.33** obtained through this approach can be recycled to give desired alkyne **2.20** by one of two strategies: a) a base-mediated epimerization/alkynylation sequence or b) conversion of the aldehyde to a redox-active phthalimide ester and subsequent Ni-catalyzed decarboxylative alkynylation, which proceeds through formation and capture of a radical intermediate at the bridgehead.

(17) For a previous report of alkyne metathesis dimerization of an α-tertiary alkyne, see: Hoffmeister, L.; Persich, P.; Fürstner, A. Formal Total Synthesis of Kendomycin by Way of Alkyne Metathesis/Gold Catalysis. *Chem. Eur. J.* **2014**, *20*, 4396–4402.

(18) Bidange, J.; Fischmeister, C.; Bruneau, C. Ethenolysis: A Green Catalytic Tool to Cleave Carbon–Carbon Double Bonds. *Chem. Eur. J.* **2016**, *22*, 12226–12244.

(19) Green, J. R. (Cycloheptyne)dicobalt Complexes in Organic Synthesis. *Eur. J. Org. Chem.* **2008**, 6053–6062.

(20) Green, J. R. Cycloheptenyne Dicobalt Hexacarbonyl Complexes by Ring Closing Metathesis. *Synlett* **2001**, *3*, 353–356.

(21) Lin, Y.-T.; Lin, F.-Y.; Isobe, M. Novel Synthesis of the ABC Rings of Solanoeclepin A. *Org. Lett.* **2014**, *16*, 5948–5951.

(22) (a) Johnson, W. S.; Semmelhack, M. F.; Sultanbawa, M. U. S.; Dolak, L. A. A New Approach to Steroid Total Synthesis. A Nonenzymic Biogenetic-Like Olefinic Cyclization Involving the Stereospecific Formation of Five Asymmetric Centers. *J. Am. Chem. Soc.* **1968**, *90*, 2994–2996. (b) Nicolaou, K. C.; Edmonds, D. J.; Bulger, P. G. Cascade Reactions in Total Synthesis. *Angew. Chem. Int. Ed.* **2006**, *45*, 7134–7186. (c) Domínguez, G.; Pérez-Castells, J. Recent Advances in [2+2+2] Cycloaddition Reactions. *Chem. Soc. Rev.* **2011**, *40*, 3430–3444.

(23) Klán, P.; Wirz, J. *Photochemistry of Organic Compounds: From Concepts to Practice*. Wiley, Chichester, 2009.

(24) Faustino, H.; Varela, I.; Mascareñas, J. L.; López, F. Gold(I)-Catalyzed [2 + 2 + 2] Cycloaddition of Allenamides, Alkenes and Aldehydes: a Straightforward Approach to Tetrahydropyrans. *Chem. Sci.* **2015**, *6*, 2903–2908.

(25) McCulley, C. H.; Geier, M. J.; Hudson, B. M.; Gagné, M. R.; Tantillo, D. J. Biomimetic Platinum-Promoted Polyene Polycyclizations: Influence of Alkene Substitution and Pre-cyclization Conformations. *J. Am. Chem. Soc.* **2017**, *139*, 11158−11164.

(26) Hoffmann, U.; Gao, Y.; Pandey, B.; Klinge, S.; Warzecha, K.-D.; Krüger, C.; Roth, H. D.; Demuth, M. Light-Induced Polyene Cyclizations via Radical Cations in Micellar Medium. *J. Am. Chem. Soc.* **1993**, *115*, 10358−10359.

(27) Wang, S. C.; Tantillo, D. J. Viability of Dodecahedrane-Forming Radical Polycyclizations. *Org. Biomol. Chem.* **2017**, *15*, 1976–1979.

CHAPTER THREE

Concise Approach to Cyclohexyne and 1,2-Cyclohexadiene Precursors

Jason V. Chari,† Francesca M. Ippoliti,† and Neil K. Garg.

J. Org. Chem. **2019**, *84*, 3652–3655.

3.1 Abstract

Silyl triflate precursors to cyclic alkynes and allenes serve as valuable synthetic building blocks. We report a concise and scalable synthetic approach to prepare the silyl triflate precursors to cyclohexyne and 1,2-cyclohexadiene. The strategy involves a retro-Brook rearrangement of an easily accessible cyclohexanone derivative, followed by triflation protocols. This simple, yet controlled, method should enable the further study of strained alkynes and allenes in chemical synthesis.

3.2 Introduction

The existence of arynes, cyclic alkynes, and cyclic allenes was once considered scientific conjecture.[1] However, following a series of seminal studies in the 1950s and 1960s by Roberts and Wittig, strained intermediates such as benzyne (**3.1**), cyclohexyne (**3.2**), and 1,2-cyclohexadiene (**3.3**) were experimentally validated (Figure 3.1).[2] In the modern era, these intermediates and their derivatives, such as heterocycles **3.4** and **3.5**, have become valuable synthetic building blocks. Indeed, these strained intermediates have been used to synthesize important ligands,[3] agrochemicals,[4] medicinal agents,[5] natural products,[6] and materials.[7] Studies

of **3.1**–**3.5** have also led to new insights regarding reactivities and selectivities,[8,9,10] particularly as a result of the distortion/interaction model investigated by Houk.[11]

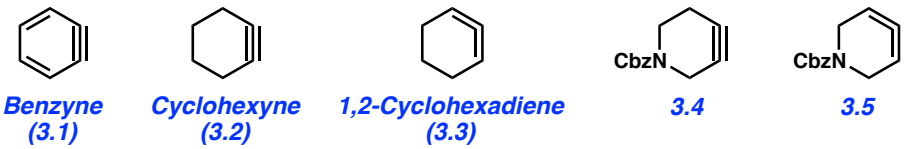

Figure 3.1. Strained cyclic alkynes and allenes.

In comparison to arynes, strained cyclic alkynes and allenes are less well-studied. However, as exemplified in Figure 3.2 in the context of **3.2** and **3.3**, cyclic alkynes and allenes can be trapped in an array of cycloadditions to give a diverse range of products.[6,9,10] For example, cycloadducts **3.7**, **3.9**, and **3.11** have been obtained by (3+2) and (4+2) cycloadditions of cyclohexyne (**3.2**).[9c,15] Analogously, **3.13**, **3.15**, and **3.16** have been prepared using (3+2), (2+2), and (4+2) cycloaddition reactions of 1,2-cyclohexadiene (**3.3**).[9b,d,12,15] In all cases, the reactions proceed by the controlled formation of two new bonds, which may be either carbon–carbon bonds or carbon–heteroatom bonds. By virtue of using heteroatom-containing trapping agents, the carbocyclic strained intermediates can be used to access heterocyclic products (e.g., **3.7**, **3.9**, **3.11**, **3.13**, **3.16**) that are of value to the pharmaceutical community. Lastly, it should be noted that the cycloadducts can bear one or more stereocenters, as seen in **3.11**, **3.13**, **3.15**, and **3.16**. In the case of substituted variants of **3.3**, it has been shown that regioselectivities, relative stereochemistry, and even absolute stereochemistry can be controlled in reactions of cyclic allenes, thus boding well for future synthetic applications.[9,10,13]

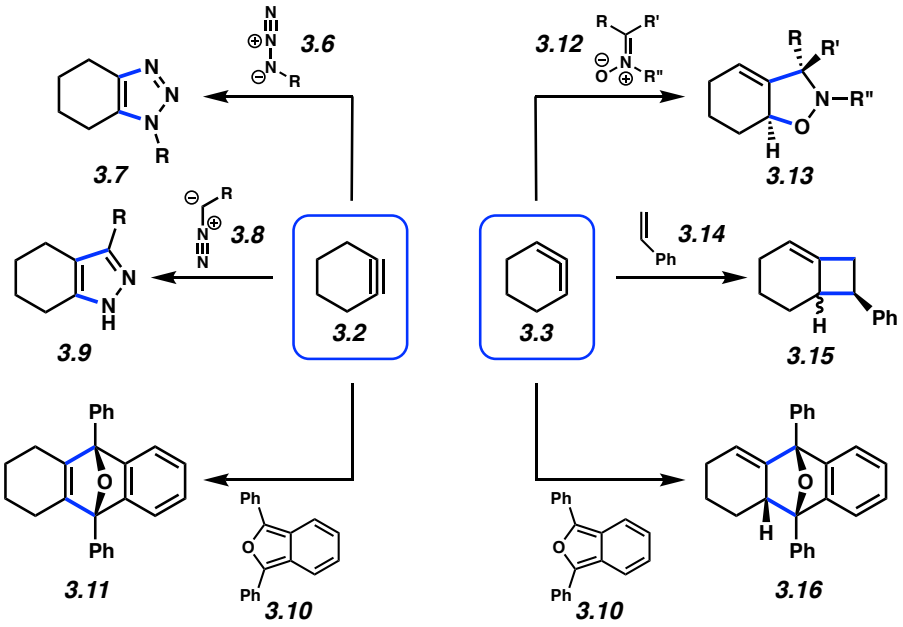

Figure 3.2. Cycloadditions of cyclohexyne (**3.2**) and 1,2-cyclohexadiene (**3.3**).

Given the synthetic utility of **3.2** and **3.3** (and derivatives thereof), chemists have sought to design practical synthetic precursors to these strained intermediates. Kobayashi's breakthrough in the context of benzyne[14] has unveiled silyl triflates as ideal precursors to strained intermediates by enabling mild reaction conditions, as will be highlighted later. In seminal studies, Guitián and co-workers demonstrated that silyl triflate precursors to **3.2** and **3.3** could be synthesized from cyclohexenone (**3.17**) (Figure 3.3).[9a,b] As depicted, Guitián's approach initially utilized trimethylsilyl groups. The sequence involves α-bromination of **3.17**, ketone protection and silylation, followed by deprotection to give **3.18**. 1,4-Reduction of **3.18** furnishes intermediate **3.19a**, which can undergo direct triflation to give cyclohexyne precursor **3.20a**. Alternatively, protonation of **3.19a**, followed by kinetic enolate formation and triflation, delivers 1,2-cyclohexadiene precursor **3.21a**. Our laboratory questioned if intermediates reminiscent of **3.19a** could be more rapidly accessed by another means. However, it should be emphasized that

during our efforts, Mori disclosed an elegant method to prepare triethylsilyl derivatives **3.20b** and **3.21b**.[15] Silyl enol ether **3.22** was treated with LDA and *t*-BuOK. This led to allylic deprotonation, followed by in situ silyl migration, to afford **3.23**. Triflation of **3.23** provided 1,2-cyclohexadiene precursor **3.21b**. On the other hand, the authors found that **3.23** could isomerize to **3.19b** under modified reaction conditions, which, in turn, underwent triflation to give cyclohexyne precursor **3.20b**. It should be noted that silyl triflates **3.20b** and **3.21b** required purification by conventional chromatography, followed by size-exclusion chromatography-HPLC. Nonetheless, Mori's use of **3.22** as the key building block offers a clever strategy.

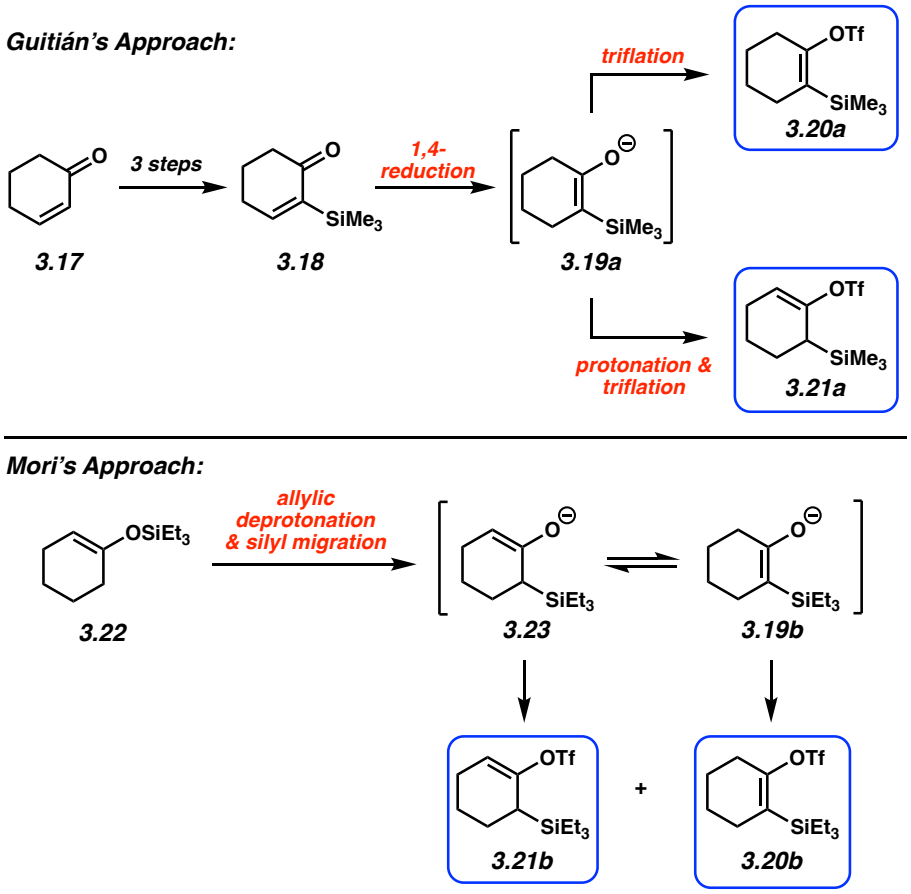

Figure 3.3. Synthetic approaches to cyclohexyne precursors **3.20a** and **3.20b** and 1,2-cyclohexadiene precursors **3.21a** and **3.21b**.

3.3 Results and Discussion

We have developed an alternative means to access **3.20b** and **3.21b**, which is depicted in Figure 3.4. Our route begins with α-bromo-cyclohexanone (**3.24**), which is commercially available or can be easily prepared from cyclohexanone.[16] Treatment of **3.24** with DABCO and triethylsilyl chloride in DMF at 0 °C gives silyl enol ether **3.25** as a single constitutional isomer. Next, we perform halogen-metal exchange using *sec*-BuLi. This proceeds with retro-Brook rearrangement to intercept anionic intermediate **3.19b** in a highly controlled and concise manner. This strategy was conceived based on the well-established retro-Brook approach to aryne precursors.[17] Following rearrangement, simply quenching **3.19b** with $PhNTf_2$ provides cyclohexyne precursor **3.20b** in 97% yield. Alternatively, **3.19b** can be quenched by the addition of aqueous sodium bicarbonate to furnish α-silyl ketone **3.26** in 95% yield. Our laboratory has previously reported the final step, wherein **3.26** can be converted to **3.21b** by kinetic enolate formation, followed by triflation. This earlier result is depicted based on the literature yield.[9d] The routes to silyl triflates **3.20b** and **3.21b** are only two and three steps from **3.24**, respectively, and notably do not require challenging chromatographic separations. Furthermore, all steps can be performed on gram scale.

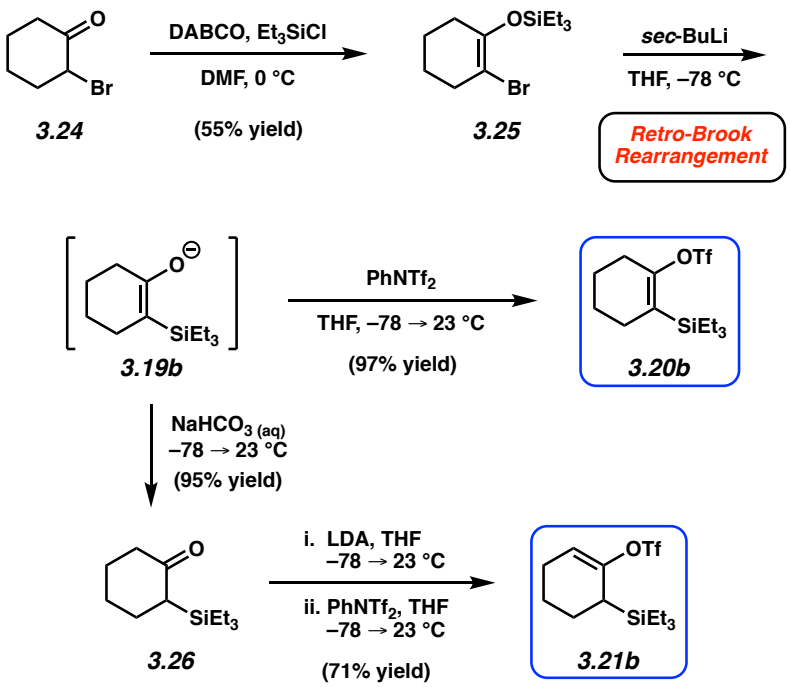

Figure 3.4. Retro-Brook approach to silyl triflates **3.20b** and **3.21b**.

To illustrate the mildness and simplicity of strained cyclic alkyne and allene chemistry using silyl triflate precursors, two known examples from the literature are depicted (Figure 3.5). In the first, silyl triflate **3.20b** is treated with **3.10** in the presence of TBAF in THF.[15] This presumably leads to the formation of **3.2** in situ, which undergoes cycloaddition to give Diels–Alder adduct **3.11**. In the second example, silyl triflate **3.21b** is treated with CsF using nitrone **3.27** as the trapping agent.[9d] Interception of 1,2-cyclohexadiene (**3.3**) gives **3.28**. The reactions proceed without the rigorous exclusion of water or oxygen, with 1.5–2.0 equivalents of the trapping agents, and with minimal byproduct formation. As such, silyl triflates **3.20b** and **3.21b** can be transformed to value-added products using simple reaction conditions.

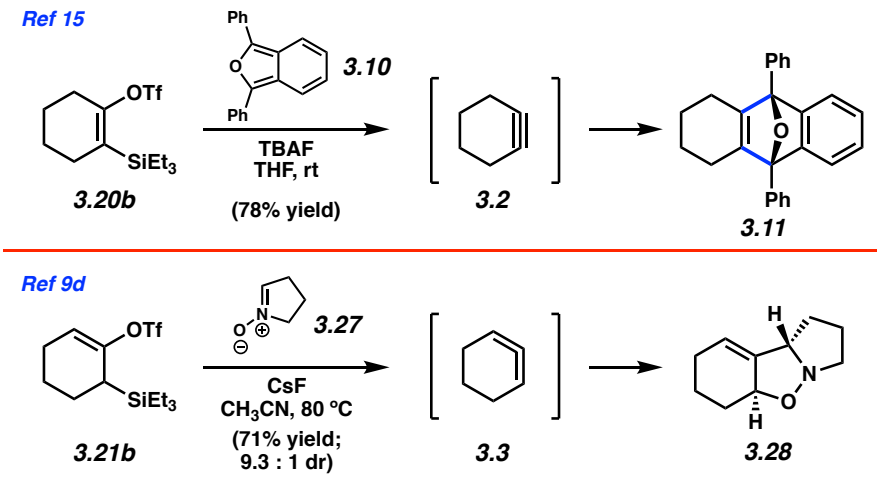

Figure 3.5. Examples of Cycloadditions Using Silyl Triflates **3.20b** and **3.21b**.

3.4 Conclusion

In summary, we have developed a concise approach to silyl triflate precursors to cyclohexyne (**3.2**) and 1,2-cyclohexadiene (**3.3**). Our strategy relies on a retro-Brook rearrangement of a readily available silyl enol ether. The resulting enolate intermediate can be diverted through two different sequences. Direct triflation gives cyclohexyne precursor **3.20b**, whereas protonation, followed kinetic enolization and triflation affords 1,2-cyclohexadiene precursor **3.21b**. We expect this concise and controlled strategy to access silyl triflate precursors will ultimately enable further studies involving strained alkynes and allenes in chemical synthesis.

3.5 Experimental Section

3.5.1 Materials and Methods. Unless stated otherwise, reactions were conducted in flame-dried glassware under an atmosphere of nitrogen using anhydrous solvents (either freshly distilled or passed through activated alumina columns). All commercially obtained reagents were used as received unless otherwise specified. 1,4-Diazabicyclo[2.2.2]octane (DABCO) was purchased from Acros Organics. *Sec*-Butyllithium 1.4 M solution in cyclohexane (*sec*-BuLi) and cyclohexanone were obtained from Sigma-Aldrich. *N*-Phenyl-bis(trifluoromethanesulfonimide) and triethylsilyl chloride (TESCl) were purchased from Oakwood Chemical. Cyclohexanone and TESCl were distilled over CaH_2 prior to use. Unless stated otherwise, reactions were performed at 23 °C. Thin-layer chromatography (TLC) was conducted with EMD gel 60 F254 pre-coated plates (0.25 mm) and visualized using anisaldehyde or potassium permanganate staining. Silicycle Siliaflash P60 (particle size 0.040–0.063 mm) was used for flash column chromatography. ^{1}H-NMR spectra were recorded on Bruker spectrometers (at 500 MHz) and are reported relative to the residual solvent signal. Data for ^{1}H-NMR spectra are reported as follows: chemical shift (δ ppm), multiplicity, coupling constant (Hz) and integration. ^{13}C-NMR spectra were recorded on Bruker spectrometers (at 100 MHz) and are reported relative to the residual solvent signal. Data for ^{13}C-NMR spectra are reported in terms of chemical shift (δ ppm). IR spectra were obtained on a Perkin-Elmer UATR Two FT-IR spectrometer and are reported in terms of frequency of absorption (cm^{-1}). DART-MS spectra were collected on a Thermo Exactive Plus MSD (Thermo Scientific) equipped with an ID-CUBE ion source, a Vapur Interface (IonSense Inc.), and an Orbitrap mass analyzer. Both the source and MSD were controlled by Excalibur software v. 3.0. The analyte was spotted onto OpenSpot sampling cards (IonSense Inc.) using $CDCl_3$ as the solvent. Ionization was accomplished using UHP He (Airgas Inc.) plasma with no additional ionization agents. The mass calibration was carried out using Pierce LTQ Velos ESI (+) and (–) Ion calibration solutions (Thermo Fisher Scientific).

3.5.2 Experimental Procedures

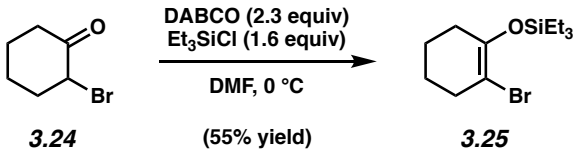

3.24 (55% yield) *3.25*

Silyl enol ether 3.25. To a stirred solution of known bromo ketone **3.24**[16] (2.01 g, 11.3 mmol, 1.00 equiv) in DMF (10.3 mL, 1.10 M) at 0 ºC was added DABCO (2.93 g, 26.1 mmol, 2.30 equiv) and TESCl (3.1 mL, 18 mmol, 1.6 equiv) sequentially. The reaction mixture was stirred for 45 min before being quenched with deionized H_2O (5 mL). The reaction was then allowed to warm to 23 ºC before being diluted with hexanes (20 mL) and H_2O (20 mL). The layers were separated and the aqueous layer was extracted with hexanes (3 x 25 mL). The combined organic layers were dried over $MgSO_4$, filtered, and concentrated under reduced pressure. The resultant crude oil was purified via flash chromatography (100% hexanes) to afford silyl enol ether **3.25** (1.81 g, 55% yield) as a colorless oil. Silyl enol ether **3.25**: R_f 0.40 (100% hexanes); ^{1}H-NMR (500 MHz, $CDCl_3$): δ 2.48–2.44 (m, 2H), 2.18–2.14 (m, 2H), 1.74–1.67 (m, 2H), 1.67–1.61 (m, 2H), 1.01 (t, J = 7.9, 9H), 0.71 (q, J = 7.9, 6H); ^{13}C{^{1}H}-NMR (100 MHz, $CDCl_3$): δ 146.7, 102.2, 34.4, 31.6, 24.6, 23.2, 6.9, 5.8; IR (film): 2937, 2876, 1666, 1215 cm^{-1}; HRMS–APCI (*m/z*) $[M + H]^+$ calcd for $C_{12}H_{24}BrOSi^+$, 291.0780; found, 291.0780.

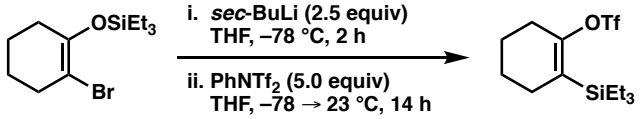

3.25 (97% yield) *3.20b*

Cyclohexyne precursor 3.20b. A solution of silyl enol ether **3.25** (1.01 g, 3.47 mmol, 1.00 equiv) in THF (25 mL, 0.14 M) was cooled to –78 °C and *sec*-BuLi (0.84 M in cyclohexane, 10 mL, 8.7 mmol, 2.5 equiv) was added dropwise over 13 min. After stirring at –78 °C for 2 h, *N*-

Phenyl-bis(trifluoromethanesulfonimide) (6.19 g, 17.3 mmol, 5.00 equiv) as a solution in THF (15 mL, 1.2 M) was added dropwise over 15 min. After stirring at –78 °C for 10 minutes, the reaction mixture was allowed to warm to 23 °C. After stirring at 23 °C for 14 h, the reaction was quenched with sat. aq. $NaHCO_3$ (40 mL). The layers were separated and the aqueous layer was extracted with EtOAc (3 x 40 mL). The combined organic layers were dried over $MgSO_4$, filtered, and concentrated under reduced pressure. The resulting crude oil was purified via flash chromatography (100% hexanes) using silica gel neutralized with triethylamine to afford cyclohexyne precursor **3.20b** (1.15 g, 97% yield) as a light yellow oil. Cyclohexyne precursor **3.20b**: R_f 0.52 (100% hexanes); Spectral data match those previously reported.[15]

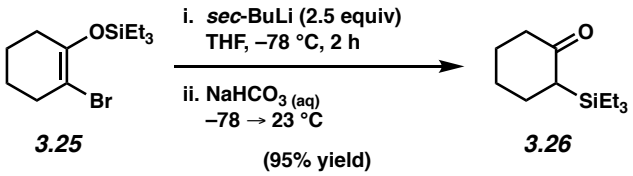

3.25 *3.26*

α-Silyl ketone 3.26. To a solution of silyl enol ether **3.25** (1.00 g, 3.43 mmol, 1.00 equiv) in THF (40 mL, 0.085 M) at –78 °C was added *sec*-BuLi (0.84 M in cyclohexane, 10 mL, 8.6 mmol, 2.5 equiv) dropwise over 13 min. The solution was stirred for 2 h at –78 °C, then the reaction was quenched with sat. aq. $NaHCO_3$ (15 mL) and allowed to warm to 23 °C. The reaction mixture was then diluted with EtOAc (15 mL) and H_2O (15 mL). The layers were then separated and the aqueous layer was extracted with EtOAc (3 x 25 mL). The combined organic layers were then dried over $MgSO_4$, filtered, and concentrated under reduced pressure. The resulting crude oil was purified by flash chromatography (100% hexanes → 9:1 hexanes:EtOAc) to afford silyl ketone **3.26** (691 mg, 95% yield) as a light yellow oil. Silyl ketone **3.26**: R_f 0.39 (9:1 hexanes:EtOAc); spectral data match those previously reported.[15]

3.6 Spectra Relevant to Chapter Three:

Concise Approach to Cyclohexyne and 1,2-Cyclohexadiene Precursors

Jason V. Chari,[†] Francesca M. Ippoliti,[†] and Neil K. Garg.

J. Org. Chem. **2019**, *84*, 3652–3655.

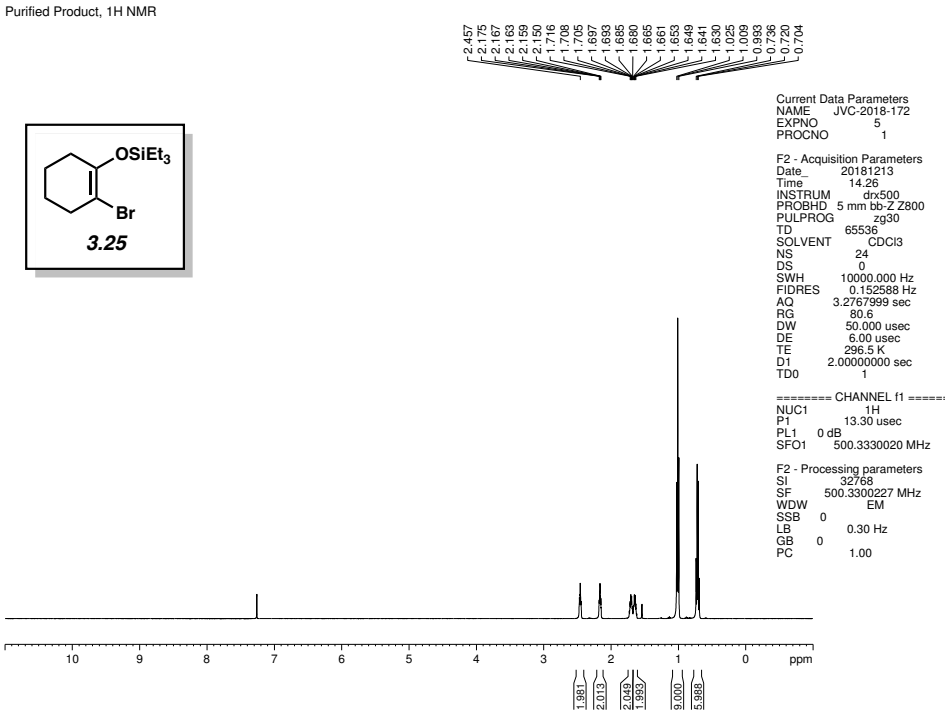

Figure 3.6 ^{1}H NMR (500 MHz, $CDCl_3$) of compound **3.25**.

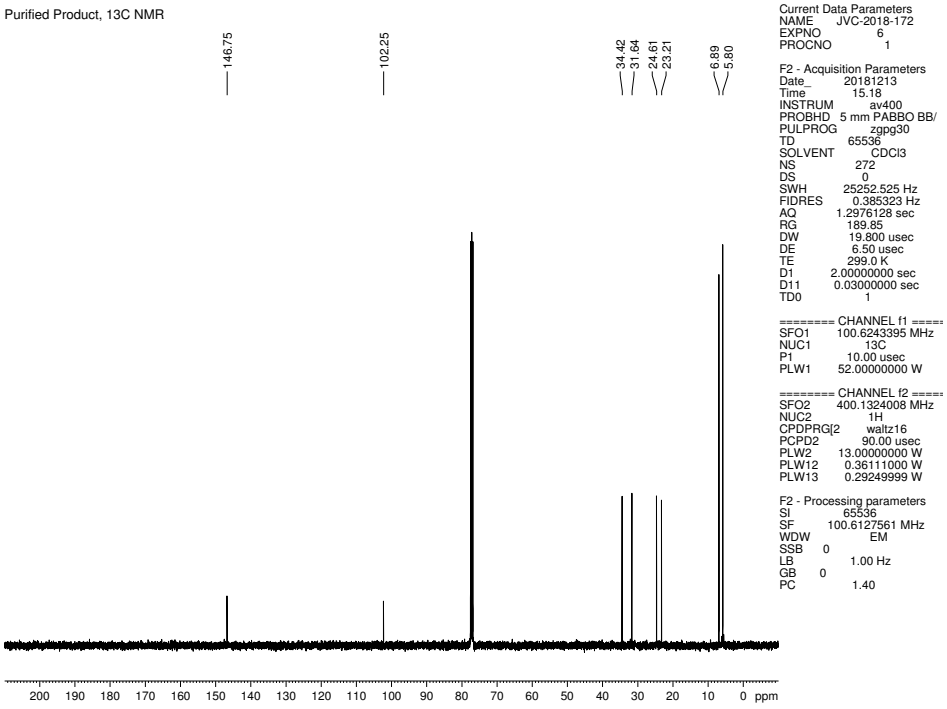

Figure 3.7 ^{13}C NMR (100 MHz, $CDCl_3$) of compound **3.25**.

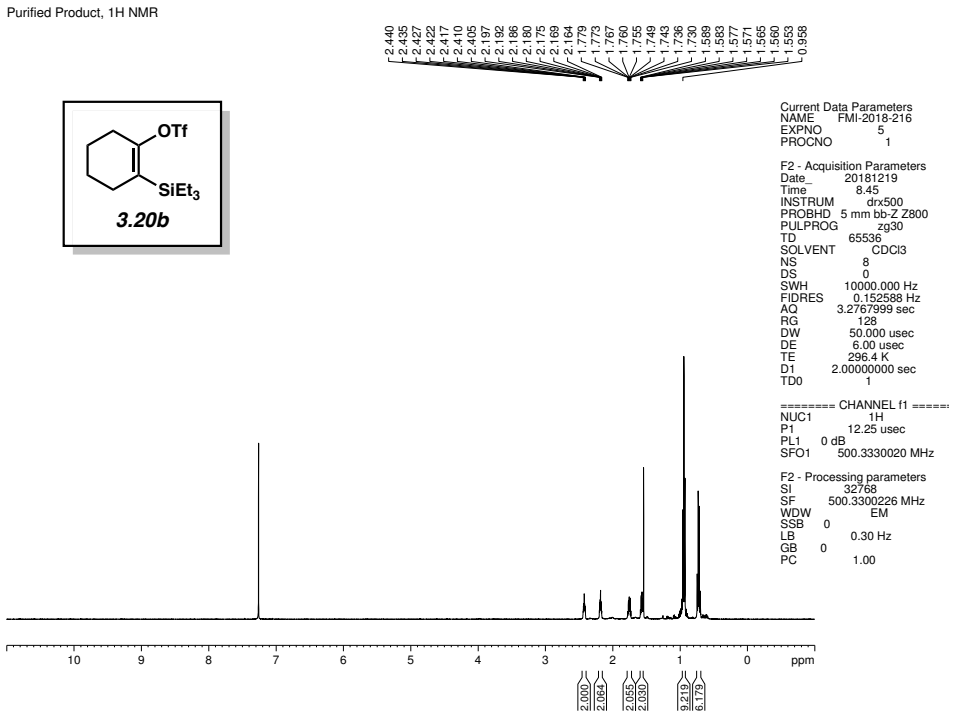

Figure 3.8 ^{1}H NMR (500 MHz, $CDCl_3$) of compound **3.20b**.

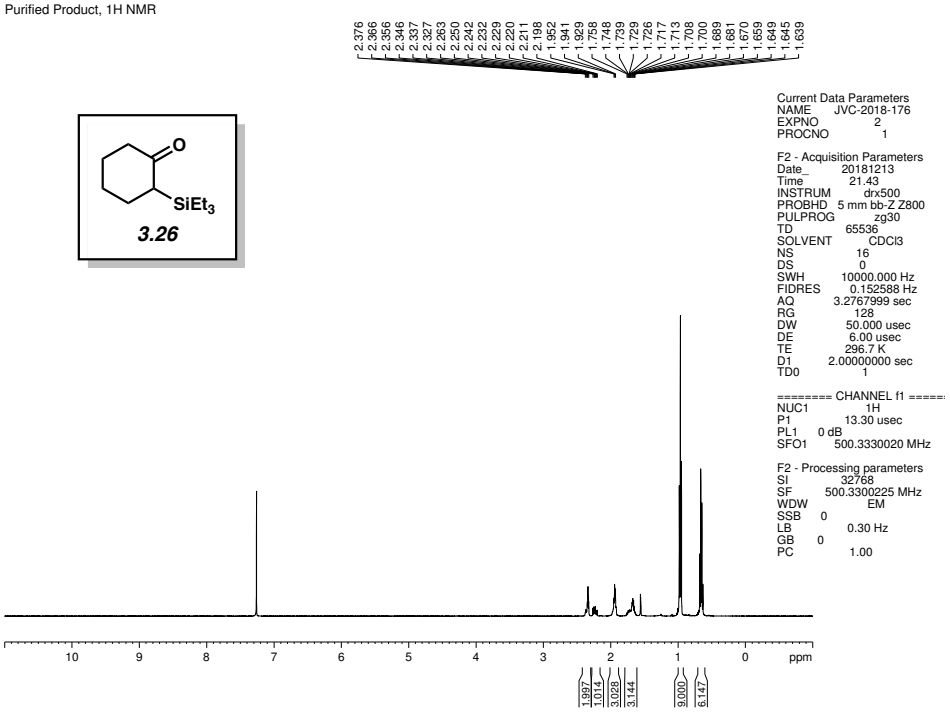

Figure 3.9 ^{1}H NMR (500 MHz, $CDCl_3$) of compound **3.26**.

3.7 Notes and References

(1) For reviews of arynes and related strained intermediates, see: (a) Bronner, S. M.; Goetz, A. E.; Garg, N. K. Understanding and Modulating Indolyne Regioselectivities. *Synlett* **2011**, *18*, 2599–2604. (b) Tadross, P. M.; Stoltz, B. M. A Comprehensive History of Arynes in Natural Product Total Synthesis. *Chem. Rev.* **2012**, *112*, 3550–3577. (c) Gampe, C. M.; Carreira, E. M. Arynes and Cyclohexyne in Natural Product Synthesis. *Angew. Chem., Int. Ed.* **2012**, *51*, 3766–3778. (d) Dubrovskiy, A. V.; Markina, N. A.; Larock, R. C. Use of Benzynes for the Synthesis of Heterocycles. *Org. Biomol. Chem.* **2013**, *11*, 191–218. (e) Hoffman, R. W.; Suzuki, K. A "Hot, Energized" Benzyne. *Angew. Chem., Int. Ed.* **2013**, *52*, 2655–2656. (f) Goetz, A. E.; Garg, N. K. Enabling the Use of Heterocyclic Arynes in Chemical Synthesis. *J. Org. Chem.* **2014**, *79*, 846–851. (g) Yoshida, S.; Hosoya, T. The Renaissance and Bright Future of Synthetic Aryne Chemistry. *Chem. Lett.* **2015**, *44*, 1450–1460. (h) Takikawa, H.; Nishii, A.; Sakai, T.; Suzuki, K. Aryne-Based Strategy in the Total Synthesis of Naturally Occurring Polycyclic Compounds. *Chem. Soc. Rev.* **2018**, *47*, 8030–8056. (i) Dhokale, R. A.; Mhaske, S. B. Transition-Metal-Catalyzed Reactions Involving Arynes. *Synthesis* **2018**, *50*, 1–16.

(2) (a) Roberts, J. D.; Simmons, H. E.; Carlsmith, L. A.; Vaughn, C. W. Rearrangement in the Reaction of Chlorobenzene-1-C^{14} with Potassium Amide. *J. Am. Chem. Soc.* **1953**, *75*, 3290–3291. (b) Scardiglia, F.; Roberts, J. D. Evidence for Cyclohexyne as an Intermediate in the Coupling of Phenyllithium with 1-Chlorocyclohexene. *Tetrahedron* **1957**, *1*, 343–344. (c) Wittig, G.; Fritze, P. On the Intermediate Occurrence of 1,2-

Cyclohexadiene. *Angew. Chem., Int. Ed.* **1966**, *5*, 846. (d) Wenk, H. H.; Winkler, M.; Sander, W. One Century of Aryne Chemistry. *Angew. Chem., Int. Ed.* **2003**, *42*, 502–528.

(3) (a) Surry, D. S.; Buchwald, S. L. Biaryl Phosphane Ligands in Palladium-Catalyzed Amination. *Angew. Chem., Int. Ed.* **2008**, *47*, 6338–6361. (b) Mauger, C. C.; Mignani, G. A. An Efficient and Safe Procedure for the Large-Scale Pd-Catalyzed Hydrazonation of Aromatic Chlorides Using Buchwald Technology. *Org. Proc. Res. Dev.* **2004**, *8*, 1065–1071.

(4) Schleth, F.; Vettiger, T.; Rommel, M.; Tobler, H. "Process for the Preparation of Pyrazole Carboxylic Acid Amides" WO2011131544 A1, Oct 27, 2011.

(5) (a) Carroll, F. I.; Robinson, T. P.; Brieaddy, L. E.; Atkinson, R. N.; Mascarella, S. W.; Damaj, M. I.; Martin, B. R.; Navarrio, H. A. Synthesis and Nicotinic Acetylcholine Receptor Binding Properties of Bridged and Fused Ring Analogues of Epibatidine. *J. Med. Chem.* **2007**, *50*, 6383–6391. (b) Kamitani, T.; Kigasawa, K.; Hiragi, M.; Wagatsuma, N.; Uryu, T.; Araki, K. Syntheses of Heterocyclic Compounds. 509. Syntheses of Analgesics. 34. Synthesis of 3-Hydroxy-*N*-Cyclopropylmethyl-9-Azamorphinan. *J. Med. Chem.* **1973**, *16*, 301–303. (c) Heindel, N. D.; Fives, W. P.; Lemke, T. F.; Rowe, J. E.; Snady, H. W. Synthesis, Transformation, and General Pharmacologic Activity in 1,4-Benzodiazepine-3,5-diones. *J. Med. Chem.* **1971**, *14*, 1233–1235. (d) Bell, M. R.; Zalay, A. W.; Oesterlin, R.; Schane, P.; Potts, G. Basic Ethers of 1-(*p*-Hydroxyphenyl)-2-Phenyl-1,2,3,4-Tetrahydroquinoline and 1-(*p*-Hydroxyphenyl)-2-Phenyl Indole. Antifertility Agents. *J. Med. Chem.* **1970**, *13*, 664–668. (e) Willis, P. G.; Pavlova, O. A.; Chefer, S. I.; Vaupel, D. B.; Mukhin, A. G.; Horti,

A. G. Synthesis and Structure-Activity Relationship of a Novel Series of Aminoalkylindoles with Potential of Imaging the Neuronal Cannabinoid Receptor by Positron Emission Tomography. *J. Med. Chem.* **2005**, *48*, 5813–5822. (f) Jacob, III, P. Sulfur Analogues of Psychotomimetic Agents. Monothio Analogues of Mescaline and Isomescaline. *J. Med. Chem.* **1981**, *24*, 1348–1353. (g) Coe, J. W.; Brooks, P. R.; Wirtz, M. C.; Bashore, C. G.; Bianco, K. E.; Vetelino, M. G.; Arnold E. P.; Lebel, L. A.; Fox, C. B.; Tingley, III, F. D.; Schulz, D. W.; Davis, T. I.; Sands, S. B.; Mansbach, R. S; Rollema, H.; O'Neill, B. T. 3,5-Bicyclic Aryl Piperidines: A Novel Class of α4β2 Neuronal Nicotinic Receptor Partial Agonists for Smoking Cessation. *Bioorg. Med. Chem. Lett.* **2005**, *15*, 4889–4897.

(6) For examples of arynes and other strained cyclic alkynes in total synthesis, see: (a) Kou, K. G. M.; Pflueger, J. J.; Kiho, T.; Morrill, L. C.; Fisher, E. L.; Clagg, K.; Lebold, T. P.; Kisunzu, J. K.; Sarpong, R. A Benzyne Insertion Approach to Hetisine-Type Diterpenoid Alkaloids: Synthesis of Cossonidine (Davisine). *J. Am. Chem. Soc.* **2018**, *140*, 8105–8109. (b) Goetz, A. E.; Silberstein, A. L.; Corsello, M. A.; Garg, N. K. Concise Enantiospecific Total Synthesis of Tubingensin A. *J. Am. Chem. Soc.* **2014**, *136*, 3036–3039. (c) Neog, K.; Borah, A.; Gogoi, P. Palladium(II)-Catalyzed C–H Bond Activation/C–C and C–O Bond Formation Reaction Cascade: Direct Synthesis of Coumestans. *J. Org. Chem.* **2016**, *81*, 11971–11977. (d) Neumeyer, M.; Kopp, J.; Brückner, R. Controlling the Substitution Pattern of Hexasubstituted Naphthalenes by Aryne/Siloxyfuran Diels–Alder Additions: Regio and Stereocontrolled Synthesis of Arizonin C1 Analogs. *Eur. J. Org. Chem.* **2017**, 2883–2915. (e) Corsello, M. A.; Kim, J.;

Garg, N. K. Total Synthesis of (–)-Tubingensin B Enabled by the Strategic Use of an Aryne Cyclization. *Nat. Chem.* **2017**, *9*, 944–949. (f) Gampe, C. M.; Carreira, E. M. Total Syntheses of Guanacastepenes N and O. *Angew. Chem., Int. Ed.* **2011**, *50*, 2962–2965.

(7) Lin, J. B.; Shah, T. J.; Goetz, A. E.; Garg, N. K.; Houk, K. N. Conjugated Trimeric Scaffolds Accessible from Indolyne Cyclotrimerizations: Synthesis, Structure, and Electronic Properties. *J. Am. Chem. Soc.* **2017**, *139*, 10447–10455.

(8) Fine Nathel, N. F.; Morrill, L. A.; Mayr, H.; Garg, N. K. Quantification of the Electrophilicity of Benzyne and Related Intermediates. *J. Am. Chem. Soc.* **2016**, *138*, 10402–10405.

(9) (a) Atanes, N.; Escudero, S.; Pérez, D.; Guitián, E.; Castedo, L. Generation of Cyclohexyne and its Diels–Alder Reaction with α-Pyrones. *Tetrahedron Lett.* **1998**, *39*, 3039–3040. (b) Quintana, I.; Peña, D.; Pérez, D.; Guitián, E. Generation and Reactivity of 1,2-Cyclohexadiene under Mild Reaction Conditions. *Eur. J. Org. Chem*. **2009**, 5519–5524. (c) Medina, J. M.; McMahon, T. C.; Jiménez-Osés, G.; Houk, K. N.; Garg, N. K. Cycloadditions of Cyclohexynes and Cyclopentyne. *J. Am. Chem. Soc.* **2014**, *136*, 14706–14709. (d) Barber, J. S.; Styduhar, E. D.; Pham, H. V.; McMahon, T. C.; Houk, K. N.; Garg, N. K. Nitrone Cycloadditions of 1,2-Cyclohexadiene. *J. Am. Chem. Soc.* **2016***, 138*, 2512–2515. (e) Lofstrand, V. A.; West, F. G. Efficient Trapping of 1,2-Cyclohexadienes with 1,3-Dipoles. *Chem. Eur. J.* **2016***, 22*, 10763–10767.

(10) (a) McMahon, T. C.; Medina, J. M.; Yang, Y.-F.; Simmons, B. J.; Houk, K. N.; Garg, N. K. Generation and Regioselective Trapping of a 3,4-Piperidyne for the Synthesis of Functionalized Heterocycles. *J. Am. Chem. Soc.* **2015**, *137*, 4082–4085. (b) Tlais, S. F.;

Danheiser, R. L. *N*-Tosyl-3-Azacyclohexyne. Synthesis and Chemistry of a Strained Cyclic Ynamide. *J. Am. Chem. Soc.* **2014**, *136*, 15489–15492. (c) Christl, M.; Braun, M.; Wolz, E.; Wagner, W. 1-Phenyl-l-aza-3,4-cyclohexadien, das erste Isodihydropyridin: Erzeugung und Abfangreaktionen. *Chem. Ber.* **1994**, *127*, 1137–1142. (d) Shah, T. K.; Medina, J. M.; Garg, N. K. Expanding the Strained Alkyne Toolbox: Generation and Utility of Oxygen-Containing Strained Alkynes. *J. Am. Chem. Soc.* **2016**, *138*, 4948–4954. (e) Barber, J. S.; Yamano, M. M.; Ramirez, M.; Darzi, E. R.; Knapp, R. R.; Liu, F.; Houk, K. N.; Garg, N. K. Diels–Alder Cycloadditions of Strained Azacyclic Allenes. *Nat. Chem.* **2018**, *10*, 953–960. (f) Johnson, R. P. Strained Cyclic Cumulenes. *Chem. Rev.* **1989**, *89*, 1111–1124. (g) Nendel, M.; Tolbert, L. M.; Herring, L. E.; Islam, M. N.; Houk, K. N. Strained Allenes as Dienophiles in the Diels–Alder Reaction: An Experimental and Computational Study. *J. Org. Chem.* **1999**, *64*, 976–983.

(11) (a) Bronner, S. M.; Goetz, A. E.; Garg, N. K. Understanding and Modulating Indolyne Regioselectivities. *Synlett* **2011**, 2599−2604. (b) Medina, J. M.; Mackey, J. L.; Garg, N. K.; Houk, K. N. The Role of Aryne Distortions, Steric Effects, and Charges in Regioselectivities of Aryne Reactions. *J. Am. Chem. Soc.* **2014**, *136*, 15798–15805. (c) Cheong, P. H.-Y.; Paton, R. S.; Bronner, S. M.; Im, G.-Y. J.; Garg, N. K.; Houk, K. N. Indolyne and Aryne Distortions and Nucleophilic Regioselectivities. *J. Am. Chem. Soc.* **2010**, *132*, 1267–1269.

(12) Moore, W. R.; Moser, W. R. The Reaction of 6,6-Dibromobicyclo[3.1.0]hexane with Methyllithium. Efficient Trapping of 1,2-Cyclohexadiene by Styrene. *J. Org. Chem.* **1970**, *35*, 908–912.

(13) Christl, M.; Fischer, H.; Arnone, M.; Engels, B. 1-Phenyl-1,2-cyclohexadiene: Astoundingly High Enantioselectivities on Generation in a Doering–Moore–Skattebøl Reaction and Interception by Activated Olefins. *Chem. Eur. J.* **2009**, *15*, 11266–11272.

(14) Himeshima, Y.; Sonoda, T.; Kobayashi, H. Fluoride-induced 1,2-Elimination of *o*-Trimethylsilylphenyl Triflate to Benzyne Under Mild Conditions. *Chem. Lett.* **1983**, *12*, 1211–1214.

(15) Inoue, K.; Nakura, R.; Okano, K.; Mori, A. One-Pot Synthesis of Silylated Enol Triflates from Silyl Enol Ethers for Cyclohexynes and 1,2-Cyclohexadienes. *Eur. J. Org. Chem.* **2018**, 3343–3347.

(16) Zhang, G.-B.; Wang, F.-X.; Du, J.-Y.; Qu, H.; Ma, X.-Y.; Wei, M.-X.; Wang, C.-T.; Li, Q.; Fan, C.-A. Toward the Total Synthesis of Palhinine A: Expedient Assembly of Multifunctionalized Isotwistane Ring System with Contiguous Quaternary Stereocenters. *Org. Lett.* **2012**, *14*, 3696–3699.

(17) Peña, D.; Cobas, A.; Pérez, D.; Guitián, E. An Efficient Procedure for the Synthesis of *ortho*-Trialkylsilylaryl Triflates: Easy Access to Precursors of Functionalized Arynes. *Synthesis* **2002**, *2002*, 1454–1458.

CHAPTER FOUR

A Platform for On-the-Complex Annulation Reactions with Transient Aryne Intermediates

Jason V. Chari,† Katie A. Spence,† Robert B. Susick, and Neil K. Garg.

Nat. Commun. **2021**, *12*, 3706.

4.1 Abstract

Organometallic complexes are ubiquitous in chemistry and biology. Whereas their preparation has historically relied on ligand synthesis followed by coordination to metal centers, the ability to efficiently diversify their structures remains a synthetic challenge. A promising yet underdeveloped strategy involves the direct manipulation of ligands that are already bound to a metal center, also known as chemistry-on-the-complex. Herein, we introduce a versatile platform for on-the-complex annulation reactions using transient aryne intermediates. In one variant, organometallic complexes undergo transition metal-catalyzed annulations with in situ generated arynes to form up to six new carbon–carbon bonds. In the other variant, an organometallic complex bearing a free aryne is generated and intercepted in cycloaddition reactions to access unique scaffolds. Our studies, centered around privileged polypyridyl metal complexes, provide an effective strategy to annulate organometallic complexes and access complex metal–ligand scaffolds, while furthering the synthetic utility of strained intermediates in chemical synthesis.

4.2 Introduction

Organometallic complexes are prevalent in chemistry and biology, with applications ranging from usage as highly selective catalysts[1] to therapeutics[2] and enzyme cofactors.[3] Key to

this versatility is the ability to tune function through manipulation of ligand structure. Fine tuning of the ligand sphere can lead to profound changes in the properties of an organometallic complex, including stereoelectronic and photophysical properties, catalyst turnover rate and stability.[4] Thus, the continued growth of organometallic chemistry is contingent on the capacity to access metal–ligand architectures with increased structural diversity and complexity.

Conventional synthetic approaches toward organometallic complexes involve reliance on ligand synthesis followed by coordination to a metal center (Figure 4.1a). This general approach remains modular and adaptable, accounting for the syntheses of the majority of known metal–ligand complexes. Nonetheless, this general strategy can have drawbacks in the syntheses of notable ligand classes. For example, the synthesis of strongly chelating ligands can be challenging due to their propensity to form stable metal–ligand chelates and, in turn, prevent the use of metal-mediated transformations such as cross-couplings, C–H functionalization, and annulation reactions.[5] In addition, highly rigid ligand systems can also have poor solubility in organic solvents, thus complicating their syntheses and subsequent coordination to metal centers.[6,7] Finally, ligand synthesis may require long, linear reaction sequences, which can render the process of synthesizing large libraries of organometallic derivatives cumbersome or impractical.

Divergent synthetic routes to organometallic complexes, analogous to those which have proven valuable in medicinal chemistry, are important for generating structurally diverse libraries of compounds. Toward this end, a nascent synthetic approach that complements traditional coordination chemistry is chemistry-on-the-complex,[8] whereby ligands are modified after being bound to a metal center. This strategy provides an attractive means for rapid

structural diversification of metal–ligand complexes and can serve to circumvent the aforementioned challenges often encountered in ligand synthesis.

Chemistry-on-the-complex has proven effective in the synthesis of heterodimetallic complexes,[9] with applications in artificial photosynthesis,[10] along with the synthesis and elaboration of ferrocenyl[11,12] and porphyrin[13] structures. These studies demonstrate the value of on-the-complex approaches in diversity-oriented synthesis, but also expose the need for further reaction development in this area. One illustrative example of chemistry-on-the-complex is highlighted in Figure 4.1b, where Davies and co-workers strategically utilized Suzuki–Miyaura cross-coupling reactions of pre-coordinated dimeric rhodium complexes toward the discovery of catalysts **4.1** used for the functionalization of unactivated C–H bonds.[14] This case demonstrates the value of the general design, but also highlights that chemistry-on-the-complex is most often used to introduce one bond relative to a given functional group. Methods that allow for the formation of more than one bond using chemistry-on-the-complex remain more limited. Examples include azide cycloadditions (click chemistry) and well-established condensation reactions, resulting in products such as **4.2**[15] and **4.3**[16], respectively.

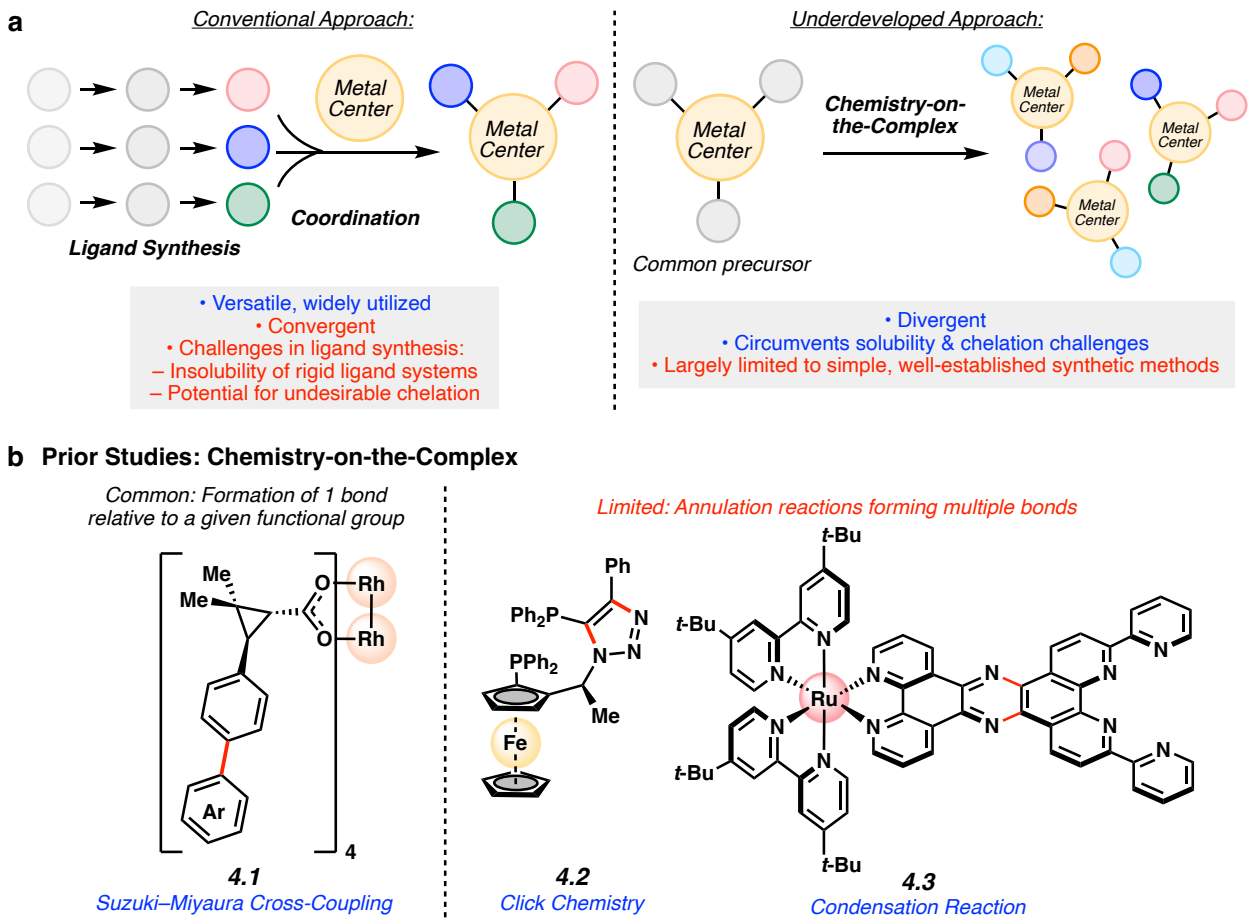

Figure 4.1. General synthetic approaches toward metal–ligand complexes. (a) Comparison of coordination chemistry and chemistry-on-the-complex. (b) Prior studies involving chemistry-on-the-complex. Me, methyl; Ph, phenyl; *t*-Bu, *tert*-butyl.

In considering the strategic generation of new ring systems on-the-complex, transient aryne intermediates provide a compelling entryway (Figure 4.2). Although arynes and related species were once avoided due to their high reactivity, they have recently gained popularity in a number of applications as useful synthons for building molecular complexity.[17,18,19,20,21,22,23,24,25,26] For example, strained cyclic intermediates such as **4.4**–**4.7** (Figure 4.2a) have been used to access heterocycles of value to medicinal chemistry,[27] widely used phosphine ligands,[28,29] agrochemicals,[30] and natural products,[31] Nonetheless, the usage of

transient aryne intermediates in chemistry-on-the-complex approaches has remained limited, with only two reports in the literature to date.[32,33] Both examples demonstrate the feasibility of aryne Diels–Alder trappings, but require that the organometallic complex bear a reactive diene ligand.

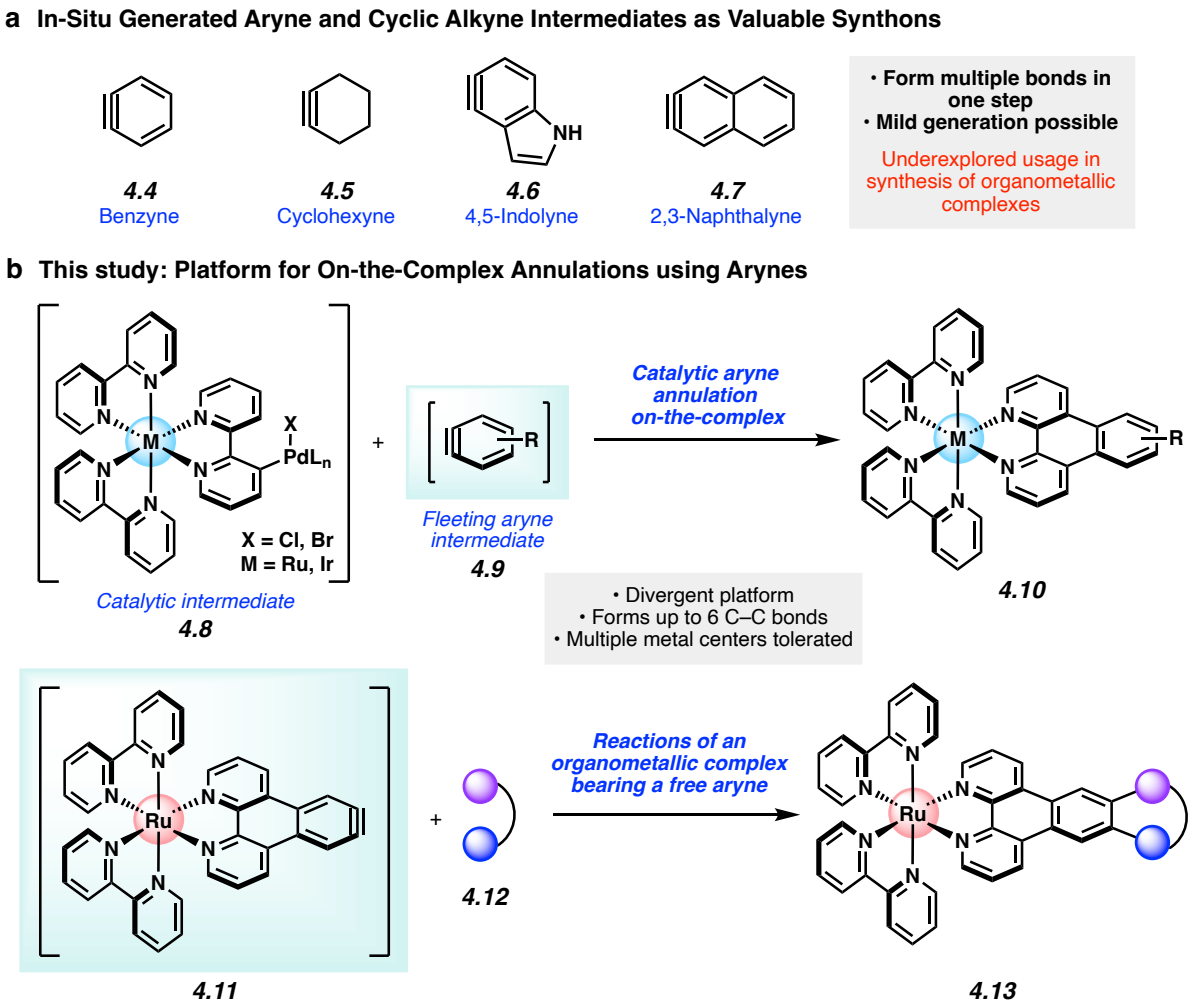

Figure 4.2. Arynes-on-the-complex approach to metal complexes. (a) Aryne and cyclic alkyne intermediates. (b) Our approach to the direct manipulation of polypyridyl metal complexes using arynes.

Herein, we show that intercepting arynes on-the-complex provides a versatile platform for the strategic manipulation of organometallic compounds. We evaluate this approach in the context of photoactive polypyridyl metal complexes, whose applications span various chemical, biological, and therapeutic disciplines[34,35,36,37,38,39,40,41,42,43] (Figure 4.2b). We disclose two variants. In the first, readily available aryl halides are embedded in the ligand framework and enable palladium-catalyzed annulations with in situ generated arynes. This proceeds via the reaction of catalytically-generated bis(metallic) species **4.8** and fleeting aryne intermediates **4.9** to give annulated products **4.10**. In the other variant, compound **4.11**, a unique organometallic complex that bears an unligated aryne, is generated transiently. In situ trapping with cycloaddition partners **4.12** gives cycloadducts **4.13**. Our approaches enable the formation of multiple carbon–carbon (C–C) bonds in a single operation, offer a means to access functionalized polypyridyl metal complexes, underscore the utility of traditionally avoided aryne intermediates, and validate the aryne on-the-complex approach for accessing a diverse range of organometallic compounds.

4.3 Development of the Pd-Catalyzed On-the-Complex Aryne Reaction

To initiate our studies, we sought to identify a versatile functional group handle for aryne on-the-complex manipulations. We settled on the use of aryl halides, given their ready availability and their prevalence in transition metal-catalyzed reactions, and prepared halogenated $Ru(bpy)_3$ derivatives **4.14** (Figure 4.3 and see Section 4.8.2.1). Although many impressive examples of Pd-catalyzed transformations of arynes have now been reported[44,45,46,47,48,49,50,51] use of this chemistry in the manipulation of organometallic complexes has remained unexplored. Inspired by Larock's impressive annulation of biaryl halides,[52,53] we

sought to perform a Pd-catalyzed annulation of **4.14** with commercially available benzyne precursor **4.15**. Initial attempts involved the use of $Pd(dba)_2$ and P(*o*-tolyl)$_3$, in the presence of CsF, but were met with limited success, as we observed formation of the desired π-extended adduct **4.16**, albeit in only 2% yield (entry 1). Instead, undesired protodehalogenation product, $Ru(bpy)_3$ (**4.17**), was observed in 48% yield. Efforts to prevent this dehalogenation pathway via reduced temperatures and rigorous exclusion of air and moisture proved unfruitful,[54] as did the use of other Pd^0 sources such as $Pd(PPh_3)_4$ (e.g., entry 2). Alternatively, the use of $Pd(OAc)_2$ led to an improved 26% yield of the desired π-extended adduct **4.16** (entry 3). By increasing the catalyst and ligand loadings to 10 mol%, we observed a further increase in yield of **4.16** to 71%, with a reaction time of just 30 minutes (entry 4). Employing modified ratios of the co-solvents, acetonitrile and toluene, resulted in decreased reaction efficiency (entries 5 and 6).[55] Finally, shifting from brominated substrate **4.14a** to chlorinated derivative **4.14b** effectively shut down the dehalogenation pathway and provided the desired product in 78% yield (entry 7). We surmise that the conversion of **4.14** + **4.15** to **4.16** proceeds via initial oxidative addition and aryne formation occurring concomitantly (see Fig 4.2b, **4.8** and **4.9**), followed by aryne insertion, palladation, and reductive elimination.[56] It is worth noting that attempts to perform the analogous annulation on uncoordinated bromo- or chlorobipyridine ligands proved unproductive, potentially owing to *N*,*N*-chelation of palladium (see Section 4.8.2.2), thus highlighting an aforementioned benefit of on-the-complex chemistry.

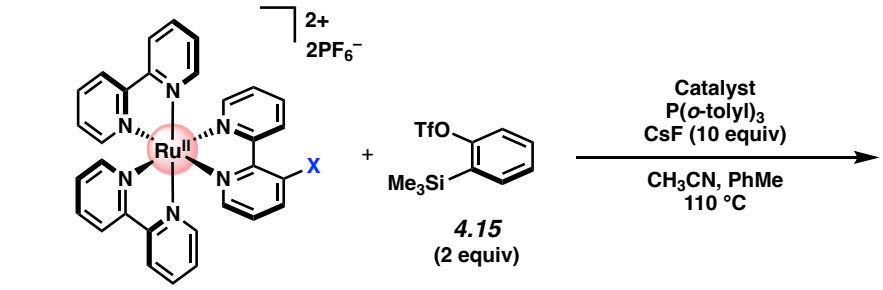

4.14
(*4.14a*: X = Br, *4.14b*: X = Cl)

4.15
(2 equiv)

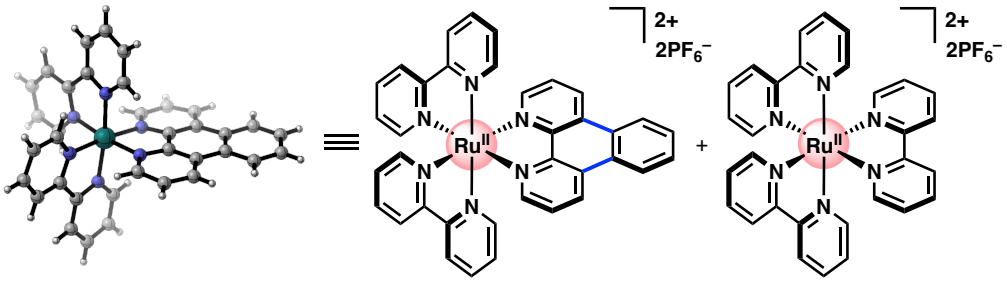

[X-ray][a]

4.16

4.17

Entry	*Catalyst*	*X*	*Catalyst Loading*	*Ligand Loading*	*CH_3CN : PhMe*	*Time*	*Yield of **4.16***[b]	*Yield of **4.17***[b]
1	$Pd(dba)_2$	Br	5 mol%	5 mol%	1 : 1	2 h	2%	48%
2	$Pd(PPh_3)_4$	Br	5 mol%	5 mol%	1 : 1	2 h	2%	48%
3	$Pd(OAc)_2$	Br	5 mol%	5 mol%	1 : 1	2 h	26%	24%
4	$Pd(OAc)_2$	Br	10 mol%	10 mol%	1 : 1	30 min	71%	16%
5	$Pd(OAc)_2$	Br	10 mol%	10 mol%	3 : 1	30 min	61%	19%
6	$Pd(OAc)_2$	Br	10 mol%	10 mol%	1 : 3	30 min	35%	28%
7	$Pd(OAc)_2$	Cl	10 mol%	10 mol%	1 : 1	30 min	78%	0%

Figure 4.3. Optimization studies for Pd-catalyzed annulation of benzyne onto Ru-polypyridyl complex **4.14**. [a] PF_6 counterions have been removed from the X-ray crystal structure for clarity. [b] Yields were determined by ^1H NMR analysis, using 1,3,5-trimethoxybenzene as an external standard. OTf, trifluoromethanesulfonate.

4.4 Scope of the Pd-Catalyzed Annulation

Variation of either the aryne or organometallic component was tolerated in the annulation, thus giving rise to a range of polypyridyl metal complexes in synthetically useful yields. With regard to the aryne component (Figure 4.4), benzyne adduct **4.16** was isolated in 81% yield (X = Cl) or 69% yield (X = Br) using standard column chromatography. Notably, the only available protocol to access the diazatriphenylene ligand found in **4.16** involves the use of hazardous reagents and exceptionally forcing conditions.[57] *N*-Me-4,5-indolyne could also be employed to deliver adduct **4.21** in 80% yield (X = Cl) or 75% yield (X = Br), thus demonstrating the expedient incorporation of a heterocycle into the π-framework of the metal complex. Naphthalynes were also deemed competent reaction partners, as judged by the formation of **4.22** and **4.23**. Prior routes to synthesize the naphthophenanthroline ligand present in **4.22** are lengthy or low yielding,[58] in part due to poor solubility of the free ligand.[6]

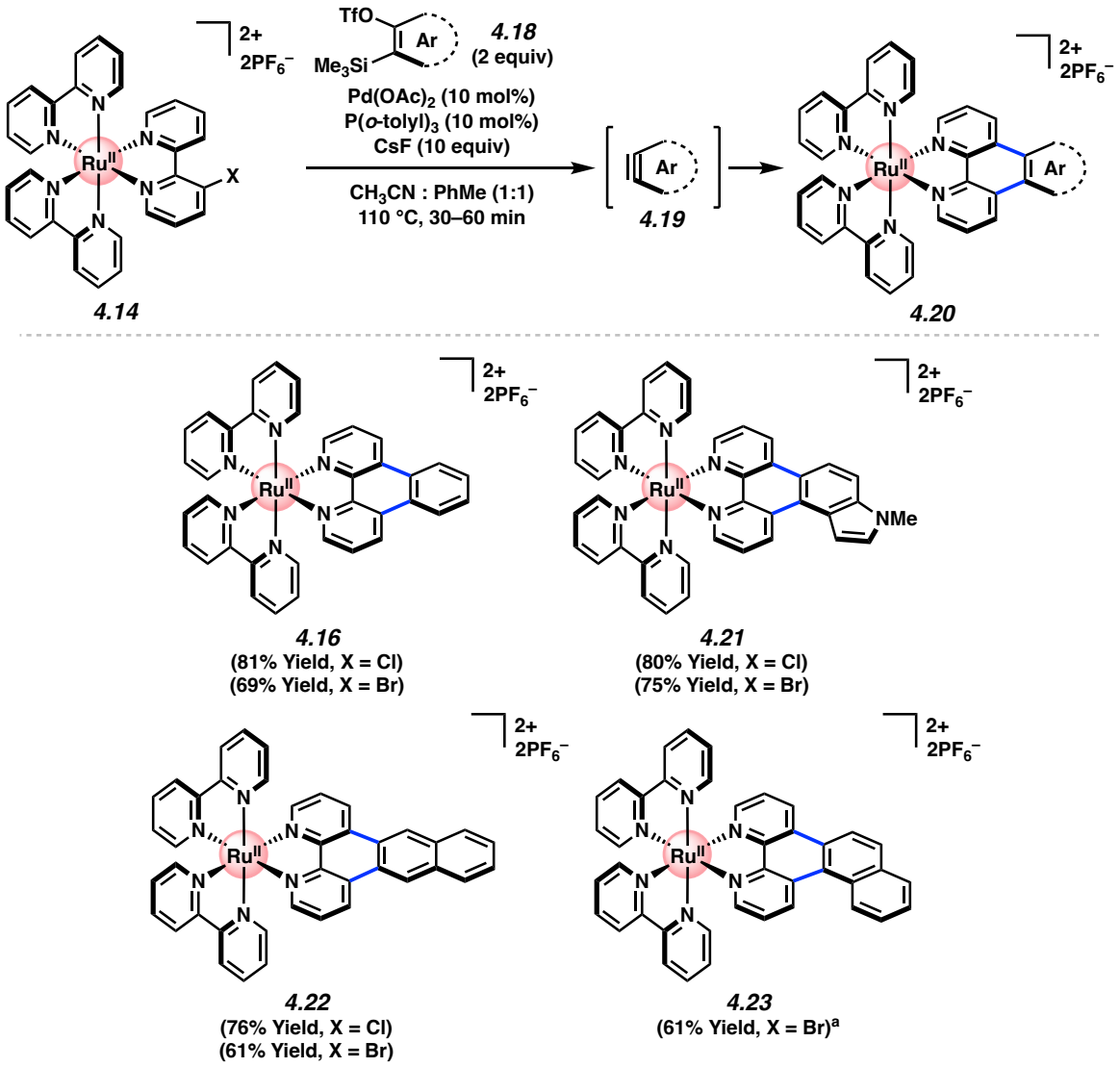

Figure 4.4. Aryne scope of the Pd-catalyzed aryne annulation. Yields shown reflect the average of two isolation experiments. [a] Significant decomposition was observed when X = Cl. Me, methyl; OTf, trifluoromethanesulfonate.

Although we primarily focused the current study on Ru complexes, we opted to probe the methodology in the context of Ir-centered polypyridyl complexes as well. Ir-centered polypyridyl complexes are prevalent in photochemistry,[59,60,61,62] with documented value of extended π-conjugation in structure–property relationship studies.[63] We were gratified to find that the

methodology could be used to access several $Ir(ppy)_2bpy$ derivatives, as delineated in Figure 4.5. Via the intermediacy of benzyne and 2,3-naphthalyne, **4.26** and **4.27** could be accessed in 75% and 71% yield, respectively. Excellent yields were also observed upon varying the phenylpyridine ligands of the substrate, as isoquinolinyl annulation product **4.28** and tetrafluorinated adduct **4.29** could each be obtained in high yields from the corresponding chloride substrates.

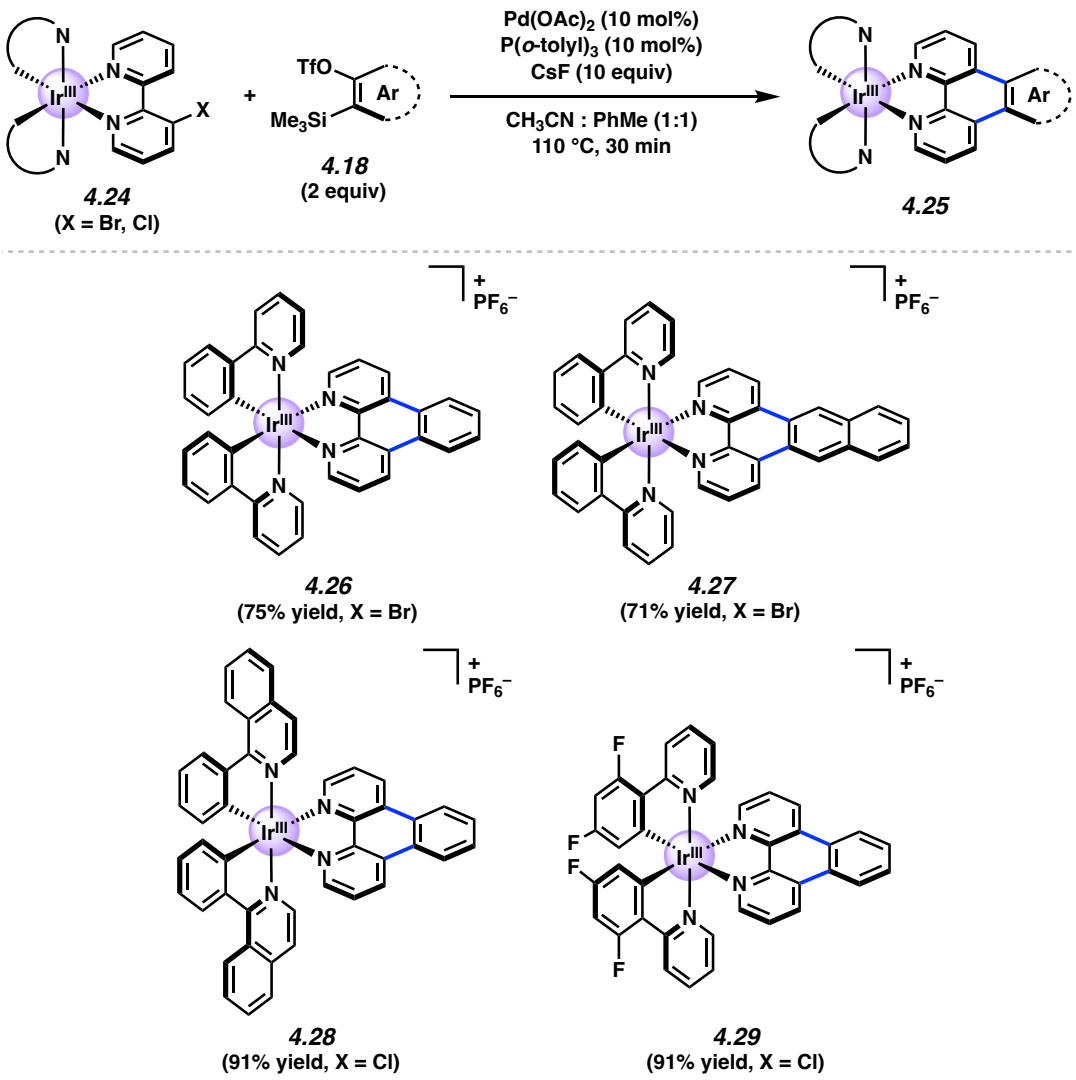

Figure 4.5. Pd-catalyzed aryne annulation of Ir-centered polypyridyl metal complexes. Yields shown reflect the average of two isolation experiments. OTf, trifluoromethanesulfonate.

To assess the possibility of carrying out multiple annulations on a given organometallic complex and test the limits of our aryne on-the-complex chemistry, we prepared Ru complexes **4.30** and **4.32**, bearing two or three chlorides, respectively (Figure 4.6). Subjecting these complexes independently to slightly modified reaction conditions delivered double and triple

annulation products **4.31** and **4.33**, via the efficient formation of four or six new C–C bonds, respectively. Half of the bonds formed in either process arise from arene C–H functionalization.

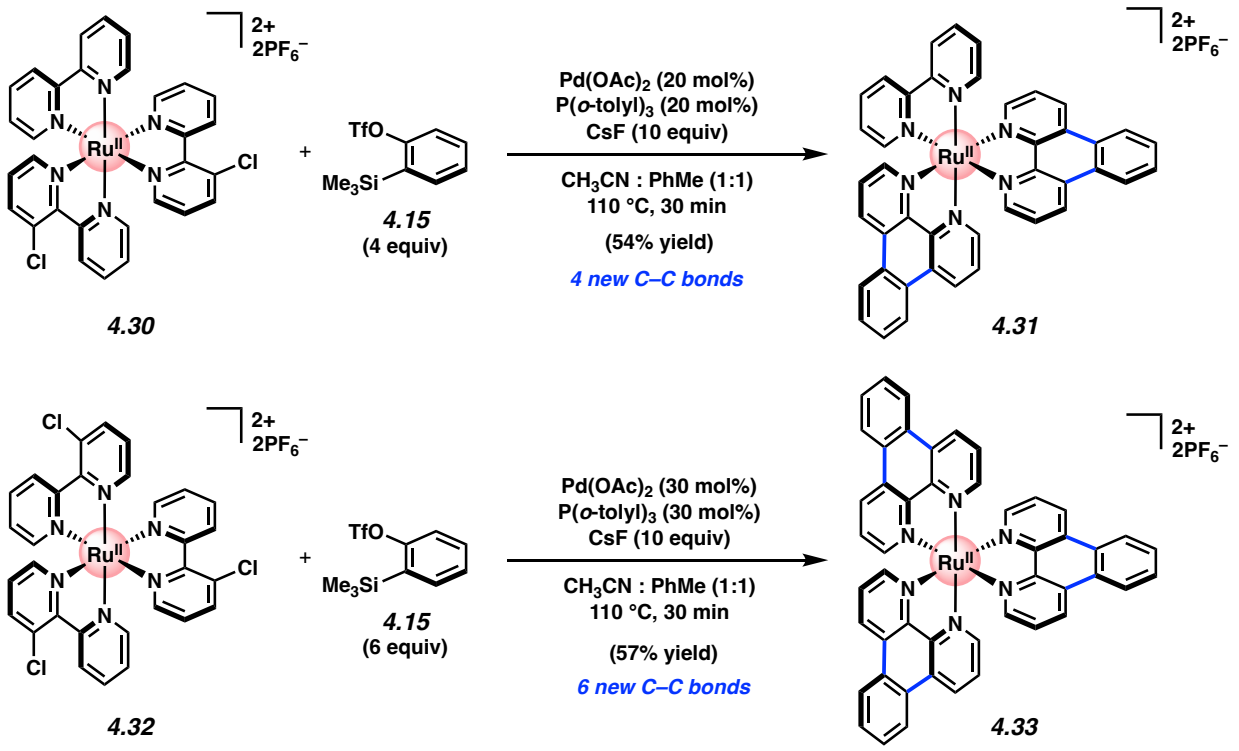

Figure 4.6. Pd-catalyzed aryne annulation at multiple sites of Ru complexes. Yields shown reflect the average of two isolation experiments. OTf, trifluoromethanesulfonate.

4.5 Generation and Trapping of an Organometallic Aryne

With an aryne-driven method for the annulation of organometallic complexes in hand, we sought to exploit this methodology to further extend the utility of aryne chemistry in accessing organometallic complexes. In particular, we sought to generate a free aryne on the organometallic complex itself and trap it in cycloaddition reactions. In contrast to arynes coordinated directly to metal centers (e.g., Zr, Ti),[64] which are well-studied, free arynes embedded in an organometallic framework have remained elusive. Notably, previous efforts

toward organometallic species bearing a free aryne have been met with difficulty,[65] and we therefore viewed the development of strategies in this area as an opportunity for advances in both aryne chemistry and chemistry on-the-complex. As shown in Figure 4.7, we targeted silyl triflate **4.35** as the suitable aryne precursor. Unfortunately, initial efforts to access **4.35** via the annulation of Ru-complex **4.14b** with bis(silyl triflate) **4.34**[66] proved unsuccessful. As a workaround, we employed methoxymethyl (MOM) ether **4.36**, prepared in two steps from commercially available materials, in the annulation reaction. After careful tuning of reaction conditions, adduct **4.37** could be generated in 80% yield with retention of both the MOM ether and trimethylsilyl group.[67] Subsequent cleavage of the MOM group, followed by triflation, delivered the desired silyl triflate **4.35** in 73% yield over two steps.

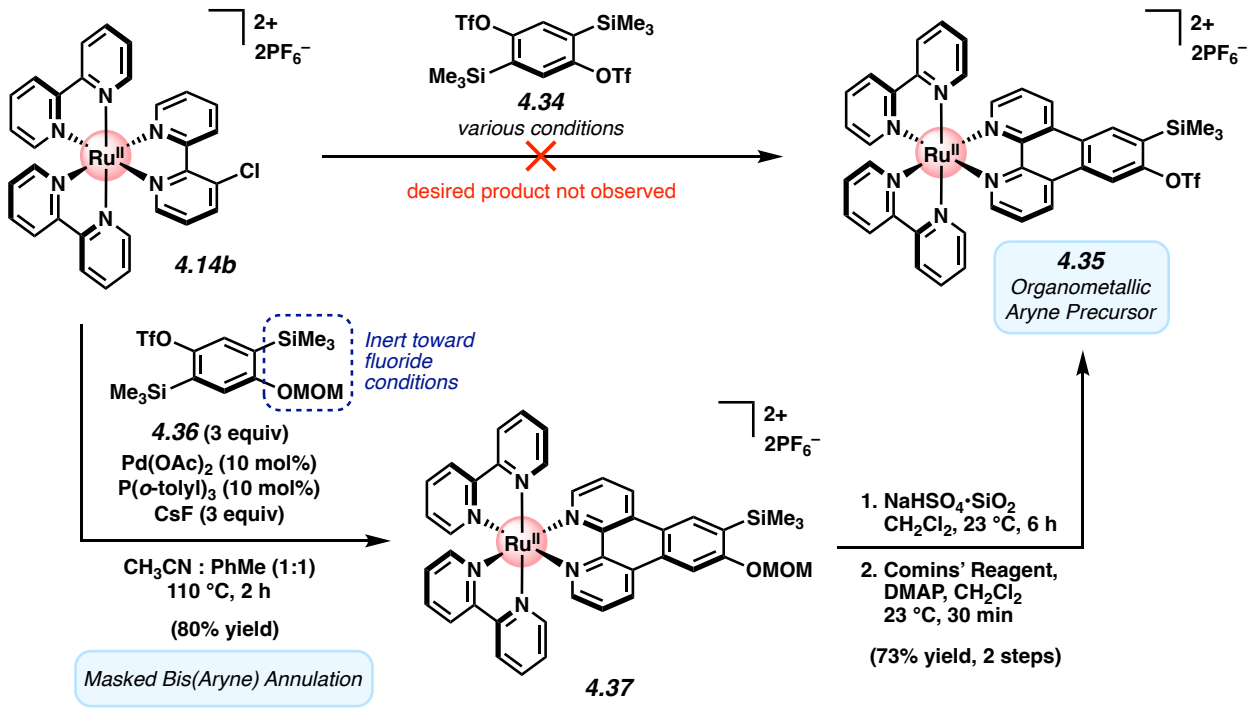

Figure 4.7. Synthesis of an organometallic aryne precursor via masked bis(aryne) annulation. OTf, trifluoromethanesulfonate; MOM, methoxymethyl; DMAP, 4-dimethylaminopyridine.

As highlighted in Figure 4.8a, we found that silyl triflate **4.35** indeed served as a suitable precursor to aryne **4.11**, which, in turn, underwent cycloaddition in situ with trapping partners **4.12**. Trapping of **4.11** in the presence of 2,5-dimethylfuran (**4.38**) gave Diels–Alder adduct **4.41** in 50% yield. In addition, a formal [2+2] cycloaddition of **4.11** with diketene acetal **4.39** was achieved, generating adduct **4.42** bearing a carbonyl functional handle. Finally, trapping of **4.11** with tetraphenylcyclopentadienone (**4.40**) gave rise to the unusual adduct **4.43** via a Diels–Alder and subsequent cheletropic cycloreversion to extrude CO. Complex **4.43** displays an excited state lifetime that is roughly two-fold longer than that of $Ru(bpy)_3$ (see Section 4.8.3.1). Overall, the ability to access **4.41**–**4.43** from aryne precursor **4.35** showcases a free aryne being generated directly on an organometallic complex and demonstrates the utility of such species to access metal complexes with a diverse array of ring systems. Moreover, the results shown in Figures 4.7 and 4.8a provide an unconventional strategy to access unique coordination complexes via two iterations of aryne on-the-complex chemistry (i.e., **4.14b** $\rightarrow$ **4.37** and **4.35** $\rightarrow$ **4.41**–**4.43**), which collectively enables the formation of four C–C bonds in each organometallic complex made.

Lastly, we explored the possibility of further manipulating the interesting organometallic complex **4.43**. Geometry optimization of **4.43** via DFT calculations suggests that its four phenyl substituents are oriented perpendicular to the plane of the bipyridyl ligand (see Figure 4.8a and Section 4.8.4). We therefore questioned whether these rings could be joined through an oxidative cyclization reaction (Figure 4.8b). Gratifyingly, treatment of **4.43** with DDQ and triflic acid facilitated triple C–C bond formation to give **4.44** in 46% yield, which notably occurs without oxidation of the Ru center. This approach to **4.44** circumvents solubility challenges historically encountered in efforts to access similar π-extended complexes through off-the-complex

protocols,[68] while providing access to a unique scaffold via a Scholl reaction[69] of a Ru-centered organometallic complex.[70]

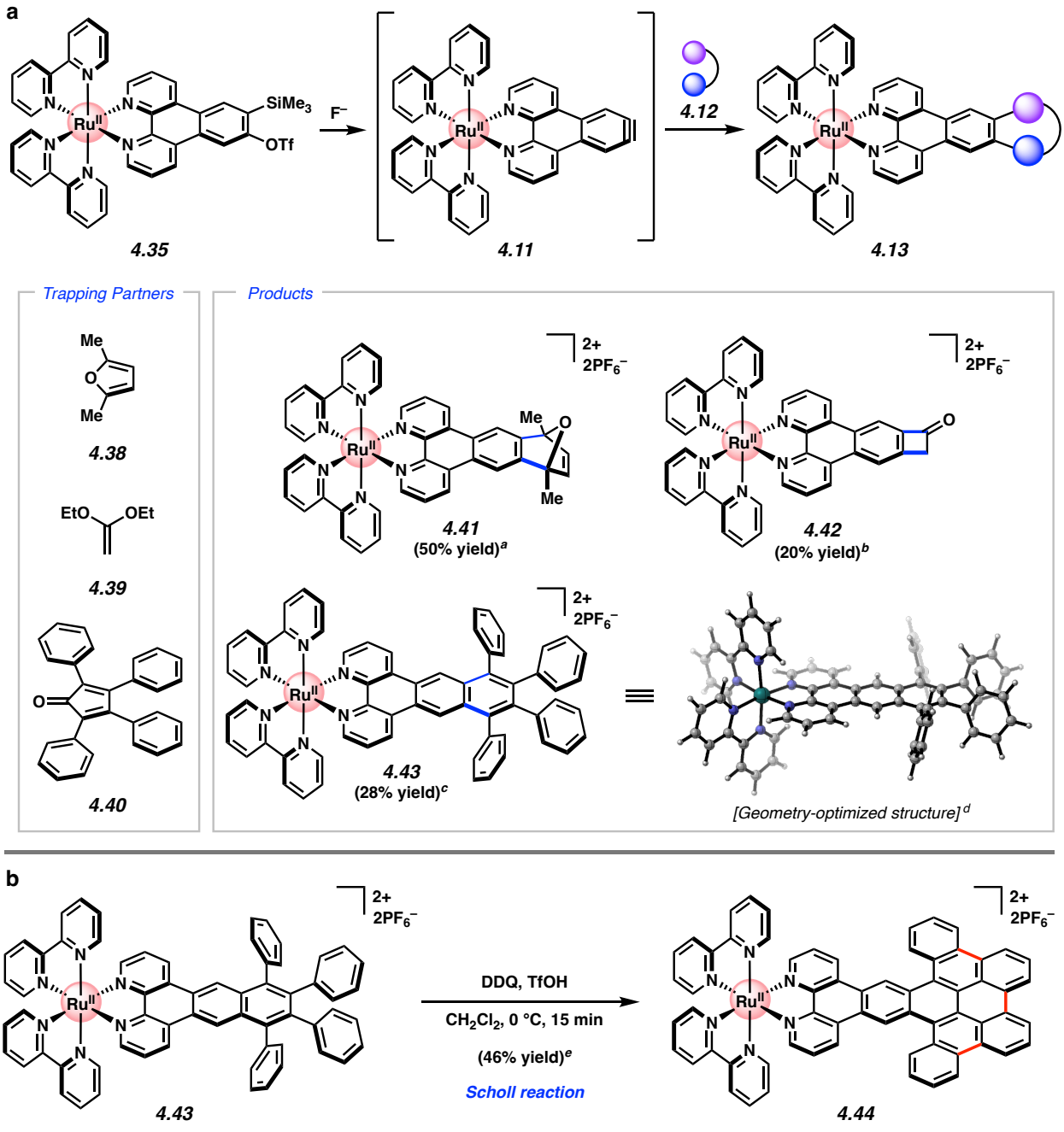

Figure 4.8. Mild generation and trapping of a Ru(II) aryne. (a) Cycloaddition reactions of organometallic aryne **4.11**. (b) Scholl reaction of **4.43** to give **4.44**. [a] Conditions: **4.35** (1 equiv),

4.38 (10 equiv), CsF (5 equiv), CH_3CN, 23 °C, 12 h. [b] Conditions: **4.35** (1 equiv), **4.39** (5 equiv), CsF (3 equiv), CH_3CN, 23 °C, 1.5 h; TFA. [c] Conditions: **4.35** (1 equiv), **4.40** (2 equiv), CsF (5 equiv), CH_3CN:CH_2Cl_2 (2:1), 50 °C, 1.5 h. [d] Geometry optimization of **4.43** (without counterions) was performed using B3LYP/6-31G(d)/LANL2DZ/CPCM(MeCN). [e] Conditions: **4.43** (1 equiv), DDQ (20 equiv), CH_2Cl_2:TfOH (40:1), 0 °C, 15 min. OTf, trifluoromethanesulfonate; Me, methyl; Et, ethyl; DDQ, 2,3-dichloro-5,6-dicyano-1,4-benzoquinone.

4.6 Photophysical Studies

Although our primary objective was to develop the fundamental synthetic methodology described above, we also sought to identify and evaluate trends in photophysical properties of the products obtained. We deemed this particularly important given the broad impact of $[Ru(bpy)_3]^{2+}$ (**4.17**) and other polypyridyl metal complexes in light-based applications, as mentioned earlier. Thus, we compared the photophysical properties of $[Ru(bpy)_3]^{2+}$ (**4.17**) to that of annulation products obtained through our methodology. Examining luminescence quantum yield and molar extinction coefficients provided useful insights and revealed adducts **4.31** and **4.33** as being particularly interesting (Figure 4.9). First, a positive trend in luminescence quantum yield was observed from $[Ru(bpy)_3]^{2+}$ (**4.17**) to bis(annulation) product **4.31** to tris(annulation) product **4.33**. In particular, **4.33** exhibits a high luminescence quantum yield of 24%, which is notably 2.5-fold greater than that of $[Ru(bpy)_3]^{2+}$ (**4.17**) at 9.5%. A high luminescence quantum yield indicates more efficient formation of a reactive excited state upon photon absorption, and is desirable in such applications as luminescence sensing, solar energy conversion, and photoredox catalysis.[36] Additionally, **4.33** displays a higher molar extinction coefficient across the visible

region (e.g., 23,500 mol^{-1} cm^{-1} at 452 nm) than that of $[Ru(bpy)_3]^{2+}$ (**4.17**) (e.g., 18,100 mol^{-1} cm^{-1} at 452 nm), which suggests that it exhibits stronger ground state absorption of light in the visible region, a desirable quality in the aforementioned applications. All three compounds exhibit a strong visible absorption peak at 452 nm, which is characteristic of the metal-to-ligand charge transfer (MLCT)-based luminescence that is typically observed in Ru(II) polypyridyl complexes. Of note, a shoulder also emerges in the region from 370–410 nm in compounds **4.31** and, more prominently, in **4.33**, and can likely be ascribed to delocalized $^1\pi$–π^* transitions that are characteristic of other π-expansive ligands (e.g., phenazine derivatives).[71] These findings bode well for the future use of our methodology to access complexes with promising and improved photophysical properties.

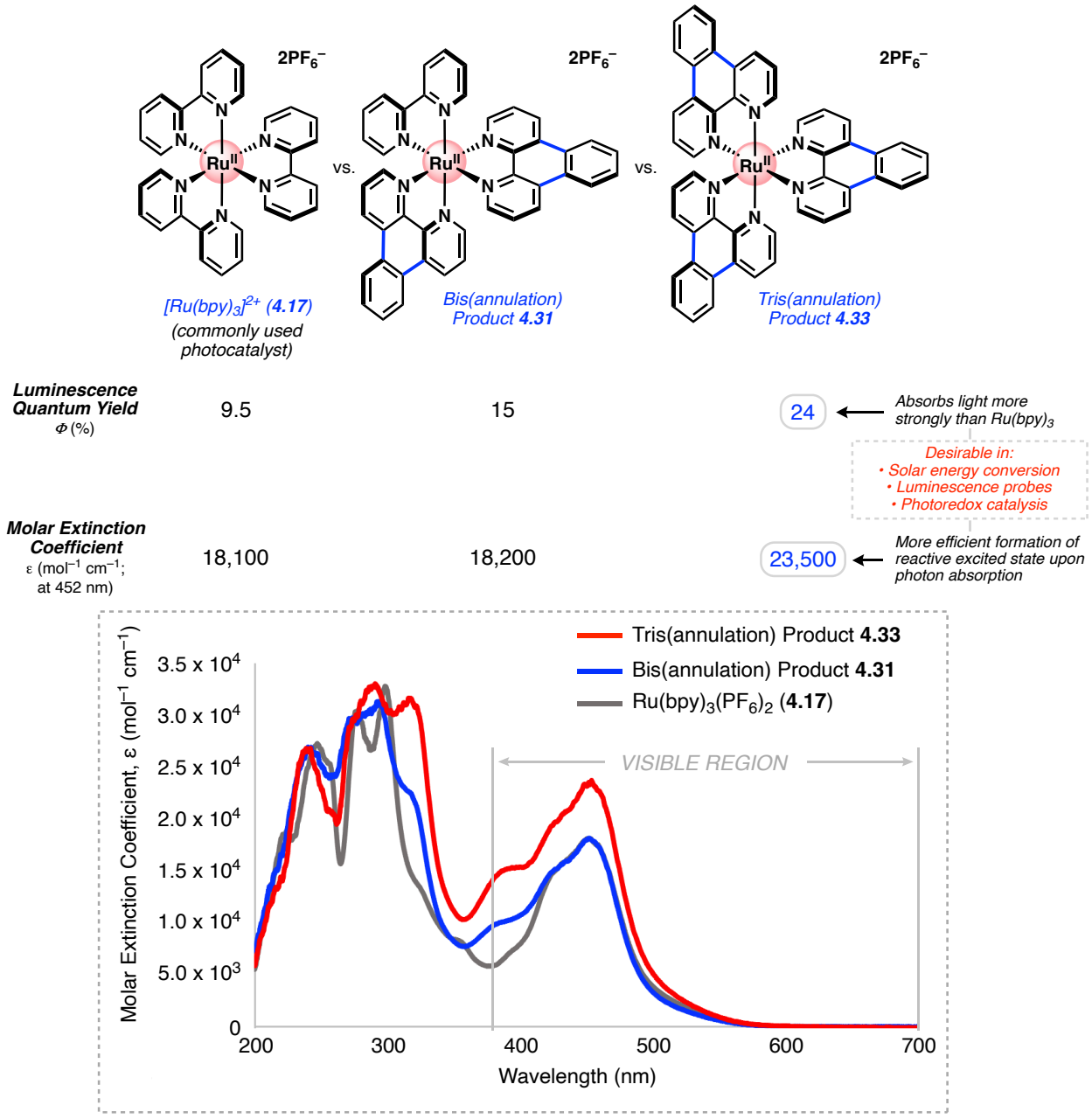

Figure 4.9. Photophysical studies of bis(annulation) product **4.31** and tris(annulation) product **4.33** relative to $[Ru(bpy)_3]^{2+}$ (**4.17**). Evaluation of luminescence quantum yield (Φ, %) and molar extinction coefficient (ε, mol^{-1} cm^{-1}). Experimental absorption spectra (molar extinction coefficient) are shown from 200–700 nm.

4.7 Conclusion

We have developed two variants of elusive aryne on-the-complex chemistry in the context of privileged polypyridyl metal complexes. In one variant, organometallic complexes bearing aryl halides undergo transition metal-catalyzed annulations with in situ, transiently-generated arynes. In the second version, an organometallic complex bearing a free aryne is intercepted in cycloaddition reactions to access complex scaffolds. Multiple C–C bonds (i.e., up to 6) can be formed in single synthetic operations, thus providing access to metal complexes bearing unique substitution patterns. These studies not only underscore the utility of traditionally avoided aryne intermediates and the value of on-the-complex aryne chemistry, but should also stimulate the development of on-the-complex reactions that enable transformations that are challenging by other means. Further studies will aim to evaluate and expand the utility of this methodology in accessing other valuable classes of organometallic complexes. From the standpoint of synthetic strategy, we hope these studies encourage the use of pre-coordinated ligands as synthons in the pursuit of complex organometallic architectures.

4.8 Experimental Section

4.8.1 Materials and Methods

Unless stated otherwise, reactions were conducted in flame-dried glassware under an atmosphere of nitrogen or argon and commercially obtained reagents were used as received. Anhydrous solvents were either freshly distilled or passed through activated alumina columns, unless otherwise stated. Reaction temperatures were controlled using an IKAmag temperature modulator, and unless stated otherwise, reactions were performed at room temperature (approximately 23 °C). Cesium fluoride (CsF), palladium(II) acetate ($Pd(OAc)_2$), and di-μ-chlorotetrakis[2-(2-pyridinyl-kN)phenyl-kC]diiridium(III) (**4.53**) were obtained from Strem Chemicals. Methyl iodide was obtained from Spectrum Chemical. Ruthenium(III) chloride trihydrate (**4.51**), 3-(trimethylsilyl)-2-naphthyl trifluoromethanesulfonate (**4.71**), 2,5-dibromohydroquinone (**4.63**), 2,5-dimethylfuran (**4.38**), and 2,3-dichloro-5,6-dicyano-1,4-benzoquinone (DDQ) were obtained from Combi-Blocks. 1-(trimethylsilyl)-2-naphthyl trifluoromethanesulfonate (**4.72**) was obtained from TCI America. Tri(*o*-tolyl)phosphine (P(*o*-tolyl)$_3$), Garg 4,5-indolyne precursor (**4.61**), *cis*-bis(2,2'-bipyridine)dichlororuthenium(II) hydrate (**4.50**), phosphorus trichloride (PCl_3), 1,1,1,3,3,3-hexamethyldisilazane (HMDS), bromomethyl methyl ether (MOMBr), tetraphenylcyclopentadienone (**4.40**), di-μ-chlorotetrakis[2-(1-isoquinolinyl-N)phenyl-C]diiridium(III) (**4.55**), and dichlorotetrakis[3,5-difluoro-2-(2-pyridinyl)phenyl]diiridium(III) (**4.57**) were obtained from Sigma-Aldrich. *N*-bromosuccinimide and *N*-chlorosuccinimide were obtained from Acros Organics. Phosphorus tribromide (PBr_3) and trifluoromethanesulfonic acid (TfOH) was obtained from Oakwood Chemical. 1,1'-Diethoxyethene (**4.39**) was obtained from Fluka. 2,2'-bipyridine *N*-oxide (**4.45**) was prepared according to literature procedures,[72] and is also commercially available. Thin-layer

chromatography (TLC) was conducted with EMD gel 60 F254 pre-coated plates (0.25 mm for analytical chromatography and 0.50 mm for preparative chromatography) and visualized using UV. Silicycle Siliaflash P60 (particle size 0.040–0.063 mm) was used for flash column chromatography. ^{1}H NMR spectra were recorded on Bruker spectrometers (at 400, 500 and 600 MHz) and are reported relative to residual solvent signals. Data for ^{1}H NMR spectra are reported as follows: chemical shift (δ ppm), multiplicity, coupling constant (Hz), integration. Data for ^{13}C NMR are reported in terms of chemical shift (at 100 Hz and 125 MHz). IR spectra were recorded on a Perkin-Elmer UATR Two FT-IR spectrometer and are reported in terms of frequency absorption (cm^{-1}). ESI-TOF measurements were carried out in positive ionization mode on a Waters LCT-Premier XE Time of Flight Instrument controlled by MassLynx 4.1 software (Waters Corporation, Milford MA). The instrument was equipped with the Multi Mode Ionization source operated in the electrospray mode. A solution of Leucine Enkephalin (Sigma Chemical, L9133) was used in the Lock-Spray to obtain accurate mass measurements. Samples were infused using direct loop injection on a Waters Acquity UPLC system. GC-MS measurements were carried out using an Agilent Model 7693 Autosampler, 7890B Gas Chromatograph, and 7250 Q-TOF Mass Selective Detector in the Electron Ionization mode. Sample injection was carried out in split mode with inlet temperature set to 280 °C. Separation was carried out on an Agilent HP5-MS column with dimensions 30m x 250 µm x 0.25 µm. Ultra High Purity Grade He (Airgas) was used as carrier gas with the flow set to 1.1 mL/min in constant flow mode. The initial oven temperature was set to 70 °C for 1 min followed by a 20 °C/min ramp to a final temperature of 300 °C which was maintained for 4 min. A 3.0 min solvent delay was used. EI energy was set to 70 eV. The MSD was set to scan the 50–500 m/z

range. Data collection and analysis were performed using Mass Hunter Acquisition and Qualitative Analysis software (Agilent).

4.8.2 Experimental Procedures

4.8.2.1 Synthesis of Halobipyridine Organometallic Complexes

Note: The following procedures for the synthesis of halobipyridines were adapted from a published literature protocol[5] to facilitate gram-scale synthesis.

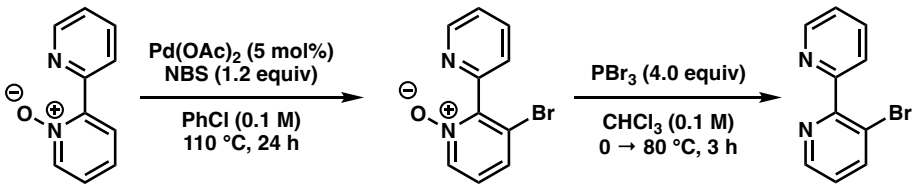

4.45 ***4.46*** ***4.47***

Bromobipyridine 4.47. To a flask containing 2,2'-bipyridyl *N*-oxide (**4.45**, 1.00 g, 5.81 mmol), $Pd(OAc)_2$ (65.4 mg, 0.291 mmol, 5 mol%), and *N*-Bromosuccinimide (1.24 g, 6.97 mmol, 1.2 equiv) was added PhCl (58 mL, 0.10 M). This suspension was then heated to 110 °C and stirred for 24 h. The reaction was then allowed to cool to 23 °C, at which point it was transferred with CH_2Cl_2 (30 mL) to a separatory funnel containing 1.0 M saturated aqueous NaOH (30 mL). The layers were separated and the aqueous layer was extracted with CH_2Cl_2 (3 x 30 mL). The combined organic layers were then dried over Na_2SO_4, filtered, and concentrated under reduced pressure to afford the corresponding bromobipyridine *N*-oxide **4.46** as a brown oil. This was carried forward without further purification.

The crude oil was dissolved in $CHCl_3$ (50 mL, 0.10 M) and cooled to 0 °C. To this stirred solution was added PBr_3 (2.0 mL, 21.0 mmol, 4.0 equiv) dropwise over 8 min. The cooling bath was then removed and the reaction was warmed to 80 °C and stirred for 3 h. It was then allowed to cool to 23 °C before being cooled further to 0 °C. The reaction was then quenched by addition

of aqueous NaOH (1.0 M, 40 mL) over 1 min before being warmed to 23 °C. 6.0 M NaOH (40 mL) was then added in one portion and the mixture was stirred at 23 °C for 5 min before being transferred to a separatory funnel. The layers were separated and the aqueous layer was extracted with CH_2Cl_2 (3 x 50 mL). The combined organic layers were then dried over Na_2SO_4, filtered, and concentrated under reduced pressure. The resulting oil was purified by flash chromatography (5% Et_3N in 9:1 hexanes:EtOAc → 5% Et_3N in 7:2 hexanes:EtOAc) using silica gel neutralized with Et_3N to afford bromobipyridine **4.47** as a beige solid (800 mg, 59% yield over two steps). **Bromobipyridine 4.47**: R_f 0.25 (3:1 EtOAc:Hexanes); ^{1}H NMR (500 MHz, $CDCl_3$): δ 8.75 (dd, J = 4.9, 0.8, 1H), 8.66 (d, J = 4.6, 1H), 8.03 (d, J = 7.9, 1H), 7.83 (td, J = 7.6, 1.4, 1H), 7.73 (d, J = 7.7, 1H), 7.36 (dd, J = 7.6, 4.9, 1H), 7.22 (dd, J = 8.3, 4.7, 1H). Spectral data match those previously reported in the literature.[5]

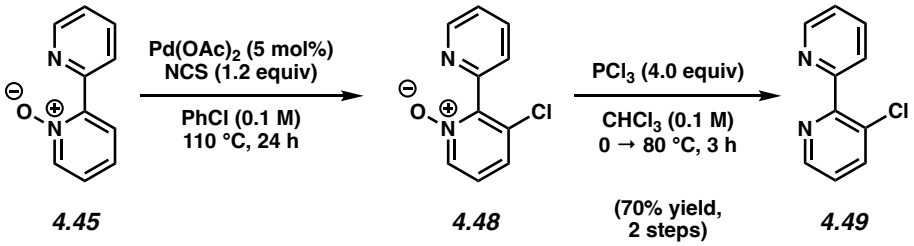

Chlorobipyridine 4.49. To a flask containing 2,2'-bipyridyl *N*-oxide (**4.45**, 3.81 g, 22.1 mmol), $Pd(OAc)_2$ (248 mg, 1.11 mmol, 5 mol%), and *N*-chlorosuccinimide (3.55 g, 26.6 mmol, 1.2 equiv) was added PhCl (220 mL, 0.10 M). This suspension was then heated to 110 °C and stirred for 24 h. The reaction mixture was then allowed to cool to 23 °C, at which point it was transferred with CH_2Cl_2 (15 mL) to a separatory funnel containing aqueous NaOH (1.0 M, 100 mL). The layers were separated and the aqueous layer was extracted with CH_2Cl_2 (3 x 60 mL). The combined organic layers were then dried over Na_2SO_4, filtered, and concentrated under

reduced pressure to afford the corresponding chlorobipyridine *N*-oxide **4.48** as a brown oil. This was carried forward without further purification.

The crude oil was dissolved in $CHCl_3$ (200 mL, 0.10 M) and cooled to 0 °C. To this stirred solution was added PCl_3 (7.28 mL, 83.2 mmol, 4.0 equiv) dropwise at 0 °C over 12 min. The cooling bath was then removed and the reaction was warmed to 80 °C and stirred for 3 h. It was then allowed to cool to 23 °C before being cooled further to 0 °C. The reaction was then quenched by addition of aqueous NaOH (1.0 M, 100 mL) over 2 min before being warmed to 23 °C. Aqueous NaOH (6.0 M, 50 mL) was then added in one portion and the mixture was stirred at 23 °C for 5 min before being transferred to a separatory funnel. The layers were separated and the aqueous layer was extracted with CH_2Cl_2 (3 x 100 mL). The combined organic layers were then dried over Na_2SO_4, filtered, and concentrated under reduced pressure. The resulting brown oil was purified by flash chromatography (5% Et_3N in 3:1 hexanes:EtOAc → 5% Et_3N in 1:1 hexanes:EtOAc → 5% Et_3N in 1:3 hexanes:EtOAc) using silica gel neutralized with Et_3N to afford chlorobipyridine **4.49** as an off-white solid (2.96 g, 70% yield over two steps). **Chlorobipyridine 4.49**: R_f 0.30 (3:1 EtOAc:hexanes); ^{1}H NMR (400 MHz, CD_3CN): δ 8.77 (d, *J* = 4.8, 1H), 8.64 (dd, *J* = 4.8, 1.4, 1H), 7.83 (td, *J* = 8.7, 1.4, 2H), 7.77 (d, *J* = 7.9, 1H), 7.36 (ddd, *J* = 7.7, 4.9, 1.3, 1H), 7.31 (dd, *J* = 8.31, 4.7, 1H). Spectral data match those previously reported in the literature.[5]

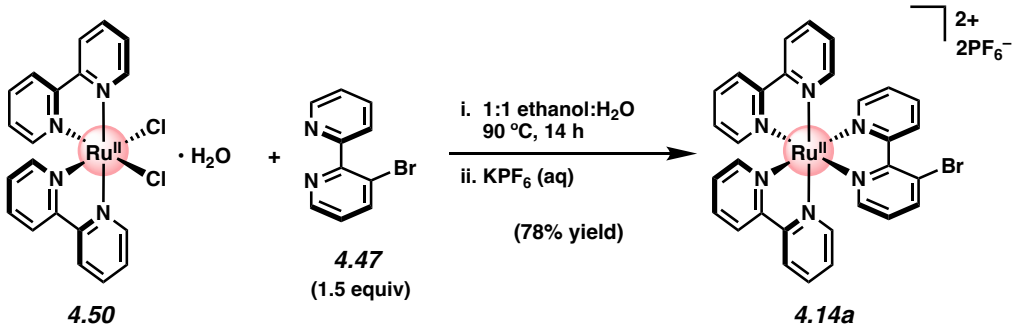

Bromo-Ru(bpy)$_3$[PF$_6$]$_2$ 4.14a. To a flask containing *cis*-bis(2,2'-bipyridine)dichlororuthenium(II) hydrate (**4.50**, 899 mg, 1.86 mmol, 1.0 equiv) and bromobipyridine **4.47** (667 mg, 2.84 mmol, 1.5 equiv) was added EtOH (120 mL) and H_2O (120 mL). The flask was topped with an air condenser and the system placed under N_2. The reaction was heated to 90 °C and stirred for 14 h, during which the solution changed in color from deep purple to red. The reaction was then allowed to cool to 23 °C before saturated aqueous KPF_6 (50 mL) was added over 1 min while stirring to produce a red precipitate. The mixture was then filtered over a pad of celite (packed with Et_2O), washed with Et_2O (3 x 20 mL), and the filtrate was discarded. The remaining solid residue was then redissolved in CH_3CN (90 mL) and passed through the same celite plug. The resulting deep red filtrate was then concentrated under reduced pressure and then passed through a pad of neutral alumina with CH_3CN (250 mL). The red band was collected and concentrated under reduced pressure to afford a red semi-solid. This material was then recrystallized from 1:1 MeOH:H_2O (10 mL) and the resulting red crystals were washed with 1:1 MeOH:H_2O (2 x 2 mL, cooled to 0 °C) and dried under reduced pressure (<1 torr) for 12 h at 60 °C to afford bromo-Ru(bpy)$_3$[PF$_6$]$_2$ **4.14a** as a red crystalline solid (1.36 g, 78% yield based on anhydrous **4.50**). **Bromo-Ru(bpy)$_3$[PF$_6$]$_2$ 4.14a**: mp >250 °C; R_f 0.64 (7:2:1 MeCN:H_2O:sat. aq. KNO_3); ^{1}H NMR (400 MHz, CD_3CN): δ 9.56 (dq, J = 8.6, 0.7, 1H), 8.49 (dd, J = 8.3, 3.4, 4H), 8.30 (dd, J = 8.3, 1.3, 1H), 8.10–8.02 (m, 5H), 7.84 (dd, J = 5.5, 1.4, 2H), 7.76 (dq, J = 5.7, 0.7, 1H), 7.70 (dq, J = 5.7, 0.7, 1H), 7.68–7.63 (m, 2H); ^{13}C NMR (125 MHz,

CD_3CN, 26 of 30 signals observed): δ 157.79, 157.78, 157.69, 157.65, 157.5, 154.9, 153.2, 152.8, 152.7, 152.5, 152.3, 145.7, 138.93, 138.91, 138.90, 138.0, 129.3, 128.7, 128.64, 128.58, 128.55, 128.46, 127.9, 125.29, 125.28, 121.8; IR (film): 1606, 1467, 1447, 1425, 837, 762 cm^{-1}; HR-ESI-MS (*m/z*) $[M - PF_6]^+$ calcd for $C_{30}H_{23}N_6BrPF_6Ru^+$, 792.98529; found 792.9849.

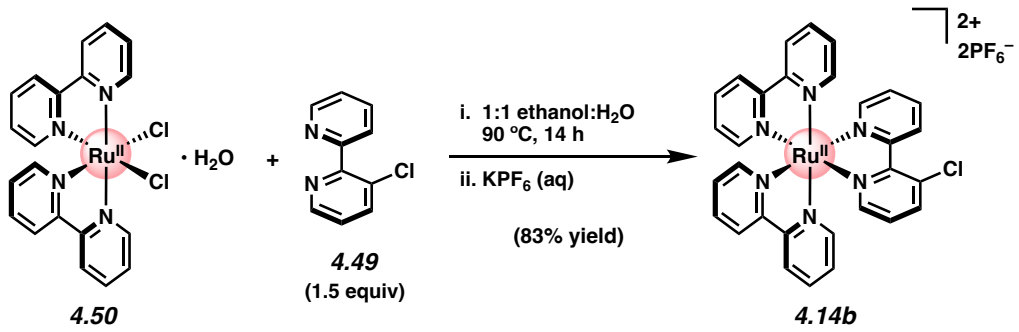

Chloro-Ru(bpy)$_3$[PF$_6$]$_2$ 4.14b. To a flask containing *cis*-bis(2,2'-bipyridine)dichlororuthenium(II) hydrate (**4.50**, 4.00 g, 8.26 mmol, 1.0 equiv) and chlorobipyridine **4.49** (2.36 g, 12.4 mmol, 1.5 equiv) was added EtOH (330 mL) and H_2O (330 mL). The flask was topped with an air condenser and the system placed under N_2. The reaction was heated to 90 °C and stirred for 14 h, during which the solution changed in color from deep purple to red. The reaction was then allowed to cool to 23 °C before saturated aqueous KPF_6 (300 mL) was added over 5 min while stirring to produce a red precipitate. The mixture was then filtered over a pad of celite (packed with Et_2O), washed with Et_2O (3 x 50 mL), and the filtrate was discarded. The remaining solid residue was redissolved in CH_3CN (200 mL) and passed through the same celite plug. The resulting deep red filtrate was then concentrated under reduced pressure and then passed through a pad of neutral alumina with CH_3CN (600 mL). The red band was collected and concentrated under reduced pressure to afford a red semi-solid. The purified material was then divided into three portions and each was recrystallized from 1:1 MeOH:H_2O (10 mL) and the resulting red crystals were washed with 1:1 MeOH:H_2O (2 x 2 mL for each

portion, cooled to 0 °C) and dried under reduced pressure (<1 torr) for 12 h at 50 °C to afford chloro-Ru(bpy)$_3$[PF$_6$]$_2$ **4.14b** as a red crystalline solid (6.13 g, 83% yield based on anhydrous **4.50**). **Chloro-Ru(bpy)$_3$[PF$_6$]$_2$ 4.14b**: mp >250 °C; R_f 0.60 (7:2:1 MeCN:H$_2$O:sat. aq. KNO$_3$); ^{1}H NMR (400 MHz, CD$_3$CN): δ 9.41 (dq, *J* = 8.5, 0.8, 1H), 8.50 (dd, *J* = 8.2, 1.0, 4H), 8.12–8.02 (m, 6H), 7.86 (dq, *J* = 5.6, 0.7, 1H), 7.81 (dd, *J* = 5.5, 1.3, 1H), 7.76 (dq, *J* = 5.6, 0.7, 1H), 7.70 (dq, *J* = 5.6, 0.7, 1H), 7.68–7.64 (m, 2H), 7.44–7.35 (m, 5H), 7.31 (dd, *J* = 8.4, 5.5, 1H); ^{13}C NMR (125 MHz, CD$_3$CN, 24 of 30 signals observed) δ 157.80, 157.78, 157.71, 157.67, 157.1, 154.0, 153.2, 152.8, 152.47, 152.45, 151.9, 142.0, 138.94, 138.91, 138.4, 134.2, 129.4, 128.7, 128.65, 128.61, 128.57, 128.5, 128.1, 125.30, 125.29; IR (film): 1604, 1467, 1447, 1427, 1243, 837 cm$^{-1;}$ HR-ESI-MS (*m/z*) [M – PF$_6$]$^+$ calcd for C$_{30}$H$_{23}$N$_6$ClPF$_6$Ru$^+$, 749.03580; found 749.0350.

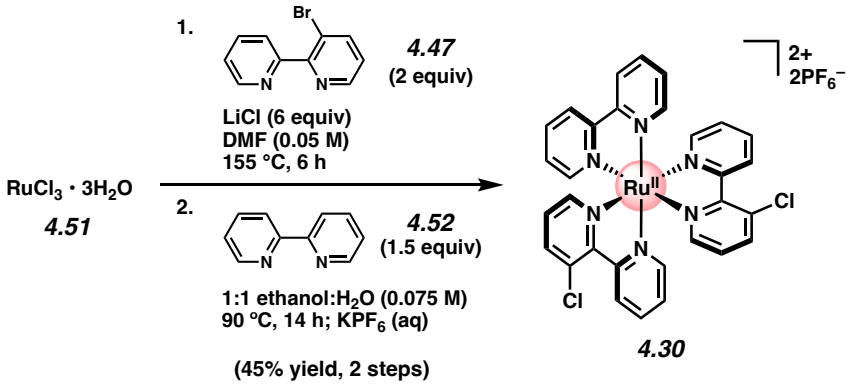

Bis(chloro)-Ru(bpy)$_3$[PF$_6$]$_2$ 4.30. To a flask containing ruthenium(III) chloride trihydrate (**4.51**, 309 mg, 1.18 mmol, 1.0 equiv), bromobipyridine **4.47** (559 mg, 2.38 mmol, 2.0 equiv), and LiCl (301 mg, 7.10 mmol, 6.0 equiv) was added DMF (25 mL, 0.05 M). The flask was topped with an air condenser and the system placed under N$_2$. The reaction was heated to 155 °C and stirred for 6 h. The reaction mixture was then allowed to cool to 23 °C before acetone (25 mL) was added in one portion and the solution was added dropwise to vigorously stirring Et$_2$O (300 mL). The

resultant mixture was then filtered over a pad of celite (packed with Et_2O) and washed with Et_2O (3 x 30 mL). The solid residue was then redissolved in CH_2Cl_2 (200 mL) and concentrated under reduced pressure to afford a deep purple solid. This was carried forward without further purification.

To the crude solid was added 2,2'-bipyridine (**4.52**, 281 mg, 1.80 mmol, 1.5 equiv), EtOH (80 mL), and H_2O (80 mL) sequentially. The flask was topped with an air condenser and the system placed under N_2. The reaction was heated to 90 °C and stirred for 14 h, during which the solution changed in color from deep purple to red. The reaction was then allowed to cool to 23 °C before saturated aqueous KPF_6 (70 mL) was added over 2 min while stirring to produce a red precipitate. The mixture was then filtered over a pad of celite (packed with Et_2O), washed with Et_2O (3 x 30 mL), and the solid residue was redissolved in MeCN (200 mL). The deep red filtrate was then concentrated under reduced pressure and then purified by flash chromatography on neutral alumina (100% MeCN). The red band was collected and concentrated under reduced pressure to afford a red semi-solid. This material was then recrystallized from 1:1 MeOH:H_2O (5 mL) and the resulting red crystals were washed with 1:1 MeOH:H_2O (2 x 2 mL, cooled to 0 °C) and dried under reduced pressure (<1 torr) for 12 h at 60 °C to afford bis(chloro)-Ru(bpy)$_3$[PF_6]$_2$ **4.30** as a red crystalline solid (491 mg, 45% yield over 2 steps). **Bis(chloro)-Ru(bpy)$_3$[PF_6]$_2$ 4.30**: mp >250 °C; R_f 0.63 (7:2:1 MeCN:H_2O:sat. aq. KNO_3); ^{1}H NMR (500 MHz, CD_3CN): δ 9.43–9.39 (m, 2H), 8.50 (d, *J* = 8.2, 2H), 8.13–8.04 (m, 6H), 7.88 (dq, *J* = 5.6, 0.7, 1H), 7.85–7.82 (m, 1H), 7.81–7.77 (m, 1H), 7.75 (ddd, *J* = 5.6, 3.7, 1.4, 1H) 7.71 (app. d, *J* = 5.6, 1H), 7.67–7.63 (m, 1H), 7.45–7.37 (m, 4H), 7.34–7.28 (m, 2H); ^{13}C NMR (125 MHz, CD_3CN) δ 157.59, 157.57, 157.56, 157.5, 156.92, 156.85, 156.81, 153.85, 153.78, 153.75, 153.3, 153.04, 153.01, 152.64, 152.63, 152.03, 152.02, 151.74, 151.71, 142.24, 142.22, 142.21, 139.13, 139.11,

139.10, 139.09, 138.58, 138.57, 134.32, 134.29, 129.53, 129.51, 128.8, 128.72, 128.67, 128.61, 128.60, 128.5, 128.2, 128.1, 128.0, 125.41, 125.39, 125.37; IR (film): 1603, 1468, 1447, 1419, 1214, 835, 797 cm^{-1}; HR-ESI-MS (*m/z*) $[M - PF_6]^+$ calcd for $C_{30}H_{22}N_6Cl_2PF_6Ru^+$, 782.99683; found 782.9984.

Note: Though unexpected, it is postulated that LiCl facilitates chloro-debromination during the reaction. ***4.30*** *was obtained as a mixture of geometric isomers; these data represent empirically observed chemical shifts from the* ^{13}C *NMR spectrum.*

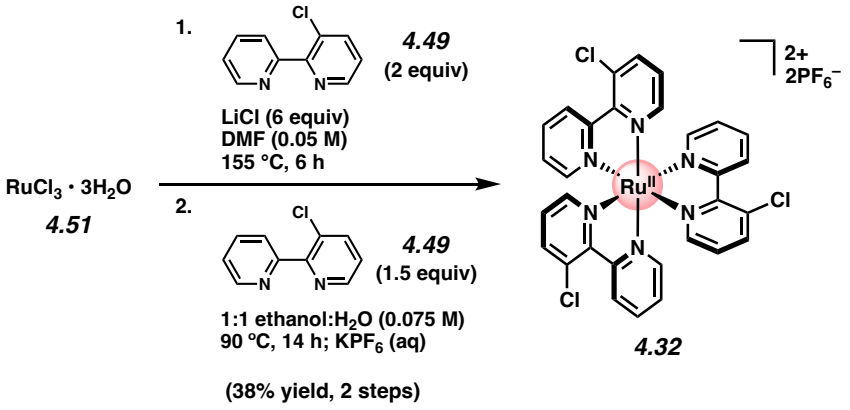

Tris(chloro)-Ru(bpy)$_3$[PF$_6$]$_2$ 4.32. To a flask containing ruthenium(III) chloride trihydrate (**4.51**, 401 mg, 1.54 mmol, 1.0 equiv), chlorobipyridine **4.49** (584 mg, 3.07 mmol, 2.0 equiv), and LiCl (390 mg, 9.21 mmol, 6.0 equiv) was added DMF (30 mL, 0.05 M). The flask was topped with an air condenser and the system placed under N_2. The reaction was heated to 155 °C and stirred for 6 h. The reaction mixture was then allowed to cool to 23 °C before acetone (35 mL) was added in one portion and the mixture was added dropwise to vigorously stirring Et_2O (300 mL). The resultant mixture was then filtered over a pad of celite (packed with Et_2O) and washed with Et_2O (4 x 30 mL). The solid residue was then redissolved in CH_2Cl_2 (250 mL) and

concentrated under reduced pressure to afford a deep purple solid. This was carried forward without further purification.

To the crude solid material was added chlorobipyridine **4.49** (443 mg, 2.32 mmol, 1.5 equiv), EtOH (100 mL), and H_2O (100 mL) sequentially. The flask was topped with an air condenser and the system placed under N_2. The reaction was heated to 90°C and stirred for 14 h, during which the solution changed in color from deep purple to red. The reaction was then allowed to cool to 23 °C before saturated aqueous KPF_6 (70 mL) was added over 2 min while stirring to produce a red precipitate. The mixture was then filtered over a pad of celite (packed with Et_2O), washed with Et_2O (3 x 30 mL), and the solid residue was redissolved in MeCN (250 mL). The deep red filtrate was then concentrated under reduced pressure and then purified by flash chromatography on neutral alumina (100% MeCN). The red band was collected and concentrated under reduced pressure to afford a red semi-solid. This material was then recrystallized from 1:1 MeOH:H_2O (5 mL) and the resulting red crystals were washed with 1:1 MeOH:H_2O (2 x 2 mL, cooled to 0 °C) and dried under reduced pressure (<1 torr) for 12 h at 60 °C to afford tris(chloro)-Ru(bpy)$_3$[PF_6]$_2$ **4.32** as a red crystalline solid (567 mg, 38% yield over 2 steps). **Tris(chloro)-Ru(bpy)$_3$[PF_6]$_2$ 4.32**: mp >250 °C; R_f 0.69 (7:2:1 MeCN:H_2O:sat. aq. KNO_3); ^{1}H NMR (500 MHz, CD_3CN): δ 9.41 (d, *J* = 8.5, 3H), 8.14–8.06 (m, 6H), 7.85–7.72 (m, 6H), 7.41–7.38 (qd, *J* = 6.8, 1.3, 3H), 7.35–7.28 (m, 3H); ^{13}C NMR (125 MHz, CD_3CN) δ 156.7, 156.5, 153.63, 153.62, 153.59, 153.20, 153.18, 151.89, 151.87, 142.40, 142.38, 142.37, 138.74, 138.71, 134.38, 134.36, 134.35, 134.34, 129.61, 129.60, 129.57, 128.83, 128.79, 128.70, 128.66, 128.3, 128.2, 128.13, 128.07; IR (film): 1473, 1428, 1420, 1215, 837, 797 cm^{-1}; HR-ESI-MS (*m/z*) [M – PF_6]$^+$ calcd for $C_{30}H_{21}N_6Cl_3PF_6Ru^+$, 816.95786; found 816.9572.

*Note: **4.32** was obtained as a mixture of geometric isomers. These data represent empirically observed chemical shifts from the ^{13}C NMR spectrum.*

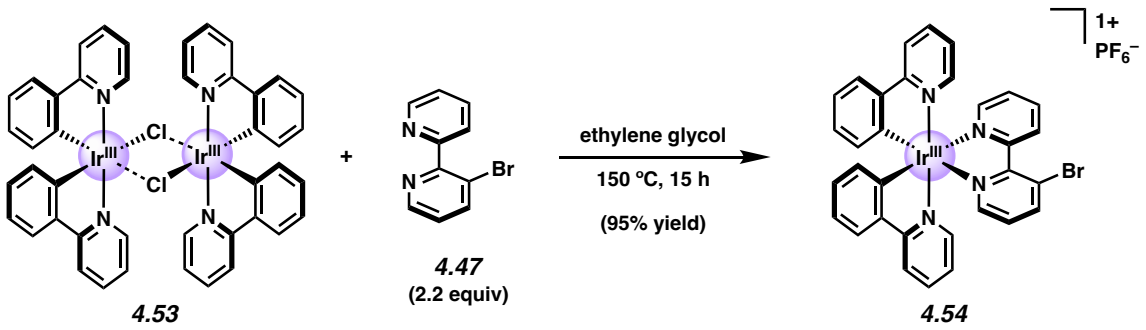

4.53 + *4.47* (2.2 equiv) → *4.54*

Bromo-Ir(ppy)$_2$bpy 4.54. To a 20 mL scintillation vial was added di-μ-chlorotetrakis[2-(2-pyridinyl-kN)phenyl-kC]diiridium(III) (**4.53**, 100.0 mg, 0.093 mmol, 1.0 equiv) in a glovebox. The vial was removed from the glovebox and placed under nitrogen. To a separate 1-dram vial was added bromobipyridine **4.47** (48.2 mg, 0.205 mmol, 2.2 equiv) and ethylene glycol (4.0 mL, 0.023 M), and the mixture was then sparged with N_2 for 15 minutes. This solution was then transferred to the vial containing **4.53**. The septa cap was replaced with a Teflon-lined screw cap and the reaction was transferred to an Al-block and stirred at 150 °C for 15 h. After cooling to 23 °C, the reaction was transferred to a separatory funnel containing deionized water (48 mL). The aqueous phase was washed with hexanes (2 x 24 mL) and then Et_2O (24 mL). The aqueous layer was then heated to 85 °C for 5 minutes to evaporate any remaining organic solvent. The solution cooled to 23 °C, and then then aqueous NH_4PF_6 (0.27 M, 12 mL) was added, resulting in an orange-yellow precipitate. This mixture was filtered through a plug of celite and washed with water (20 mL) to remove ethylene glycol. The celite pad was then eluted with acetonitrile (50 mL) to redissolve the product, and the resulting filtrate was collected and concentrated under reduced pressure to afford bromo-Ir(ppy)$_2$bpy complex **4.54** as a dark yellow solid (156 mg, 95% yield). **Bromo-Ir(ppy)$_2$bpy 4.54**. R_f 0.60 (7:2:1 CH_3CN:H_2O:sat. aq. KNO_3); ^1H NMR (500

MHz, CD_3CN): δ 9.42 (dt, *J* = 8.3, 1.6, 0.9, 1H), 8.36 (dd, *J* = 8.4, 1.4, 1H), 8.13 (ddd, *J* = 8.7, 7.9, 1.8 1H), 8.09–8.04 (m, 4H), 7.88–7.83 (m, 2H), 7.78 (ddd, *J* = 7.9, 3.3, 1.1, 2H), 7.73–7.70 (m, 2H), 7.49 (ddd, *J* = 7.7, 5.5, 1.2, 1H), 7.29 (dd, *J* = 8.6, 5.4, 1H), 7.06–7.01 (m, 4H), 6.90 (tdd, *J* = 7.4, 2.4, 1.3, 2H), 6.22 (ddd, *J* = 7.6, 4.6, 1.0, 2H); ^{13}C NMR (125 MHz, CD_3CN) δ 168.6, 168.5, 156.2, 154.9, 152.6, 151.7, 151.5, 150.83, 150.79, 150.7, 147.5, 145.4, 145.3, 140.1, 140.0, 139.8, 132.9, 132.8, 131.9, 131.8, 130.2, 129.9, 129.5, 126.3, 124.9, 124.8, 124.1, 124.0, 123.8, 123.0, 121.3, 121.2; IR (film): 3064, 2921, 1607, 1478, 1420, 1342 cm^{-1}; HR-ESI-MS (*m/z*) $[M - PF_6]^+$ calcd for $C_{32}H_{23}BrN_4Ir^+$, 735.0735; found 735.0738.

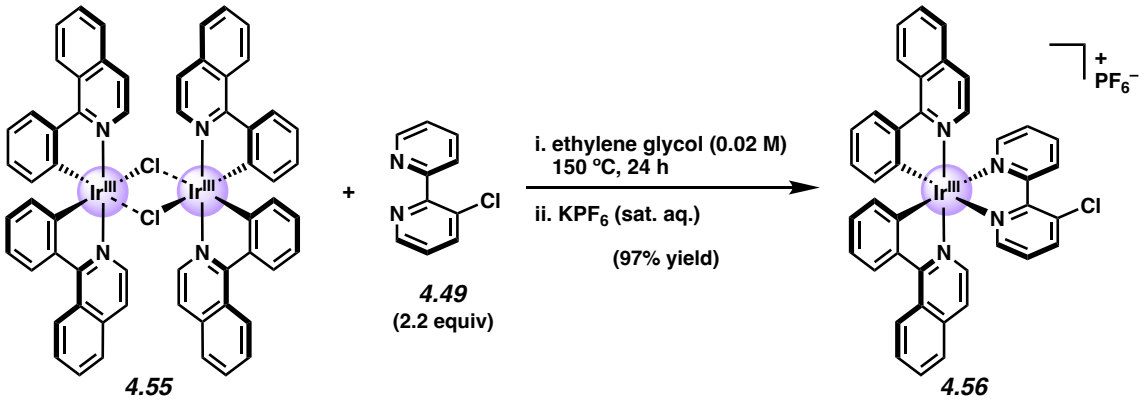

Isoquinolinyl Complex 4.56. To an 8-dram vial containing di-μ-chlorotetrakis[2-(1-isoquinolinyl-N)phenyl-C]diiridium(III) (**4.55**, 200.0 mg, 0.157 mmol, 1.0 equiv) and chlorobipyridine **4.49** (65.9 mg, 0.346 mmol, 2.2 equiv) was added ethylene glycol (6.8 mL, 0.023 M). The resulting suspension was then sparged with N_2 for 15 minutes before being transferred to an Al-block and stirred at 150 °C for 24 h. After cooling to 23 °C, the reaction was diluted with water (20 mL) before being transferred with water (5 mL) to a flask containing sat. aq. KPF_6 (50 mL), resulting in formation of a red precipitate. This mixture was then filtered through a plug of celite and washed sequentially with water (300 mL), hexanes (200 mL), and Et_2O (200 mL). The celite pad was then eluted with CH_2Cl_2 (200 mL) to redissolve the product,

and the resulting filtrate was collected, dried over Na_2SO_4, concentrated under reduced pressure, and dried under reduced pressure (<1 torr) at 100 °C for 12 h to afford Ir(ppy)$_2$bpy complex **4.56** as a red solid (286.3 mg, 97% yield). **Isoquinolinyl Complex 4.56**. R_f 0.62 (14:1:1 CH_3CN:H_2O:sat. aq. KNO_3); ^{1}H NMR (500 MHz, CD_3CN): δ 9.34 (dt, *J* = 8.5, 1.0, 1H), 9.06–8.94 (m, 2H), 8.37 (d, *J* = 8.1, 2H), 8.16–8.08 (m, 2H), 8.02–7.98 (m, 2H), 7.97 (ddd, *J* = 5.4, 1.7, 0.8, 1H), 7.93 (dd, *J* = 5.3, 1.4, 1H), 7.87–7.80 (m, 4H), 7.63 (d, *J* = 6.4, 1H), 7.61 (d, *J* = 6.5, 1H), 7.47–7.40 (m, 3H), 7.35 (dd, *J* = 8.3, 5.2, 1H), 7.11 (dddd, *J* = 8.8, 6.6, 1.6, 1.4, 2H), 6.86 (t, *J* = 7.4, 2H), 6.25 (ddd, *J* = 7.7, 4.4, 1.1, 2H); ^{13}C NMR (125 MHz, CD_3CN, 35 of 40 signals observed) δ 169.3, 169.1, 155.2, 154.4, 153.7, 153.2, 152.2, 150.8, 146.5, 146.4, 143.4, 141.93, 141.90, 139.7, 138.1, 138.05, 134.8, 132.92, 132.87, 132.7, 131.8, 131.53, 131.47, 129.9, 129.8, 129.4, 129.2, 128.51, 128.50, 127.7, 127.1, 123.4, 123.3, 122.9, 122.8; IR (film): 3080, 3045, 1576, 1541, 1433, 840 cm^{-1}; HR-ESI-MS (*m/z*) [M – PF_6]$^+$ calcd for $C_{40}H_{27}ClN_4Ir^+$, 791.1553; found 791.1603.

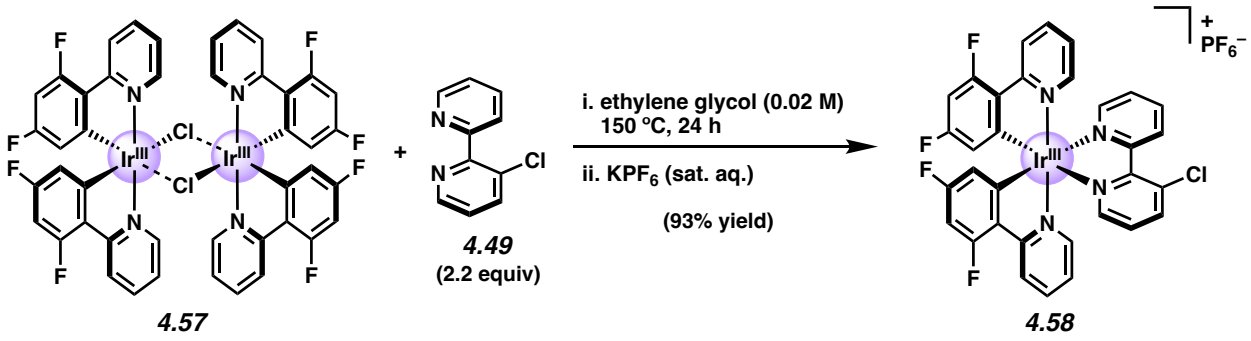

Fluorinated Ir Complex 4.58. To an 8-dram vial containing dichlorotetrakis[3,5-difluoro-2-(2-pyridinyl)phenyl]diiridium(III) (**4.57**, 200.0 mg, 0.165 mmol, 1.0 equiv) and chlorobipyridine **4.49** (69.0 mg, 0.362 mmol, 2.2 equiv) was added ethylene glycol (7.2 mL, 0.023 M). The resulting suspension was then sparged with N_2 for 15 minutes before being transferred to an Al-

block and stirred at 150 °C for 24 h. After cooling to 23 °C, the reaction was diluted with water (20 mL) before being transferred with water (5 mL) to a flask containing sat. aq. KPF_6 (50 mL), resulting in formation of a red precipitate. This mixture was then filtered through a plug of celite and washed sequentially with water (300 mL), hexanes (200 mL), and Et_2O (200 mL). The celite pad was then eluted with CH_2Cl_2 (200 mL) to redissolve the product, and the resulting filtrate was collected, dried over Na_2SO_4, concentrated under reduced pressure, and dried under reduced pressure (<1 torr) at 100 °C for 12 h to afford Ir(ppy)$_2$bpy complex **4.58** as a yellow solid (277.7 mg, 93% yield). **Fluorinated Ir Complex 4.58**. R_f 0.64 (14:1:1 CH_3CN:H_2O:sat. aq. KNO_3); ^{1}H NMR (500 MHz, CD_3CN): δ 9.36 (dt, *J* = 8.4, 0.9, 1H), 8.31 (d, *J* = 8.5, 2H), 8.23–8.15 (m, 2H), 8.12 (ddd, *J* = 5.4, 1.7, 0.7, 1H), 8.07 (dd, *J* = 5.3, 1.4, 1H), 7.95–7.87 (ddddd, *J* = 8.5, 7.9, 4.2, 1.6, 0.7, 2H), 7.71 (d, *J* = 5.8, 2H), 7.54 (ddd, *J* = 7.8, 5.5, 1.2, 1H), 7.45 (dd, *J* = 8.6, 5.3, 1H), 7.09 (dddd, *J* = 10.9, 7.8, 5.9, 1.4, 2H), 6.69 (dddd, *J* = 12.8, 9.4, 2.5, 2.1), 5.69 (ddd, *J* = 8.6, 7.2, 2.4); ^{13}C NMR (125 MHz, CD_3CN) δ 165.5, 165.4. 164.43, 164.38, 164.34, 164.28, 163.5, 163.43, 163.40, 163.38, 163.3, 161.31, 161.26, 155.21, 155.15, 155.1, 154.43, 154.37, 153.0, 152.6, 151.3, 150.84, 150.75, 144.1, 140.59, 140.57, 140.4, 135.1, 130.0, 129.8, 129.5, 128.91, 128.89, 128.87, 128.85, 128.81, 128.79, 128.77, 128.75, 125.0, 124.8, 124.7, 114.81, 114.79, 114.67, 114.65, 114.6, 114.51, 114.48, 100.03, 99.98, 99.81, 99.76, 99.6, 99.5; IR (film): 3088, 2973, 1739, 1604, 1575, 1479, 1430, 1406, 840 cm^{-1}; HR-ESI-MS (*m/z*) [M – PF_6]$^+$ calcd for $C_{32}H_{19}ClF_4N_4Ir^+$, 763.0864; found 763.0864.

(Note: Complex splitting patterns observed due to presence of fluorine atoms; these data represent empirically observed chemical shifts from the ^{13}C NMR spectrum)

4.8.2.2 Optimization of on-the-Complex Annulation with Benzyne

Representative Procedure for reaction optimization. Benzyne adduct 4.16 (Table 4.1, entry 11): To a 1-dram vial was added $Pd(OAc)_2$ (1.6 mg, 7.3 μmol, 10 mol%), bromo-$Ru(bpy)_3[PF_6]_2$ **4.14a** (68.6 mg, 73.1 μmol, 1.0 equiv), P(*o*-tolyl)$_3$ (2.2 mg, 7.3 μmol, 10 mol%), MeCN (0.50 mL, 0.15 M), PhMe (0.50 mL, 0.15 M), silyl triflate (43.6 mg, 73.1 μmol, 2.0 equiv, **4.15**), an oven-dried magnetic stir bar, and CsF (111 mg, 731 μmol, 10.0 equiv) sequentially. The reaction was then purged with N_2 for 5 min before being sealed with a Teflon-lined screw cap under a flow of N_2, sealed with Teflon tape and electrical tape, transferred to an Al-block, and stirred at 110 °C for 30 min. After cooling to 23 °C, the mixture was filtered through a plug of celite with MeCN (6 mL) and concentrated under reduced pressure. The yield was determined by ^{1}H NMR analysis with 1,3,5-trimethoxybenzene as an external standard.

Optimization efforts that deviate from the above conditions are indicated below.

Table 4.1. Optimization studies of on-the-complex annulation with benzyne. Yields were determined using ^{1}H NMR analysis with 1,3,5-trimethoxybenzene (TMB) as an external standard.

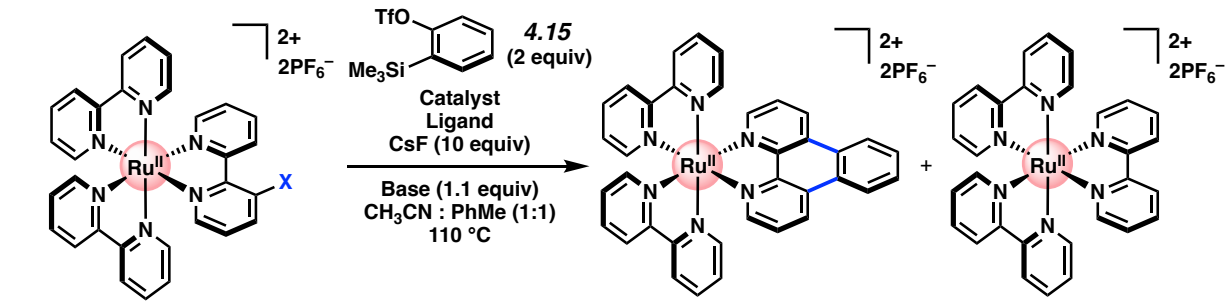

4.14 (***4.14a***: X = Br, ***4.14b***: X = Cl) ***4.16*** ***4.17***

Entry	*Catalyst*	*Ligand*	***X***	*Catalyst Loading*	*Ligand Loading*	*Base*	*CH_3CN : PhMe*	*Time*	***4.16***	***4.17***
1	$Pd(dba)_2$	P(*o*-tolyl)$_3$	Br	5 mol%	5 mol%	–	1 : 1	2 h	2%	48%
2	$Pd(PPh_3)_4$	P(*o*-tolyl)$_3$	Br	5 mol%	5 mol%	–	1 : 1	2 h	2%	48%
3	XPhos Pd G2		Br	5 mol%	5 mol%	–	1 : 1	2 h	4%	40%
4	$Pd(OAc)_2$	P(*o*-tolyl)$_3$	Br	5 mol%	5 mol%	–	1 : 1	2 h	26%	24%
5	$Pd(OAc)_2$	P(*o*-tolyl)$_3$	Br	10 mol%	30 mol%	–	1 : 1	2 h	60%	18%
6	$Pd(OAc)_2$	P(*o*-tolyl)$_3$	Br	10 mol%	30 mol%	Ag_2CO_3	1 : 1	2 h	54%	16%
7	$Pd(OAc)_2$	P(*o*-tolyl)$_3$	Br	10 mol%	30 mol%	K_2CO_3	1 : 1	2 h	41%	19%
8	$Pd(OAc)_2$	P(4-ClC_6H_4)$_3$	Br	10 mol%	30 mol%	–	1 : 1	2 h	32%	29%
9	$Pd(OAc)_2$	P(4-MeOC_6H_4)$_3$	Br	10 mol%	30 mol%	–	1 : 1	2 h	16%	35%
10	$Pd(OAc)_2$	SPhos	Br	10 mol%	30 mol%	–	1 : 1	2 h	44%	26%
11	$Pd(OAc)_2$	P(*o*-tolyl)$_3$	Br	10 mol%	10 mol%	–	1 : 1	30 min	71%	16%
12	$Pd(OAc)_2$	P(*o*-tolyl)$_3$	Br	10 mol%	10 mol%	–	3 : 1	30 min	61%	19%
13	$Pd(OAc)_2$	P(*o*-tolyl)$_3$	Br	10 mol%	10 mol%	–	9 : 1	30 min	44%	18%
14	$Pd(OAc)_2$	P(*o*-tolyl)$_3$	Br	10 mol%	10 mol%	–	100% CH_3CN	30 min	47%	16%
15	$Pd(OAc)_2$	P(*o*-tolyl)$_3$	Br	10 mol%	10 mol%	–	1 : 3	30 min	35%	28%
16	$Pd(OAc)_2$	P(*o*-tolyl)$_3$	Cl	10 mol%	10 mol%	–	1 : 1	30 min	78%	0%

Significant decomposition was observed when the halogenated bipyridyl ligand was not pre-ligated to the Ru complex (see below). It is postulated that deleterious intermediates such as ***4.51*** *may form under these conditions due to the propensity for bipyridyl ligands to undergo N,N'-chelation to transition metals.*

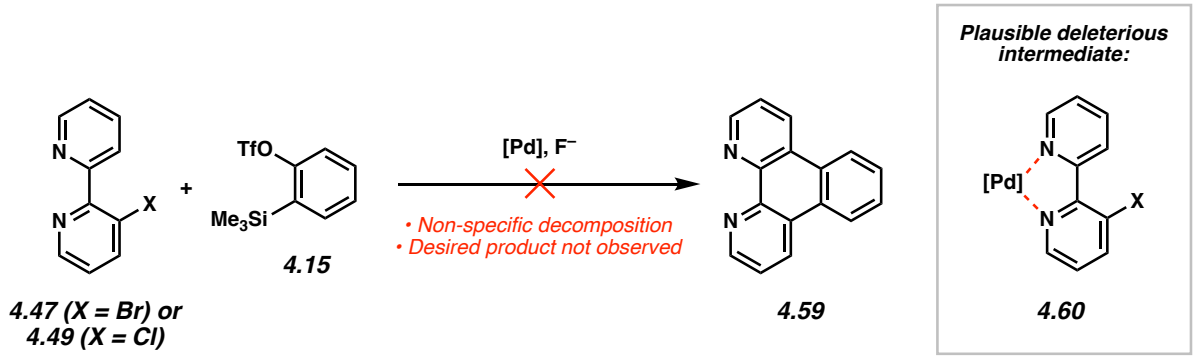

Figure 4.10. Unsuccessful aryne annulation of free ligands **4.47** and **4.49**.

4.8.2.3 Crystallographic Data

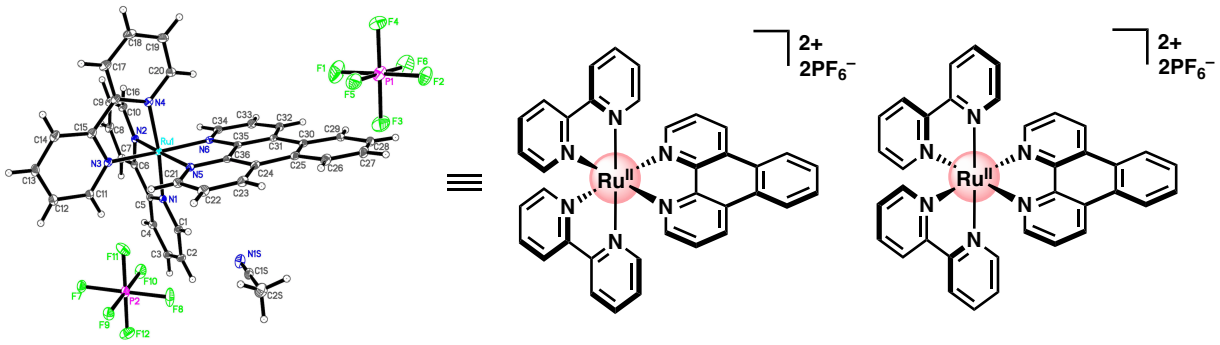

4.16
(crystallized as mixture of Δ- and Λ-isomers)

Figure 4.11. ORTEP representation of X-ray crystallographic structure **4.16**.

(CCDC Registry #2048567).

Table 4.2. Crystal data and structure refinement for compound **4.16**.

Identification code	cu_garg1904_a_sq_s	
Empirical formula	C38 H29 F12 N7 P2 Ru	
Formula weight	974.69	
Temperature	100(2) K	
Wavelength	1.54178 Å	
Crystal system	Monoclinic	
Space group	$P2_1/c$	
Unit cell dimensions	a = 11.6931(3) Å	α = 90°.
	b = 30.8685(9) Å	β = 112.4510(10)°.
	c = 12.4524(3) Å	γ = 90°.
Volume	4154.01(19) $Å^3$	
Z	4	
Density (calculated)	1.559 Mg/m^3	
Absorption coefficient	4.611 mm^{-1}	
F(000)	1952	
Crystal size	.16 x .08 x .04 mm^3	
Theta range for data collection	2.863 to 70.067°.	
Index ranges	-13<=h<=12, -36<=k<=37, -14<=l<=15	
Reflections collected	34574	
Independent reflections	7544 [R(int) = 0.0345]	
Completeness to theta = 67.679°	96.9 %	
Absorption correction	Semi-empirical from equivalents	
Max. and min. transmission	0.75 and 0.62	
Refinement method	Full-matrix least-squares on F^2	
Data / restraints / parameters	7544 / 0 / 542	
Goodness-of-fit on F^2	1.060	
Final R indices [I>2sigma(I)]	R1 = 0.0259, wR2 = 0.0644	
R indices (all data)	R1 = 0.0302, wR2 = 0.0657	
Extinction coefficient	n/a	
Largest diff. peak and hole	0.464 and -0.490 e.$Å^{-3}$	

4.8.2.4 Synthesis of Silyl Triflate Aryne Precursors

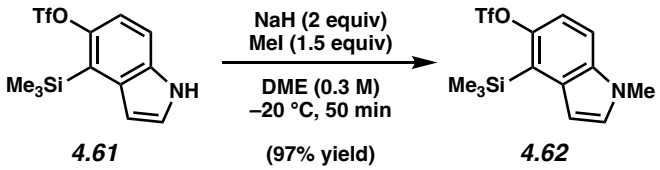

4.61 **(97% yield)** ***4.62***

Silyl triflate 4.62. To a solution of Garg 4,5-indolyne precursor (**4.61**, 913 mg, 2.71 mmol, 1.0 equiv) in DME (9 mL, 0.3 M) at –20 °C was added MeI (256 µL, 4.10 mmol, 1.5 equiv) and

NaH (60 wt% dispersion in mineral oil; 215 mg, 5.41 mmol, 2.0 equiv) sequentially. The reaction mixture was then stirred at –20 °C for 50 min before being quenched by addition of saturated aqueous NH_4Cl (5 mL). It was then allowed to warm to 23 °C before being transferred to a separatory funnel with H_2O (10 mL) and EtOAc (10 mL). The layers were then separated and the aqueous layer was extracted with EtOAc (3 x 15 mL). The combined organic layers were dried over $MgSO_4$, filtered, and concentrated under reduced pressure. The crude residue was then purified by flash chromatography (100% hexanes → 100:1 hexanes:EtOAc → 50:1 hexanes:EtOAc) to afford silyl triflate **4.62** as a viscous, pale yellow oil (927 mg, 97% yield). ***N*-Me silyl triflate 4.62**: R_f 0.63 (4:1 hexanes:EtOAc); ^1H NMR (500 MHz, $CDCl_3$): δ 7.33 (d, J = 9.0, 0.9, 1H), 7.20–7.14 (m, 2H), 6.68 (dd, J = 3.4, 0.6, 1H), 3.81 (s, 3H), 0.50 (s, 9H). Spectral data match those previously reported in the literature.[73]

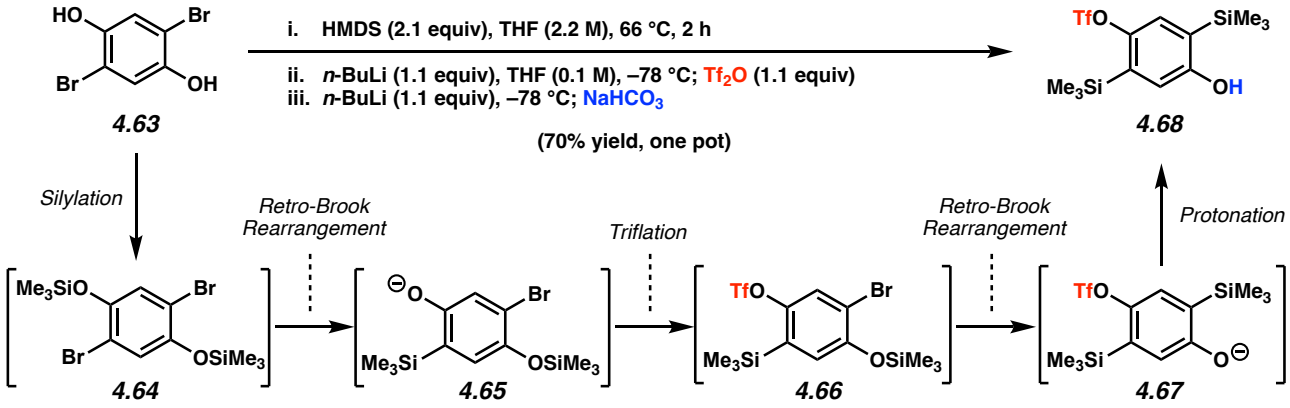

Silyl alcohol 4.68. To a stirred solution of 2,5-dibromohydroquinone (**4.63**, 2.60 g, 9.71 mmol, 1.0 equiv) in THF (4.40 mL, 2.20 M) was added HMDS (4.25 mL, 20.4 mmol, 2.1 equiv). The flask was topped with an air condenser and the system placed under N_2. The reaction was heated to 66 °C and stirred for 2 h. Then, the reaction mixture was allowed to cool to 23 °C and the volatiles were removed. THF (69 mL, 0.14 M) was then added and the mixture was cooled to –78 °C. *n*-BuLi (2.49 M in hexanes; 4.29 mL, 10.7 mmol, 1.1 equiv) was then added dropwise

over 8 min. The reaction mixture was then stirred at –78 °C for 25 min. Tf_2O (1.80 mL, 10.7 mmol, 1.1 equiv) was then added dropwise over 5 min at –78 °C, and the mixture was allowed to stir at this temperature for 25 min. *n*-BuLi (2.49 M in hexanes; 4.29 mL, 10.7 mmol, 1.1 equiv) was then added dropwise over 8 min. The reaction mixture was then stirred at –78 °C for 25 min. Finally, the reaction was quenched by addition of saturated aqueous $NaHCO_3$ (40 mL) in one portion and the mixture was allowed to warm to 23 °C before being transferred to a separatory funnel with Et_2O (100 mL) and the layers were separated. The aqueous layer was then extracted with Et_2O (2 x 100 mL) and the combined organic layers were dried over Na_2SO_4, filtered, and concentrated under reduced pressure. The crude residue was then purified by flash chromatography (100% hexanes → 3% EtOAc in hexanes → 5% EtOAc in hexanes) to afford silyl alcohol **4.68** as a viscous yellow oil (2.62 g, 70% yield). **Silyl alcohol 4.68**: R_f 0.39 (9:1 hexanes:EtOAc) ^{1}H NMR (600 MHz, $CDCl_3$): δ 7.23 (s, 1H), 6.74 (s, 1H), 4.88 (s, 1H), 0.35 (s, 9H), 0.31 (s, 9H). Spectral data match those previously reported in the literature.[67]

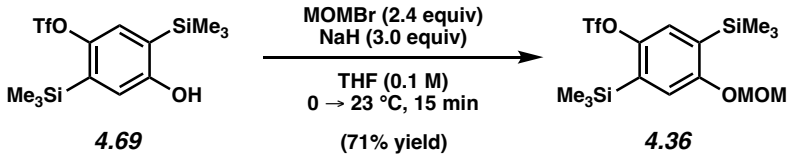

Methoxymethyl ether 4.36. To a stirred solution of silyl alcohol **4.69** (1.03 g, 2.66 mmol, 1.0 equiv) in THF (25 mL, 0.10 M) at 0 °C was added sodium hydride (dry, 95%; 202 mg, 7.99 mmol, 3.0 equiv) in one portion. The solution was then stirred at 0 °C for 15 min, followed by dropwise addition of bromomethyl methyl ether (522 μL, 6.39 mmol, 2.40 equiv) over 1 minute. Following addition, the reaction was allowed to warm to 23 °C and stirred for 15 min before being diluted with Et_2O (30 mL). H_2O (30 mL) was then added over 30 seconds and the mixture was transferred with Et_2O (5 mL) to a separatory funnel. The layers were separated and the

aqueous layer was extracted with Et_2O (3 x 30 mL). The combined organic layers were then washed with H_2O (30 mL), dried over Na_2SO_4, and concentrated under reduced pressure. The crude residue was then purified by flash chromatography (100% hexanes) to afford methoxy methyl ether **4.36** as a white solid (814 mg, 71% yield). **Methoxymethyl ether 4.36**: mp: 37.5–38.5 ºC; R_f 0.56 (9:1 hexanes:EtOAc); ^{1}H NMR (500 MHz, $CDCl_3$): δ 7.25 (s, 1H), 7.14 (s, 1H), 5.19 (s, 2H), 3.48 (s, 3H), 0.36 (s, 9H), 0.28 (s, 9H); ^{13}C NMR (125 MHz, CD_3CN) δ 160.5, 149.6, 135.3, 132.8, 126.1, 126.0, 119.2, 118.7 (q, J = 320.5 Hz), 94.3, 56.3, –0.7, –1.2; IR (film): 2957, 1468, 1420, 1341, 1246, 1210, 1144, 1082, 1013, 945, 841, 757, 633 cm^{-1}; HR-GC-MS (*m/z*) $[M]^+$ calcd for $C_{15}H_{25}F_3O_5SSi_2^+$ 430.09133; found 430.0908.

4.8.2.5 Scope of Pd-Catalyzed Aryne Annulation

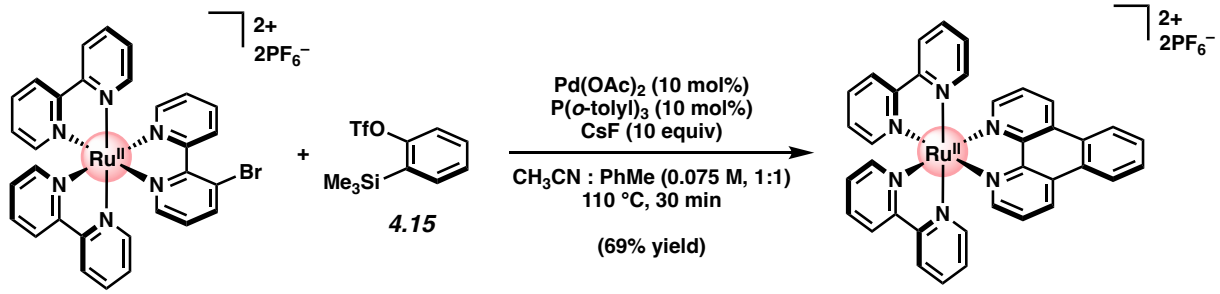

Representative Procedure A for aryne annulations (Figure 4.3, benzyne adduct 4.16 used as an example). To a 1-dram vial was added $Pd(OAc)_2$ (1.5 mg, 6.7 µmol, 10 mol%), Bromo-Ru(bpy)$_3$[PF_6]$_2$ **4.14a** (62.2 mg, 0.066 mmol, 1.0 equiv), P(*o*-tolyl)$_3$ (2.2 mg, 7.2 µmol, 10 mol%), MeCN (0.50 mL, 0.15 M), PhMe (0.50 mL, 0.15 M), silyl triflate **4.15** (40.1 mg, 0.134 mmol, 2.0 equiv), an oven-dried magnetic stir bar, and CsF (101 mg, 0.663 mmol, 10.0 equiv) sequentially. The reaction was then purged with N_2 for 5 min before being capped with a Teflon-

lined screw cap under a flow of N_2, sealed with Teflon tape and electrical tape, transferred to an Al-block, and stirred at 110 °C for 30 min. After cooling to 23 °C, the mixture was filtered through a plug of celite with MeCN (6 mL), and concentrated under reduced pressure. The crude residue was adsorbed onto silica gel (500 mg) under reduced pressure and purified by flash chromatography (100% EtOAc → 14:1:1 MeCN:H_2O:sat. aq. KNO_3). To the concentrated aqueous mixture was added saturated aqueous KPF_6 (50 mL) to precipitate the desired product, and the resultant mixture was transferred to a separatory funnel with CH_2Cl_2 (50 mL). The layers were separated and the aqueous layer was extracted with CH_2Cl_2 (2 x 50 mL). The combined organic layers were then dried over Na_2SO_4, concentrated under reduced pressure and dried under reduced pressure (<1 torr) at 100 °C for 12 h to afford benzyne adduct **4.16** as a deep red solid (69% yield, average of two experiments). **Benzyne adduct 4.16**: mp >250 °C; R_f 0.68 (7:2:1 MeCN:H_2O:sat. aq. KNO_3); ^{1}H NMR (500 MHz, CD_3CN): δ 9.23 (dd, *J* = 8.4, 0.9, 2H), 8.92–8.88 (m, 2H), 8.55 (d, *J* = 8.3, 2H), 8.51 (d, *J* = 8.3, 2H), 8.11 (td, *J* = 7.9. 1.5, 2H), 8.07 (dd, *J* = 5.3, 0.9, 2H), 8.02–7.98 (m, 4H), 7.85 (d, *J* = 5.8, 2H), 7.79 (dd, *J* = 8.2, 5.3, 2H), 7.63 (d, *J* = 5.6, 2H), 7.46 (td, *J* = 6.9, 1.3, 2H), 7.23 (td, *J* = 6.9, 1.2, 2H); ^{13}C NMR (125 MHz, CD_3CN) δ 158.09, 153.11, 152.91, 152.82, 149.00, 148.82, 138.70, 133.18, 133.03, 131.32, 131.26, 131.21, 129.14, 128.34, 127.42, 127.28, 125.64, 125.60, 125.13; IR (film): 1604, 1466, 1447, 1437, 838, 761, 731, 557 cm^{-1}; HR-ESI-MS (*m/z*) $[M - PF_6]^+$ calcd for $C_{36}H_{26}F_6N_6PRu^+$, 789.09043; found 789.0905.

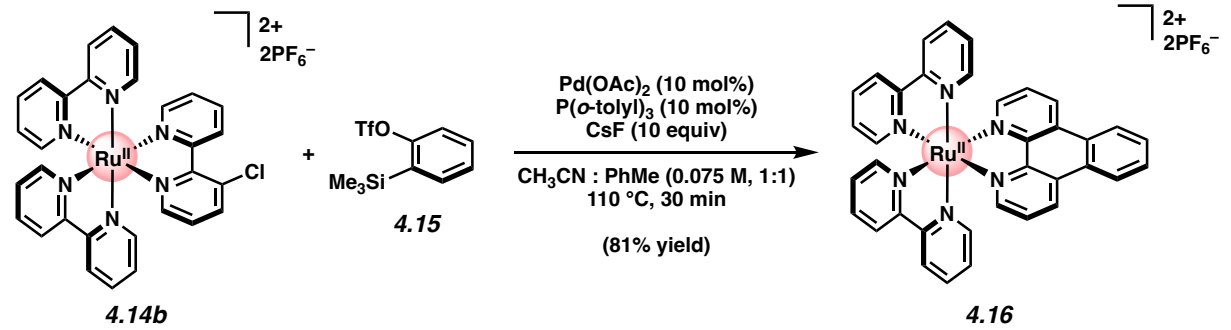

Benzyne adduct 4.16. Followed representative procedure A. Purification by flash chromatography (100% EtOAc → 14:1:1 CH_3CN:H_2O:sat. aq. KNO_3) afforded benzyne adduct **4.16** (81% yield, average of two experiments) as a red solid. Spectral data matched those provided above.

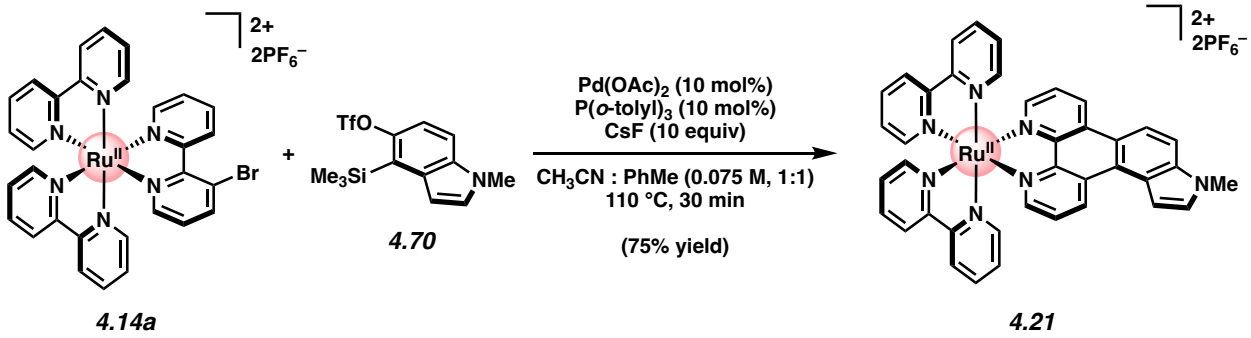

Indolyne adduct 4.21. Followed representative procedure A. Purification by flash chromatography (7:2:1 CH_3CN:H_2O:sat. aq. KNO_3) afforded indolyne adduct **4.21** (75% yield, average of two experiments) as a red solid. **Indolyne adduct 4.21**: mp >250 °C; R_f 0.63 (7:2:1 CH_3CN:H_2O:sat. aq. KNO_3); ^{1}H NMR (600 MHz, CD_3CN): δ 9.71 (dd, J = 8.8, 1.1, 1H), 9.27 (d, J = 8.8, 1H), 8.73 (d, J = 9.1, 1H), 8.54 (ddt, J = 8.3, 4.4, 1.1, 2H), 8.51–8.48 (m, 2H), 8.12–8.07 (m, 3H), 8.06 (dd, J = 5.2, 1.1, 1H), 8.01 (dd, J = 5.3, 1.1, 1H), 8.00–7.96 (m, 2H), 7.87–7.81 (m, 3H), 7.75 (dd, J = 8.6, 5.2, 1H), 7.67 (d, J = 3.3, 1H), 7.64–7.60 (m, 2H), 7.57 (d, J = 3.3, 1H), 7.57–7.43 (m, 2H), 7.22–7.18 (m, 2H), 4.04 (s, 3H); ^{13}C NMR (125 MHz, CD_3CN): δ

158.6, 158.5, 158.4, 153.23, 153.22, 151.71, 151.66, 149.1, 147.8, 139.1, 139.0, 138.7, 136.2, 133.6, 133.4, 132.8, 132.6, 128.92, 128.90, 128.76, 128.75, 127.6, 127.3, 125.61, 125.60, 125.5, 125.1, 123.9, 123.6, 115.2, 103.9, 34.4; IR (film): 3707, 2681, 2973, 2923, 1055, 1033; HR-ESI-MS (*m/z*) $[M - PF_6]^+$ calcd for $C_{39}H_{29}N_7P\,F_6Ru^+$, 842.1180; found 842.1110.

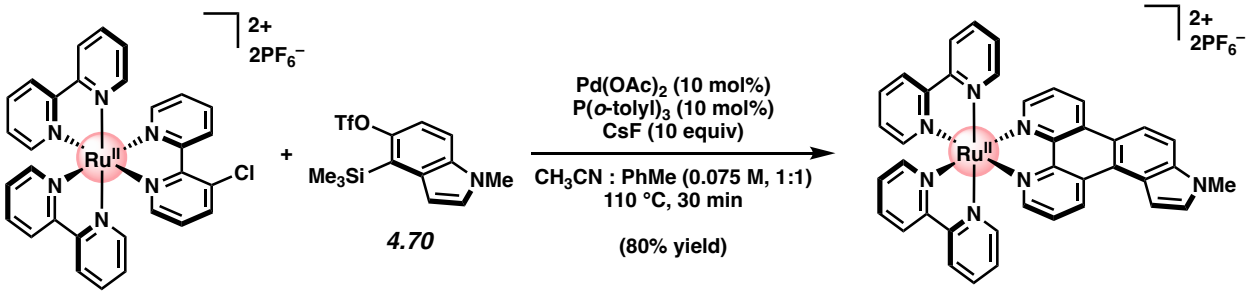

4.14b *4.70* *4.21*

Indolyne adduct 4.21. Followed representative procedure A. Purification by flash chromatography (7:2:1 CH_3CN:H_2O:sat. aq. KNO_3) afforded indolyne adduct **4.21** (80% yield, average of two experiments) as a red solid. Spectral data matched those provided above.

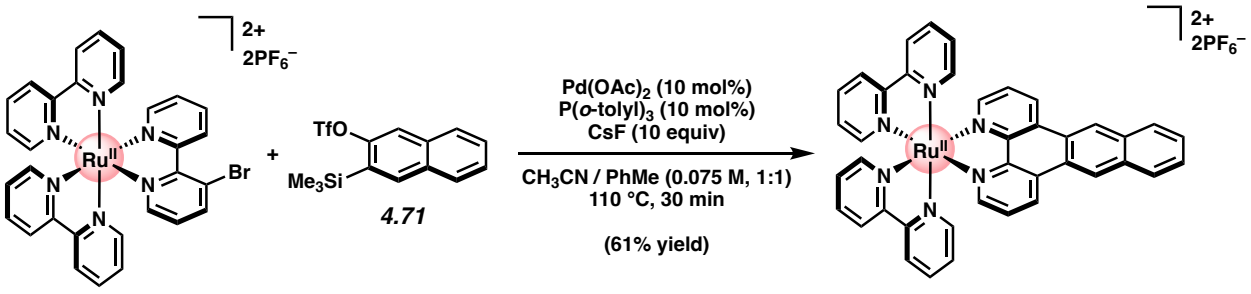

4.14a *4.71* *4.22*

Representative Procedure B for aryne annulations (Figure 4.3, naphthalyne adduct 4.22 used as an example). To a 1-dram vial was added $Pd(OAc)_2$ (1.4 mg, 6.4 μmol, 10 mol%), Bromo-Ru(bpy)$_3$[PF_6]$_2$ **4.14a** (60.0 mg, 0.064 mmol, 1.0 equiv), P(*o*-tolyl)$_3$ (2.0 mg, 6.4 μmol, 10 mol%), MeCN (0.50 mL, 0.15 M), PhMe (0.50 mL, 0.15 M), silyl triflate **4.71** (44.6 mg,

0.128 mmol, 2.0 equiv), an oven-dried magnetic stir bar, and CsF (97.1 mg, 0.639 mmol, 10.0 equiv) sequentially. The reaction was then purged with N_2 for 5 min before being sealed with a Teflon-lined screw cap under a flow of N_2, sealed with Teflon tape and electrical tape, transferred to an Al-block, and stirred at 110 °C for 30 min. After cooling to 23 °C, the mixture was filtered through a plug of celite with MeCN (6 mL), and concentrated under reduced pressure. The crude residue was adsorbed onto silica gel (500 mg) under reduced pressure and purified by flash chromatography (100% EtOAc → 7:2:1 MeCN:H_2O:sat. aq. KNO_3). To the concentrated aqueous mixture was added saturated aqueous KPF_6 (50 mL) to precipitate the desired product, and the resultant mixture was transferred to a separatory funnel with CH_2Cl_2 (50 mL). The layers were separated and the aqueous layer was extracted with CH_2Cl_2 (2 x 50 mL). The combined organic layers were then concentrated under reduced pressure before being redissolved in CH_3CN (10 mL). Activated charcoal (150 mg) was then added the mixture was agitated for 10 seconds before being filtered over celite, concentrated under reduced pressure, and dried under reduced pressure (<1 torr) at 100 °C for 12 h to afford naphthalyne adduct **4.22** as a deep red solid (61% yield, average of two experiments). **Naphthalyne adduct 4.22**: mp >250 °C; R_f 0.57 (7:2:1 CH_3CN:H_2O:saturated aqueous KNO_3); ^{1}H NMR (500 MHz, CD_3CN): δ 9.41 (s, 2H), 9.29 (dd, *J* = 8.0, 1.2, 2H), 8.56–8.51 (m, 4H), 8.30–8.27 (m, 2H), 8.11 (td, *J* = 10, 1.4, 2H), 8.03–7.99 (m, 4H), 7.85 (dd, *J* = 5.5, 0.5, 2H), 7.79–7.76 (m, 4H), 7.72 (dd, *J* = 5.6, 0.5, 2H), 7.46 (ddd, *J* = 7.8, 5.7, 1.3, 2H), 7.27 (ddd, *J* = 7.8, 5.7, 1.3, 2H); ^{13}C NMR (125 MHz, CD_3CN): δ 158.0, 157.9, 152.9, 152.8, 152.3, 149.5, 138.8, 138.6, 133.9, 133.0, 132.2, 129.3, 129.1, 128.5, 128.4, 127.7, 126.4, 125.5, 125.2, 125.1; IR (film): 3681, 2981, 2923, 1332, 1054, 1033, 1013 cm^{-1}; HR-ESI-MS (*m/z*) $[M - PF_6]^+$ calcd for $C_{40}H_{27}N_6PF_6Ru^+$, 839.1061; found 839.1050.

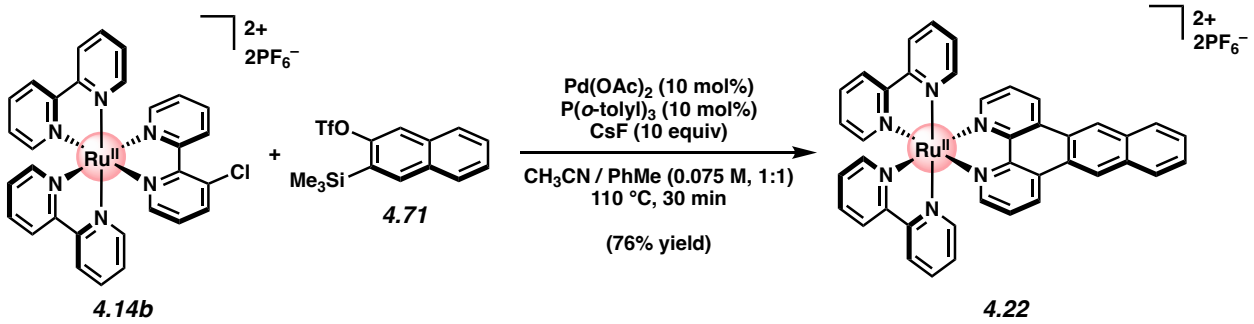

Naphalyne adduct 4.22. Followed representative procedure B. Purification by flash chromatography (7:2:1 CH_3CN:H_2O:sat. aq. KNO_3) afforded naphthalyne adduct **4.22** (76% yield, average of two experiments) as a red solid. Spectral data matched those provided above.

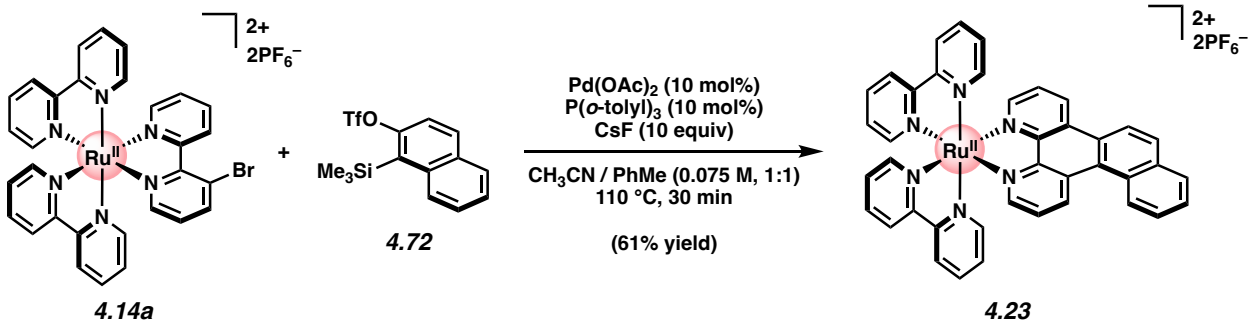

Naphthalyne adduct 4.23. Followed representative procedure B. Purification by flash chromatography (14:2:1 CH_3CN:H_2O:sat. aq. KNO_3) afforded naphthalyne adduct **4.23** (61% yield, average of two experiments) as a red solid. **Naphthalyne adduct 4.23**: mp >250 °C; R_f 0.70 (7:2:1 CH_3CN:H_2O:sat. aq. KNO_3); ^{1}H NMR (600 MHz, CD_3CN): δ 9.52 (d, J = 8.7, 1H), 9.29 (d, J = 8.7, 1H), 8.96 (d, J = 8.3, 1H), 8.82 (d, J = 8.7, 1H), 8.57–8.50 (m, 4H), 8.37 (d, J = 8.8, 1H), 8.24 (d, J = 7.9, 1H), 8.15–8.09 (m, 4H) 8.00 (t, J = 7.8, 2H), 7.89–7.78 (m, 6H), 7.69 (d, J = 5.2, 1H), 7.64 (d, J = 5.6, 1H), 7.49–7.44 (m, 2H), 7.23–7.20 (m, 2H); ^{13}C NMR (125 MHz, CD_3CN): δ 158.1, 157.9, 152.92, 152.86, 152.8, 152.0, 149.1, 148.6, 138.8, 138.7, 138.0, 135.3, 133.7, 132.0, 130.8, 130.6, 130.5, 130.0, 129.1, 128.9, 128.6, 128.5, 128.3, 127.3, 126.9,

126.3, 125.2, 125.1, 121.6; IR (film): 3663, 3589, 3084, 2925, 2854 cm^{-1}; HR-ESI-MS (*m/z*) [M – PF_6]$^+$ calcd for $C_{40}H_{27}N_6PF_6Ru^+$, 839.1061; found 839.1119.

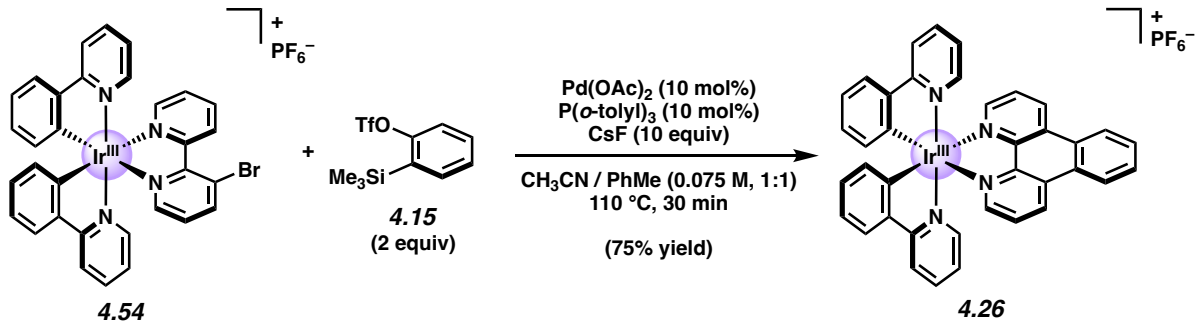

4.54 *4.26*

Ir-benzyne adduct 4.26. Followed representative procedure A. Purification by flash chromatography (9:1 benzene:acetonitrile → 3:2 benzene:acetonitrile) afforded Ir-benzyne adduct **4.26** (75% yield, average of two experiments) as a dark orange solid. **Ir-benzyne adduct 4.26**: mp >250 °C; R_f 0.59 (7:2:1 CH_3CN:H_2O:sat. aq. KNO_3); ^1H NMR (600 MHz, CD_3CN): δ 9.30 (dd, *J* = 8.6, 0.9, 1H), 8.92–8.88 (m, 1H), 8.29 (dd, *J* = 5.1, 1.3, 1H), 8.06 (d, *J* = 8.3, 1H), 8.00–7.98 (m, 1H), 7.89 (dd, *J* = 8.6, 5.1, 1H), 7.84 (dd, *J* = 8.0, 1.1, 1H), 7.79 (ddd, *J* = 8.2, 7.6, 1.5, 1H), 7.49 (ddd, *J* = 6.0, 1.5, 0.7, 1H), 7.29 (dd, *J* = 8.4, 5.3, 1H), 7.06–7.00 (m, 4H), 6.90 (tdd, *J* = 7.5, 2.5, 1.3, 2H), 6.22 (ddd, 7.5, 4.8, 1.2, 2H); ^{13}C NMR (125 MHz, CD_3CN): δ 168.33, 151.5, 151.2, 150.4, 147.9, 145.1, 139.3, 134.7, 132.6, 131.7, 131.3, 131.1, 129.1, 128.2, 125.8, 125.5, 124.3, 123.5, 120.7; IR (film): 2981, 1735, 1689, 1368, 1149 cm^{-1}; HR-ESI-MS (*m/z*) [M – PF_6]$^+$ calcd for $C_{38}H_{26}N_4Ir^+$, 731.1787; found 731.1704.

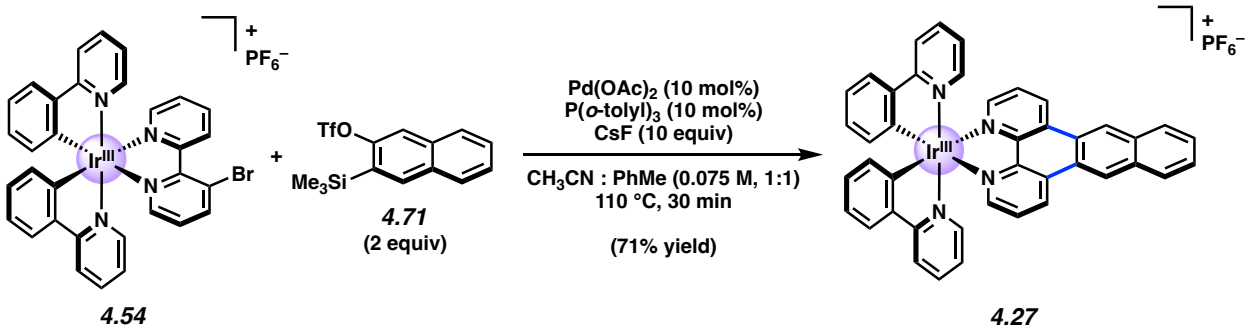

Ir-naphthalyne adduct 4.27. Followed representative procedure B. Purification by flash chromatography (100% EtOAc → 14:2:1 MeCN:H_2O:sat. aq. KNO_3) afforded naphthalyne adduct **4.27** as an orange solid (71% yield, average of two experiments). **Naphthalyne adduct 4.27**: mp >200 °C; R_f 0.70 (14:2:1 CH_3CN:H_2O:saturated aqueous KNO_3); ^{1}H NMR (500 MHz, CD_3CN): δ 9.41 (s, 2H), 9.36 (dd, *J* = 8.6, 1.2, 2H), 8.30–8.27 (m, 2H), 8.24 (dd, *J* = 5.4, 1.3, 2H), 8.07 (d, *J* = 8.3, 2H), 7.89–7.77 (m, 10H), 7.59 (ddd, *J* = 6.0, 1.5, 0.8, 2H), 7.09 (td, *J* = 7.2, 1.5, 2H), 6.97 (td, *J* = 7.7, 1.4, 2H), 6.91 (td, *J* = 6.8, 1.5, 2H), 6.38 (dd, *J* = 7.5, 0.8, 2H); ^{13}C NMR (125 MHz, CD_3CN): δ 167.8, 150.71, 150.65, 149.8, 148.1, 144.6, 138.8, 134.0, 133.4, 132.2, 132.0, 130.7, 128.7, 128.5, 128.0, 125.8, 125.2, 124.9, 123.7, 122.9, 120.2; IR (film): 3050, 2924, 2855, 1608, 1479 cm^{-1}; HR-ESI-MS (*m/z*) $[M - PF_6]^+$ calcd for $C_{42}H_{27}N_4Ir^+$, 780.1859; found 780.1835.

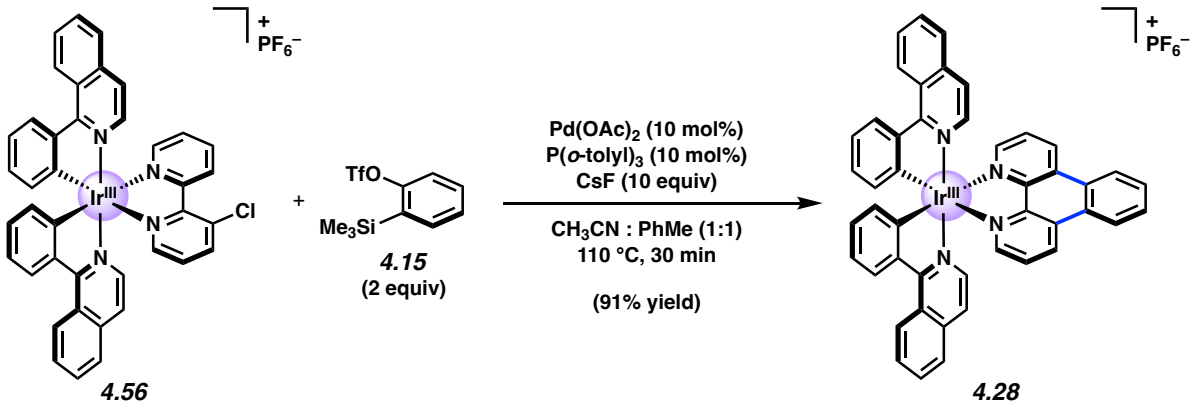

Isoquinolinyl adduct 4.28. Followed representative procedure A. Purification by flash chromatography (100% EtOAc → 14:1:1 MeCN:H_2O:sat. aq. KNO_3) afforded isoquinolinyl adduct **4.28** as a red solid (91% yield, average of two experiments). **Isoquinolinyl adduct 4.28**: mp >200 °C; R_f 0.63 (14:1:1 CH_3CN:H_2O:saturated aqueous KNO_3); ^1H NMR (500 MHz, CD_3CN): δ 9.30 (dd, *J* = 8.5, 1.3, 2H), 9.04 (d, *J* = 8.5, 2H), 8.92–8.84 (m, 2H), 8.42 (d, *J* = 8.0, 2H), 8.18 (dd, *J* = 5.1, 1.3, 2H), 8.01–7.97 (m, 2H), 7.93–7.90 (m, 2H), 7.87–7.78 (m, 6H), 7.40 (d, *J* = 6.5, 2H), 7.26 (d, *J* = 6.5, 2H), 7.18 (ddd, *J* = 8.1, 7.0, 1.3, 2H), 6.93 (td, *J* = 7.5, 1.2, 2H), 6.40 (dd, *J* = 7.6, 1.2, 2H); ^{13}C NMR (125 MHz, CD_3CN): δ 169.5, 154.6, 151.6, 147.8, 146.7, 141.9, 138.0, 134.8, 133.1, 132.8, 131.8, 131.4, 131.2, 129.9, 129.1, 128.4, 128.3, 127.7, 127.1, 125.5, 123.3, 122.7; IR (film): 3047, 1577, 1541, 1435, 841 cm^{-1}; HR-ESI-MS (*m/z*) $[M - PF_6]^+$ calcd for $C_{46}H_{30}N_4Ir^+$, 831.2100; found 831.2111.

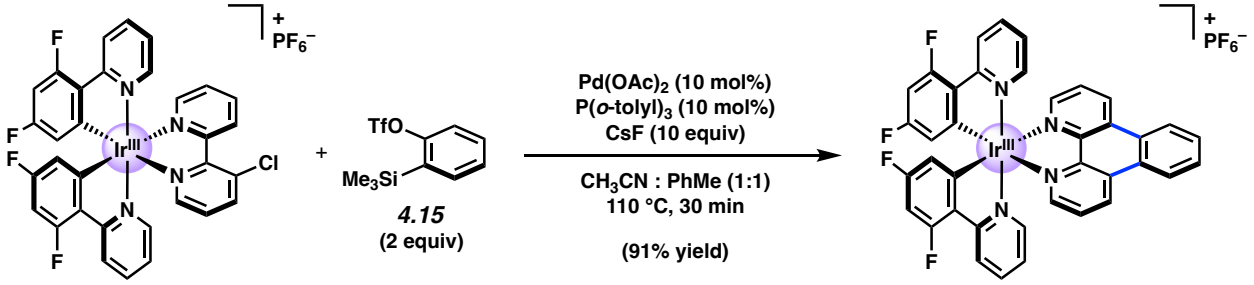

Fluorinated Ir adduct 4.29. Followed representative procedure A. Purification by flash chromatography (100% EtOAc → 14:1:1 MeCN:H_2O:sat. aq. KNO_3) afforded fluorinated Ir adduct **4.29** as a golden solid (91% yield, average of two experiments). **Fluorinated Ir adduct 4.29**: mp >200 °C; R_f 0.64 (14:1:1 CH_3CN:H_2O:saturated aqueous KNO_3); ^1H NMR (500 MHz, CD_3CN): δ 9.33 (dd, *J* = 8.6, 1.3, 2H), 8.94–8.82 (m, 2H), 8.35–8.30 (m, 4H), 8.01–7.97 (m, 2H), 7.92 (dd, *J* = 8.5, 5.1, 2H), 7.85 (td, *J* = 8.0, 1.3, 2H), 7.54 (ddd, *J* = 5.9, 1.6, 0.7, 2H), 6.93 (ddd, *J* = 7.8, 6.0, 1.4, 2H), 6.72 (ddd, *J* = 12.5, 9.5, 2.5, 2H), 5.84 (dd, *J* = 8.6, 2.4, 2H); ^{13}C

NMR (125 MHz, CD_3CN): δ 165.5, 165.4, 164.7, 164.6, 163.5, 163.43, 163.40, 163.3, 161.4, 161.3, 155.33, 155.28, 151.9, 150.8, 147.6, 140.4, 135.3, 132.0, 131.3, 129.12, 129.11, 129.09, 129.05, 128.4, 125.5, 124.8, 124.7, 124.5, 114.91, 114.89, 114.77, 114.75, 99.9, 99.7, 99.5; IR (film): 3082, 1739, 1603, 1406, 1105, 840 cm^{-1}; HR-ESI-MS (*m/z*) $[M - PF_6]^+$ calcd for $C_{38}H_{22}F_4N_4Ir^+$, 803.1410; found 803.1416.

(Note: Complex splitting patterns observed due to presence of fluoride substituents; these data represent empirically observed chemical shifts from the ^{13}C NMR spectrum)

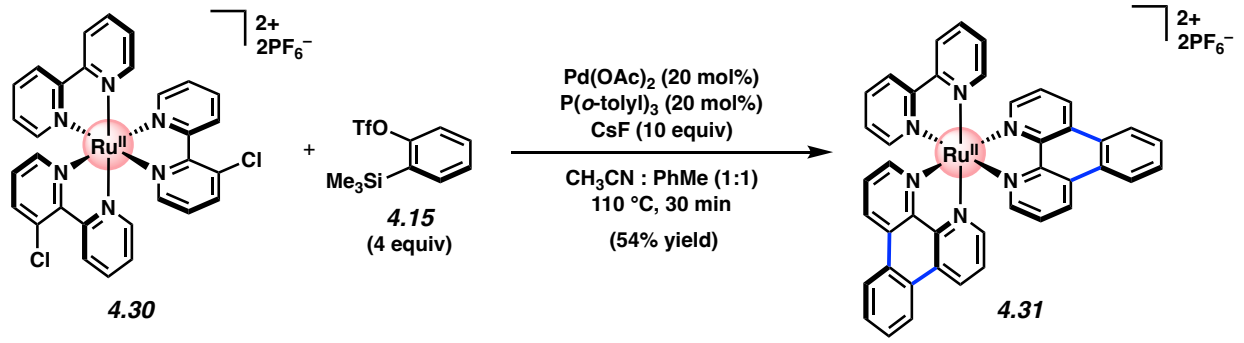

Bis(annulation) adduct 4.31. Followed representative procedure A. Purification by flash chromatography (100% EtOAc → 14:1:1 CH_3CN:H_2O:sat. aq. KNO_3) afforded adduct **4.31** (54% yield, average of two experiments) as a red solid. **Bis(annulation adduct) 4.31**: mp >250 °C; R_f 0.77 (7:2:1 MeCN:H_2O:sat. aq. KNO_3); ^1H NMR (500 MHz, CD_3CN): δ 9.27 (d, *J* = 8.6, 1H), 9.16 (d, *J* = 8.6, 1H), 8.96–8.85 (m, 2H), 8.54 (d, *J* = 8.4, 1H), 8.17 (d, *J* = 5.2, 1H), 8.07–7.92 (m, 4H), 7.83 (dd, *J* = 8.5, 5.3, 1H), 7.74 (d, *J* = 5.3, 1H), 7.61 (dd, *J* = 8.2, 5.4, 1H), 7.28 (t, *J* = 6.4, 1H); ^{13}C NMR (125 MHz, CD_3CN, 19 of 21 signals observed) δ 158.1, 153.1, 152.9, 152.8, 149.0, 148.8, 138.7, 133.2, 133.0, 131.32, 131.26, 131.2, 129.14, 128.3, 127.4, 127.3,

125.64, 125.60, 125.1; IR (film): 1467, 1436, 1407, 840, 762 cm^{-1}; HR-ESI-MS (*m/z*) $[M - PF_6]^+$ calcd for $C_{42}H_{28}N_6F_6PRu^+$, 863.10662; found 863.1080.

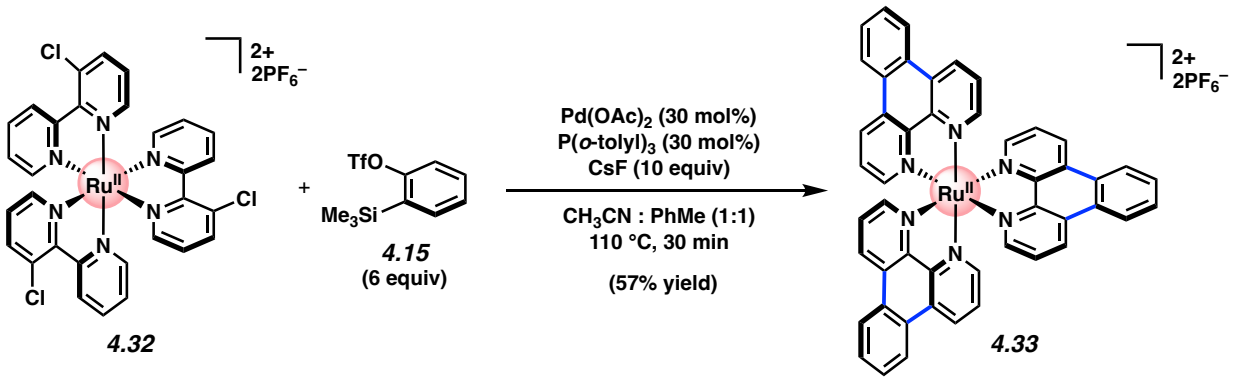

(Tris)annulation adduct 4.33. Followed representative procedure B. Purification by flash chromatography (100% EtOAc → 14:1:1 CH_3CN:H_2O:sat. aq. KNO_3) afforded adduct **4.33** (57% yield, average of two experiments) as a red solid. (**Tris)annulation adduct 4.33**: mp >250 °C; R_f 0.78 (7:2:1 CH_3CN:H_2O:sat. aq. KNO_3); ^1H NMR (500 MHz, CD_3CN): δ 9.22 (dd, *J* = 8.7, 0.7, 6H), 8.93–8.90 (m, 6H), 8.08 (dd, *J* = 5.3, 1.0, 6H), 8.03–7.99 (m, 6H), 7.68 (dd, *J* = 8.3, 5.3, 6H); ^{13}C NMR (125 MHz, CD_3CN) δ 153.1, 149.0, 133.1, 131.3, 131.2, 129.2, 127.3, 125.6; IR (film): 2962, 1435, 1407, 1260, 1211, 1084, 1021, 840, 805, 758, 557; HR-ESI-MS (*m/z*) $[M - PF_6]^+$ calcd for $C_{48}H_{30}F_6N_6PRu^+$, 937.12227; found 937.1227.

4.8.2.6 Synthesis and Trapping Experiments of Ru-Centered Aryne

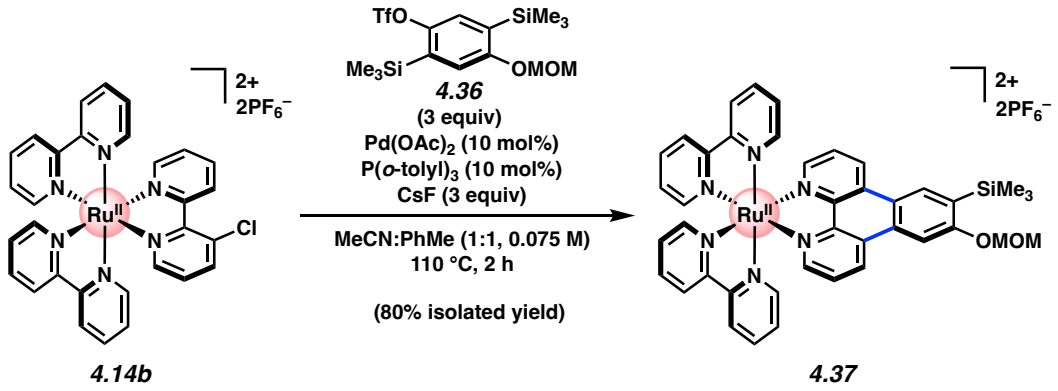

Methoxymethyl ether adduct 4.37. To a 20 mL scintillation vial was added $Pd(OAc)_2$ (10.1 mg, 44.8 µmol, 10 mol%), chloro-Ru(bpy)$_3$[PF_6]$_2$ **4.14b** (400.5 mg, 0.448 mmol, 1.0 equiv), P(*o*-tolyl)$_3$ (13.6 mg, 44.8 mmol, 10 mol%), MeCN (3.0 mL), PhMe (3.0 mL), silyl triflate **4.36** (564 mg, 1.31 mmol, 3.0 equiv), an oven-dried magnetic stir bar, and CsF (204 mg, 1.34 mmol, 3.0 equiv) sequentially. The reaction was then purged with N_2 for 5 min before being sealed with a Teflon-lined screw cap under a flow of N_2, sealed with Teflon tape and electrical tape, transferred to an Al-block, and stirred at 110 °C for 2 h. After cooling to 23 °C, the mixture was filtered through a plug of celite with MeCN (10 mL), and concentrated under reduced pressure. The crude residue was adsorbed onto SiO_2 and purified by flash chromatography (100% EtOAc → 14:1:1 MeCN:H_2O:sat. aq. KNO_3). To the concentrated aqueous mixture was added saturated aqueous KPF_6 (100 mL) to precipitate the desired product, and the resultant mixture was transferred to a separatory funnel with CH_2Cl_2 (50 mL). The layers were separated and the aqueous layer was extracted with CH_2Cl_2 (2 x 50 mL). The combined organic layers were then concentrated under reduced pressure before being redissolved in CH_3CN (10 mL). Activated charcoal (500 mg) was then added and the mixture was agitated for 10 seconds before being filtered over celite, concentrated under reduced pressure, and dried under reduced pressure (<1 torr) at 100 °C for 12 h to afford methoxymethyl ether adduct **4.37** as a red solid (380 mg, 80%

yield). **Methoxymethyl ether adduct 4.37**: mp >250 °C; R_f 0.79 (7:2:1 CH_3CN:H_2O:saturated aqueous KNO_3); ^1H NMR (500 MHz, CD_3CN): δ 9.25 (dd, *J* = 12.0, 8.5, 2H), 8.88 (s, 1H), 8.60 (dd, *J* = 8.2, 2H), 8.56 (dd, *J* = 8.2, 2H), 8.34 (s, 1H), 8.16–8.11 (m, 3H), 8.08 (d, *J* = 5.2, 1H), 8.03 (tt, *J* = 7.9, 1.7, 2H), 7.91 (d, *J* = 5.8, 2H), 7.82 (td, *J* = 8.4, 5.3, 2H), 7.69 (t, *J* = 6.8, 2H), 7.50 (td, *J* = 6.6, 1.0, 2H), 7.28 (dd, *J* = 12.9, 5.5, 2H), 5.58 (q, *J* = 5.5, 2H), 3.54 (s, 3H), 0.48 (s, 9H); ^{13}C NMR (100 MHz, CD_3CN) δ 163.8, 158.1, 157.9, 152.9, 152.84, 152.79, 152.8, 152.7, 151.6, 149.2, 147.7, 138.7, 138.6, 134.4, 133.2, 132.7, 132.6, 131.8, 131.2, 130.8, 128.5, 128.3, 128.3, 127.3, 127.1, 125.2, 125.1, 122.6, 106.7, 94.9, 57.0, 55.2, -1.02; IR (film): 3464, 3079, 1604, 1369, 1345 cm^{-1}; HR-ESI-MS (*m/z*) $[M - PF_6]^+$ calcd for $C_{41}H_{38}F_6N_6O_2PRuSi^+$, 921.15163; found 921.1541.

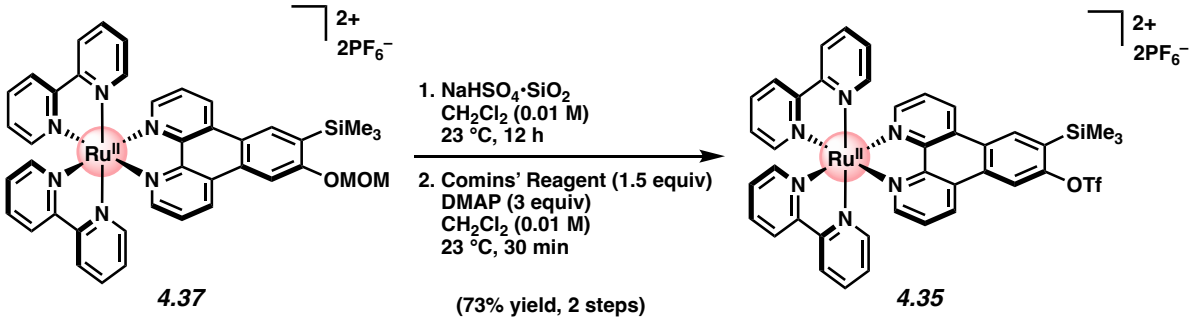

Silyl triflate 4.35. To a stirred solution of methoxymethyl ether **4.37** (259 mg, 0.243 mmol, 1.0 equiv) in CH_2Cl_2 (25 mL, 0.01 M) at 23 °C was added solid supported catalyst[74] $NaHSO_4$•SiO_2 (2.63 g, stored in the oven for >48 h and added while hot) in one portion. The reaction mixture was then stirred for 6 h at 23 °C. The mixture was then filtered through a plug of silica gel with 7:2:1 MeCN:H_2O:sat. aq. KNO_3 (100 mL). The eluate was concentrated under reduced pressure before being crashed out with sat. aq. KPF_6 (100 mL) and transferred to a separatory funnel with CH_2Cl_2 (100 mL). The layers were separated and the aqueous layer was extracted with CH_2Cl_2 (2

x 100 mL). The combined organic layers were then concentrated under reduced pressure to afford the intermediate silyl alcohol as a red solid.

The intermediate silyl alcohol was then dissolved in CH_2Cl_2 (25 mL, 0.01 M) and while stirring at 23 °C, DMAP (89.3 mg, 0.731 mmol, 3.0 equiv) and Comins' reagent (144 mg, 0.366 mmol, 1.5 equiv) were added sequentially, each in single portions. After stirring at 23 °C for 30 min, the reaction was concentrated under reduced pressure and then loaded onto a silica plug. The silica plug was washed with EtOAc (200 mL; eluate discarded) before being eluted with 7:2:1 MeCN:H_2O:sat. aq. KNO_3 (100 mL). The red eluate was then concentrated under reduced pressure and transferred with CH_2Cl_2 (100 mL) to a separatory funnel containing aqueous HCl (2.0 M, 100 mL). The layers were separated and the organic layer was washed with aqueous HCl (2.0 M, 2 x 40 mL). The combined aqueous layers were then extracted with CH_2Cl_2 (2 x 100 mL). The organic layers were then combined, dried over Na_2SO_4, and concentrated under reduced pressure. The residue was then filtered over a pad of neutral alumina (200 mL CH_3CN eluent) and concentrated under reduced pressure before being dried under reduced pressure (<1 torr) at 100 °C for 1 h to afford silyl triflate **4.35** as a red solid (204 mg, 73% yield). **Silyl triflate 4.35**: mp: >250 °C; R_f 0.34 (14:1:1 MeCN:H_2O:sat. aq. KNO_3); ^{1}H NMR (500 MHz, CD_3CN): δ 9.29 (d, *J* = 8.6, 1H), 9.11 (d, *J* = 8.5, 1H), 9.02 (s, 1H), 8.69 (s, 1H), 8.53 (d, *J* = 8.2, 2H), 8.49 (d, *J* = 8.2, 2H), 8.13–8.08 (m, 4H), 8.00 (tt, *J* = 7.9, 1.7, 2H), 7.84–7.78 (m, 4H), 7.60 (t, *J* = 5.3, 2H), 7.45 (t, *J* = 6.8, 2H), 7.22 (qt, *J* = 6.6, 1.3, 2H), 0.55 (s, 9H); ^{13}C NMR (125 MHz, CD_3CN) δ 158.1, 157.9, 156.2, 153.7, 153.3, 153.00, 152.97, 152.9, 152.8, 149.5, 149.1, 138.9, 138.7, 136.7, 134.7, 133.6, 133.2, 131.8, 130.3, 130.1, 128.5, 128.4, 128.0, 127.7, 125.24, 125.16, 116.1; IR (film): 3359, 3310, 3193, 2920, 2851, 1632 cm^{-1}; HR-ESI-MS (*m/z*) [M – PF_6]$^+$ calcd for $C_{40}H_{33}F_9N_6O_3PRuSSi^+$, 1009.07470; found 1009.0704.

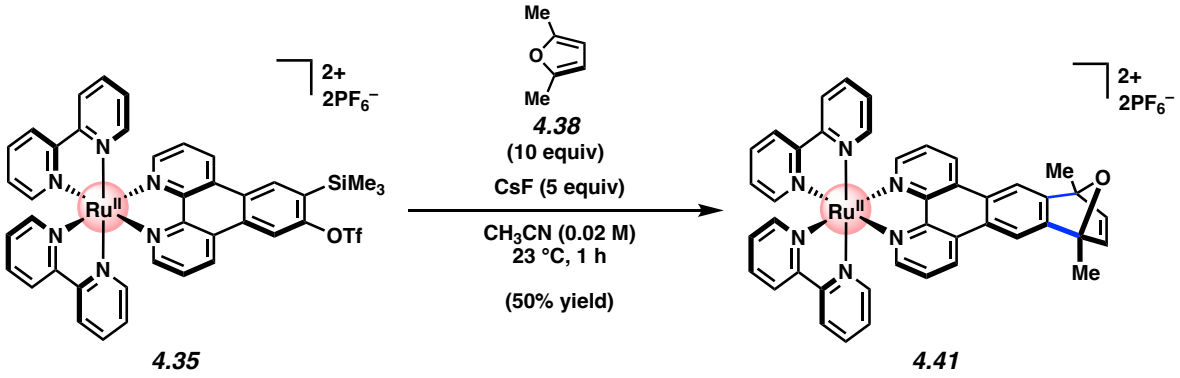

Cycloadduct 4.41. To a 1-dram vial was added silyl triflate **4.35** (19.5 mg, 16.9 μmol) and dissolved in MeCN (0.8 mL, 0.02 M). 2,5-dimethylfuran (**4.38**) (16.2 mg, 0.17 mmol, 10 equiv) was then added in one portion. While stirring, CsF (12.8 mg, 0.085 mmol, 5 equiv) was added in one portion and the reaction was stirred at 23 ªC for 1 h. After 1 h, the reaction mixture was then filtered through a plug of celite with MeCN (10 mL), adsorbed onto silica gel (500 mg) under reduced pressure, and purified by flash chromatography (100% EtOAc → 14:1:1 MeCN:H_2O:sat. aq. KNO_3). To the resultant concentrated aqueous mixture was added saturated aqueous KPF_6 (50 mL) to precipitate the desired product, and the resultant mixture was transferred to a separatory funnel with CH_2Cl_2 (50 mL). The layers were separated and the aqueous layer was extracted with CH_2Cl_2 (2 x 50 mL). The combined organic layers were then concentrated under reduced pressure, dried over sodium sulfate, and dried under reduced pressure (<1 torr) at 100 °C for 12 h to afford cycloadduct **4.41** as a red solid (4.1 mg, 25% yield). **Cycloadduct 4.41**: mp: >250 °C; R_f 0.31 (14:1:1 MeCN:H_2O:sat. aq. KNO_3); ^{1}H NMR (500 MHz, CD_3CN): δ 9.23 (dt, *J* = 8.6, 1.3, 2H), 8.59 (d, *J* = 1.4, 2H), 8.52 (dq, *J* = 8.3, 0.8, 2H), 8.49 (ddt, *J* = 8.3, 3.0, 1.1, 2H), 8.09 (td, *J* = 8.0, 1.4, 2H), 8.04 (ddd, *J* = 5.2, 4.3, 1.1, 2H), 8.01–7.94 (m, 2H), 7.83 (dddd, *J* = 5.6, 3.3, 1.5, 0.8, 2H), 7.76 (dd, *J* = 8.6, 5.2, 2H), 7.57 (dddd, *J* = 11.8, 5.7, 1.6, 0.7, 2H), 7.44 (ddt, *J* = 7.7, 5.6, 1.3, 2H), 7.19 (dddd, *J* = 11.1, 7.8, 5.8, 1.3,

2H), 6.92 (app dd, J = 5.4, 3.4, 2H), 2.044 (s, 3H), 2.037 (s, 3H); ^{13}C NMR (125 MHz, CD_3CN): δ 158.1, 157.90. 157.88, 156.2, 152.90, 152.89, 152.8, 152.3, 148.6, 147.41, 147.38, 138.8, 138.62, 138.59, 133.3, 131.3, 128.5, 128.33, 128.32, 127.2, 127.1, 125.2, 125.11, 125.09, 114.9, 114.8, 89.6; IR (film): 2931, 1467, 1447, 1390, 1141, 839, 762, 558 cm^{-1}; HR-ESI-MS (*m/z*) [M – PF_6]$^+$ calcd for $C_{42}H_{32}F_6N_6OPRu^+$, 883.13284; found 883.1326.

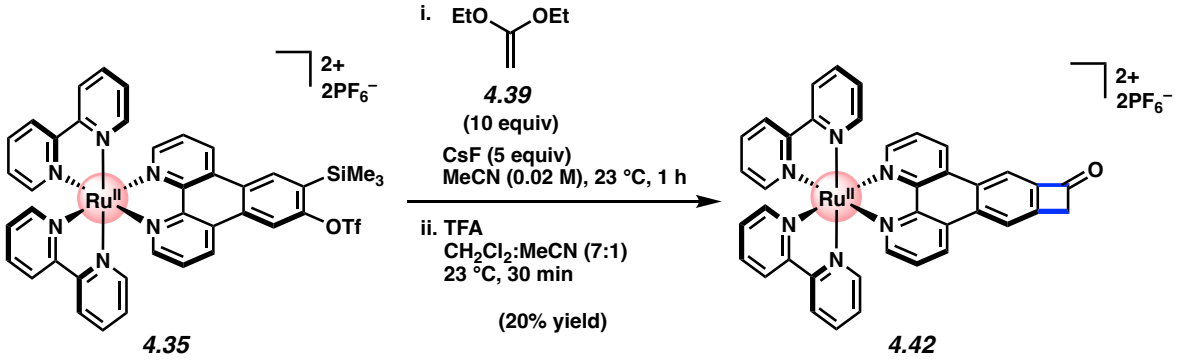

Cyclobutanone 4.42. To a stirred solution of silyl triflate **4.35** (20.5 mg, 17.8 µmol, 1.0 equiv) and 1,1-diethoxyethene (**4.39**) (24.9 µL, 178 µmol, 10.0 equiv) in MeCN (0.9 mL, 0.02 M) at 23 °C was added CsF (13.5 mg, 88.8 µmol, 5.0 equiv) in one portion. After stirring at 23 °C for 1 h, the reaction was filtered through a plug of celite with MeCN (10 mL) and then concentrated under reduced pressure. To the resulting residue was added CH_2Cl_2 (2.1 mL) and MeCN (0.3 mL) and while stirring at 23 °C, TFA (0.5 mL) was added dropwise over 20 seconds and the mixture was stirred at 23 °C for 30 min. The reaction was then quenched by slow addition of saturated aqueous $NaHCO_3$ (2.5 mL) over 30 seconds. The reaction was then transferred to a separatory funnel with CH_2Cl_2 (25 mL) and saturated aqueous KPF_6 (20 mL). The layers were separated and the aqueous layer was extracted with CH_2Cl_2 (3 x 50 mL). The combined organic layers were then dried over Na_2SO_4, filtered, and concentrated under reduced pressure. Purification by preparative TLC (14:1:1 MeCN:H_2O:sat. aq. KNO_3) afforded cyclobutanone **4.42**

as a red solid (3.4 mg, 20% yield). **Cyclobutanone 4.42**: mp >250 °C; R_f 0.34 (14:1:1 MeCN:H_2O:sat. aq. KNO_3); ^{1}H NMR (500 MHz, CD_3CN): δ 9.29 (d, *J* = 8.4, 1H), 9.21 (d, *J* = 8.4, 1H), 9.07 (s, 1H), 8.89 (s, 1H), 8.53 (d, *J* = 8.4, 2H), 8.50 (d, *J* = 8.4, 2H), 8.14–8.05 (m, 4H), 8.00 (t, *J* = 8.2, 2H), 7.84–7.76 (m, 4H), 7.62 (d, *J* = 5.0, 2H), 7.45 (t, *J* = 6.4, 2H), 7.23 (t, *J* = 6.0, 2H), 4.37 (s, 2H); ^{13}C NMR (125 MHz, CD_3CN): δ 189.2, 158.1, 157.9, 153.7, 153.1, 152.99, 152.95, 152.83, 152.81, 151.7, 150.7, 149.7, 148.7, 138.9, 138.7, 134.7, 134.1, 133.3, 131.9, 131.1, 130.1, 128.5, 128.4, 127.63, 127.58, 125.23, 125.16, 120.5, 117.3; IR (film): 2923, 1772, 1618, 1469, 1449, 839, 558 cm^{-1}; HR-ESI-MS (*m/z*) [M – PF_6]$^+$ calcd for $C_{38}H_{26}F_6N_6OPRu^+$, 829.08589; found 829.0845.

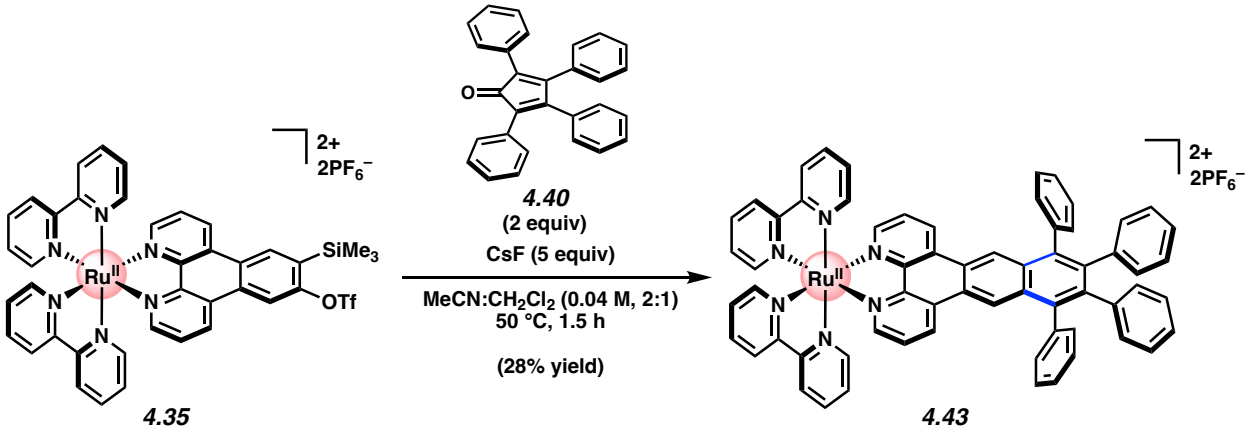

Cycloadduct 4.43. To a 1-dram vial was added silyl triflate **4.35** (99.7 mg, 86.4 µmol, 1.0 equiv), tetraphenylcyclopentadienone (**4.40**, 66.4 mg, 173 µmol, 2.0 equiv), MeCN (1.4 mL, 0.06 M), CH_2Cl_2 (0.7 mL, 0.12 M), and CsF (65.6 mg, 432 µmol, 5.0 equiv) were added sequentially. The reaction vessel was purged with N_2, sealed with a Teflon cap, and placed in a preheated, 50 °C aluminum heating block. After stirring for 1.5 h, the reaction was cooled to 23 °C. The reaction mixture was then filtered through a plug of celite with MeCN (10 mL), adsorbed onto silica gel (750 mg) under reduced pressure, and purified by flash chromatography

(100% EtOAc → 14:1:1 MeCN:H_2O:sat. aq. KNO_3). To the concentrated aqueous mixture was added saturated aqueous KPF_6 (50 mL) to precipitate the desired product, and the resultant mixture was transferred to a separatory funnel with CH_2Cl_2 (50 mL). The layers were separated and the aqueous layer was extracted with CH_2Cl_2 (1 x 50 mL). The combined organic layers were then dried over sodium sulfate, filtered, concentrated under reduced pressure, and dried under reduced pressure (<1 torr) at 100 °C for 12 h to afford cycloadduct **4.43** as a red solid (30.7 mg, 28% yield). **Cycloadduct 4.43**: mp >250 °C; R_f 0.84 (7:2:1 MeCN:H_2O:sat. aq. KNO_3); ^{1}H NMR (600 MHz, CD_3CN): δ 8.94 (s, 2H), 8.60 (dd, *J* = 8.6, 1.1, 2H), 8.51 (dt, *J* = 8.2, 1.0, 2H), 8.48 (dt, *J* = 8.2, 1.0, 2H), 8.08 (td, *J* = 8.0, 1.4, 2H), 8.00 (td, *J* = 7.9, 1.5, 2H), 7.94 (dd, *J* = 5.3, 1.1, 2H), 7.79 (ddd, *J* = 5.6, 1.4, 0.6, 2H), 7.64 (ddd, *J* = 5.7, 1.4, 0.6, 2H), 7.60 (dd, *J* = 8.3, 5.4, 2H), 7.44–7.34 (m, 12H), 7.23 (ddd, *J* = 7.7, 5.8, 1.3, 2H), 7.06–6.97 (m, 4H), 6.96–6.89 (m, 6H); ^{13}C NMR (125 MHz, CD_3CN): δ 158.0, 157.9, 152.8, 152.7, 152.4, 149.6, 142.2, 141.1, 140.0, 139.5, 138.8, 138.7, 133.0, 132.6, 132.24, 132.18, 132.00, 131.98, 131.8, 128.91, 128.88, 128.5, 128.4, 128.2, 127.8, 127.6, 126.8, 126.2, 125.2, 125.1, 124.2; IR (film): 2929, 1606, 1469, 1447, 840, 763, 701, 558 cm^{-1}; HR-ESI-MS (*m/z*) [M – PF_6]$^+$ calcd for $C_{64}H_{44}F_6N_6PRu^+$, 1143.23182; found 1443.2338.

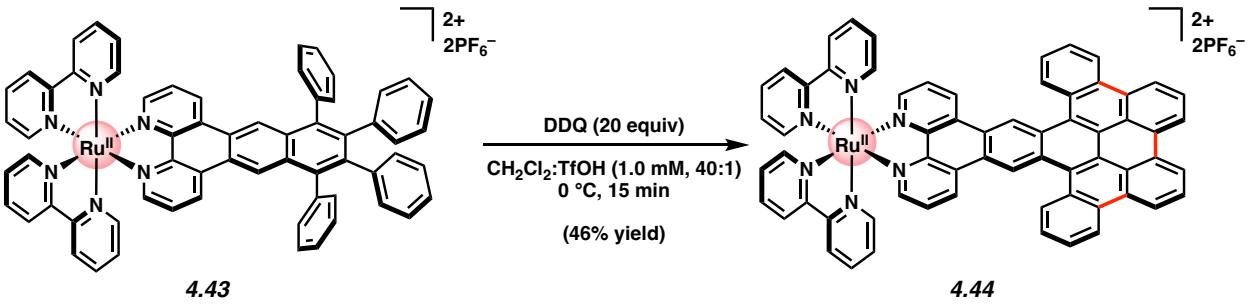

4.43 *4.44*

Scholl Product 4.44. To a stirred solution of **4.43** (6.3 mg, 4.9 µmol, 1.0 equiv), in CH_2Cl_2 (4.0 mL) at 0 °C was added DDQ (22 mg, 98 µmol, 20 equiv) in one portion. Then, TfOH (0.1 mL)

was added dropwise over 1 min, whereupon the reaction turned deep green in color. The reaction was then stirred at 0 °C for 15 min, followed by addition of saturated aqueous $NaHCO_3$ (4.0 mL) slowly, over 10 seconds. The resulting mixture was then stirred at 0 °C for 5 min before being allowed to warm to 23 °C. It was then transferred with CH_2Cl_2 (30 mL) to a separatory funnel containing saturated aqueous KPF_6 (30 mL). The layers were separated and the aqueous layer was extracted with CH_2Cl_2 (2 x 30 mL). The combined organic layers were then concentrated under reduced pressure and loaded onto a silica plug, which was washed with EtOAc (25 mL) before being eluted with 7:2:1 MeCN:H_2O:sat. aq. KNO_3 (30 mL). The red eluate was then concentrated under reduced pressure, saturated aqueous KPF_6 (30 mL) was added to precipitate the desired product, and the resultant mixture was transferred to a separatory funnel with CH_2Cl_2 (30 mL). The layers were separated and the aqueous layer was extracted with CH_2Cl_2 (1 x 30 mL). The combined organic layers were then concentrated under reduced pressure, dried over Na_2SO_4, filtered, and concentrated under reduced pressure to afford **Scholl Product 4.44** as a red solid (2.9 mg, 46% yield). **Scholl Product 4.44**: R_f 0.41 (14:1:1 MeCN:H_2O:sat. aq. KNO_3); ^{1}H NMR (500 MHz, CD_3CN): δ 10.03 (s, 2H), 9.05 (d, *J* = 8.3, 2H), 8.75 (d, *J* = 8.3, 2H), 8.71–8.64 (m, 4H), 8.61 (d, *J* = 8.2, 2H), 8.57 (d, *J* = 8.2, 2H), 8.50 (d, *J* = 7.8, 2H), 8.16 (td, *J* = 8.1, 1.4, 2H), 8.08 (dd, *J* = 5.3, 0.8, 2H), 8.05 (td, *J* = 8.0, 1.4, 2H), 7.91 (d, *J* = 5.5, 2H), 7.87–7.81 (m, 4H), 7.75 (t, *J* = 7.8, 2H), 7.69 (t, *J* = 7.6, 2H), 7.61 (t, *J* = 7.4, 2H), 7.51 (ddd, *J* = 7.8, 5.5, 1.3, 2H), 7.35 (t, *J* = 6.8, 2H); ^{13}C NMR (125 MHz, CD_3CN, 31 of 32 signals observed): δ 157.20, 157.19, 152.0, 151.9, 151.5, 148.6, 138.0, 137.9, 132.2, 131.0, 130.9, 129.9, 129.5, 129.1, 128.7, 127.9, 127.7, 127.6, 127.41, 127.37, 126.9, 124.6, 124.5, 124.42, 124.39, 124.3, 124.0, 123.3, 122.9, 122.2, 122.0; IR (film): 2925, 1468, 1447, 1425, 841, 761, 558 cm^{-1}; HR-ESI-MS (*m/z*) $[M - PF_6]^+$ calcd for $C_{64}H_{44}F_6N_6PRu^+$, 1143.23182; found 1143.2338.

*Note: **4.44** readily decomposes upon removal of solvent, and must therefore be carefully handled as a dilute solution. We surmise that its instability may be a consequence of its highly π-expansive nature, which introduces numerous sites for oxidation or dimerization.*

4.8.3 Photophysical Data

UV–vis absorption spectra were recorded on an Ocean Optics Flame-T spectrometer with the OceanView software package. Dynamic light scattering (DLS) data were collected using a Beckman-Coulter N4 Plus particle analyzer. Quartz cuvettes (1 cm) were used for absorbance and photoluminescence measurements. Relative quantum yields were determined in degassed acetonitrile relative to $Ru(bpy)_3[PF_6]_2$.

Nanosecond transient absorption experiments were performed using an Edinburgh Instruments LP920 laser flash photolysis spectrometer in conjunction with a Q-switched Nd:YAG Brilliant b laser from Quantel with a 266 nm output wavelength, a 5−8 ns pulse width, a 1 Hz repetition rate, and a 36−40 mJ pulse energy. Transient absorption detection is based on a 450 W pulsed xenon arc lamp, a Czerny-Turner TMS300 monochromator, a Hamamatsu R928 photomultiplier detector, and a Tektronix TDS3012C digital oscilloscope. Transient absorption data were collected and processed using the L900 software package provided by Edinburgh Instruments. Samples were prepared as solutions in acetonitrile and degassed by sparging with argon in a quartz cuvette. Reported transient absorption lifetime (τ_{TA}) values are reported as the average of three experiments. Phosphorescence spectra were recorded using an Edinburgh Instruments FLSP920 fluorimeter with a 450 W xenon lamp in CW (continuous wave) emission source.

4.8.3.1 Compiled Photophysical Data Table

Table 4.3. Photophysical data for selected Ru complexes. Samples were prepared as solutions in acetonitrile and degassed by sparging with argon in a quartz cuvette.

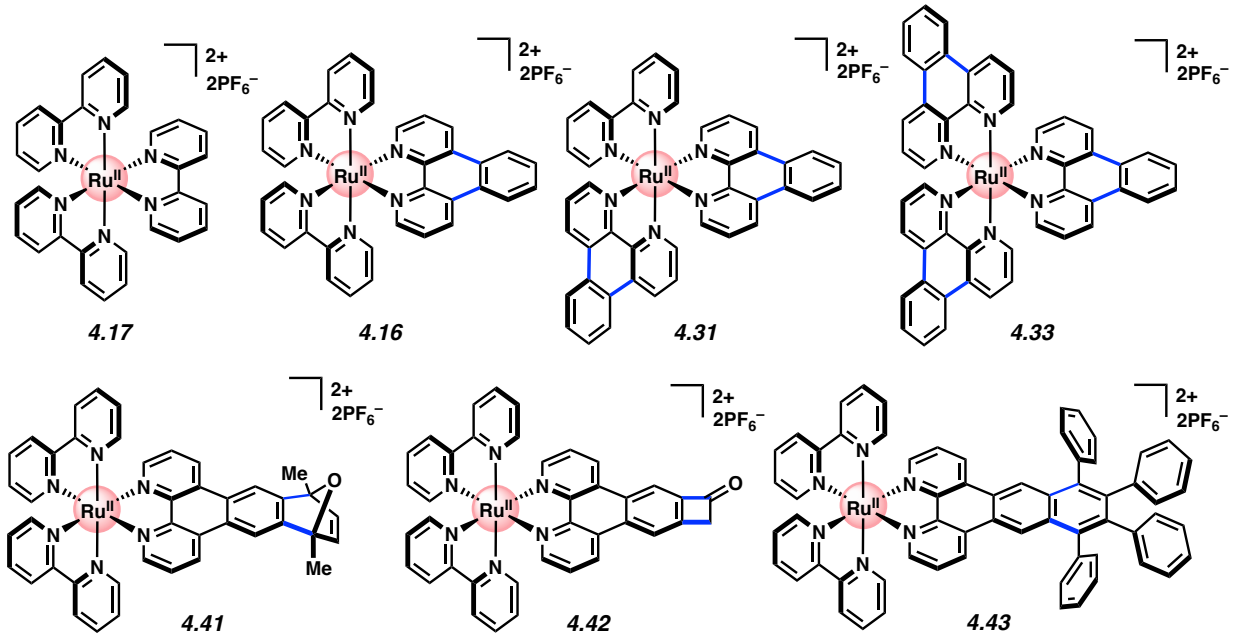

4.17 ***4.16*** ***4.31*** ***4.33***

4.41 ***4.42*** ***4.43***

Ru Complex	$\lambda_{max\ em.}$ (nm)	ε × 10^3 (mol^{-1} cm^{-1}; at 452 nm)	Φ_P (%)	τ_{TA} *(ns)*
4.17	593	18.1	9.5 (lit.)[6]	1115
4.16	592	7.7	15	1077
4.31	589	18.2	15	1382
4.33	586	23.5	24	1479
4.41	592	14.7	14	1100
4.42	594	11.5	14	1339
4.43	591	15.8	16	2006

4.8.3.2 UV–Vis Spectra

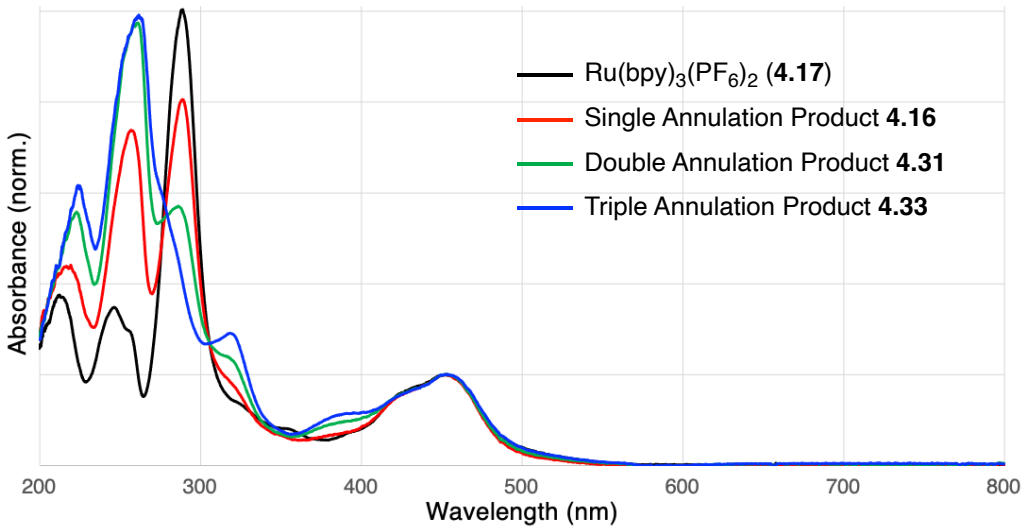

Figure 4.12. UV−vis absorption spectra of compounds **4.17**, **4.16**, **4.31**, and **4.33**. Spectra are normalized to OD = 1 at the MLCT maximum (452 nm) to compare the band shapes.

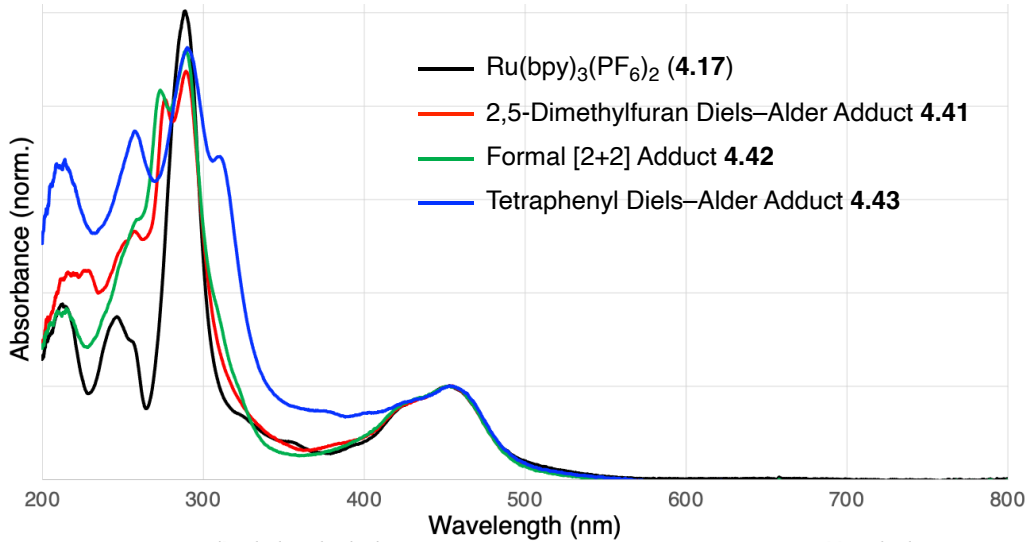

Figure 4.13. UV−vis absorption spectra of compounds **4.17**, **4.41**, **4.42**, and **4.43**. Spectra are normalized to OD = 1 at the MLCT maximum (452 nm) to compare the band shapes.

4.8.3.3 Molar Extinction Coefficient Measurements

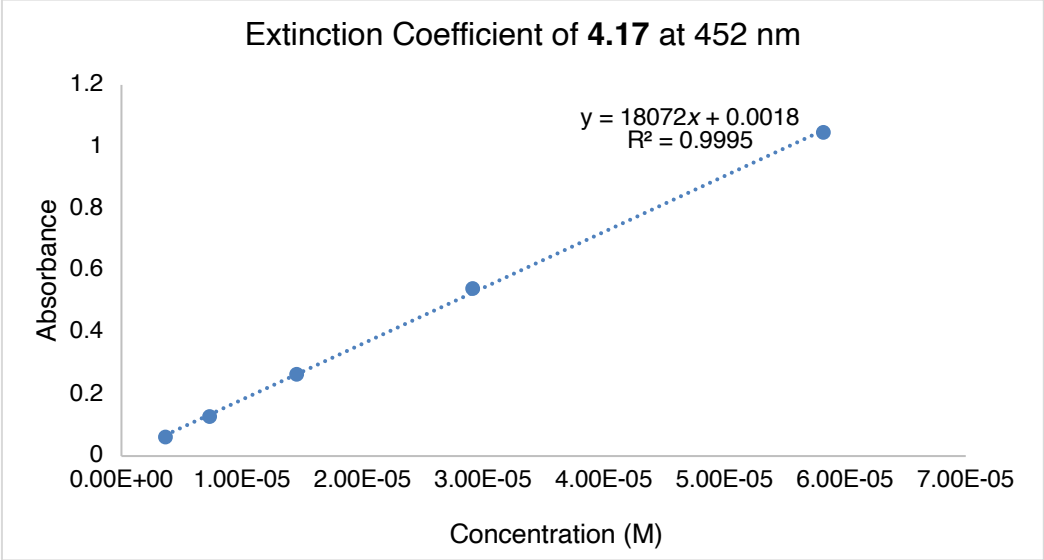

Figure 4.14. Beer-Lambert plot of **4.17** at 452 nm. (ε = 18.1 x 10^4 M^{-1} cm^{-1}).

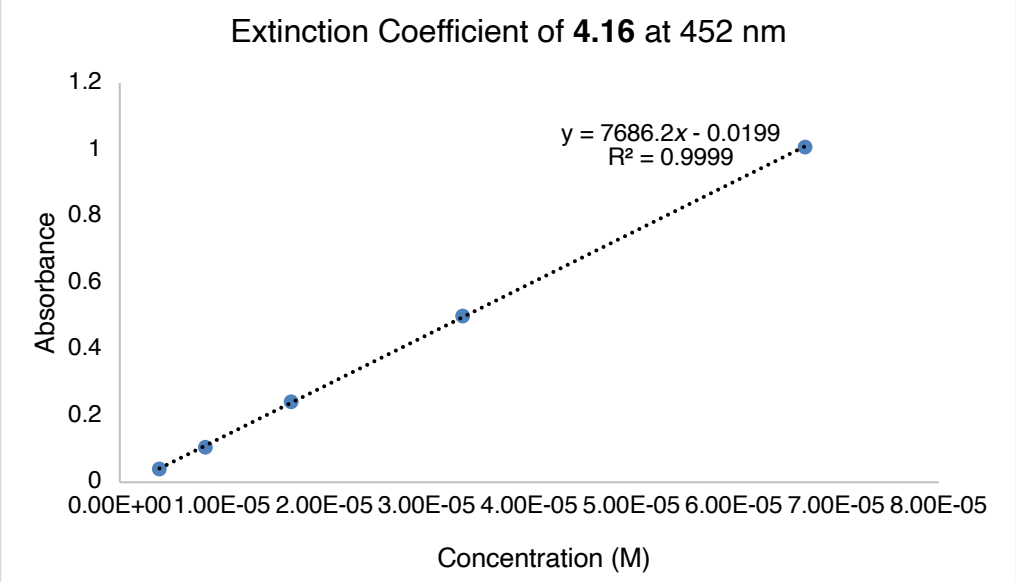

Figure 4.15. Beer-Lambert plot of **4.16** at 452 nm. (ε = 7.69 x 10^3 M^{-1} cm^{-1}).

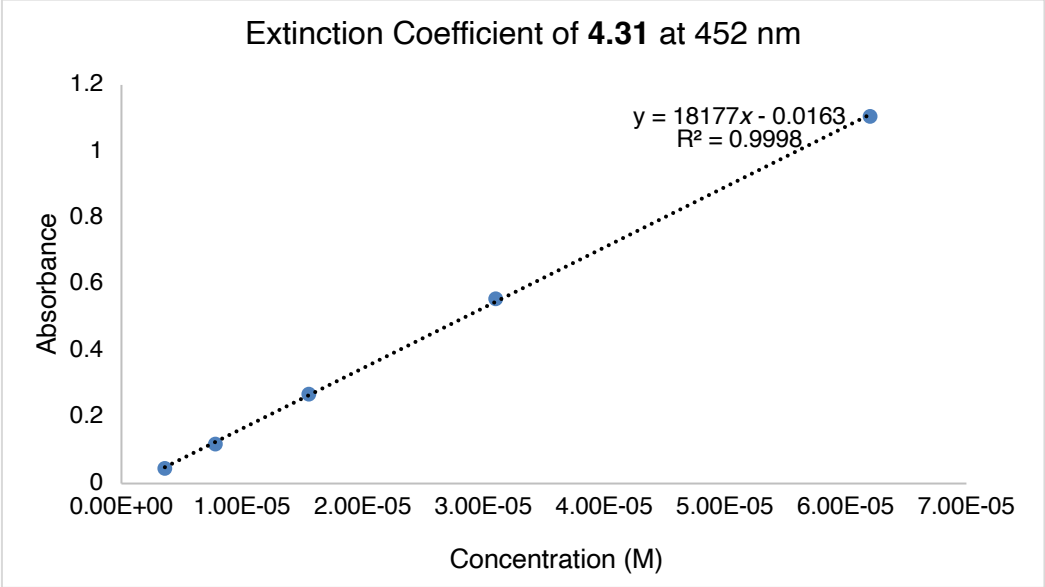

Figure 4.16. Beer-Lambert plot of **4.31** at 452 nm. ($\varepsilon = 18.2 \times 10^4\ M^{-1}\ cm^{-1}$).

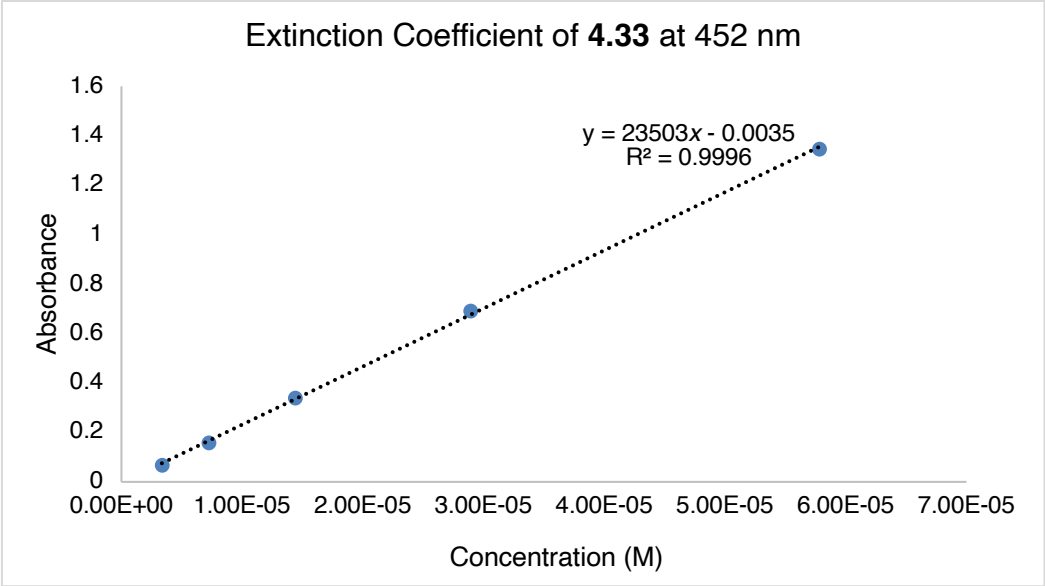

Figure 4.17. Beer-Lambert plot of **4.33** at 452 nm. ($\varepsilon = 23.5 \times 10^4\ M^{-1}\ cm^{-1}$).

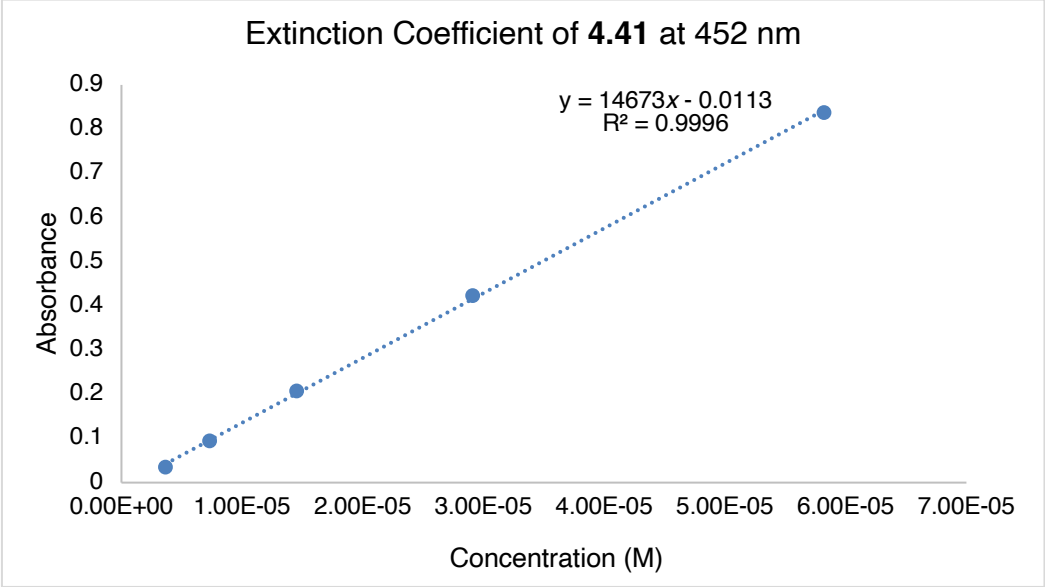

Figure 4.18. Beer-Lambert plot of **4.41** at 452 nm. ($\varepsilon = 14.7 \times 10^4\ M^{-1}\ cm^{-1}$).

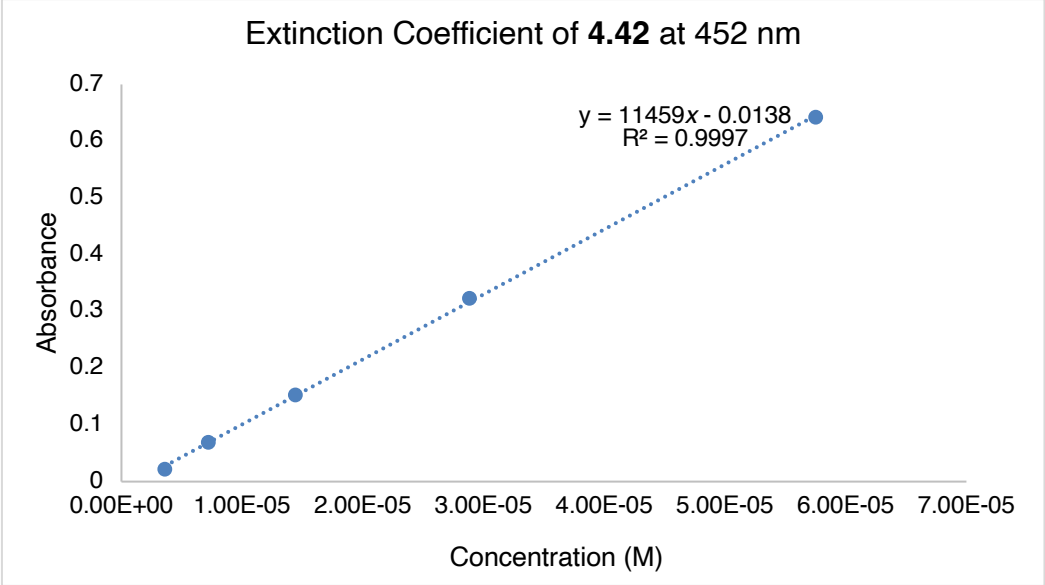

Figure 4.19. Beer-Lambert plot of **4.42** at 452 nm. ($\varepsilon = 11.5 \times 10^3\ M^{-1}\ cm^{-1}$).

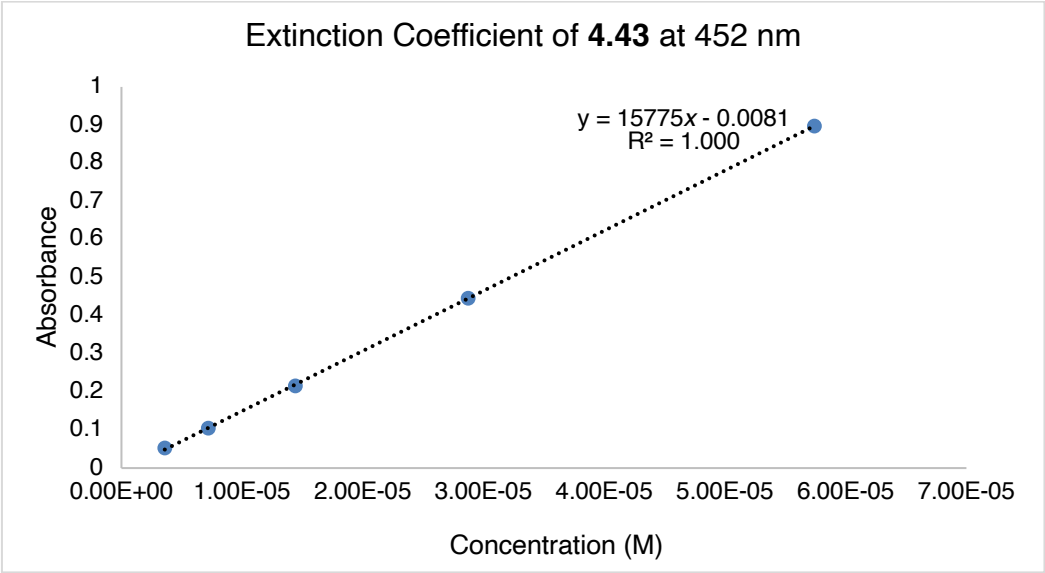

Figure 4.20. Beer-Lambert plot of **4.43** at 452 nm. (ε = 15.8 x 10^4 M^{-1} cm^{-1}).

4.8.3.4 Quantum Yield Measurements

The phosphorescence quantum yield (Φ_P) of a molecule or material is defined as follows:

$$\Phi_P = \frac{PE}{PA}$$

Where PE and PA represent the number of photons emitted and absorbed, respectively. To determine the quantum yield, we used a relative method with $Ru(bpy)_3[PF_6]_2$ as a known standard in the same region of the electromagnetic spectrum.

To compare an unknown to a reference with a known quantum yield, the following relationship was used:

$$\Phi_{P,x} = \Phi_{P,r}\left(\frac{m_x}{m_r}\right)\left(\frac{n_x}{n_r}\right)$$

Where m represents the slope of the line (y = mx + b) obtained from graphing integrated phosphorescence intensity versus optical density across a series of samples, η is the refractive index of the solvent and the subscripts x and r represent values of the unknown and reference,

respectively. The $\Phi_{P,r}$ of $Ru(bpy)_3[PF_6]_2$ in degassed acetonitrile was taken to be 9.5%, as previously determined.[75]

To obtain a plot of integrated phosphorescence intensity versus absorbance for the reference and unknown, five solutions and a solvent blank were prepared with absorbance at 452 nm between 0.02 and 0.30 au. Absorbance and emission spectra (with an excitation wavelength of 450 nm) were acquired for all samples. $Ru(bpy)_3[PF_6]_2$ and the unknown Ru complexes were diluted in acetonitrile to concentrations with optical densities at 452 nm of less than 0.3 to minimize effects of reabsorption. The phosphorescence traces were integrated, and the raw integrals were corrected by subtracting the integral over an identical range from phosphorescence traces of the blank solvent. The integrated phosphorescence intensities were then plotted against the baseline corrected absorbance values at the relevant wavelength (450 nm), and the slope and error in slope were obtained ($R^2 > 0.98$ for all traces).

4.8.4 Computational Data

Calculations were carried out with the Gaussian 16 package. Geometry optimization was performed with B3LYP with LANL2DZ basis set for Ru atom and 6-31G(d) basis set for all other atoms (C, H, N); CPCM (MeCN) solvation model was utilized.[76] Computed structures are illustrated using CYLView.[77]

4.8.4.1 Complete Citation of Gaussian 16

M. J. Frisch, G. W. Trucks, H. B. Schlegel, G. E. Scuseria, M. A. Robb, J. R. Cheeseman, G. Scalmani, V. Barone, G. A. Petersson, H. Nakatsuji, X. Li, M. Caricato, A. V. Marenich, J. Bloino, B. G. Janesko, R. Gomperts, B. Mennucci, H. P. Hratchian, J. V. Ortiz, A. F. Izmaylov, J. L. Sonnenberg, D. Williams-Young, F. Ding, F. Lipparini, F. Egidi, J. Goings, B. Peng, A.

Petrone, T. Henderson, D. Ranasinghe, V. G. Zakrzewski, J. Gao, N. Rega, G. Zheng, W. Liang, M. Hada, M. Ehara, K. Toyota, R. Fukuda, J. Hasegawa, M. Ishida, T. Nakajima, Y. Honda, O. Kitao, H. Nakai, T. Vreven, K. Throssell, J. A. Montgomery, Jr., J. E. Peralta, F. Ogliaro, M. J. Bearpark, J. J. Heyd, E. N. Brothers, K. N. Kudin, V. N. Staroverov, T. A. Keith, R. Kobayashi, J. Normand, K. Raghavachari, A. P. Rendell, J. C. Burant, S. S. Iyengar, J. Tomasi, M. Cossi, J. M. Millam, M. Klene, C. Adamo, R. Cammi, J. W. Ochterski, R. L. Martin, K. Morokuma, O. Farkas, J. B. Foresman, and D. J. Fox, Gaussian, Inc., Wallingford CT, **2016**.

4.8.4.2 Energy and Cartesian Coordinates for Optimized Structure

Diels–Alder Product **4.43**:

Ru	4.40809	-0.00012	-0.00007
C	6.22913	2.03055	-1.16572
C	6.57862	1.88488	1.13838
C	7.22284	3.00866	-1.27044
C	7.57559	2.85342	1.09803
H	6.28918	1.4164	2.07072
C	7.90368	3.42517	-0.13021
H	7.46637	3.44296	-2.23182
H	8.0771	3.1454	2.01373
H	8.67631	4.18324	-0.20307
C	3.79384	0.04896	-3.03046
C	5.45287	1.52931	-2.31722
C	3.91518	0.47135	-4.34978
H	3.08641	-0.72173	-2.75111
C	5.62078	1.99568	-3.62464
C	4.8463	1.46386	-4.65154
H	3.28956	0.02634	-5.11515
H	6.34779	2.76764	-3.84278
H	4.97009	1.82056	-5.66857
N	5.91592	1.4774	0.03975
N	4.54011	0.55823	-2.03255
C	2.82646	2.63885	0.39094
C	1.54248	0.71709	0.10359
C	1.67673	3.42417	0.49829
H	3.81553	3.07389	0.46351
C	0.33237	1.43315	0.2052
C	0.432	2.82417	0.40613

H	1.77165	4.49286	0.65347
H	-0.45666	3.43751	0.48978
C	1.54243	-0.71674	-0.10598
C	2.82622	-2.63856	-0.39372
C	0.33226	-1.43263	-0.20813
C	1.67643	-3.42364	-0.50206
H	3.81525	-3.07373	-0.46595
C	0.43176	-2.82352	-0.40997
H	1.77126	-4.49225	-0.65788
H	-0.45695	-3.43667	-0.49444
N	2.76551	1.31566	0.19906
N	2.76539	-1.31546	-0.20122
C	6.57918	-1.8862	-1.13547
C	6.22731	-2.03073	1.16837
C	7.57612	-2.85472	-1.09362
H	6.29059	-1.41823	-2.06831
C	7.22103	-3.00865	1.2746
C	7.90306	-3.4257	0.13528
H	8.07852	-3.14723	-2.00866
H	7.46367	-3.44245	2.23641
H	8.67569	-4.18365	0.20936
C	3.78911	-0.04915	3.02935
C	5.44945	-1.52931	2.31874
C	3.90846	-0.4715	4.34886
H	3.0819	0.72136	2.74891
C	5.61538	-1.99563	3.62644
C	4.83922	-1.46387	4.65211
H	3.28151	-0.02659	5.1132
H	6.34199	-2.76762	3.8458
H	4.96142	-1.82058	5.66933
N	4.53702	-0.55834	2.03263
N	5.91542	-1.47812	-0.0377
C	-0.94068	-0.7112	-0.10227
C	-2.15871	-1.37413	-0.19101
C	-0.94063	0.71175	0.09983
C	-3.40002	-0.71029	-0.0907
H	-2.17855	-2.44455	-0.34277
C	-2.15863	1.37467	0.18934
C	-3.40002	0.71086	0.08954
H	-2.17834	2.44503	0.34148
C	-4.64711	-1.41775	-0.17557
C	-4.64718	1.41819	0.17521
C	-5.84149	0.71582	0.08873
C	-5.84144	-0.71559	-0.0883
C	-4.63266	2.90284	0.38001
C	-4.86062	3.45042	1.6518

C	-4.36913	3.77147	-0.69099
C	-4.8351	4.83305	1.84646
H	-5.05974	2.78886	2.49018
C	-4.34524	5.15448	-0.49708
H	-4.18771	3.36037	-1.68052
C	-4.57877	5.68918	0.77241
H	-5.01456	5.24032	2.83779
H	-4.14515	5.81256	-1.3383
H	-4.56001	6.76491	0.9238
C	-7.14919	1.4443	0.18504
C	-7.91079	1.39474	1.36243
C	-7.63273	2.1922	-0.89888
C	-9.12462	2.07862	1.45487
H	-7.54854	0.82046	2.21048
C	-8.84906	2.87265	-0.80915
H	-7.05386	2.23849	-1.81699
C	-9.59862	2.81872	0.36851
H	-9.69914	2.03299	2.37618
H	-9.20965	3.44464	-1.65989
H	-10.54421	3.34923	0.43948
C	-7.14903	-1.44432	-0.18437
C	-7.63259	-2.19184	0.89979
C	-7.9104	-1.39549	-1.36194
C	-8.84875	-2.87261	0.81015
H	-7.05387	-2.23758	1.81802
C	-9.12407	-2.07969	-1.45429
H	-7.54813	-0.82149	-2.21017
C	-9.59811	-2.81939	-0.36768
H	-9.20936	-3.4443	1.66108
H	-9.69843	-2.03462	-2.37573
H	-10.54355	-3.35015	-0.43858
C	-4.6325	-2.9024	-0.38056
C	-4.85892	-3.44969	-1.65275
C	-4.37033	-3.77125	0.69058
C	-4.83324	-4.83229	-1.84767
H	-5.057	-2.78793	-2.49123
C	-4.34628	-5.15422	0.49641
H	-4.19003	-3.36036	1.6804
C	-4.57825	-5.68864	-0.77348
H	-5.01154	-5.23934	-2.83929
H	-4.14723	-5.81249	1.33773
H	-4.55935	-6.76434	-0.92507

4.9 Spectra Relevant to Chapter Four:

A Platform for On-the-Complex Annulation Reactions with Transient Aryne Intermediates

Jason V. Chari,† Katie A. Spence,† Robert B. Susick, and Neil K. Garg.

Nat. Commun. **2021**, *12*, 3706.

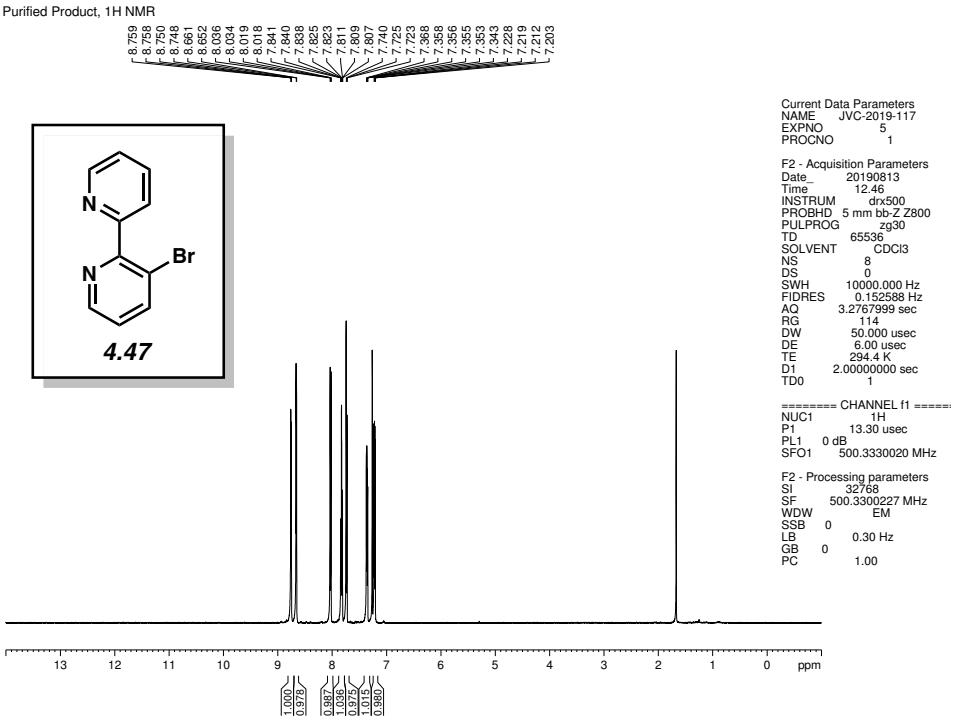

Figure 4.21 ^{1}H NMR (500 MHz, $CDCl_3$) of compound **4.47**.

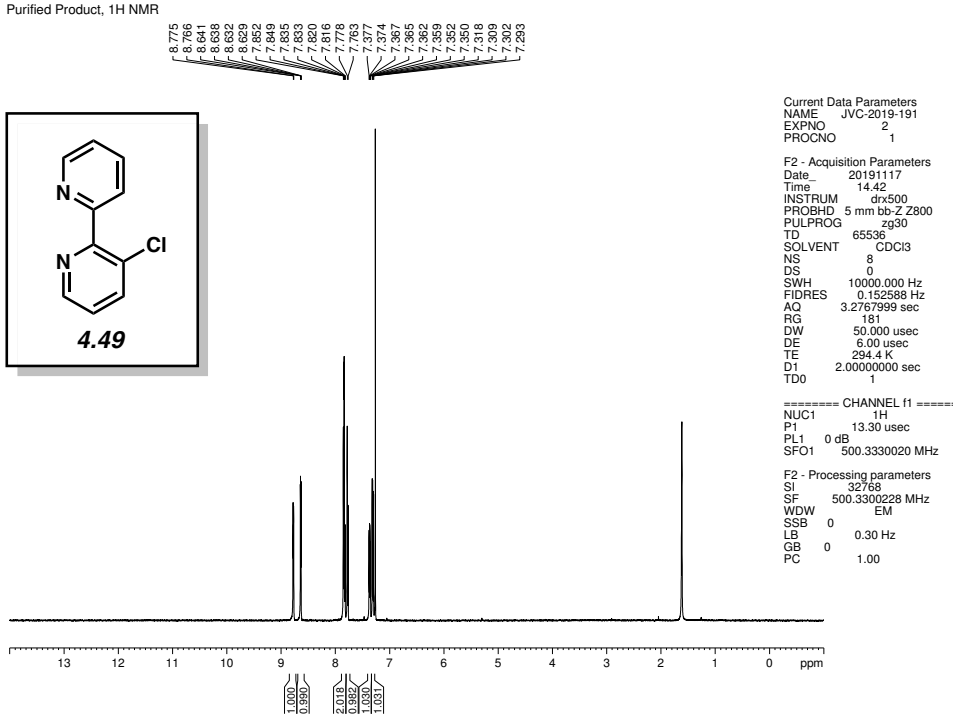

Figure 4.22 ^{1}H NMR (500 MHz, $CDCl_3$) of compound **4.49**.

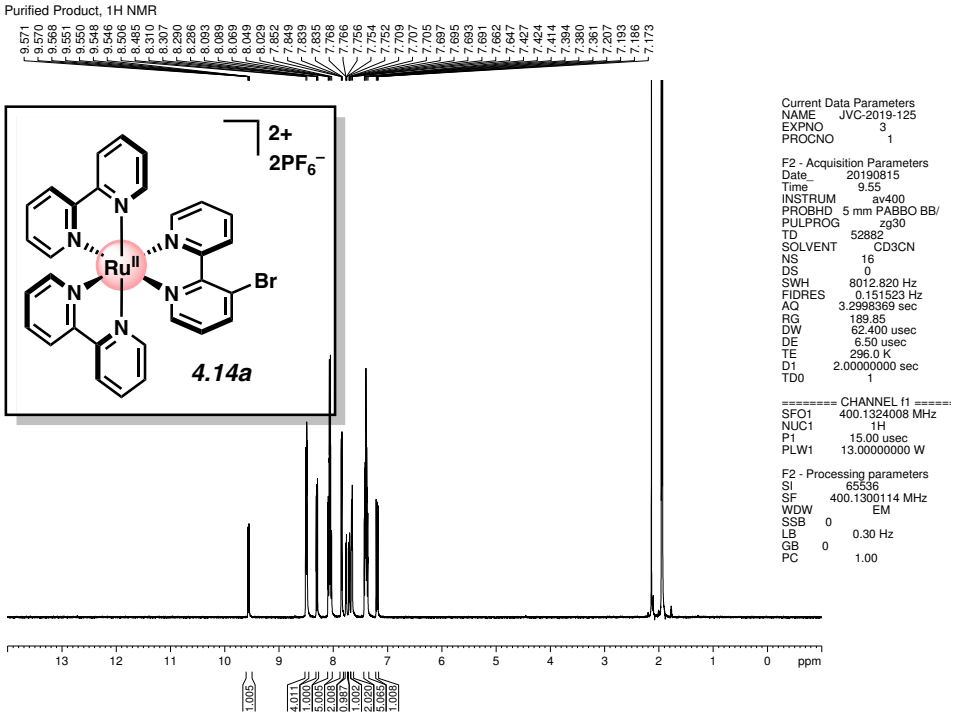

Figure 4.23 ^{1}H NMR (400 MHz, $CDCl_3$) of compound **4.14a**.

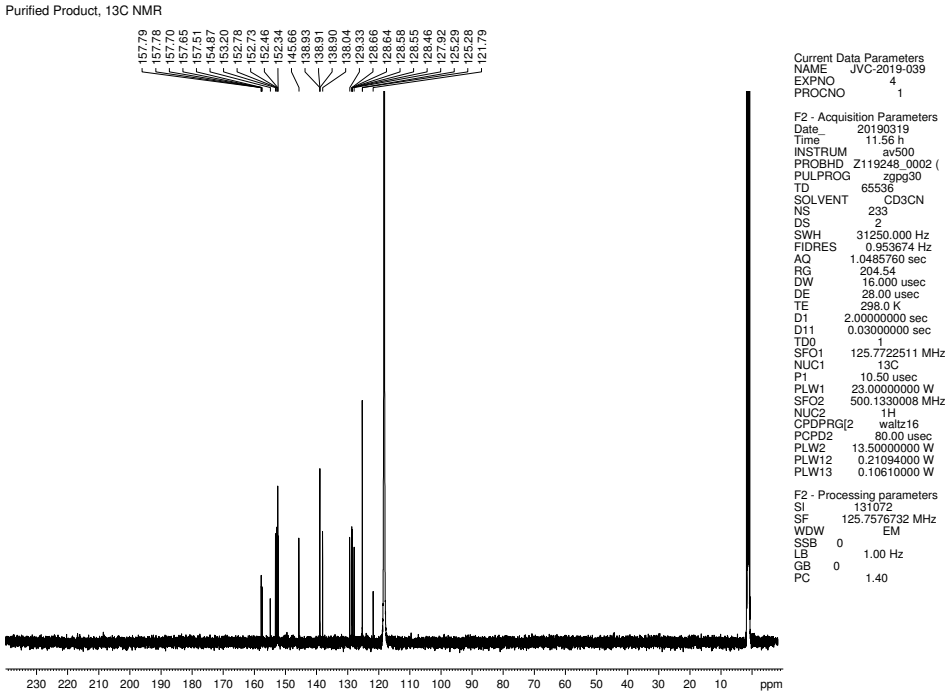

Figure 4.24 ^{13}C NMR (125 MHz, $CDCl_3$) of compound **4.14a**.

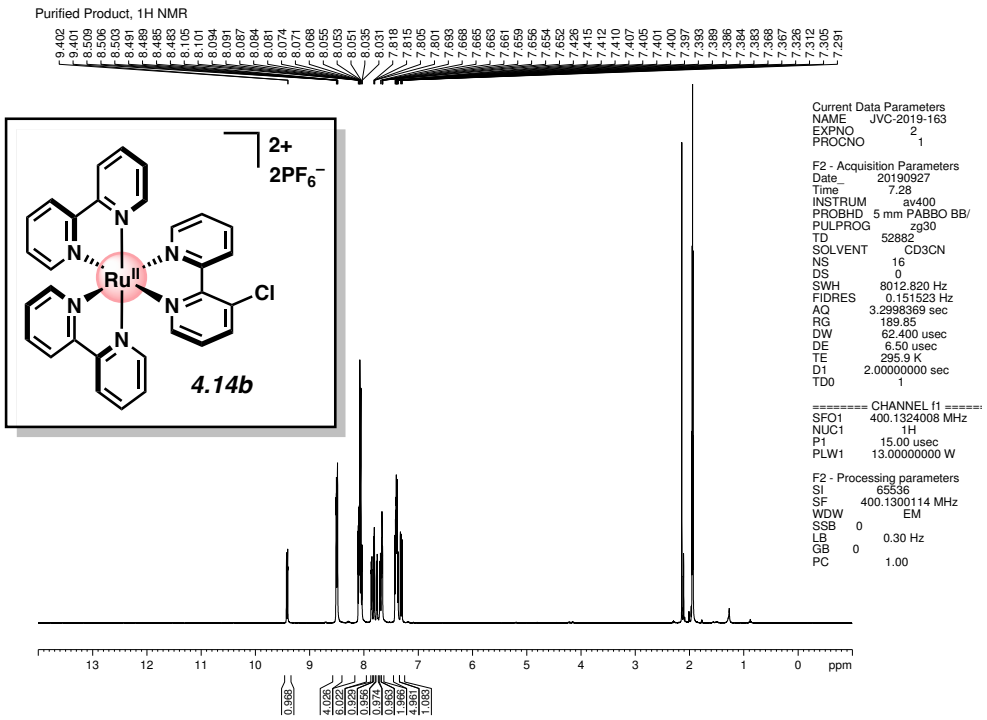

Figure 4.25 ^{1}H NMR (400 MHz, CD_3CN) of compound **4.14b**.

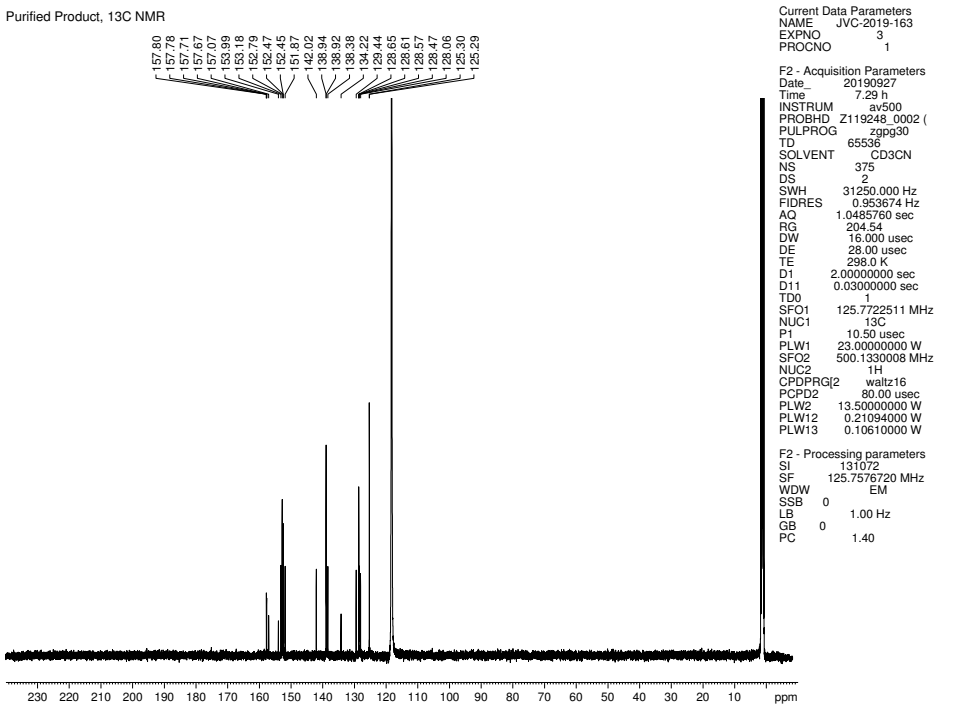

Figure 4.26 ^{13}C NMR (125 MHz, CD_3CN) of compound **4.14b**.

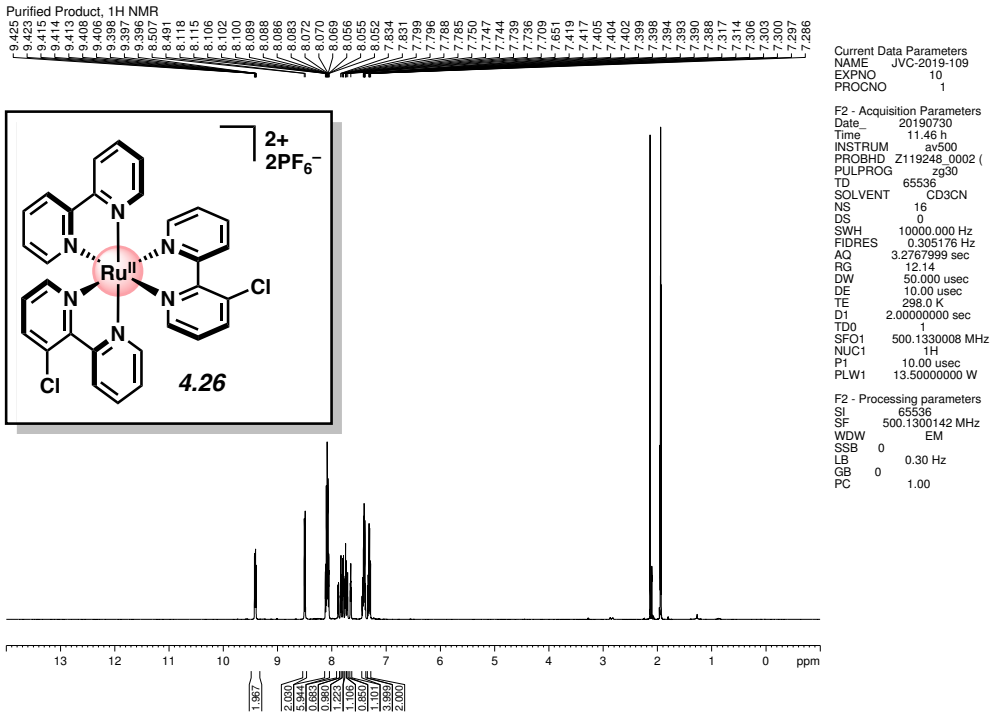

Figure 4.27 ^{1}H NMR (500 MHz, CD_3CN) of compound **4.26**.

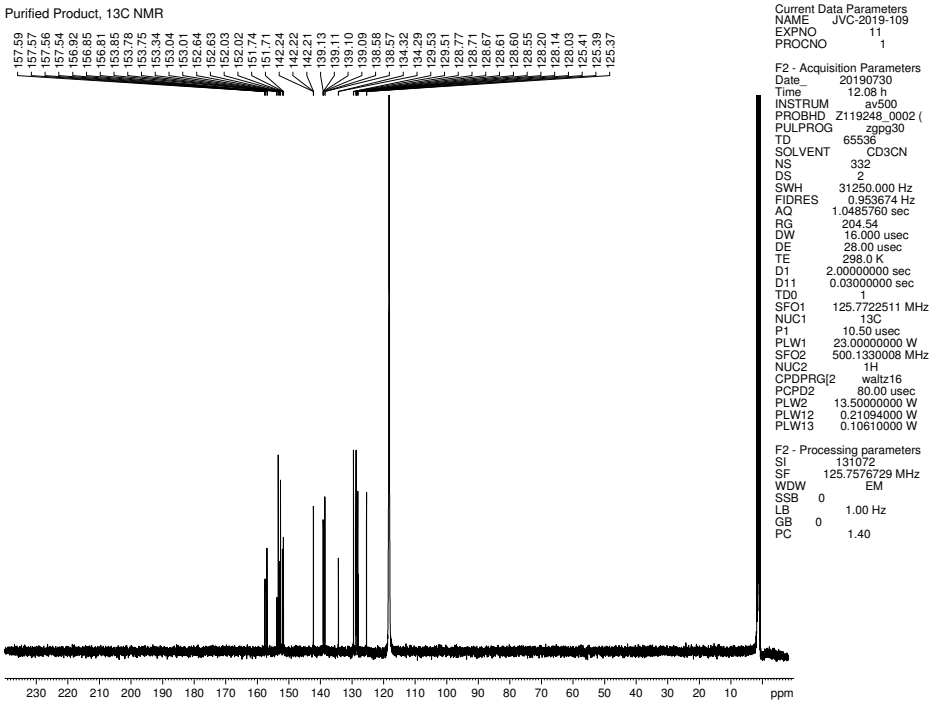

Figure 4.28 ^{13}C NMR (125 MHz, CD_3CN) of compound **4.26**.

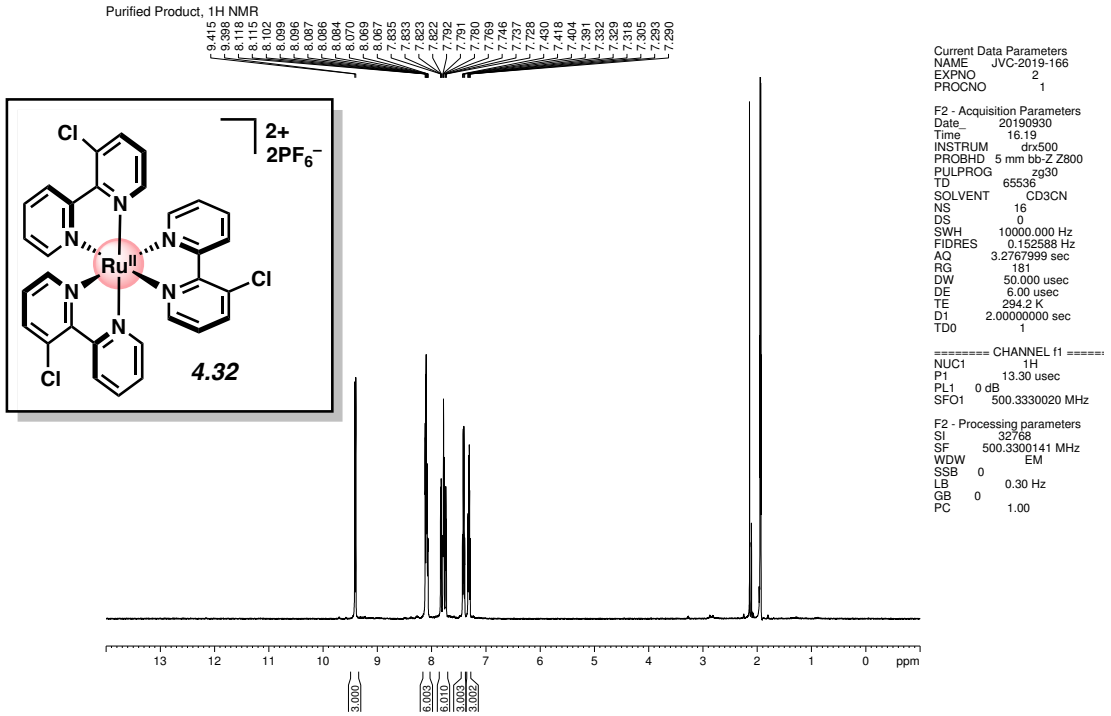

Figure 4.29 ^{1}H NMR (500 MHz, CD_3CN) of compound **4.32**.

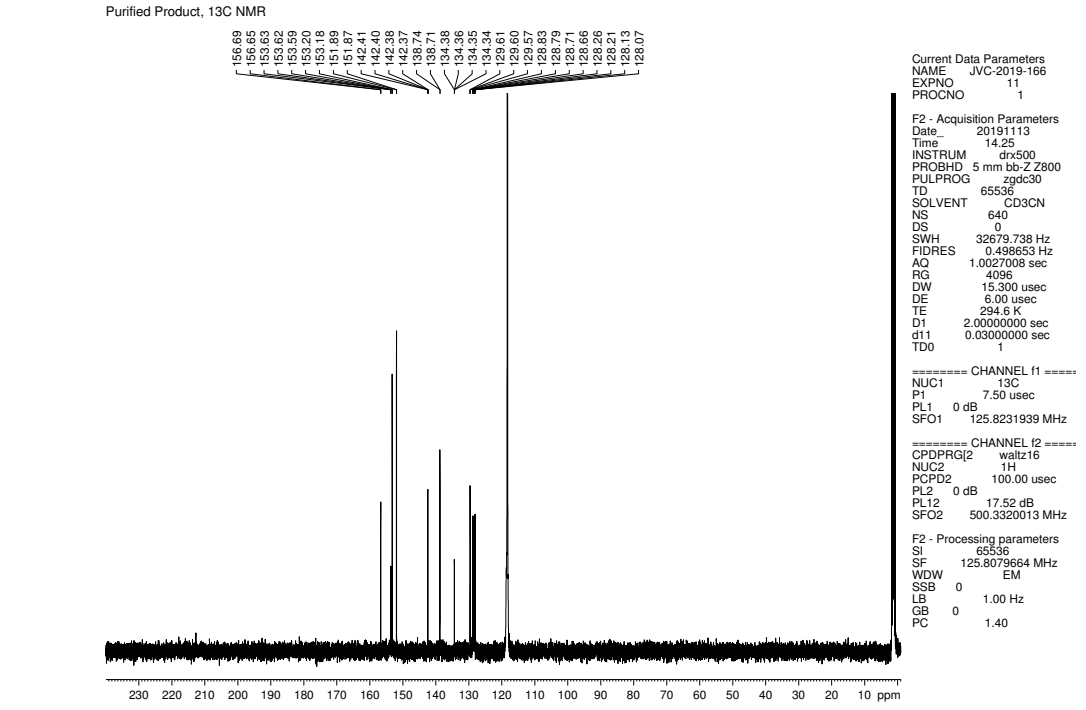

Figure 4.30 ^{13}C NMR (125 MHz, CD_3CN) of compound **4.32**.

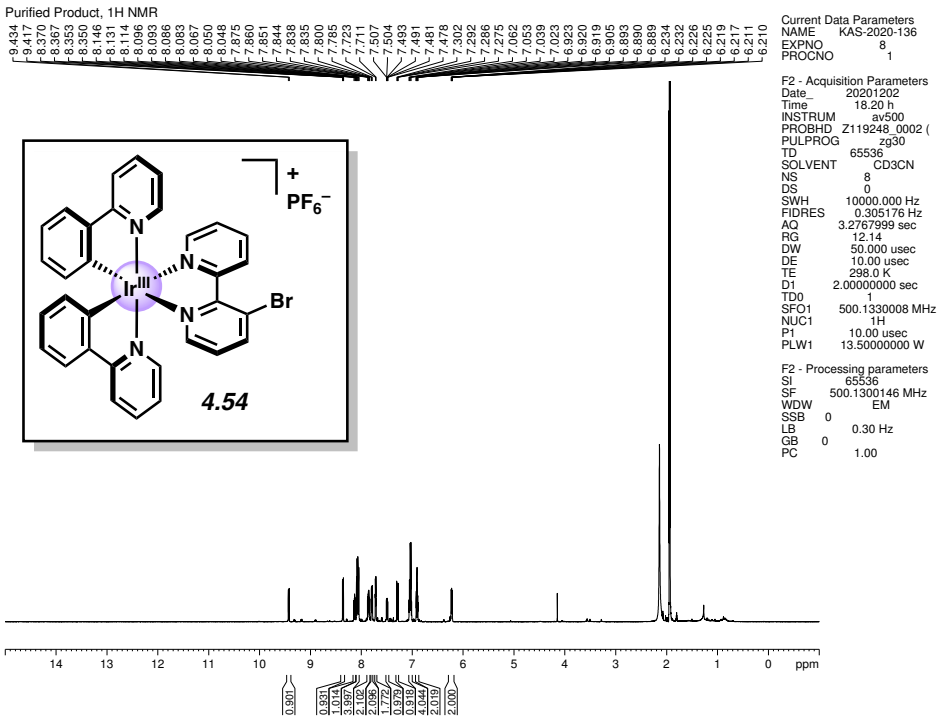

Figure 4.31 ^{1}H NMR (500 MHz, CD_3CN) of compound **4.54**.

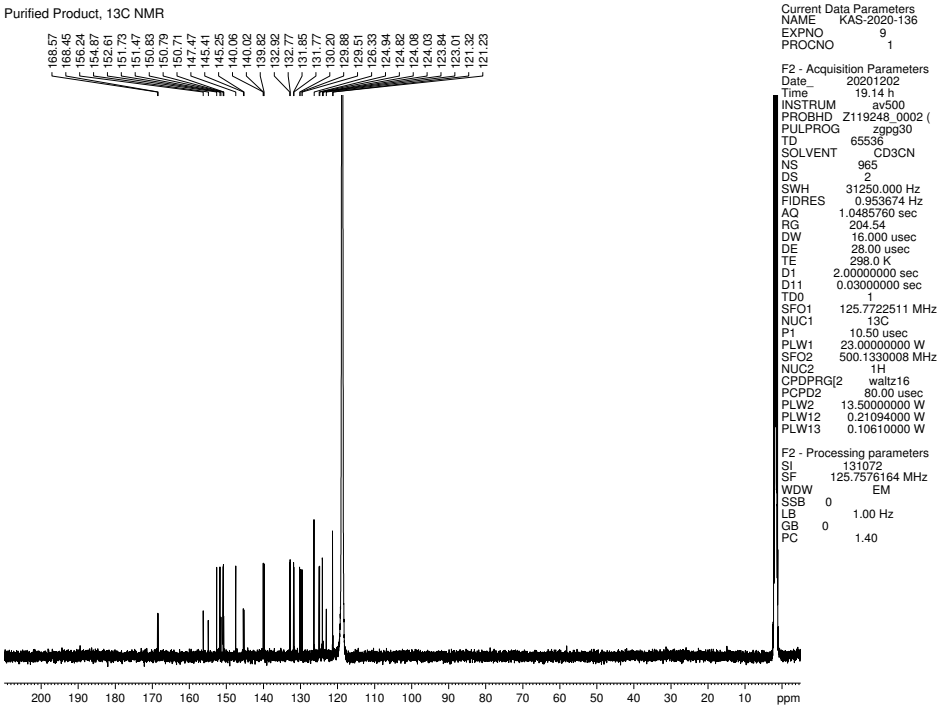

Figure 4.32 ^{13}C NMR (125 MHz, CD_3CN) of compound **4.54**.

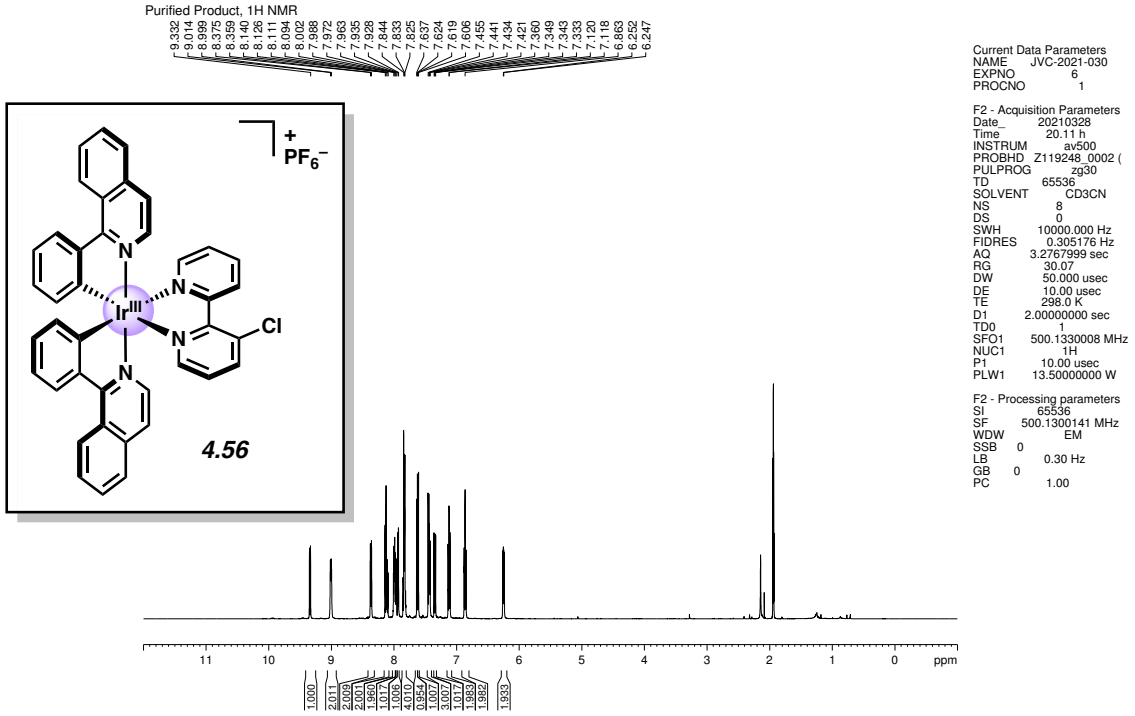

Figure 4.33 ^{1}H NMR (500 MHz, CD_3CN) of compound **4.56**.

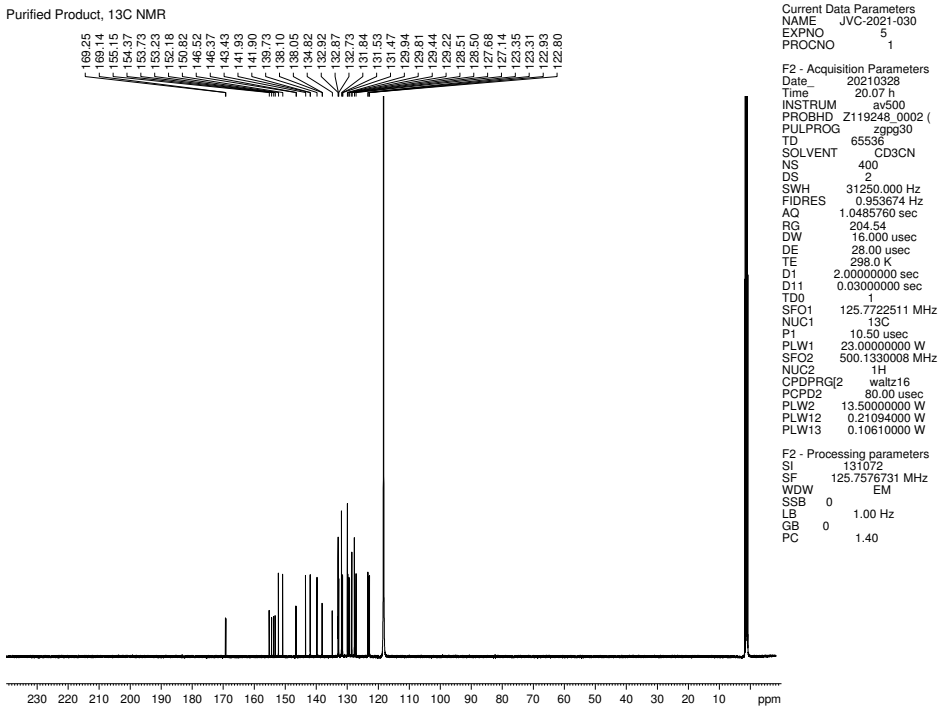

Figure 4.34 ^{13}C NMR (125 MHz, CD_3CN) of compound **4.56**.

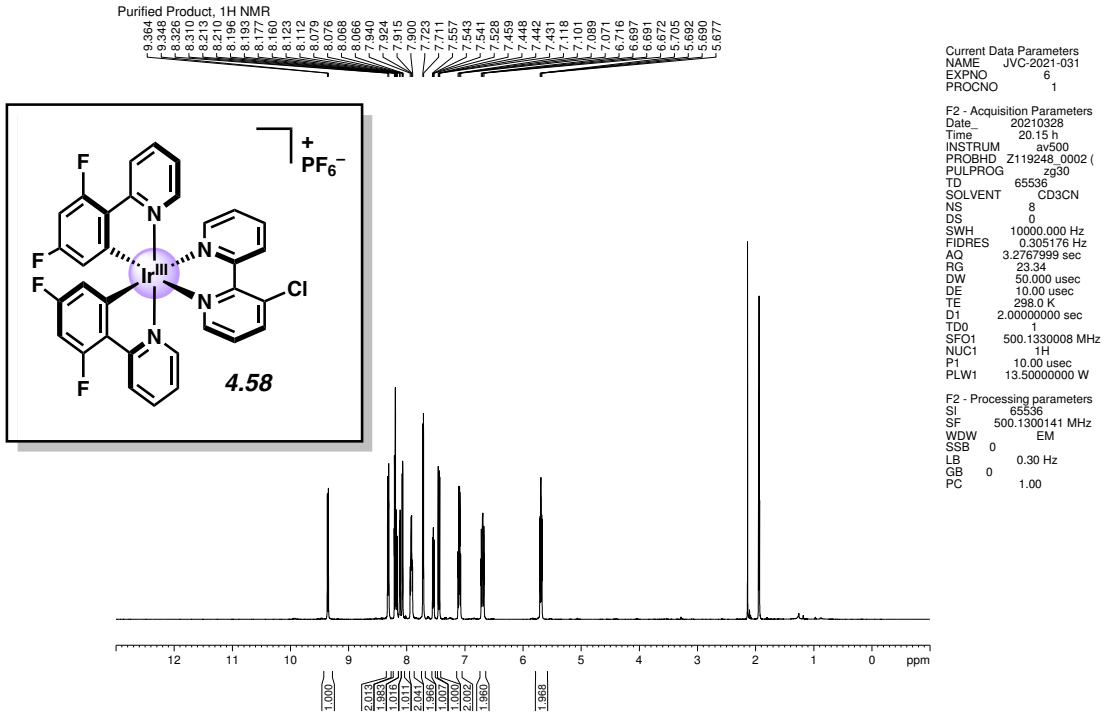

Figure 4.35 ^{1}H NMR (500 MHz, CD_3CN) of compound **4.58**.

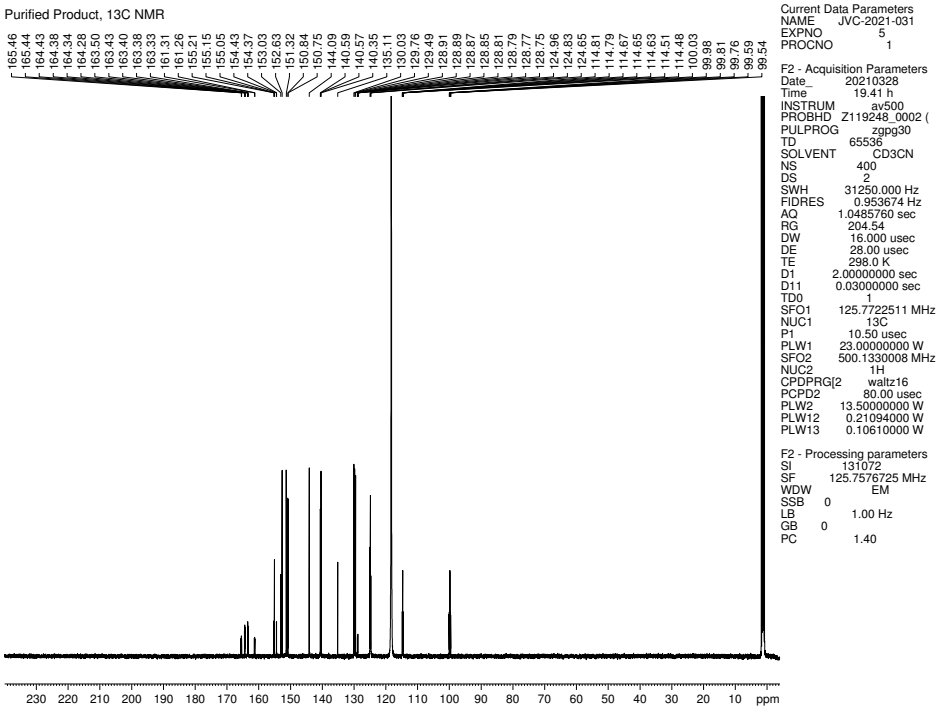

Figure 4.36 ^{13}C NMR (125 MHz, CD_3CN) of compound **4.58**.

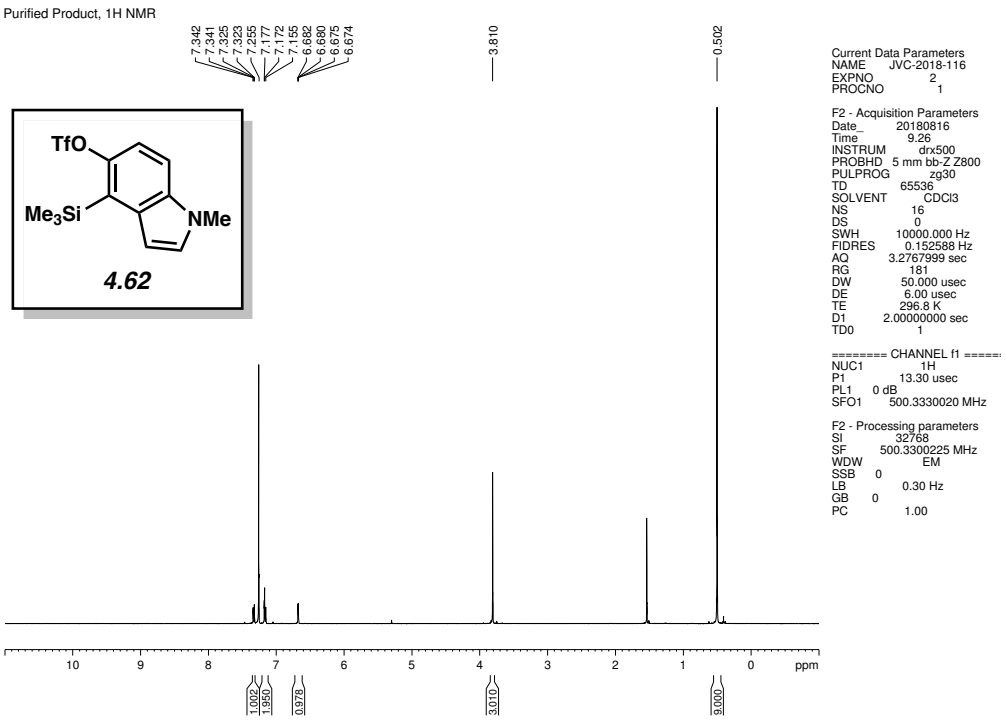

Figure 4.37 ^{1}H NMR (500 MHz, $CDCl_3$) of compound **4.62**.

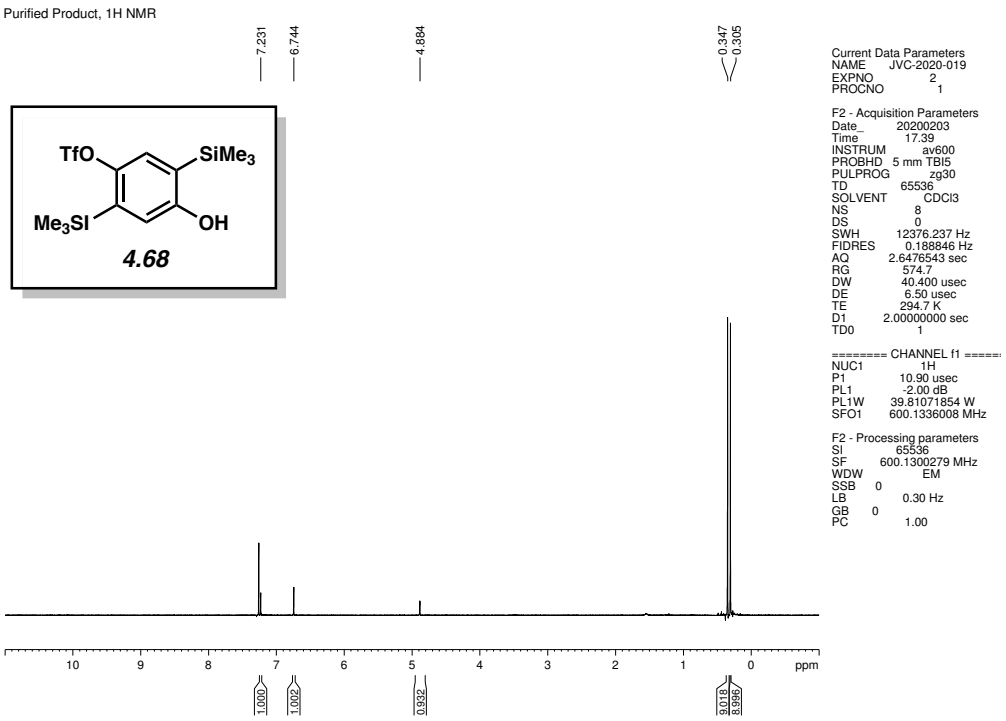

Figure 4.38 ^{1}H NMR (600 MHz, $CDCl_3$) of compound **4.68**.

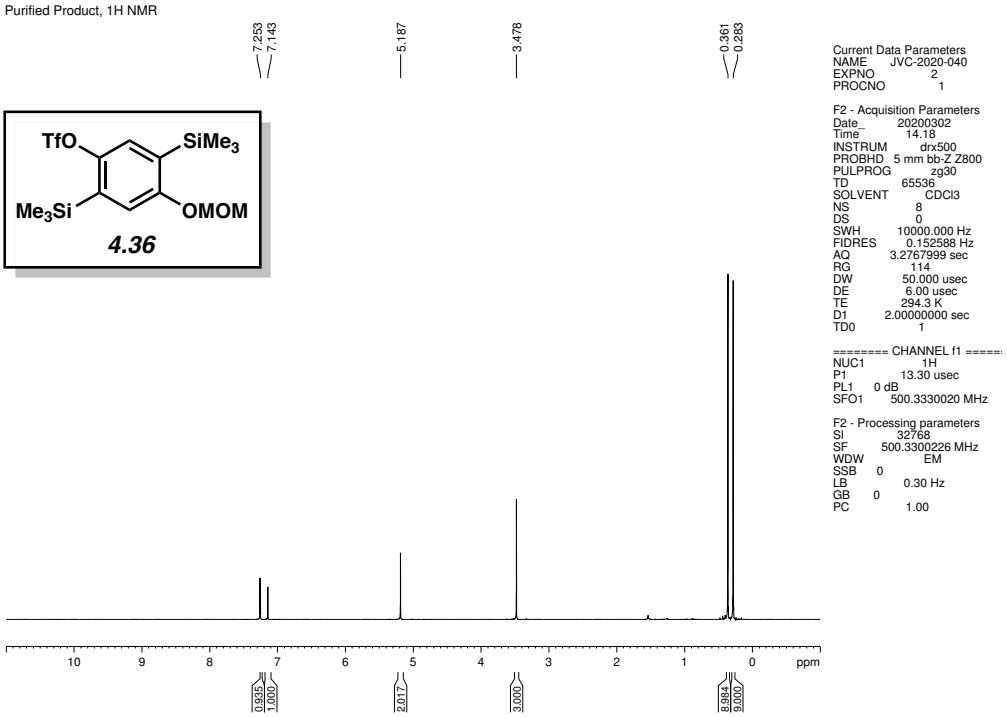

Figure 4.39 ^{1}H NMR (500 MHz, CD_3CN) of compound **4.36**.

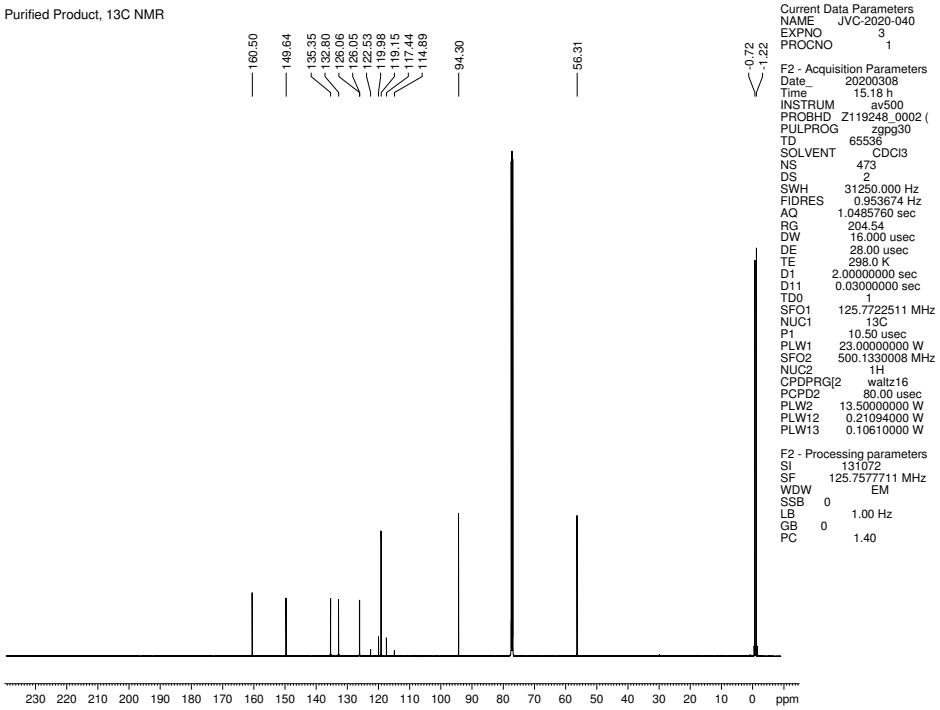

Figure 4.40 ^{13}C NMR (125 MHz, CD_3CN) of compound **4.36**.

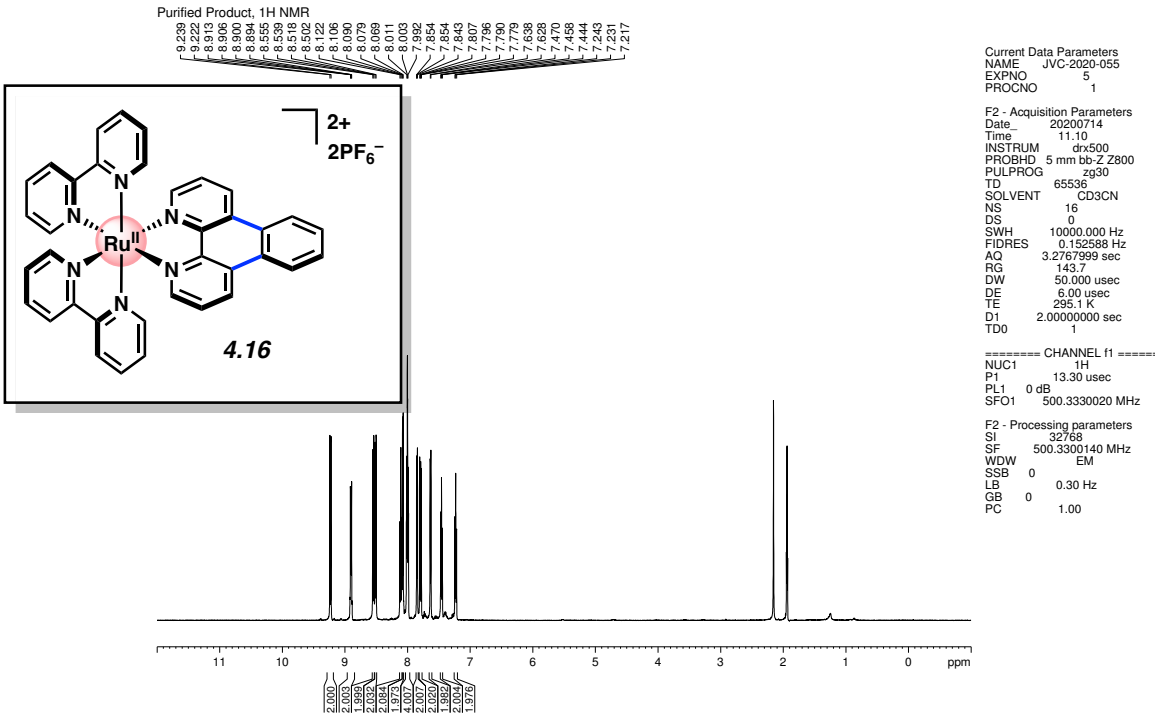

Figure 4.41 ^{1}H NMR (500 MHz, CD_3CN) of compound **4.16**.

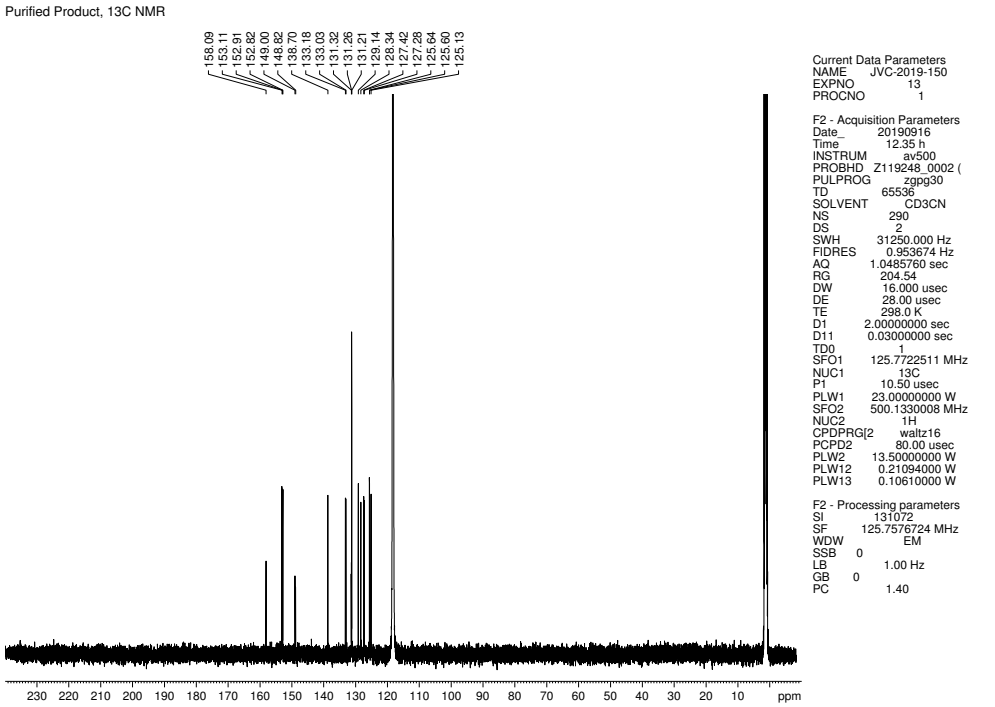

Figure 4.42 ^{13}C NMR (125 MHz, CD_3CN) of compound **4.16**.

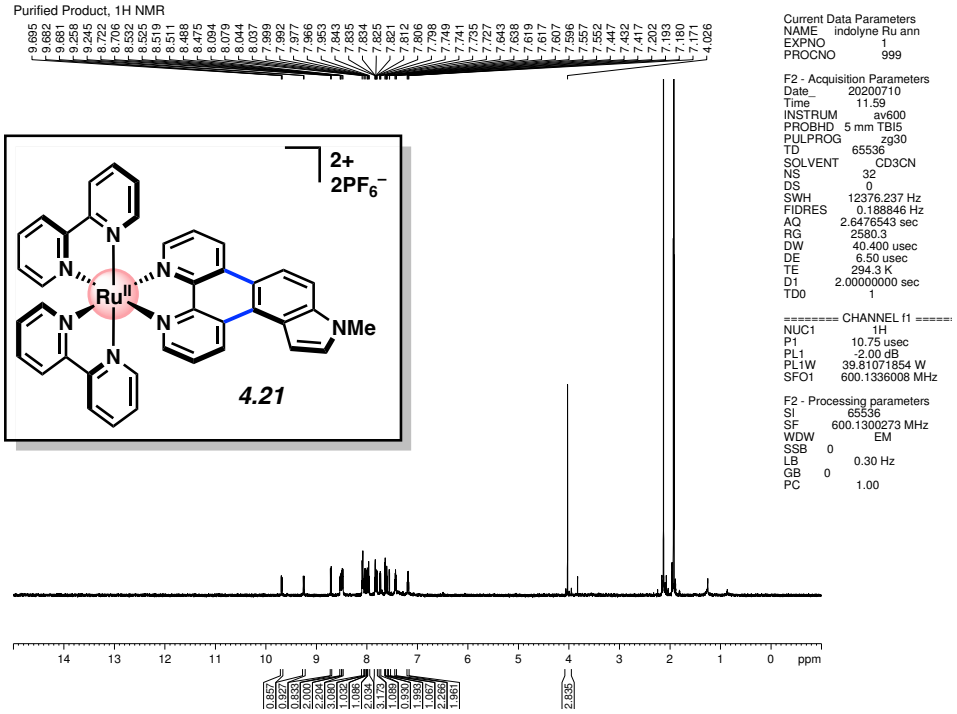

Figure 4.43 ^{1}H NMR (600 MHz, CD_3CN) of compound **4.21**.

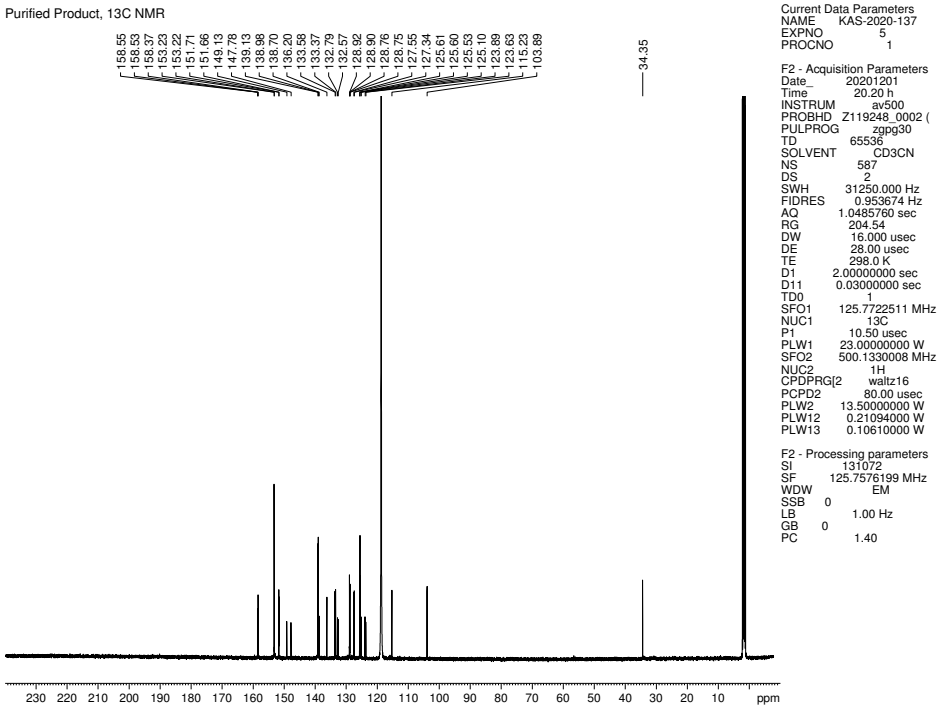

Figure 4.44 ^{13}C NMR (125 MHz, CD_3CN) of compound **4.21**.

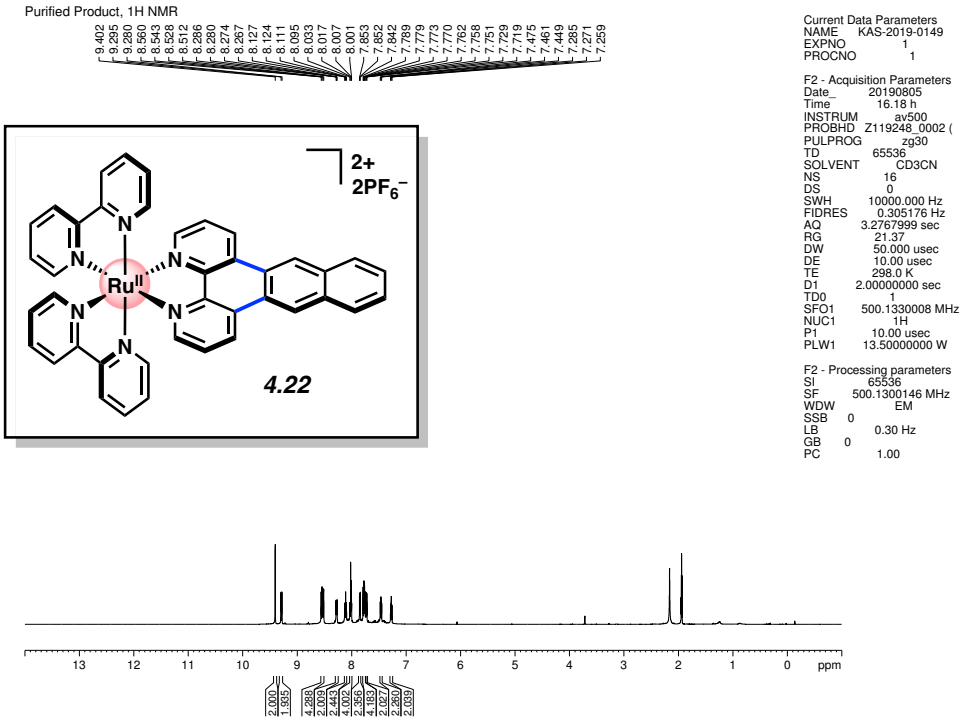

Figure 4.45 ^{1}H NMR (500 MHz, CD_3CN) of compound **4.22**.

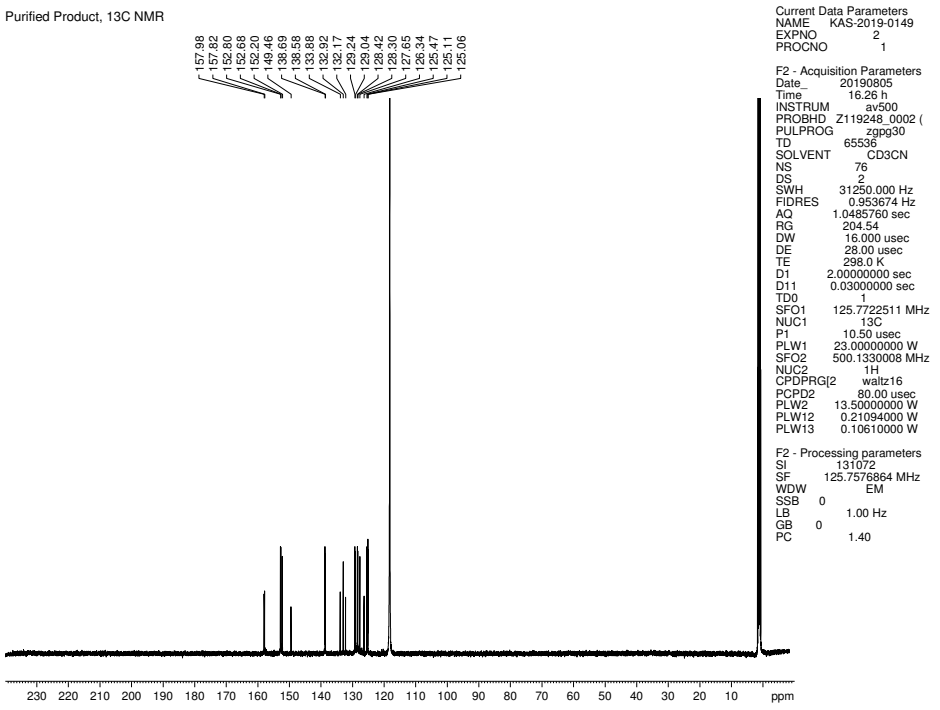

Figure 4.46 ^{1}H NMR (500 MHz, CD_3CN) of compound **4.22**.

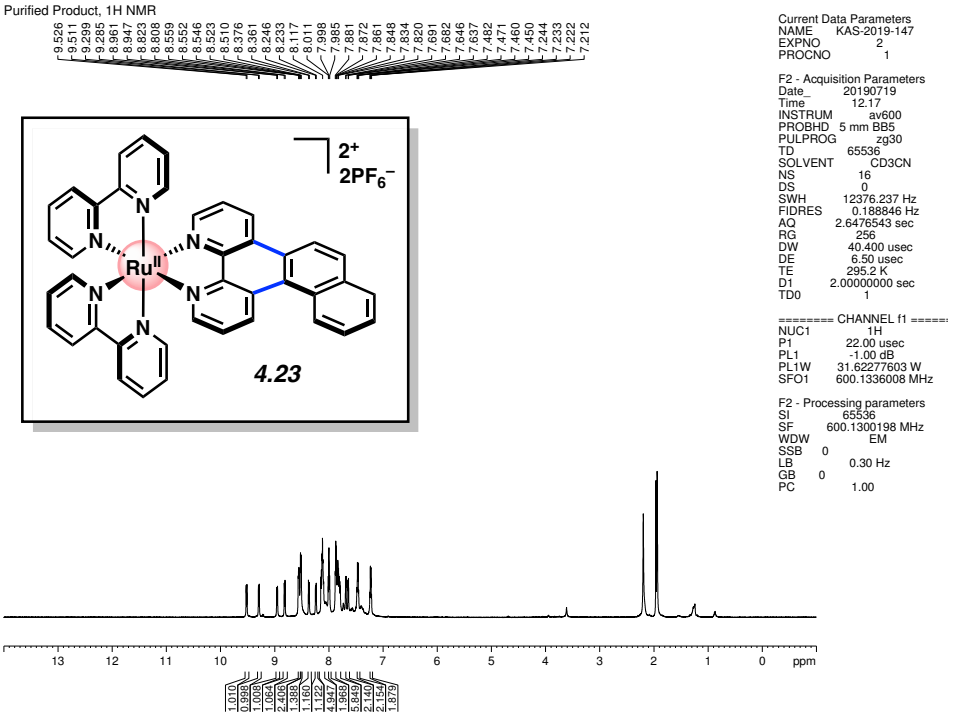

Figure 4.47 ^{1}H NMR (600 MHz, CD_3CN) of compound **4.23**.

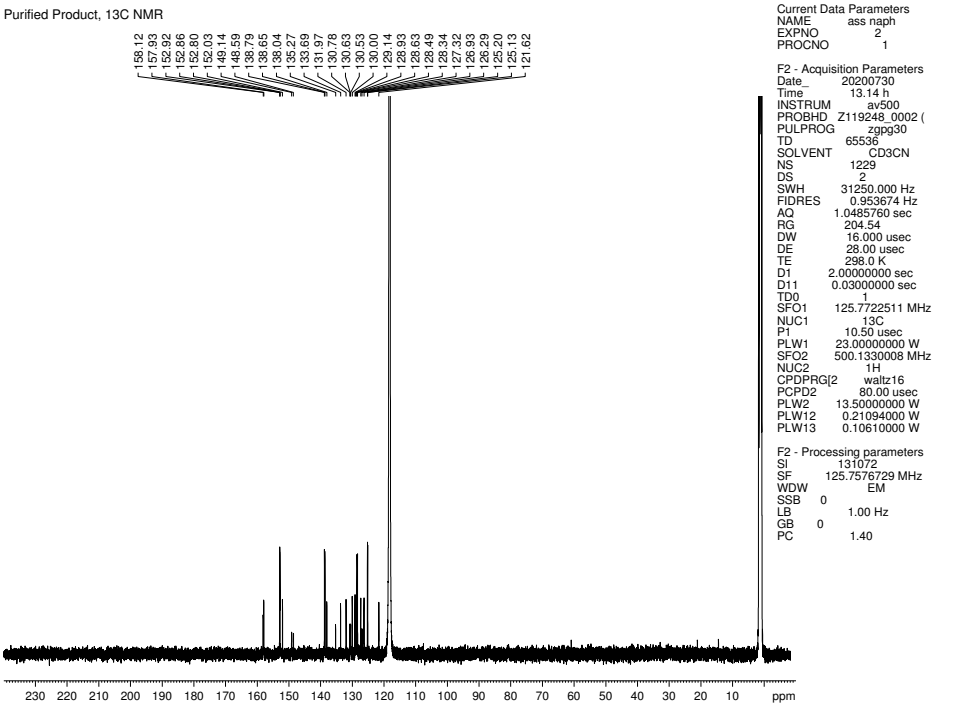

Figure 4.48 ^{13}C NMR (125 MHz, CD_3CN) of compound **4.23**.

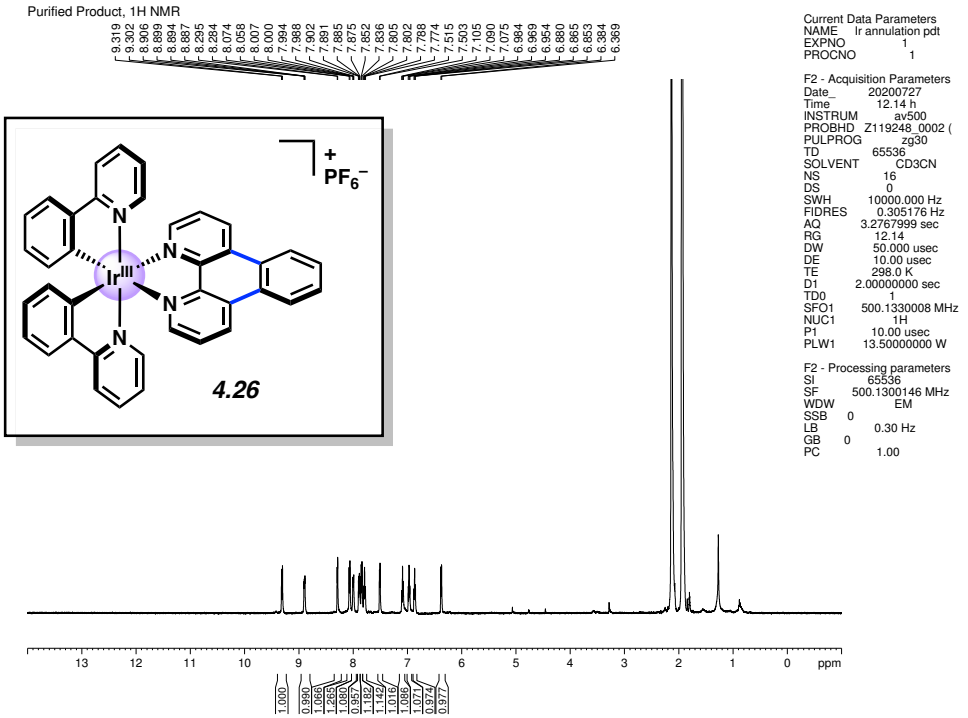

Figure 4.49 ^{1}H NMR (500 MHz, CD_3CN) of compound **4.26**.

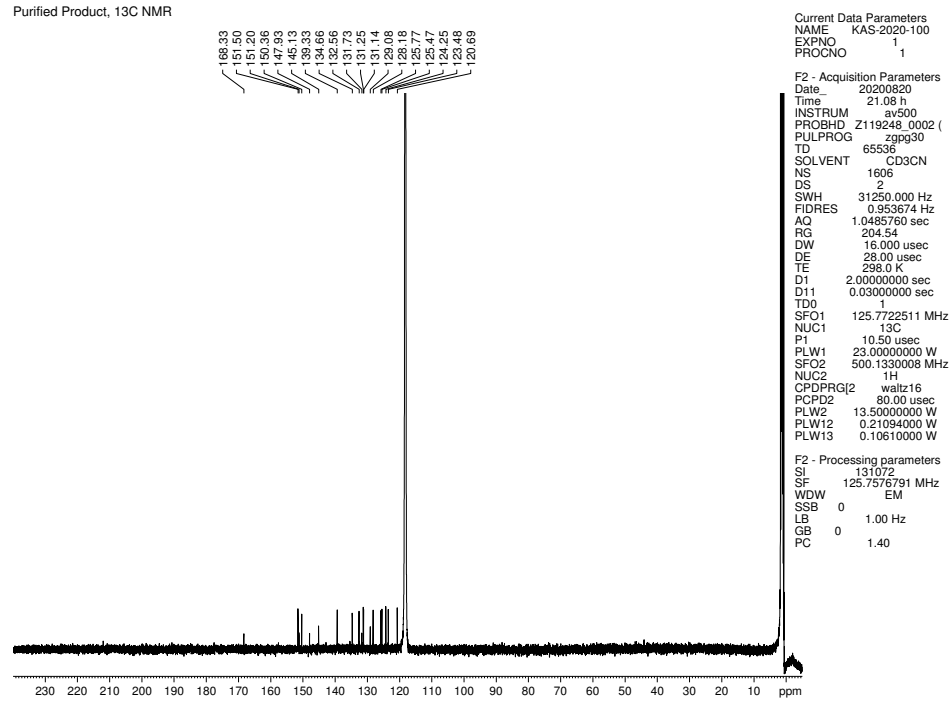

Figure 4.50 ^{13}C NMR (125 MHz, CD_3CN) of compound **4.26**.

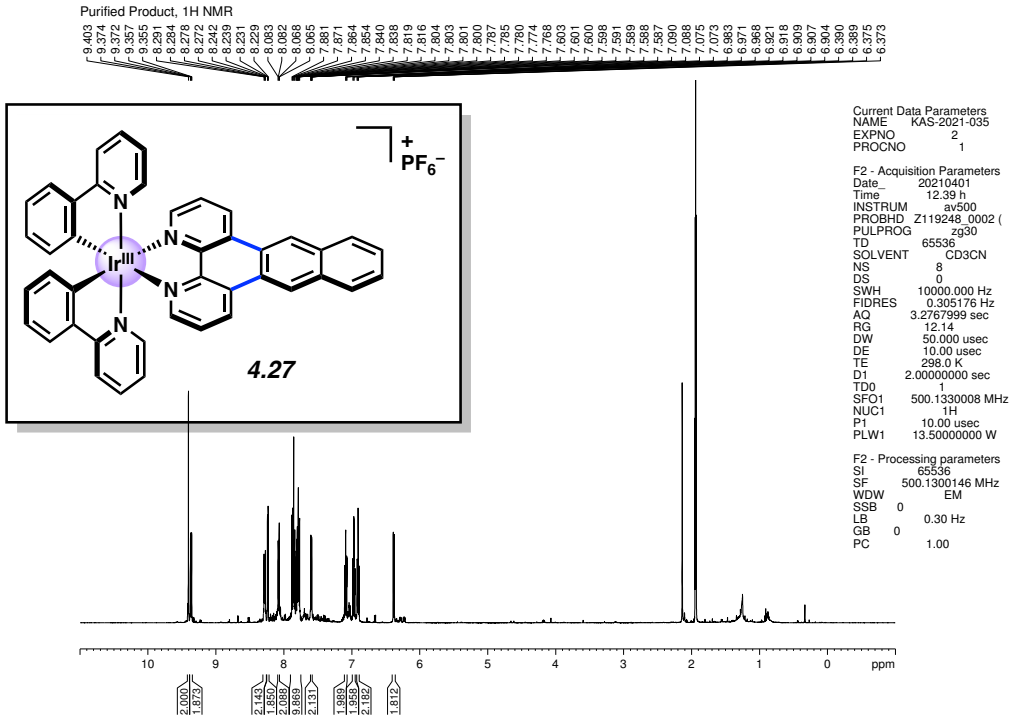

Figure 4.51 ^{1}H NMR (500 MHz, CD_3CN) of compound **4.27**.

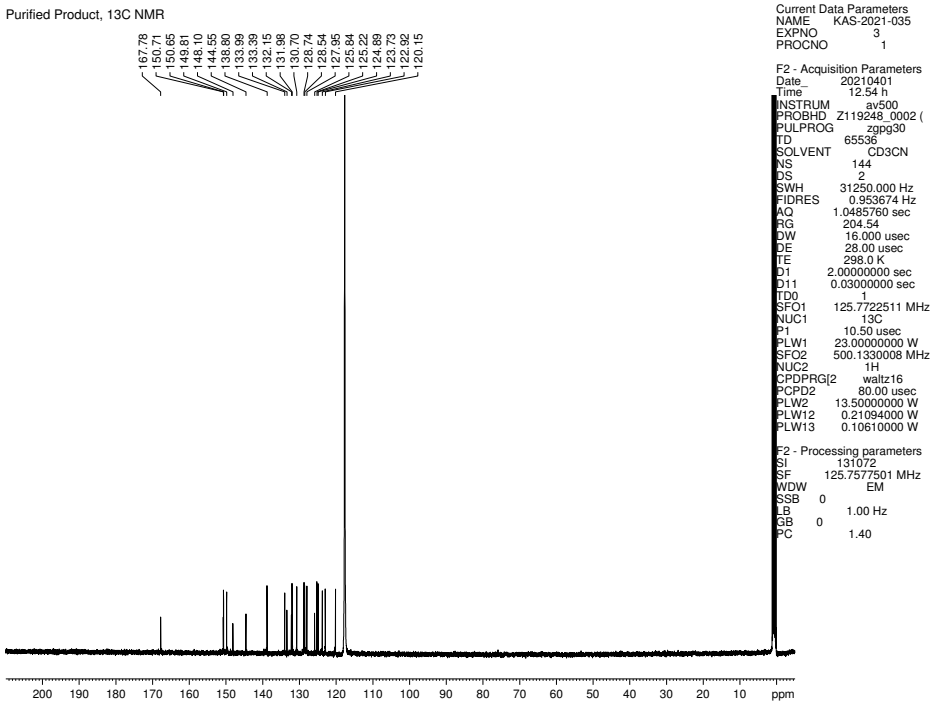

Figure 4.52 ^{13}C NMR (125 MHz, CD_3CN) of compound **4.27**.

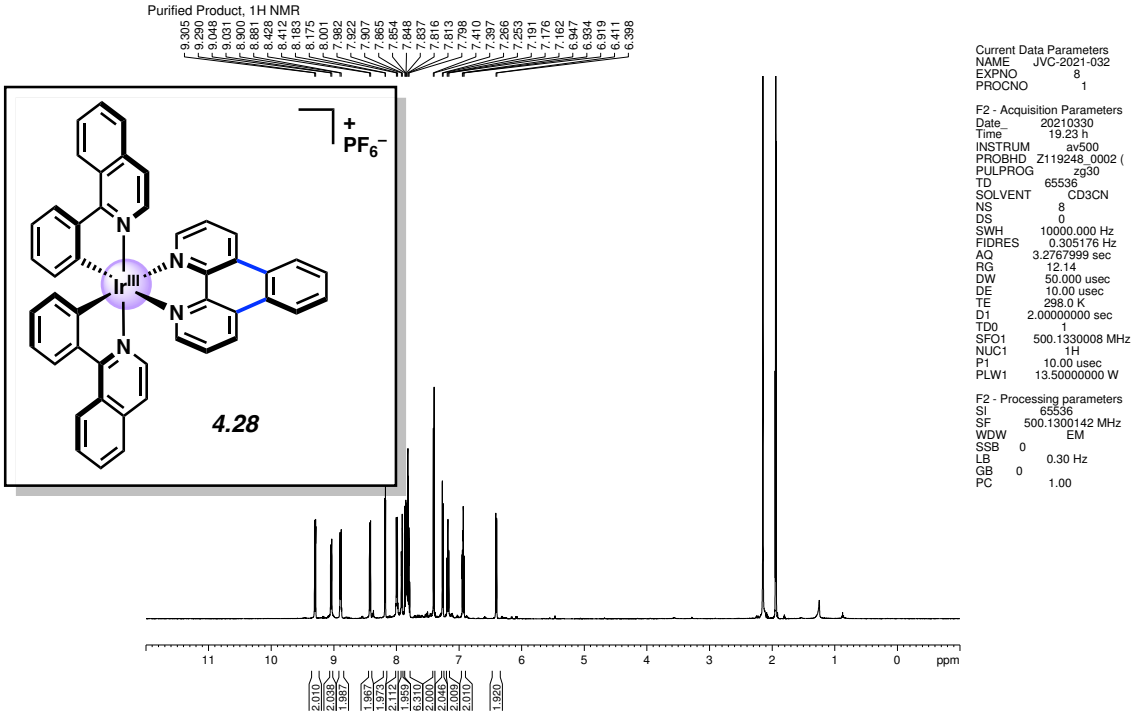

Figure 4.53 ^{1}H NMR (500 MHz, CD_3CN) of compound **4.28**.

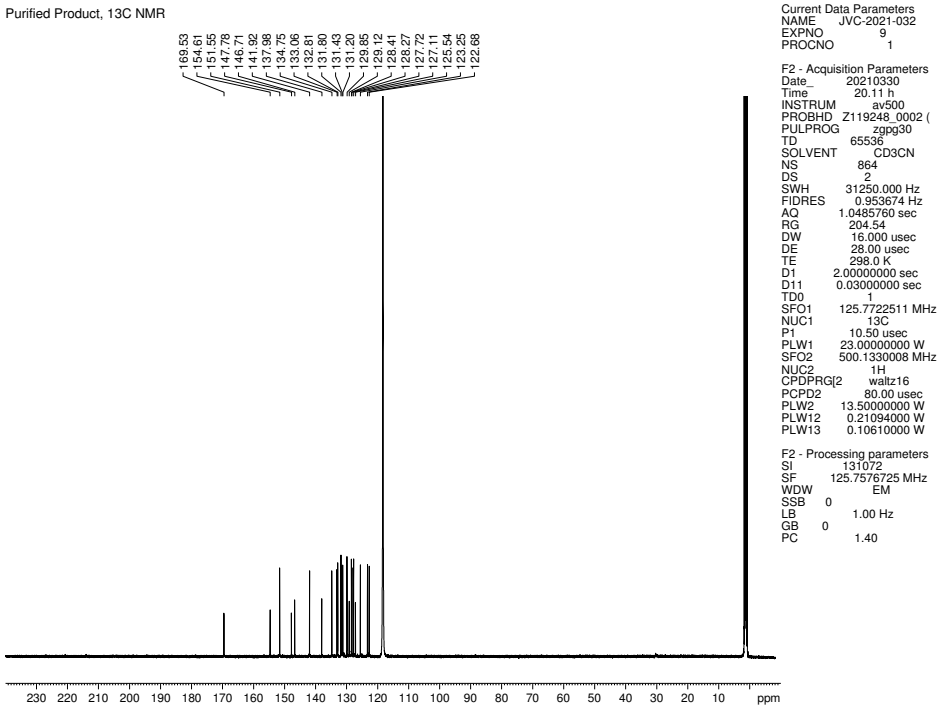

Figure 4.54 ^{1}H NMR (125 MHz, CD_3CN) of compound **4.28**.

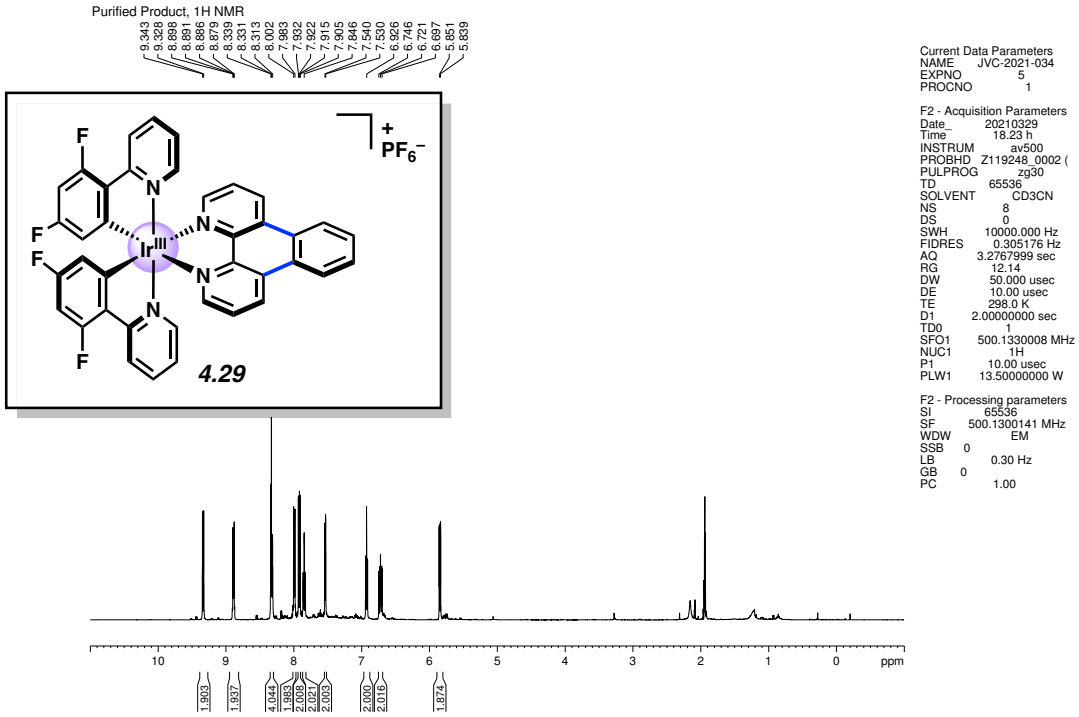

Figure 4.55 ^{1}H NMR (500 MHz, CD_3CN) of compound **4.29**.

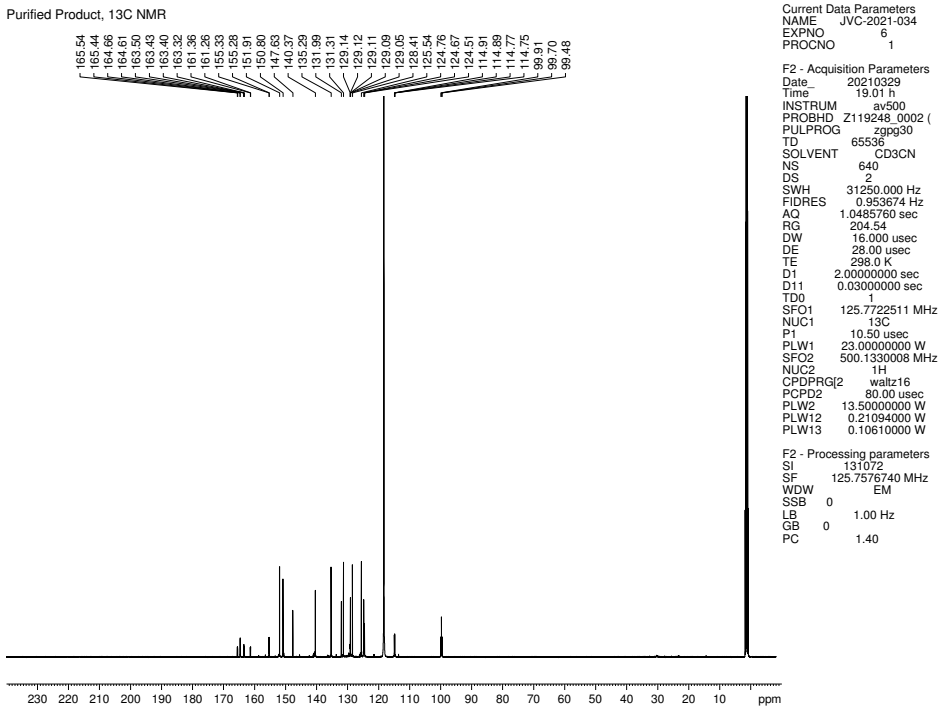

Figure 4.56 ^{13}C NMR (125 MHz, CD_3CN) of compound **4.29**.

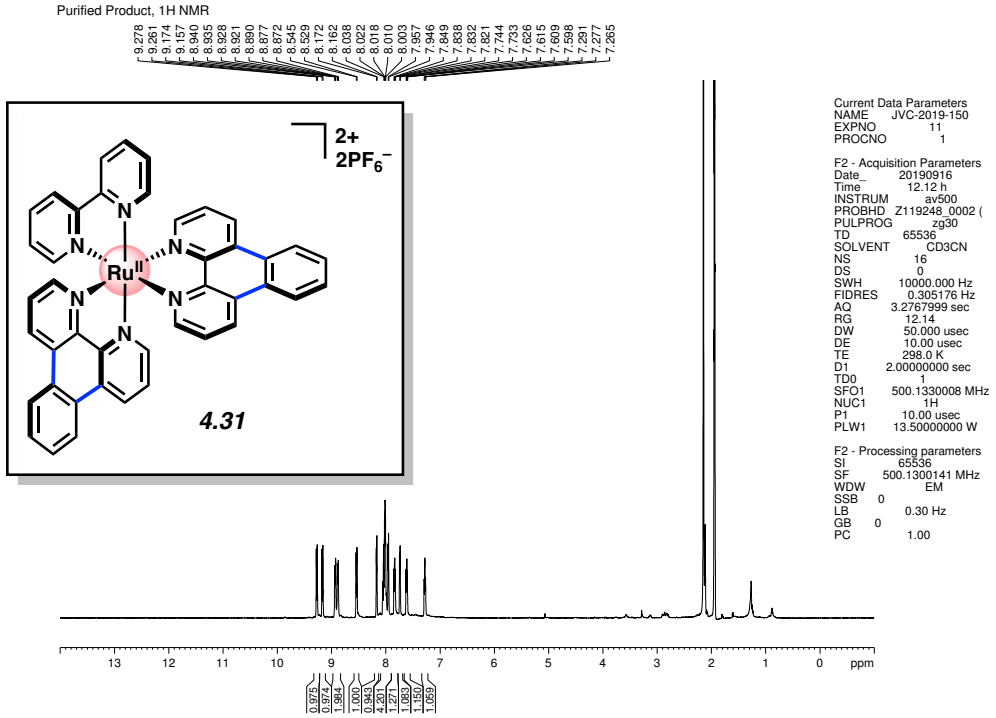

Figure 4.57 ^{1}H NMR (500 MHz, CD_3CN) of compound **4.31**.

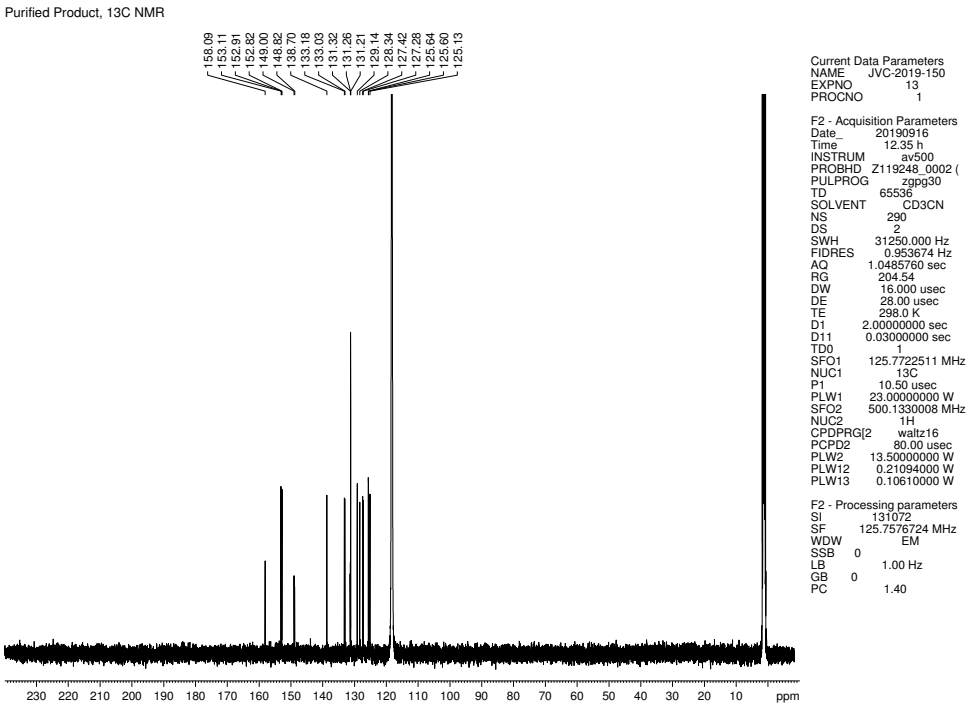

Figure 4.58 ^{13}C NMR (125 MHz, CD_3CN) of compound **4.31**.

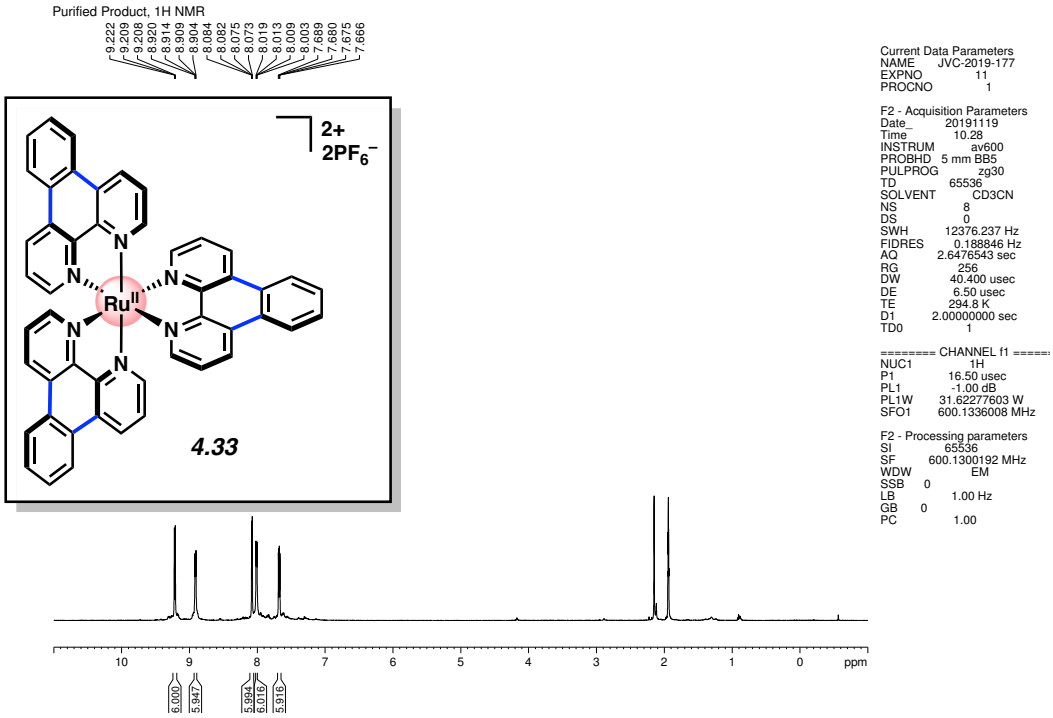

Figure 4.59 ^{1}H NMR (600 MHz, CD_3CN) of compound **4.33**.

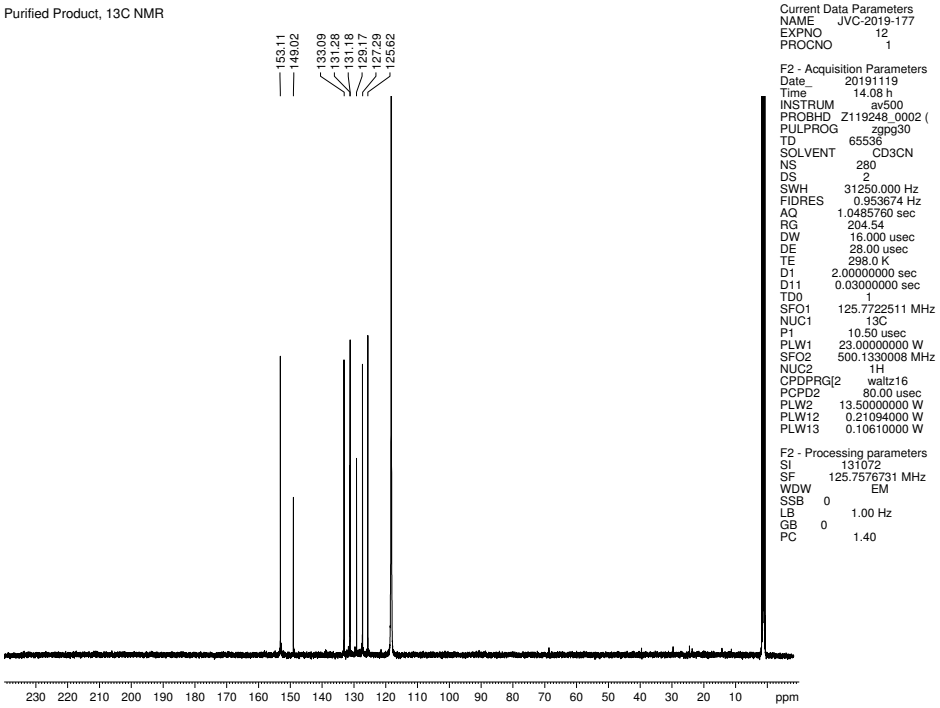

Figure 4.60 ^{13}C NMR (125 MHz, CD_3CN) of compound **4.33**.

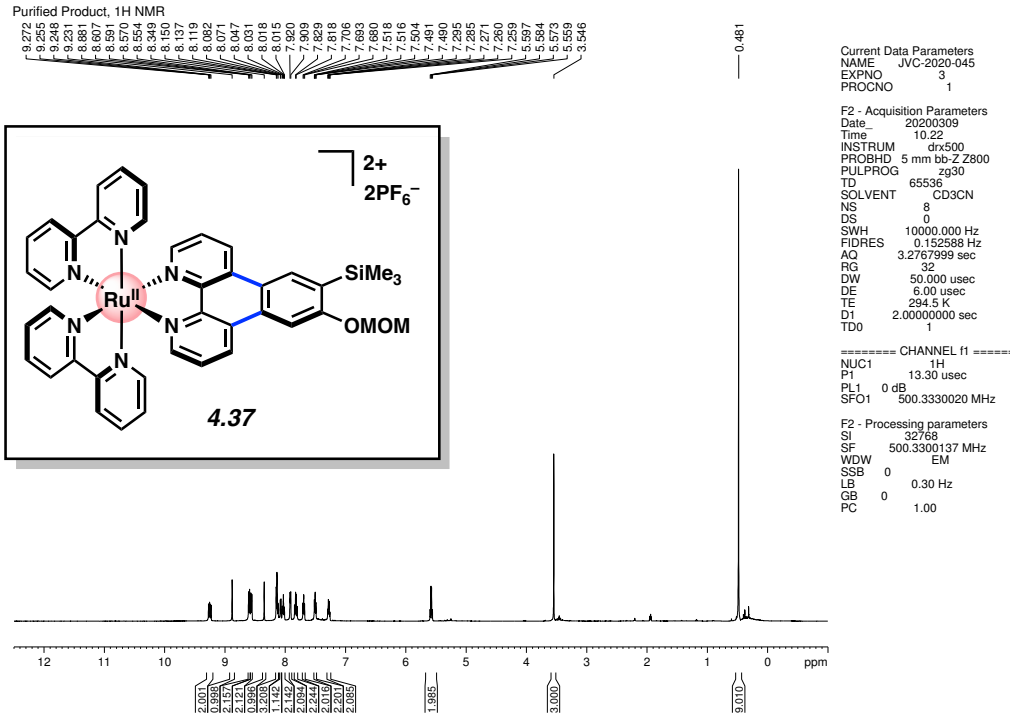

Figure 4.61 ^{1}H NMR (500 MHz, CD_3CN) of compound **4.37**.

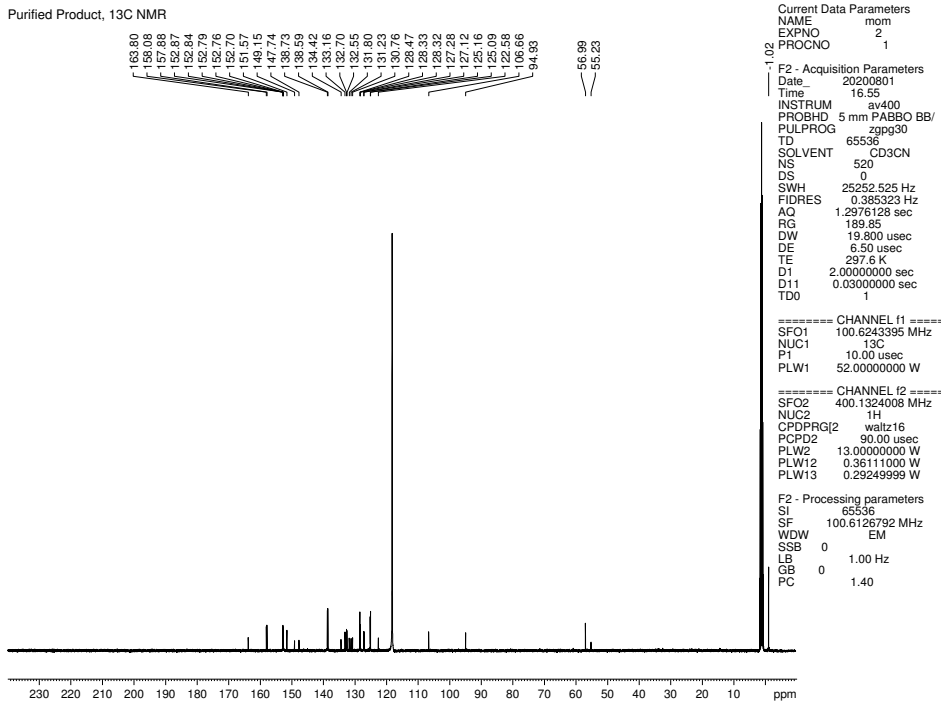

Figure 4.62 ^{13}C NMR (100 MHz, CD_3CN) of compound **4.37**.

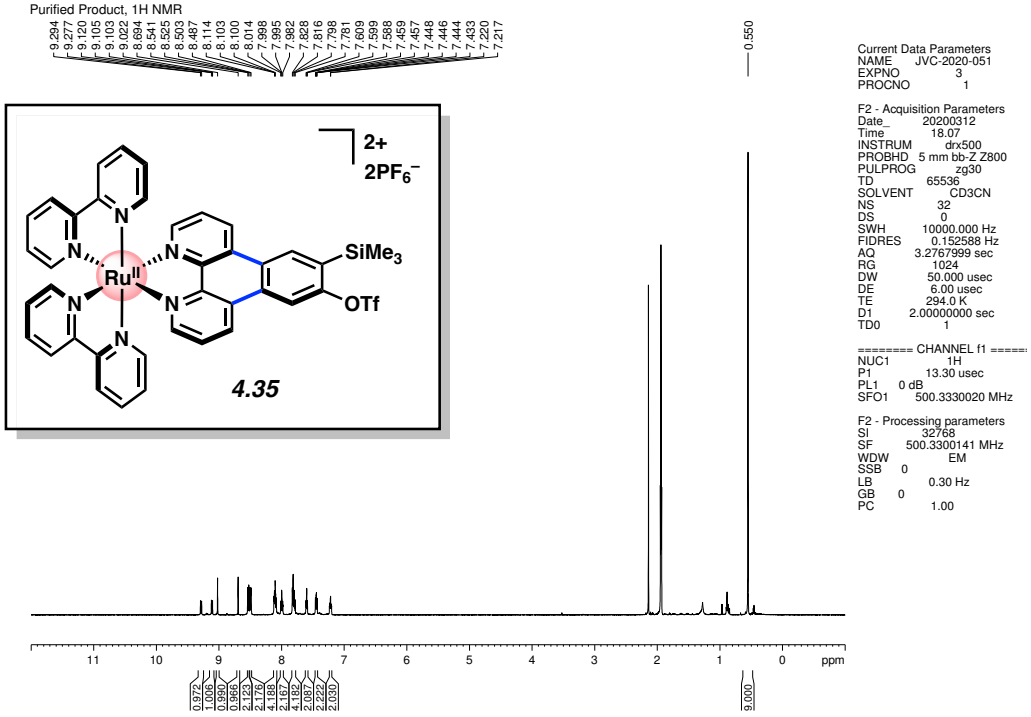

Figure 4.63 ^{1}H NMR (500 MHz, CD_3CN) of compound **4.35**.

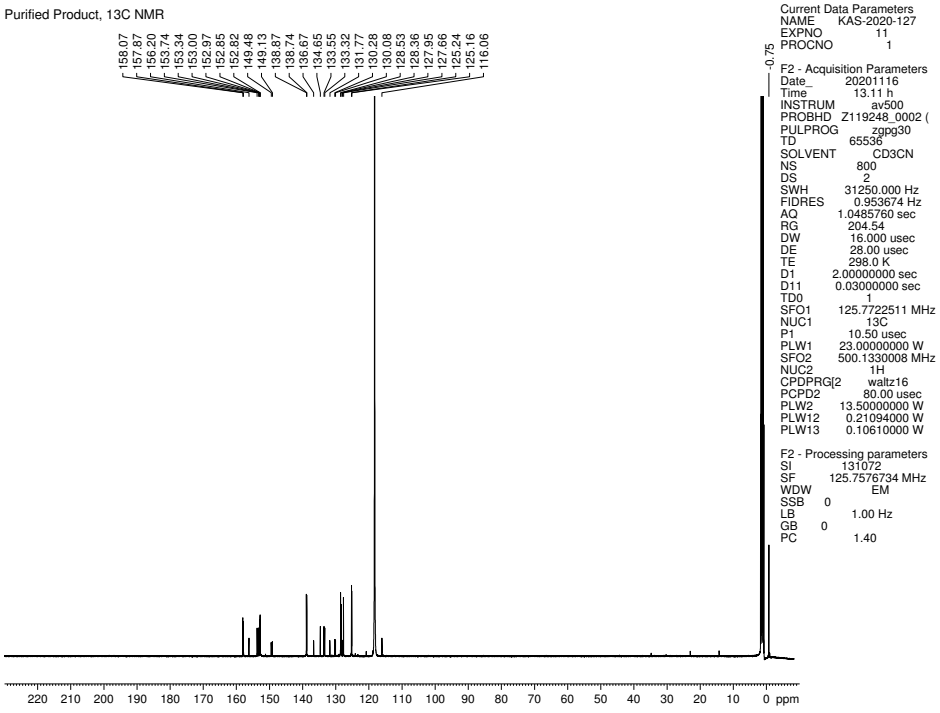

Figure 4.64 ^{13}C NMR (125 MHz, CD_3CN) of compound **4.35**.

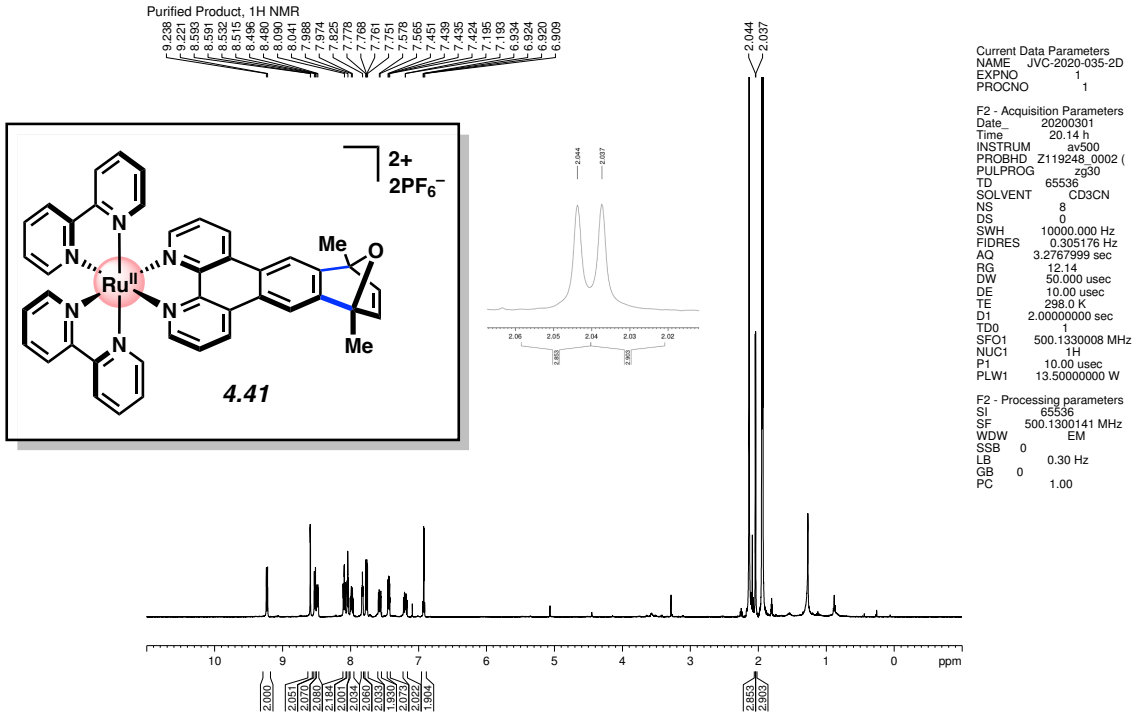

Figure 4.65 ^{1}H NMR (500 MHz, CD_3CN) of compound **4.41**.

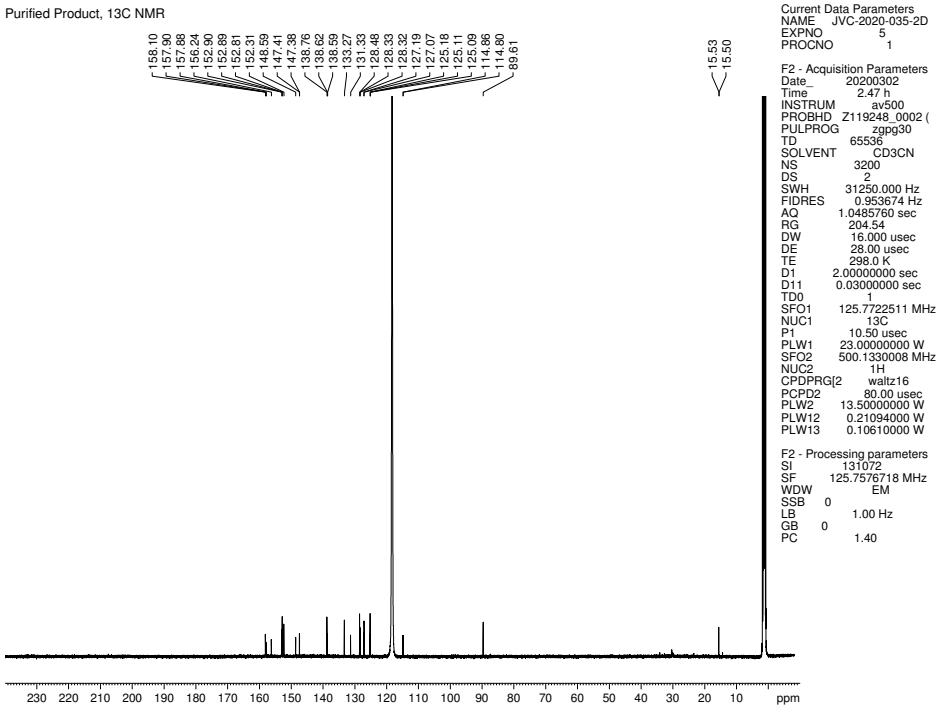

Figure 4.66 ^{13}C NMR (125 MHz, CD_3CN) of compound **4.41**.

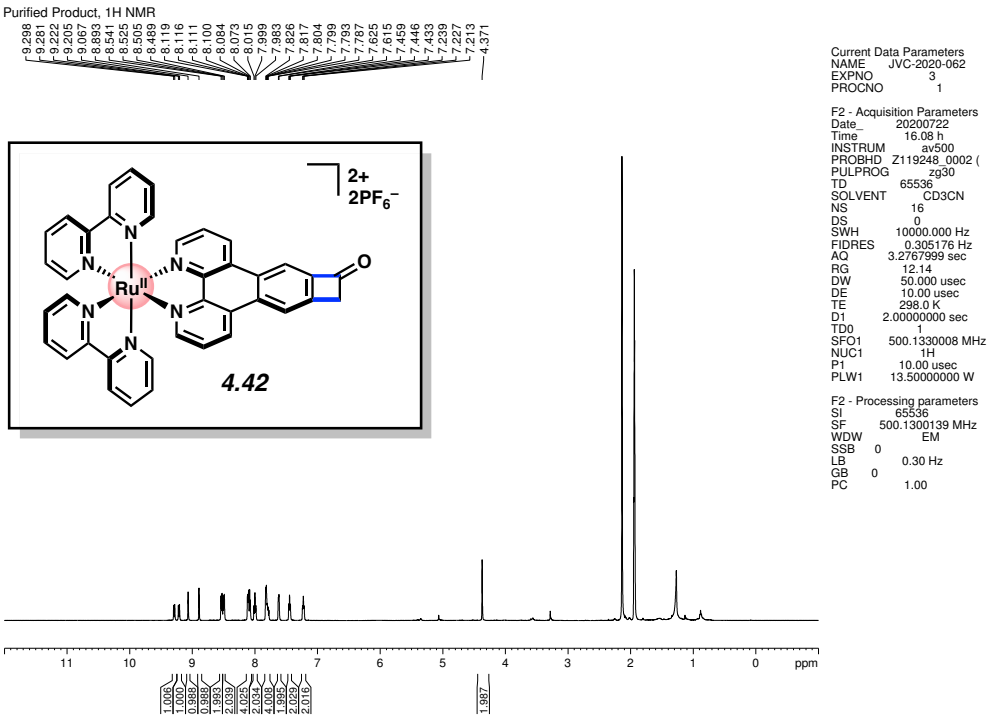

Figure 4.67 ^{1}H NMR (500 MHz, CD_3CN) of compound **4.42**.

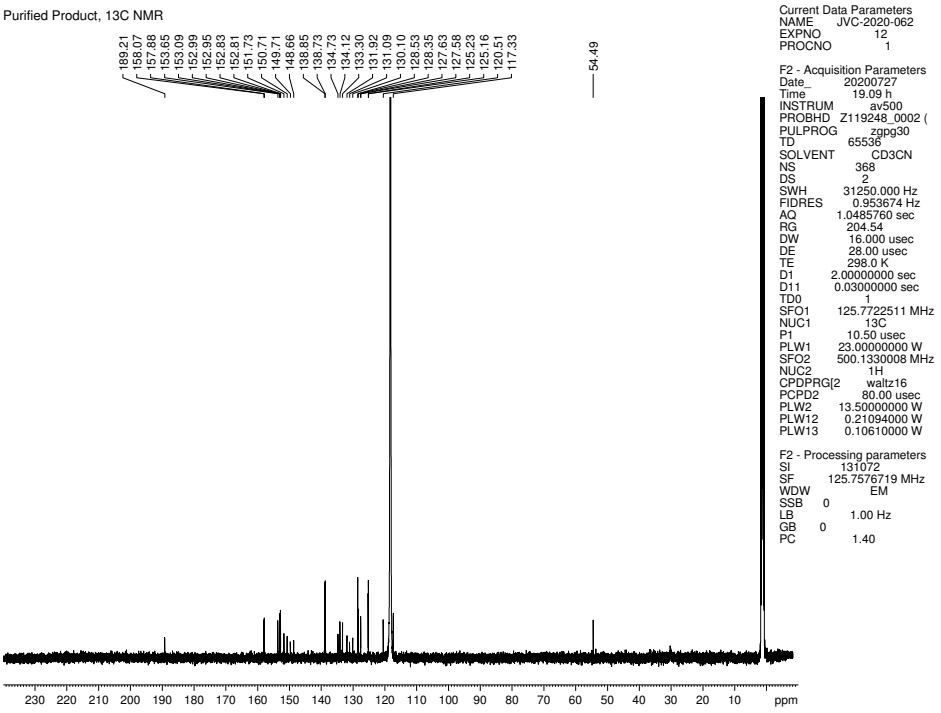

Figure 4.68 ^{13}C NMR (125 MHz, CD_3CN) of compound **4.42**.

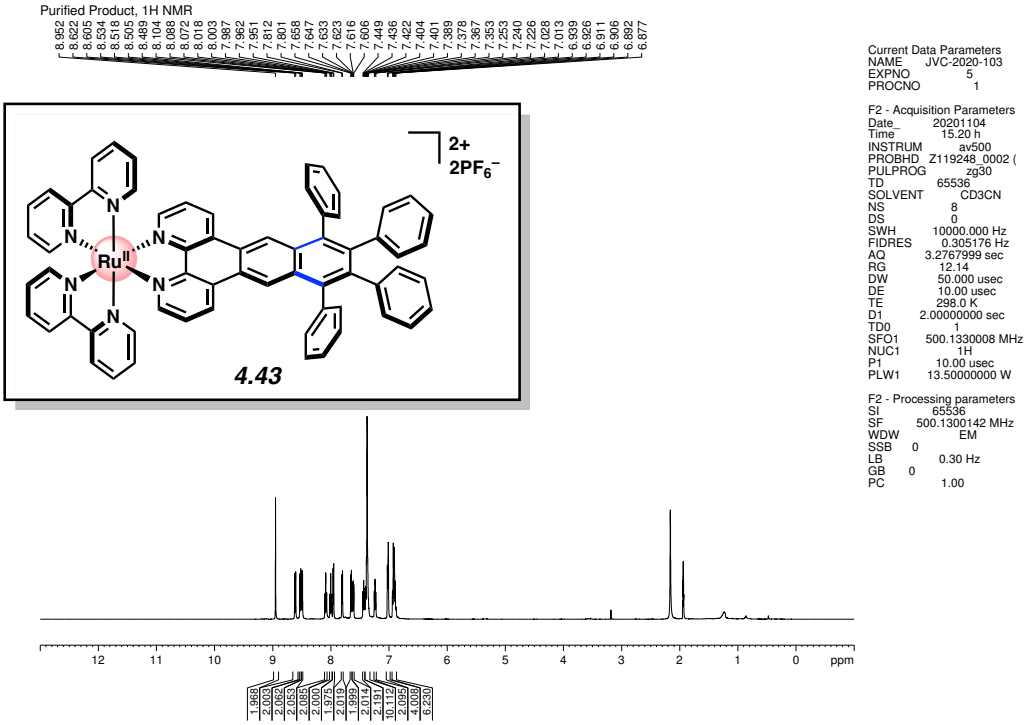

Figure 4.69 ^{1}H NMR (500 MHz, CD_3CN) of compound **4.43**.

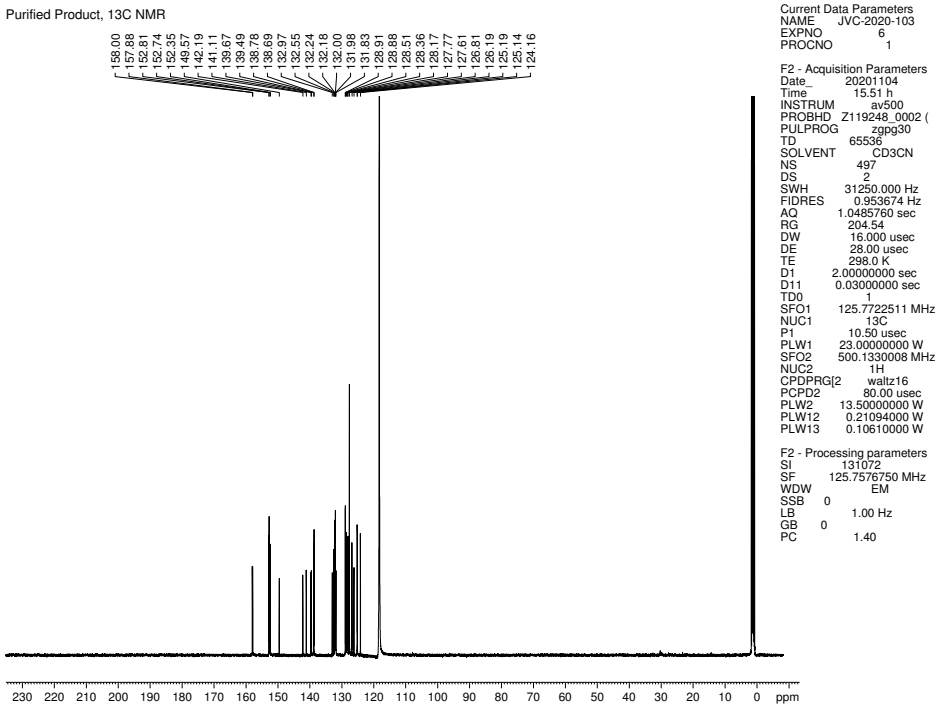

Figure 4.70 ^{13}C NMR (125 MHz, CD_3CN) of compound **4.43**.

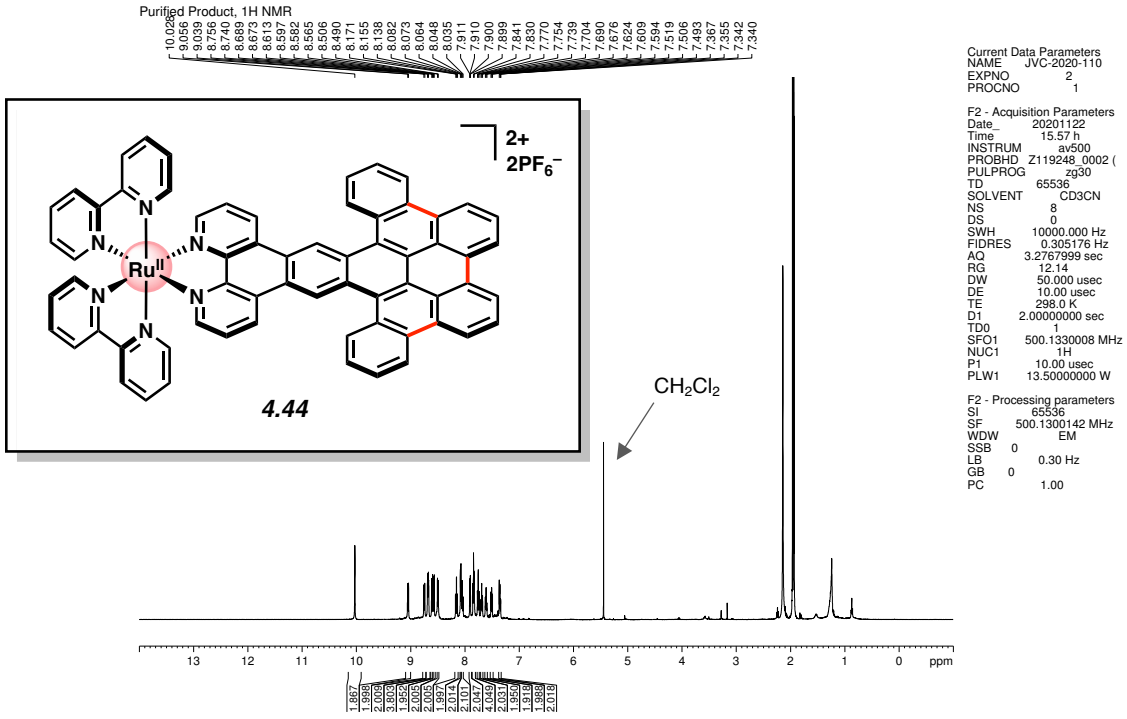

Figure 4.71 ^{1}H NMR (500 MHz, CD_3CN) of compound **4.44**.

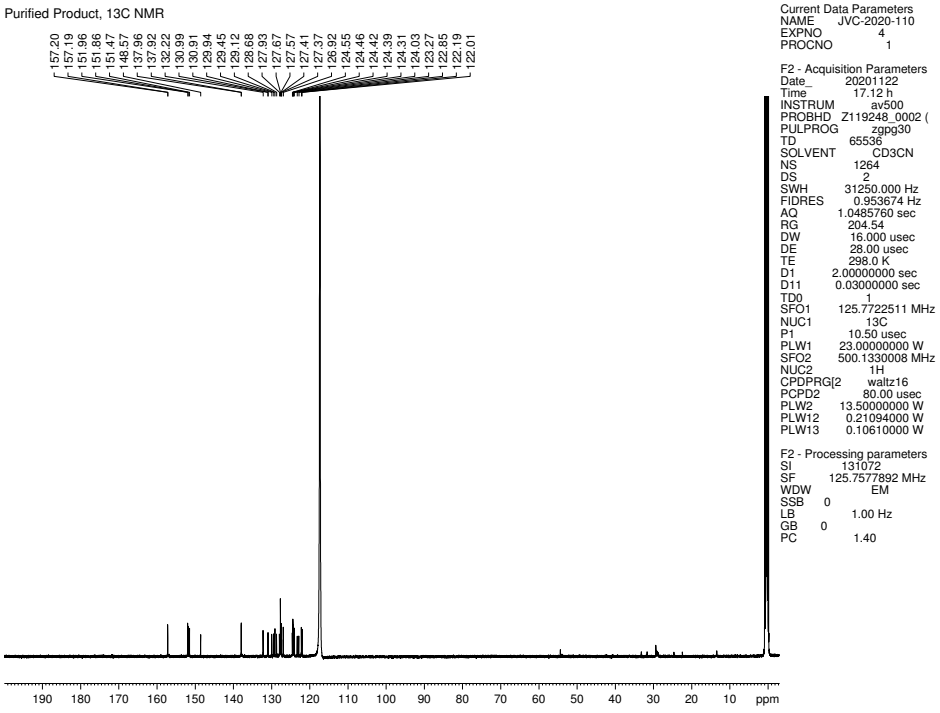

Figure 4.72 ^{13}C NMR (125 MHz, CD_3CN) of compound **4.44**.

4.10 Notes and References

(1) Noyori, R.; Kitamura, M.; Ohkuma, T. Toward Efficient Asymmetric Hydrogenation: Architectural and Functional Engineering of Chiral Molecular Catalysts. *Proc. Natl. Acad. Sci. U.S.A.* **2004**, *101*, 5356–5362.

(2) Monro, S.; Colón, K. L.; Yin, H.; Roque, J., III.; Konda, P.; Gujar, S.; Thummel, R. P.; Lilge, L.; Cameron, C. G.; McFarland, S. A. Transition Metal Complexes and Photodynamic Therapy from a Tumor-Centered Approach: Challenges, Opportunities, and Highlights from the Development of TLD1433. *Chem. Rev.* **2019**, *119*, 797–828.

(3) Linck, R. C.; Rauchfuss, T. B. In *Bioorganometallics: Biomolecules, Labeling, Medicine;* Wiley–VCH; Weinheim, 2005; pp 403–435.

(4) Braunstein, P. Functional Ligands and Complexes for New Structures, Homogeneous Catalysts and Nanomaterials. *J. Organomet. Chem.* **2004**, *689*, 3953–3967.

(5) Zucker, S. P.; Wossidlo, F.; Weber, M.; Lentz, D.; Tzschucke, C. C. Palladium-Catalyzed Directed Halogenation of Bipyridine *N*-Oxides. *J. Org. Chem.* **2017**, *82*, 5616–5635.

(6) Soulis, K.; Gourlaouen, C.; Daniel, C.; Quatela, A.; Odobel, F.; Blart, E.; Pellegrin, Y. New Luminescent Copper(I) Complexes with Extended π-Conjugation. *Polyhedron* **2018**, *140*, 42–50.

(7) Bolger, J.; Gourdon, A.; Ishow, E.; Launay, J.-P. Stepwise Syntheses of Mono- and Di-Nuclear Ruthenium tpphz Complexes $[(bpy)_2Ru(tpphz)]^{2-}$ and $[(bpy)_2Ru(tpphz)Ru(bpy)_2]^{4+}$ {tpphz = tetrapyrido[3,2-a: 2′,3′-c: 3″,2″-h: 2″,3‴-j]phenazine}. *J. Chem. Soc., Chem. Commun.* **1995**, 1799–1800.

(8) Mede, T.; Jäger, M.; Schubert, U. S. "Chemistry-on-the-Complex": Functional Ru^{II} Polypyridyl-Type Sensitizers as Divergent Building Blocks. *Chem. Soc. Rev.* **2018**, *47*, 7577–7627.

(9) Fang, Y.-Q.; Polson, M. I. J.; Hanan, G. S. Creating New Binding Sites in Ligands and Metal Complexes Using the Negishi Cross-Coupling Reaction. *Inorg. Chem.* **2003**, *42*, 5–7.

(10) Zedler, L.; Mengele, A. K.; Ziems, K. M.; Zhang, Y.; Wächtler, M.; Gräfe, S.; Pascher, T.; Rau, S.; Kupfer, S.; Dietzek, B. Unraveling the Light-Activated Reaction Mechanism in a Catalytically Competent Key Intermediate of a Multifunctional Molecular Catalyst for Artificial Photosynthesis. *Angew. Chem., Int. Ed.* **2019**, *58*, 13140–13148.

(11) Anderson, S. C.; Grounds, H.; Szalóki, G. Synthesis of Planar Chiral Ferrocenyl Cyclopentadienyl Chelate Ligand Precursors. *Tetrahedron: Asymmetry* **2013**, *24*, 1023–1034.

(12) Teimuri-Mofrad, R.; Mirzaei, F.; Abbasi, H.; Safa, K. D. Synthesis of new binuclear ferrocenyl compounds by hydrosilylation reactions. *C. R. Chimie.* **2017**, *20*, 197–205.

(13) Hiroto, S.; Miyake, Y.; Shinokubo, H. Synthesis and Functionalization of Porphyrins through Organometallic Methodologies. *Chem. Rev.* **2017**, *117*, 2910–3043.

(14) Liao, K.; Yang, Y.-F.; Li, Y.; Sanders, J. N.; Houk, K. N.; Musaev, D. G.; Davies, H. M. L. Design of Catalysts for Site-Selective and Enantioselective Functionalization of Non-Activated Primary C–H Bonds. *Nat. Chem.* **2018**, *10*, 1048–1055.

(15) Fukuzawa, S.; Oki, H.; Hosaka, M.; Sugasawa, J.; Kikuchi, S. ClickFerrophos: New Chiral Ferrocenyl Phosphine Ligands Synthesized by Click Chemistry and the Use of

Their Metal Complexes as Catalysts for Asymmetric Hydrogenation and Allylic Substitution. *Org. Lett.* **2007**, *9*, 5557–5560.

(16) Huber, F. L.; Nauroozi, D.; Mengele, A. K.; Rau, S. Synthesis and Characterization of a Ruthenium(II) Complex for the Development of Supramolecular Photocatalysts Containing Multidentate Coordination Spheres. *Eur. J. Inorg. Chem.* **2017**, 4020–4027.

(17) Nakamura, Y.; Yoshida, S.; Hosoya, T. Recent Advances in Synthetic Hetaryne Chemistry. *Heterocycles* **2019**, *98*, 1623–1677.

(18) Pellissier, H.; Santelli, M. The Use of Arynes in Organic Synthesis. *Tetrahedron* **2003**, *59*, 701–730.

(19) Wenk, H. H.; Winkler, M.; Sander, W. One Century of Aryne Chemistry. *Angew. Chem., Int. Ed.* **2003**, *42*, 502–528.

(20) Sanz, R. Recent Applications of Aryne Chemistry to Organic Synthesis. A Review. *Org. Prep. Proced. Int.* **2008**, *40*, 215–291.

(21) Gampe, C. M.; Carreira, E. M. Arynes and Cyclohexyne in Natural Product Synthesis. *Angew. Chem., Int. Ed.* **2012**, *51*, 3766–3778.

(22) Bhunia, A.; Yetra, S. R.; Biju, A. T. Recent Advances in Transition-Metal-Free Carbon–Carbon and Carbon–Heteroatom Bond-Forming Reactions Using Arynes. *Chem. Soc. Rev.* **2012**, *41*, 3140–3152.

(23) Yoshida, H.; Takaki, K. Aryne Insertion Reactions into Carbon–Carbon σ-bonds. *Synlett* **2012**, 1725–1732.

(24) Dubrovskiy, A. V.; Markina, N. A.; Larock, R. C. Use of Benzynes for the Synthesis of Heterocycles. *Org. Biomol. Chem.* **2013**, *11*, 191–218.

(25) Wu, C.; Shi, F. A Closer Look at Aryne Chemistry: Details that Remain Mysterious. *Asian J. Org. Chem.* **2013**, *2*, 116–125.

(26) Hoffmann, R. W.; Suzuki, K. A "Hot, Energized" Benzyne. *Angew. Chem., Int. Ed.* **2013**, *52*, 2655–2656.

(27) Goetz, A. E.; Garg, N. K. Enabling the Use of Heterocyclic Arynes in Chemical Synthesis. *J. Org. Chem.* **2014**, *79*, 846–851.

(28) Surry, D. S.; Buchwald, S. L. Biaryl Phosphane Ligands in Palladium-Catalyzed Amination. *Angew. Chem., Int. Ed.* **2008**, *47*, 6338–6361.

(29) Mauger, C. C.; Mignani, G. A. An Efficient and Safe Procedure for the Large-Scale Pd-Catalyzed Hydrazonation of Aromatic Chlorides using Buchwald Technology. *Org. Process Res. Dev*. **2004**, *8*, 1065–1071.

(30) Schleth, F.; Vettiger, T.; Rommel, M.; Tobler, H. Process for the Preparation of Pyrazole Carboxylic Acid Amides. WO2011131544 A1 (2011).

(31) Tadross, P. M.; Stoltz, B. M. A Comprehensive History of Arynes in Natural Product Total Synthesis. *Chem. Rev.* **2012**, *112*, 3550–3577.

(32) Wang, B.; Mu, B.; Chen, D.; Xu, S.; Zhou, X. Diels−Alder Reactions of Benzyne with Indenyl Iron Complexes. *Organometallics* **2004**, *23*, 6225–6230.

(33) Luo, S.; Zhao, X.; Mu, B.; Song, H.; Xu, S.; Wang, B. Diels−Alder Reactions of Benzyne with Indenyl and Fluorenyl Ruthenium Complexes. *Organometallics* **2009**, *28*, 4602–4605.

(34) Grätzel, M. Dye-Sensitized Solar Cells. *J. Photochem. Photobiol., C* **2003**, *4*, 145–154 (2003).

(35) Shaw, M. H.; Twilton, J.; MacMillan, D. W. C. Photoredox Catalysis in Organic Chemistry. *J. Org. Chem.* **2016**, *81*, 6898–6926.

(36) Arias-Rotondo, D. M.; McCusker, J. K. The Photophysics of Photoredox Catalysis: a Roadmap for Catalyst Design. *Chem. Soc. Rev.* **2016**, *45*, 5804–5820.

(37) Balzani, V.; Bergamini, G.; Marchioni, F.; Ceroni, P. Ru(II)-Bipyridine Complexes in Supramolecular Systems, Devices and Machines. *Coord. Chem. Rev.* **2006**, *250*, 1254–1266.

(38) McAtee, R. C.; McClain, E. J.; Stephenson, C. R. J. Illuminating Photoredox Catalysis. *Trends Chem.* **2019**, *1*, 111–125.

(39) Gill, M. R.; Thomas, J. A. Ruthenium(II) Polypyridyl Complexes and DNA--From Structural Probes to Cellular Imaging and Therapeutics. *Chem. Soc. Rev.* **2012**, *41*, 3179–3192.

(40) Zeglis, B.; Pierre, V. C.; Barton, J. K. Metallo-Intercalators and Metallo-insertors. *Chem. Commun.* **2007**, 4565–4579.

(41) Song, H.; Kaiser, J. T.; Barton, J. K. Crystal Structure of Δ-$[Ru(bpy)_2dppz]^{2+}$ Bound to Mismatched DNA Reveals Side-by-Side Metalloinsertion and Intercalation. *Nat. Chem.* **2012**, *4*, 615–620.

(42) Keefe, M. H.; Benkstein, K. D.; Hupp, J. T. Luminescent Sensor Molecules Based on Coordinated Metals: A Review of Recent Developments. *Coord. Chem. Rev.* **2000**, *205*, 201–228.

(43) Kozhenvnikov, V. N.; Deary, M. E.; Mantso, T.; Panayiotidis, M. I.; Sims, M. T. Iridium(iii) Complexes of 1,2,4-triazines as Potential Bioorthogonal Reagents: Metal

Coordination Facilitates Luminogenic Reaction with Strained Cyclooctynes. *Chem. Commun.* **2019**, *55*, 14283–14286.

(44) Peña, D.; Pérez, D.; Guitián, E.; Castedo, L. Palladium-Catalyzed Cocyclization of Arynes with Alkynes: Selective Synthesis of Phenanthrenes and Naphthalenes. *J. Am. Chem. Soc.* **1999**, *121*, 5827–5828.

(45) Yoshida, H.; Ikadai, J.; Shudo, M.; Ohshita, J.; Kunai, A. Palladium-Catalyzed Bissilylation of Arynes with Cyclic Disilanes: Synthesis of Benzo-Annulated Disilacarbocycles. *J. Am. Chem. Soc.* **2003**, *125*, 6638–6639.

(46) Jeganmohan, M.; Bhuvaneswari, S.; Cheng, C.-H. A Cooperative Copper- and Palladium-catalyzed Three-Component Coupling of Benzynes, Allylic Epoxides, and Terminal Alkynes. *Angew. Chem., Int. Ed.* **2009**, *48*, 391–394.

(47) Liu, Y.-L.; Liang, Y.; Pi, S.-F.; Huang, X.-C.; Li, J.-H. Palladium-Catalyzed Cocyclotrimerization of Allenes with Arynes: Selective Synthesis of Phenanthrenes. *J. Org. Chem.* **2009**, *74*, 3199–3202.

(48) Garve, L. K. B.; Werz, D. B. Pd-Catalyzed Three-Component Coupling of Terminal Alkynes, Arynes, and Vinyl Cyclopropane Dicarboxylate. *Org. Lett.* **2015**, *17*, 596–599.

(49) Feng, M.; Tang, B.; Xu, H.-X.; Jiang, X. Collective Synthesis of Phenanthridinone through C–H Activation Involving a Pd-Catalyzed Aryne Multicomponent Reaction. *Org. Lett.* **2016**, *18*, 4352–4355.

(50) Yao, T.; He, D. Palladium-Catalyzed Domino Heck/Aryne Carbopalladation/C–H Functionalization: Synthesis of Heterocycle-Fused 9,10-Dihydrophenanthrenes. *Org. Lett.* **2017**, *19*, 842–845.

(51) Pozo, I.; Guitián, E.; Pérez, D.; Peña, D. Synthesis of Nanographenes, Starphenes, and Sterically Congested Polyarenes by Aryne Cyclotrimerization. *Acc. Chem. Res.* **2019**, *52*, 2472–2481.

(52) Liu, Z.; Zhang, X.; Larock, R. C. Synthesis of Fused Polycyclic Aromatics by Palladium-Catalyzed Annulation of Arynes using 2-Halobiaryls. *J. Am. Chem. Soc.* **2005**, *127*, 15716–15717.

(53) Liu, Z.; Larock, R. C. Highly Efficient Route to Fused Polycyclic Aromatics via Palladium-Catalyzed Aryne Annulation by Aryl Halides. *J. Org. Chem.* **2007**, *72*, 223–232.

(54) For a prior report of dehalogenation in $Ru(bpy)_3$ derivatives, see: Iranmanesh, H.; Arachchige, K. S. A.; Bhadbhade, M.; Donald, W. A.; Liew, J. Y.; Liu, K. T.-C.; Luis, E. T.; Moore, E. G.; Price, J. R.; Yan, H.; Yang, J.; Beves, J. E. Chiral Ruthenium(II) Complexes as Supramolecular Building Blocks for Heterometallic Self-Assembly. *Inorg. Chem.* **2016**, *55*, 12737–12751.

(55) CsF, which governs aryne formation, has sparing solubility in organic solvents. By modulating the solvent mixture, one can tune the effective concentration of aryne in solution. In a catalytic reaction, such as that reported herein, it is critical to balance the amount of aryne in solution relative to the reactive organometallic species.

(56) For a pertinent report and proposed mechanism for Pd-catalyzed annulation of arynes with halobiaryl substrates, see reference 64.

(57) Verhoeven, J. W.; van der Tol, E. B.; Steemers, F. J.; Verboom, W.; Reinhoudt, D. N.; Hofstraat, J. W. Complex Comprising a Rare-Earth Metal Ion and a Complexing Moiety. EP1019401 B1 (1998).

(58) Lu, W.; Vicic, D. A.; Barton, J. K. Reductive and Oxidative DNA Damage by Photoactive Platinum(II) Intercalators. *Inorg. Chem.* **2005**, *44*, 7970–7980.

(59) Geri, J. B.; Oakley, J. V.; Reyes-Robles, T.; Wang, T.; McCarver, S. J.; White, C. H.; Rodriguez-Rivera, F. P.; Parker, D. L., Jr.; Hett, E. C.; Fadeyi, O. O.; Oslund, R. C.; MacMillan, D. W. C. Microenvironment Mapping via Dexter Energy Transfer on Immune Cells. *Science* **2020**, *367*, 1091–1097.

(60) Colombo, M. G.; Hauser, A.; Guedel, H. U. Evidence for Strong Mixing Between the LC and MLCT Excited States in bis(2-phenylpyridinato-C2,N')(2,2'-bipyridine)iridium(III). *Inorg. Chem.* **1993**, *32*, 3088–3092.

(61) Wang, C.; deKrafft, K. E.; Lin, W. Pt Nanoparticles@Photoactive Metal−Organic Frameworks: Efficient Hydrogen Evolution via Synergistic Photoexcitation and Electron Injection. *J. Am. Chem. Soc.* **2012**, *134*, 7211–7214.

(62) Bolink, H. J.; Coronado, E.; Costa, R. D.; Ortí, E.; Sessolo, M.; Graber, S.; Doyle, K.; Neuburger, M.; Housecroft, C. E.; Constable, E. C. Long-Living Light-Emitting Electrochemical Cells – Control through Supramolecular Interactions. *Adv. Mater.* **2008**, *20*, 3910–3913.

(63) Li, Y.; Dandu, N.; Liu, R.; Li, Z.; Kilina, S.; Sun, W. Effects of Extended π-Conjugation in Phenanthroline (N^N) and Phenylpyridine (C^N) Ligands on the Photophysics and

Reverse Saturable Absorption of Cationic Heteroleptic Iridium(III) Complexes. *J. Phys. Chem. C* **2014**, *118*, 6372–6384.

(64) Bennett, M. A.; Schwemlein, H. P. Metal Complexes of Small Cycloalkynes and Arynes. *Angew. Chem., Int. Ed. Engl.* **1989**, *28*, 1296–1320.

(65) Werner, G.; Lehmann, C. W.; Butenschön, H. The First Anionic Thia-Fries Rearrangements at Ferrocene: Ready Access to Trifluoromethylsulfonyl-Substituted Hydroxyferrocenes and an Extremely High Interannular Stereoinduction Between Cyclopentadienyl Ligands. *Adv. Synth. Catal.* **2010**, *352*, 1345–1355.

(66) Duong, H. M.; Bendikov, M.; Steiger, D.; Zhang, Q.; Sonmez, G.; Yamada, J.; Wudl, F. Efficient Synthesis of a Novel, Twisted and Stable, Electroluminescent "Twistacene." *Org. Lett.* **2003**, *5*, 4433–4436.

(67) Suzuki, S.; Itami, K.; Yamaguchi, J. Synthesis of Octaaryl Naphthalenes and Anthracenes with Different Substituents. *Angew. Chem., Int. Ed.* **2017**, *56*, 15010–15013.

(68) Graczyk, A.; Murphy, F. A.; Nolan, D.; Fernández-Moreira, V.; Lundin, N. J.; Fitchett, C. M.; Draper, S. M. Terpyridine-Fused Polyaromatic Hydrocarbons Generated via Cyclodehydrogenation and used as Ligands in Ru(II) Complexes. *Dalton Trans.* **2012**, *41*, 7746–7754.

(69) Grzybowski, M.; Sadowski, B.; Butenschön, H.; Gryko, D. T. Synthetic Applications of Oxidative Aromatic Coupling—from Biphenols to Nanographenes. *Angew. Chem., Int. Ed.* **2020**, *59*, 2998–3027.

(70) Polypyridyl metal complexes bearing highly π-expanded ligand systems have historically demonstrated unique coordinating properties and photophysical characteristics. For a

notable example, see: Draper, S. M.; Gregg, D. J.; Schofield, E. R.; Browne, W. R.; Duati, M.; Vos, J. G.; Passaniti, P. Complexed Nitrogen Heterosuperbenzene: The Coordinating Properties of a Remarkable Ligand. *J. Am. Chem. Soc.* **2004**, *126*, 8694–8701.

(71) Reichardt, C.; Monro, S.; Sobotta, F. H.; Colón, K. L.; Sainuddin, T.; Stephenson, M.; Sampson, E.; Roque, J., III.; Yin, H.; Brendel, J. C.; Cameron, C. G.; McFarland, S.; Dietzek, B. Predictive Strength of Photophysical Measurements for in Vitro Photobiological Activity in a Series of Ru(II) Polypyridyl Complexes Derived from π-Extended Ligands. *Inorg. Chem.* **2019**, *58*, 3156–3166.

(72) Young, M. C.; Liew, E.; Ashby, J.; McCoy, K. E.; Hooley, R. J. Spin State Modulation of Iron Spin Crossover Complexes via Hydrogen Bonding Self-Assembly. *Chem. Commun.* **2013**, *49*, 6331–6333.

(73) Cheong, P. H.-Y.; Paton, R. S.; Bronner, S. M.; Im, G.-Y. J.; Garg, N. K.; Houk, K. N. Indolyne and Aryne Distortions and Nucleophilic Regioselectivites. *J. Am. Chem. Soc.* **2010**, *132*, 1267–1269.

(74) Breton, G. W. Selective Monoacetylation of Unsymmetrical Diols Catalyzed by Silica Gel Supported Sodium Hydrogen Sulfate. *J. Org. Chem.* **1997**, *62*, 8952–8954.

(75) Suzuki, K.; Kobayashi, A.; Kaneko, S.; Takehira, K.; Yoshihara, T.; Ishida, H.; Shiina, Y.; Oishi, S.; Tobita, S. Reevaluation of Absolute Luminescence Quantum Yields of Standard Solutions using a Spectrometer with an Integrating Sphere and a Back-Thinned CCD Detector. *Phys. Chem. Chem. Phys.* **2009**, *11*, 9850–9860.

(76) Méndez-Hernández, D. D.; Gillmore, J. G.; Montano, L. A.; Gust, D.; Moore, T. A.; Moore, A. L.; Mujica, V. Building and Testing Correlations for the Estimation of One-Electron Reduction Potentials of a Diverse Set of Organic Molecules. *J. Phys. Org. Chem.* **2015**, *28*, 320–328 (2015).

(77) CYLview20; Legault, C. Y., Université de Sherbrooke, 2020 (http://www.cylview.org).

CHAPTER FIVE

π-Extension of Heterocycles via a Pd-Catalyzed Heterocyclic Aryne Annulation: π-Extended Donors for TADF Emitters

Katie A. Spence,[†] Jason V. Chari,[†] Mattia Di Niro, Robert B. Susick, Narcisse Ukwitegetse, Peter I. Djurovich, Mark E. Thompson, and Neil K. Garg.

Chem. Sci. **2022**, *13*, 5884–5892.

5.1 Abstract

We report the annulation of heterocyclic building blocks to access π-extended polycyclic aromatic hydrocarbons (PAHs). The method involves the trapping of short-lived hetarynes with catalytically-generated biaryl palladium intermediates and allows for the concise appendage of three or more fused aromatic rings about a central heterocyclic building block. Our studies focus on annulating the indole and carbazole heterocycles through the use of indolyne and carbazolyne chemistry, respectively, the latter of which required the synthesis of a new carbazolyne precursor. Notably, these represent rare examples of transition metal-catalyzed reactions of *N*-containing hetarynes. We demonstrate the utility of our methodology in the synthesis of heterocyclic π-extended PAHs, which were then applied as ligands in two-coordinate metal complexes. As a result of these studies, we identified a new thermally-activated delayed fluorescence (TADF) emitter that displays up to 81% photoluminescence efficiency, along with insight into structure-property relationships. These studies underscore the utility of heterocyclic strained intermediates in the synthesis and study of organic materials.

5.2 Introduction

Polycyclic aromatic hydrocarbons (PAHs) have had a remarkable impact on materials science due to their desirable electronic and self-assembly properties.[1] A privileged subset of PAHs, heterocyclic PAHs, are highly valued in solar cells,[2] electroluminescent materials[3] and organic light emitting diodes (OLEDs)[4] (e.g., **5.1**–**5.3**, Figure 5.1). Indeed, heteroatom incorporation in these systems provides several functional and electronic advantages. This includes the introduction of nitrogen functional handles for synthetic manipulations, capacity for *N*-coordination to metal centers, the potential for donor-acceptor systems and usage as stimuli-responsive materials.[5] Accordingly, concise and diversifiable synthetic methods for accessing heterocyclic PAHs are highly desirable.[6]

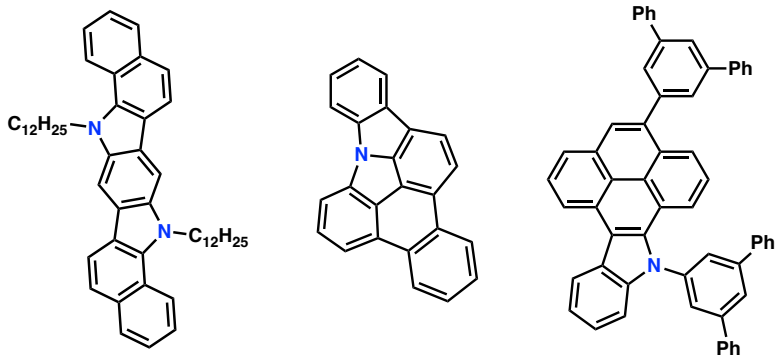

Figure 5.1. Examples of heteroatom-containing PAHs with applications in materials chemistry.

An attractive approach toward heterocyclic PAHs involves assembling fused rings about a central heterocyclic building block through annulative π-extension (APEX).[6] A compelling means to achieve this objective involves the use of in situ generated arynes, although such intermediates were historically avoided because of their high reactivity. However, the strain driven reactivity of

arynes, along with the ability to form multiple bonds in a single step under mild conditions, has prompted the recent usage of arynes as modular building blocks in a wide array of applications, including in the synthesis of PAHs.[7,8,9,10,11] In contrast, heterocyclic arynes (hetarynes) have only been used sparingly in PAH synthesis. This is in part due to the mild, fluoride-mediated generation of heterocyclic arynes (hetarynes) only becoming widespread in the past decade.[12] Moreover, the ability to access and manipulate indole-derived arynes (indolynes) and their derivatives differs considerably from that of benzyne chemistry. The pyrrole ring can influence aryne structure and reactivity,[13] and its nucleophilicity can often result in side reactions,[14] posing numerous challenges for methodology development. Specifically, the reaction rate of pyrrole in electrophilic aromatic substitution reactions has been approximated to be roughly 3×10^{18} times faster than that of benzene.[15] Figure 5.2A highlights two recent examples of the generation and capture of indolyne **5.5**, which arises from indolyne silyl triflate precursor **5.4**.[16,17,18]

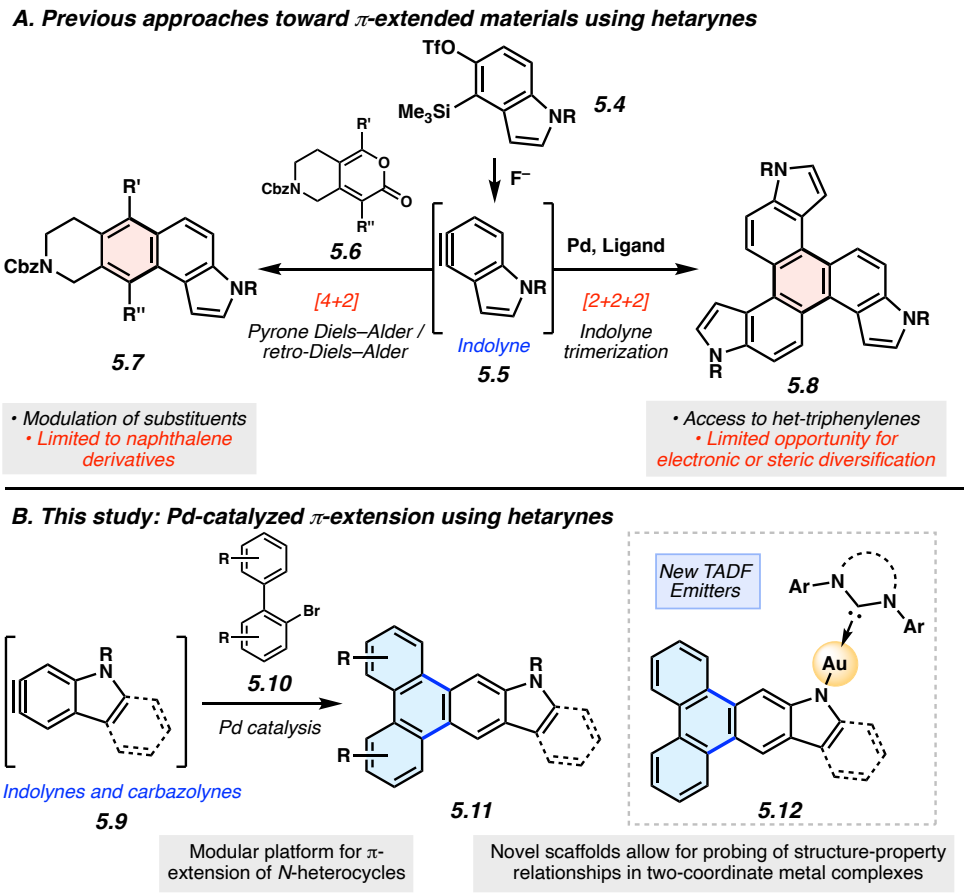

Figure 5.2. Approaches for π-extension of hetarynes.

In the present study, we aimed to develop a rapid, convergent approach to access heteroatom-containing PAH scaffolds. In particular, a method was devised that allows for the appendage of multiple aromatic rings to important heterocyclic building blocks in a controlled bimolecular reaction. This reaction provides access to a diverse set of aromatic products with electronic and steric modifications. The sequence we devised, inspired by pioneering studies by Larock,[19] is shown in Figure 5.2B. In situ generated hetarynes **5.9** would be united with bromobiaryl partners **5.10** using palladium catalysis to furnish heterocyclic PAHs **5.11**.[20] This annulative π-extension of hetarynes would expand on existing applications of hetaryne chemistry, create two new carbon–carbon (C–C) bonds, allow for the addition of three aromatic rings (shown

in blue) to important heterocycles, and permit rapid access to heterocyclic triphenylene derivatives. Of note, this type of Larock annulation[19] had not previously been achieved using nitrogen-containing, hetaryne intermediates. Additionally, metal-catalyzed transformations that utilize hetarynes are rare. Iwayama and Sato have reported [2+2+2] reactions of pyridynes.[21] Only one study involving metal-catalyzed reactions of electron-rich *N*-containing hetarynes is available in the literature, as developed by our laboratory.[17]

Herein, we describe the development of this methodology to access π-extended heterocyclic adducts, in addition to a concise synthetic route to a new carbazolyne precursor. We also show the utility of our methodology in the synthesis of π-extended ligands, which were utilized in novel two-coordinate metal complexes **5.12**. Rapid access to complexes **5.12** allowed us to study the influence of extended conjugation on the efficiency of thermally activated delayed fluorescence (TADF) processes, which have received notable interest in recent years in the context of OLEDs.[22] As described in Scheme 5.1, in OLEDs, singlets (S_1) and triplets (T_1) are generated upon hole and electron recombination. Fluorescence describes prompt decay from the S_1 state, whereas phosphorescence describes delayed decay from the T_1 state. In TADF emitters, T_1 is thermally promoted to the S_1 state, followed by radiative decay from S_1. We show that extended π-conjugation can influence the performance of the TADF complex by modulating either the steric or electronic features of the ligand. Moreover, our studies permit access to a new TADF emitter that displays up to 81% photoluminescence efficiency.

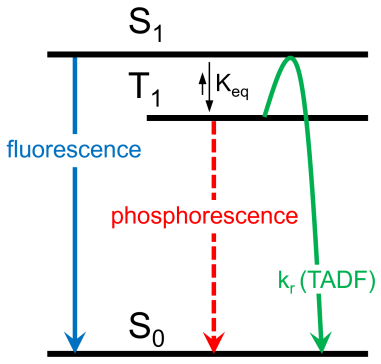

Scheme 5.1. Mechanism for TADF emission in comparison to fluorescence and phosphorescence.

5.3 Results and Discussion

5.3.1 Pd-Catalyzed Annulations of Indolyne

We initiated our synthetic studies by pursuing a Pd-catalyzed annulation reaction of bromobiaryls **5.13**[23] with *N*-Me-4,5-indolyne precursor **5.14** (Figure 5.3), the latter of which is accessible in a single step from its commercially available N–H derivative. In our initial studies, we used 2-bromobiphenyl as the aryl halide coupling partner and examined conditions reported by Larock for the annulation of carbocyclic arynes.[19] This led to the formation of **5.16** in only 43% yield, highlighting the aforementioned challenges associated with using *N*-containing hetarynes in metal-catalyzed reactions, as compared to simpler arynes. In prior studies,[24,25,26] we found that metal-catalyzed trappings of heterocyclic strained intermediates necessitate careful optimization, as such reactions require that a transient strained intermediate be generated at a rate that allows for efficient reaction with an in situ generated organometallic species (i.e., after **5.13** undergoes oxidative addition with Pd), while minimizing decomposition pathways commonly seen in strained intermediate chemistry. We ultimately found the desired reaction took place more efficiently by employing 5 mol% $Pd(dba)_2$, 5 mol% P(*o*-tolyl)$_3$, a 1:1 ratio of co-solvents acetonitrile and toluene,

and 10 equivalents of cesium fluoride (CsF). The mixture of co-solvents, in particular, is thought to be important for modulating the rate of hetaryne formation.[27] With optimal conditions, **5.16** could be accessed in 90% yield. Substituted biaryls could also be employed in the methodology. For example, methoxy- and nitro-substituted biaryls underwent the annulation smoothly to deliver adducts **5.17** and **5.18** in 62% and 80% yields, respectively. In these cases, mixtures of regioisomers are formed in roughly equal quantities.[28] We also sought to incorporate additional heteroatoms into the products by employing heterocyclic derivatives of 2-bromobiphenyls. Use of a pyridyl substrate furnished **5.19** in 76% yield, which is an interesting aza-analog of parent compound **5.16**. We were also able to replace one of the phenyl rings with pyrrole or indole units, as exemplified by the formation of **5.20**–**5.22**. Lastly, we performed the annulation of 2-bromobiphenyl (**5.23**) with 5,6-indolyne precursor **5.24**, which delivered adduct **5.25** in 81% yield. The results shown in Figure 5.3 not only provide access to electronically and structurally diverse heteroatom-containing PAHs, but also validate our strategy to achieve the π-extension of heterocyclic building blocks.

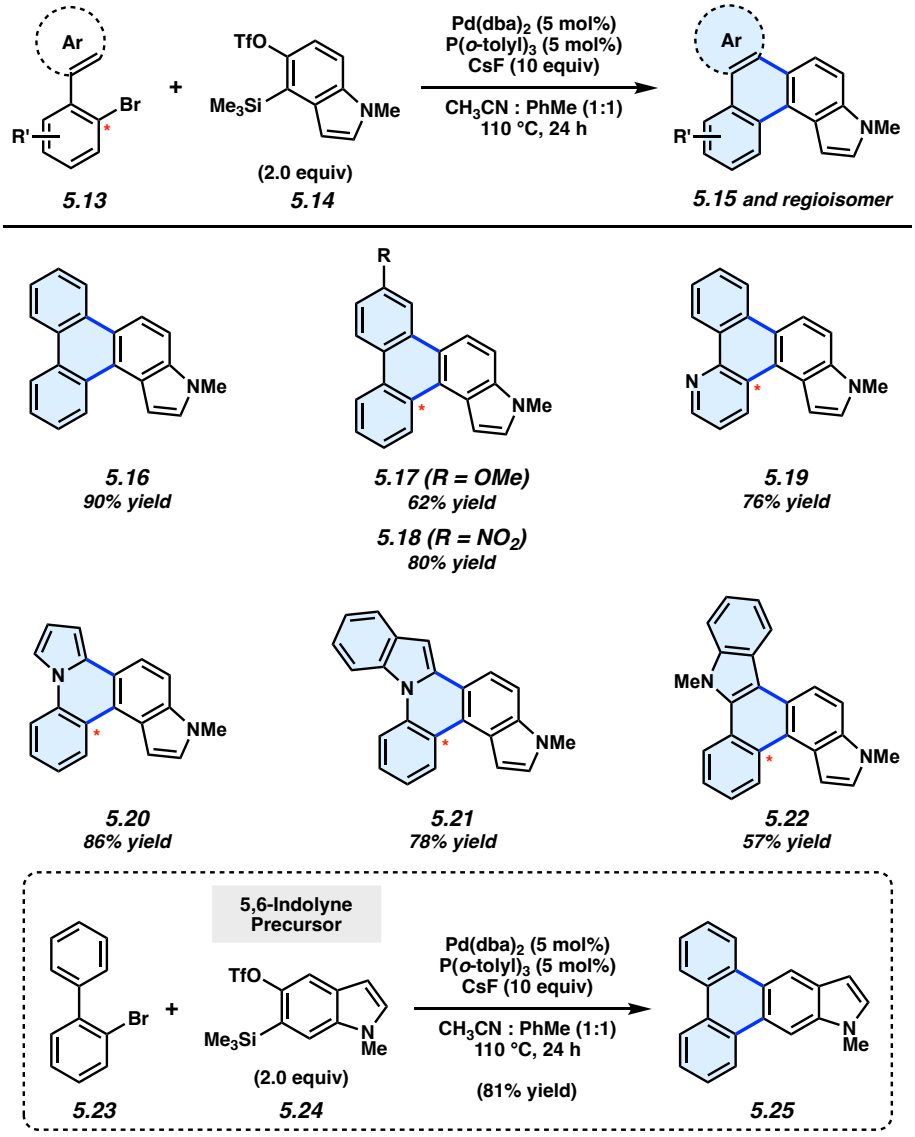

Figure 5.3. π-Extension of indolynes. Yields for **5.17**–**5.22** reflect isolated yields of a mixture of regioisomers (1–1.5:1; see Section 5.5.2.1 for details).

5.3.2 Carbazolyne Studies

Having validated the π-extension of indoles via the use of indolynes, we sought to develop analogous chemistry using the carbazole heterocycle. Carbazoles bear an additional aromatic ring in comparison to their indole counterparts and are valuable in materials-based applications,[29]

medicinal chemistry,[30] and natural product total synthesis.[31] However, aryne-derived carbazoles (carbazolynes) have seen sparce use in chemical synthesis. Recent examples involve carbazolyne generation from the hexadehydro-Diels–Alder reaction,[32] the use of a silyl nonaflate precursor,[33] and via classic dehydrohalogenation chemistry.[31,34]

As silyl triflate precursors to carbazolynes were not known in the literature, we developed the concise approach to carbazolyne precursors **5.29**–**5.31** shown in Figure 5.4. 3-Bromo-2-hydroxycarbazole (**5.26**)[31,34] was treated with HMDS to afford silyl ether **5.27**, which, in turn, was carried forward in a retro-Brook rearrangement sequence to afford silyl alcohol **5.28**. Triflation proceeded smoothly to deliver silyl triflate **5.29** in 69% yield. N–H compound **5.29** was elaborated to protected derivatives **5.30** and **5.31** via methylation and Boc-protection, respectively. *N*-Me-carbazolyne precursor **5.30** was employed in our π-extension methodology using our previously optimized conditions. We were delighted to find that reaction of 2-bromobiphenyl (**5.23**) and *N*-Me-carbazolyne precursor **5.30** using Pd-catalysis furnished π-extended carbazole **5.32** in 86% yield. This is the first example of a transition metal-catalyzed trapping of a carbazolyne intermediate. Notably, this permits the one-step installment of a carbazole moiety into a π-extended system.

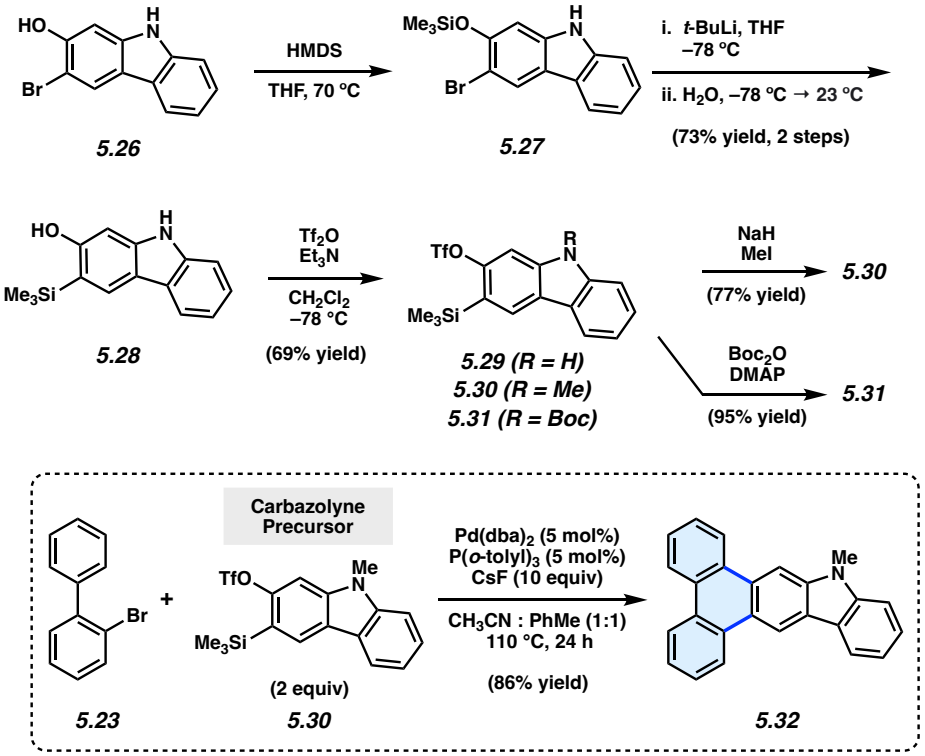

Figure 5.4. Synthesis of carbazolyne precursors.

We also sought to determine if N–H derivatives of our indole and carbazole annulation products could be accessed using our methodology. It was ultimately found that N–H products were accessible by employing *N*-Boc protected hetaryne precursors in our methodology (Figure 5.5).[35] Subjection of **5.23** and indolyne precursor **5.33** to our standard reactions conditions, followed by treatment with trifluoroacetic acid (TFA) to remove the Boc protecting group, gave deprotected indole scaffold **5.34** in 34% yield. Similarly, N–H carbazole adduct **5.35** was accessed in 65% yield via the corresponding reaction of **5.23** and *N*-Boc-carbazolyne precursor **5.31**. The ability to access π-extended N–H products (e.g., **5.34** and **5.35**) is expected to prove generally useful, as the *N*-position can be easily substituted. PAHs **5.34** and **5.35** also proved useful in our subsequent studies (vide infra) pertaining to the synthesis and evaluation of thermally activated delayed fluorescence (TADF) complexes.

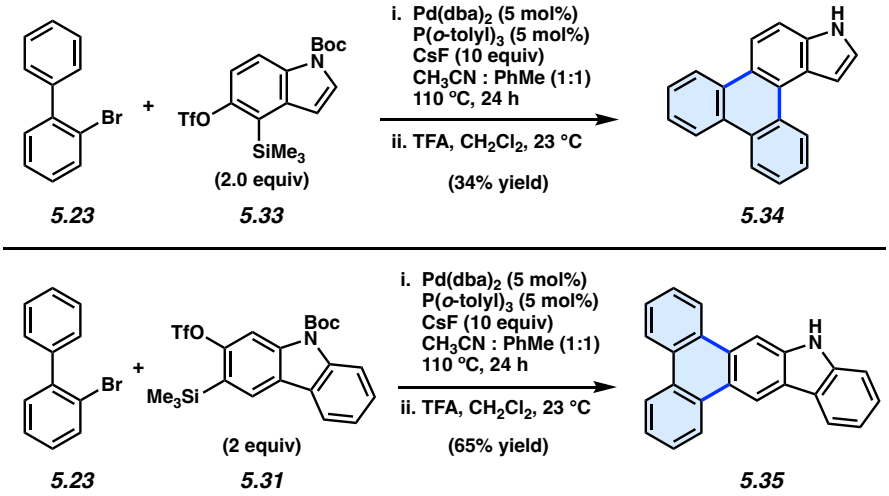

Figure 5.5. Synthesis of N–H products **5.34** and **5.35**.

5.3.3 Application of π-Extended Products as TADF Emitters

A potential application of indole- and carbazole-based PAHs is in organic light emitting diodes (OLEDs), which are crucial for high-performance display technologies and solid-state lighting applications. Specifically, the recent development of TADF complexes of the general structure donor–M–acceptor, where M is Cu(I), Ag(I), or Au(I), and where the donor and acceptor are amide and carbene ligands, respectively, (e.g., **5.36** and **5.37**, Figure 5.6),[36,37,38,39,40] has allowed access to emissive dopants with high photoluminescence efficiencies (Φ_{PLQY} up to 100% in both solution and in the solid state) and short-lived excited states ($\tau < 1$ ms). These compounds also offer potential economic advantages over Ir- or Pt-centered phosphorescent dopants.[41,42]

The photophysical properties of these two-coordinate complexes can be manipulated by altering either the donor or acceptor ligands.[43] For example, compounds **5.36** and **5.37** have the same amide donor ligand (carbazolyl) but different acceptor carbene ligands. Consequently, the energy for the interligand charge transfer (ICT) transition is different in each complex. Compound

5.36, with the carbene BZI (1,3-bis(2,6-diisopropylphenyl)-1-H-benzo[d]imidazole-2-ylidene) as an acceptor ligand emits at 432 nm when doped in polystyrene (PS) films whereas **5.37**, which has MAC (1,3-bis(2,6-diisopropylphenyl)-5,5-dimethyl-4-keto-tetrahydropyridylidene) as an acceptor, emits at 506 nm in the same media. The difference in energy for the ICT state is due to the poorer electrophilicity of BZI (**5.36**, E_{red} = –2.82 V vs. Fc^+/Fc) relative to MAC (**5.37**, E_{red} = –2.50 V). The low electron affinity of BZI raises the energy of the ^{3}ICT state such that it is near resonant with that of the locally excited triplet state (^{3}LE) of carbazolyl (^{3}LE = 415 nm). It follows that altering the nature of amide donor will also modify the energy of the ICT state, and consequently the photophysical properties of the complex.

Previous studies on carbazolyl donor ligands have focused on electronic modifications of carbazole using electron-donating or withdrawing groups, steric hindrance, and structural flexibility, leading to important structure-property relationships.[36c,40,43,44,45] Moreover, extending the conjugation in aromatic π-systems by benzannulation has been shown to impact relative HOMO and LUMO energy levels in ways that sometimes lead to counterintuitive changes in emission color.[42,46,47] Thus, the effect of similar π-extension on the photophysical properties of donor–M–acceptor complexes may not be obvious. Heterocyclic PAHs accessible by our π-extension methodology provide an opportunity to study and compare new π-extended TADF complexes.

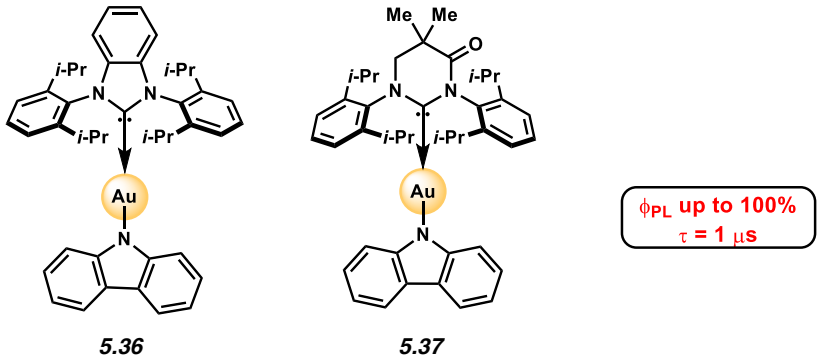

Figure 5.6. Heterocyclic PAHs as donor ligands in TADF complexes.[48,49]

Two-coordinate donor-Au-acceptor complexes were prepared by treatment of **5.34** or **5.35** with sodium *tert*-butoxide in the presence of the NHC-Au-Cl complex (Figure 5.7A). The metal complexes evaluated in the present study (Figure 5.7B) are Au complexes due to their superior stability compared to Ag or Cu analogs.[40] Complexes **5.36+π** and **5.37+π** were obtained in 68% and 78% yields, respectively, whereas the respective indolyl complexes **5.38** and **5.38+π** were prepared in 60% and 45% yields using this protocol. Complexes **5.36+π** and **5.37+π** enable comparison of the new π-extended phenanthrocarbazolyl donors to their respective carbazolyl counterparts, **5.36**[48] and **5.37**.[43,49] The methylindolyl (**5.38**) and phenanthroindolyl (**5.38+π**) derivatives allow us to assess the impact of π-extension within a new indole series of complexes, as well as compare the carbazolyl and indolyl complexes.

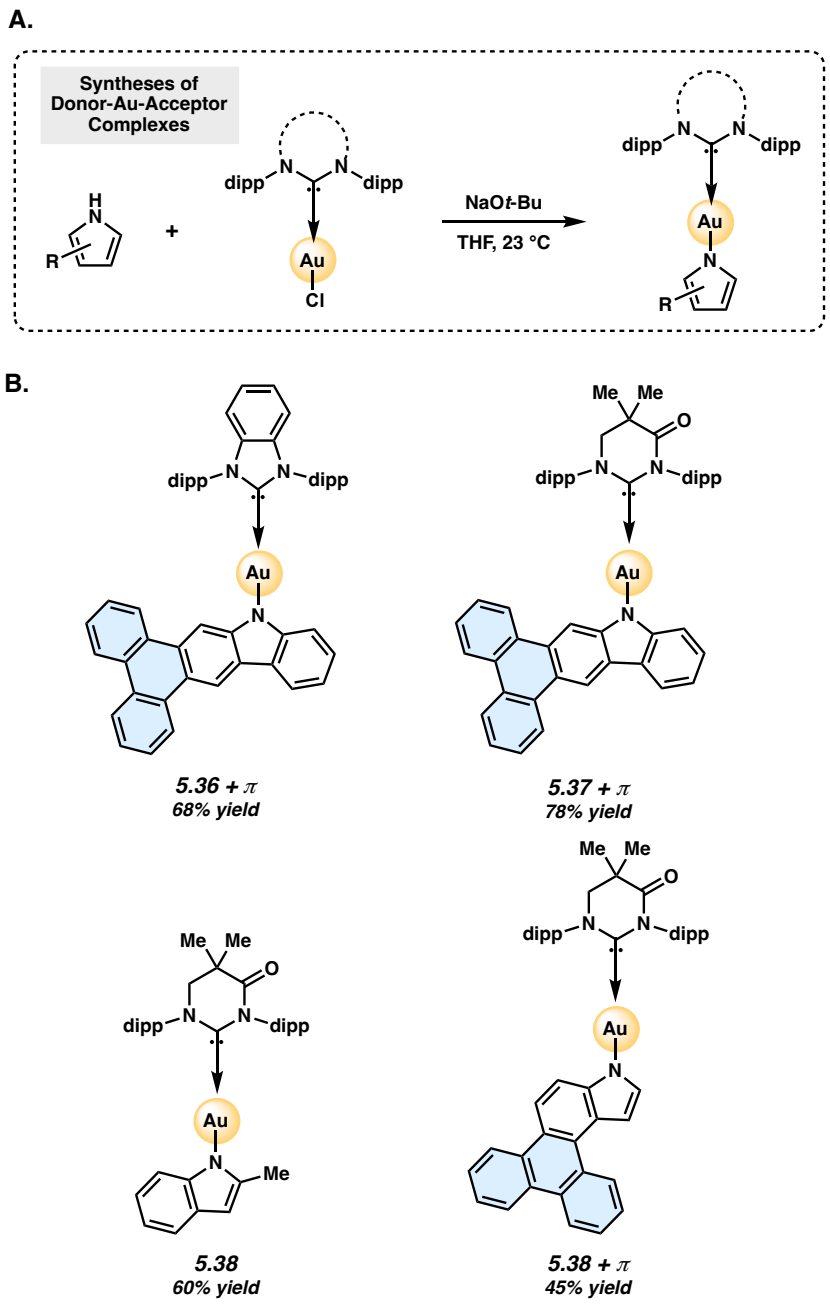

Figure 5.7. Preparation (A) and structures (B) of two-coordinate gold complexes. dipp = 2,6-diisopropylphenyl, as shown in Figure 5.6.

The photophysical properties of the π-extended carbazolyl-based complexes, **5.36+π** and **5.37+π**, were examined in different media (Figure 5.8) and compared to data of the parent

carbazole-containing complexes **5.36** and **5.37** (Table 5.1).[43,49,49] The UV-visible absorption spectra of **5.36+π** and **5.37+π** display a strong solvent-independent band at 320 nm attributed to a π–π* transition localized on the phenanthrocarbazolyl ligand. Weaker bands at lower energy are more structured and display a pronounced negative solvatochromism (e.g., **5.36+π** at 416 nm in MeCy and 382 nm in MeTHF; **5.37+π** at 460 nm in MeCy and 417 nm in MeTHF). This band is assigned to the ICT transition between the π-extended carbazole donor and carbene acceptor ligand that is overlapped with π–π* transitions on the phenanthrocarbazolyl ligand. The solvatochromic behavior of the ICT band is ascribed to the dipole moment interactions between the solvent and complex molecules, in which the dipole of the excited state is larger and is oriented in the opposite direction as that of the ground state. The energy of the ICT transition in **5.36+π** and **5.37+π** is comparable to values for **5.36** and **5.37** (see Table 5.1) indicating that the donor strength of the phenanthrocarbazolyl and carbazolyl ligands are nearly equivalent.

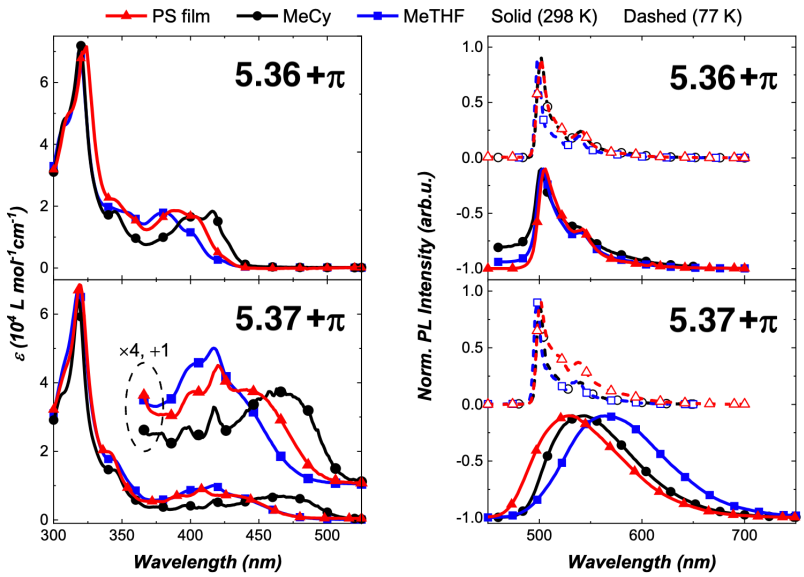

Figure 5.8. Absorption (left) and emission spectra (right) for the carbene-Au-carbazolyl complexes. Note that the absorption spectra of the PS films were scaled to match the intensity of the MeCy solution at λ_{max} = 320 nm. This feature is assigned to a solvent insensitive transition localized on the carbazolyl ligand.

Table 5.1. Photophysical data for carbene-Au-carbazolyl complexes.

complex	solvent	λ_{abs}[a]	$\lambda_{em,\ 298K}$ (λ_{77K})	Φ_{PLQY}	τ_{298K} (10^{-6} s)	k_r (10^5 s^{-1})	k_{nr} (10^5 s^{-1})	τ_{77K} (10^{-3} s)
5.36[48]	1% PS film	385	452 (426)	1.00	3.6 (54%) 0.74 (46%)	4.4[b]	<0.04[b]	0.19
	MeCy	405	424 (424)	0.89	1.2	7.8	0.9	0.34
	MeTHF	365	452 (426)	0.79	2.6	3.0	0.8	0.64
5.36+π	1% PS film	388	506 (502)	0.52	5.1 (70%) 6.7 (30%)	3.1[b]	11[b]	1.8
	MeCy	416	502 (504)	0.03	30.0	0.01	0.3	2.9 (90%) 14 (8%) 100 (2%)
	MeTHF	382	504 (498)	0.02	57	0.004	0.2	3.2 (94%) 33 (6%)
5.37[49]	1% PS film	425[c]	512 (506)	0.85	0.83	10.0	1.8	0.043
	MeCy	450	522 (456)	0.88	1.1	8.0	1.1	0.068
	MeTHF	412	544 (428)	0.50	0.79	6.3	6.3	0.26
5.37+π	1% PS film	420	529 (500)	0.74	3.3 (47%) 1.0 (45%)[d]	3.4[b]	1.2[b]	4.4 (43%) 2.2 (33%) 0.7 (24%)
	MeCy	460	544 (500)	0.81	0.9 (91%)[d]	9.1	2.1	1.8 (59%) 3.1 (41%)
	MeTHF	417	566 (498)	0.39	0.6 (96%)[d]	6.9	11	2.4 (72%) 5.3 (28%)

[a] ICT band. [b] Calculated from the weighted averages of both contributions. [c] Obtained from excitation spectrum. [d] An additional minor contribution from a longer lifetime component is needed to fit the observed data and assigned to p-type delayed fluorescence. See Section 5.6.2.

The effect of π-extension on the amide ligand is manifested more evidently in the luminescence properties of the complexes. In particular, whereas luminescence from **5.36** is broad and solvatochromic, emission spectra of **5.36+π** are narrow, red-shifted and independent of solvent polarity. Radiative (k_r) and non-radiative (k_{nr}) rate constants are calculated using the relationship $k_r = \Phi_{PL}/\tau$, where $\Phi_{PL} = k_r/(k_r + k_{nr})$. The radiative rate for emission from **5.36** is rapid (k_r = 3.0×10^5 s^{-1} in MeTHF) as opposed to being markedly slow in **5.36+π** ($k_r = 4 \times 10^2$ s^{-1} in MeTHF). Unlike the photophysical properties of **5.36**, which are characteristic of emission from an ICT state, luminescence from **5.36+π** indicates that the excited state transitions are localized on the donor ligand, and hence undergo conventional phosphorescence rather than TADF. This

assignment for the luminescence is confirmed by the minimal shift in energy and millisecond emission lifetime found upon cooling to 77 K. The difference in properties for **5.36+π** versus **5.36** is caused by the lower energy for ^{3}LE state of the phenanthrocarbazolyl moiety (see section 5.6) compared to that for the carbazolyl ligand. In contrast, complex **5.37+π** is capable of efficient TADF from the ICT state as borne out by emission spectra (Figure 5.8) that are similar, albeit redshifted, to spectra reported for **5.37**. The fast radiative rate (k_r = 9.1 × 10^5 s^{-1}) and high photoluminescence efficiency (Φ_{PLQY} = 0.81) at room temperature in MeCy, along with luminescence that is redshifted from polar solvent (MeTHF) to non-polar solvent (MeCy and polystyrene film), is also consistent with emission from an ICT state.[50] Emission at 77 K (500 nm) is structured and polarity-independent. In this case, solvent molecules are frozen as a glass around the complex molecules, thus restricting stabilization of the excited ICT triplet.[43] Therefore, the triplet state localized on the donor becomes the lowest-lying emissive state and precludes ICT events. Notably, **5.37+π** achieved 81% photoluminescence efficiency in MeCy (Figure 5.8).

Next, we compared the optical properties of **5.38** and **5.38+π** (Figure 5.9 and Table 5.2). The ICT and π–π* absorption bands are more resolved in complex **5.38** than in **5.38+π**. The high extinction coefficients for the ICT band of **5.38** suggest strong electronic coupling between the acceptor carbene and the 2-methylindolyl donor ligands. Emission spectra for both complexes at 298 K show broad featureless bands and radiative rates are relatively fast (k_r > 10^5 s^{-1}), both characteristics consistent with decay from an ICT excited state. The luminescence from **5.38** is slightly red-shifted (e.g., λ_{MeTHF} = 600 nm) relative to spectra from **5.38+π** (e.g., λ_{MeTHF} = 566 nm), indicating that 2-methylindole is a stronger donor than the phenanthroindolyl ligand, which can be attributed to the different position of the π-extension in **5.38+π** compared to **5.36+π** and **5.37+π**. Luminescence from the methylindolyl-based complex remains broad and

featureless upon cooling from 298 K to 77 K, indicating that the transition retains ICT character even in frozen matrix. For **5.38**, note that the destabilization of the ICT state upon going from 298 K to 77 K is greater in MeCy and MeTHF than in the PS film. This is likely due to enhanced solute-solute interactions on cooling the fluid solutions to 77 K, whereas the relative orientations of the solutes are fixed in a more random fashion at room temperature in the PS film. In contrast, the emission spectrum of **5.38+π** is structured at 77 K and assigned to a low-lying ^{3}LE transition on the phenanthroindolyl ligand. The short lifetime measured for **5.38** at 77 K in MeTHF (τ = 1.1 × 10^{-4} s) compared to that for **5.38+π** (τ = 1.5 × 10^{-2} s) is consistent with an ^{3}ICT transition for the former complex and ^{3}LE phosphorescence for the latter derivative.

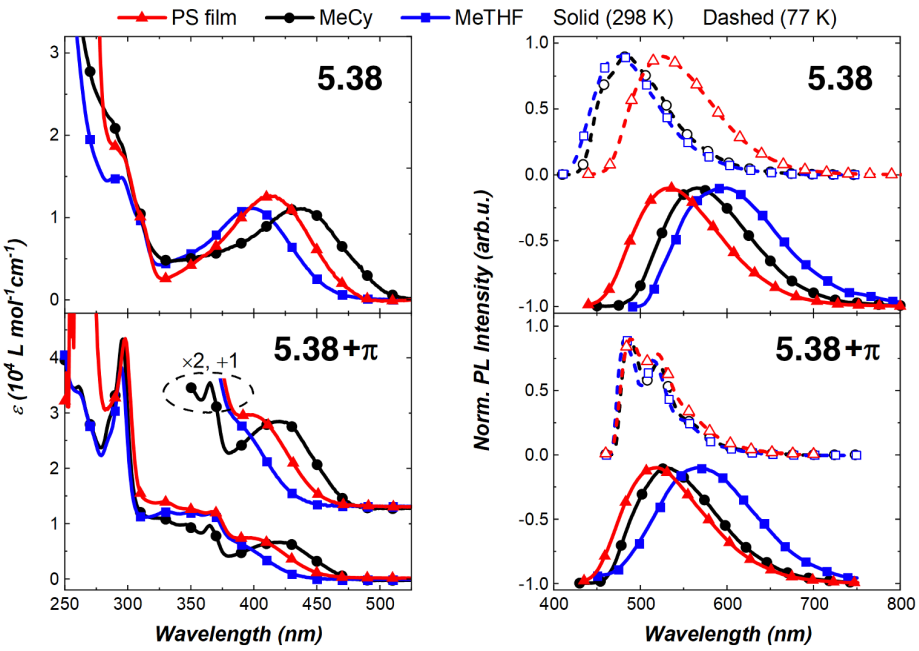

Figure 5.9. Absorption (left) and emission spectra (right) for carbene-Au-indolyl complexes. Note that the absorption spectra of the PS films were scaled to match the peak at λ_{max} = 295 nm in MeCy solution, which is assigned to a solvent insensitive transition localized on the indolyl ligand.

Complex **5.38+π** exhibits higher photoluminescence quantum yields in all media compared to **5.38**. The yields increase from MeTHF (Φ_{PLQY} = 1.4%) to MeCy (Φ_{PLQY} = 24.2%) to the PS film (Φ_{PLQY} = 49%). The lower emission efficiency in polar solvents is attributed to the greater reorganization of the excited state structure in polar solvents. Generally, complex **5.38** displays comparable, although slower radiative rates (k_r) and faster non-radiative rates (k_{nr}) in all solvents relative to **5.38+π**. The slower k_{nr} of **5.38+π** is likely due to a slower rate of rotation or exchange caused by the larger free volume of the **5.38+π** ligand.

Table 5.2. Photophysical data for carbene-Au-indolyl complexes.

complex	solvent	λ_{abs}[a]	$\lambda_{em,\ 298K}$ (λ_{77K})	Φ_{PLQY}	τ_{298K} (10^{-6} s)	k_r (10^5 s^{-1})	k_{nr} (10^5 s^{-1})	τ_{77K} (10^{-3} s)
5.38	1% PS film	414	534 (525)	0.12	0.71 (80%) 0.25 (20%)	2.5[b]	14[b]	0.067 (78%) 0.025 (22%)
	MeCy	435	565 (484)	0.03	0.13	2.5	74	0.10
	MeTHF	399	600 (476)	0.004	0.011	3.6	910	0.11
5.38+π	1% PS film	394	519 (495)	0.49	1.7 (65%) 0.41 (35%)	3.9[b]	2.1[b]	7.0 (74%) 3.0 (26%)
	MeCy	420	530 (486)	0.24	0.54	4.1	14	9.3 (62%) 13 (38%)
	MeTHF	380[a]	566 (482)	0.01	0.024	5.8	4100	14 (73%) 19 (27%)

[a] *ICT band.* [b] *Calculated from the weighted averages of both contributions.*

Comparing the carbazolyl and indolyl MAC complexes, it is noted that both appear to undergo TADF emission; however, the former (carbazolyl) family exhibits higher photoluminescence efficiencies due to lower rates of non-radiative decay. In comparing **5.38** to **5.38+π**, the low steric profile about the indolyl ligand appears to have a greater influence on the photophysical performance than any energetic differences. In contrast, the discrepancy in performance between **5.36** and **5.36+π** is attributed primarily to the energetics induced by π-

conjugation. In other words, the photophysical properties of indolyl-based complexes are primarily influenced by decreased steric hindrance of the indolyl ligand, whereas the performance of the carbazolyl-based complexes is primarily dictated by the π-conjugation thermodynamics.

5.4 Conclusions

In summary, we have developed a modular platform to access *N*-heterocycles with extended π-conjugation by leveraging hetarynes and Pd-catalysis. Of note, these represent rare examples of metal-mediated transformations of *N*-heterocyclic arynes. Through the construction of two C–C bonds in a single operation, this methodology allows for the direct π-extension of heterocyclic scaffolds through the appendage of three or more aromatic rings. The methodology offers a convergent platform for accessing important heterocycles with structural and electronic diversity. Notably, a new carbazolyne precursor, whose synthesis relies on a key retro-Brook rearrangement, can also be leveraged in this reaction to access carbazole derivatives. Heterocycles accessed in our methodology were ligated to Au-NHC complexes to give new two-coordinate metal complexes.

We find that extending the π-conjugation of the donor ligand influences the photophysical properties of the two-coordinate Au(I)-NHC complexes. The principal effect of π-extension in these compounds is stabilization of the triplet energy as opposed to only a minor perturbation of the donor strength. Therefore, depending on the nature of the carbene paired with the donor ligand, luminescence can be tuned to achieve emission from either the ^{3}LE or ICT state. Thus, a relatively weak electron accepting carbene such as BZI in **5.36** and **5.36+π** gives only inefficient ^{3}LE emission, whereas the stronger electron accepting MAC carbene in **5.37** and **5.37+π** leads to efficient emission from the ICT state. The carbazolyl (**5.37** and **5.37+π**) and indolyl (**5.38** and

5.38+π) complexes allow for the direct comparison of two systems that undergo TADF emission from the ICT state. The π-extension of the carbazolyl ligand in **5.37+π** leads to a red-shift in emission. However, π-extending the indolyl-based ligand in **5.38+π** results in an unexpected blue-shift in emission energy that may owe to the different position of substitution.[42]

These studies should prompt further structure–photophysical property studies of donor ligands in these metal complexes to enhance OLED stability and efficiency. Furthermore, these studies demonstrate that hetarynes can be strategically leveraged as central building blocks for accessing π-extended scaffolds with notable properties.

5.5 Experimental Section

5.5.1 Materials and Methods

Unless stated otherwise, reactions were conducted in flame-dried glassware under an atmosphere of nitrogen or argon and commercially obtained reagents were used as received. Anhydrous solvents were either freshly distilled or passed through activated alumina columns, unless otherwise stated. Reaction temperatures were controlled using an IKAmag temperature modulator and, unless stated otherwise, reactions were performed at room temperature (approximately 23 °C). Cesium Fluoride (CsF) and Bis(dibenzylidenacetone)palladium(0) ($Pd(dba)_2$) were obtained from Strem Chemicals and stored in a desiccator. Tri(*o*-tolyl)phosphine ($P(o\text{-tolyl})_3$), 1,1,1,3,3,3-hexamethyldisilazane (HMDS), *tert*-butyllithium (*t*-BuLi), sodium hydride (NaH), and sodium *ter*-butoxide (NaO*t*-Bu) were obtained from Sigma Aldrich. Methyl iodide (MeI) was acquired from Spectrum Chemical. Triflic anhydride was purchased from Oakwood Chemical and distilled over phosphorous pentoxide prior to use. Di-tert-butyl decarbonate and 4-dimethylaminopyridine (DMAP) were obtained from Oakwood Chemical. Triethylamine was purchased from Fischer Scientific and passed through an activated alumina column prior to use. 2-Bromobiphenyl (**5.23**) was obtained from Combi-Blocks and purified by flash chromatography (100% Hexanes) prior to use. 3-Bromo-2-phenylpyridine (**5.43**) was obtained from Combi-Blocks. Bromobiaryls **5.39**,[51] **5.41**,[52] **5.45**,[53] **5.47**,[54] and **5.49**,[55] were prepared according to literature procedures. The silyl triflates **5.14**,[16] **5.33**,[56] and **5.24**[56] were prepared following literature procedures. 3-Bromo-2-hydroxycarbazole (**5.26**) was prepared in one step from 2-hydroxycarbazole following a literature protocol.[31] NHC–Au–Cl complexes **5.51**[48] and **5.52**[43] were prepared following literature procedures. Regioisomeric ratios for indolyne annulation products were determined by analysis of the ^{1}H NMR spectra of the crude reaction mixtures. Thin-layer chromatography (TLC) was

conducted with EMD gel 60 F254 pre-coated plates (0.25 mm for analytical chromatography and 0.50 mm for preparative chromatography) and visualized using UV(254 nm). Celite® was purchased from Fischer Scientific and used as received. Silicycle Siliaflash P60 (particle size 0.040–0.063 mm) was used for flash column chromatography. ^{1}H NMR spectra were recorded on Bruker spectrometers (at 400, 500 and 600 MHz) and are reported relative to residual solvent signals. Data for ^{1}H NMR spectra are reported as follows: chemical shift (δ ppm), multiplicity, coupling constant (Hz), integration. Data for ^{13}C NMR are reported in terms of chemical shift (at 101 and 125 MHz). IR spectra were recorded on a Perkin-Elmer UATR Two FT-IR spectrometer and are reported in terms of frequency absorption (cm^{-1}). DART-MS spectra were collected on a Thermo Exactive Plus MSD (Thermo Scientific) equipped with an ID-CUBE ion source and a Vapur Interface (IonSense Inc.). Both the source and MSD were controlled by Excalibur software v. 3.0. The analyte was spotted onto OpenSpot sampling cards (IonSense Inc.) using CH_2Cl_2 as the solvent. Ionization was accomplished using UHP He plasma with no additional ionization agents. The mass calibration was carried out using Pierce LTQ Velos ESI (+) and (–) Ion calibration solutions (Thermo Fisher Scientific). UV-visible absorption spectra were recorded by using Hewlett-Packard 4853 diode array spectrometer. Steady state emission spectra were recorded on Quanta-Master Photon Technology International phosphorescence/fluorescence spectrofluorometer. Emission quantum yields were measured using Hamamatsu C9920 system equipped with a xenon lamp, integrating sphere and model C10027 photonic multichannel analyzer (PMA). Emission lifetimes were acquired on IBH Fluorocube instrument by using time-correlated single photon counting (TCSPC) method.

5.5.2 Experimental Procedures

5.5.2.1 Scope of Pd-Catalyzed Annulation with *N*-Me-4,5-Indolyne

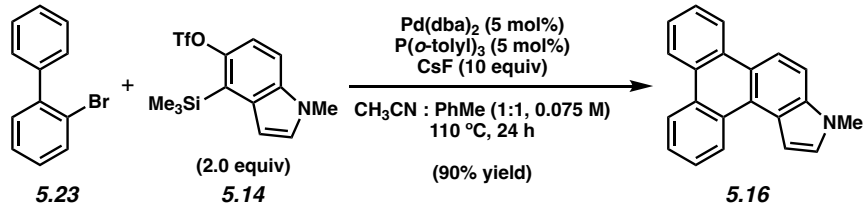

5.23 *5.14* *5.16*

Representative Procedure A for hetaryne annulations (Figure 5.3, annulation product 5.16 used as an example). A 1-dram vial was charged with $Pd(dba)_2$ (3.7 mg, 0.064 mmol, 5 mol%). Next, toluene (0.86 mL), P(*o*-tolyl)$_3$ (2.0 mg, 0.064 mmol, 5 mol%), 2-bromobiphenyl (**5.23**) (30.0 mg, 0.129 mmol, 1.0 equiv), silyl triflate **5.14** (90.5 mg, 0.257 mmol, 2.0 equiv), and acetonitrile (0.86 mL) were added, followed by an oven-dried magnetic stirbar and then CsF (195 mg, 1.29 mmol, 10 equiv). The vial was purged with nitrogen for 3 minutes, then sealed with a Teflon-lined screw cap and stirred at 110 °C for 24 h. Then, after cooling to 23 °C, the mixture was transferred with CH_2Cl_2 (10 mL) and H_2O (2 mL) to a 150 mL separatory funnel containing brine (15 mL). The layers were separated and the aqueous layer was extracted with CH_2Cl_2 (3 x 15 mL). The combined organic layers were dried over $MgSO_4$, filtered, and concentrated *in vacuo*. The resulting crude product was purified by flash chromatography (100% Hexanes → 200:1 Hexanes:EtOAc) to afford annulation product **5.16** (90% yield, average of two experiments) as an off-white solid. Indole **5.16**: mp: 139–144 °C; R_f 0.41 (4:1 Hexanes:EtOAc); ^{1}H NMR (500 MHz, $CDCl_3$): δ 9.24 (d, *J* = 8.0, 1H), 8.78 (d, *J* = 8.0, 1H), 8.72 (t, *J* = 7.0, 2H), 8.57 (d, *J* = 9.0, 1H), 7.74 (t, *J* = 7.4, 1H), 7.73–7.62 (m, 4H), 7.53 (d, *J* = 2.8, 1H), 7.28 (d, *J* = 3.0, 1H), 3.92 (s, 3H); ^{13}C NMR (125 MHz, $CDCl_3$): δ 136.4, 131.3, 131.2, 130.4, 128.9, 128.8, 127.17, 127.15, 126.7, 126.4, 125.9, 124.6, 124.1, 123.8, 123.6, 123.28, 123.25, 117.7, 110.5, 104.0, 33.3; IR (film): 3069, 2924, 2850,

1514, 1492, 1441, 1417, 1351, 1248, 754, 740, 718 cm^{-1}; HRMS-APCI (*m/z*) $[M + H]^+$ calcd for $C_{21}H_{16}N^+$, 282.12773; found 282.12717.

Any modifications of the conditions shown in the representative procedure above are specified in the following schemes, which depict all of the results shown in Figure 5.3.

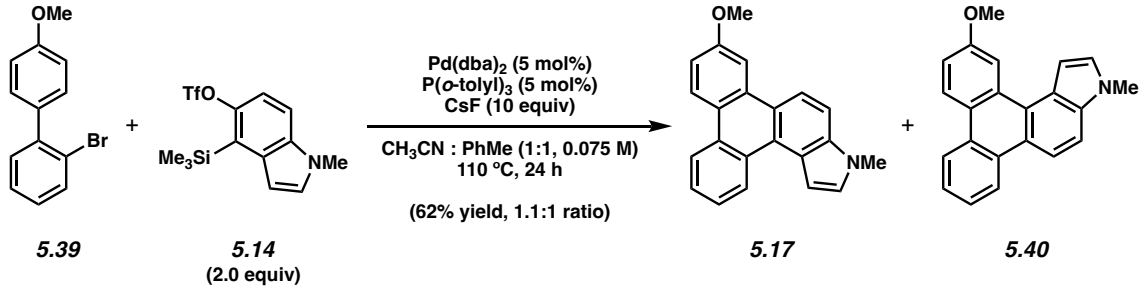

5.39 ***5.14*** (2.0 equiv) ***5.17*** ***5.40***

Indoles 5.17 and 5.40. Followed representative procedure A. Purification by flash chromatography (50:1 Hexanes:EtOAc) afforded an inseparable mixture of indoles **5.17** and **5.40** (62% yield, average of two experiments, 1.1:1 ratio, unassigned) as a white solid. Indoles **5.17** and **5.40**: R_f 0.27 (4:1 Hexanes:EtOAc); ^{1}H NMR (500 MHz, C_6D_6, combined): δ 9.42 (dd, *J* = 8.3, 1.3, 1H), 8.93 (d, *J* = 2.6, 1H), 8.69 (dd, *J* = 7.9, 1.3, 1H), 8.57–8.50 (m, 5H), 8.48 (d, *J* = 9.0, 1H), 8.22 (d, *J* = 2.5, 1H), 7.60–7.47 (m, 6H), 7.30–7.26 (m, 3H), 7.21 (dd, *J* = 9.2, 2.6, 1H), 6.72 (d, *J* = 6.7, 1H), 6.69 (d, *J* = 3.2, 1H), 3.61 (s, 3H), 3.55 (s, 3H), 3.001 (s, 3H), 2.995 (s, 3H); ^{13}C NMR (125 MHz, C_6D_6, combined): δ 159.6, 159.3, 136.8, 136.6, 133.32, 133.31, 131.2, 131.0, 130.8, 129.7, 128.6, 128.5, 127.6, 126.6, 126.4, 126.2, 126.0, 125.8, 125.4, 125.3, 125.2, 125.1, 125.0, 124.6, 124.5, 124.4, 124.0, 123.6, 123.27, 123.25, 118.1, 118.0, 115.5, 115.0, 110.8, 110.5, 110.1, 106.5, 104.5, 104.0, 55.0, 54.9, 32.31, 32.28; IR (film): 2934, 2834, 1614, 1510, 1414, 1246, 1227 cm^{-1}; HRMS-APCI (*m/z*) $[M + H^+]$ calcd for $C_{22}H_{18}NO^+$, 312.13829; found 312.13897.

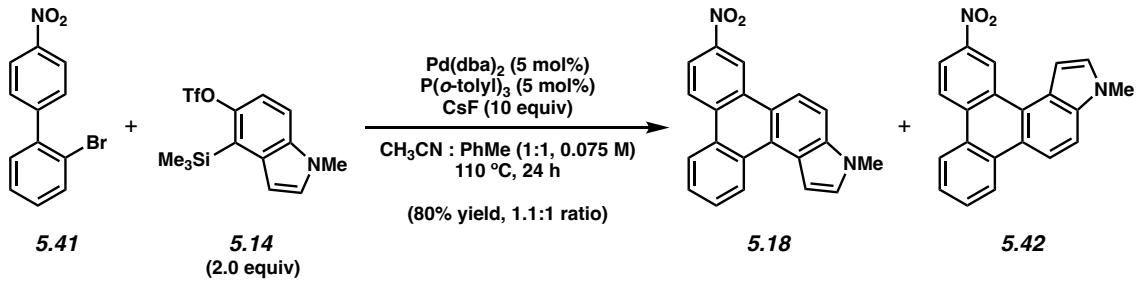

5.41 *5.14* (2.0 equiv) *5.18* *5.42*

Indoles 5.18 and 5.42. Followed representative procedure A. Purification by flash chromatography (50:1 Hexanes:EtOAc → 20:1 Hexanes:EtOAc) afforded an inseparable mixture of indoles **5.18** and **5.42** (80% yield, average of two experiments, 1.4:1 ratio, unassigned) as a yellow solid. Indoles **5.18** and **5.42**: R_f 0.45 (4:1 Hexanes:EtOAc); ^{1}H NMR (600 MHz, $CDCl_3$, major): δ 10.10 (d, *J* = 2.4, 1H), 8.79 (d, *J* = 9.1, 1H), 8.71 (d, *J* = 8.3, 1H), 8.66 (d, *J* = 8.2, 1H), 8.55 (d, *J* = 9.2, 1H), 8.41 (dd, *J* = 9.0, 2.3, 1H), 7.78–7.72 (m, 2H), 7.67 (ddd, *J* = 8.1, 7.0, 1.2, 1H), 7.54 (d, *J* = 3.1, 1H), 7.39 (d, *J* = 3.2, 1H), 4.00 (s, 3H); ^{1}H NMR (600 MHz, $CDCl_3$, minor): δ 9.54 (d, *J* = 2.3, 1H), 9.21 (d, *J* = 8.3, 1H), 8.75 (d, *J* = 9.1, 1H), 8.70 (d, *J* = 8.3, 1H), 8.55 (d, *J* = 8.9, 1H), 8.35 (dd, *J* = 9.0, 2.3, 1H), 7.82 (ddd, *J* = 8.1, 7.0, 1.3, 1H), 7.76–7.71 (m, 2H), 7.51 (d, *J* = 3.1, 1H), 7.36 (d, *J* = 3.2, 1H), 4.00 (s, 3H); ^{13}C NMR (125 MHz, $CDCl_3$, combined): δ 146.4, 146.0, 136.8, 136.4, 134.8, 133.3, 132.51, 132.48, 131.3, 131.0, 129.9, 129.4, 129.0, 128.7, 128.6, 127.4, 127.3, 126.8, 126.4, 125.2, 124.6, 124.4, 124.21, 124.17, 124.1, 123.8, 123.60, 123.55, 123.5, 123.1, 122.8, 119.9, 119.53, 119.47, 117.5, 117.4, 111.7, 111.1, 104.0, 103.4, 33.4, 33.3; IR (film): 2919, 2852, 1597, 1515, 1346, 854, 747 cm^{-1}; HRMS-APCI (*m/z*) [M + H^+] calcd for $C_{21}H_{15}N_2O_2^+$, 327.11280; found 327.11387.

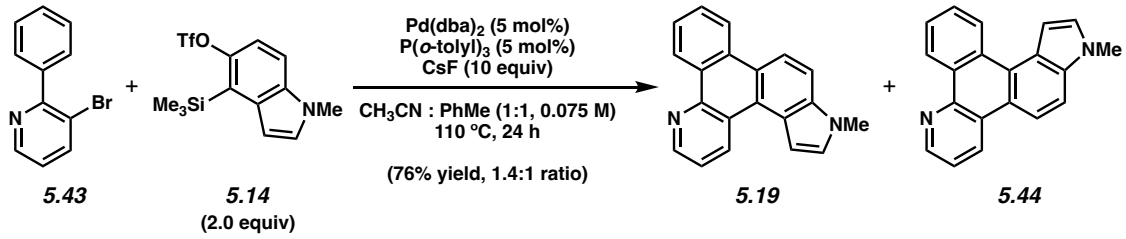

5.43 *5.14* (2.0 equiv) *5.19* *5.44*

Indoles 5.19 and 5.44. Followed representative procedure A. Purification by flash chromatography (100% Hexanes → 50:1 Hexanes:EtOAc → 9:1 Hexanes:EtOAc) afforded an inseparable mixture of indoles **5.19** and **5.44** (76% yield, 1.4:1 ratio, average of two experiments) as a pale yellow solid. Indole **5.19**: R_f 0.34 (4:1 Hexanes:EtOAc); ^{1}H NMR (500 MHz, $CDCl_3$): δ 9.40 (ddd, *J* = 8.2, 4.7, 1.4, 2H), 8.99 (dd, *J* = 4.3, 1.6, 1H), 8.66 (d, 8.2, 1H), 8.54 (d, 8.5, 1H), 7.76 (ddd, *J* = 8.1, 6.9, 1.6, 1H), 7.71 (ddd, *J* = 8.3, 6.8, 1.2, 1H), 7.65 (d, *J* = 9.0, 1H), 7.64–7.60 (m, 1H), 7.38 (d, *J* = 2.9, 1H), 7.27 (d, *J* = 3.2, 1H), 3.90 (s, 3H). Indole **5.44**: R_f 0.34 (4:1 Hexanes:EtOAc); ^{1}H NMR (500 MHz, $CDCl_3$): δ 9.46 (dd, *J* = 8.1, 1.3, 1H), 9.18 (d, *J* = 8.2, 1H), 8.95 (dd, *J* = 4.3, 1.6, 1H), 8.89 (dd, *J* = 8.4, 1.3, 1H), 8.41 (d, *J* = 9.0, 1H), 7.83 (ddd, *J* = 8.2, 7.0, 1.7, 1H), 7.77 (ddd, *J* = 7.2, 5.6, 1.2, 1H), 7.64–7.60 (m, 1H), 7.55 (dd, *J* = 8.3, 4.3, 1H), 7.53 (d, *J* = 3.1, 1H), 7.29 (d, *J* = 3.2, 1H), 3.91 (s, 3H); ^{13}C NMR (125 MHz, $CDCl_3$, combined): 147.69, 147.66, 146.9, 145.6, 136.6, 136.3, 134.2, 132.8, 132.7, 131.4, 131.0, 130.1, 129.3, 129.2, 128.8, 128.4, 126.6, 126.4, 126.2, 126.1, 125.8, 125.4, 125.2, 124.6, 124.2, 124.0, 123.9, 123.2, 122.9, 122.8, 122.1, 121.5, 117.7, 117.3, 111.1, 110.6, 104.0, 103.2, 33.3 (2C); IR (film): 3059, 2920, 1739, 1609, 1579, 1513, 1477, 1444, 1418, 1399, 1349, 1290, 1241 cm^{-1}; HRMS-APCI (*m/z*) [M + H^+] calcd for $C_{20}H_{15}N_2^+$, 283.12297; found 283.11932.

The structure of **5.19** was verified by 2D-NOESY and 2D-COSY of the mixture, as the following interactions were observed:

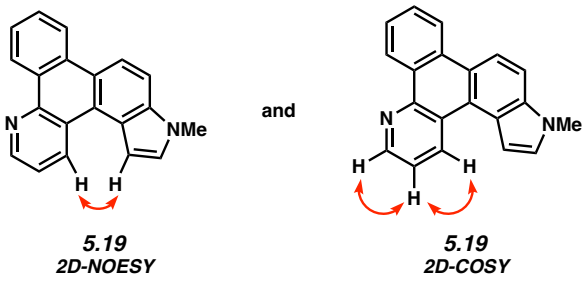

5.19 ***2D-NOESY*** ***5.19*** ***2D-COSY***

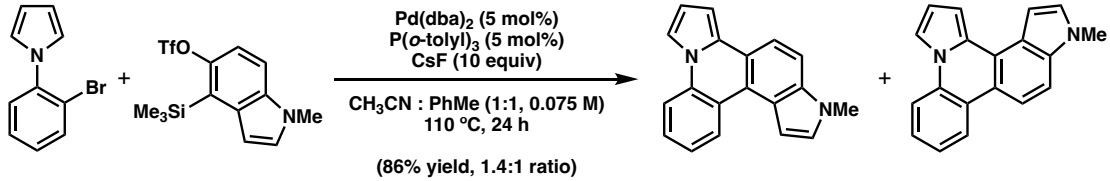

5.45 ***5.14*** **(2.0 equiv)** ***5.20*** ***5.46***

Pyrroles 5.20 and 5.46. Followed representative procedure A. Purification by flash chromatography (20:1 Hexanes:Benzene) afforded an inseparable mixture of pyrroles **5.20** and **5.46** (86% yield, 1.4:1 ratio, average of two experiments, unassigned) as a yellow solid. Pyrroles **5.20** and **5.46**: R_f 0.56 (4:1 Hexanes:EtOAc); ^{1}H NMR (500 MHz, C_6D_6, combined): δ 9.01 (dd, *J* = 8.0, 1.5, 1H), 8.33–8.28 (m, 1H), 8.13 (d, *J* = 8.9, 1H), 8.01 (d, *J* = 8.7, 1H), 7.65 (dd, *J* = 3.0, 1.4, 1H), 7.58 (dd, *J* = 3.0, 1.4, 1H), 7.4 (m, 3H), 7.28 (dd, *J* = 3.2, 0.7, 1H), 7.27–7.23 (m, 2H), 7.22–7.19 (m, 1H), 7.19–7.17 (m, 2H), 7.10 (t, *J* = 0.9, 1H), 7.09 (m, 2H), 6.92 (dd, *J* = 4.0, 2.9, 1H), 6.84 (dd, *J* = 3.9, 2.8, 1H), 6.67 (d, *J* = 3.0, 1H), 6.62 (d, *J* = 3.3, 1H), 2.96 (s, 3H), 2.92 (s, 3H); ^{13}C NMR (125 MHz, C_6D_6, combined): δ 136.7, 136.2, 134.0, 132.9, 131.5, 129.6, 128.9, 128.8, 127.60, 127.58, 127.0, 124.3, 124.2, 124.0, 123.7, 123.5, 123.4, 122.9, 121.5, 120.4, 118.9, 118.6, 117.9, 117.0, 115.3, 115.2, 113.0, 112.9, 112.7, 112.2, 111.5, 108.8, 105.6, 102.94, 102.88, 101.0, 32.22, 32.19; IR (film): 3102, 2923, 1500, 1441, 1355 cm^{-1}; HRMS-APCI (*m/z*) [M + H$^+$] calcd for $C_{19}H_{15}N_2^+$, 271.12297; found 271.12191.

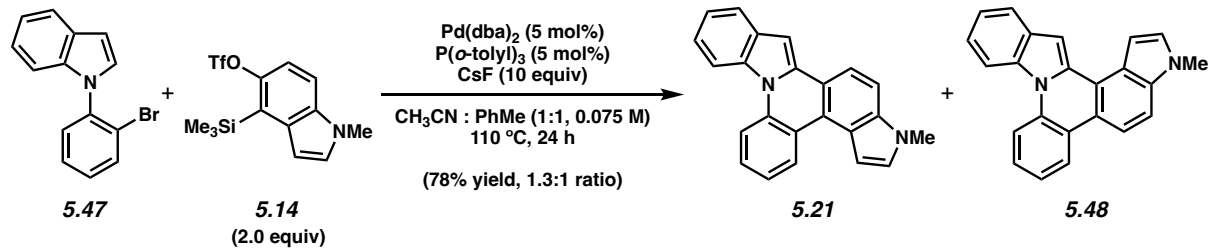

Indoles 5.21 and 5.48. Followed representative procedure A. Purification by flash chromatography (100% Hexanes → 100:1 Hexanes:EtOAc → 25:1 Hexanes:EtOAc → 9:1 Hexanes:EtOAc, followed by a second column of 9:1 Hexanes:EtOAc) afforded an inseparable mixture of indoles **5.21** and **5.48** (78% yield, 1.3:1 ratio, average of two experiments, unassigned) as a bright yellow solid. Indoles **5.21** and **5.48**: R_f 0.32 (4:1 Hexanes:EtOAc); ^{1}H NMR (500 MHz, C_6D_6, major): δ 8.43 (dd, *J* = 8.2, 1.0, 1H), 8.28 (dd, *J* = 8.0, 1.1, 2H), 8.04 (d, *J* = 9.0, 1H), 7.98 (d, *J* = 8.6, 1H), 7.79 (s, 1H), 7.41 (ddd, *J* = 7.8, 6.8, 0.9, 1H), 7.36–7.31 (m, 1H), 7.30–7.17 (m, 3H), 7.08 (dd, *J* = 8.9, 0.6, 1H), 6.63 (d, *J* = 3.2, 1H), 2.94 (s, 3H); ^{1}H NMR (500 MHz, C_6D_6, minor): δ 8.95 (dd, *J* = 8.0, 1.6, 1H), 8.41 (dd, *J* = 8.0, 1.1, 1H), 8.23 (d, *J* = 8.4, 1H), 7.98 (d, *J* = 7.6, 1H), 7.91 (d, *J* = 7.9, 1H), 7.41 (ddd, *J* = 7.5, 6.9, 0.9, 1H), 7.36–7.31 (m, 1H), 7.30–7.17 (m, 4H), 7.04 (dd, *J* = 8.7, 0.7, 1H), 6.58 (d, *J* = 3.2, 1H), 2.92 (s, 3H); ^{13}C NMR (125 MHz, C_6D_6, combined; 44 of 46 signals observed): δ 137.6, 137.2, 136.7, 136.5, 135.6, 135.5, 134.1, 133.9, 131.7, 131.6, 129.3, 129.2, 127.6, 127.3, 124.6, 124.3, 124.0, 123.8, 123.7, 123.04, 122.95, 122.3, 122.11, 122.06, 121.6, 121.5, 121.4, 121.1, 121.0, 120.7, 119.9, 118.7, 116.8, 116.7, 116.6, 114.8, 111.3, 110.5, 103.2, 102.9, 99.8, 95.2, 32.21, 32.18; IR (film): 3040, 2923, 1738, 1601, 1550, 1509, 1490, 1447, 1419, 1355; HRMS-APCI (*m/z*) $[M + H]^+$ calcd for $C_{23}H_{17}N_2^+$, 321.13862; found 321.13951.

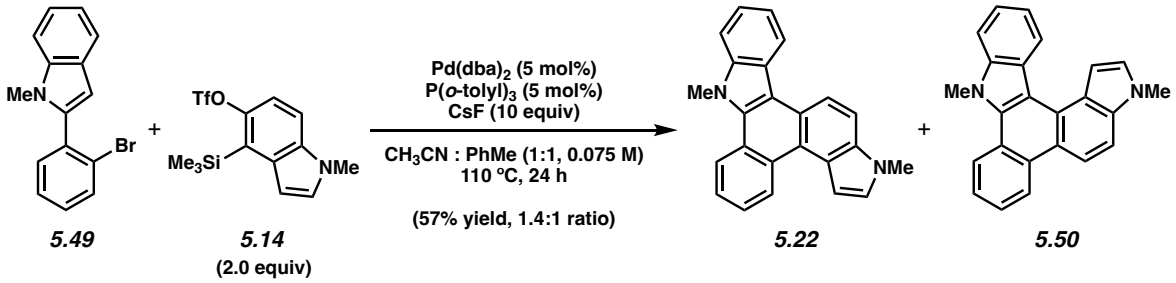

Indoles 5.22 and 5.50. Followed representative procedure A. Purification by flash chromatography (100% Hexanes → 200:1 Hexanes:EtOAc → 100:1 Hexanes:EtOAc) afforded an inseparable mixture of indoles **5.22** and **5.50** (57% yield, 1.4:1 ratio, average of two experiments) as a yellow amorphous solid. Indole **5.22**: R_f 0.40 (3:1 Hexanes:EtOAc); ^{1}H NMR (500 MHz, C_6D_6): δ 9.74 (d, *J* = 8.5, 1H), 9.09 (d, *J* = 8.8, 1H), 8.92–8.88 (m, 1H), 8.48 (dd, *J* = 8.3, 0.9, 1H) 7.70–7.65 (m, 2H), 7.59–7.43 (m, 4H), 7.29 (dd, *J* = 7.5, 1.5, 1H), 6.81 (d, *J* = 3.1, 1H), 3.57 (s, 3H), 3.11 (s, 3H); ^{13}C NMR (125 MHz, C_6D_6; 22 of 24 signals observed): 141.8, 134.8, 134.2, 132.7, 125.7, 125.3, 125.2, 124.4, 123.9, 123.8, 123.6, 123.3, 122.6, 122.1, 120.3, 118.8, 115.7, 111.4, 109.9, 103.9, 34.0, 32.4. Indole **5.50**: R_f 0.40 (3:1 Hexanes:EtOAc); ^{1}H NMR (500 MHz, C_6D_6): δ 9.37 (d, *J* = 8.1, 1H), 8.92–8.88 (m, 1H), 8.68 (d, *J* = 9.1, 1H), 8.38 (dd, *J* = 8.4, 0.9, 1H), 7.95 (d, *J* = 3.1, 1H), 7.59–7.43 (m, 3H), 7.40 (ddd, *J* = 7.9, 7.1, 1.1, 1H), 7.34 (dd, *J* = 9.1, 0.6, 1H), 7.26 (d, *J* = 8.1, 1H), 6.72 (d, *J* = 3.1, 1H), 3.54 (s, 3H), 3.10 (s, 3H); ^{13}C NMR (125 MHz, C_6D_6; 23 of 24 signals observed): 141.5, 136.5, 136.2, 132.8, 126.3, 125.8, 125.1, 124.8, 124.54, 124.51, 124.46, 123.7, 123.6, 123.1, 121.7, 119.2, 118.3, 115.3, 109.7, 108.1, 105.8, 34.0, 32.4; IR (film, entire mixture): 3055, 2923, 2854, 1737, 1509, 1472, 1374, 1342, 1245, 1102 cm^{-1}; HRMS-APCI (*m/z*) $[M + H]^+$ calcd for $C_{24}H_{19}N_2^+$, 335.15428; found 335.15396.

The structure of **5.22** was verified by 2D-NOESY of the mixture, as the following interaction was observed:

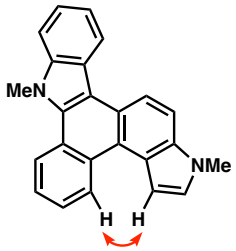

5.22

2D-NOESY

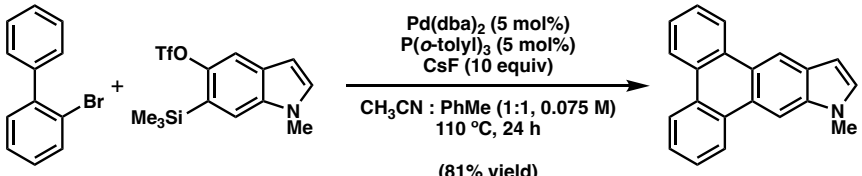

5.23 ***5.24*** (2.0 equiv) ***5.25***

Indole 5.25. Followed representative Procedure A. Purification by flash chromatography (Hexanes → 1:1 Hexanes:Benzene) afforded indole **5.25** (81% yield, average of two experiments) as an off-white solid. Indole **5.25**: mp 169.6–172.0 °C; R_f 0.25 (9:1 Hexanes:EtOAc); ^{1}H NMR (500 MHz, $CDCl_3$): δ 8.92 (s, 1H), 8.73 (d, J = 8.3, 2H), 8.62 (t, J = 7.7, 2H), 8.51 (s, 1H), 7.66–7.56 (m, 4H), 7.27 (d, J = 2.6, 1H), 6.70 (dd, J = 0.8, 3.1, 1H), 3.99 (s, 3H); ^{13}C NMR (125 MHz, $CDCl_3$; 27 of 28 signals observed): δ 137.4, 132.0, 131.4, 131.2, 129.6, 129.3, 129.0, 127.3, 127.1, 126.6, 126.1, 125.7, 123.56, 123.55, 123.4, 123.22, 123.15, 115.1, 102.3, 101.1, 33.2; IR (film): 3081, 2928, 2811, 1628, 1601, 1520, 1446, 1218, 1085, 754 cm^{-1}; HRMS–APCI (m/z) $[M]^+$ calcd for $C_{21}H_{16}N^+$, 281.11990; found 281.12065.

5.5.2.2 Synthesis of Silyl Triflate Precursor to 2,3-Carbazolyne

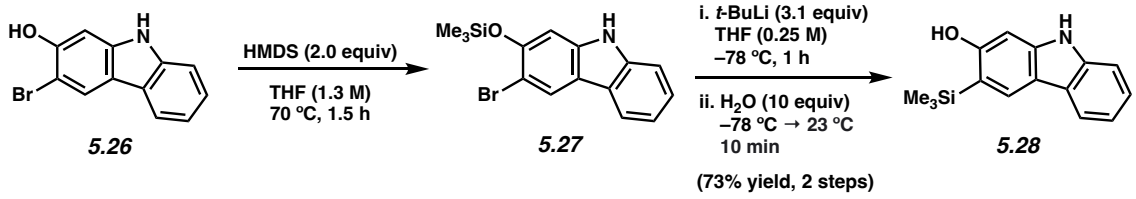

Silyl alcohol 5.28. A 20 mL scintillation vial was charged with 3-bromo-2-hydroxycarbazole (**5.26**, 4.3 g, 16 mmol, 1.0 equiv) and THF (5.6 mL, 1.3 M). HMDS (6.9 mL, 2.0 equiv, 33 mmol) was added in one portion. The vial was sealed with a Teflon cap, and subsequently placed in an aluminum block preheated to 70 °C, where it was allowed to stir for 1.5 h. After stirring for 1.5 h, the reaction mixture was cooled to 23 °C and concentrated under reduced pressure to afford the intermediate silyl enol ether **5.27** as a pink solid. This was carried forward without further purification.

The crude solid was dissolved in THF (8.5 mL, 0.25 M) and purged with nitrogen for 3 minutes, before being cooled to –78 °C. *tert*-Butyllithium (1.70 M, 4.17 mL, 7.09 mmol, 3.1 equiv) was then added dropwise over 10 min. The solution was allowed to stir for 1 hour at –78 °C. After the allotted time, deionized H_2O (408 μL, 22.5 mmol, 10 equiv) was added dropwise over 2 min. The solution was then allowed to warm to 23 °C over 10 min and the mixture was transferred to a separatory funnel with H_2O (20 mL) and CH_2Cl_2 (20 mL). The layers were then separated and the aqueous layer was extracted with CH_2Cl_2 (2 x 20 mL). The combined organic layers were dried over $MgSO_4$, filtered, and concentrated under reduced pressure. The crude residue was then purified by flash chromatography (100% Benzene) to afford silyl alcohol **5.28** as a white solid (3.1 g, 73% yield over two steps). Silyl alcohol **5.28**: mp: >200 °C; R_f 0.15 (100% Benzene); ^{1}H NMR (600 MHz, $CDCl_3$): δ 8.03 (s, 1H), 8.00 (d, J = 7.7, 1H), 7.84 (s, 1H), 7.36–7.32 (m, 2H), 7.21 (dd, J = 6.6, 2.2, 1H), 6.72 (d, J= 2.4, 1H), 4.94 (s, 1H), 0.39 (s, 9H); ^{13}C NMR (125 MHz, $CDCl_3$): δ

159.4, 141.8, 139.2, 126.9, 124.4, 123.4, 119.6, 119.3, 117.5, 117.2, 110.2, 96.0, –0.7; IR (film): 3416, 3016, 2970, 2926, 2854, 1738, 1366 cm^{-1}; HRMS-APCI (*m/z*) $[M + H]^+$ calcd for $C_{13}H_{18}NOSi^+$, 256.1152; found 256.1171.

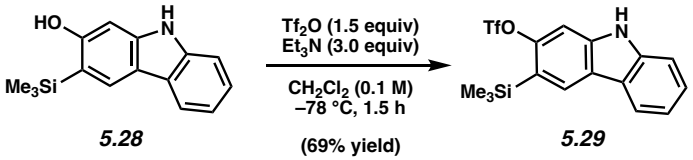

Silyl triflate 5.29. Silyl alcohol **5.28** (403 mg, 1.58 mmol, 1.00 equiv) was suspended in CH_2Cl_2 (15 mL). The solution was purged with nitrogen for 3 minutes, then cooled to –78 °C. Triethylamine (0.66 mL, 4.7 mmol, 3.0 equiv) was then added in one portion followed by trifluoromethanesulfonic anhydride (400 μL, 2.37 mmol, 1.5 equiv), which was added dropwise over 5 min. The solution was allowed to stir for 1.5 h at –78 °C. After the allotted time, saturated aqueous $NaHCO_3$ (20 mL) was added over 1 minute. The solution was then allowed to warm to 23 °C over 10 min and the mixture was transferred to a separatory funnel with H_2O (10 mL) and CH_2Cl_2 (20 mL). The layers were then separated and the aqueous layer was extracted with CH_2Cl_2 (2 x 20 mL). The combined organic layers were dried over $MgSO_4$, filtered, and concentrated under reduced pressure. The crude residue was then purified by flash chromatography (100% Benzene) to afford silyl triflate **5.29** as a clear oil (375 mg, 69% yield). Silyl triflate **5.29**: R_f = 0.59 (100% Benzene); ^1H NMR (500 MHz, $CDCl_3$): δ 8.22 (s, 1H), 8.16 (s, 1H), 8.08 (d, J = 7.9, 1H), 7.46–7.44 (m, 3H), 7.28 (ddd, J = 7.8, 5.0, 3.1, 1H), 0.44 (s, 9H); ^{13}C NMR (125 MHz, $CDCl_3$): δ 153.3, 140.4, 140.2, 127.5, 126.6, 122.7, 122.3, 121.9, 120.43, 120.41, 110.9, 102.0, 0.40; IR (film): 3443, 3016, 2970, 2948, 1739, 1217 cm^{-1}; HRMS-APCI (*m/z*) $[M + H]^+$ calcd for $C_{16}H_{17}NO_3F_3SSi^+$, 388.0645; found 388.0659.

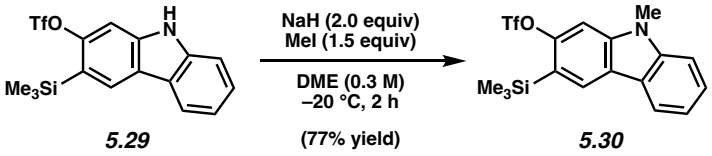

5.29 *5.30*

***N*-Me-Carbazole Silyl Triflate 5.30**. To a 2-dram vial was added carbazole silyl triflate **5.29** (196 mg, 0.506 mmol, 1.00 equiv) and DME (1.7 mL, 0.3 M). The resulting mixture was stirred under positive nitrogen pressure. The mixture was cooled to –20 °C in a dry ice and water/methanol (7:3) bath for 5 min. To the cooled solution was added iodomethane (48 μL, 0.76 mmol, 1.5 equiv) in a single portion. Next, the septum was removed and NaH (60% dispersion in mineral oil, 40.5 mg, 1.01 mmol, 2.0 equiv) was added in a single portion, then the septum was quickly replaced. The reaction continued to stir under nitrogen at –20 °C for 2 h, at which point the reaction was quenched with sat. aq. NH_4Cl (5 mL) and allowed to stir at 23 °C for 5 min. The mixture was transferred to a separatory funnel containing water (10 mL) and EtOAc (10 mL). The layers were separated and the aqueous layer was extracted with EtOAc (3 x 10 mL). The organic layers were combined, dried over $MgSO_4$, filtered, and concentrated under reduced pressure to afford a yellow solid. The crude residue was purified by flash chromatography (16:1 Hexanes:Benzene) to afford *N*-Me-carbazole silyl triflate **5.30** (156 mg, 77% yield) as a white solid. *N*-Me-carbazole silyl triflate **5.30**: mp 128.2–130.3 °C; R_f 0.79 (9:1 Hexanes:EtOAc); ^{1}H NMR (600 MHz, $CDCl_3$): δ 8.18 (s, 1H), 8.11 (d, J = 7.9, 1H), 7.53–7.50 (m, 1H), 7.43 (d, J = 8.3, 1H), 7.38 (s, 1H), 7.30 (td, J = 7.5, 0.9, 1H), 3.85 (s, 3H), 0.44 (s, 9H); ^{13}C NMR (125 MHz, $CDCl_3$; 14 of 15 signals observed): δ 153.5, 142.1, 141.9, 127.4, 126.4, 122.1, 121.9, 121.0, 120.4, 119.9, 108.8, 100.0, 29.3, –0.4; IR (film): 3017, 2955, 1739, 1596, 1414, 1206 cm^{-1}; HRMS-APCI (*m/z*) $[M + H]^+$ calcd for $C_{17}H_{19}F_3NO_3SSi^+$, 402.0802; found 402.0690.

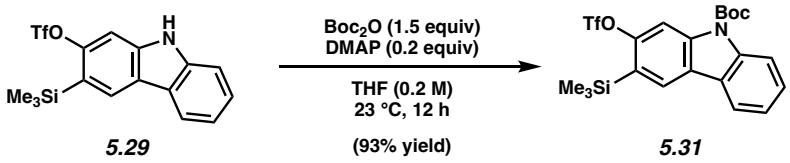

***N*-Boc-Carbazole Silyl Triflate 5.31**. To a 50 mL round bottom flask was added carbazole silyl triflate **5.29** (1.00 g, 2.58 mmol, 1.0 equiv), THF (13 mL, 0.2 M), 4-dimethylaminopyridine (63 mg, 0.51 mmol, 0.2 equiv), and di-*tert*-butyl dicarbonate (839 mg, 3.84 mmol, 1.5 equiv). The resulting mixture was purged with nitrogen for 3 minutes, then allowed to stir under positive nitrogen pressure at 23 °C for 2 h. The mixture was then quenched with deionized water (10 mL). The solution was transferred to a separatory funnel and the layers were separated. The aqueous layer was subsequently extracted with CH_2Cl_2 (3 x 10 mL). The organic layers were combined, dried over Na_2SO_4, filtered, and concentrated under reduced pressure to afford a crude, yellow solid. The crude material was purified by flash chromatography (100:1 Hexanes:EtOAc) to yield *N*-Boc-carbazole silyl triflate **5.31** (1.17 g, 93% yield) as a white solid. *N*-Boc-carbazole silyl triflate **5.31**: mp: 170.5–172.3 °C; R_f 0.57 (9:1 Hexanes:EtOAc); ^{1}H NMR (600 MHz, $CDCl_3$): δ 8.36 (d, J = 8.6, 1H), 8.35 (s, 1H), 8.08 (s, 1H), 8.00 (d, J = 7.9, 1H), 7.51 (td, J = 7.6, 1.0, 1H), 7.39 (td, J = 7.5, 1.0, 1H), 1.76 (s, 9H), 0.44 (s, 9H); ^{13}C NMR (125 MHz, $CDCl_3$; 16 of 17 signals observed): δ 153.9, 150.6, 139.6, 127.8, 126.6, 126.4, 124.9, 124.5, 123.6, 119.9, 119.8, 116.5, 108.3, 85.1, 28.4, –0.5; IR (film): 2983, 1728, 1393, 1355, 1212, 1155, 1140 cm^{-1}; HRMS-APCI (*m/z*) $[M + H]^+$ calcd for $C_{21}H_{25}F_3NO_5SSi^+$, 488.1169; found 488.1198.

5.5.2.3 Annulation of *N*-Me-Carbazolyne

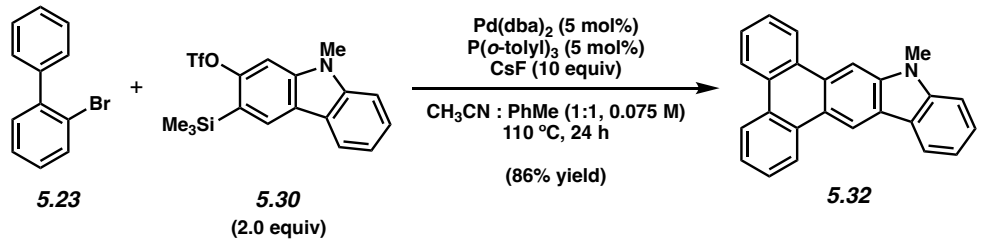

5.23 *5.30* (2.0 equiv) *5.32*

Carbazole 5.32. Followed representative procedure A. Purification by flash chromatography (100% Hexanes → 1:1 Hexanes:Benzene) afforded carbazole **5.32** (86% yield) as an off-white solid. Carbazole **5.32**: mp >200 °C; R_f 0.74 (4:1 Hexanes:EtOAc); ^{1}H NMR (400 MHz, $CDCl_3$): δ 9.38 (s, 1H), 8.86 (d, J = 8.2, 1H), 8.81 (d, J = 7.8, 1H), 8.68 (td, J = 8.6, 1.5, 2H), 8.54 (s, 1H), 8.31 (dt, J = 7.8, 0.9, 1H), 7.72–7.60 (m, 4H), 7.63 (td, J = 7.8, 1.1, 1H), 7.58 (td, J = 7.8, 1.1, 1H), 7.47 (d, J = 8.1, 1H), 7.33 (td, J = 7.4, 0.8, 1H), 4.03 (s, 3H); ^{13}C NMR (100 MHz, $CDCl_3$; 27 of 28 signals observed): δ 142.9, 141.3, 131.1, 130.6, 130.0, 128.85, 128.78, 127.4, 127.1, 127.0, 126.8, 126.1, 123.9, 123.6, 123.5, 123.4, 123.1, 123.0, 122.9, 120.8, 119.2, 114.8, 108.5, 101.1, 29.3; IR (film): 3049, 2923, 2854, 1638, 1603, 1500, 1443, 1258, 754 cm^{-1}; HRMS-APCI (m/z) $[M]^+$ calcd for $C_{25}H_{17}N^+$, 331.13555; found 331.13609.

5.5.2.4 Synthesis of N–H Annulation Products for Metal Coordination

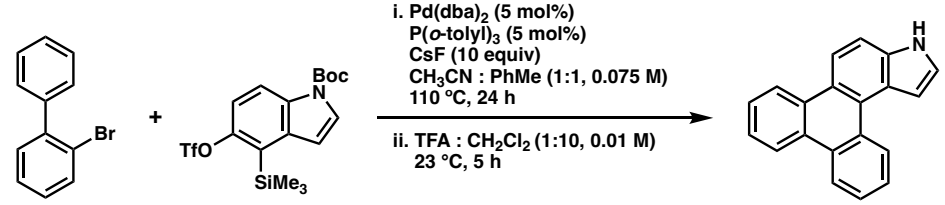

5.23 *5.33* (2.0 equiv) *5.34*

Indole 5.34. A 2-dram vial was charged with $Pd(dba)_2$ (7.0 mg, 0.012 mmol, 5 mol%). Next, toluene (1.5 mL), P(*o*-tolyl)$_3$ (3.7 mg, 0.012 mmol, 5 mol%), 2-bromobiphenyl (**5.23**) (56.4 mg, 0.242 mmol, 1.0 equiv), silyl triflate **5.33** (318 mg, 0.495 mmol, 2.0 equiv), and acetonitrile (1.5

mL) were added sequentially, followed by an oven-dried magnetic stirbar and then CsF (333 mg, 8.26 mmol, 10.0 equiv). The vial was purged with nitrogen for 3 minutes, then sealed with a Teflon-lined screw cap and stirred at 110 °C for 24 h. After allowing to cool to 23 °C, the mixture was transferred with CH_2Cl_2 (20 mL) and H_2O (10 mL) to a separatory funnel containing brine (15 mL). The layers were separated and the aqueous layer was extracted with CH_2Cl_2 (3 x 30 mL). The combined organic layers were dried over Na_2SO_4, filtered, and concentrated under reduced pressure to afford a brown residue that was carried forward without further purification.

The crude material was dissolved in 10:1 CH_2Cl_2:TFA (24.2 mL, 0.01 M) and stirred at 23 °C for 5 h. The reaction was then slowly transferred to a separatory funnel containing sat. aq. sodium bicarbonate (30 mL). The mixture was further diluted with CH_2Cl_2 (10 mL) and the layers were separated. The organic phase was dried over Na_2SO_4 and filtered. To the filtrate was added silica (500 mg). The resulting mixture was dried under reduced pressure until a free-flowing solid was obtained. The crude material purified by flash chromatography (2:3 CH_2Cl_2:Hexanes → 3:1 CH_2Cl_2:Hexanes) to afford indole **5.34** (22.0 mg, 34% yield) as a yellow solid. Indole **5.34**. mp: >200 °C; R_f 0.22 (2:3 CH_2Cl_2:Hexanes); ^{1}H NMR (600 MHz, DMSO-d_6): δ 9.23 (dd, *J* = 8.6, 1.4, 1H), 8.77 (dd, *J* = 8.3, 1.7, 1H), 8.74–8.79 (m, 2H), 8.55 (d, *J* = 8.9, 1H), 8.50 (s, 1H), 7.76–7.60 (m, 6H), 7.41 (t, *J* = 3.6, 2.8, 1H); ^{13}C NMR (100 MHz, $CDCl_3$): δ 135.5, 131.1, 131.0, 130.3, 128.9, 127.1, 127.0, 126.7, 126.3, 125.9, 124.5, 124.4, 124.1, 123.5, 123.19, 123.18, 123.13, 118.1, 112.3, 105.6; IR (film): 3416, 3026, 3073, 2956, 1725, 1350 cm^{-1}; HRMS-APCI (*m/z*) $[M + H]^+$ calcd for $C_{20}H_{14}N^+$, 268.1121; found 267.6527.

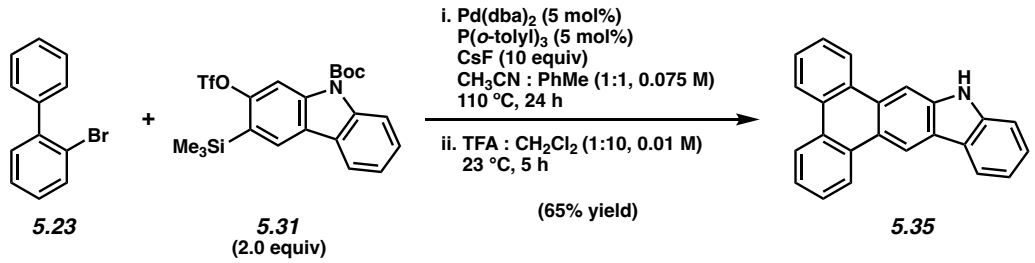

5.23 + *5.31* (2.0 equiv) → *5.35*

Carbazole 5.35. A 2-dram vial was charged with $Pd(dba)_2$ (7.1 mg, 0.012 mmol, 5 mol%). Next, toluene (1.3 mL), P(*o*-tolyl)$_3$ (3.8 mg, 0.012 mmol, 5 mol%), 2-bromobiphenyl (**5.23**) (58.0 mg, 0.248 mmol, 1.0 equiv), silyl triflate **5.31** (241 mg, 0.495 mmol, 2.0 equiv), and acetonitrile (1.6 mL) were added, followed by an oven-dried magnetic stirbar and then CsF (376 mg, 2.48 mmol, 10 equiv). The vial was purged with nitrogen for 3 minutes, then sealed with a Teflon-lined screw cap and stirred at 110 °C for 24 h. After allowing to cool to 23 °C, the mixture was transferred with CH_2Cl_2 (20 mL) and H_2O (10 mL) to a separatory funnel containing brine (15 mL). The layers were separated and the aqueous layer was extracted with CH_2Cl_2 (3 x 30 mL). The combined organic layers were dried over Na_2SO_4, filtered, and concentrated under reduced pressure to afford a brown residue that was carried forward without further purification.

The crude material was dissolved in 10:1 CH_2Cl_2:TFA (24.2 mL, 0.01 M) and stirred at 23 °C for 5 h. The reaction was then slowly transferred to a separatory funnel containing sat. aq. sodium bicarbonate (30 mL). The mixture was further diluted with CH_2Cl_2 (10 mL) and the layers were separated. The organic phase was dried over Na_2SO_4 and filtered. To the filtrate was added silica (500 mg). The resulting mixture was dried under reduced pressure until a free-flowing solid was obtained. The crude material purified by flash chromatography (100% Hexanes → 9:1 Hexanes:EtOAc → 1:1 Hexanes:Benzene) to yield carbazole **5.35** (51 mg, 65% yield) as an off-white solid. Carbazole **5.35**. mp >200 °C; R_f 0.63 (4:1 Hexanes:EtOAc); ^{1}H NMR (600 MHz, $CDCl_3$): δ 11.35 (s, 1H), 9.62 (s, 1H), 9.0 (d, J = 8.0, 1H), 8.82 (d, J = 8.3, 1H), 8.76 (dd, J = 12.5,

8.3, 2H), 8.72 (s, 1H), 8.43 (d, J = 7.5, 1H), 7.73–7.69 (m, 2H), 7.67 (t, J = 6.9, 1H), 7.62 (t, J = 7.5, 1H), 7.55 (d, J = 8.0, 1H), 7.46 (t, J = 7.5, 1H), 7.24 (t, J = 7.5, 1H); ^{13}C NMR (100 MHz, $CDCl_3$; 22 of 24 signals observed): δ 141.3, 139.8, 131.0, 130.3, 129.9, 129.0, 128.8, 127.3, 127.1, 127.0, 126.9, 126.2, 124.4, 123.5, 123.43, 123.36, 123.0, 120.8, 119.8, 114.8, 110.6, 103.4; IR (film): 3413, 2923, 2852, 1611, 1435, 751 cm^{-1}; HRMS-APCI (m/z) $[M + H]^+$ calcd for $C_{24}H_{16}N^+$, 318.12773; found 318.12843.

5.5.2.5 Synthesis of Two-Coordinate Metal Complexes

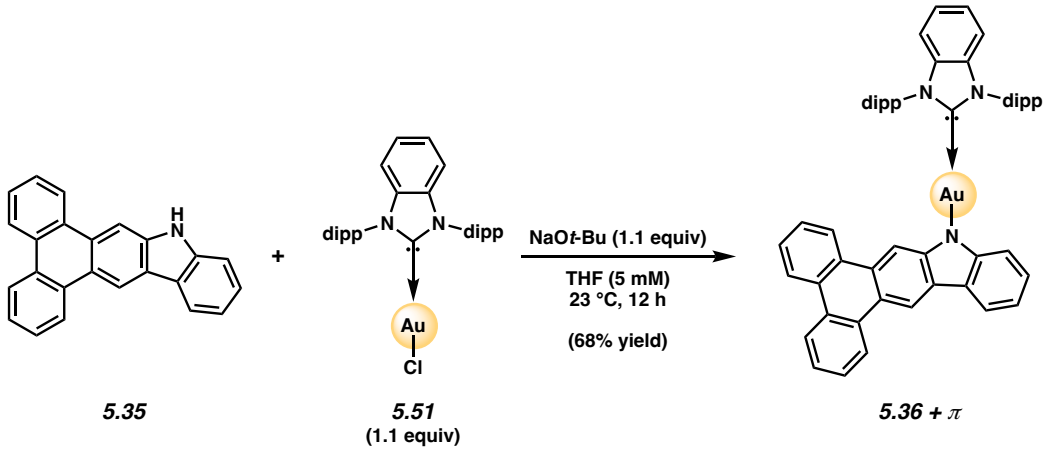

5.35 | *5.51* (1.1 equiv) | *5.36* + π

Representative Procedure B for metal coordination (Figure 5.7, complex 5.36+π used as an example). Sodium *tert*-butoxide (6.4 mg, 67 µmol, 1.1 equiv) was added to a solution of ligand **5.35** (20 mg, 63 µmol, 1.0 equiv) in THF (10 mL). **5.51** (44.4 mg, 66.2 µmol, 1.1 equiv) was added to the reaction flask in one portion and the mixture was left stirring under inert gas at 23 ºC for 12 hours. The solution was filtered through a plug of celite (2 cm in a 15 mL fritted funnel), washed with THF (10 mL), and the volatiles were removed under reduced pressure. The resulting product was recrystallized from CH_2Cl_2 and hexanes to afford an off-white precipitate (47 mg, 68% yield). Carbazole–Au–BZI **5.36+π**: ^{1}H NMR (400 MHz, $CDCl_3$): δ 9.25 (s, 1H), 8.77 (dd, J = 8.5, 1.3, 1H), 8.60 (ddd, J = 16.7, 8.4, 1.4, 2H), 8.28 (dd, J = 8.5, 1.4, 1H), 8.17 (dd, J = 7.6, 1.0, 1H), 8.13

(s, 1H), 7.86 (t, J = 7.8, 2H), 7.72 (ddd, J = 8.2, 6.9, 1.3, 1H), 7.65–7.56 (m, 6H), 7.52–7.47 (m, 3H), 7.29–7.26 (m, 2H), 7.16 (ddd, J = 8.2, 7.0, 1.3, 1H), 7.01 (ddd, J = 7.9, 7.0, 1.0, 1H), 6.67 (dd, J = 8.1, 0.9, 1H), 2.60 (hept, J = 6.9, 4H), 1.40 (d, J = 6.9, 12H), 1.19 (d, J = 6.8, 12H). ^{13}C NMR (150 MHz, $CDCl_3$): δ 207.21, 206.89, 185.66, 151.68, 149.68, 147.17, 146.43, 134.96, 132.19, 131.63, 131.44, 131.04, 129.51, 128.02, 127.23, 126.88, 126.05, 125.74, 125.54, 125.33, 124.75, 124.64, 123.80, 123.73, 123.17, 123.07, 122.78, 120.55, 119.85, 116.11, 113.50, 111.90, 105.58, 30.89, 29.19, 24.64, 24.08. Anal. Calcd for $C_{55}H_{52}AuN_3$: C, 69.39; N, 4.41; H, 5.51. Found: C, 68.05; N, 4.27; H, 5.30. MALDI-TOF (m/z) $[M]^+$ calcd for $C_{55}H_{52}AuN_3^+$, 951.38; found, 951.22.

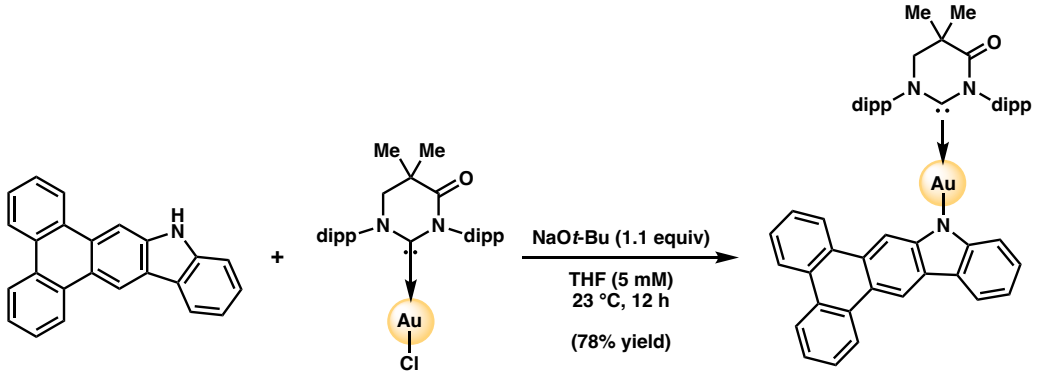

Annulated Carbazole–Au–MAC 5.37+π. Representative procedure B was followed to yield **5.37+π** (42 mg, 78% yield) as a yellow solid. Annulated Carbazole–Au–MAC **5.37+π**: ^{1}H NMR (400 MHz, $CDCl_3$): δ 9.17 (s, 1H), 8.73 (d, J = 7.8 Hz, 1H), 8.57 (ddd, J = 18.5, 8.3, 1.1 Hz, 2H), 8.38 (d, J = 8.1 Hz, 1H), 8.08 (d, J = 0.7 Hz, 1H), 7.82 – 7.70 (m, 3H), 7.65 – 7.44 (m, 8H), 7.04 – 6.91 (m, 2H), 5.81 (d, J = 7.6 Hz, 1H), 3.86 (s, 2H), 3.36 (hept, J = 6.5 Hz, 2H), 3.08 (hept, J = 6.8 Hz, 2H), 1.56 (s, 6H), 1.45 – 1.33 (m, 18H), 1.26 (d, J = 6.8 Hz, 6H). ^{13}C NMR (100 MHz, $CDCl_3$): δ 204.87, 171.43, 151.72, 149.54, 146.05, 144.95, 140.12, 135.57, 132.07, 131.35, 130.60,

130.44, 129.45, 127.98, 127.33, 126.87, 125.86, 125.79, 125.65, 125.63, 124.82, 124.73, 124.54, 124.16, 123.54, 123.14, 123.02, 122.80, 120.63, 119.41, 116.24, 114.06, 113.35, 105.48, 77.19, 62.27, 37.95, 29.35, 28.98, 24.70, 24.61, 24.58, 24.13, 23.93. Anal. Calcd for $C_{54}H_{56}AuN_3O$: C, 67.56; N, 4.38; H, 5.88. Found: C, 67.41; N, 4.35; H, 5.93. MALDI-TOF (*m/z*) $[M]^+$ calcd for $C_{54}H_{56}AuN_3O^+$, 959.41; found, 959.16.

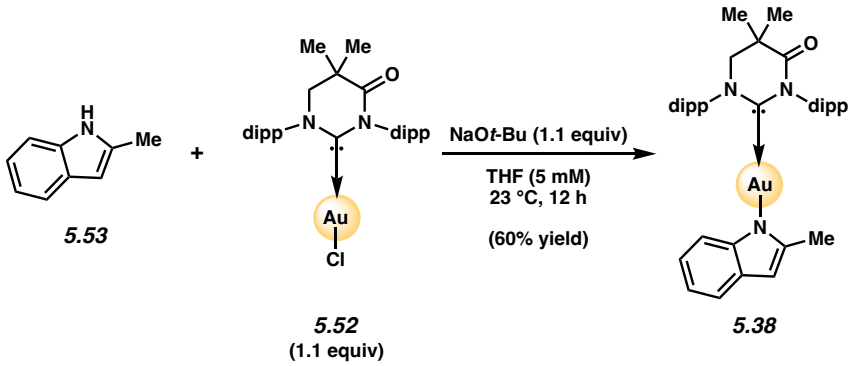

5.53

5.52
(1.1 equiv)

5.38

2-Methyl Indole–Au–MAC 5.38. Representative procedure B was followed to yield **5.38** (110 mg, 60% yield) as an off-white solid. 2-Methylindole–Au–MAC **5.38**: ^{1}H NMR (400 MHz, acetone-d_6): δ 7.64 (dt, J = 17.7, 7.7, 2H), 7.52 (d, J = 7.8, 2H), 7.46 (d, J = 7.7, 2H), 7.09 (dd, J = 7.6, 1.2, 1H), 6.62–6.53 (m, 1H), 6.49 (td, J = 7.5, 1.3, 1H), 5.84 (d, J = 8.0, 1H), 5.74 (d, J = 1.0, 1H), 4.25 (s, 2H), 3.50 (hept, J = 6.8, 2H), 3.24 (hept, J = 6.8, 2H), 1.69 (s, 6H), 1.48–1.43 (m, 8H), 1.42 (d, J = 3.2, 7H), 1.40 (d, J = 6.8, 6H), 1.25 (d, J = 6.8, 6H). ^{13}C NMR (100 MHz, acetone-d_6): δ 205.18, 171.91, 146.16, 145.94, 144.96, 144.43, 140.69, 136.56, 130.54, 130.07, 129.77, 125.29, 124.30, 117.03, 116.77, 116.13, 113.55, 98.29, 61.12, 37.98, 28.49, 23.94, 23.70, 23.65, 23.25, 15.60. Anal. Calcd for $C_{39}H_{50}AuN_3O$: C, 60.54; N, 5.43; H, 6.51. Found: C, 60.49; N, 5.32; H, 6.67. MALDI-TOF (*m/z*) $[M]^+$ calcd for $C_{39}H_{50}AuN_3O^+$, 773.36; found, 773.45.

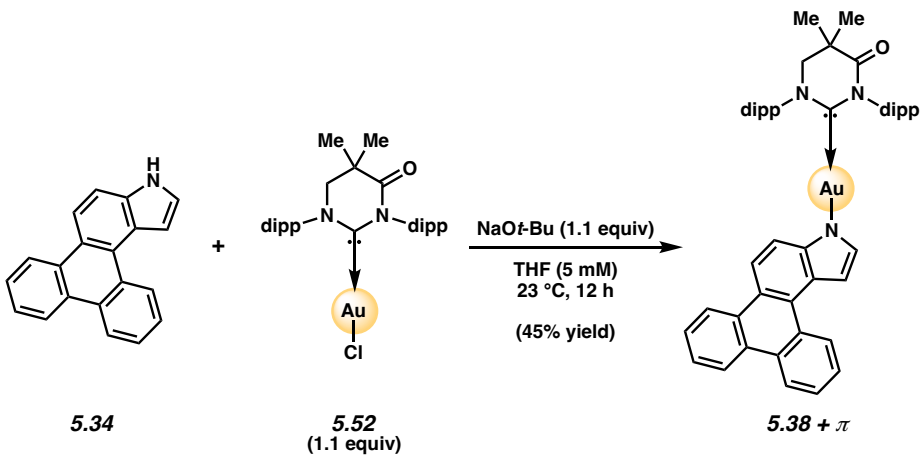

Annulated Indole–Au–MAC 5.38+π. Representative procedure B was followed to yield **5.38** (120 mg, 45% yield) as an off-white solid. Annulated Indole–Au–MAC **5.38+π**: ^{1}H NMR (400 MHz, acetone-d_6): δ 9.18–9.11 (m, 1H), 8.77–8.62 (m, 3H), 8.05 (d, J = 9.1 Hz, 1H), 7.72 (dt, J = 20.8, 7.8 Hz, 2H), 7.65–7.45 (m, 8H), 7.16–7.10 (m, 1H), 6.52 (d, J = 2.8 Hz, 1H), 6.49 (dd, J = 8.9, 1.0 Hz, 1H), 4.29 (s, 2H), 3.48 (h, J = 6.8 Hz, 2H), 3.24 (hept, J = 6.8 Hz, 2H), 1.68 (s, 6H), 1.50–1.31 (m, 18H), 1.22 (d, J = 6.8 Hz, 6H). ^{13}C NMR (150 MHz, acetone-d_6): δ 205.19, 203.69, 171.81, 146.27, 145.07, 145.00, 140.59, 136.57, 135.92, 132.09, 131.87, 130.31, 129.95, 129.45, 128.12, 126.78, 126.61, 126.17, 125.36, 125.10, 124.71, 124.37, 124.18, 124.05, 123.32, 123.20, 122.94, 122.74, 122.49, 117.26, 113.45, 103.02, 60.96, 38.13, 28.85, 28.35, 24.04, 23.97, 23.92, 23.86, 23.79, 23.72, 23.53, 23.21, 23.07. Anal. Calcd for $C_{50}H_{54}AuN_3O$: C, 66.00; N, 4.62; H, 5.98. Found: C, 65.50; N, 4.49; H, 6.09. MALDI-TOF (*m/z*) $[M]^+$ calcd for $C_{50}H_{54}AuN_3O^+$, 909.39; found, 909.27.

5.5.2.6 General Procedure for Photophysical Property Analyses

General Procedure for 1% Polystyrene Films. A mixture of polystyrene pellets (99 mg) and toluene (2 mL) was sonicated for 1 h, until all pellets are dissolved. Two-coordinate metal complex (1 mg) was dissolved in the solution. Using a pipet, ~0.5 mL of the solution was drop-casted onto

a glass substrate (2 cm x 2 cm) to achieve an even surface. The film was left to air-dry for 30 min and then placed in the vacuum chamber for further drying overnight. The resulting film was used to acquire the photophysical data.

5.5.2.7 Absorption Spectra of Donor Ligands

The extinction coefficient for the donor ligands was measured in 2-MeTHF. The molar absorptivity values for the donor ligands are comparable in magnitude to the molar absorptivity values for the transitions localized on the donor ligands in the metal complexes.

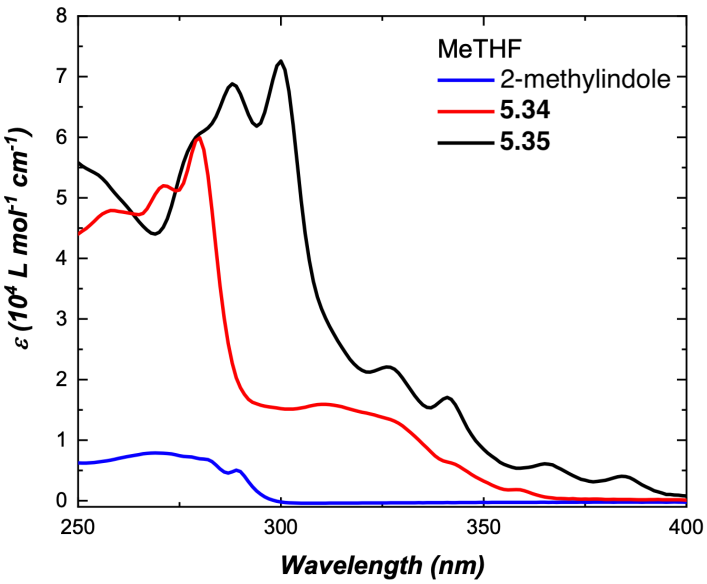

Figure 5.10. Extinction coefficients for the donor ligands in 2-MeTHF.

5.5.2.8 Emission Spectra of Deprotonated Donor Ligands

A few milligrams of donor ligand (1–3 mg) were dissolved in THF (10 mL). The solution was cooled in an ice bath. Once completely dissolved, a solution containing 1.2 equivalents of *n*-BuLi diluted in THF was added. Although a color change was immediately observable, the reaction was

allowed to stir for 1 h. The solvent was then evaporated under reduced pressure, and the solid obtained was dissolved in 2-MeTHF.

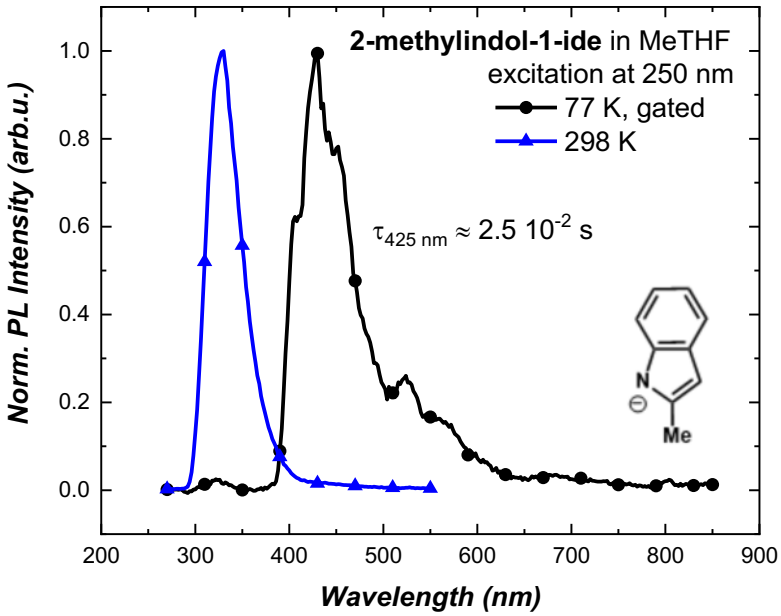

Figure 5.11. Emission spectra of 2-methylindol-1-ide in 2-MeTHF.

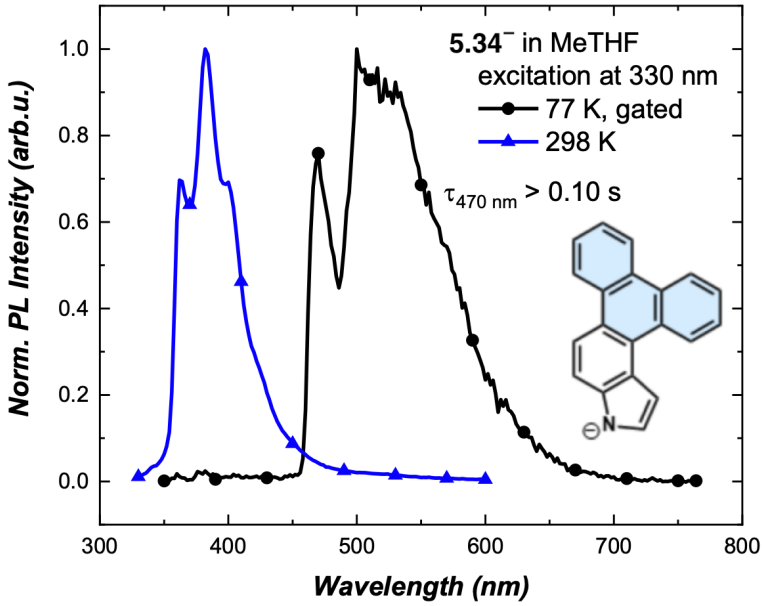

Figure 5.12. Emission spectra of ligand **5.34**⁻ in 2-MeTHF.

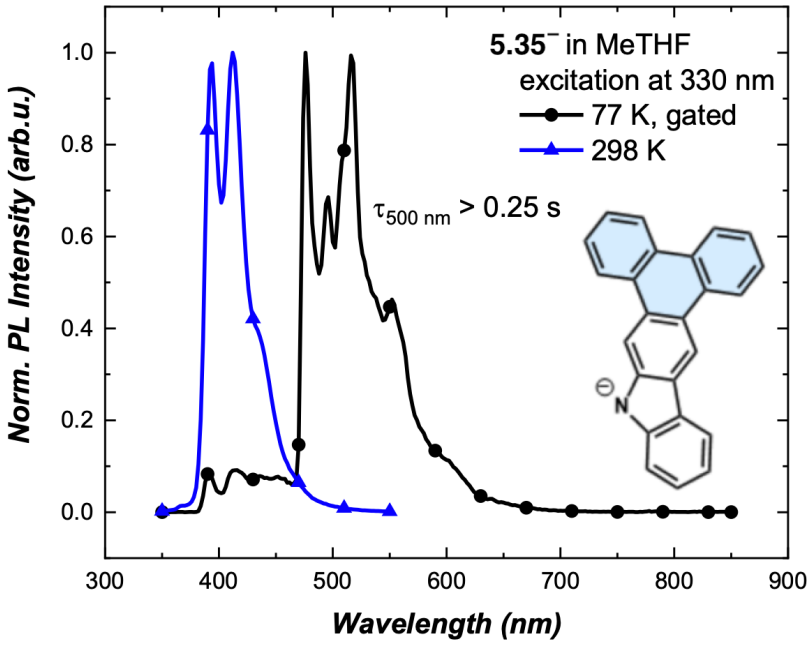

Figure 5.13. Emission spectra of ligand **5.35**⁻ in 2-MeTHF.

5.6 Computational Methods

5.6.1 Complete Citation of Q-Chem 5.1

Density functional theory (DFT) calculations were executed using Q-Chem 5.1 program[57] at the B3LYP/6-31G** level for ground state geometry optimization of the organic ligands and at the B3LYP/LACVP level for the metal complexes. Time-dependent density functional theory (TD-DFT) calculations were performed on the ground state optimized geometries at the CAM-B3LYP/LACVP** level for a balanced description of both charge-transfer and locally excited (LE) states (Table 5.3).

5.6.2 Calculated Frontier Molecular Orbital Energies

Table 5.3. Calculated frontier molecular orbital, singlet (S_1), and triplet (T_1) energies. CT = Charge Transfer state, LE = Locally Excited state.

	HOMO (eV)	**LUMO (eV)**	**$\Delta E_{HOMO-LUMO}$ (eV)**	**S_1 (eV)**	**Nature of S_1 transition**	**T_1 (eV)**	**Nature of T_1 transition**
2-methylindole	-5.28	0.00	5.28	5.21	-	3.16	-
5.34	-5.28	-0.90	4.38	4.24	-	2.55	-
carbazole	-5.47	-0.65	4.82	4.58	-	3.09	-
5.35	-5.28	-1.20	4.08	4.04	-	2.53	-
5.36	-4.22	-1.44	2.78	3.50	CT	3.07	LE
5.36+π	-4.27	-1.52	2.75	3.46	CT	2.48	LE
5.37	-4.30	-1.96	2.34	3.10	CT	2.85	CT
5.37+π	-4.35	-2.07	2.29	3.07	CT	2.48	LE
5.38	-4.16	-1.96	2.20	3.11	CT	2.87	CT
5.38+π	-4.38	-2.10	2.29	3.27	CT	2.51	LE

5.7 Photoluminescence (PL) Decay Lifetime Data

5.7.1 Lifetime Plots

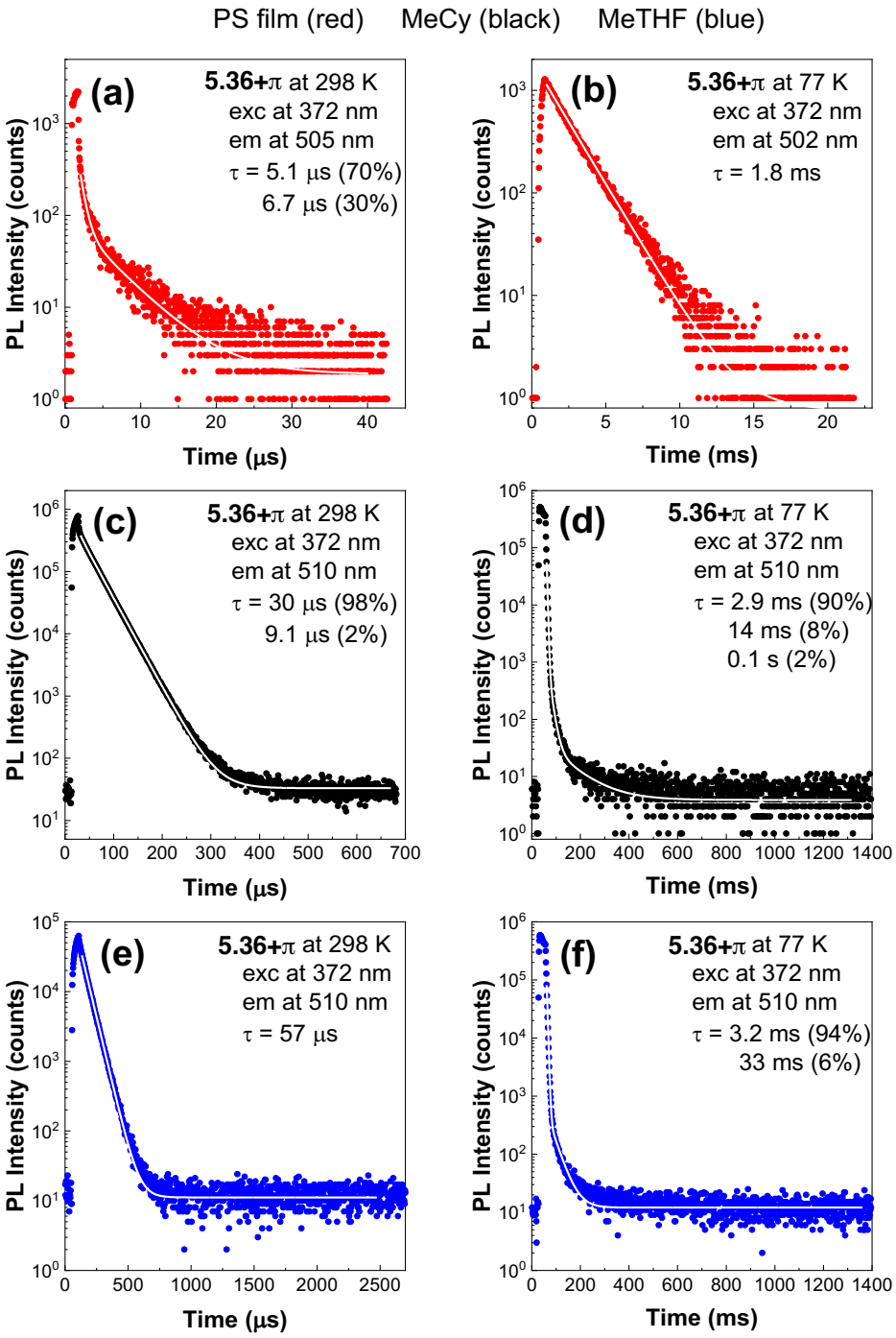

Figure 5.14. Emission lifetime decay for **5.36+π** in (a-b) PS film, (c-d) MeCy, and (e-f) MeTHF at 298 K (left side) and 77 K (right side).

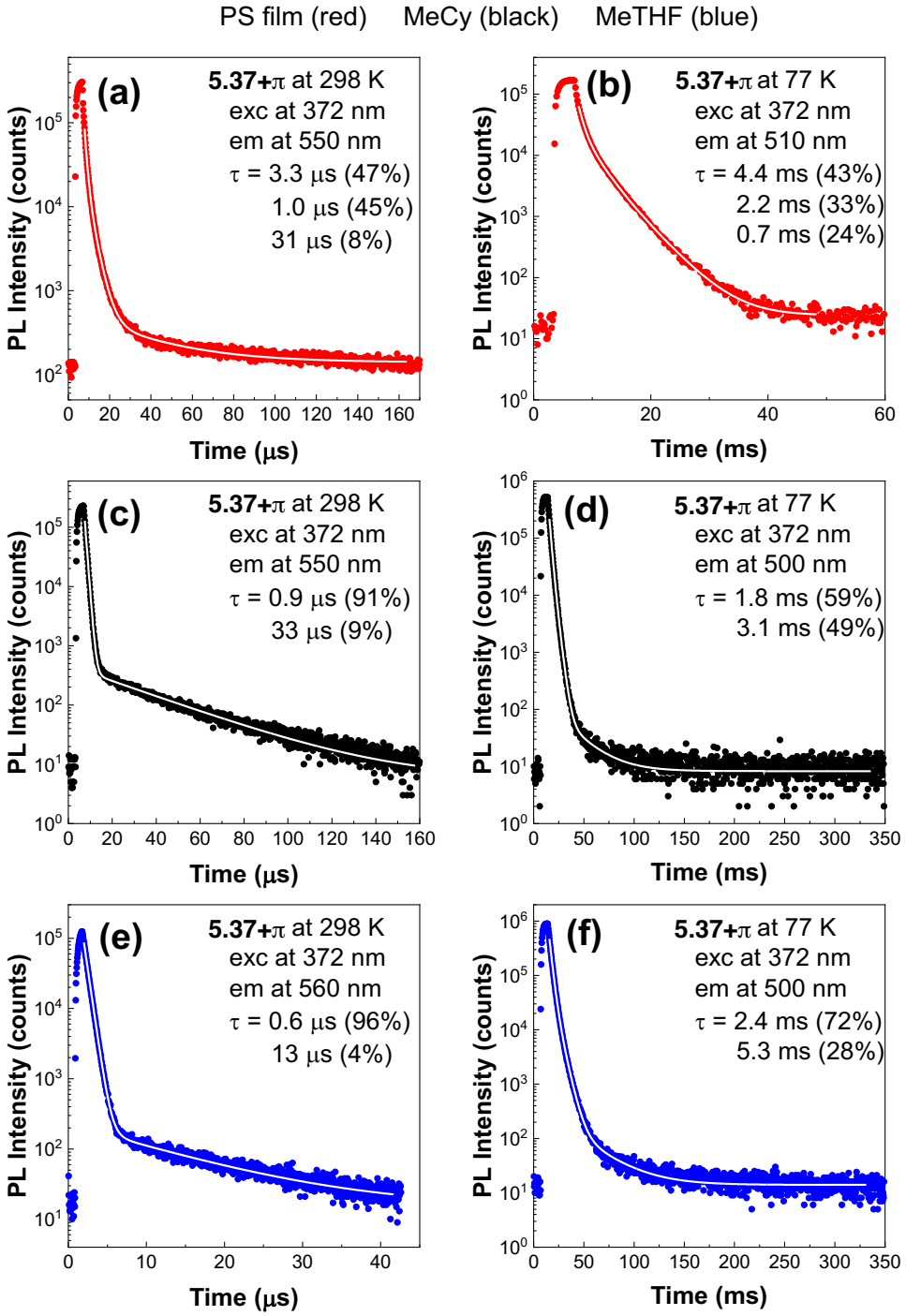

Figure 5.15. Emission lifetime decay for **5.37+π** in (a-b) PS film, (c-d) MeCy, and (e-f) MeTHF at 298 K (left side) and 77 K (right side).

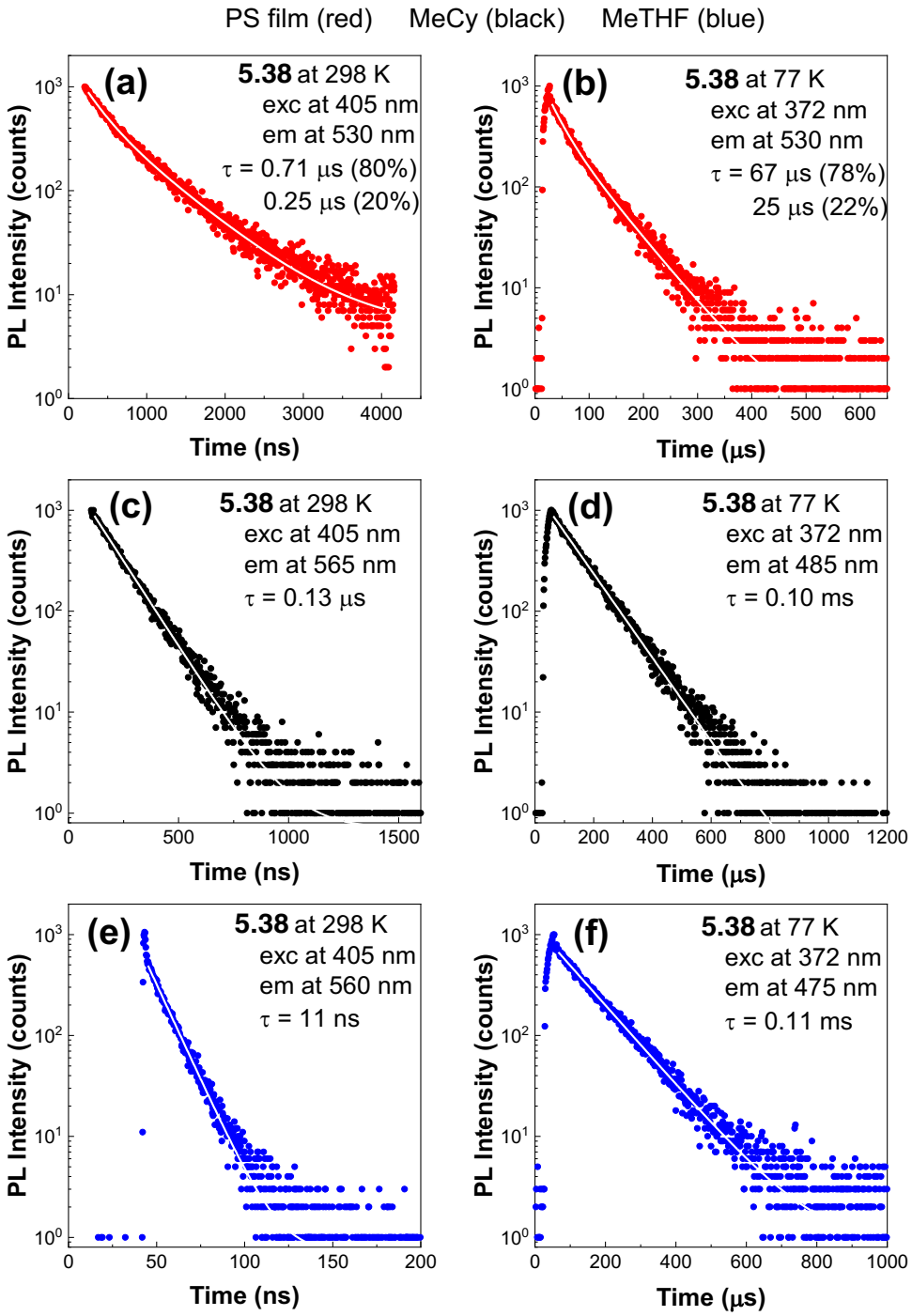

Figure 5.16. Emission lifetime decay for **5.38** in (a-b) PS film, (c-d) MeCy, and (e-f) MeTHF at 298 K (left side) and 77 K (right side).

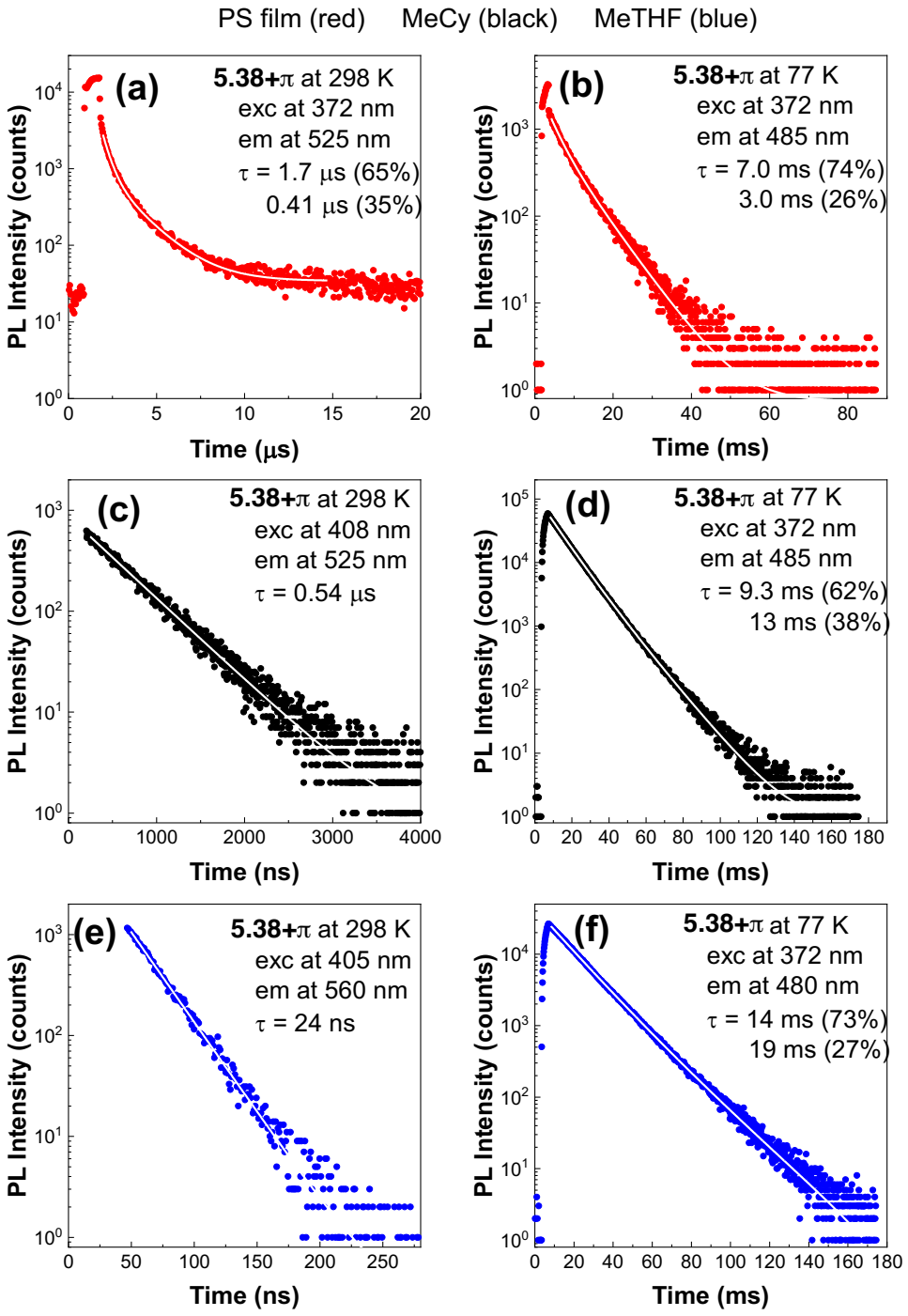

Figure 5.17. Emission lifetime decay for **5.38+π** in (a-b) PS film, (c-d) MeCy, and (e-f) MeTHF at 298 K (left side) and 77 K (right side). In **5.37+π**, in both MeCy and MeTHF at 298 K a

biexponential decay is observed. The slow lifetime is in the range of tens of microseconds. It is assigned to p-type delayed fluorescence caused by a bimolecular triplet-triplet annihilation.

5.8 Spectra Relevant to Chapter Five:

π-Extension of Heterocycles via a Pd-Catalyzed Heterocyclic Aryne Annulation: π-Extended Donors for TADF Emitters

Katie A. Spence,† Jason V. Chari,† Mattia Di Niro, Robert B. Susick, Narcisse Ukwitegetse, Peter I. Djurovich, Mark E. Thompson, and Neil K. Garg.

Chem. Sci. **2022**, *13*, 5884–5892.

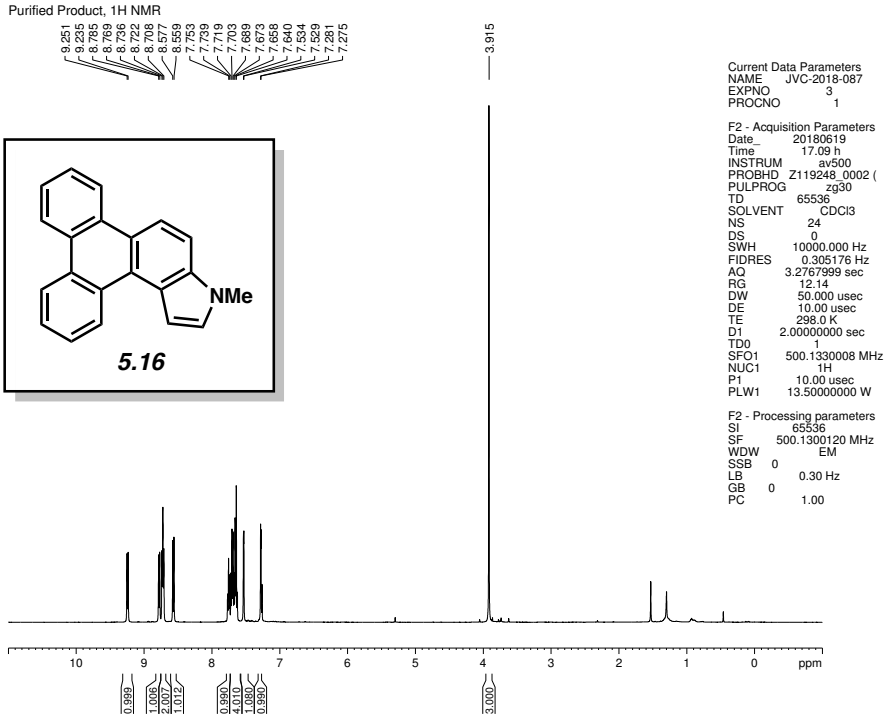

Figure 5.18 ^{1}H NMR (500 MHz, $CDCl_3$) of compound **5.16**.

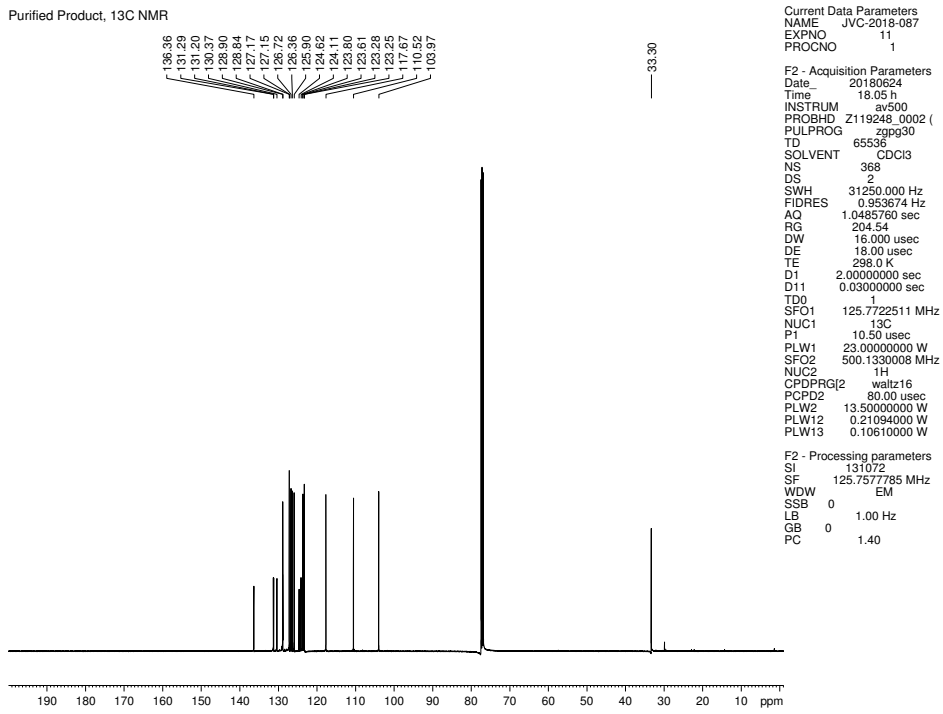

Figure 5.19 ^{13}C NMR (125 MHz, $CDCl_3$) of compound **5.16**.

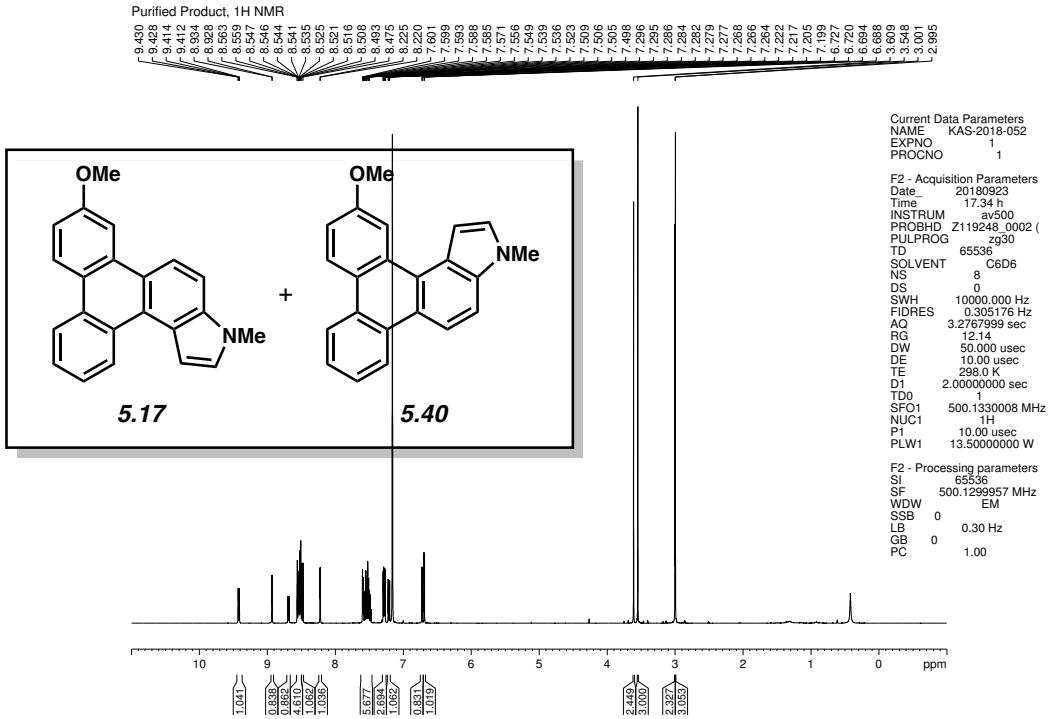

Figure 5.20 ^{1}H NMR (500 MHz, C_6D_6) of compounds **5.17** and **5.40**.

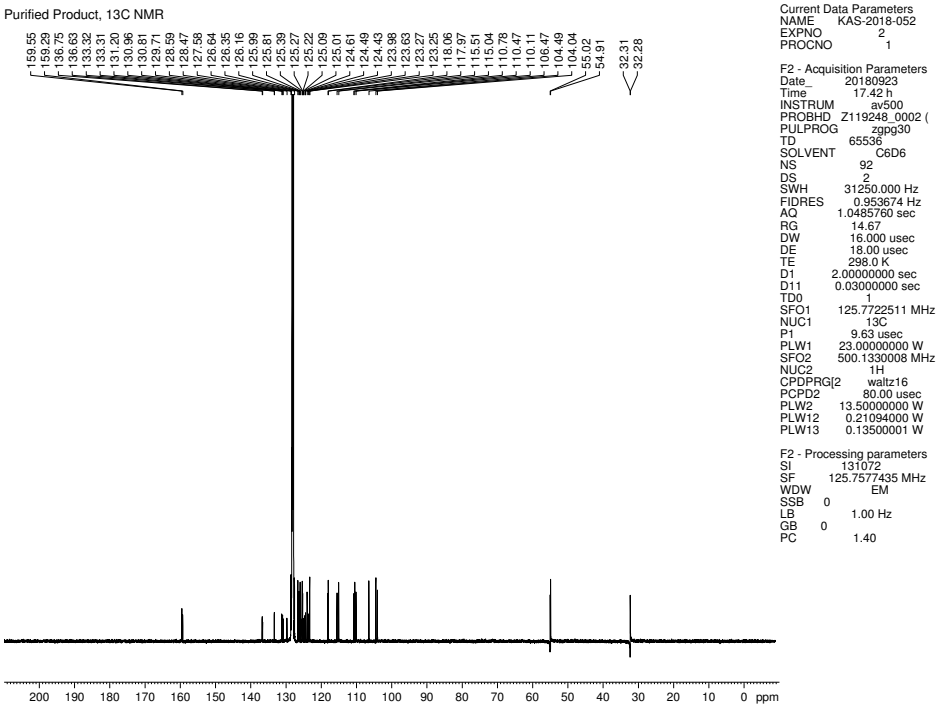

Figure 5.21 ^{13}C NMR (125 MHz, C_6D_6) of compounds **5.17** and **5.40**.

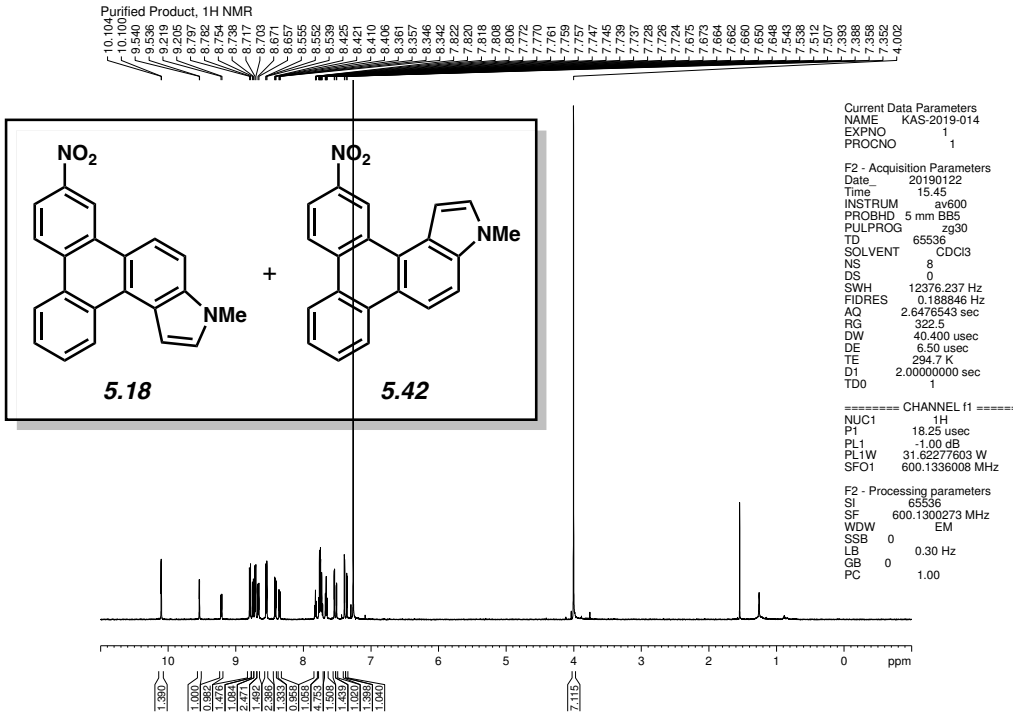

Figure 5.22 ^{1}H NMR (600 MHz, $CDCl_3$) of compounds **5.18** and **5.42**.

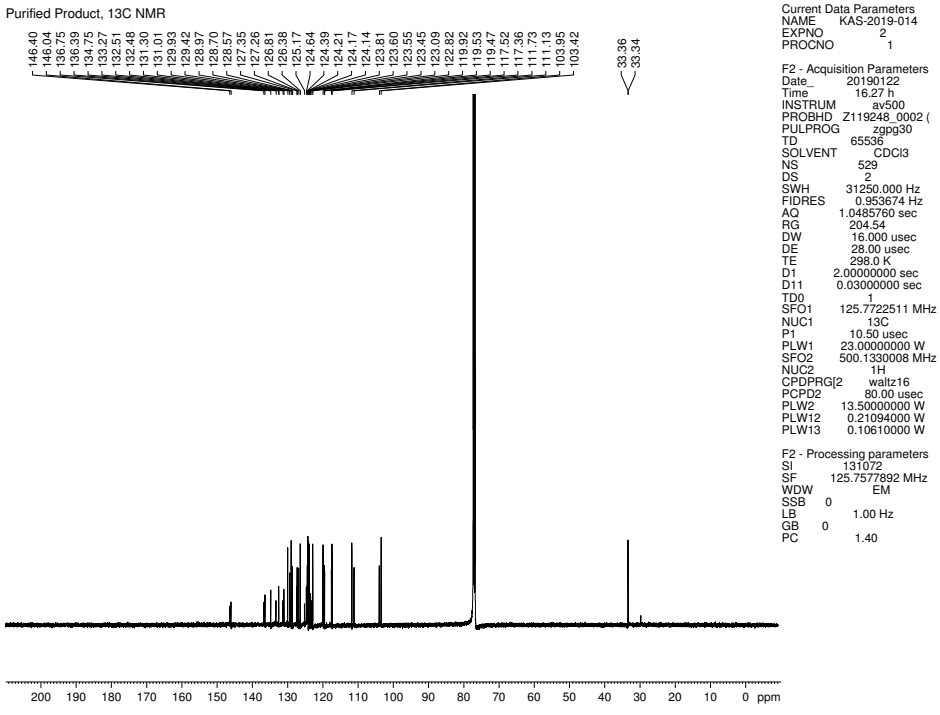

Figure 5.23 ^{13}C NMR (125 MHz, $CDCl_3$) of compounds **5.18** and **5.42**.

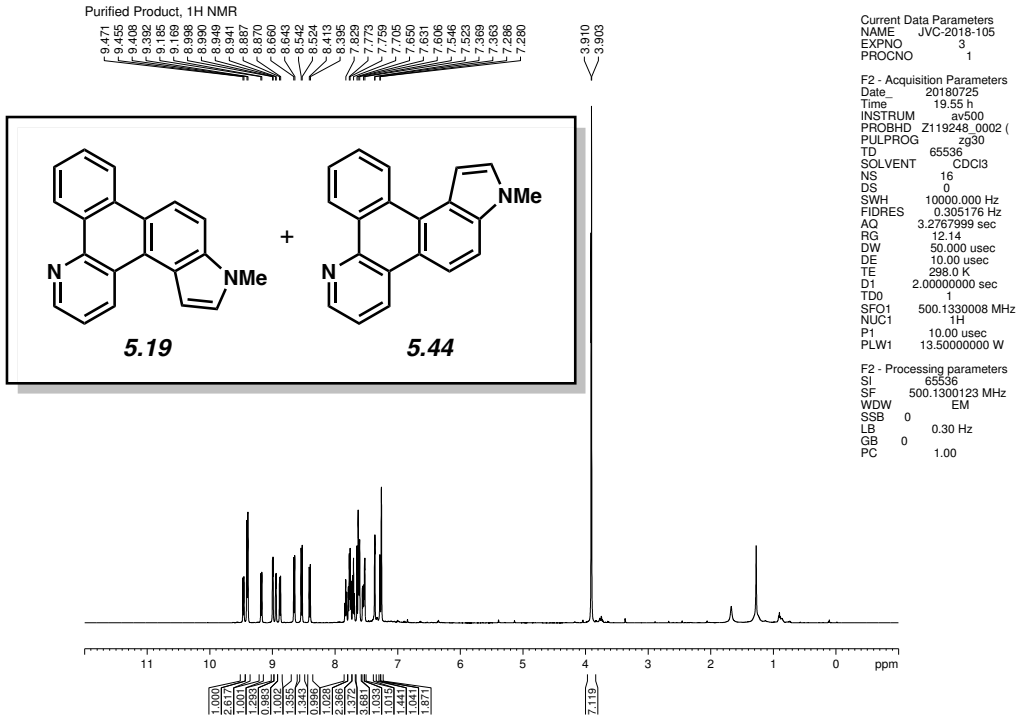

Figure 5.24 ^{1}H NMR (500 MHz, $CDCl_3$) of compounds **5.19** and **5.44**.

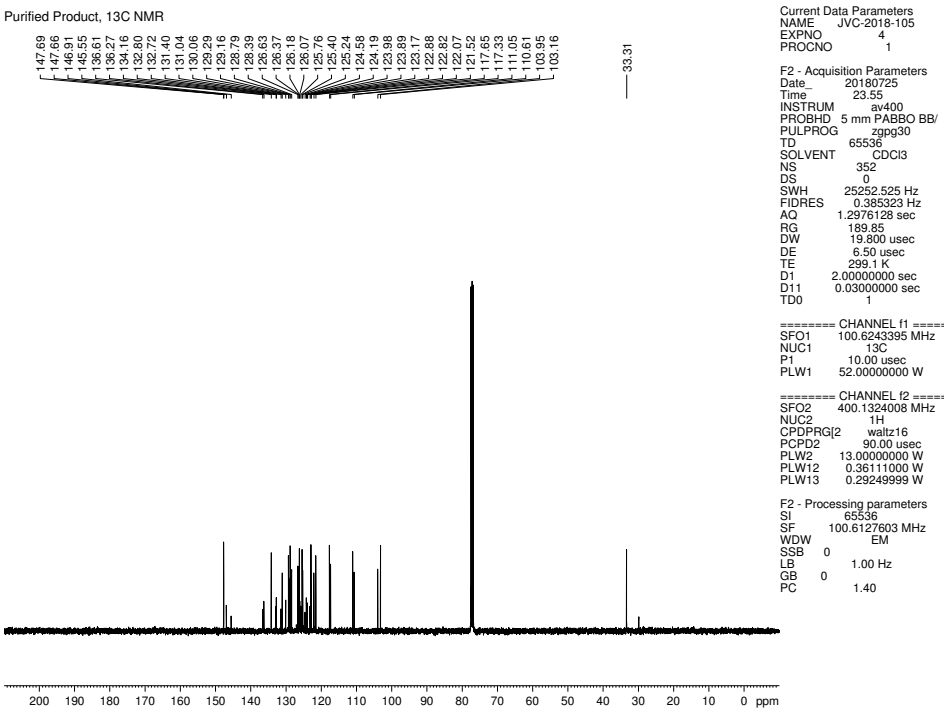

Figure 5.25 ^{13}C NMR (100 MHz, $CDCl_3$) of compounds **5.19** and **5.44**.

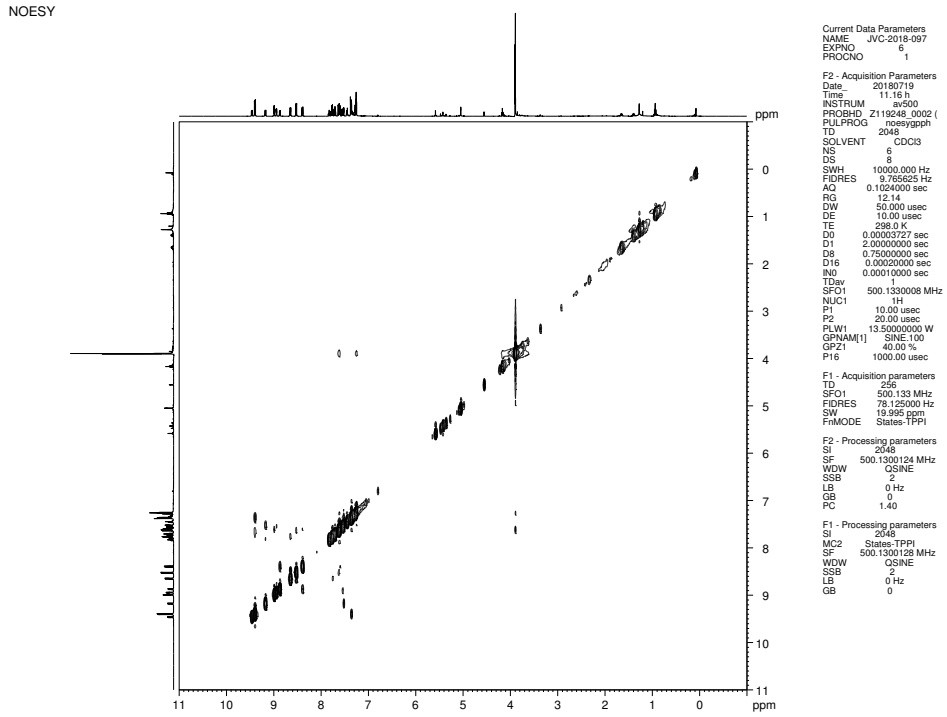

Figure 5.26 NOESY NMR (500 MHz, $CDCl_3$) of compounds **5.19** and **5.44**.

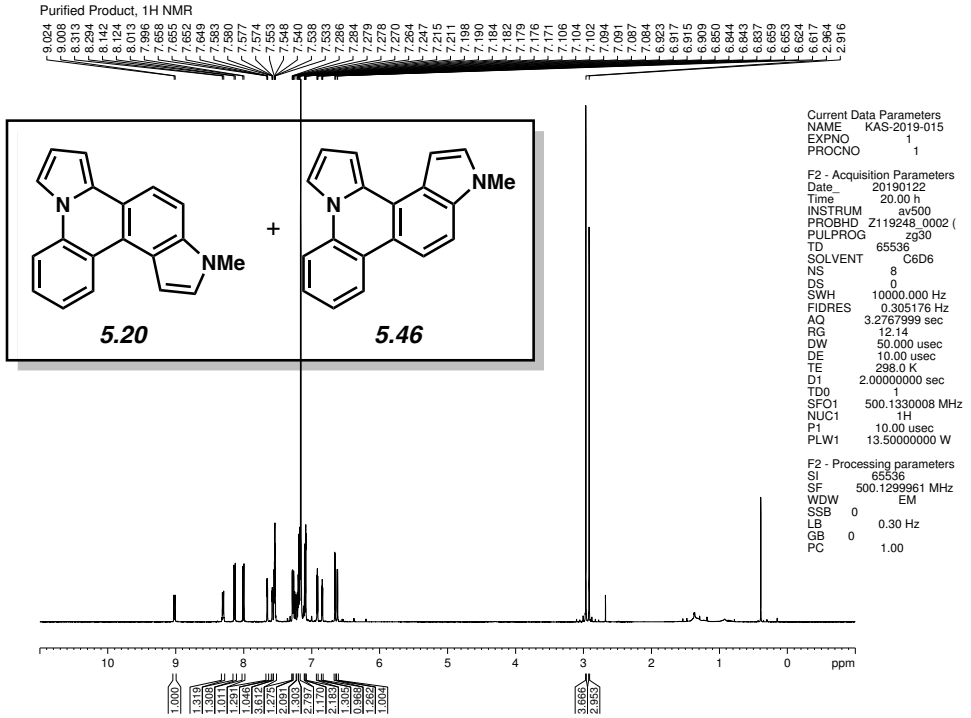

Figure 5.27 ^{1}H NMR (500 MHz, C_6D_6) of compounds **5.20** and **5.46**.

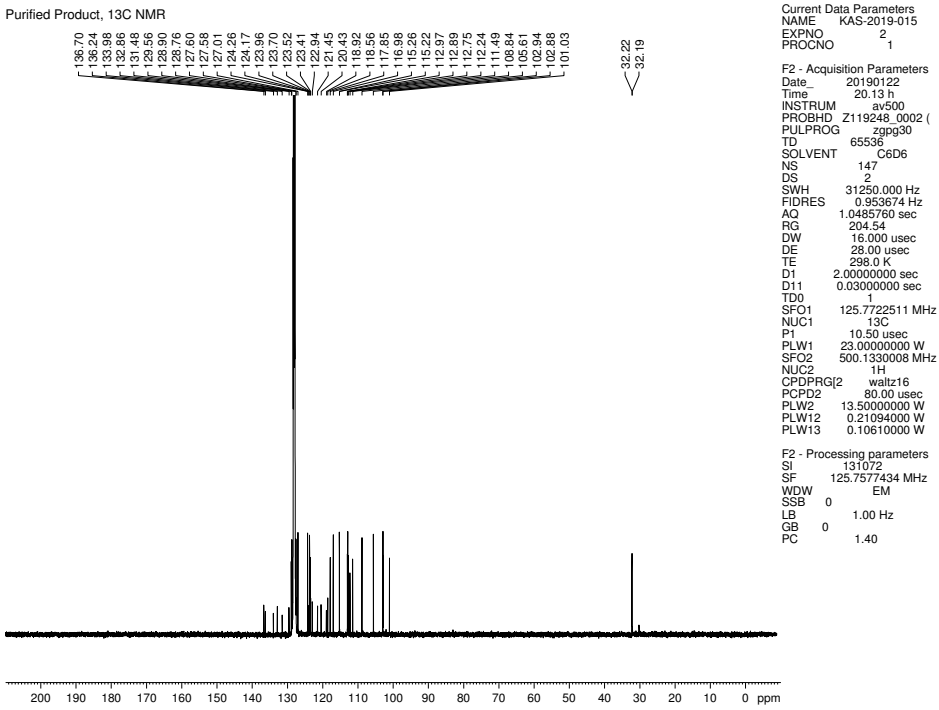

Figure 5.28 ^{13}C NMR (125 MHz, C_6D_6) of compounds **5.20** and **5.46**.

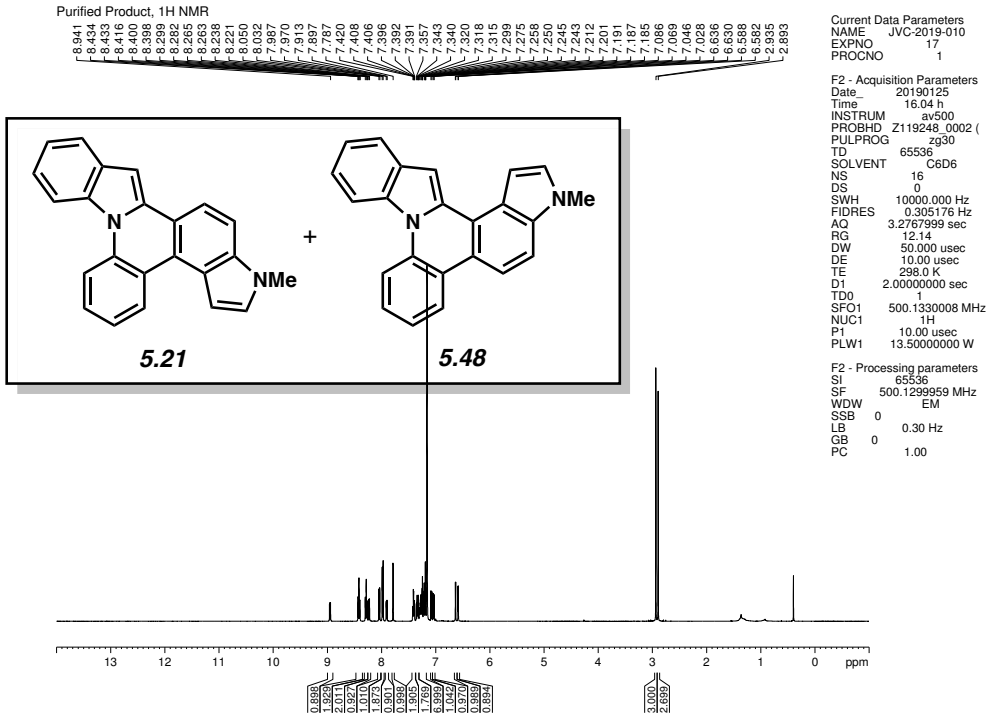

Figure 5.29 ^{1}H NMR (500 MHz, C_6D_6) of compounds **5.21** and **5.48**.

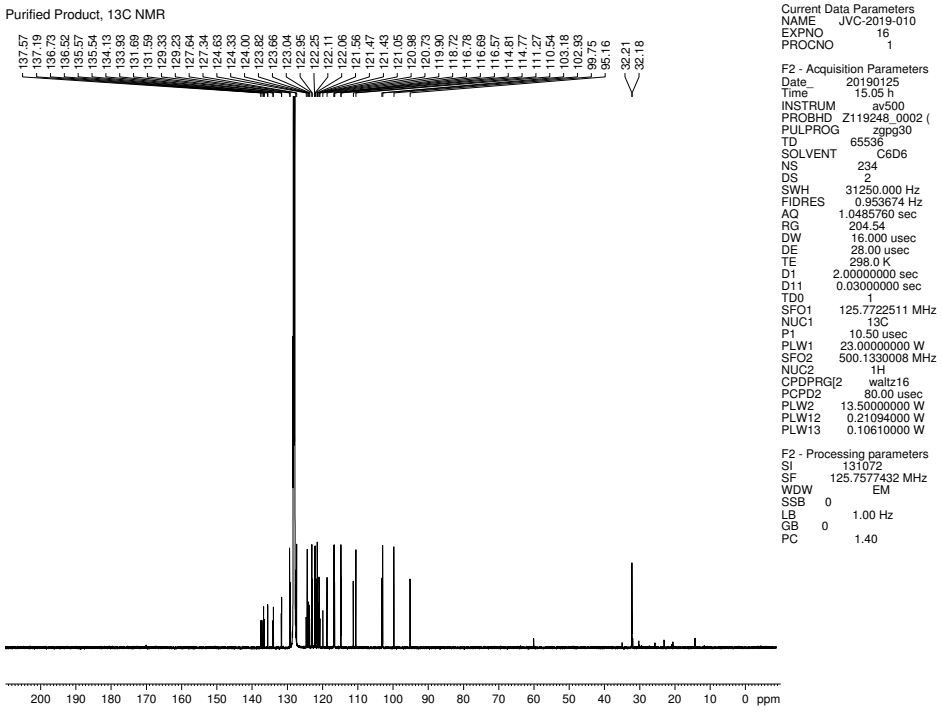

Figure 5.30 ^{13}C NMR (125 MHz, C_6D_6) of compounds **5.21** and **5.48**.

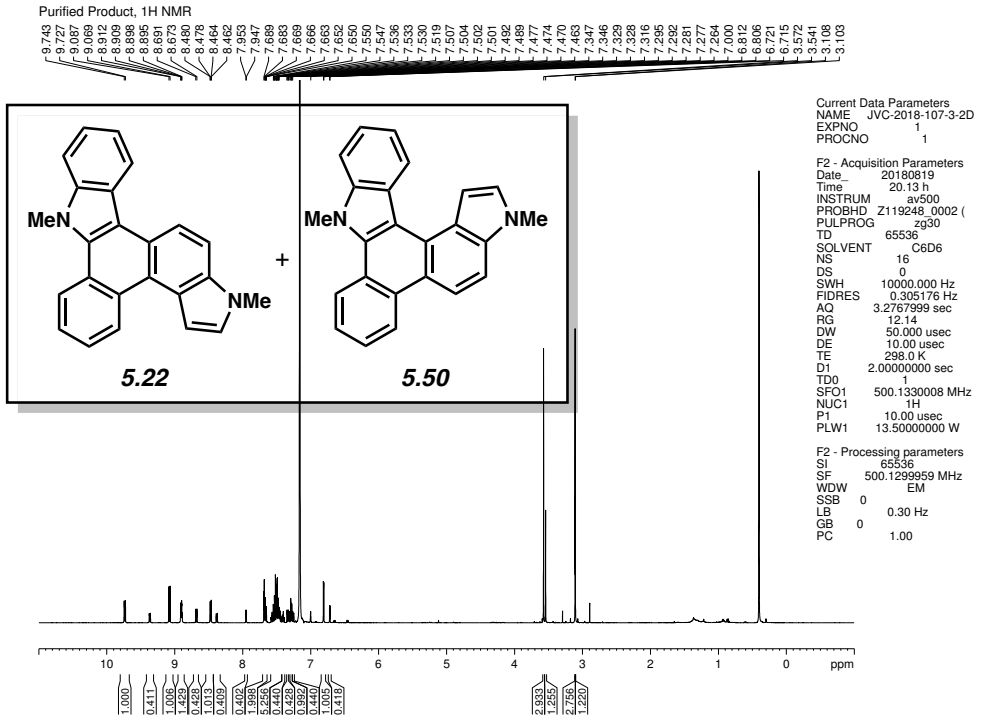

Figure 5.31 ^{1}H NMR (500 MHz, C_6D_6) of compounds **5.22** and **5.50**.

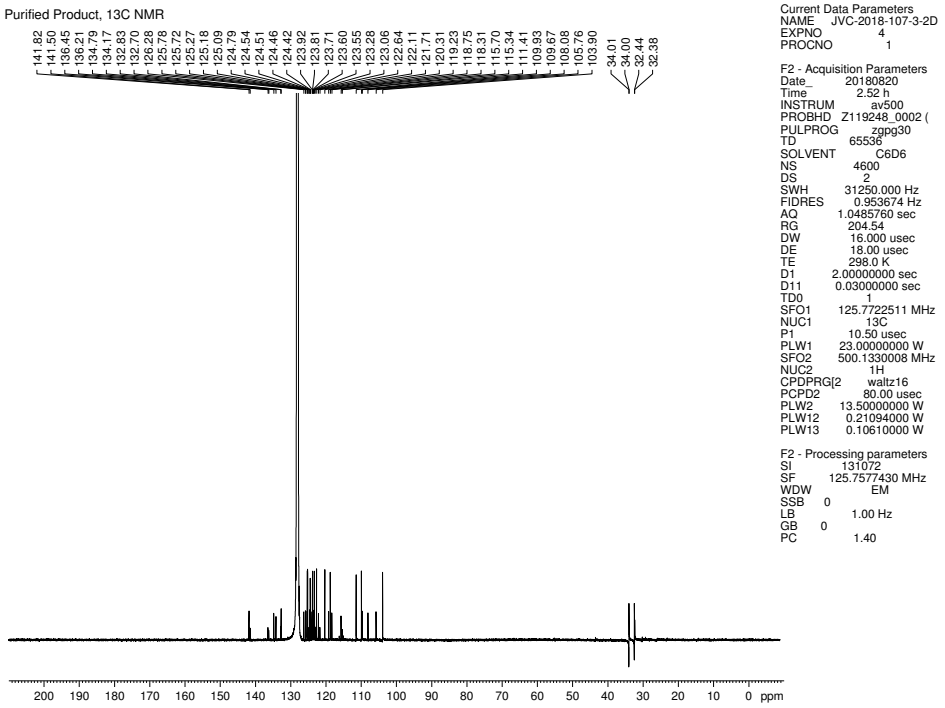

Figure 5.32 ^{13}C NMR (125 MHz, C_6D_6) of compounds **5.22** and **5.50**.

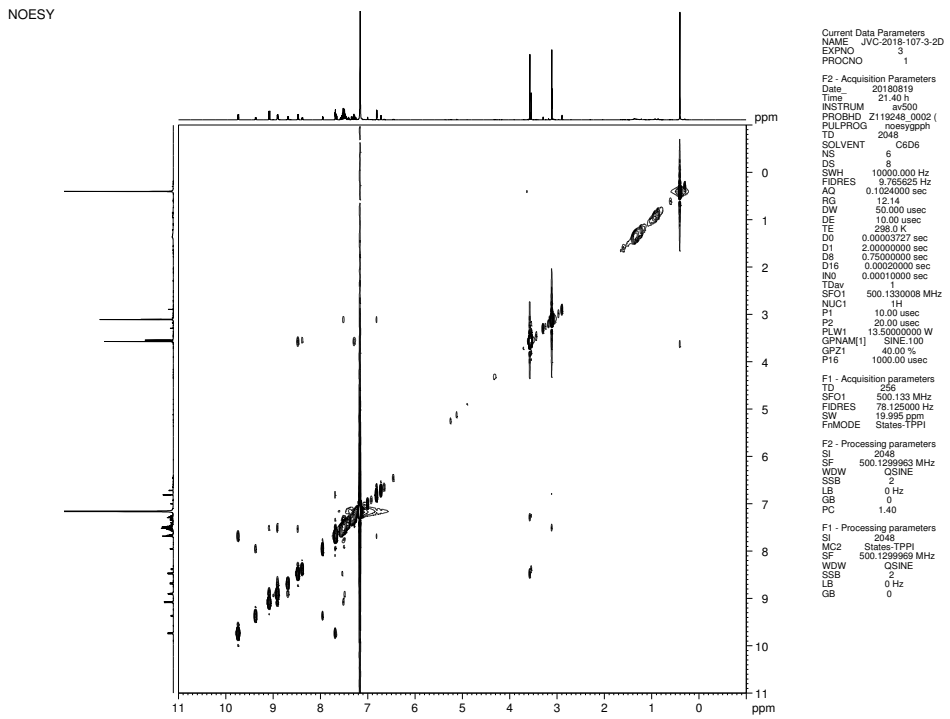

Figure 5.33 NOESY NMR (125 MHz, C_6D_6) of compounds **5.22** and **5.50**.

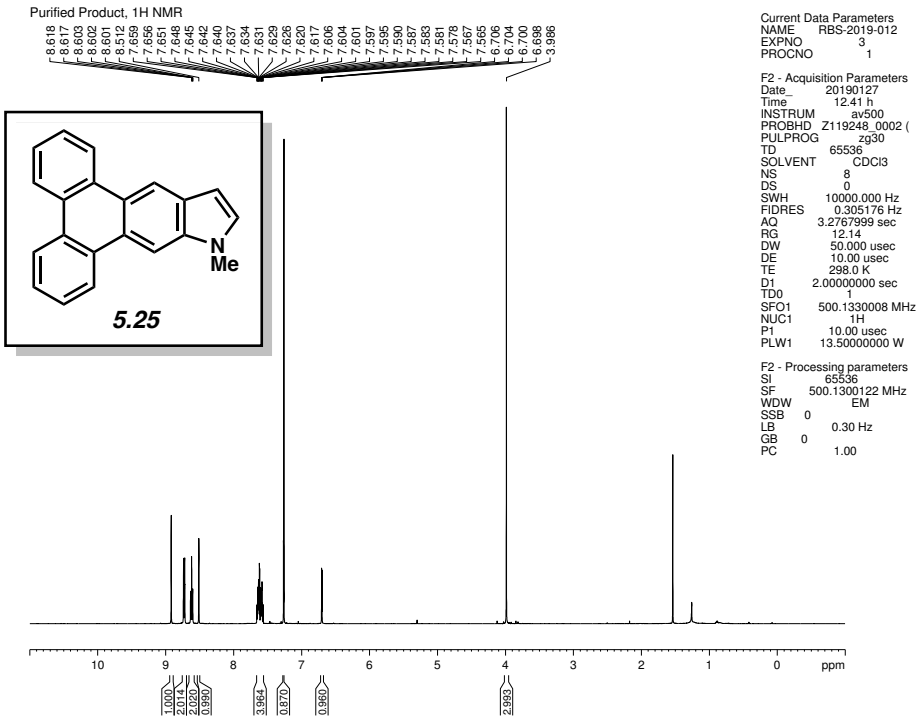

Figure 5.34 ^{1}H NMR (500 MHz, $CDCl_3$) of compound **5.25**.

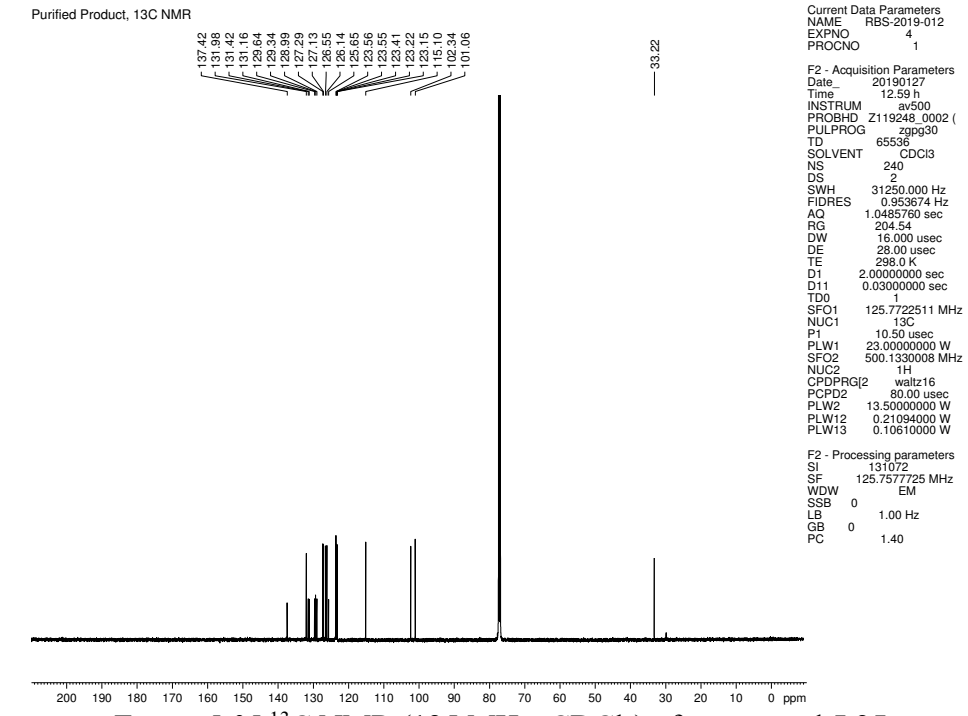

Figure 5.35 ^{13}C NMR (125 MHz, $CDCl_3$) of compound **5.25**.

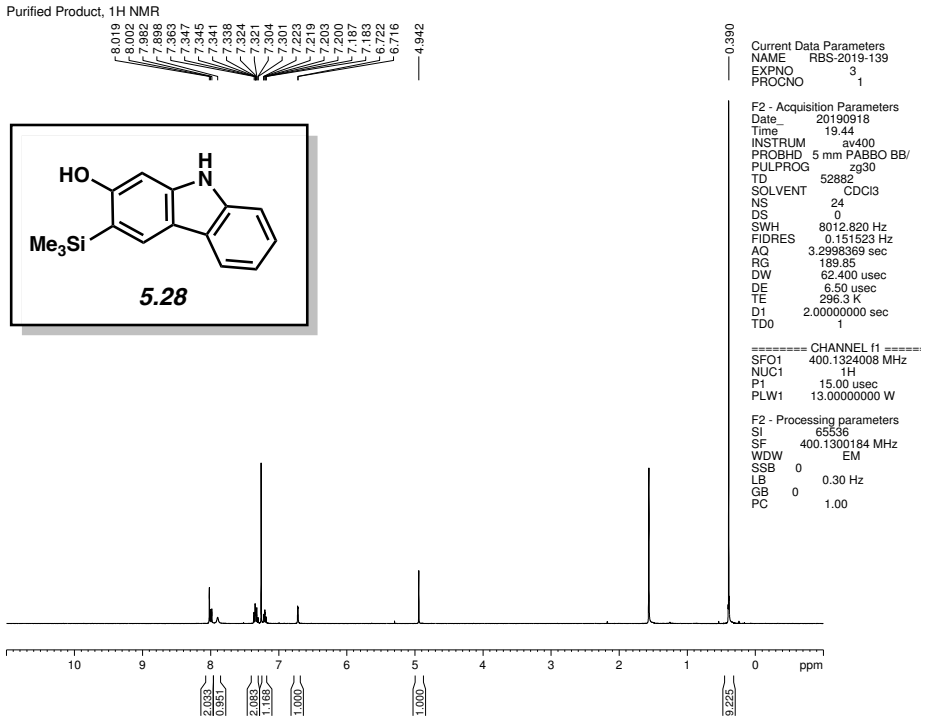

Figure 5.36 ^{1}H NMR (400 MHz, $CDCl_3$) of compound **5.28**.

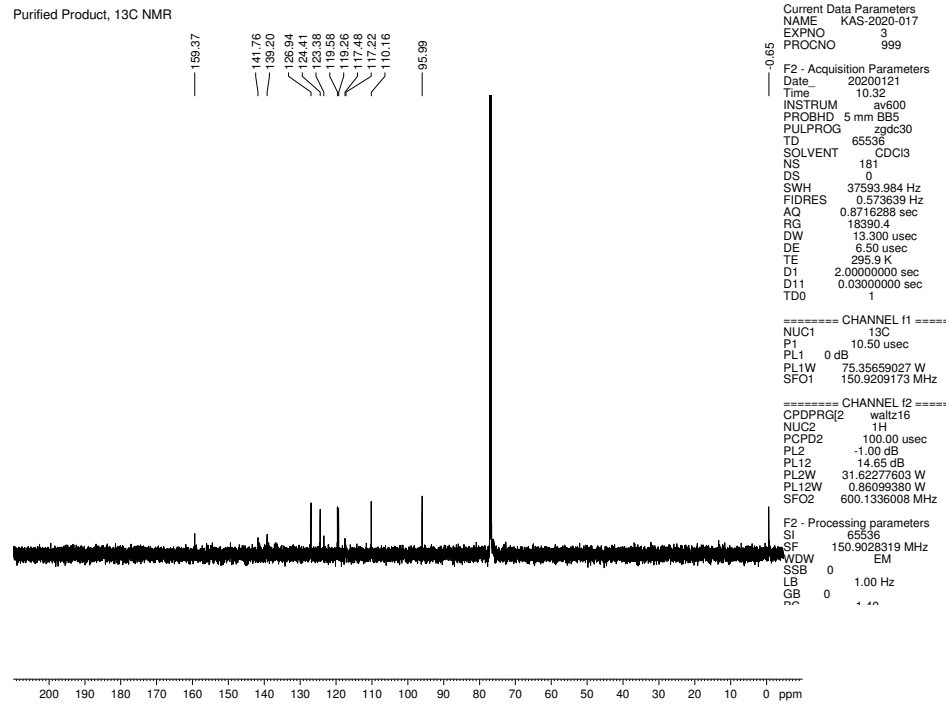

Figure 5.37 ^{13}C NMR (150 MHz, $CDCl_3$) of compound **5.28**.

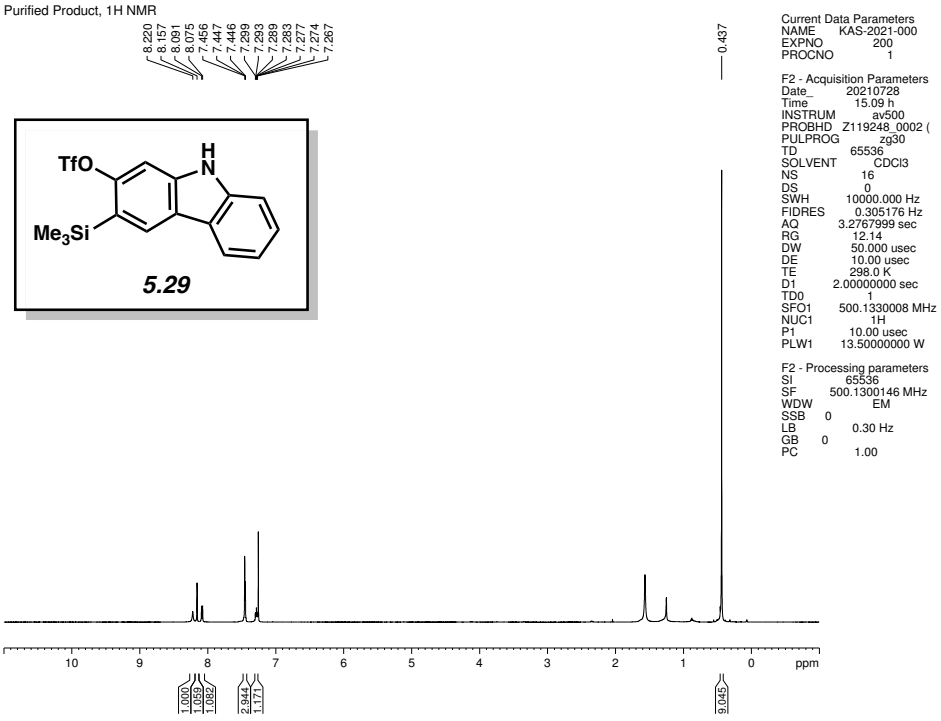

Figure 5.38 ^{1}H NMR (400 MHz, $CDCl_3$) of compound **5.29**.

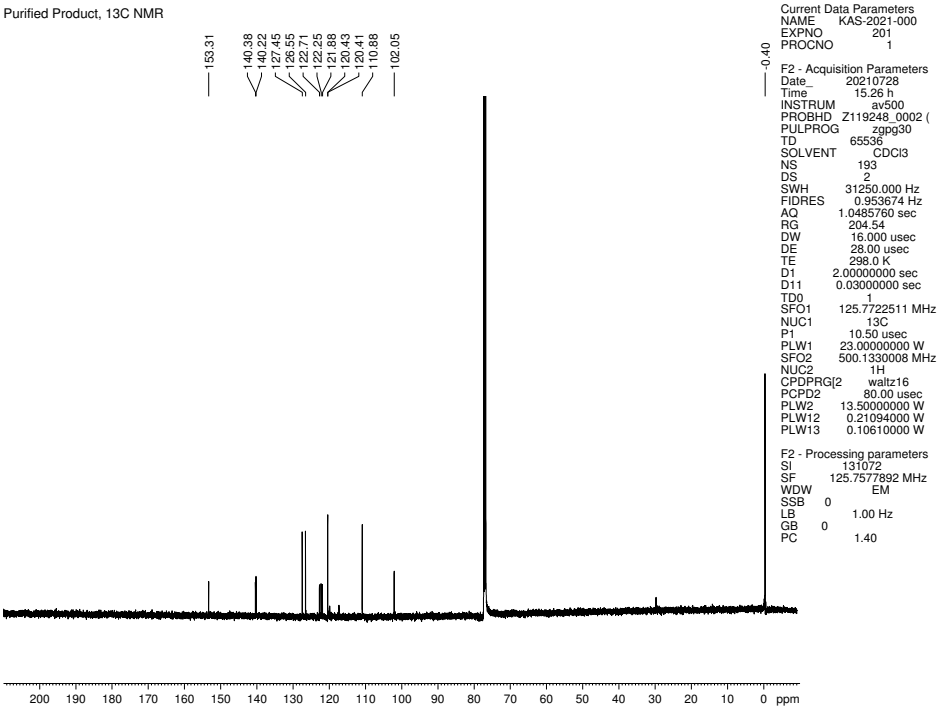

Figure 5.39 ^{13}C NMR (125 MHz, $CDCl_3$) of compound **5.29**.

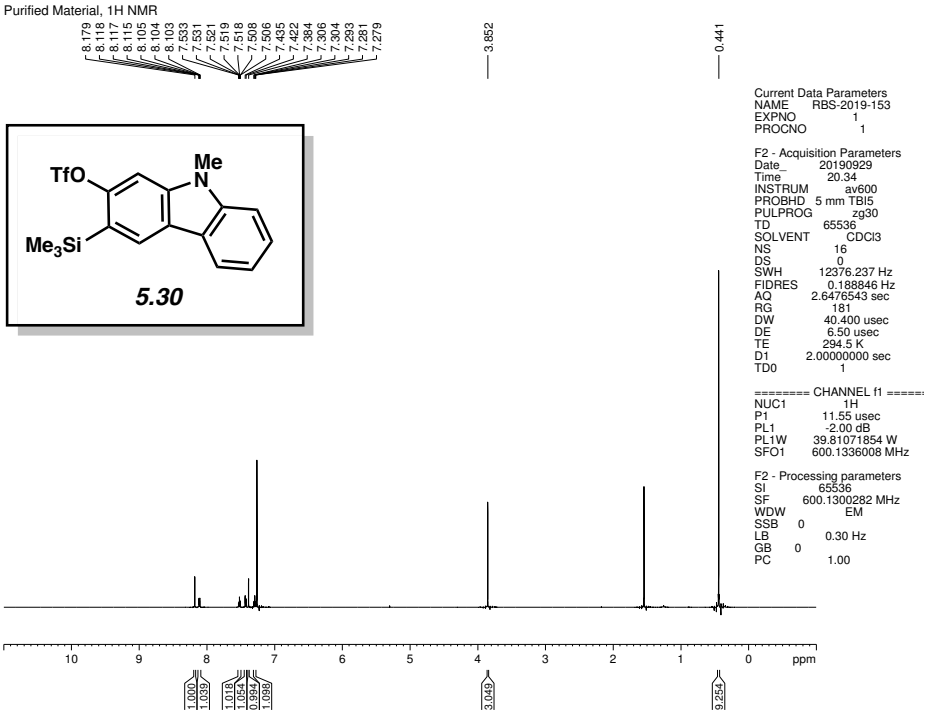

Figure 5.40 ^{1}H NMR (600 MHz, $CDCl_3$) of compound **5.30**.

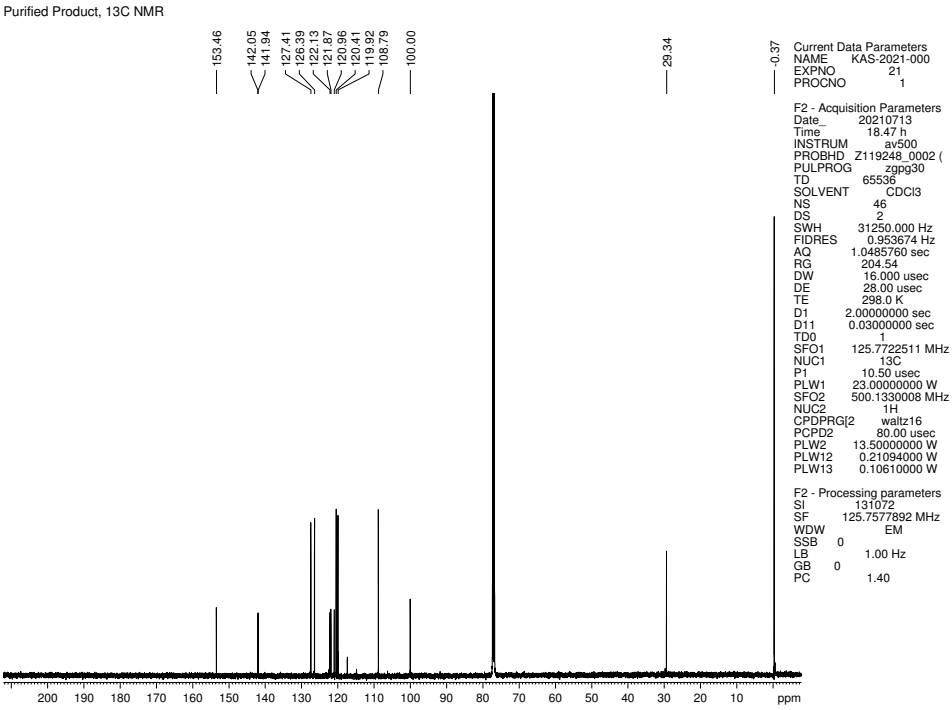

Figure 5.41 ^{13}C NMR (125 MHz, $CDCl_3$) of compound **5.30**.

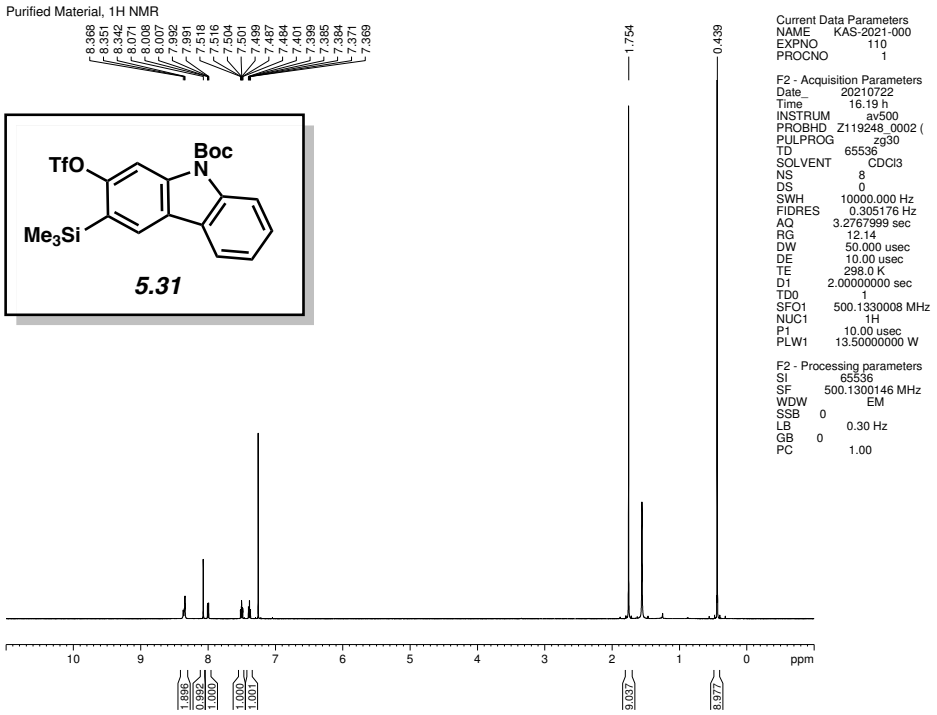

Figure 5.42 ^{1}H NMR (500 MHz, $CDCl_3$) of compound **5.31**.

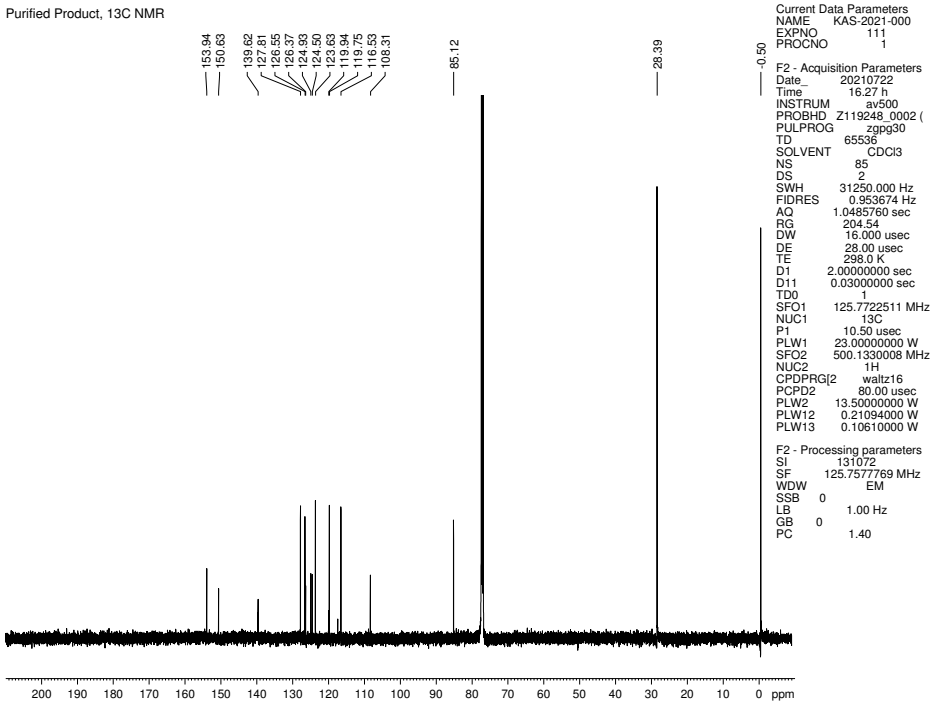

Figure 5.43 ^{13}C NMR (125 MHz, $CDCl_3$) of compound **5.31**.

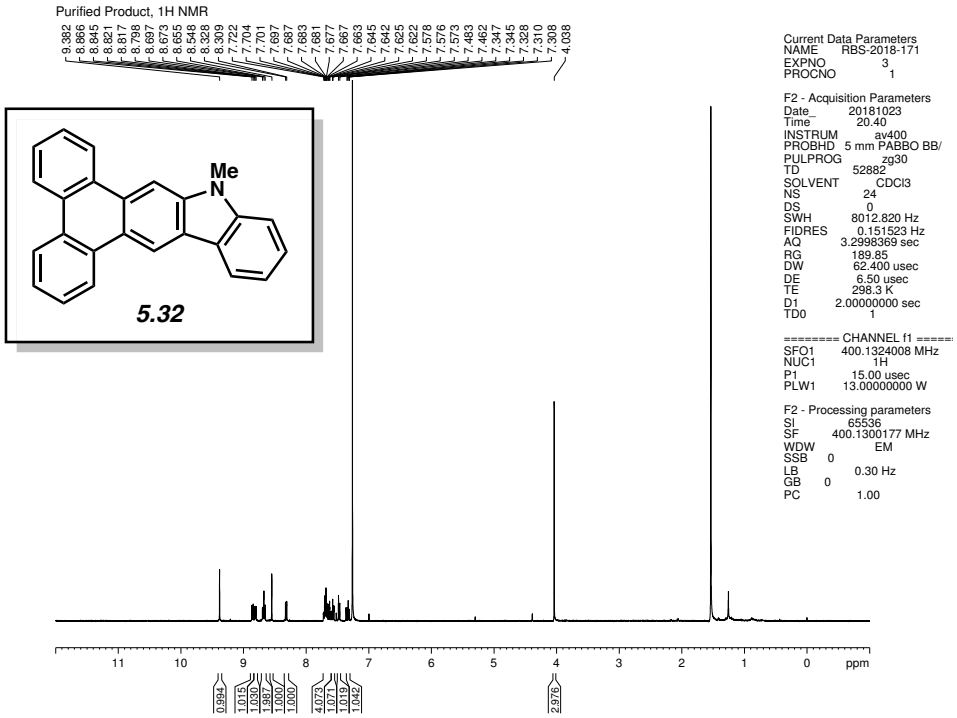

Figure 5.44 ^{1}H NMR (400 MHz, $CDCl_3$) of compound **5.32**.

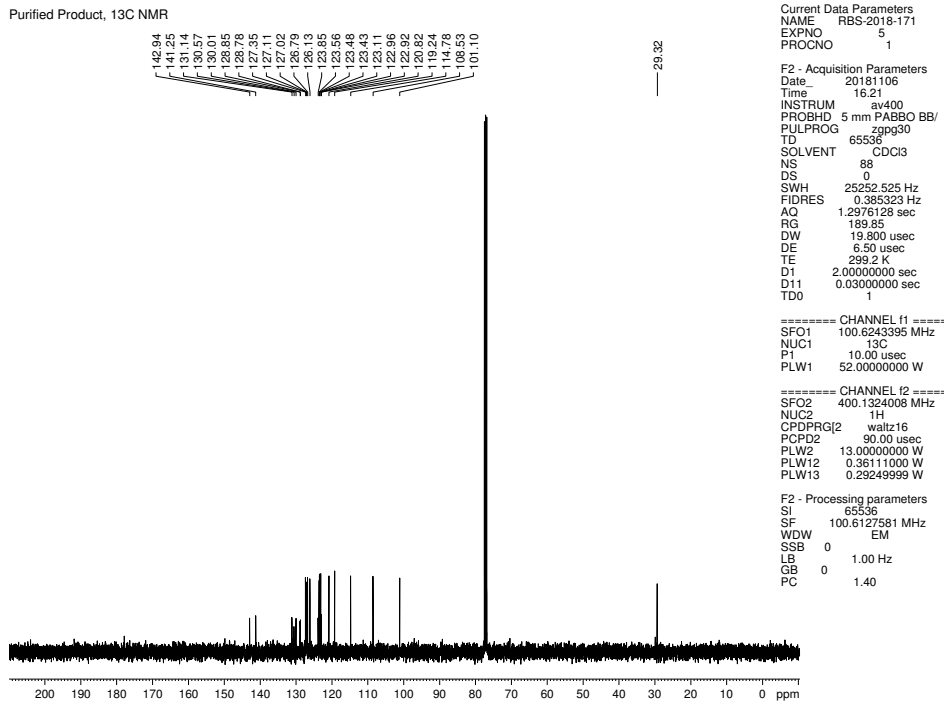

Figure 5.45 ^{13}C NMR (100 MHz, $CDCl_3$) of compound **5.32**.

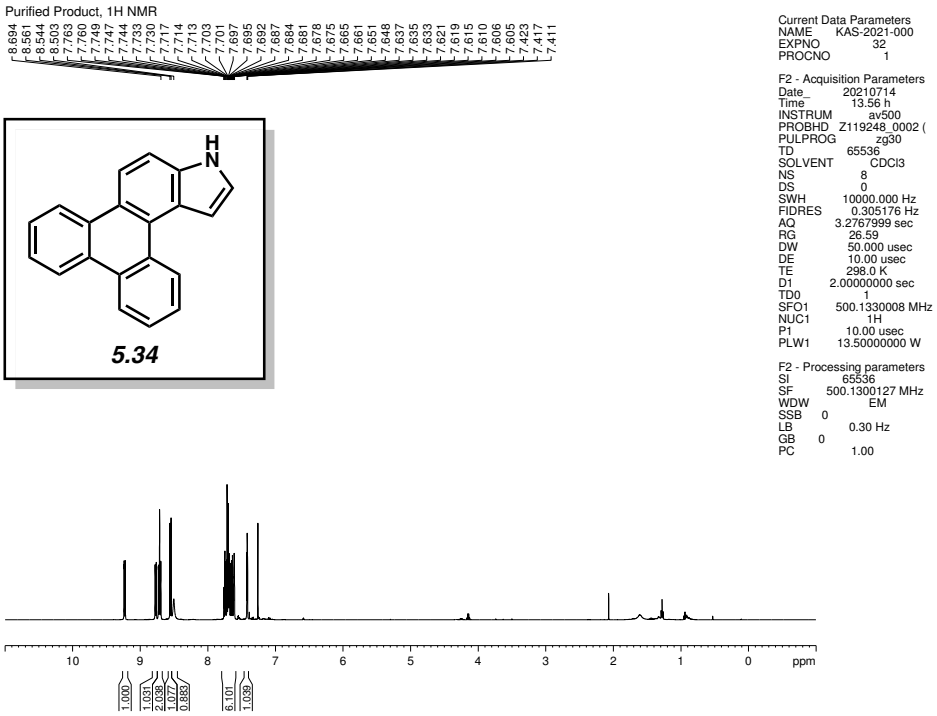

Figure 5.46 ^{1}H NMR (500 MHz, $CDCl_3$) of compound **5.34**.

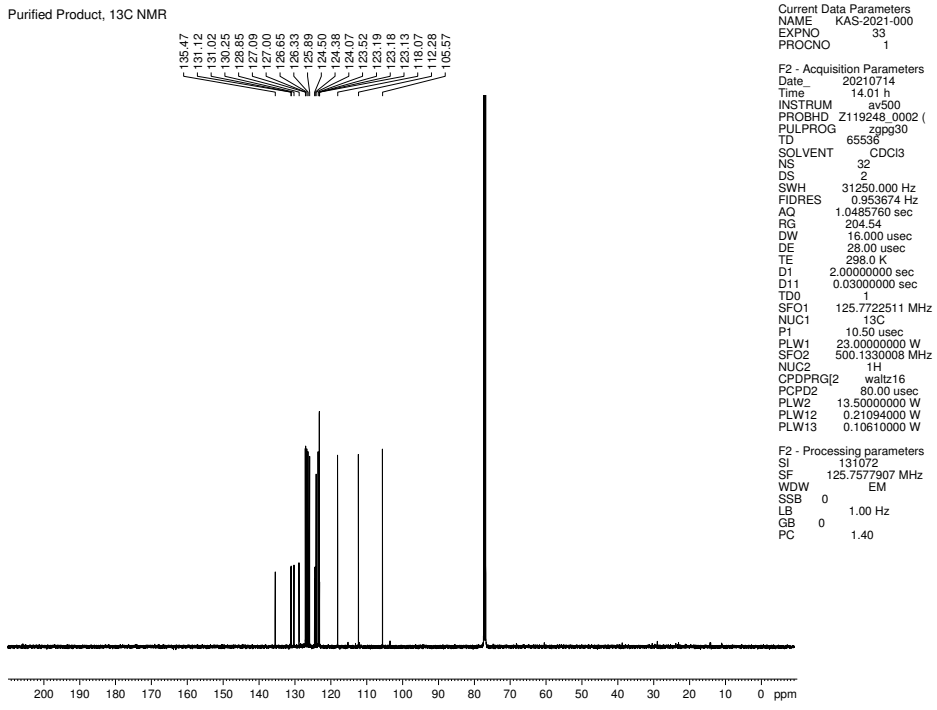

Figure 5.47 ^{13}C NMR (125 MHz, $CDCl_3$) of compound **5.34**.

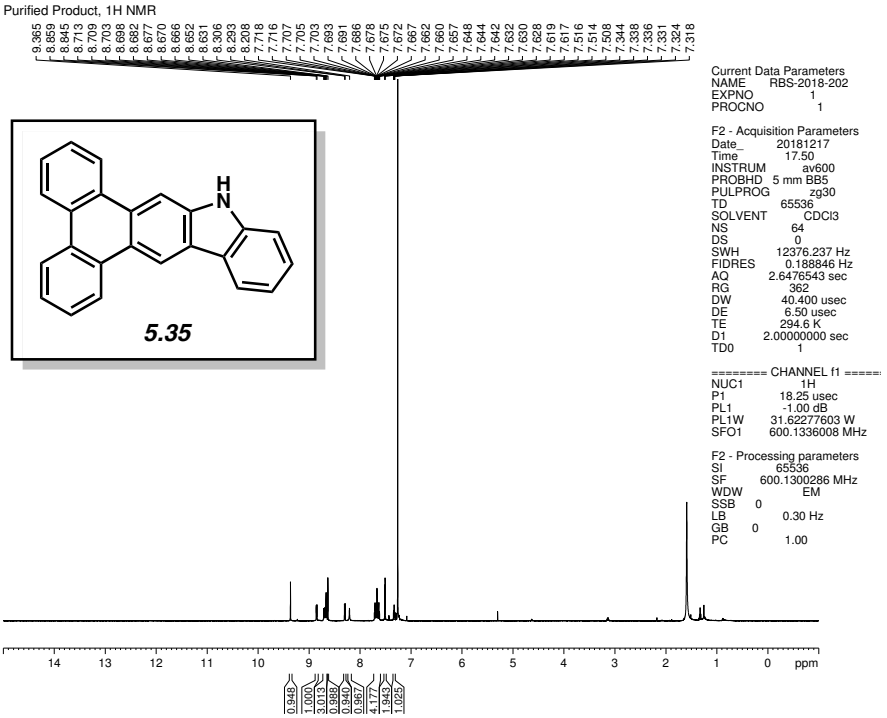

Figure 5.48 ^{1}H NMR (600 MHz, $CDCl_3$) of compound **5.35**.

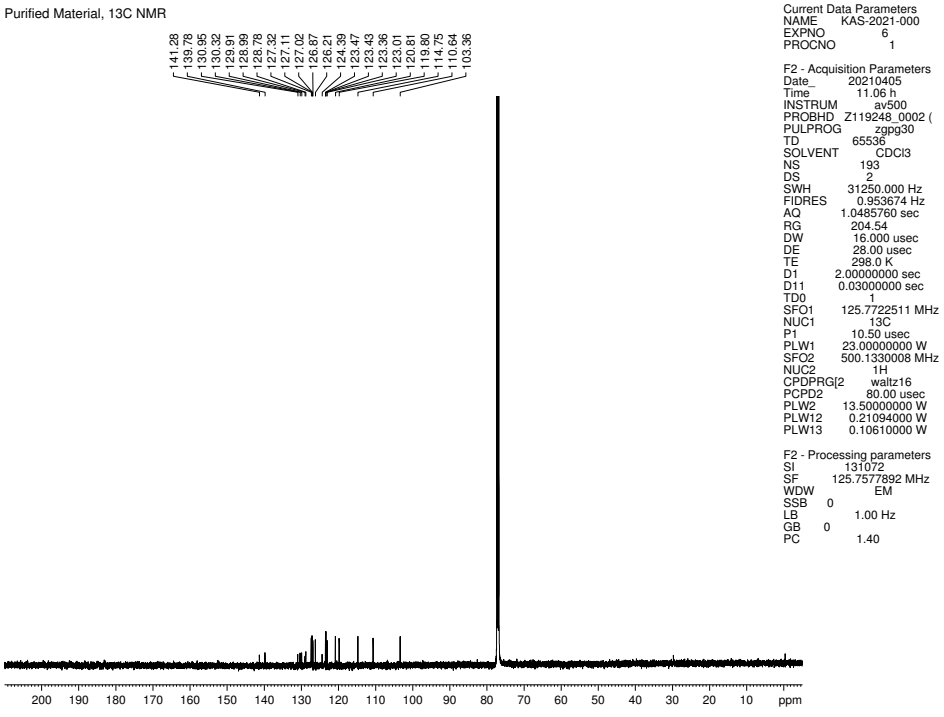

Figure 5.49 ^{13}C NMR (125 MHz, $CDCl_3$) of compound **5.35**.

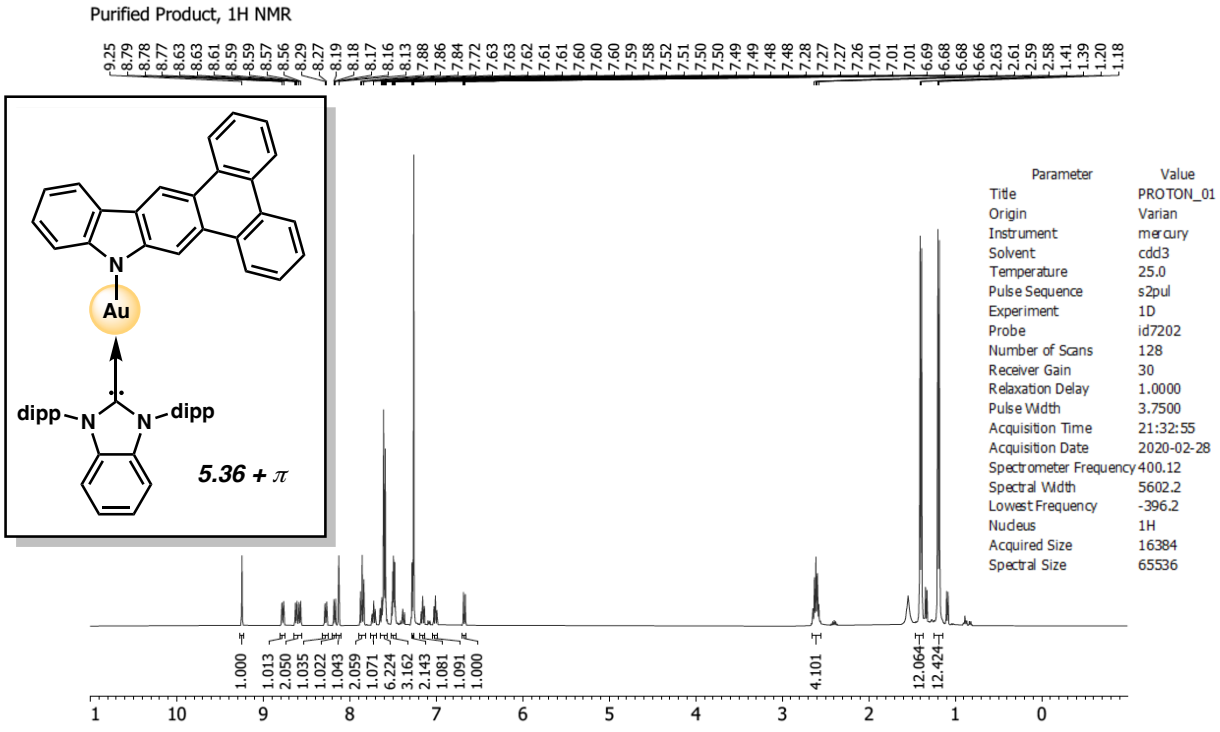

Figure 5.50 ^{1}H NMR (400 MHz, $CDCl_3$) of compound **5.36+π**.

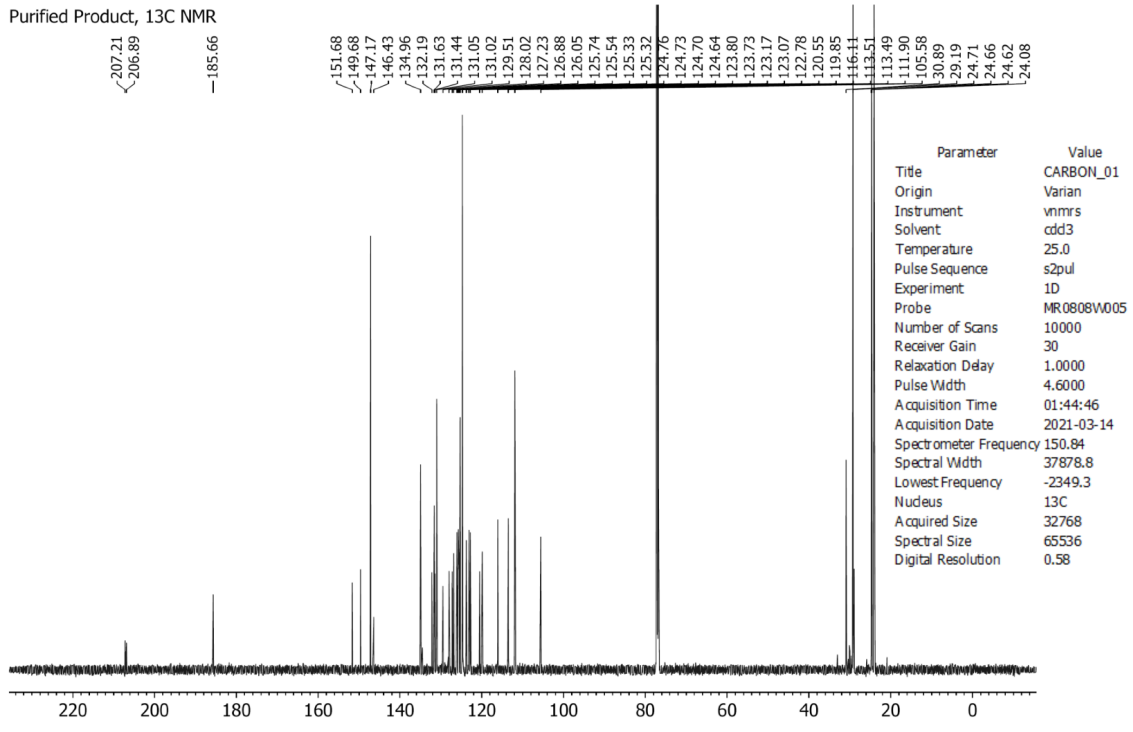

Figure 5.51 ^{13}C NMR (150 MHz, $CDCl_3$) of compound **5.36+π**.

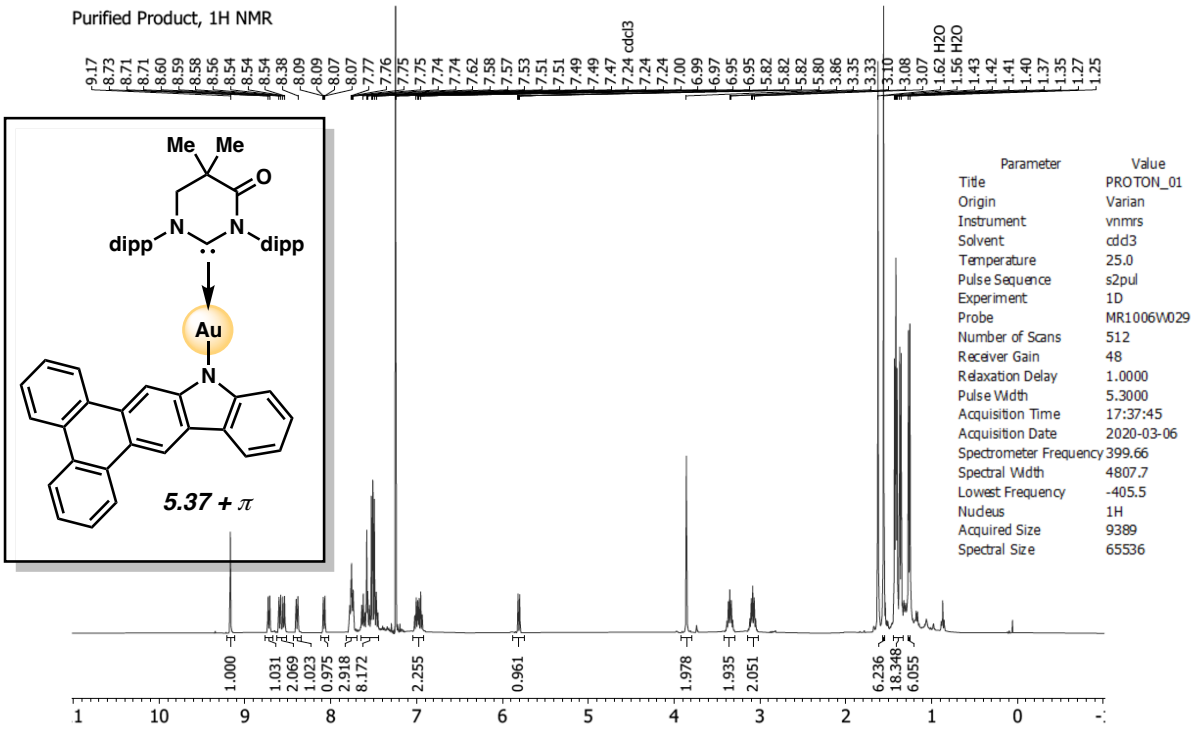

Figure 5.52 ^{1}H NMR (400 MHz, $CDCl_3$) of compound **5.37+π**.

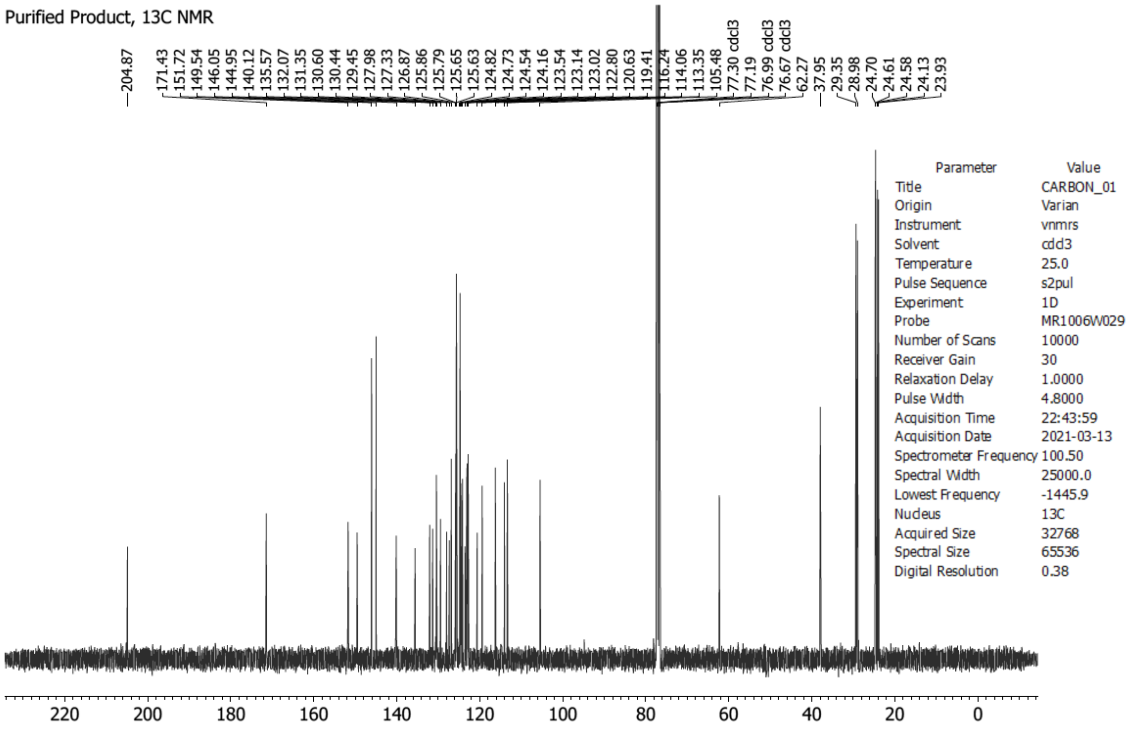

Figure 5.53 ^{13}C NMR (100 MHz, $CDCl_3$) of compound **5.37+π**.

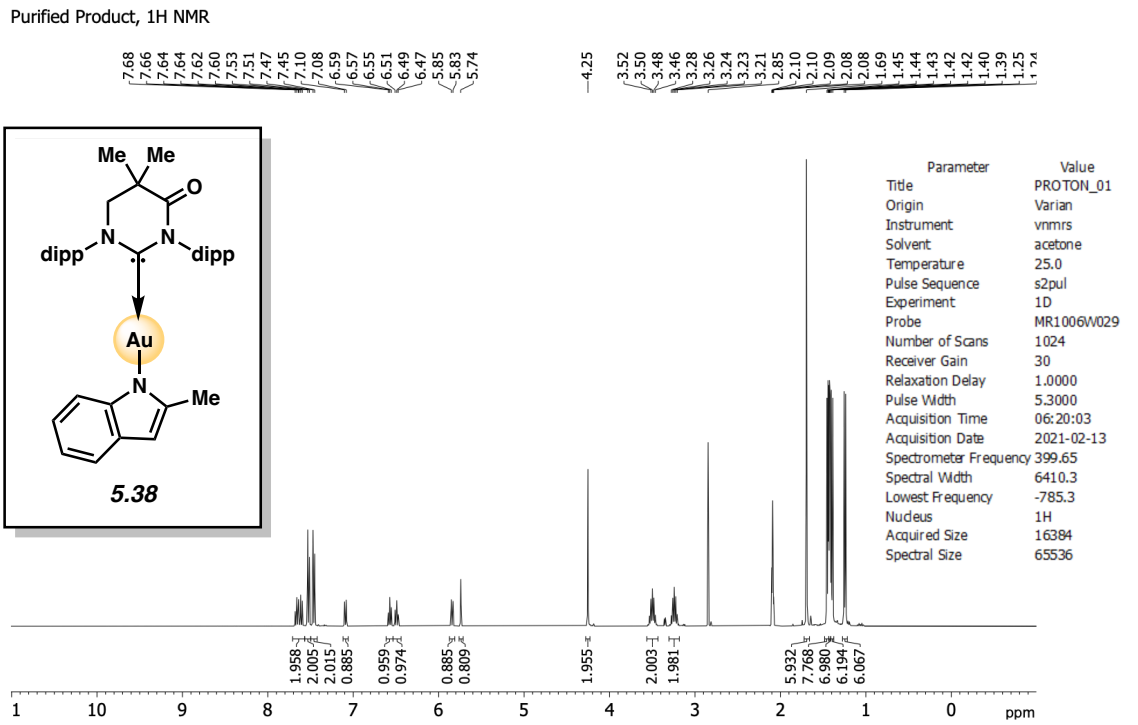

Figure 5.54 ^{1}H NMR (400 MHz, acetone-d_6) of compound **5.38**.

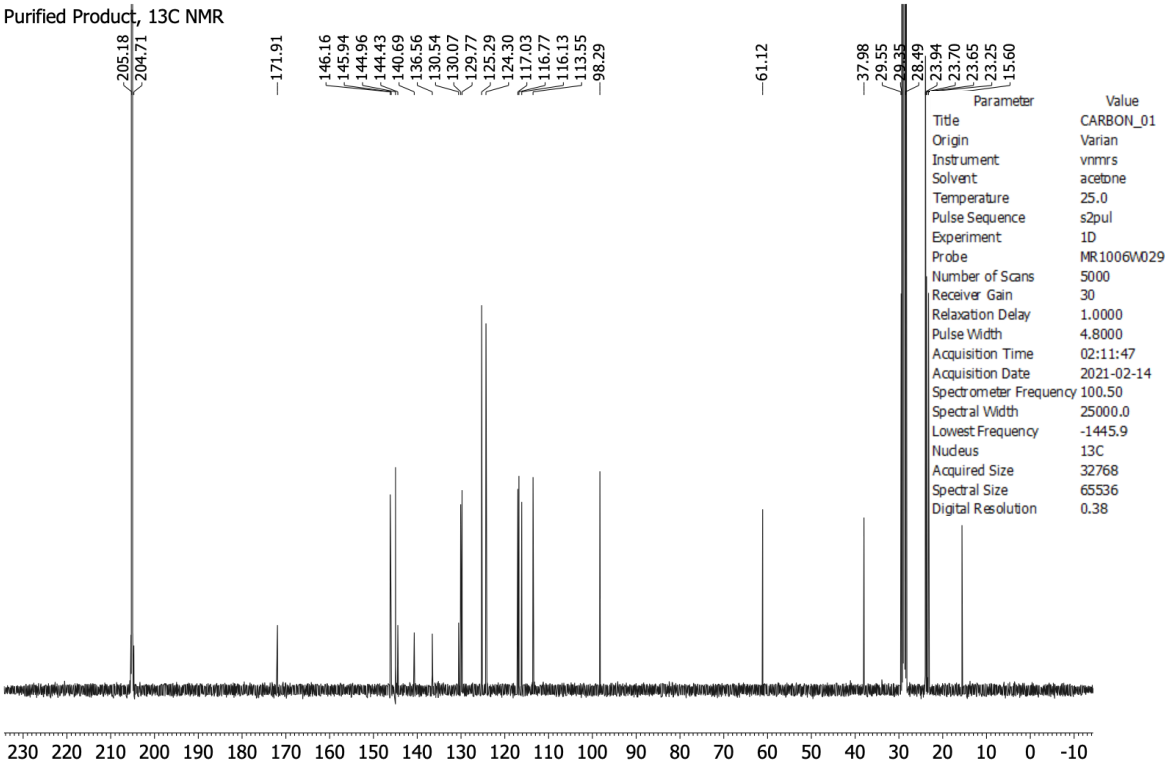

Figure 5.55 ^{13}C NMR (100 MHz, acetone-d_6) of compound **5.38**.

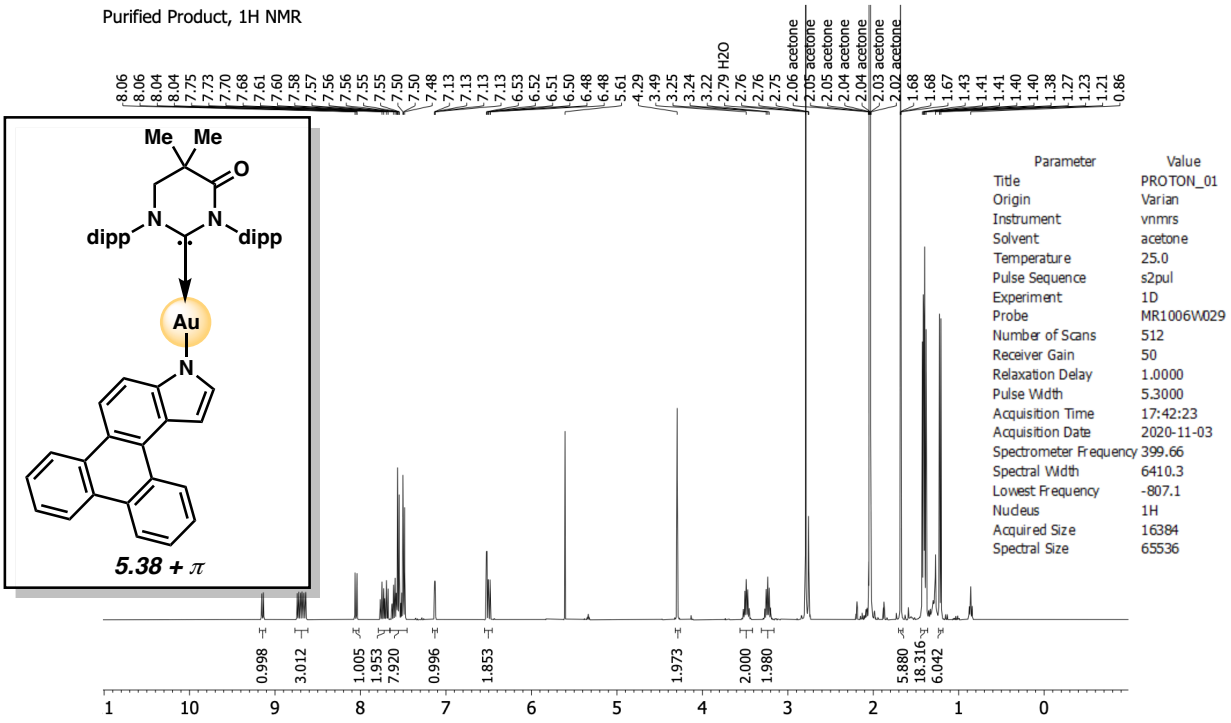

Figure 5.56 ^{1}H NMR (400 MHz, acetone-d_6) of compound **5.38+π**.

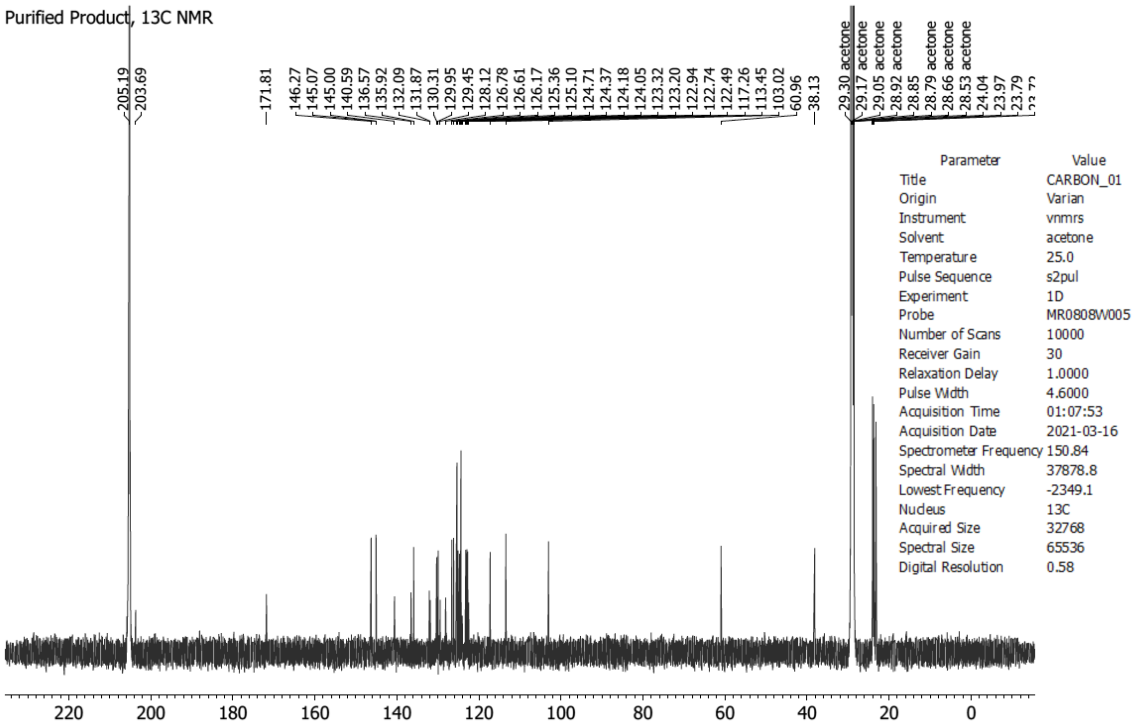

Figure 5.57 ^{13}C NMR (150 MHz, acetone-d_6) of compound **5.38+π**.

5.9 Notes and References

(1) Keyte, I. J.; Harrison, R. M.; Lammel, G. Chemical Reactivity and Long-Range Transport Potential of Polycyclic Aromatic Hydrocarbons – A Review. *Chem. Soc. Rev.* **2013**, *42*, 9333–9391.

(2) Park, K. S.; Salunkhe, S. M.; Lim, I.; Cho, C.-G.; Han, S. H.; Sung, M. High-Performance Air-Stable Single-Crystal Organic Nanowires Based on a New Indolocarbazole Derivative for Field-Effect Transistors. *Adv. Mater.* **2013**, *25*, 3351–3356.

(3) Ji, Z.; Layek, S.; Ma, B. *US Pat.*, 0315759 A1, 2019.

(4) Lee, J.; Park, J. Synthesis and Electroluminescence of Novel Pyrene-Fused Chromophores. *Org. Lett.* **2015**, *17*, 3960–3963.

(5) Wang, Y.; Zhang, Y.-M.; Zhang, S. X.-A. Stimuli-Induced Reversible Proton Transfer for Stimuli-Responsive Materials and Devices. *Acc. Chem. Res.* **2021**, *54*, 2216–2226.

(6) Traditional synthetic approaches to heterocyclic PAH scaffolds rely on sequential C–C bond formation. For a review of recent advances, see: Ito, H.; Ozaki, K.; Itami, K. Annulative π-Extension (APEX): Rapid Access to Fused Arenes, Heteroarenes, and Nanographenes. *Angew. Chem., Int. Ed.* **2017**, *56*, 11144–11164.

(7) Nakamura, Y.; Yoshida, S.; Hosoya, T. Recent advances in synthetic hetaryne chemistry. *Heterocycles* **2019**, *98*, 1623–1677.

(8) Pellissier, H.; Santelli, M. The use of arynes in organic synthesis. *Tetrahedron* **2003**, *59*, 701–730.

(9) Wenk, H. H.; Winkler, M.; Sander, W. One century of aryne chemistry. *Angew. Chem., Int. Ed.* **2003**, *42*, 502–528.

(10) Sanz, R. Recent applications of aryne chemistry to organic synthesis. A review. *Org. Prep. Proced. Int.* **2008**, *40*, 215–291.

(11) Perez, D.; Pena, D.; Guitian, E. Aryne Cycloaddition Reactions in the Synthesis of Large Polycyclic Aromatic Compounds. *Eur. J. Org. Chem.* **2013**, *27*, 5981–6013.

(12) Goetz, A. E.; Shah, T. K.; Garg, N. K. Pyridynes and indolynes as building blocks for functionalized heterocycles and natural products. *Chem. Commun.* **2015**, *51*, 34–45.

(13) Cheong, P. H.-Y.; Paton, R. S.; Bronner, S. M.; Im, G.-Y. J.; Garg, N. K.; Houk, K. N. Indolyne and Aryne Distortions and Nucleophilic Regioselectivities. *J. Am. Chem. Soc.* **2010**, *132,* 1267–1269.

(14) Lakhdar, S.; Westermaier, M.; Terrier, F.; Goumont, R.; Boubaker, T.; Ofial, A. R.; Mayr, H. Nucleophilic Reactivities of Indoles. *J. Org. Chem.* **2006**, *71*, 9088–9095.

(15) Loudon, G. M.; Parise, J. *Organic Chemistry*, 6th ed.; Roberts and Company Publishers, Inc., 2016.

(16) Bronner, S. M.; Bahnck, K. B.; Garg, N. K. Indolynes as Electrophilic Indole Surrogates: Fundamental Reactivity and Synthetic Applications. *Org. Lett*. **2009** *11*, 1007–1010.

(17) Lin, J. B.; Shah, T. K.; Goetz, A. E.; Garg, N. K.; Houk, K. N. Conjugated Trimeric Scaffolds Accessible from Indolyne Cyclotrimerizations: Synthesis, Structures, and Electronic Properties. *J. Am. Chem. Soc.* **2017**, *139*, 10447–10455.

(18) Darzi, E. R.; Barber, J. S.; Garg, N. K. Cyclic Alkyne Approach to Heteroatom-Containing Polycyclic Aromatic Hydrocarbon Scaffolds. *Angew. Chem., Int. Ed.* **2019**, *58*, 9419–9424.

(19) a) Liu, Z.; Zhang, X.; Larock, R. C. Synthesis of Fused Polycyclic Aromatics by Palladium-Catalyzed Annulation of Arynes Using 2-Halobiaryls. *J. Am. Chem. Soc.* **2005**, *127*,

15716–15717. b) Liu, Z.; Larock, R. C. Highly Efficient Route to Fused Polycyclic Aromatics via Palladium-Catalyzed Aryne Annulation by Aryl Halides. *J. Org. Chem.* **2007**, *72*, 223–232.

(20) For examples of Pd-catalyzed transformations of arynes, see: a) Peña, D.; Pérez, D.; Guitián, E.; Castedo, L. Palladium-Catalyzed Cocyclization of Arynes with Alkynes: Selective Synthesis of Phenanthrenes and Naphthalenes. *J. Am. Chem. Soc.* **1999**, *121*, 5827–5828. b) Yoshida, H.; Ikadai, J.; Shudo, M.; Ohshita, J.; Kunai, A. Palladium-Catalyzed Bissilylation of Arynes with Cyclic Disilanes: Synthesis of Benzo-Annulated Disilacarbocycles. *J. Am. Chem. Soc.* **2003**, *125*, 6638–6639. c) Jeganmohan, M.; Bhuvaneswari, S.; Cheng, C.-H. A Cooperative Copper- and Palladium-catalyzed Three-Component Coupling of Benzynes, Allylic Epoxides, and Terminal Alkynes. *Angew. Chem., Int. Ed.* **2009**, *48*, 391–394. d) Liu, Y.-L.; Liang, Y.; Pi, S.-F.; Huang, X.-C.; Li, J.-H. Palladium-Catalyzed Cocyclotrimerization of Allenes with Arynes: Selective Synthesis of Phenanthrenes. *J. Org. Chem.* **2009**, *74*, 3199–3202. e) Garve, L. K. B.; Werz, D. B. Pd-Catalyzed Three-Component Coupling of Terminal Alkynes, Arynes, and Vinyl Cyclopropane Dicarboxylate. *Org. Lett.* **2015**, *17*, 596–599. f) Feng, M.; Tang, B.; Xu, H.-X.; Jiang, X. Collective Synthesis of Phenanthridinone through C–H Activation Involving a Pd-Catalyzed Aryne Multicomponent Reaction. *Org. Lett.* **2016**, *18*, 4352–4355. g) Yao, T.; He, D. Palladium-Catalyzed Domino Heck/Aryne Carbopalladation/C–H Functionalization: Synthesis of Heterocycle-Fused 9,10-Dihydrophenanthrenes. *Org. Lett.* **2017**, *19*, 842–845. h) Pozo, I.; Guitián, E.; Pérez, D.; Peña, D. Synthesis of

Nanographenes, Starphenes, and Sterically Congested Polyarenes by Aryne Cyclotrimerization. *Acc. Chem. Res.* **2019**, *52*, 2472–2481.

(21) For notable examples, see ref. 16 and a) Iwayama, T.; Sato, Y. Nickel(0)-catalyzed [2 + 2 + 2] cycloaddition of diynes and 3,4-pyridynes: novel synthesis of isoquinoline derivatives. *Chem. Commun.* **2009**, 5245−5247. b) Iwayama, T.; Sato, Y. Synthesis of Substituted Isoquinolines *via* Nickel-Catalyzed [2+2+2] Cycloaddition of Alkynes and 3,4-Pyridynes. *Heterocycles* **2010**, *80*, 917−924.

(22) For a review on yellow/orange phosphors, see: a) Fan, C.; Yang, C. Yellow/Orange Emissive Heavy-Metal Complexes as Phosphors in Monochromatic and White Organic Light-Emitting Devices. *Chem. Soc. Rev.* **2014**, *43*, 6439–6469. For a review on blue phosphors, see: b) Im, Y.; Byun, S. Y.; Kim, J. H.; Lee, D. R.; Oh, C. S.; Yook, K. S.; Lee, J. Y. Recent Progress in High-Efficiency Blue-Light-Emitting Materials for Organic Light-Emitting Diodes. *Adv. Funct. Mater.* **2017***, 27*, 1603007.

(23) We elected to utilize aryl bromides for our studies due to their ease of preparation and success in our preliminary studies. Other studies have demonstrated the viability of using aryl iodides (see ref. 19). Our laboratory has also demonstrated the use of aryl chlorides, albeit in the context of metal-complexed bipyridyl ligands (see ref. 24).

(24) Chari, J. V.; Spence, K. A.; Susick, R. B.; Garg, N. K. A Platform for On-the-Complex Annulation Reactions with Transient Aryne Intermediates. *Nat. Commun.* **2021***, 12*, 3706.

(25) Yamano, M. M.; Kelleghan, A. V. Shao, Q.; Giroud, M.; Simmons, B. J.; Li, B.; Chen, S.; Houk, K. N.; Garg, N. K. Intercepting Fleeting Cyclic Allenes with Asymmetric Nickel Catalysis. *Nature* **2020**, *586*, 242–247.

(26) Kelleghan, A. V.; Witkowski, D. C.; McVeigh, M. S.; Garg, N. K. Palladium-Catalyzed Annulations of Strained Cyclic Allenes. *J. Am. Chem. Soc.* **2021**, *143*, 9338–9342.

(27) We have experimentally observed that the addition of toluene leads to slower consumption of silyltriflate precursors, presumably by reducing the solubility of CsF in the reaction medium. The solubility of CsF in acetonitrile is roughly 5000x greater compared to the solubility of CsF in benzene, a close relative of toluene with a comparable dielectric constant. For a study of CsF solubility, see: Wynn, D. A.; Roth, M. M.; Pollard, B. D. The solubility of alkali-metal fluorides in non-aqueous solvents with and without crown ethers, as determined by flame emission spectrometry. *Talanta* **1984**, *31*, 1036–1040.

(28) In prior studies of indolynes, we have observed lower regioselectivities for processes that are concerted. As such, we believe the reaction proceeds by oxidative addition, followed by a concerted insertion across the reactive triple bond of the indolyne. This step is also consistent with the general mechanism proposed by Larock (see ref. 19a).

(29) Cha, M. S.; Park, J. E.; Kim, S.; Han, S.-H.; Shin, S.-H.; Yang, S. H.; Kim, T.-H.; Yu, D. M.; So, S.; Hong, Y. T.; Yoon, S. J.; Oh, S.-G.; Kang, S. Y.; Kim, O.-H.; Park, H. S.; Bae, B.; Sung, Y.E.; Cho, Y.-H.; Lee, J. Y. Poly(carbazole)-based Anion-Conducting Materials with High Performance and Durability for Energy Conversion Devices. *Energy Environ. Sci.* **2020**, *13*, 3633–3645.

(30) Tsutsumi, L. S.; Gündisch, D.; Sun, D. Carbazole Scaffolds in Medicinal Chemistry and Natural Products: A Review from 2010–2015. *Curr. Top. Med. Chem.* **2016**, *16*, 1290–1313.

(31) Goetz, A. E.; Silberstein, A. L.; Corsello, M. A.; Garg, N. K. Concise Enantiospecific Total Synthesis of Tubingensin A. *J. Am. Chem. Soc.* **2014**, *136*, 3036–3039.

(32) Wang, T.; Hoye, T. R. Hexadehydro-Diels–Alder (HDDA)-Enabled Carbazolyne Chemistry: Single Step, de Novo Construction of the Pyranocarbazole Core of Alkaloids of the *Murraya koenigii* (Curry Tree) Family. *J. Am. Chem. Soc.* **2016**, *138*, 13870–13873.

(33) Devaraj, K.; Ingner, F. J. L.; Sollert, C.; Gates, P. J.; Orthaber, A.; Pilarski, L. T. Arynes and Their Precursors from Arylboronic Acids via Catalytic C−H Silylation. *J. Org. Chem.* **2019**, *84*, 5863–5871.

(34) Corsello, M. A.; Kim, J.; Garg, N. K. Total Synthesis of (–)-Tubingensin B Enabled by the Strategic Use of an Aryne Cyclization. *Nat. Chem.* **2017**, *9*, 944–949.

(35) When the N–H variant of the 4,5-indolyne precursor was utilized in our general annulation conditions, only minimal amounts of the desired product were observed.

(36) Jones, S.; Thomas, T. H.; Jalebi, M. A.; Friend, R. H.; Linnolahti, M.; Bochmann, M.; Credgington, D. High-Performance Light-Emitting Diodes Based on Carbene-Metal-Amides. *Science* **2017**, *356*, 159–163. b) Hamze, R.; Peltier, J. L.; Sylvinson, D.; Jun, M.; Cardenas, J.; Haiges, R.; Soleilhavoup, M.; Jazzar, R.; Djurovich, P. I.; Bertrand, G.; Thompson, M. E. Eliminating Nonradiative Decay in Cu(I) Emitters: >99% Quantum Efficiency and Microsecond Lifetime. *Science* **2019**, *363*, 601–606. c) Hamze, R.; Shi, S.; Kapper, S. C.; Ravinson, D. S. M.; Estergreen, L.; Jung, M.-C.; Tadle, A. C.; Haiges, R.; Djurovich, P. I.; Peltier, J. L.; Jazzar, R.; Bertrand, G.; Bradforth, S. E.; Thompson, M. E. "Quick-Silver" from a Systematic Study of Highly Luminescent, Two-Coordinate, d^{10} Coinage Metal Complexes. *J. Am. Chem. Soc.* **2019***, 141*, 8616–8626.

(37) Gernert, M.; Balles-Wolf, L.; Kerner, F.; Müller, U.; Schmiedel, A.; Holzapfel, M.; Marian, C. M.; Pflaum, J.; Lambert, C.; Steffen, A. Cyclic (Amino)(aryl)carbenes Enter the Field of Chromophore Ligands: Expanded π System Leads to Unusually Deep Red Emitting Cu^{I} Compounds. *J. Am. Chem. Soc.* **2020**, *142*, 8897–8909.

(38) Romanov, A. S.; Becker, C. R.; James, C. E.; Di, D.; Credgington, D.; Linnolahti, M.; Bochmann, M. Copper and Gold (Alkyl)(amino)carbene Complexes with Sub-Microsecond Photoemissions: Structure and Substituent Effects on Redox and Luminescent Properties. *Chem. Eur. J.* **2017**, *23*, 4625–4637.

(39) Conaghan, P. J.; Matthews, C. S. B.; CHotard, F.; Jones, S. T. E.; Greenham, N. C.; Bochmann, M.; Credgington, D.; Romanov, A. S. Highly Efficient Blue Organic Light-Emitting Diodes Based on Carbene-Metal-Amides. *Nat. Commun.* **2020**, *11*, 1758.

(40) Chotard, F.; Sivchik, V.; Linnolahti, M.; Bochmann, M.; Romanov, A. S. Mono- versus Bicyclic Carbene Metal Amide Photoemitters: Which Design Leads to the Best Performance? *Chem. Mater.* **2020**, *32*, 6114–6122.

(41) Yersin, H.; Rausch, A. F.; Czerwieniec, R.; Hofbek, T.; Fischer, T. The Triplet State of Organo-Transition Metal Compounds. Triplet Harvesting and Singlet Harvesting for Efficient OLEDs. *Coord. Chem. Rev.* **2011**, *255*, 2622–2652.

(42) Hanson, K.; Roskop, L.; Djurovich, P. I.; Zahariev, F.; Gordon, M. S.; Thompson, M. E. A Paradigm for Blue- or Red-Shifted Absorption of Small Molecules Depending on the Site of π-Extension. *J. Am. Chem. Soc.* **2010**, *132*, 16247–16255.

(43) Shi, S.; Jung, M. C.; Coburn, C.; Tadle, A.; Ravinson, D. S. M.; Djurovich, P. I.; Forrest, S. R.; Thompson, M. E. Highly Efficient Photo- and Electroluminescence from Two-

Coordinate Cu(I) Complexes Featuring Nonconventional *N*-Heterocyclic Carbenes. *J. Am. Chem. Soc.* **2019**, *141*, 3576–3588.

(44) Romanov, A. S.; Yang, L.; Jones, S. T. E.; Di, D.; Morley, O. J.; Drummond, B. H.; Reponen, A. P. M.; Linnolahti, M.; Credgington, D.; Bochmann, M. Dendritic Carbene Metal Carbazole Complexes as Photoemitters for Fully Solution-Processed OLEDs. *Chem. Mater.* **2019**, *31*, 3613–3623.

(45) Ying, A.; Huang, Y.-H.; Lu, C.-H.; Chen, Z.; Lee, W.-K.; Zeng, X.; Chen, T.; Cao, X.; Wu, C.-C.; Gong, S.; Yang, C. High-Efficiency Red Electroluminescence Based on a Carbene-Cu(I)-Acridine Complex. **2021**, *13*, 13478–13486.

(46) Bossi, A.; Rausch, A. F.; Leitl, M. J.; Czerwieniec, R.; Whited, M. T.; Djurovich, P. I.; Yersin, H.; Thompson, M. E. Photophysical Properties of Cyclometalated Pt(II) Complexes: Counterintuitive Blue Shift in Emission with an Expanded Ligand p System. *Inorg. Chem.* **2013**, *52*, 12403–12415.

(47) Mandapati, P.; Giesbrecht, P. K.; Davis, R. L.; Herbert, D. E. Phenanthridine-Containing Pincer-like Amido Complexes of Nickel, Palladium, and Platinum. *Inorg. Chem.* **2017**, *56*, 3674–3685.

(48) Hamze, R.; Idris, M.; Ravinson, D. S. M.; Jung, M. C.; Haiges, R.; Djurovich, P. I.; Thompson, M. E. Highly Efficient Deep Blue Luminescence of 2-Coordinate Coinage Metal Complexes Bearing Bulky NHC Benzimidazolyl Carbene. *Front. Chem.* **2020**, *8*, 401.

(49) Hamze, R.; Shi, S.; Kapper, S.; Ravinson, D. S. M.; Estergreen, L.; Jung, M.-C.; Tadle, A. C.; Haiges, R.; Djurovich, P. I.; Peltier, J. L.; Jazzar, R.; Bertrand, G.; Bradforth, S. E.;

Thompson, M. E. “Quick-Silver” from a Systematic Study of Highly Luminescent, Two-Coordinate, d^{10} Coinage Metal Complexes. *J. Am. Chem. Soc.* **2019**, *141*, 8616–8626.

(50) See Section 5.5.2.6 for preparation of 1 wt% polystyrene film.

(51) Zhang, Q.-W.; An, K.; Liu, L.-C.; Guo, S.; Jiang, C.; Guo, H.; He, W. Rhodium-Catalyzed Intramolecular C−H Silylation by Silacyclobutanes. *Angew. Chem., Int. Ed.* **2016**, *55*, 6319–6323.

(52) Wang, T.-F.; Lin, C.-L.; Chen, C.-N.; Wang, T.-C. Easily Accessible 2-(2-Bromophenyl)-4,4,5,5-Tetramethyl-[1,3,2]Dioxaborolane for Suzuki-Miyaura Reactions. *J. Chin. Chem. Soc.* **2007**, *54*, 811–816.

(53) Wu, D.; Chen, L.; Ma, S.; Luo, H.; Cao, J.; Chen, R.; Duan, Z.; Mathey, F. Synthesis of 1,3-Azaphospholes with Pyrrolo[1,2-*a*]quinoline Skeleton and Their Optical Applications. *Org. Lett.* **2018**, *20*, 4103−4106.

(54) Panteleev, J.; Geyer, K.; Aguilar-Aguilar, A.; Wang, L.; Lautens, M. C−H Bond Functionalization in the Synthesis of Fused 1,2,3-Triazoles. *Org. Lett.* **2010**, *12*, 5092–5095.

(55) Wong, S. M.; Yuen, O. Y.; Choy, P. Y.; So, C. M.; Kwong, F. Y. Preparation of 2-(2-(Dicyclohexylphosphino)phenyl)-1-methyl-1H-indole (CM-phos). *Org. Synth.* **2016**, *93*, 14–28.

(56) Im, G.-Y. J.; Bronner, S. M.; Goetz, A. E.; Paton, R. S.; Cheong, P. H.-Y.; Houk, K. N.; Garg, N. K. Indolyne Experimental and Computational Studies: Synthetic Applications and Origins of Selectivities of Nucleophilic Additions. *J. Am. Chem. Soc.* **2010**, *132*, 17933–17944.

(57) Shao, Y. H.; Gan, Z. T.; Epifanovsky, E.; Gilbert, A. T. B.; Wormit, M.; Kussmann, J.; Lange, A. W.; Behn, A.; Deng, J.; Feng, X. T.; Ghosh, D.; Goldey, M.; Horn, P. R.; Jacobson, L. D.; Kaliman, I.; Khaliullin, R. Z.; Kus, T.; Landau, A.; Liu, J.; Proynov, E. I.; Rhee, Y. M.; Richard, R. M.; Rohrdanz, M. A.; Steele, R. P.; Sundstrom, E. J.; Woodcock, H. L.; Zimmerman, P. M.; Zuev, D.; Albrecht, B.; Alguire, E.; Austin, B.; Beran, G. J. O.; Bernard, Y. A.; Berquist, E.; Brandhorst, K.; Bravaya, K. B.; Brown, S. T.; Casanova, D.; Chang, C. M.; Chen, Y. Q.; Chien, S. H.; Closser, K. D.; Crittenden, D. L.; Diedenhofen, M.; DiStasio, R. A.; Do, H.; Dutoi, A. D.; Edgar, R. G.; Fatehi, S.; Fusti-Molnar, L.; Ghysels, A.; Golubeva-Zadorozhnaya, A.; Gomes, J.; Hanson-Heine, M. W. D.; Harbach, P. H. P.; Hauser, A. W.; Hohenstein, E. G.; Holden, Z. C.; Jagau, T. C.; Ji, H. J.; Kaduk, B.; Khistyaev, K.; Kim, J.; King, R. A.; Klunzinger, P.; Kosenkov, D.; Kowalczyk, T.; Krauter, C. M.; Lao, K. U.; Laurent, A. D.; Lawler, K. V.; Levchenko, S. V.; Lin, C. Y.; Liu, F.; Livshits, E.; Lochan, R. C.; Luenser, A.; Manohar, P.; Manzer, S. F.; Mao, S. P.; Mardirossian, N.; Marenich, A. V.; Maurer, S. A.; Mayhall, N. J.; Neuscamman, E.; Oana, C. M.; Olivares-Amaya, R.; O'Neill, D. P.; Parkhill, J. A.; Perrine, T. M.; Peverati, R.; Prociuk, A.; Rehn, D. R.; Rosta, E.; Russ, N. J.; Sharada, S. M.; Sharma, S.; Small, D. W.; Sodt, A.; Stein, T.; Stuck, D.; Su, Y. C.; Thom, A. J. W.; Tsuchimochi, T.; Vanovschi, V.; Vogt, L.; Vydrov, O.; Wang, T.; Watson, M. A.; Wenzel, J.; White, A.; Williams, C. F.; Yang, J.; Yeganeh, S.; Yost, S. R.; You, Z. Q.; Zhang, I. Y.; Zhang, X.; Zhao, Y.; Brooks, B. R.; Chan, G. K. L.; Chipman, D. M.; Cramer, C. J.; Goddard, W. A.; Gordon, M. S.; Hehre, W. J.; Klamt, A.; Schaefer, H. F.; Schmidt, M. W.; Sherrill, C. D.; Truhlar, D. G.; Warshel, A.; Xu, X.; Aspuru-Guzik, A.; Baer, R.; Bell, A. T.; Besley, N. A.; Chai, J. D.;

Dreuw, A.; Dunietz, B. D.; Furlani, T. R.; Gwaltney, S. R.; Hsu, C. P.; Jung, Y. S.; Kong, J.; Lambrecht, D. S.; Liang, W. Z.; Ochsenfeld, C.; Rassolov, V. A.; Slipchenko, L. V.; Subotnik, J. E.; Van Voorhis, T.; Herbert, J. M.; Krylov, A. I.; Gill, P. M. W.; Head-Gordon, M. Advances in Molecular Quantum Chemistry Contained in the Q-Chem 4 Program Package. *Mol. Phys.* **2015,** *113*, 184–215.

CHAPTER SIX

An Enzymatic Alder-ene Reaction

Adapted from: Masao Ohashi,† Cooper S. Jamieson,† Yujuan Cai,† Dan Tan, Daiki Kanayama, Man-Cheng Tang, Sarah M. Anthony, Jason V. Chari, Joyann S. Barber, Elias Picazo, Thomas B. Kakule, Shugeng Cao, Neil K. Garg, Jiahai Zhou, K. N. Houk, and Yi Tang.

Nature **2020**, *586*, 64–69.

6.1 Abstract

An ongoing challenge in chemical research is to design catalysts that select the outcomes of the reactions of complex molecules. Chemists rely on organo- or transition metal catalysts to control stereo-, regio-, and periselectivity (selectivity among possible pericyclic reactions). Nature achieves these types of selectivity with a variety of enzymes such as the recently discovered pericyclases – a family of enzymes that catalyze pericyclic reactions.[1] To date, the majority of characterized enzymatic pericyclic reactions are cycloadditions, and it has been difficult to rationalize how observed selectivities are achieved.[2–13] We report here the discovery of two homologous groups of pericyclases that catalyze distinct reactions: one group catalyzes an Alder-ene reaction, previously unknown in biology; the second catalyzes a stereoselective hetero-Diels–Alder reaction. Guided by computational studies, we rationalized the observed differences in reactivities and designed mutants that reverse periselectivities from Alder-ene to hetero-Diels–Alder and *vice versa*. A combination of *in vitro* biochemical characterizations,

computational studies, enzyme co-crystal structures, and mutational studies provide a picture of how high regio- and periselectivities are achieved in nearly identical active sites.

6.2 Introduction

Pericyclic reactions are concerted chemical transformations in which all bonding changes occur in a cyclic array of atoms (Fig. 6.1a).[14] Diels–Alder and hetero-Diels–Alder reactions are classics in synthesis, and form cyclohexenes and pyrans, respectively.[15,16] Recently, these pericyclic reactions have been discovered to be catalyzed by enzymes in nature (Fig. 6.1a, b).[4] The Alder-ene reaction (Fig. 6.1a),[17] originally named the 'substituting addition' reaction by Kurt Alder's laboratory in 1943 and subject of his Nobel prize lecture,[18] is an efficient method for carbon–carbon bond formation and has been applied to total syntheses of complex polycyclic natural products.[19,20] While this reaction has been postulated to be involved in several biological processes,[21] there are no characterized examples of enzyme-catalyzed Alder-ene reactions in biology despite the frequency of substituted pentenes in natural products.[22] To this end, we set out to discover the enzymatic Alder-ene reaction in biosynthesis.

6.3 Results and Discussion

Chemical syntheses of racemic pyridoxatin (**6.1**)[23,24] and cordypyridone[25] and our previous work on related leporin 2-pyridone alkaloids[4,26] led us to hypothesize that the vinyl cyclohexane core of **6.1** could be formed by an Alder-ene reaction of a reactive (*E*)- or (*Z*)-quinone methide (QM) (Fig. 6.1c).[27] The activated QM can also undergo various hetero-Diels–Alder reactions involving either oxygen atom on the pyridone ring. To understand factors controlling the periselectivity, we expanded our study to include related natural products with the identical carbon

backbones asperpyridone A (**6.2**)[28] and fusaricide (**6.3**)[29,30] that presumably derive from the hetero-Diels–Alder reaction of the same reactive QM. Because Alder-ene reactions are less exothermic (~ –27 kcal·mol^{-1}) than cycloadditions (~ –38 kcal·mol^{-1}), we anticipated that the Alder-ene reaction would be intrinsically more difficult than hetero-Diels–Alder reactions and periselectivity would strongly favor the latter.

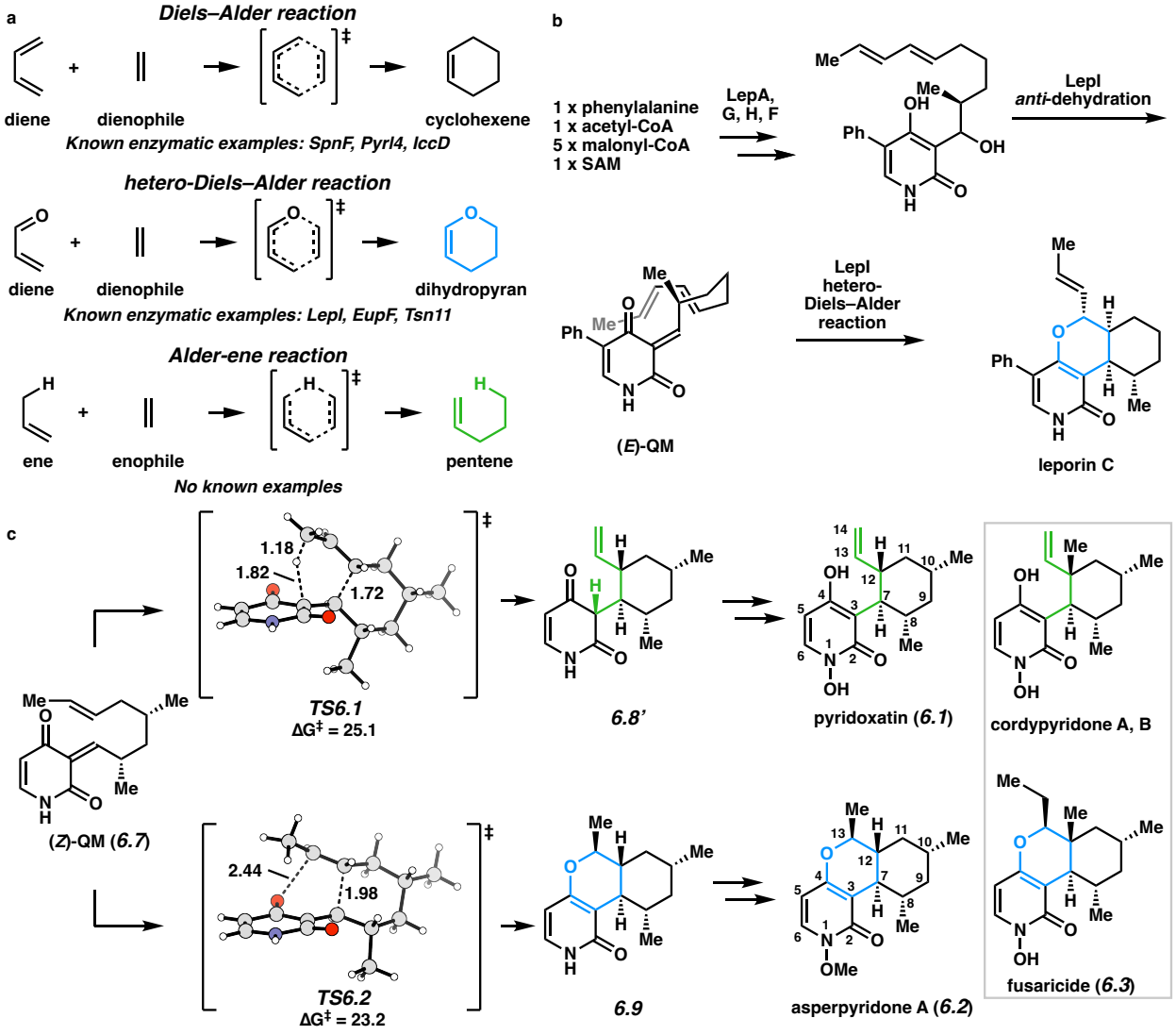

Figure 6.1. Pericyclic reactions in natural product biosynthesis.

To understand the reactivity of the QM in pericyclic reactions, we performed quantum mechanical calculations to determine transition state (TS) geometries and to quantify the barriers of possible pericyclic reactions from (*E*)- and (*Z*)-QM. Calculations indicate that the Alder-ene reaction has a slight preference (0.4 kcal·mol^{-1}) to occur from the (*Z*)- over the (*E*)-QM. From the (*Z*)-QM **6.7**, the Alder-ene reaction via **TS6.1** is 1.9 kcal·mol^{-1} higher in energy than preferred hetero-Diels–Alder **TS6.2** (Fig. 6.1c). This difference in Gibbs free energy corresponds to a nonenzymatic ratio of 1:9 Alder-ene to hetero-Diels–Alder adducts, and indicates that a dedicated pericyclase with strong periselectivity must be involved in each of the biosynthetic pathways for the exclusive formation of either **6.1** or **6.2** (and **6.3**) from the producing strains.

To identify the potential pericyclases, we searched the genomes of **6.1**-producing strain *Albophoma yamanashiensis* and the related pyran-containing, **6.3**-producing strain *Epicoccum sorghinum* FT1062, as the **6.2**-producing strain was unavailable.[30,31] As shown in Figure 6.2, the two genomes of *A. yamanashiensis* and *E. sorghinum* FT1062 both encode a homologous biosynthetic gene cluster (*adx* and *epi*, respectively) containing a polyketide synthase-nonribosomal peptide synthetase (*adxC*/*epiC*), a partnering enoylreductase (*adxD*/*epiD*), a ring expansion P450 (*adxA*/*epiA*), a putative *N*-hydroxylation P450 (*adxB*/*epiB*), a short-chain dehydrogenase/reductase (SDR) (*adxG*/*epiG*) and a putative *O*-methyltransferase (OMT) (*adxI*/*epiI*). We searched the National Center for Biotechnology Information (NCBI) database for other homologous clusters, which are conserved in many sequenced fungal strains such as *Aspergillus bombycis* (*pdx*), *Monosporascus cannonballus* (*modx*), *Uncinocarpus reesii* (*upi*) and *Hymenoscyphus scutula* (*hpi*) (Figure 6.2). Based on the sequence of previously discovered pericyclase LepI in leporin biosynthesis (Figure 6.1b and Figure 6.2),[4] we hypothesized that the predicted OMT-fold enzymes in these pathways, which are AdxI, EpiI, PdxI, ModxI, UpiI and

HpiI, are potential pericyclases. We proposed that each enzyme catalyzes the stereoselective dehydration of alcohol **6.6** to **6.7**; AdxI from the **6.1**-producing strain would then catalyze the subsequent Alder-ene reaction; while EpiI from the **6.3**-producing strain would catalyze the hetero-Diels–Alder reaction (Fig. 6.3). While there is a high sequence identity between these enzymes (59–83%), they all display very low identity to LepI (~15%).

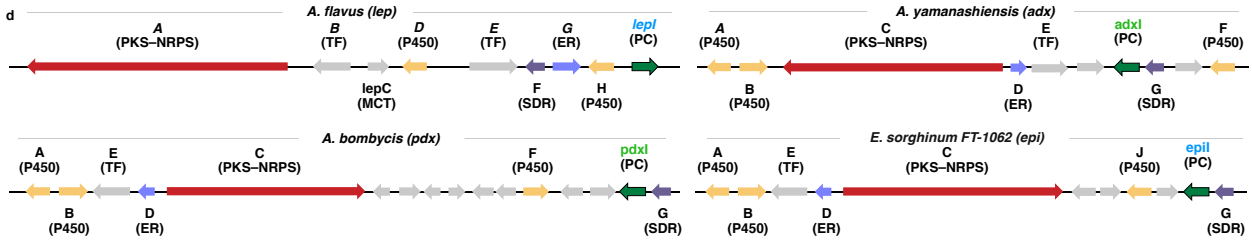

Figure 6.2. Genomes of *A. yamanashiensis* and *E. sorghinum*.

We performed the coupled *in vitro* reactions using enzymatically and chemoenzymatically prepared ketone **6.5**, the SDR PdxG as the putative ketoreductase, and one of the proposed pericyclases. In the presence of PdxG and cofactor NADPH, **6.5** is reduced to the alcohol **6.6** (Figure 6.3). In solution, **6.6** readily underwent nonenzymatic dehydration to generate both (*E*)- and (*Z*)-QM that rehydrate to form **6.6** and the C7 diastereomer.[32] After 2 h, small amounts of O4-hetero-Diels–Alder product **6.9** and atropisomeric Alder-ene product **6.8** were detected in a 3:1 ratio (Figure 6.3) along with three other unidentified minor products. Extended incubation times (10 h) with PdxG generated the overreduced **6.10**, which is presumably derived from a reduction of the QM (Figure 6.3). When AdxI, PdxI or ModxI was incubated with PdxG, NADPH and **6.5**, **6.8** was predominantly formed (>98:2, **6.8**:**6.9**) (Figure 6.3). On the other hand, when we added EpiI, UpiI or HpiI to the reaction mixtures containing PdxG, NADPH, and **6.5**, the periselectivity was switched with **6.9** as the predominant product (<5:95, **6.8**:**6.9**) (Figure 6.3).

Since **6.8** and **6.9** can be chemically interconverted in harsh acidic conditions,[25] we investigated whether these pericyclases could catalyze such a transformation. However, no enzyme was able to catalyze the interconversion (Figure 6.3), which indicates these enzymes catalyze the observed reactions with strong periselectivity. Although these new pericyclases are predicted *S*-adenosyl-L-methionine (SAM)-dependent *O*-MTs,[4,33] none were copurified with SAM, nor was SAM or *S*-adenosyl-L-homocysteine (SAH) required for catalysis. Overall, our biochemical data show that the group of AdxI, PdxI and ModxI are the first characterized enzymes to catalyze the Alder-ene reaction forming a *bona fide* Alder-ene adduct. The group of EpiI, UpiI and HpiI were characterized as SAM-independent enzymes that catalyze a hetero-Diels–Alder reaction to form a *trans*-fused hexahydroisochromene, which is in contrast to LepI that forms a *cis*-fused hexahydroisochromene. These discoveries expand the repertoire of reactions catalyzed in Nature.

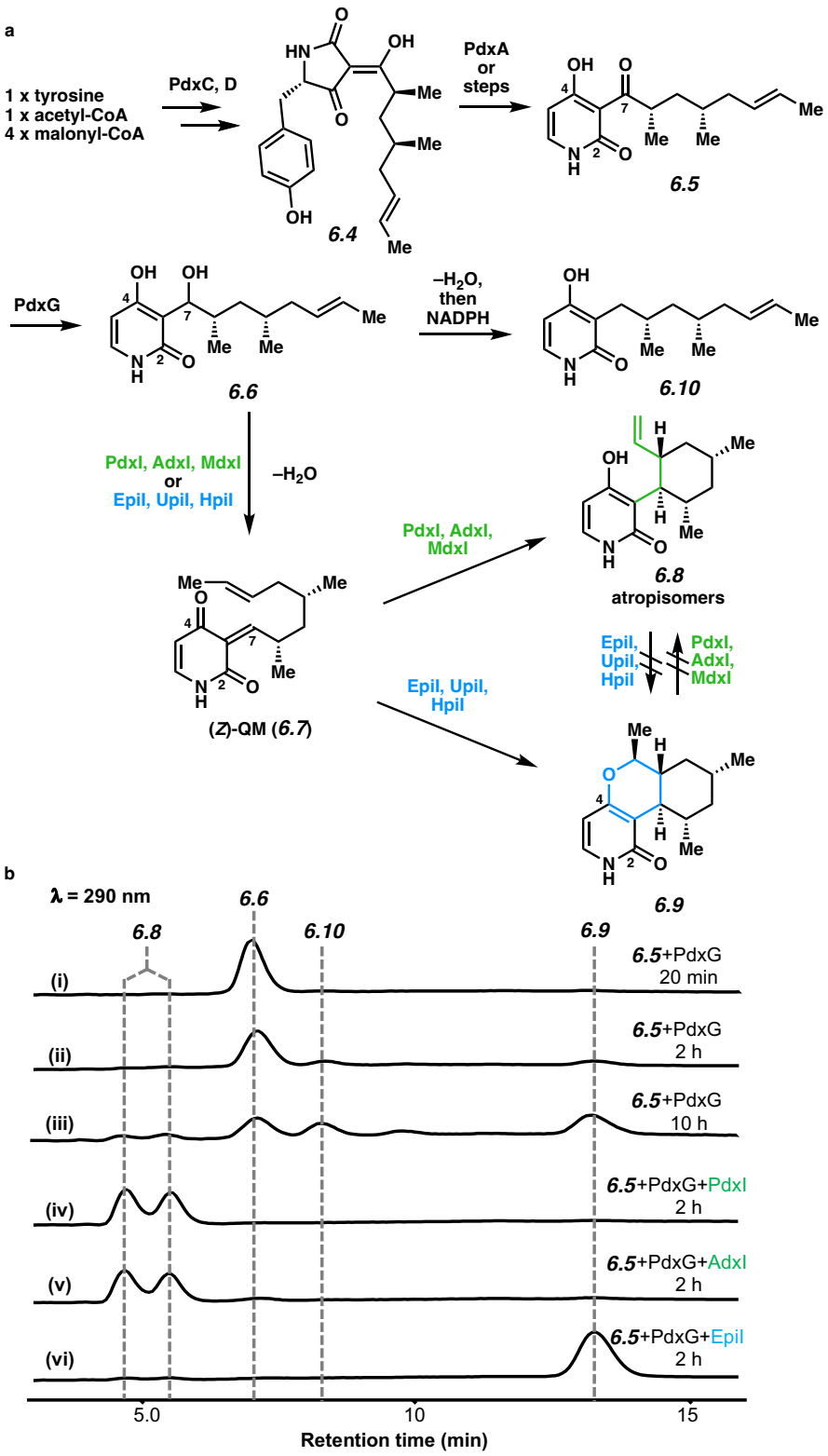

Figure 6.3. The proposed biosynthesis of the Alder-ene product (**6.8**) and the hetero-Diels–Alder product (**6.9**) from the common intermediate **6.7**.

To gain mechanistic insight into the enzyme-catalyzed Alder-ene reaction, X-ray crystal structures of *apo*-PdxI, substrate analogue complex PdxI-**6.5**, and product complex PdxI-**6.8** were solved and refined to 2.0 Å, 2.0 Å, and 2.4 Å resolutions, respectively. The *apo*-PdxI structure adopts a classic α,β-Rossman *O*-MT fold (Figure 6.4a)[26] and forms a woven dimer structure by interlocking the *N*-terminal helices (lime and royal blue, Figure 6.4b). The PdxI-**6.5** and PdxI-**6.8** structures are overall very similar to *apo*-PdxI (root mean squared deviation (r.m.s.d.) of 0.162 and 0.202 for 831 Cα atoms, respectively). The chain A active site of PdxI-**6.5** and PdxI-**6.8** are shown in Figure 6.4c. The pyridone ring forms hydrogen bonds with the side chains of K337, H161 and Q412, as well as water molecules via T232, D233 and H336 in the active site. The extended alkyl chain of **6.5** is pointed towards hydrophobic residue I366 and is not in a near attack conformation for the pericyclic reaction. The C7 ketone of substrate analogue **6.5** is positioned *syn* to the C4-hydroxyl and is indicative that the alcohol substrate undergoes a *syn*-dehydration facilitated by K337 to generate (*Z*)-QM **6.7**. In order to generate an (*E*)-QM the C7 alcohol would need to rotate 180º and be *syn* to the C2-oxygen. The fact that this (*E*)-QM geometry differs greatly from that of the substrate analogue indicates that it is most probable that **6.7** is generated *in situ*. Substitution of K337 to alanine completely abolished the dehydration activity but can be rescued by mutation to arginine, which supports the role of K337 as a general base for the dehydration step.

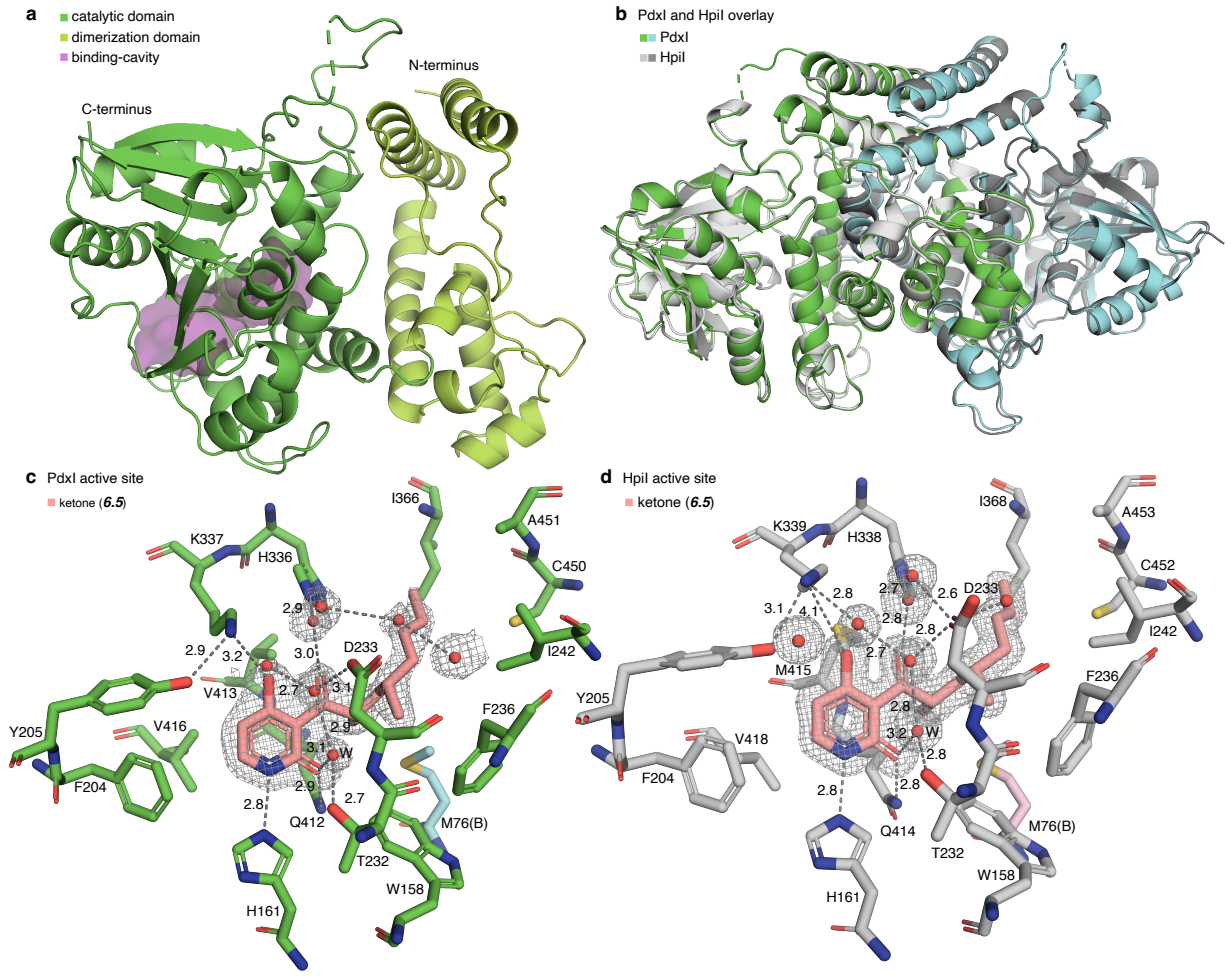

Figure 6.4. Crystal structures of PdxI and HpiI.

To investigate how the active site of PdxI catalyzes the energetically unfavorable Alder-ene reaction and suppresses the hetero-Diels–Alder reaction, we performed multiple 500 ns classical molecular dynamics (MD) simulations of **6.7** docked into PdxI. Since K337 is expected to be protonated after dehydration of **6.6** to **6.7**, we modeled side chain of K337 as an ammonium ion. We analyzed the conformation of the alkyl chain of the reactive **6.7** throughout the simulations and found that the alkyl chain can reorganize from the extended, unreactive conformation seen in PdxI-**6.5** into a reactive near attack conformation for 50–100 ns of the 500 ns simulation. In all simulations, H161 and Q412 hydrogen bond to N1 and C2-carbonyl of the pyridone, respectively,

whereas K337 and H336 hydrogen bond to the C4-carbonyl. K337 maintains this hydrogen bond to the pyridone C4-carbonyl of **6.7** for longer durations in the simulation, which implies the protonated K337 may facilitate the Alder-ene reaction by hydrogen bond catalysis.

Next, we quantified how the K337 and H161 hydrogen bonds affect the reaction rate with a truncated catalytic-residue 'theozyme' model; K337 is modeled as a methyl ammonium and H161 as an imidazole (Figure 6.5a). The calculations indicate that the energetic barrier for the Alder-ene transition state in the theozyme (**TS6.3**) is reduced by 11.7 kcal·mol^{-1}, a rate acceleration of >10^8, when compared to the nonenzymatic reaction. Protonation of the carbonyl makes C7 highly electrophilic and decreases the nucleophilicity of the carbonyl oxygen. Both of these factors suppress the hetero-Diels–Alder transition state (**TS6.4**) and favor **TS6.3** by 3.4 kcal·mol^{-1}, a 5.8 kcal·mol^{-1} shift in $\Delta\Delta G^{\ddagger}$ relative to the nonenzymatic reactions (Figure 6.5a). Mechanistically, calculations indicate that **6.7** undergoes protonation by K337 and concomitant Alder-ene reaction via **TS6.3** with an overall enthalpic barrier of 9.2 kcal·mol^{-1}. In comparison, the O4-hetero-Diels–Alder via **TS6.4** has a higher enthalpic barrier of 12.6 kcal·mol^{-1}. This indicates that the PdxI active site alters the electronics of the reaction, by protonation of O4, to favor the Alder-ene reaction and achieve the observed periselectivity.

It should be noted that the Alder-ene theozyme model also predicts a distinct, yet favorable hetero-Diels–Alder reaction via **TS6.5** to form the *cis*-fused O2-hetero-Diels–Alder 4-pyridone adduct **6.11** (Figure 6.5a). However, **6.11** is not found in the *in vitro* PdxI reaction mixtures (Figure 6.3b). This implies an additional degree of regio- and periselectivity exerted by PdxI to disfavor formation of **TS6.5**. The PdxI structure with a docked **TS6.5** indicates that the side chain of T232 and water molecule (**W**) cause unfavorable interactions with the terminal C14 methyl in **TS6.5**. The threonine residue acts as a steric wall to prevent **6.7** from accessing the **TS6.5** conformation.

To test this hypothesis, we prepared the PdxI T232A/S/V mutants and performed the coupled *in vitro* reactions. Indeed, the less hindered T232A and T232S mutants generated an appreciable amount of a new compound as compared to the WT PdxI (Fig. 6.6). Large scale *in vitro* reaction of PdxI T232S mutant led to the isolation and determination of structure as the expected **6.11**, which is one of the minor, nonenzymatic cyclized products from **6.7**. Mutation to valine (PdxI T232V), the steric isostere of threonine, did not produce any **6.11** (Figure 6.6) supporting the role of T232 residue in sterically preventing the formation of **TS6.5**.

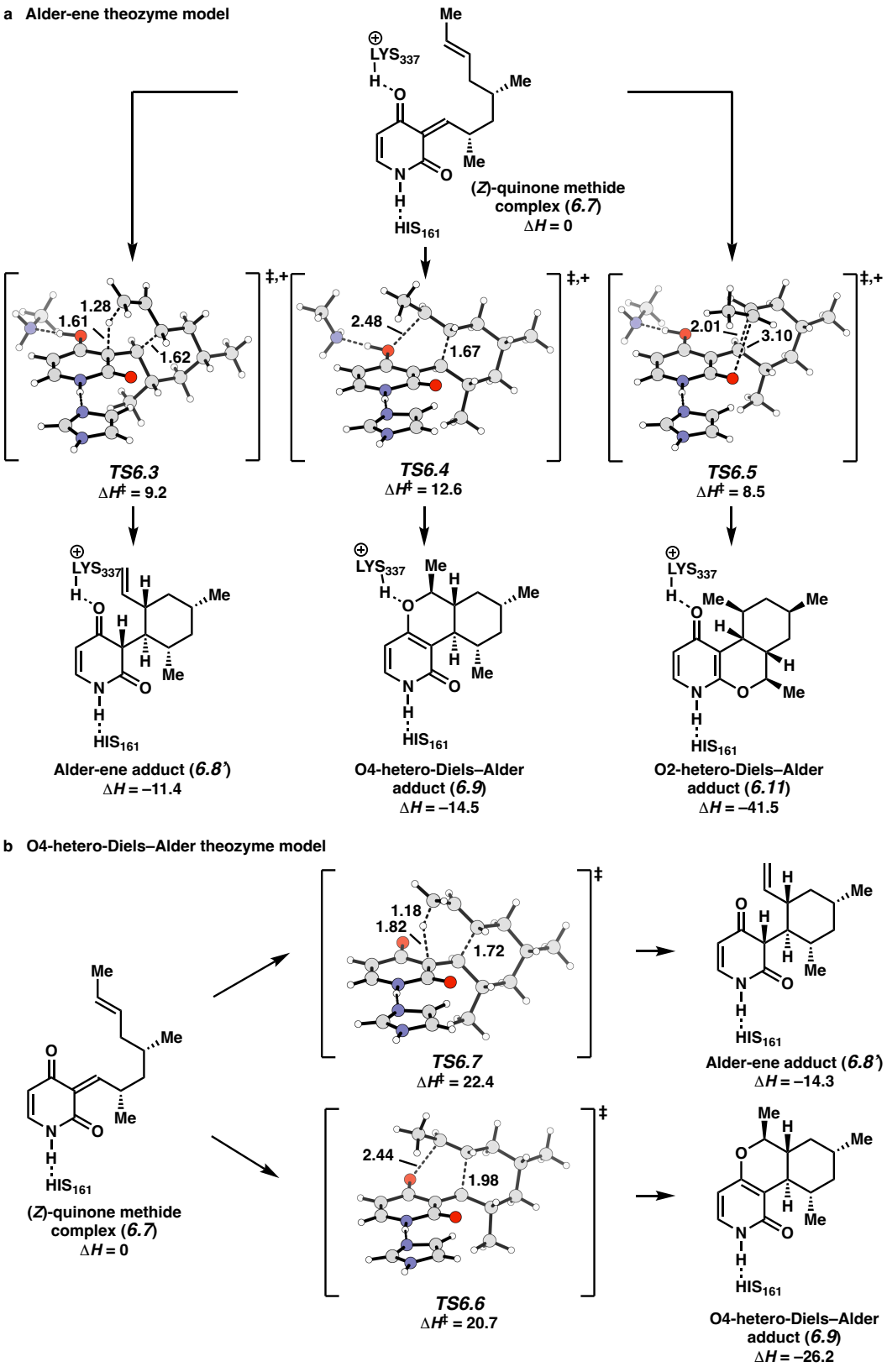

Figure 6.5. Mechanism of periselective and regioselective pericyclic reactions.

PdxI crystal structures, molecular dynamics, and the 'theozyme' model indicate that the K337 residue acts as a general acid catalyst to favor the Alder-ene reaction over the O4-hetero-Diels–Alder reaction. Then, we calculated the O4-hetero-Diels–Alder 'theozyme' model (Figure 6.5b) by removing the lysine from the PdxI K337 and H161 theozyme model (Figure 6.5a), and indeed the O4-hetero-Diels–Alder reaction is preferred by 1.7 kcal·mol^{-1} (**TS6.6** vs. **TS6.7**). This suggests that the group of enzymes (EpiI, HpiI and UpiI) that catalyze the O4-hetero-Diels–Alder reaction, in contrast to PdxI, must avoid proton transfer to the pyridone C4 carbonyl to achieve the opposite periselectivity. Nevertheless, the corresponding lysine is conserved in these three enzymes as well. We solved and refined the crystal structures of *apo*-HpiI and HpiI-**6.5** to 1.3 Å and 1.5 Å resolution, respectively (Figure 6.4d). These structures are highly similar to that of PdxI (r.m.s.d of 0.468 for 415 Cα atoms) (Figure 6.4b–d). Notably, the binding modes of **6.5** in PdxI and HpiI are essentially identical (Figure 6.4c, d) and nearly all amino acid residues in the active site between PdxI and HpiI are conserved except for V413 in PdxI and the corresponding residue M415 in HpiI (Figure 6.4c,d). This key residue sits below the pyridone binding site and neighbors the aforementioned lysine (K337 in PdxI, K338 in EpiI and K339 in HpiI). The HpiI-**6.5** complex clearly shows that K339, unlike K337 in PdxI, does not form a hydrogen bond to the 4-hydroxy on the pyridone ring; this distance is stretched out from 3.2 Å in PdxI to 4.1 Å in HpiI (Figure 6.4d). To verify the lysine residue is not catalytic, we prepared the more stable mutant K338A of EpiI. In contrast to PdxI K337A mutant, EpiI K338A mutant retained the majority of the enzymatic activity (~80%) and showed the same periselectivity as WT EpiI (Figure 6.6). Thus, the EpiI-catalyzed reactions do not require hydrogen bonding between the C4-oxygen on the pyridone ring and K338. From the crystal structure of HpiI, this loss of a hydrogen bond is caused by the bulkier side chain of M415, which shifts the lysine side chain further away from the substrate

(Figure 6.4d). Consistently, homologous pericyclases such as EpiI, UpiI, and HpiI all catalyze the hetero-Diels–Alder reaction to form **6.9**, and the methionine residue is conserved (M411, M413, and M415, respectively). By contrast, pericyclases such as PdxI, AbxI and ModxI catalyze the Alder-ene reaction, and the valine residue (V413) is conserved.

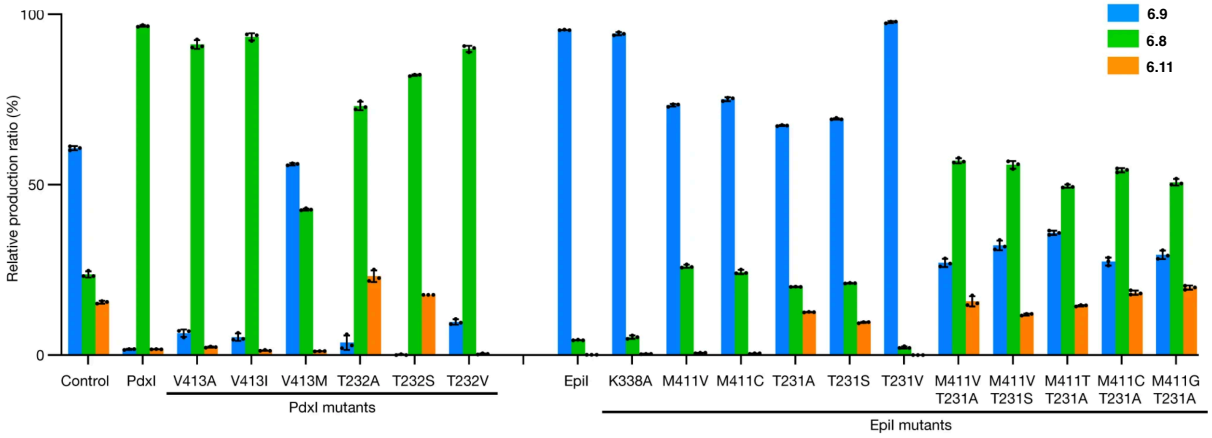

Figure 6.6. Mutagenesis: enzymatic periselectivity and regioselectivity.

We next explored if the periselectivity of PdxI could be switched to favor the hetero-Diels–Alder reaction by replacement of V413 residue with alanine, isoleucine or methionine. Mutating valine to alanine and isoleucine, residues that are smaller than methionine, retained the periselectivity of PdxI for the Alder-ene reaction (Figure 6.6). In contrast, the V413M mutant showed reversed periselectivity, switching the major reaction type from Alder-ene to hetero-Diels–Alder, forming **6.8** and **6.9** in a ratio of 40:60 compared to the wild-type ratio of >98:2 (Figure 6.6). On the other hand, the mutation of M411 in EpiI to the less bulky valine or cysteine altered the product ratio (**6.8**:**6.9**) from 5:95 to 25:75 (Figure 6.6). The mutation of M411 alone in EpiI is not sufficient to reverse the periselectivity, suggesting that other factors such as shape complementarity to restrict the movement of **6.7** would also contribute to maintaining the observed periselectivity for the hetero-Diels–Alder reaction.

Since the conformational flexibility of **6.7** is expected to be restricted by both M411 and T231 residues in the EpiI active site based on the HpiI-**6.5** complex (Figure 6.4d), we mutated the T231 residue to smaller alanine and serine residues. This mutation would increase the conformational flexibility of **6.7** in the EpiI active site to form the key hydrogen bonding with K338 for the Alder-ene reaction. Indeed, while the hetero-Diels–Alder product **6.9** still remains the major product, EpiI T231A and T231S mutants increased the ratio of Alder-ene product **6.8** along with the O2-hetero-Diels–Alder product **6.11** as seen in PdxI T232A/S mutants (Figure 6.6). Intriguingly, the double mutant M411V/T231A showed the reversed periselectivity with the ratio (**6.8**:**6.9**) of 66:33. Other less bulky double mutants such as M411V/T231S, M411T/T231A. M411C/T231A, and M411G/T231A showed similarly reversed periselectivities. Based on these results, we conclude that the replacement of the methionine and threonine with smaller residues enlarges the enzyme active site and allows for greater conformational sampling of **6.7** and protonation of the C4 carbonyl, thus leading to the opposite periselectivity.

Our results show that the group of PdxI, AdxI, and ModxI are multifunctional enzymes that catalyze the stereoselective *syn*-dehydration of **6.6** to **6.7** and the subsequent Alder-ene reaction of **6.7** to **6.8** in a stereo-, regio- and periselective manner. In contrast, the group of EpiI, UpiI, and HpiI catalyze the same stereoselective *syn*-dehydration of **6.6** to **6.7** but with orthogonal periselectivity and catalyze the hetero-Diels–Alder reaction of **6.7** to **6.9**. Computational studies, comparative analysis of the enzyme-cocrystal structures, and site-directed mutagenesis provided a detailed picture of the catalytic mechanism for PdxI and EpiI. PdxI utilizes K337 as general acid catalyst to facilitate the otherwise energetically unfavorable Alder-ene reaction, while the methionine substitution in EpiI abolishes this interaction to allow only the O4-hetero-Diels–Alder

reaction. The steric effect of T232 in PdxI and T231 in EpiI inhibits the formation of the O2-hetero-Diels–Alder product **6.11** to further control regioselectivity.

6.4 Conclusion

In conclusion, we have characterized two homologous groups of enzymes and identified how subtle evolutionary divergence leads to the production of different natural products. The insight gained from our research serves as a basis for developing new biocatalysts that catalyze various natural and unnatural Alder-ene and hetero-Diels–Alder reactions that are valuable synthetic transformations.

6.5 Experimental Section

6.5.1 Materials and Methods

Unless stated otherwise, reactions were conducted in flame-dried glassware under an atmosphere of nitrogen using anhydrous solvents (either freshly distilled or passed through activated alumina columns). Commercially obtained reagents were used as received unless otherwise specified. Reaction temperatures were controlled using an IKAmag temperature modulator, and unless stated otherwise, reactions were performed at room temperature (rt, approximately 23 °C). Thin-layer chromatography (TLC) was conducted with EMD gel 60 F254 pre-coated plates (0.25 mm) and visualized using a combination of UV, anisaldehyde, iodine, phosphomolybdic acid and cerium (IV) sulfate in water with sulfuric acid (Seebach), and potassium permanganate staining. Silicycle P60 (particle size 0.040–0.063 mm) silica gel was used for flash column chromatography. ^{1}H NMR spectra were recorded on Bruker spectrometers (at 500 MHz) and are reported relative to deuterated solvent signals (7.26 ppm for $CDCl_3$, 7.16 ppm for C_6D_6, 4.78 ppm for CD_3OD). Data

for ^{1}H NMR spectra are reported as follows: chemical shift (δ ppm), multiplicity, coupling constant (Hz), and integration. ^{13}C NMR spectra were recorded on Bruker spectrometers (at 125 MHz) and are reported relative to deuterated solvent signals (77.16 ppm for $CDCl_3$). Data for ^{13}C NMR spectra are reported in terms of chemical shift, and when necessary, multiplicity, coupling constant (Hz) and carbon type.

6.5.2 Experimental Procedures.

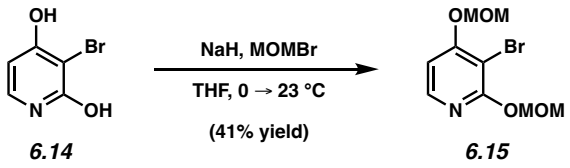

6.14 *6.15*

Bromopyridine 6.15: To a solution of diol **6.14** (3.0 g, 1.0 equiv, 15.8 mmol) in THF (160 mL, 0.10 M) at 0 °C was added sodium hydride (7.6 g, 12.0 equiv, 189 mmol, 60% dispersion in mineral oil) and bromomethyl methyl ether (7.7 mL, 6.0 equiv, 94.7 mmol) sequentially, in single portions. The reaction was stirred for 1 h at 0 °C before being warmed to 23 °C and stirred for 18 h. Upon completion, the reaction was quenched by addition of saturated aqueous NH_4Cl (20 mL) and the layers were separated. The aqueous layer was extracted with EtOAc (3 x 25 mL) and the combined organic layers were dried over Na_2SO_4 and concentrated under reduced pressure. Purification by flash chromatography (4:1 hexanes:EtOAc) followed by recrystallization from hexanes afforded bromopyridine **6.15** (1.8 g, 41% yield) as a white solid. Bromopyridine **6.15**: ^{1}H NMR (500 MHz, $CDCl_3$): δ 7.99 (dd, *J* = 5.5, 1H), 6.76 (dd, *J* = 5.5, 1H), 5.58 (s, 2H), 5.31 (s, 2H), 3.55 (s, 3H), 3.51 (s, 3H).

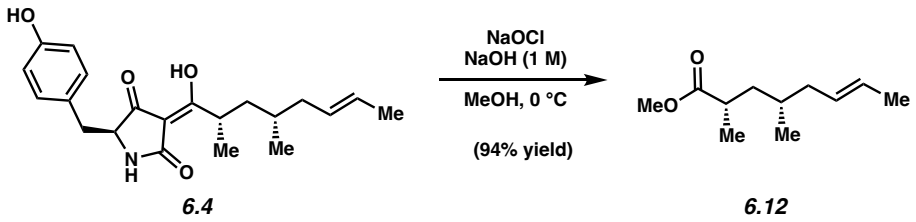

6.4 *6.12*

Methyl Ester 6.12: To solution of tetramic acid **6.4** (7.60 mg, 1.00 equiv, 21.3 μmol) in methanol (425 μL, 0.05 M) at 0 °C was added aq. NaOH (35.4 μL, 1 M) in one portion. Then, aq. NaOCl (106 μL, 0.2 M) was added dropwise over 30 seconds. After 3 minutes of stirring, a solution of aq. Na_2SO_3 (142 μL, 1 M) and a solution of aq. HCl (35.4 μL, 1 M) were added sequentially. The mixture was diluted with EtOAc (1 mL) and then warmed to 23 °C. The layers were separated and the aqueous layer was extracted with EtOAc (3 x 1 mL). The organic layers were combined and dried over Na_2SO_4 and concentrated under reduced pressure. Methyl ester **6.12** (3.7 mg, 94% yield) was used without further purification. Methyl Ester **6.12**: ^{1}H NMR (500 MHz, $CDCl_3$): δ 5.45–5.31 (m, 2H), 3.66 (s, 3H), 2.60–2.51 (m, 1H), 2.00–1.93 (m, 1H), 1.84–1.76 (m, 1H), 1.75–1.67 (m, 2H), 1.65 (d, *J* = 5.15, 3H), 1.48–1.39 (m, 1H), 1.14 (d, *J* = 7.03, 3H), 0.86 (d, *J* = 6.61, 3H); ^{13}C NMR (125 MHz, $CDCl_3$): δ 177.7, 129.5, 126.5, 51.6, 41.1, 40.2, 37.4, 31.2, 19.4, 18.1, 18.1.

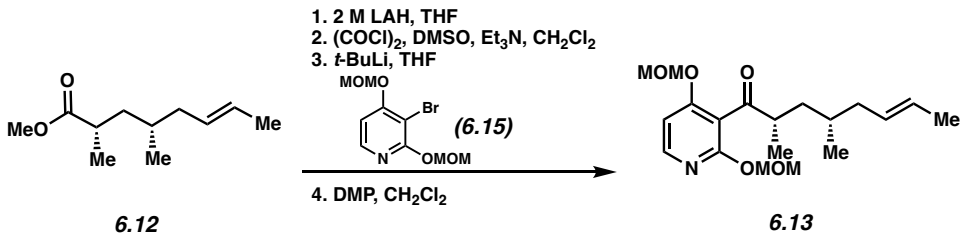

6.12 *6.13*

To a solution of methyl ester **6.12** (3.70 mg, 1.0 equiv, 20.1 μmol) in THF (669 μL, 0.030 M) at 0 °C was added a solution of lithium aluminum hydride in THF (20.1 μL, 2.0 equiv, 40.2 μmol, 2.0 M) dropwise over 1 minute. The reaction was stirred at 0 °C for 5 minutes and then warmed to 23 °C and stirred for 5 minutes. The reaction was then cooled to 0 °C and then quenched by the

addition water (0.5 mL) dropwise over 5 minutes and then diluted with EtOAc (1 mL) and warmed to 23 °C. The layers were separated and the aqueous layer was extracted with EtOAc (3 x 1 mL). The organic layers were combined and dried over Na_2SO_4 and concentrated under reduced pressure. The primary alcohol was used without further purification. Primary alcohol: ^{1}H NMR (500 MHz, $CDCl_3$): δ 5.42–5.37 (m, 2H), 3.51 (dd, *J* = 5.1, 10.6, 1H), 3.37 (dd, *J* = 6.7, 10.6, 1H), 1.79–1.69 (m, 2H), 1.66–1.63 (m, 3H), 1.58–1.50 (m, 2H), 1.33–1.29 (m, 2H), 0.92 (d, *J* = 6.67, 3H), 0.86 (d, *J* = 6.67, 3H).

To a solution of oxalyl chloride (34.9 μL, 1.5 equiv, 398 μmol) in CH_2Cl_2 (0.31 mL) at –78 °C was added a solution of DMSO (47.2 μL, 2.5 equiv, 664 μmol) in CH_2Cl_2 (76.8 μL, 3.5 M) dropwise over 1 minute. This solution was allowed to stir at –78 °C for 30 minutes and then previously prepared primary alcohol (41.5 mg, 1.0 equiv, 0.266 mmol) was added dropwise over 1 minute. The reaction was allowed to stir for 30 additional minutes. Triethylamine (0.18 mL, 1.33 mmol, 5.00 equiv) was then added dropwise over 1 minute and the reaction was stirred for an additional 30 minutes and then warmed to 23 °C. The reaction was then quenched with water (1 mL) and the layers were separated. The aqueous layer was extracted with CH_2Cl_2 (3 x 1 mL). The organic layers were combined and washed with aq. 2% HCl (1 x 1 mL), aq. 5% Na_2CO_3 (1 x 1 mL), and brine (1 x 1 mL). The organic layer was dried over Na_2SO_4 and concentrated under reduced pressure. The aldehyde was used without further purification.

To a solution of bromopyridine **6.15** (20.0 mg, 1.0 equiv, 71.9 μmol) in THF (719 μL, 0.1 M) at –78 °C was added *t*-BuLi (84.6 μL, 2.00 equiv, 1.7 M, 144 μmol) to the reaction over 1 minute. After stirring at –78 °C for 45 minutes, the previously prepared aldehyde (13.3 mg, 1.2 equiv, 86.3

μmol) was added. The reaction was stirred at –78 °C for 20 minutes and then was allowed to warm to 23 °C and stirred for 40 minutes. Methanol (1 mL) was added to the reaction and the solution was stirred for 5 minutes at 23 °C. The reaction was filtered through a small plug of $MgSO_4$ using EtOAc (10 mL) as the eluent. The volatiles were removed under reduced pressure and the crude mixture was purified by prep TLC (2:1 hexanes:EtOAc) to yield the secondary alcohol (6.7 mg, 26% yield).

To a solution of the secondary alcohol (20.3 mg, 1.0 equiv, 57.2 μmol) in CH_2Cl_2 (1.15 mL, 0.050 M) was added DMP (36.5 mg, 1.5 equiv, 36.5 mmol). The reaction was allowed to stir at 23 °C for 45 minutes and then was quenched with sat. aq. $Na_2S_2O_3$ (1 mL) and sat. aq. $NaHCO_3$ (1 mL). The layers were separated and the aqueous layer was extracted with CH_2Cl_2 (3 x 2 mL). The organic layer was filtered through a plug of Na_2SO_4 and concentrated under reduced pressure. The crude mixture was purified via prep TLC (2:1 hexanes:EtOAc) to afford ketone **6.13** (12.3 mg, 61% yield). ^{1}H NMR (500 MHz, $CDCl_3$): δ 8.06 (d, *J* = 6.0, 1H), 6.77 (d, *J* = 6.0, 1H), 5.53 (d, *J* = 6.1, 1H), 5.48 (m, *J* = 6.1, 1H), 5.39–5.32 (m, 2H), 5.19 (s, 2H), 3.47 (s, 3H), 3.44 (s, 3H), 3.14 (sextuplet, *J* = 7.1, 1H), 2.02–1.98 (m, 1H), 1.85 (quintuplet, *J* = 6.8, 1H), 1.80–1.73 (m, 1H), 1.62–1.59 (m, 5H), 1.19–1.10 (m, 4H), 0.88 (d, *J* = 6.67, 3H).

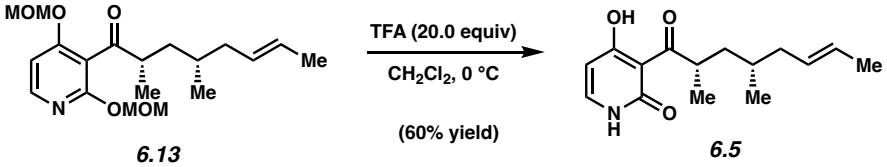

Pyridone 6.5: To a solution of ketone **6.13** (12.0 mg, 1.0 equiv, 34.1 μmol) in CH_2Cl_2 (683 μL, 0.050 M) at 0 °C was added TFA (52.6 μL, 20.0 equiv, 683 μmol). The reaction was stirred at this

temperature for 75 minutes and then quenched with sat. aq. $NaHCO_3$ (1 mL). The layers were separated and the aqueous layer was extracted with CH_2Cl_2 (3 x 1 mL). The combined organic layers were dried over Na_2SO_4 and concentrated under reduced pressure. The crude mixture was purified by prep TLC (2:1 hexanes:EtOAc) to afford pyridone **6.5** (5.5 mg, 60% yield). The spectral data matched the authentic sample.

6.5.3 Synthetic Biology Details

The details for DNA manipulation, protein expression, protein crystallization and structure determination and other extended and supplemental tables and figures are reported in the literature.[34] The atomic coordinates of PdxI, PdxI with **6.5**, PdxI with **6.8**, HpiI, and HpiI with **6.5** have been deposited in the Protein Data Bank (http://www.rcsb.org) under the accession code 7BQJ, 7BQK, 7BQL, 7BQP, and 7BQO, respectively.

6.5.4 Computational Details

Molecular coordinates of calculated structures using density functional theory (DFT) for both the non-enzymatic and enzymatic reactions are reported in the literature.[34] Initial conformational searches were conducted using Schrodinger's Maestro 2017-2 version 11.2.01441. The geometry of conformers were recalculated with the density functional and basis set ωB97X-D/6-31G(d,p) as implemented in Gaussian 16. This functional was chosen for its ability to reproduce CCSD geometry calculations of asynchronous Diels–Alder reactions as well as its general applicability for accurately calculating reaction barriers. Structures of interest were further optimized at the reported level of theory, ωB97X-D/6-311+G(d,p). Following Head-Gordon's suggested basis set for energetics, we computed single point energies at the ωB97X-D/def2-

QZVPP level of theory. We believe these methods to accurately calculate energetics for the reported systems and recommend them for use.

Classical molecular dynamics (MD) simulations were performed with the GPU code pmemd from the AMBER 16 package. Parameters for ligands were generated within the antechamber module with the general Amber force field (gaff) using RESP partial charges calculated at the HF/6-311+G(d,p) level of theory. Each simulation was solvated using the leap module in a pre-equilibrated TIP3P truncated octahedral box with a 17 Å buffer and neutralized by Na^+ counter ions. Subsequent calculations used the Stony Brook modification of the Amber14 force field (ff14sb). All dynamics simulations used a standard minimization, heating and equilibration protocol before beginning the 500-ns production run.

6.6 Notes and References

(1) Jamieson, C. S.; Ohashi, M.; Liu, F.; Tang, Y.; Houk, K. N. The Expanding World of Biosynthetic Pericyclases: Cooperation of Experiment and Theory for Discovery. *Nat. Prod. Rep.* **2019**, *36*, 698–713.

(2) Kim, H. J.; Ruszczycky, M. W.; Choi, S.; Liu, Y.; Liu, H.; Enzyme-Catalysed [4+2] Cycloaddition is a Key Step in the Biosynthesis of Spinosyn A. *Nature* **2011**, *473*, 109–112.

(3) Wever, W. J.; Bogart, J. W.; Baccile, J. A.; Chan, A. N.; Schroeder, F. C.; Bowers, A. A. Chemoenzymatic Synthesis of Thiazolyl Peptide Natural Products Featuring an Enzyme-Catalyzed Formal [4 + 2] Cycloaddition. *J. Am. Chem. Soc.* **2015**, *137*, 3494–3497.

(4) Ohashi, M.; Liu, F.; Hai, Y.; Chen, M.; Tang, M.-C.; Yang, Z.; Sato, M.; Watanabe, K.; Houk, K. N.; Tang, Y. SAM-Dependent Enzyme-Catalysed Pericyclic Reactions in Natural

Product Biosynthesis. *Nature* **2017**, *549*, 502–506.

(5) Bailey, S. S.; Payne, K. A.; Saaret, A.; Marshall, S. A.; Gostimaskaya, I.; Kosov, I.; Fisher, K.; Hay, S.; Leys, D. Enzymatic Control of Cycloadduct Conformation Ensures Reversible 1,3-Dipolar Cycloaddition in a prFMN-Dependent Decarboxylase. *Nat. Chem.* **2019**, *11*, 1049–1057.

(6) Chen, Q.; Gao, J.; Jamieson, C.; Liu, J.; Ohashi, M.; Bai, J.; Yan, D.; Liu, B.; Che. Y.; Wang, Y.; Houk, K. N.; Hu, Y. Enzymatic Intermolecular Hetero-Diels–Alder Reaction in the Biosynthesis of Tropolonic Sesquiterpenes. *J. Am. Chem. Soc.* **2019**, *141*, 14052–14056.

(7) Zhang, B.; Wang, K. B.; Wang, W.; Wang, X.; Liu, F.; Shu, J.; Shi, J.; Li, L. Y.; Han, H.; Xu, K.; Qiao, H. Y.; Shang, X.; Jiao, R. H.; Houk, K. N.; Liang, Y.; Tan, R. X.; Ge, H. M. Enzyme-Catalysed [6+4] Cycloadditions in the Biosynthesis of Natural Products. *Nature* **2019**, *568*, 122–126.

(8) Little, R.; Paiva, F. C. R.; Jenkins, R.; Hong, H.; Sun, Y.; Demydchuk, Y.; Samborskyy, M.; Tosin, M.; Leeper, F. J.; Dias, M. V. B.; Leadlay, P. F. Unexpected Enzyme-Catalysed [4+2] Cycloaddition and Rearrangement in Polyether Antibiotic Biosynthesis. *Nat. Catal.* **2019**, *2*, 1045–1054.

(9) Dan, Q.; Newmister, S. A.; Klas, K. R.; Fraley, A. E.; McAfoos, T. J.; Somoza, A. D.; Sunderhaus, J. D.; Ye, Y.; Shende, V. V.; Yu, F.; Sanders, J. N.; Brown, W. C.; Zhao, L.; Paton. R. S.; Houk, K. N.; Smith, J. L.; Sherman, D. H.; Williams, R. M. Fungal Indole Alkaloid Biogenesis Through Evolution of a Bifunctional Reductase/Diels–Alderase. *Nat. Chem.* **2019**, *11*, 972–980.

(10) Zhang, Z.; Jamieson, C. S.; Zhao, Y.-L.; Li, D.; Ohashi, M.; Houk, K. N.; Yang, Y.

Enzyme-Catalyzed Inverse-Electron Demand Diels–Alder Reaction in the Biosynthesis of Antifungal Ilicicolin H. *J. Am. Chem. Soc.* **2019**, *141*, 5659–5663.

(11) Gustin, D. J.; Mattei, P.; Kast, P.; Wiest, O.; Lee, L.; Cleland, W. W.; Hilvert, D. Heavy Atom Isotope Effects Reveal a Highly Polarized Transition State for Chorismate Mutase. *J. Am. Chem. Soc.* **1999**, *121*, 1756–1757.

(12) DeClue, M. S.; Baldridge, K. K.; Künzler, D. E.; Kast, P.; Hilvert, D. Isochorismate Pyruvate Lyase: A Pericyclic Reaction Mechanism? *J. Am. Chem. Soc.* **2005**, *127*, 15002–15003.

(13) Tian, Z.; Sun, P.; Yan, Y.; Wu, Z.; Zheng, Q.; Zhou, S.; Zhang, H.; Yu, F.; Jia, X.; Chen, D.; Mandi, A.; Kurtan, T.; Liu, W. An Enzymatic [4+2] Cyclization Cascade Creates the Pentacyclic Core of Pyrroindomycins. *Nat. Chem. Biol.* **2015**, *11*, 259–265.

(14) Woodward, R. B.; Hoffmann, R. The Conservation of Orbital Symmetry. *Angew. Chem., Int. Ed. Engl.* **1969**, *8*, 781–853.

(15) Nicolaou, K. C.; Snyder, S. A.; Montagnon, T.; Vassilikogiannakis, G. The Diels–Alder Reaction in Total Synthesis. *Angew. Chem., Int. Ed.* **2002**, *41*, 1668–1698.

(16) Corey, E. J.; Cheng, X. M. *The Logic of Chemical Synthesis*; Wiley: New York, New York, 1989.

(17) Hoffmann, H. M. R. The Ene Reaction. *Angew. Chem., Int. Ed. Engl.* **1969**, *8*, 556–577.

(18) Alder, K. Diene Synthesis and Related Reaction Types. *Nobel Lectures, Chemistry* 1950, 267–303.

(19) Niu, D.; Hoye, T. R. The Aromatic Ene Reaction. *Nat. Chem.* **2014**, *6*, 34–40.

(20) Mikami, K.; Shimizu, M. Asymmetric Ene Reactions in Organic Synthesis. *Chem. Rev.*

1992, *92*, 1021–1050.

(21) Jensen, A. W.; Mohanty, D. K.; Dilling, W. L. The Growing Relevance of Biological Ene Reactions. *Bioorg. Med. Chem.* **2019**, *27*, 686–691.

(22) Lin, C.-I.; McCarty, R. M.; Liu, H. The Enzymology of Organic Transformations: A Survey of Name Reactions in Biological Systems. *Angew. Chem., Int. Ed.* **2017**, *56*, 3446–3489.

(23) Snider, B. B.; Lu, Q. Total Synthesis of (±)-Pyridoxatin. *J. Org. Chem.* **1994**, *59*, 8065–8070.

(24) Snider, B. B.; Qing, L. A Two-Step Synthesis of Pyridoxatin Analogues. *Tetrahedron Lett.* **1994**, *35*, 531–534.

(25) Jones, I. L.; Moore, F. K.; Chai, C. L. L. Total Synthesis of (±)-Cordypyridones A and B and Related Epimers. *Org. Lett.* **2009**, *11*, 5526–5529.

(26) Cai, Y.; Hai, Y.; Ohashi, M.; Jamieson, C. S.; Garcia-Borras, M.; Houk, K. N.; Zhou, J.; Tang, Y. Structural Basis for Stereoselective Dehydration and Hydrogen-Bonding Catalysis by the SAM-dependent Pericyclase LepI. *Nat. Chem.* **2019**, *11*, 812–820.

(27) Appendino, G.; Cravotto, G.; Toma, L.; Annunziata, R.; Palmisano, G. The Chemistry of Coumarin Derivatives. Part VI. Diels–Alder Trapping of 3-Methylene-2,4-chromandione. A New Entry to Substituted Pyrano[3,2-c]coumarins. *J. Org. Chem.* **1994**, *59*, 5556–5564.

(28) Qiao, Y.; Xu, Q.; feng, W.; Tao, L.; Li, X.-N.; Liu, J.; Zhu, H.; Lu, Y.; Wang, J.; Qi, C.; Xue, Y.; Zhang, Y. Asperpyridone A: An Unusual Pyridone Alkaloid Exerts Hypoglycemic Activity through the Insulin Signaling Pathway. *J. Nat. Prod.* **2019**, *82*, 2925–2930.

(29) McBrien, K. D.; Gao, Q.; Huang, S.; Klohr, S. E.; Wang, R. R.; Pirnik, D. M.; Neddermann,

K. M.; Bursuker, I.; Kadow, K. F.; Leet, J. L. Fusaricide, a New Cytotoxic *N*-Hydroxypyridone from *Fusarium* sp. *J. Nat. Prod.* **1996**, *59*, 1151–1153.

(30) Li, C.; Sarotti, A. M.; Yang, B.; Turkson, J.; Cao, S. A New *N*-methoxypyridone from the Co-Cultivation of Hawaiian Endophytic Fungi *Camporesia sambuci* FT1061 and *Epicoccum sorghinum* FT1062. *Molecules (Basel, Switzerland)*, **2017**, *22*, 1166.

(31) Kho, Y.-H.; Chun, H-K.; Kim, H.-M.; Lee, H.-J.; Chung, M.-C.; Lee, C.-H. Pyridoxatin, an Inhibitor of Gelatinase A with Cytotoxic Activity. *J. Microbiol. Biotechnol.* **1996**, *6*, 445–450.

(32) Singh, M. S.; Nagaraju, A.; Anand, N.; Chowdhury, S. *ortho*-Quinone methide (*o*-QM): a Highly Reactive, Ephemeral and Versatile Intermediate in Organic Synthesis. *RSC Adv.* **2014**, *4*, 55924–55959.

(33) Singh, S.; Chang, A.; Goff, R. D.; Bingman, C. A.; Grüschow, S.; Sherman, D. H.; Phillips, G. N., Jr.; Thorson, J. S. Structural Characterization of the Mitomycin 7-*O*-Methyltransferase. *Proteins: Struct., Funct., Genet.* **2011**, *79*, 2181–2188.

(34) Ohashi, M.; Jamieson, C. S.; Cai, Y.; Tan, D.; Kanayama, D.; Tang, M.-C.; Anthony, S. M.; Chari, J. V.; Barber, J. S.; Picazo, E.; Kakule, T. B.; Cao, S.; Garg, N. K.; Zhou, J.; Houk, K. N.; Tang, Y. An Enzymatic Alder-ene Reaction. *Nature* **2020**, *586*, 64–69.

CHAPTER SEVEN

Thioesterase-Catalyzed Aminoacylation and Thiolation of Polyketides in Fungi

Adapted from: Man-Cheng Tang,† Curt R. Fischer,† Jason V. Chari, Dan Tan, Sundari Suresh, Angela Chu, Molly Miranda, Justin Smith, Zhuan Zhang, Neil K. Garg, Robert P. St. Onge, and Yi Tang.

J. Am. Chem. Soc. **2019**, *141*, 8198–8206.

7.1 Abstract

Fungal highly reducing polyketide synthases (HRPKSs) biosynthesize polyketides using a single set of domains iteratively. Product release is a critical step in HRPKS function to ensure timely termination and enzyme turnover. Nearly all of the HRPKSs characterized to date employ a separate thioesterase (TE) or acyltransferase enzyme for product release. In this study, we characterized two fungal HRPKSs that have fused C-terminal TE domains, a new domain architecture for fungal HRPKSs. We showed that both HRPKS-TEs synthesize aminoacylated polyketides in an ATP-independent fashion. The KU42 TE domain selects cysteine and homocysteine and catalyzes transthioesterification using the side-chain thiol group as the nucleophile. In contrast, the KU43 TE domain selects leucine methyl ester and performs a direct amidation of the polyketide, a reaction typically catalyzed by nonribosomal peptide synthetase (NRPS) domains. The characterization of these HRPKS-TE enzymes showcases the functional diversity of HRPKS enzymes and provides potential TE domains as biocatalytic tools to diversify HRPKS structures.

7.2 Introduction

In thiol-templated biosynthesis catalyzed by polyketide synthases (PKSs) and nonribosomal peptide synthetases (NRPSs), product release is an essential step in ensuring enzyme turnover. In bacterial PKSs where multidomain modules are arranged in an assembly-line-like fashion, C-terminal thioesterase (TE) domains are used to release the polyketide product via hydrolysis or macrocyclization.[1] Fungal highly reducing PKSs (HRPKSs),[2] on the other hand, consist of a single set of catalytic domains that are used iteratively. The domain architecture of fungal HRPKSs resembles a single module of bacterial type I modular PKSs. In contrast to bacterial product release strategies, many fungal HRPKSs studied to date use a separate, dissociated TE enzyme or acyltransferase to release the polyketide chain through hydrolysis or transesterification (Figure 7.1A).[3] Both examples are represented in the lovastatin biosynthetic pathway:[4] TE LovG hydrolyzes dihydromonacolin L acid from LovB, and acyltransferase LovD transfers α-methylbutyrate from LovF to monacolin L acid and affords lovastatin acid (Figure 7.1A). In tandem PKS systems, the product of the HRPKS can be offloaded by the *N*-terminal starter unit–ACP transacylase (SAT) domain of a nonreducing PKS (NRPKS).[5] Other modes of product release from HRPKS not catalyzed by TE have been reported in several recent studies.[6]

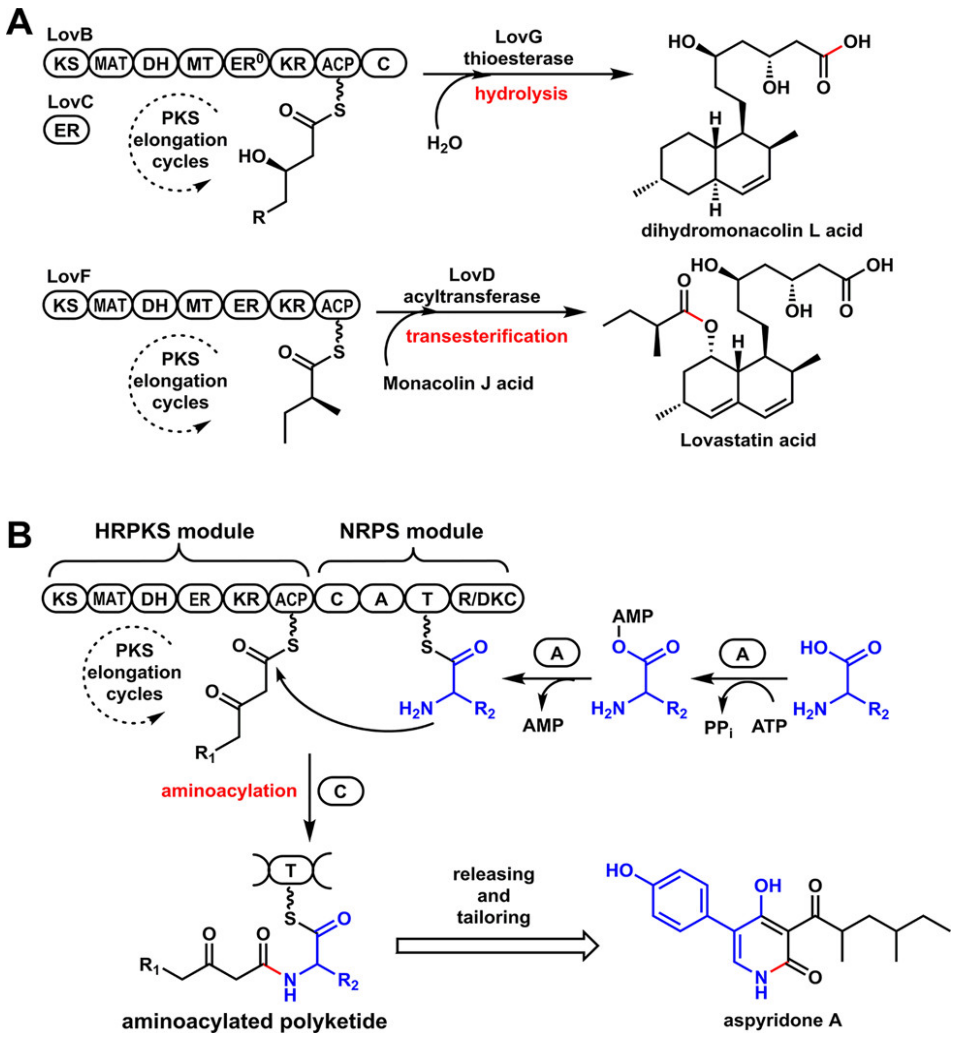

Figure 7.1. Known product-releasing mechanisms of fungal HRPKSs. (A) Product release is catalyzed by a separate TE or acyltransferase through hydrolysis or transesterification. (B) The C domain serves as the releasing domain in the biosynthesis of fungal aminoacylated polyketide products. Domain abbreviations: KS, ketosynthase; MAT, malonyl-CoA:ACP transacylase; DH, dehydratase; MT, methyltransferase; ER, enoyl reductase; KR, ketoreductase; ACP, acyl carrier protein; C, condensation; A, adenylation; T, thiolation; R, reductase.

Many fungal polyketides are aminoacylated and further modified to have significant biological activities, as exemplified by cytochalasin E (antiangiogensis),[7] pseurotin A

(immunosuppressant),[8] and UCS1025A (anticancer).[9] These natural products are synthesized by HRPKS-NRPS hybrid enzymes.[10] The adenylation domain in the *C*-terminal NRPS module uses one ATP molecule to activate a specific amino acid followed by acyl transfer to the thiolation (T) domain. The condensation domain (C) then serves as an HRPKS-releasing domain in principle by transferring the completed polyketide acyl chain from the ACP domain of the HRPKS module to the T domain in the NRPS module as an aminoacylated polyketide, forming an amide bond (Figure 7.1B).[10]

The iterative nature of fungal HRPKSs dictates that a single set of domains is used repeatedly during elongation and tailoring of the polyketide chain. Hence, the releasing domain/enzyme is necessary to ensure that the correct polyketide product, once formed, is released promptly. Previous studies showed that in the absence of releasing domains, the HRPKS comes to a halt because of the occupancy of the ACP domain[11] or functions aberrantly to yield products of incorrect sizes.[12] Therefore, understanding the different mechanisms of product release is a key aspect of decoding HRPKS programming rules. Genome mining of fungal HRPKSs with an emphasis on finding unusual product release domains can lead to the discovery of new products. For example, we previously identified a clade of HRPKSs that are terminated with a *C*-terminal domain with sequence homology to carnitine *O*-acyltransferase (cAT).[13] The reversible nature of the cAT was a key feature that enabled the complete execution of Tv6-931 programming steps.

Recently, our genome mining efforts identified a group of fungal HRPKSs with fused terminal TE domains that differ from all characterized HRPKSs to date. These architecturally distinct HRPKSs had no known associated products.[14] Two such gene clusters, KU42 and KU43, mined from the genomes of basidiomycete fungal species *Punctularia strigosozonata* and

Hydnomerulius pinastri, respectively, contain genes encoding HRPKS-TE belonging to this family (Figure 7.2).[14] Bioinformatic analysis indicated that within the KU42 cluster, genes encoding an HRPKS-TE, three P450s, an oxidoreductase, a PAP2-like protein, a hypothetical protein, and a major facilitator superfamily transporter (Figure 7.2A) are found. When KU42 HRPKS-TE and the three P450s were introduced together into engineered yeast strain RC01, two aminoacylated products (**7.1** and **7.2**, as shown in Figure 7.2A) were identified.[14] In parallel, genes from KU43 clusters encode an HRPKS-TE, four P450s, two carboxyl methyltransferases (C-MTs), and others (Figure 7.2B). The expression of the KU43 HRPKS-TE together with the four P450s and two C-MTs in engineered yeast strains resulted in the production of an aminoacylated polyketide **7.3** (Figure 7.2B).[14] The structures of aminoacylated polyketides were surprising based on known fungal HRPKS programming rules because enzymes responsible for amino acid activation and incorporation, such as NRPS and CoA-ligase, are absent in the two gene clusters.

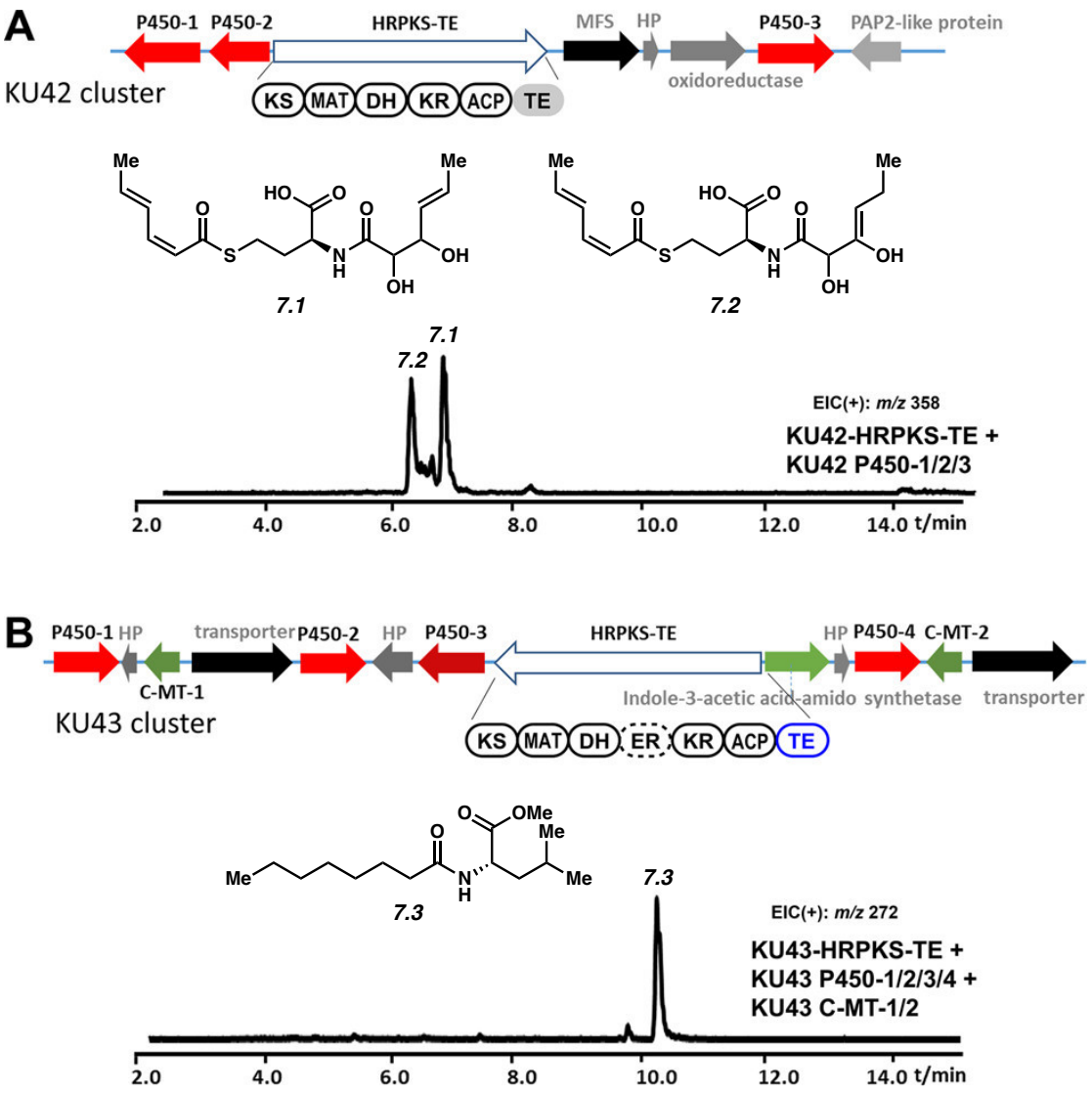

Figure 7.2. Genome mining of fungal secondary metabolite biosynthetic gene clusters containing a gene encoding HRPKS-TE megasynthase. (A) KU42 cluster mined from *P. strigosozonata* and the production of **7.1** and **7.2** in yeast. (B) KU43 cluster mined from *H. pinastri* and the production of **7.3** in yeast. HP, hypothetical protein; PAP2, type 2 phosphatidic acid phosphatase; MFS, major facilitator superfamily; C-MT, carboxyl methyltransferase. Shown are the traces of an extracted-ion chromatogram. In control traces from strains transformed with a vector only, these compounds were not found.

Here we studied the biosynthetic mechanisms of these HRPKS-TE enzymes and showed that the amino acids are directly incorporated by the fused TE domains. In the case of KU42, we demonstrate that the TE domain can catalyze a transthioesterification with thiol-containing amino acids followed by an S–N shift to form the amide bond.

7.3 Results and Discussion

7.3.1 Sequence Analysis of the KU42 TE Domain

7.1 and **7.2** are closely related compounds containing an *S*,*N*-diacylated homocysteine. The acyl groups appear to originate from the same dienoyl triketide precursor. In the absence of any apparent amino acid activation domain, we hypothesized that **7.1** and **7.2** were formed by the KU42 HRPKS-TE domain and that homocysteine is used to release the polyketide chains. The amino and the thiol groups of homocysteine serve as nucleophiles to perform aminoacylation and thiolation, respectively, to form the diacylated adduct. We propose that the amino acid specificity is likely controlled by the TE domain. Sequence analysis revealed that the TE domain, like many other PKS TE domains, is a member of the serine α/β hydrolase domain superfamily.[15] The TE domain contains a cysteine residue (C2040) instead of serine as the conserved active site nucleophile, while the other two residues of the conserved catalytic triad, D2056 and H2225, have the usual identity.[1b,16]

Homology searches against predicted fungal protein sequences revealed that similar TE domains are encoded on a diverse set of fungal genomes. Of 500 BLAST hits retrieved (with *E* values of between 2×10^{-41} and 0.127), 37 coded for cysteine as the active site nucleophile while 452 had serine (7 coded for alanine at this position; 3 other sequences had other residues or alignment gaps in the conserved position). The occurrence of cysteine or serine in this key active

site position was independent of phylogeny, suggesting that the mutation to cysteine has occurred multiple times in the evolution of this domain. Cysteine active site nucleophiles have been observed in some starter-unit:ACP transacylase domains in fungal nonreducing PKSs, although the biochemical reason for this substitution over serine is unclear.[17] A recent report from the Wencewicz group reported that a cysteine nucleophile in a TE domain is required for the cyclization of β-lactone product obafluorin.[18] It was proposed that the thioester intermediate is at a higher ground-state energy compared to the oxyester, and thus is favorable in driving β-lactone formation.[18]

7.3.2 Functional Characterization of KU42-HRPKS-TE

To identify the product synthesized by KU42-HRPKS-TE alone, the gene was cloned under the ADH2 promoter on a 2 μ plasmid and transformed to engineered *S. cerevisiae* strain BJ5464-NpgA.[11] After 4 days of culturing followed by extraction with ethyl acetate (containing 1% acetic acid), we observed the accumulation of several new metabolites (Figure 7.3A). The major product is **7.4** with a molecular weight (MW) of 309, and the minor product is **7.5** with a MW of 323. These compounds were isolated and characterized by NMR. Compound **7.4** was elucidated to be disorbyl cysteine, in which both of the thiol group and the amine group of cysteine were acylated with sorbic acid (Figure 7.3A). On the basis of the value of proton coupling constants obtained from the ^{1}H NMR spectrum (J = 11.2 Hz for H2–H3 and H2′–H3′, 14.0 Hz for H4–H5 and H4′–H5′) and published literature values for sorbate with different olefin stereochemistry,[19] the double-bond configurations in **7.4** were assigned to be 2-*cis*-4-*trans*-sorbyl. Similar to **7.4**, the structure of **7.5** was also elucidated in which the L-cysteine unit in

compound **7.4** was replaced by L-homocysteine (Figure 7.3A). **7.5** is therefore likely oxidized to **7.1** and **7.2** when the P450 enzymes were coexpressed in yeast (Figure 7.2A).

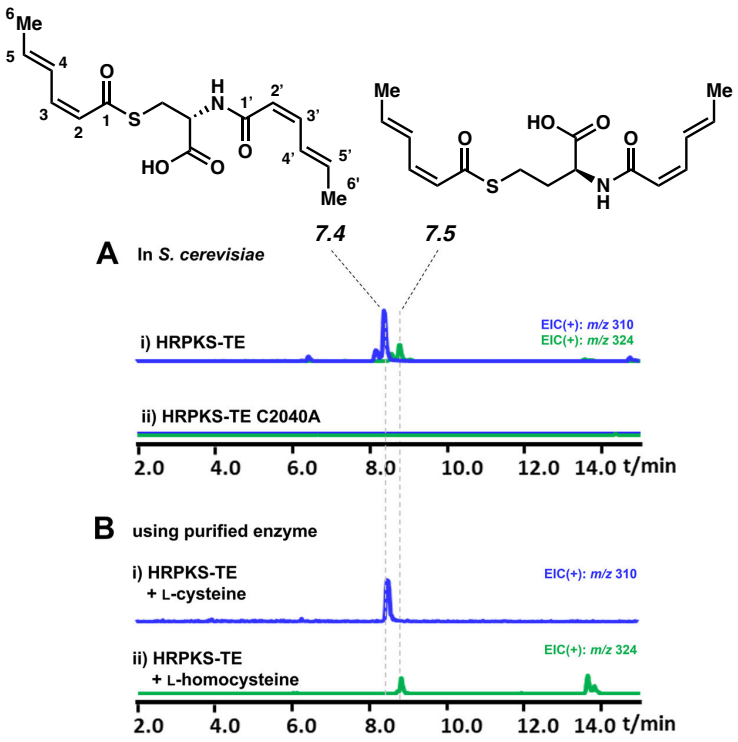

Figure 7.3. Characterization of KU42 HRPKS-TE in vivo and in vitro. Shown are the extracted-ion chromatograms. (A) Expression of HRPKS-TE and C2040A mutants in yeast and the structures of the compounds produced. (B) LC–MS analysis of the in vitro assays of purified HRPKS-TE in the presence of malonyl-CoA, NADPH, and L-cysteine or L-homocysteine.

To confirm that KU42 HRPKS-TE alone is sufficient for the biosynthesis of **7.4** and **7.5**, recombinant enzyme (246.2 kDa) was purified from yeast to homogeneity by anti-FLAG resin column chromatography. An assay of the enzyme in the presence of malonyl-CoA, NADPH, and L-cysteine yielded **7.4** as expected (Figure 7.3B). When L-cysteine was replaced by L-homocysteine, the production of **7.5** was confirmed (Figure 7.3B). When the enzyme was

assayed in the presence of equimolar amounts of L-cysteine and L-homocysteine (1 mM), the production of both **7.4** and **7.5** was detected, with **7.4** as the predominant product. ATP was not necessary in these assays to activate the amino acids, as expected because there is no adenylation domain in the enzyme. The collective in vivo and in vitro assays confirm that HRPKS-TE alone is able to add two molecules of the polyketide product onto either cysteine (preferred substrate) or homocysteine, forming the *S*,*N*-diacylated products without the use of a condensation or adenylation domain.

7.3.3 KU42 HRPKS-TE Substrate Scope and Proposed Reaction Mechanism

We then investigated the function of the TE domain in KU42 HRPKS-TE. We first constructed TE active-site mutant C2040A in which the putative cysteine nucleophile was mutated into alanine. When transformed into yeast, the mutant lost the ability to biosynthesize **7.4** and **7.5** (Figure 7.3A), indicating that both polyketide chain release and amino acid incorporation require the cysteine nucleophile. The mutation of putative general base H2225 to either Ala or Asn similarly abolished the function of the enzyme. When the active-site nucleophile was changed from cysteine to serine (C2040S) and expressed in yeast, we also did not observe the formation of either **7.4** or **7.5**. We further subjected these culture supernatants to untargeted metabolite analysis using XCMS.[20] This analysis revealed that the C2040S mutant, but not C2040A or H2225A, produced a unique compound not produced by wild-type HRPKS-TE and has an ion mass of 113.0597 Da, corresponding to the molecular formula of sorbic acid ($C_6H_8O_2$) plus a proton. This peak indicates that the C2040S mutant retained the ability to synthesize the polyketide product but is unable to perform aminoacylation or thiolation. Instead, the product appears to be prone to hydrolysis, analogous to the cysteine to serine mutation

observed in the obafluorin TE domain.[18] Although it is not clear whether such hydrolysis occurs as a S2040-sorbyl oxyester or via direct hydrolysis from the ACP, this result confirms the necessity of the cysteine as an active site nucleophile.

We attempted to express and purify the standalone TE domain from *E. coli* BL21(DE3) but failed to obtain soluble protein. We were successful in the expression of the TE domain together with the upstream ACP domain, ACP-TE, as an *N*-terminal His_6-tagged fusion protein. To test the function of ACP-TE, acyl-*S*-*N*-acetyl cysteamine (SNAC) compounds were added to the enzyme and analyzed by LC–MS to determine whether one or two acyl groups are transferred to the amino acid nucleophile. Because of the instability of sorbyl-SNAC, we used an available acyl-SNAC, (*S*)-3-hydroxyoctanoyl-SNAC (**7.12**),[21] as a substrate analog (Figure 7.4A). Compared to the negative control, we were able to detect the formation of three different products: one has a MW of 419, which is expected for diacylated product **7.13**; another product has a MW of 277, which corresponds to the MW of the monoacylated product **7.14**; the third compound has a MW of 552, which corresponds to that of **7.15**, a dimer of **7.14** formed though the oxidative coupling of free thiol groups to form a disulfide (Figure 7.4A). When tris(2-carboxyethyl)phosphine (TCEP) was included in the assay, the formation of **7.15** was no longer detected and only **7.13** and **7.14** were formed. This supports the proposed relationship of **7.14** and **7.15**. Together with the mutagenesis results, these results confirmed that the TE domain is indeed responsible for the acylation reactions.

A

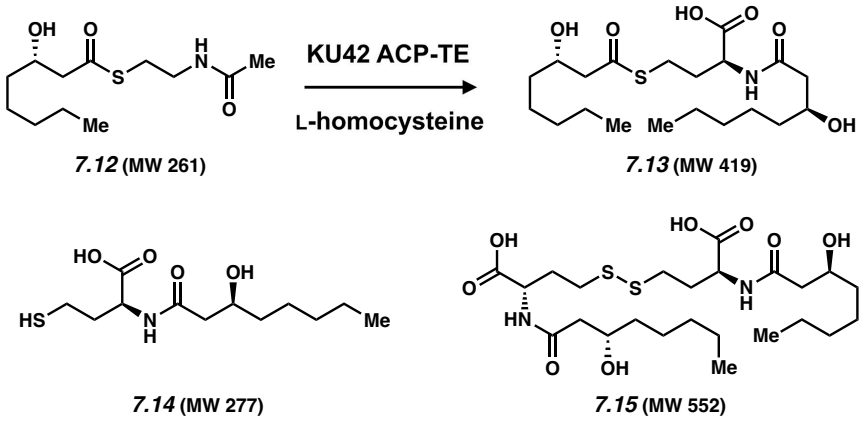

B

acyl-SNAC	nucleophile	product	yield
butyryl-SNAC	L-cysteine	*N,S*-dibutyryl	+++
butyryl-SNAC	D-cysteine	*N,S*-dibutyryl	+++
butyryl-SNAC	L-homocysteine	*N,S*-dibutyryl	++
butyryl-SNAC	L-methionine	-	-
butyryl-SNAC	L-serine	-	-
butyryl-SNAC	*N*-acetyl-L-cysteine	*S*-butyryl	++
butyryl-SNAC	mercaptoethanol	-	-
butyryl-SNAC	β-alanine	-	-
3-oxo-butyryl-SNAC	L-cysteine	-	-
3-OH-butyryl-SNAC	L-cysteine	-	-
3-oxo-hexanoyl-SNAC	L-cysteine	*N,S*-di-3-oxo-hexanoyl	+
3-OH-octanoyl-SNAC ***7.12***	L-cysteine	*N,S*-di-3-OH-octanoyl	+++

Figure 7.4. Assaying the KU42 TE domain with different acyl and amino acid substrates reveals the biochemical mechanism. (A) Product analysis of the in vitro assays of KU42 ACP-TE in the presence of L-homocysteine and **7.12**. In the negative control, boiled enzyme was used. (B) Summary of products formed by using different amino acids and acyl-SNAC substrates.

The substrate scope of the TE domain was further assayed using different acyl-SNAC and amino acid substrates (Figure 7.4B). When L-cysteine was used as the nucleophile, several acyl-SNAC substrates with different acyl chain lengths (from C4 to C8) could be used as the acyl donors by the TE domain. Among the C4 substrates, only butyryl-SNAC was accepted by the TE domain. Using butyryl-SNAC as the acyl donor, different amino acid nucleophiles were tested

for the formation of mono- and dibutyryl adducts. One key trend that emerged, which is consistent with amino acid incorporated into **7.4** and **7.5**, is that amino acids without a free thiol group cannot be used as nucleophiles, such as L-serine and L-methionine. Interestingly, D-cysteine can also be accepted by the TE domain as a nucleophile to form the dibutyryl-D-cysteine product. Importantly, when *N*-acetyl-L-cysteine was used as the nucleophile, we observed the formation of a monobutyryl adduct by LC–MS. This product, unlike **7.14**, does not undergo air oxidation to form a dimer, suggesting that the free thiol group is acylated by the butyryl unit.

From these in vitro assay results of the TE domain with different substrates, a possible catalytic mechanism for the formation of diacylated products **7.4** and **7.5** can be proposed. We propose that the TE domain is a bona fide acyltransferase that can catalyze the transthioesterification between the side-chain thiol nucleophile and the sorbyl-*S*-ACP thioester to release the product. When L-homocysteine is used as the releasing nucleophile, the TE domain would catalyze the transthioesterification reaction to yield *S*-sorbyl homocysteine. This is followed by a spontaneous intramolecular *S*- to *N*-acyl shift to form the *N*-sorbyl homocysteine to regenerate a free thiol group. This type of uncatalyzed rearrangement reaction is widely used in native chemical ligation to synthesize peptides and small proteins.[22] With the thiol group now free to react, the TE domain catalyzes the second transthioesterification reaction of *N*-sorbyl homocysteine to form disorbyl homocysteine **7.5** (Figure 7.6). Therefore, the TE domain does not catalyze direct aminoacylation but instead catalyzes the unprecedented release of polyketide products using the side-chain thiol of cysteine or homocysteine.

7.3.4 Delineating the Stereoselectivity of KR and DH Domains of KU42 HRPKS-TE in the Synthesis of 2-*cis*-4-*trans*-Sorbyl Polyketide Chain

A surprise in the structures of **7.4** and **7.5** is that they contain both *cis*- and *trans*-double bonds. Several HRPKSs have been proposed to biosynthesize polyketides with both *cis* and *trans* olefins, such as in the sordarin pathway.[23] Cox and co-workers recently reported that StPKS1 from *Strobilurus tenacellus* can produce a polyketide containing both *cis*- and *trans*-olefins.[24] However, the programming rules that govern the formation of mixed olefins from a single set of KR and DH domains are unknown. A working hypothesis is that the KR domain reduces the β-keto functionality with opposite stereochemistry after the two chain elongation steps. The two oppositely configured alcohol substrates bind in the DH active site differently for *syn* elimination, leading to either *cis* or *trans* products. We previously showed in the hypothemycin HRPKS, the stereochemistry (L or D) of KR-catalyzed β-ketoreduction is chain-length-dependent.[25] It is also well documented that the stereochemistry of the reduced alcohol can affect the stereoselectivity of the DH-catalyzed dehydration reaction.[26]

To test this hypothesis, we first verified that the HRPKS product is indeed the 2-*cis*-4-*trans* sorbyl chain and that the TE domain is not involved in the *trans–cis* isomerization of the second olefin. We constructed a truncated version of KU42 HRPKS-TE lacking the TE domain (HRPKS ΔTE). An assay of the truncated enzyme in the presence of only malonyl-CoA yielded triacetic acid lactone (see Section 7.5.2), confirming that the elongation domains are active. The addition of NADPH led to no detectable polyketide products because there is no releasing domain (see Section 7.5.2). To enable release, we added a heterologous TE domain from an unrelated PKS13, which was previously demonstrated to have promiscuous substrate specificity in ACP-thioester hydrolysis,[27] to the reaction mixture. Under this condition, we observed the

turnover of a new product that had a UV spectrum similar to that of 2-*trans*-4-*trans*-sorbic acid but a different retention time (see Section 7.5.2). We synthesized an authentic standard of 2-*cis*-4-*trans*-sorbic acid (see Section 7.5.1), which matched that released from the enzymatic assay. This confirmed that the polyketide produced by KU42 HRPKS is indeed the 2-*cis*-4-*trans*-sorbate, and no post-PKS isomerization of a *trans–trans* product is required.

We next examined the stereoselectivity of the KR domain toward β-keto substrates of different sizes. We assayed the HRPKS-TE with three different β-ketoacyl-SNAC compounds in the presence of NADPH and analyzed the β-keto reduced products using chiral HPLC and synthetic standards (Figure 7.5). Diketide acetoacetyl-SNAC (**7.6**)[25] and triketide 3-oxohexanoyl-SNAC (**7.7**)[25] were both reduced to the corresponding β-hydroxyacyl-SNAC, and the retention time matched that of **7.6D** and **7.7D** (the D configuration of the hydroxyl products),[25] respectively (Figure 7.5). Hence the KR specificity does not vary with chain length. We then assayed the product stereochemistry using 3-oxo-4-*trans*-hexenoyl-SNAC (**7.8**),[28] of which the acyl chain is the natural triketide of the KR domain. Surprisingly, the product elution time matched that of **7.8L**. To further verify the stereochemistry of this product, we scaled up the reaction and purified sufficient amounts of **7.8L** by HPLC. The structure was verified by NMR analysis, and the optical rotation ($[\alpha]_D^{27}$ +13, c = 0.2, $CHCl_3$) matched the reported value of **7.8L** ($[\alpha]_D^{25}$ +17, c = 0.42, CH_2Cl_2).[28] Our studies therefore revealed an unexpected layer of fungal HRPKS programming complexity in that the stereoselectivity of the KR domain depends on the degree of unsaturation of the substrate. In this case, changing from a single bond in the substrate (in **7.7**) to the double bond (in **7.8**) completely reversed the stereochemical outcome. The stereochemical switch from diketide **7.6** (in the D configuration) to triketide **7.8** (in the L

configuration) is most likely the cause of the subsequent different dehydration stereochemical outcomes.

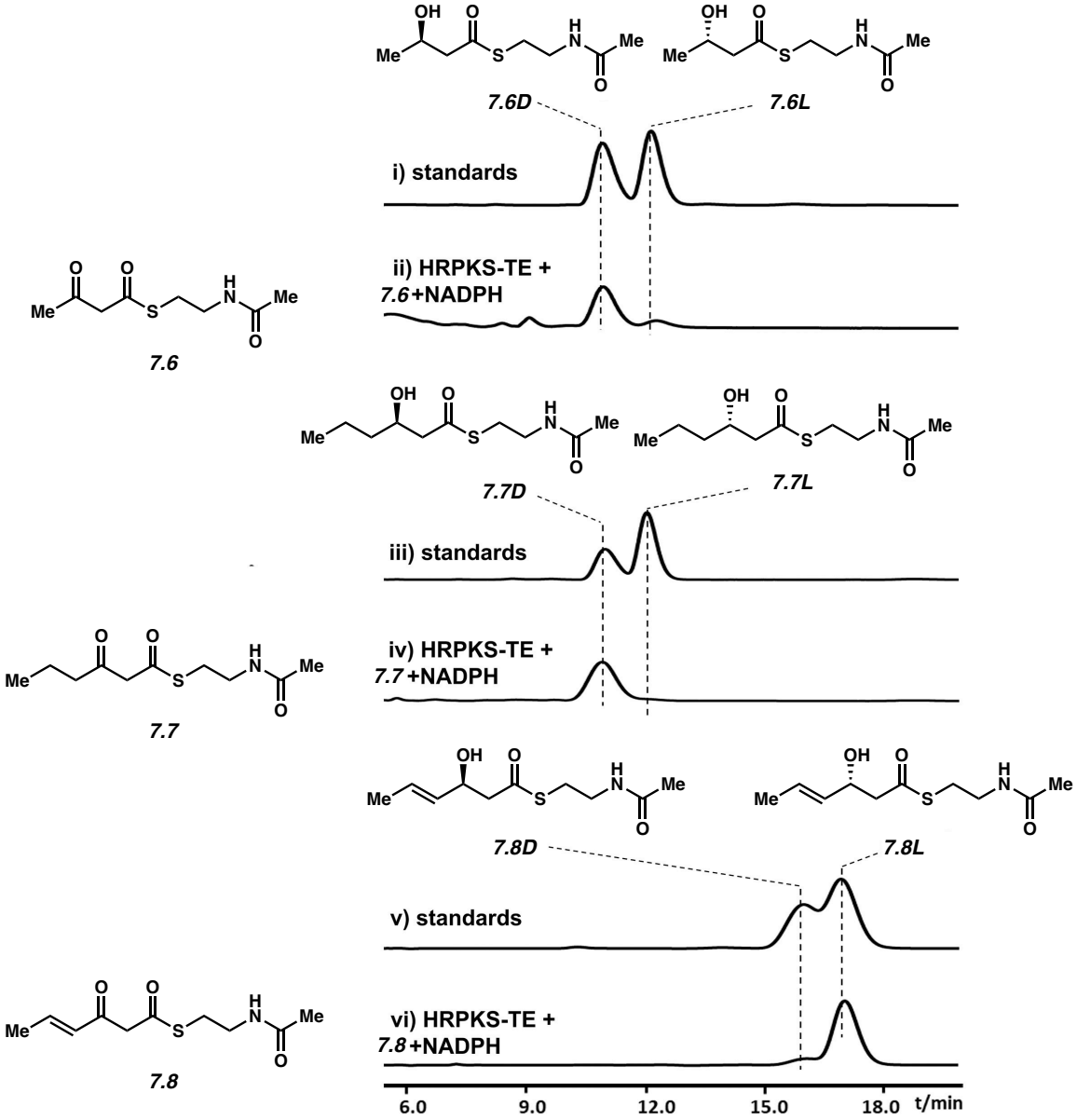

Figure 7.5. Biochemical characterization of the function of KU42-HRPKS-TE KR domain in vitro. Shown are the HPLC traces at 240 nm.

PKS DH domains generally catalyze the syn dehydration of their substrates.[29] Cane and co-workers showed that in the biosynthesis of fostriecin, the double-bond configurations

produced by DH domains were determined by the stereoconfiguration of the β-hydroxy group that is controlled by KR domains.[26b] We therefore propose that because of the different stereochemistry of the β-hydroxyl group in **7.6D** and **7.8L**, the substrates will bind differently in the active site of the DH domain, leading to *trans* and *cis* geometry of the dehydrated olefin, respectively. When diketide substrate **7.6D** was incubatesd with KU42 HRPKS-TE, we detected the formation of new product **7.9** (MW 187). The compound was purified from scaled-up in vitro assays and was shown to be *trans*-crotonoyl-SNAC. No dehydration product was detected when **7.6L** was used as the substrate, indicating strict substrate specificity of the DH domain in the diketide stage. When **7.8L** was tested as the substrate, we also detected the formation of dehydration product **7.10** (MW 213). However, after purification from scaled-up in vitro assays, the product was shown to be 2-*trans*-4-*trans*-sorbyl-SNAC, not the expected 2-*cis*-4-*trans*-sorbyl-SNAC. Assaying DH domains that produce *cis*-configured olefin have documented difficulties due to the isomerization of the double bond, that is, α,β to the thioester.[26d,30] Similarly, we proposed that the formation of 2-*trans*-4-*trans*-sorbyl-SNAC is due to the rapid cis-to-trans isomerization of 2-*cis*-4-*trans* sorbyl product, which could be catalyzed by nucleophiles such as *N*-acetylcysteamine through a Michael addition and a retro-Michael addition.[31] *N*-Acetylcysteamine itself could form through the decomposition of acyl-SNAC substrates. Although we were not able to prove the dehydration specificity of the DH domain in these experiments directly, our demonstration of unexpected KR programming rules and comparison to knowledge accumulated for the bacterial DH domains can rationalize the formation of *cis* and *trans* olefins in the same polyketide product by a single fungal HRPKS (Figure 7.6).

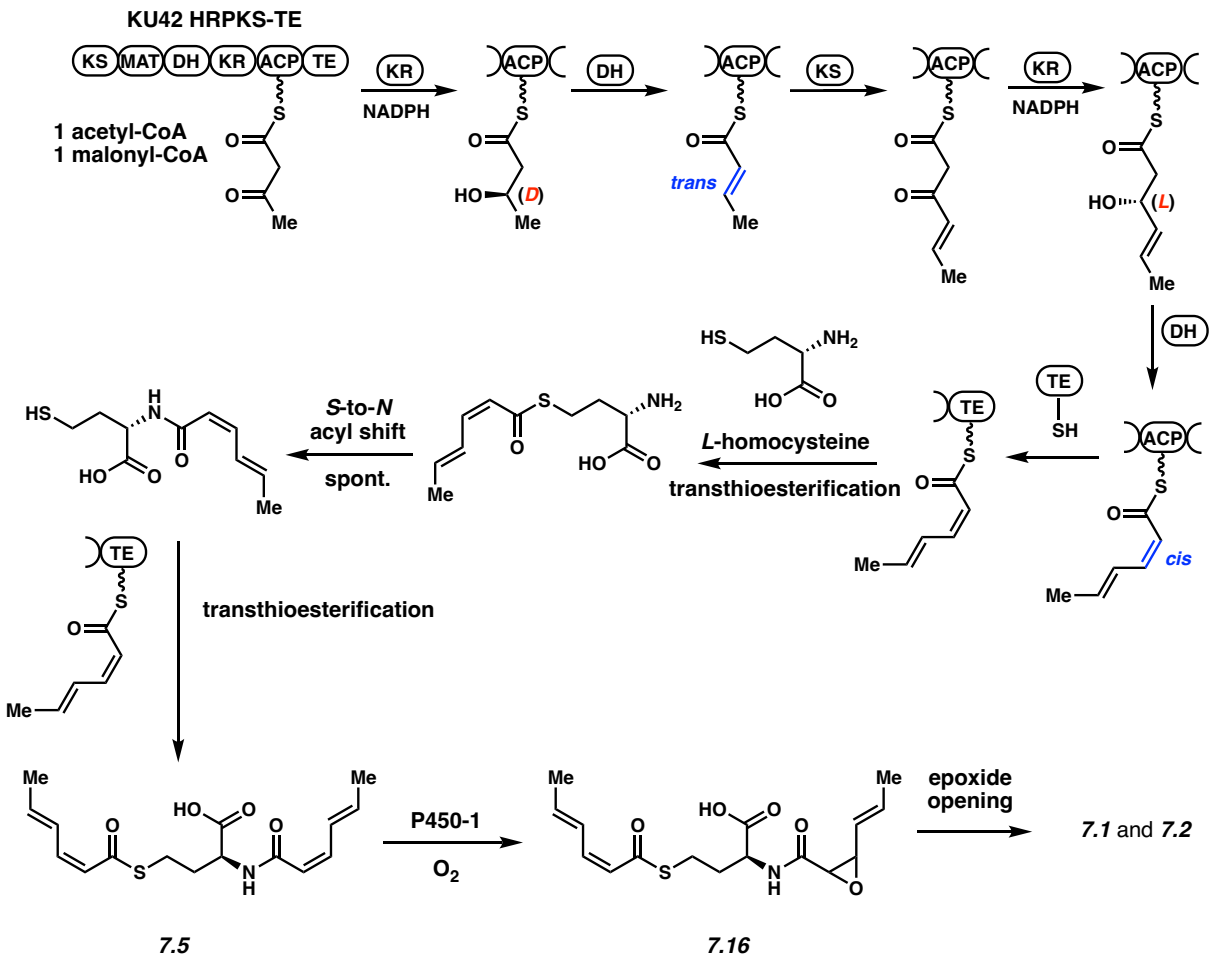

Figure 7.6. Proposed biosynthetic pathway for **7.5**.

7.3.5 Characterization of the Roles of the Three P450s from the KU42 Cluster

Our results showed that the major product of KU42 HRPKS-TE when expressed in yeast or assayed in vitro is **7.4**, the disorbyl-L-cysteine. However, we also showed that when KU42 HRPKS-TE was coexpressed with three P450s enzymes from the KU42 cluster in yeast, the products were **7.1** and **7.2**, which are derived from the homocysteine containing **7.5** (Figure 7.2A).[13] The two hydroxyl groups in **7.1** and **7.2** are presumably formed from the water-mediated opening of an epoxide precursor. To explore the roles of these P450s in the biosynthesis of **7.1** and **7.2**, coexpression experiments of the HRPKS-TE and individual P450 in *S. cerevisiae*

RC01[32] were performed. Coexpression with either P450-2 or P450-3 did not lead to the formation of **7.1** and **7.2**. When KU42 HRPKS was coexpressed with P450-1, both **7.1** and **7.2** could be detected. Therefore, we assign P450-1 to be an epoxidase that catalyzes the selective epoxidation of one of the *cis* olefin in **7.5** to form unstable product **7.16**, which can be readily hydrolyzed to form **7.1** and **7.2** under a culturing condition (Figure 7.6). P450-1 appears to be selective for homocysteine adduct **7.5** because no cysteine-derived analogs of **7.1** and **7.2** can be detected in the culture.

The overall biosynthetic pathway to **7.1** and **7.2** from KU42 HRPKS-TE is shown in Figure 7.6. Formation of the 2-*cis*-4-*trans*-sorbyl polyketide chain is proposed to involve the programmed stereoselectivities of the KR domain, which in turn influences the dehydration stereochemistry. The TE domain then catalyzes two transthioesterification steps using either cysteine or homocysteine. The second transthioesterification follows an *S–N* rearrangement to afford **7.4** or **7.5**, respectively. While **7.4** does not appear to be further processed, **7.5** is selectively epoxidized by P450-1 to **7.16**, which can be attacked by water to afford both **7.1** and **7.2**. The exact natural product of the KU42 pathway is unknown and is the subject of future studies.

7.3.6 Factors That Influence Cysteine to Homocysteine Incorporation Levels

Our in vitro experiments clearly indicated that HRPKS-TE in fact prefers cysteine over homocysteine, yet on the basis of in vivo reconstitution results with P450-1, homocysteine is the preferred substrate for yielding the natural product of the pathway. Therefore, the in vivo ratio of cysteine to homocysteine should impact product distributions and the roles of other enzymes in the cluster. To test this idea, we utilized CRISPRi-mediated gene repression, coupled to a

targeted metabolomics readout. We integrated the KU42 HRPKS-TE gene into a yeast haploid strain and mated this strain to 41 CRISPRi strains[33] expressing different guide RNAs directed against 1 of 17 genes involved in homocysteine and cysteine biosynthetic pathways. The resulting diploid strains were then cultured in 96-well plates in the presence or absence of anhydrotetracycline (ATc, which induces guide RNA expression). The relative titers of cysteine-derived **7.4** and homocysteine-derived **7.5** in each well were measured via LC–MS. Among the genes tested, the repression of CYS4, which encodes for cystathionine β-synthase that converts homocysteine to cystathionine (a cysteine precursor), was found to result in the greatest shift in relative abundance of each product. We observed an ~5-fold increase in the titer of **7.5** and an ~2-fold decrease in the titer of **7.4** for an overall ~10-fold change in the relative amounts of **7.5** and **7.4**.

7.3.7 KU43-HRPKS-TE Is Responsible for the Biosynthesis of 7.3

Our studies above showed how the KU42 HRPKS-TE can synthesize disorbyl homocysteine products using TE to catalyze transthioesterification and release the HRPKS product. In contrast, the product of KU43 HRPKS-TE, **7.3**, is formed by a direct amidation between octanoate and leucine methyl ester (Figure 7.7). An analysis of KU43-HRPKS-TE indicated that it contains the domain organization of KS-MAT-DH-ER-KR-ACP-TE. We reasoned that the TE domain could be responsible for the amidation reaction because no enzyme responsible for amino acid activation and incorporation is present in the KU43 gene cluster. Different from KU42-HRPKS TE, sequence alignment results indicated that the active site of KU43-HRPKS TE is serine, the same as for the canonical TEs.

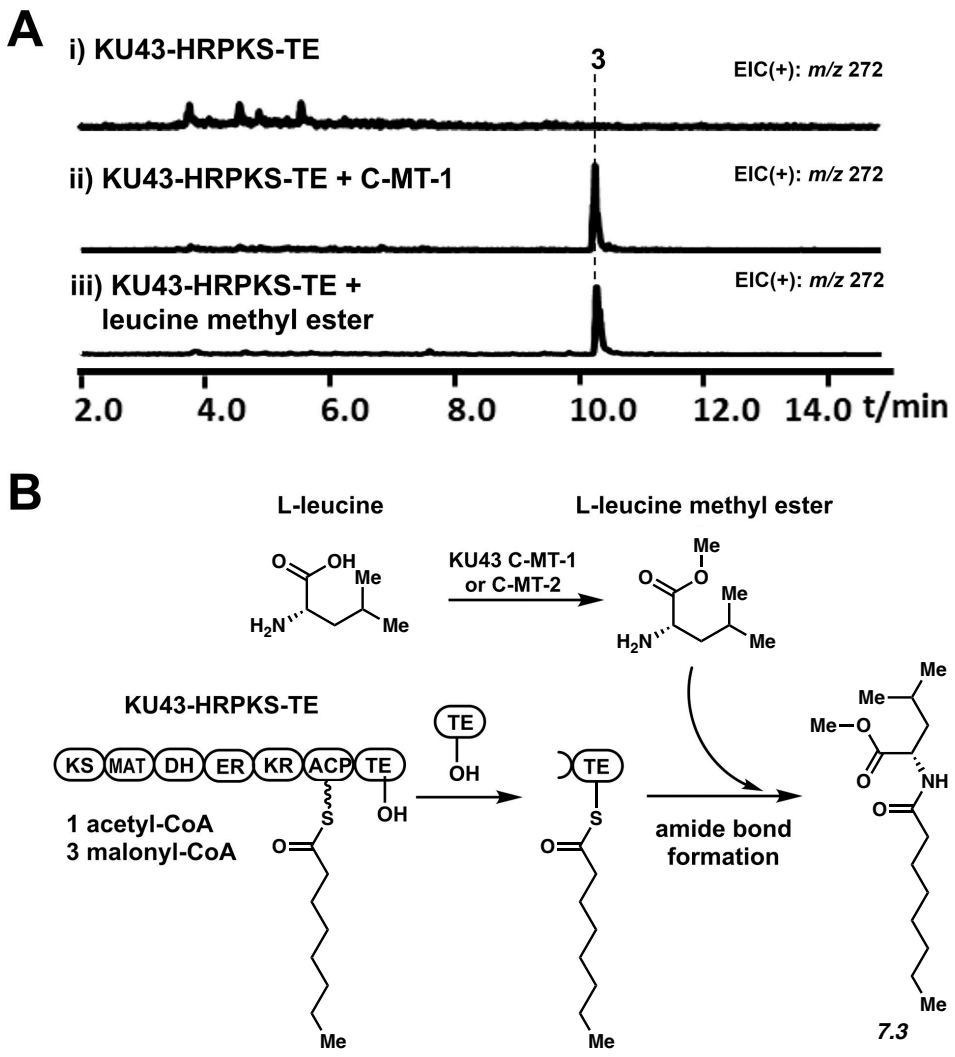

Figure 7.7. Biosynthesis of **7.3**. (A) Product profiles of *S. cerevisiae* BJ5464-NpgA transformed with KU43 cluster genes. Shown are the extracted MS spectra. (B) Proposed biosynthetic pathway for **7.3**.

The expression of HRPKS-TE alone in BJ5464-NpgA did not yield any new products (Figure 7.7A). When either C-MT-1 or C-MT-2 (Figure 7.2B), which are nearly identical to each other (96% protein sequence identity), from the cluster was coexpressed with KU43 HRPKS-TE, we detected the production of **7.3** (Figure 7.7A). On the basis of these results, we proposed that

C-MT-1 or C-MT-2 is responsible for the biosynthesis of L-leucine methyl ester, which could be used as the nucleophile by KU43 HRPKS-TE to release the octanoate chain biosynthesized by KU43-HRPKS (Figure 7.7B). To support this hypothesis, we repeated the heterologous expression experiment of KU43 HRPKS-TE with the addition of L-leucine methyl ester as the releasing substrate. As expected, the production of **7.3** was detected (Figure 7.7A). On the basis of these results, we proposed that the TE domain of KU43 HRPKS-TE catalyzes polyketide chain release by using L-leucine methyl ester to yield **7.3** (Figure 7.7B). Different from the KU42 HRPKS TE, which uses cysteine as the active site nucleophile to catalyze the transthioesterification reaction to yield thiolated polyketide, the KU43 HRPKS TE uses serine as the active-site nucleophile to capture the polyketide product as an oxyester, followed by amide bond formation to yield the aminoacylated polyketide. This is in sharp contrast to the ATP-dependent aminoacylation catalyzed by NRPS domains. The requirement of the serine nucleophile in catalysis was verified by site-directed mutagenesis. Mutation of the active site serine of KU43-HRPKS TE to alanine resulted in no detectable production of **7.3** when mutant HRPKS-TE was coexpressed with C-MT-1 in yeast.

7.4 Conclusions

In this study, we characterized two fungal HRPKSs with fused *C*-terminal TE domains, a new domain architecture among fungal PKSs. Both KU42 and KU43 HRPKS-TEs produced products that have not been reported previously, showing the potential of studying novel HRPKS enzymes for natural product mining. We demonstrated that both TE domains are involved in product release to synthesize aminoacylated polyketides in an ATP-independent fashion. The reactions catalyzed by the two TE domains, however, are very different. The KU42 TE

recognizes thiol-containing amino acids and uses the side-chain thiol as a nucleophile for performing chain release via transthioesterification. The product can then undergo an *S–N* acyl shift, followed by a second transthioesterification to produce the diacylated amino acid. Although the transthioesterification reactions are known for TE enzymes, the use of a cysteine or homocysteine side-chain thiol for polyketide product release is reported for the first time. In contrast, the KU43 TE recognizes leucine methyl ester and uses its amino group as a nucleophile to release the polyketide chain produced by the HRPKS.

In conclusion, our results show that novel programming rules are present in HRPKS-TEs to biosynthesize different natural products. These TE domains, along with others that can be mined from uncharacterized biosynthetic pathways, can serve as potential biocatalytic tools for diversifying polyketide structures.

7.5 Experimental Section

7.5.1 Experimental Procedures

2-*cis*-4-*trans*-sorbic acid (**7.17**) was chemically synthesized according to modified literature protocols.[19] A spectrum of the authentic sample of **7.17** obtained through chemical synthesis is shown below.

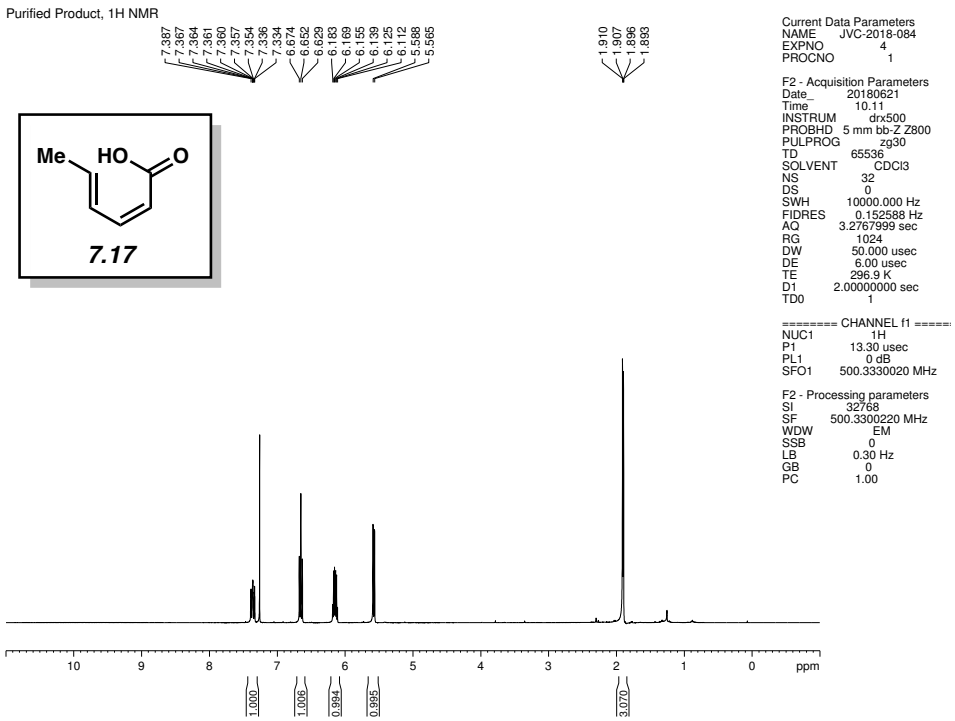

Figure 7.8 ^{1}H NMR (500 MHz, $CDCl_3$) of compound **7.17**.

7.5.2 Characterization of KU42 HRPKS *Δ*TE *in vitro*

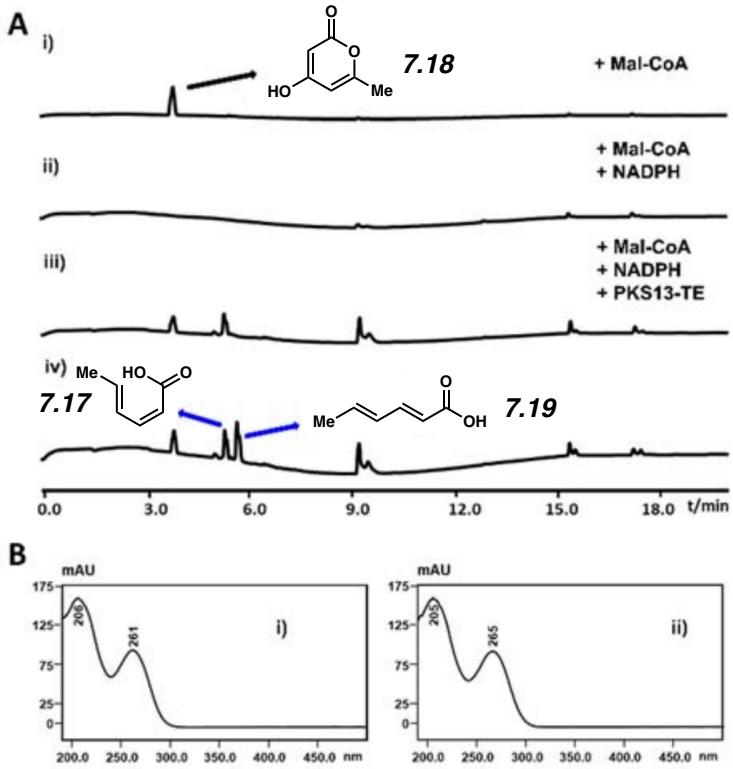

Figure 7.9. Characterization of KU42 HRPKS *Δ*TE *in vitro*. (A) LC-MS analysis of the KU42 HRPKS *Δ*TE *in vitro* assays. Shown are HPLC traces at 265 nm. i) KU42 HRPKS *Δ*TE in the presence of Mal-CoA; ii) KU42 HRPKS *Δ*TE in the presence of Mal-CoA and NADPH; iii) KU42 HRPKS *Δ*TE in the presence of Mal-CoA, NADPH, and PKS13-TE; iv) reaction products from iii) were co-injected with the standards of 2-*trans*-4-*trans*-sorbic acid (**7.19**) and 2-*cis*-4-*trans*-sorbic acid (**7.17**). (B) The UV spectra of 2-*trans*-4-*trans*-sorbic acid (**7.19**) (i) and the polyketide product released by PKS13-TE from KU42 HRPKS *Δ*TE (ii).

7.5.3 Synthetic Biology Details

The details for DNA manipulation, protein expression, activity assays, structure determination and other extended and supplemental tables and figures are reported in the literature.[34]

7.6 Notes and References

(1) (a) Du, L.; Lou, L. PKS and NRPS release mechanisms. *Nat. Prod. Rep.* **2010**, *27*, 255−278. (b) Horsman, M. E.; Hari, T. P.; Boddy, C. N. Polyketide Synthase and Non-Ribosomal Peptide Synthetase Thioesterase Selectivity: Logic Gate or a Victim of Fate? *Nat. Prod. Rep.* **2016**, *33*, 183−202.

(2) Cox, R. J. Polyketides, Proteins and Genes in Fungi: Programmed Nano-Machines Begin to Reveal Their Secrets. *Org. Biomol. Chem.* **2007**, *5*, 2010−2026.

(3) Chooi, Y.-H.; Tang, Y. Navigating the Fungal Polyketide Chemical Space: From Genes to Molecules. *J. Org. Chem.* **2012**, *77*, 9933−9953.

(4) (a) Xie, X.; Watanabe, K.; Wojcicki, W. A.; Wang, C. C.; Tang, Y. Biosynthesis of Lovastatin Analogs with a Broadly Specific Acyltransferase. *Chem. Biol.* **2006**, *13*, 1161−1169. (b) Xu, W.; Chooi, Y.-H.; Choi, J. W.; Li, S.; Vederas, J. C.; Da Silva, N. A.; Tang, Y. LovG: the Thioesterase Required for Dihydromonacolin L Release and Lovastatin Nonaketide Synthase Turnover in Lovastatin Biosynthesis. *Angew. Chem., Int. Ed.* **2013**, *52*, 6472−6475.

(5) Crawford, J. M.; Dancy, B. C. R.; Hill, E. A.; Udwary, D. W.; Townsend, C. A. Identification of a Starter Unit Acyl-Carrier Protein Transacylase Domain in an Iterative Type I Polyketide Synthase. *Proc. Natl. Acad. Sci. U. S. A.* **2006**, *103*, 16728−16733.

(6) (a) Fujii, R.; Matsu, Y.; Minami, A.; Nagamine, S.; Takeuchi, I.; Gomi, K.; Oikawa, H. Biosynthetic Study on Antihypercholesterolemic Agent Phomoidride: General Biogenesis of Fungal Dimeric Anhydrides. *Org. Lett.* **2015**, *17*, 5658−5661. (b) Bonsch, B.; Belt, V.; Bartel, C.; Duensing, N.; Koziol, M.; Lazarus, C. M.; Bailey, A. M.; Simpson, T. J.; Cox, R. J. Identification of Genes Encoding Squalestatin S1 Biosynthesis and In Vitro Production of New Squalestatin Analogues. *Chem. Commun.* **2016**, *52*, 6777−6780. (c) Liu, N.; Hung, Y.-S.; Gao, S.-S.; Hang, L.; Zou, Y.; Chooi, Y.-H.; Tang, Y. Identification and Heterologous Production of a Benzoyl-Primed Tricarboxylic Acid Polyketide Intermediate from the Zaragozic Acid A Biosynthetic Pathway. *Org. Lett.* **2017**, *19*, 3560−3563. (d) Bai, J.; Yan, D.; Zhang, T.; Guo, Y.; Liu, Y.; Zou, Y.; Tang, M.; Liu, B.; Wu, Q.; Yu, S.; Tang, Y.; Hu, Y. A Cascade of Redox Reactions Generates Complexity in the Biosynthesis of the Protein Phosphatase-2 Inhibitor Rubratoxin A. *Angew. Chem., Int. Ed.* **2017**, *56*, 4782−4786. (e) Ugai, T.; Minami, A.; Fujii, R.; Tanaka, M.; Oguri, H.; Gomi, K.; Oikawa, H. Heterologous Expression of Highly Reducing Polyketide Synthase Involved in Betaenone Biosynthesis. *Chem. Commun.* **2015**, *51*, 1878−1881.

(7) Büchi, G.; Kitaura, Y.; Yuan, S.-S.; Wright, H. E.; Clardy, J.; Demain, A. L.; Ginsukon, T.; Hunt, N.; Wogan, G. N. Structure of Cytochalasin E, a Toxic Metabolite of *Aspergillus clavatus*. *J. Am. Chem. Soc.* **1973**, *95*, 5423−5425.

(8) Bloch, P.; Tamm, C.; Bollinger, P.; Petcher, T. J.; Weber, H. P. Pseuotin, a New Metabolite of *Pseudeurotium ovalis* STOLK Having an Unusual Hetero-Spirocyclic System. *Helv. Chim. Acta* **1976**, *59*, 133−137.

(9) (a) Nakai, R.; Ogawa, H.; Asai, A.; Ando, K.; Agatsuma, T.; Matsumiya, S.; Yamashita, Y.; Mizukami, T. UCS1025A, a Novel Antibiotic Produced by *Acremonium* sp. *J. Antibiot.* **2000**, *53*, 294−296. (b) Agatsuma, T.; Akama, T.; Nara, S.; Matsumiya, S.; Nakai, R.; Ogawa, H.; Otaki, S.; Ikeda, S.; Saitoh, Y.; Kanda, Y. UCS1025A and B, New Antitumor Antibiotics from the Fungus *Acremonium* Species. *Org. Lett.* **2002**, *4*, 4387−4390.

(10) (a) Song, Z.; Cox, R. J.; Lazarus, C. M.; Simpson, T. J. Fusarin C Biosynthesis in *Fusarium moniliforme* and *Fusarium venenatum*. *ChemBioChem* **2004**, *5*, 1196−1203. (b) Sims, J. W.; Fillmore, J. P.; Warner, D. D.; Schmidt, E. W. Equisetin Biosynthesis in *Fusarium heterosporum*. *Chem. Commun.* **2005**, 186−188. (c) Eley, K. L.; Halo, L. M.; Song, Z.; Powles, H.; Cox, R. J.; Bailey, A. M.; Lazarus, C. M.; Simpson, T. J. Biosynthesis of the 2-Pyridone Tenellin in the Insect Pathogenic Fungus *Beauveria bassiana*. *ChemBioChem* **2007**, *8*, 289−297. (d) Boettger, D.; Hertweck, C. Molecular Diversity Sculpted by Fungal PKS-NRPS Hybrids. *ChemBioChem* **2013**, *14*, 28−42.

(11) Ma, S. M.; Li, J. W.; Choi, J. W.; Zhou, H.; Lee, K. K.; Moorthie, V. A.; Xie, X.; Kealey, J. T.; Da Silva, N. A.; Vederas, J. C.; Tang, Y. Complete Reconstitution of a Highly Reducing Iterative Polyketide Synthase. *Science* **2009**, *326*, 589−592.

(12) Zabala, A. O.; Chooi, Y.-H.; Choi, M. S.; Lin, H.-C.; Tang, Y. Fungal Polyketide Synthase Product Chain-Length Control by Partnering Thiohydrolase. *ACS Chem. Biol.* **2014**, *9*, 1576−1586.

(13) Hang, L.; Tang, M.-C.; Harvey, C. J. B.; Page, C. G.; Li, J.; Hung, Y.-S.; Liu, N.; Hillenmeyer, M. H.; Tang, Y. Reversible Product Release and Recapture by a Fungal Polyketide Synthase Using a Carnitine Acyltransferase Domain. *Angew. Chem., Int. Ed.* **2017**, *56*, 9556−9560.

(14) Harvey, C. J. B.; Tang, M.; Schlecht, U.; Horecka, J.; Fischer, C. R.; Lin, H.-C.; Li, J.; Naughton, B.; Cherry, J.; Miranda, M.; Li, Y. F.; Chu, A. M.; Hennessy, J. R.; Vandova, G. A.; Inglis, D.; Aiyar, R.; Steinmetz, L. M.; Davis, R. W.; Medema, M. H.; Sattely, E.; Khosla, C.; St.Onge, R. P.; Tang, Y.; Hillenmeyer, M. H. HEx: A Heterologous Expression Platform for the Discovery of Fungal Natural Products. *Sci. Adv.* **2018**, *4*, No. eaar5459.

(15) Cantu, D. C.; Chen, Y.; Reilly, P. J. Thioesterases: A New Perspective Based on Their Primary and Tertiary Structures. *Protein Sci.* **2010**, *19*, 1281−1295.

(16) (a) Holmquist, M. Alpha/Beta-Hydrolase Fold Enzymes: Structures, Functions and Mechanisms. *Curr. Protein Pept. Sci.* **2000**, *1*, 209−235. (b) Rauwerdink, A.; Kazlauskas, R. J. How the Same Core Catalytic Machinery Catalyzes 17 Different Reactions: the Serine-Histidine-Aspartate Catalytic Triad of α/β-Hydrolase Fold Enzymes. *ACS Catal.* **2015**, *5*, 6153−6176.

(17) Winter, J. M.; Cascio, D.; Dietrich, D.; Sato, M.; Watanabe, K.; Sawaya, M. R.; Vederas, J. C.; Tang, Y. Biochemical and Structural Basis for Controlling Chemical Modularity in Fungal Polyketide Biosynthesis. *J. Am. Chem. Soc.* **2015**, *137*, 9885−9893.

(18) Schaffer, J. E.; Reck, M. R.; Prasad, N. K.; Wencewicz, T. A. β-Lactone Formation During Product Release from a Nonribosomal Peptide Synthetase. *Nat. Chem. Biol.* **2017**, *13*, 737−744.

(19) (a) Crombie, L.; Crombie, W. M. L. Stereochemistry of Thermolytic Base-Catalysed Decarboxylation to Form Conjugated Diene−Acids: Synthesis Using Ethylidenemalonic Ester Condensation. *J. Chem. Soc., Perkin Trans. 1* **1994**, *1*, 1267−1274. (b) Schmidt, B.; Kunz, O. One-Flask Tethered Ring Closing Metathesis−Electrocyclic Ring Opening for the Highly Stereoselective Synthesis of Conjugated *Z*/*E*-Dienes. *Eur. J. Org. Chem.* **2012**, *2012*, 1008−1018.

(20) Smith, C. A.; Want, E. J.; O'Maille, G.; Abagyan, R.; Siuzdak, G. XCMS: Processing Mass Spectrometry Data for Metabolite Profiling Using Nonlinear Peak Alignment, Matching, and Identification. *Anal. Chem.* **2006**, *78*, 779−787.

(21) Cochrane, R. V.; Sanichar, R.; Lambkin, G. R.; Reiz, B.; Xu, W.; Tang, Y.; Vederas, J. C. Production of New Cladosporin Analogues by Reconstitution of the Polyketide Synthases Responsible for the Biosynthesis of this Antimalarial Agent. *Angew. Chem., Int. Ed.* **2016**, *55*, 664−668.

(22) (a) Dawson, P. E.; Muir, T. W.; Clark-Lewis, I.; Kent, S. B. Synthesis of Proteins by Native Chemical Ligation. *Science* **1994**, *266*, 776−779. (b) Conibear, A. C.; Watson, E.

E.; Payne, R. J.; Becker, C. F. W. Native Chemical Ligation in Protein Synthesis and Semi-Synthesis. *Chem. Soc. Rev.* **2018**, *47*, 9046−9068.

(23) Kudo, F.; Matsuura, Y.; Hayashi, T.; Fukushima, M.; Eguchi, T. Genome Mining of the Sordarin Biosynthetic Gene Cluster from *Sordaria araneosa* Cain ATCC 36386: Characterization of Cycloaraneosene Synthase and GDP-6-deoxyaltrose Transferase. *J. Antibiot.* **2016**, *69*, 541−548.

(24) Nofiani, R.; de Mattos-Shipley, K.; Lebe, K. E.; Han, L. C.; Iqbal, Z.; Bailey, A. M.; Willis, C. L.; Simpson, T. J.; Cox, R. J. Strobilurin Biosynthesis in Basidiomycete Fungi. *Nat. Commun.* **2018**, *9*, 3940.

(25) Zhou, H.; Gao, Z.; Qiao, K.; Wang, J.; Vederas, J. C.; Tang, Y. A Fungal Ketoreductase Domain that Displays Substrate-Dependent Stereospecificity. *Nat. Chem. Biol.* **2012**, *8*, 331−333.

(26) (a) Xie, X.; Cane, D. E. Stereospecific Formation of Z-Trisubstituted Double Bonds by the Successive Action of Ketoreductase and Dehydratase Domains from trans-AT Polyketide Synthases. *Biochemistry* **2018**, *57*, 3126−3129. (b) Shah, D. D.; You, Y.-O.; Cane, D. E. Stereospecific Formation of E- and Z-Disubstituted Double Bonds by Dehydratase Domains from Modules 1 and 2 of the Fostriecin Polyketide Synthase. *J. Am. Chem. Soc.* **2017**, *139*, 14322−14330. (c) Liddle, E.; Scott, A.; Han, L. C.; Ivison, D.; Simpson, T. J.; Willis, C. L.; Cox, R. J. In Vitro Kinetic Study of the Squalestatin Tetraketide Synthase Dehydratase Reveals the Stereochemical Course of a Fungal Highly Reducing Polyketide Synthase. *Chem. Commun.* **2017**, *53*, 1727−1730. (d) Gay, D.; You, Y.-O.; Keatinge-Clay, A.; Cane, D. E. Structure and Stereospecificity of the Dehydratase

Domain from the Terminal Module of the Rifamycin Polyketide Synthase. *Biochemistry* **2013**, *52*, 8916−8928. (e) Valenzano, C. R.; You, Y.-O.; Garg, A.; Keatinge-Clay, A.; Khosla, C.; Cane, D. E. Stereospecificity of the Dehydratase Domain of the Erythromycin Polyketide Synthase. *J. Am. Chem. Soc.* **2010**, *132*, 14697−14699.

(27) Wang, M.; Zhou, H.; Wirz, M.; Tang, Y.; Boddy, C. N. A Thioesterase from an Iterative Fungal Polyketide Synthase Shows Macrocyclization and Cross Coupling Activity and May Play a Role in Controlling Iterative Cycling through Product Offloading. *Biochemistry* **2009**, *48*, 6288−6290.

(28) Ge, H.-M.; Huang, T.; Rudolf, J. D.; Lohman, J. R.; Huang, S.- X.; Guo, X.; Shen, B. Enediyne Polyketide Synthases Stereoselectively Reduce the *β*-Ketoacyl Intermediates to *β*-D-Hydroxyacyl Intermediates in Enediyne Core Biosynthesis. *Org. Lett.* **2014**, *16*, 3958−3961.

(29) Labonte, J. W.; Townsend, C. A. Active Site Comparisons and Catalytic Mechanisms of the Hot Dog Superfamily. *Chem. Rev.* **2013**, *113*, 2182−2204.

(30) (a) Vergnolle, O.; Hahn, F.; Baerga-Ortiz, A.; Leadlay, P. F.; Andexer, J. N. Stereoselectivity of Isolated Dehydratase Domains of the Borrelidin Polyketide Synthase: Implications for *cis* Double Bond Formation. *ChemBioChem* **2011**, *12*, 1011−1014. (b) Hahn, F.; Kandziora, N.; Friedrich, S.; Leadlay, P. F. Synthesis of Complex Intermediates for the Study of a Dehydratase from Borrelidin Biosynthesis. *Beilstein J. Org. Chem.* **2014**, *10*, 634−640.

(31) Reeves, C. D.; Hu, Z.; Reid, R.; Kealey, J. T. Genes for the Biosynthesis of the Fungal Polyketides Hypothemycin from *Hypomyces subiculosus* and Radicicol from *Pochonia chlamydosporia*. *Appl. Environ. Microbiol.* **2008**, *74*, 5121−5129.

(32) Tang, M.-C.; Lin, H.-C.; Li, D.; Zou, Y.; Li, J.; Xu, W.; Cacho, R. A.; Hillenmeyer, M. E.; Garg, N. K.; Tang, Y. Discovery of Unclustered Fungal Indole Diterpene Biosynthetic Pathways through Combinatorial Pathway Reassembly in Engineered Yeast. *J. Am. Chem. Soc.* **2015**, *137*, 13724−13727.

(33) Smith, J. D.; Schlecht, U.; Xu, W.; Suresh, S.; Horecka, J.; Proctor, M. J.; Aiyar, R. S.; Bennett, R. A.; Chu, A.; Li, Y. F.; Roy, K.; Davis, R. W.; Steinmetz, L. M.; Hyman, R. W.; Levy, S. F.; St. Onge, R. P. A Method for High-Throughput Production of Sequence-Verified DNA Libraries and Strain Collections. *Mol. Syst. Biol.* **2017**, *13*, 913.

(34) Tang, M.-C.; Fischer, C. R.; Chari, J. V.; Tan, D.; Suresh, S.; Chu, A.; Miranda, M.; Smith, J.; Zhang, Z.; Garg, N. K.; St. Onge, R. P.; Tang, Y. Thioesterase-Catalyzed Aminoacylation and Thiolation of Polyketides in Fungi. *J. Am. Chem. Soc.* **2019**, *141*, 8198–8206

CHAPTER EIGHT

Catalysis in Modern Drug Discovery: Insights from a Graduate Student-Taught Undergraduate Course

Jason V. Chari,† Rachel R. Knapp,† Timothy B. Boit, and Neil K. Garg.

J. Chem. Educ. **2022**, *99*, 1296–1303.

8.1 Abstract

A course centered around transition-metal catalysis in modern drug discovery was designed to illustrate the central role of organic chemistry in driving small-molecule drug development. The course highlighted both fundamental and applied concepts, first with a focus on the drug discovery process, followed by foundational principles in catalysis and modern catalytic methods. Finally, these topics were unified in the last portion of the course, where case studies served to highlight the use of transition-metal catalysis in the synthesis of modern drugs. Three graduate students designed and taught the course, with mentorship from a faculty member, leading to several notable teaching outcomes. Additionally, experts in the fields of catalysis and drug discovery served as guest lecturers throughout the duration of the course. This approach spotlighted the various careers that organic chemists play in the development of new medicines. We hope that this course motivates the creation of other courses in STEM that unify fundamental concepts with applications and career outcomes.

8.2 Introduction

Organic synthesis plays an integral role in small molecule drug development.[1] Indeed, chemists trained in organic synthesis execute both the design and synthesis of small molecules that treat widespread ailments and address global health crises.[2] Comprising 71% of the 53 drugs approved by the FDA in 2020,[3] small molecule therapeutics continue to represent the majority of drugs approved in the US. In addition, multiple phases of the drug development pipeline require expertise in synthetic organic chemistry. For example, the discovery phase of small molecule drug development necessitates the synthesis and design of numerous analogs, whereas the process chemistry phase warrants the creation and optimization of a highly efficient synthetic route to the desired drug molecule.

In spite of the connections between organic synthesis and the drug discovery process, this fundamental relationship is not always directly or thoroughly explored in undergraduate courses. Traditionally, undergraduate organic chemistry coursework centers around fundamental synthetic transformations, whereas discussions of applications are often limited or receive minimal context. Although there have been exciting advances that bring these connections into organic laboratory courses,[4] as well as courses in computational drug design,[5] considerably fewer initiatives have been reported in lecture-based courses. This can leave undergraduate students with a narrow perspective on the relevance of organic chemistry, as well as career opportunities. Articulating both the modern drug discovery process and careers in organic chemistry can serve to both empower students to consider its connection to human health and lead to greater student engagement overall.

In addition to connecting organic chemistry to improving human health, an area that is often underemphasized or omitted from undergraduate coursework is transition-metal catalysis.

As reflected in the awarding of three Nobel Prizes in chemistry over the past two decades,[6] transition-metal catalysis has had a widespread impact across many disciplines of science, enabling access to new pharmaceuticals, polymers, agrochemicals, and materials. In the area of drug discovery, transition-metal catalysis represents a ubiquitous and indispensable tool that has greatly improved the ability to establish structure–activity relationships in drug leads.[7] As an example, 22% of representative medicinal chemistry publications in 2014 described a Suzuki–Miyaura cross-coupling reaction.[8] In comparison, data from 1984 revealed no examples of transition-metal catalysis in medicinal chemistry publications.[8] In spite of the dramatic impact and evolution of transition-metal catalysis in drug development, it often receives less attention than "classical" reactions (e.g., S_N2, Diels–Alder, etc.) and their fundamental principles in undergraduate lecture courses.[9] As such, students may not have the opportunity to learn fundamental concepts in catalysis, or perhaps more importantly, understand the applications of these concepts in important areas such as pharmaceutical development. Teaching transition-metal catalysis in the context of drug discovery offers a means for students to connect chemistry to human health, and to equip students with the conceptual tools necessary to devise syntheses of drug scaffolds. By clearly articulating the direct connection between transition-metal catalysis and improving human health, students can begin to appreciate the driving force of organic chemistry in the world around them.

8.3 Course Rationale

We sought to design a virtual course that teaches fundamental concepts in both drug discovery and catalysis, while also being engaging and impactful for students from diverse backgrounds. To achieve this, we pursued an approach that highlights both young researchers and established experts in the field. First, rather than being led by a professor or lecturer, the course

was designed and taught by senior graduate students, under the advisement of a faculty member. This offered notable advantages for both the undergraduate students in the course and the graduate student instructors themselves. Indeed, previous studies have demonstrated that "undergraduates who take their first course in a given subject from a graduate student are nearly twice as likely to subsequently major in that subject compared to their peers who take the same course from full-time faculty."[10] This finding supports the idea that receiving instruction from graduate students can serve as a valuable supplement to professor-led courses. Of note, this model is by no means meant to replace faculty teaching responsibilities, nor should it be used by faculty to skirt or delegate their teaching responsibilities. Additionally, this approach is likely most suitable for summer course offerings, when faculty are ordinarily not expected to teach and greater flexibility may be available. This can also positively impact the graduate student instructors themselves, as "graduate students who teach more frequently are more likely to graduate in a timely manner and more likely to subsequently be employed by a college or university in their early careers."[10] To ensure that the graduate students were well-equipped to lead this course, they received important mentorship from a faculty member in teaching, scientific communication, and management. In particular, the faculty member provided insight and advice on refining the course design as well as depth and difficulty of content, managing student issues, and providing advice on grading. In addition to this mentorship, the senior graduate students who led the course were also either pursuing research directly involved in transition-metal catalysis or had career aspirations of entering the pharmaceutical industry. This ensured that the instructors were both confident in the material and passionate about the topics discussed.

It should also be noted that graduate student instructors are often similar in age to their undergraduate counterparts and can therefore appear more approachable, and additionally offer

insight into the motivations and experiences of a graduate student. Demystifying the graduate student experience[11] proved to be a defining feature of the course, as the majority of those enrolled were third- or fourth-year undergraduate students in the process of making important decisions about their post-graduation plans.

In addition to placing a focus on graduate student instruction, we also sought to include perspectives, insights, and stories from established leaders in the fields of drug discovery and catalysis through invited guest lectures.[12] We envisioned that this would allow the course to more fully and accurately portray the field of drug discovery by serving as a supplement to the graduate student-produced lectures. Furthermore, this would provide an opportunity to showcase scientists from diverse backgrounds, including women and scientists of color, highlighting their unique experiences and career trajectories.[13] Achieving diversity and inclusion in science remains a critical goal, and showcasing the empowering stories of chemists from underrepresented backgrounds in leadership positions has proven to be a powerful mechanism to address equity in chemistry.[14] Indeed, many of the guest lecturers featured in our course had non-linear career paths and stories, but that still led to successful outcomes. Hearing these stories can provide important inspiration for students considering potential career paths and create an open space for students to pose questions and interact directly with leaders in the field. This fostered a unique environment for the students, who may not have otherwise had the opportunity to connect with chemists in this capacity. In addition to the positive impact on students, this design also appealed to the guest lecturers by providing a space for them to gain more exposure and visibility for their company or research group, as well as connect with students who are early in their careers. Likewise, the graduate student instructors for the course were able to broaden their professional network by connecting with leaders in industry.

Beyond the overall learning experience of the undergraduate students, several administrative benefits can arise through the creation of virtual courses led by graduate students. Namely, the virtual, asynchronous design enables students outside of the university to participate in the course. Of note, this can provide students from smaller schools, which may have fewer available elective courses, exposure to applications of organic chemistry in drug discovery. Moreover, individuals outside of academia would also have the opportunity to participate. This course garnered enrollment from the University of California, Los Angeles (UCLA) students as well as non-UCLA-enrolled undergraduate students and even individuals currently working in the pharmaceutical industry. In so doing, the virtual approach brought visibility to the department and university at large. Overall, the course was designed to not only better contextualize important concepts in organic chemistry, but also to provide a unique and positive experience for all participating groups.

8.4 Course Design

Catalysis in Modern Drug Discovery was offered as a 4-unit elective course that would take place over six weeks. The course was designed at UCLA and garnered an enrollment of 53 students in its first year (summer of 2020) and 43 students in its second year (summer of 2021). The prerequisites for the course were general chemistry and introductory organic chemistry.

The decision to render this course virtual, which was made prior to the COVID-19 pandemic, was motivated by several guiding factors.[15] First, this would offer UCLA students who were not on campus during the summer the opportunity to complete the course remotely. Moreover, this format would allow students outside of the UCLA community, both in academia and in industry, to participate. The virtual format would additionally provide flexibility regarding

time commitment. In particular, the lectures, which were 30 to 60 minutes in length, were posted three times per week, and could be viewed at any time. These lectures were provided in the form of pre-recorded videos featuring narrated presentations and interactive clips. The lectures were supplemented with small-group, virtual discussion sections. Two one-hour sessions were offered per week, each of which was attended by 20–30 students. These sessions were focused on answering questions from students, as well as reviewing challenging course content. These discussion sections served to maintain student engagement, provide important support to students, and create a sense of community, given the virtual nature of the course. As mentioned earlier, these sessions were optional, but attendance was rewarded with extra credit. Office hours were also conducted virtually in a one-on-one setting by student request.

As mentioned, in addition to the core pre-recorded lecture content, a guest lecture series was incorporated into the course and featured five guest lectures delivered by experts in academia and the pharmaceutical industry. These live, virtual lectures featured a vice president at a major pharmaceutical company, an established academic medicinal chemist, a rising star at a small biotechnology company, a prominent process chemist, and an established academic researcher in the area of catalysis. The faculty advisor for the course provided important suggestions for potential guest lecturers and, in some cases, directly connected the graduate student instructors with these individuals. The first guest lecture took place during the second week of the course, ensuring that students were introduced to key principles in drug discovery prior to this lecture. The format of the guest lectures varied depending on the invited individual, but generally involved a 30-minute lecture followed by a 30-minute question-and-answer session. The guest lecturers typically placed a large emphasis on illustrating the story of their journey to their current career, as well as providing advice and insights along the way. In addition to detailing empowering success

stories in catalysis or drug discovery, these guest lectures and question-and-answer sessions sprouted meaningful discussions around topics such as diversity in STEM, how to engage in undergraduate research, and even advice on applying and interviewing for jobs. By conducting the course in a virtual setting, several speakers were able to attend from various parts of the country.

8.5 Course Content

The course was segmented into three main parts, as illustrated in Figure 8.1. Overall, this structure would allow students to gain a foundational understanding of the drug discovery process (Part I) before learning about catalysis as a field, and more specifically, the principles of transition-metal catalysis (Part II). Equipped with knowledge of both drug development and important concepts in catalysis, the students would then be capable of combining all elements of these topics in the final portion of the course (Part III). More specifically, this latter section would challenge students to apply their knowledge of transition-metal catalysis in order to strategically build drug molecules. With three graduate students teaching the course, each graduate student spearheaded one of the three sections and was tasked with designing course content, recording lecture content, and leading discussion sections for those two weeks.

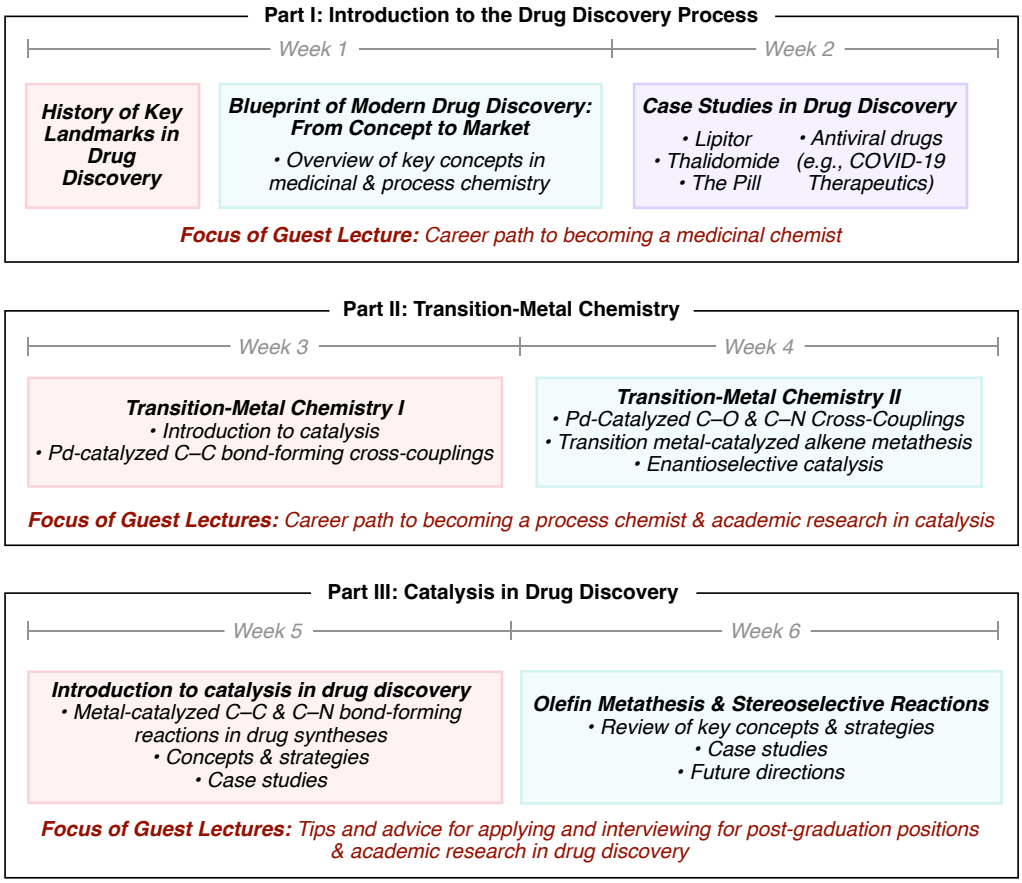

Figure 8.1. Structure of course content, including core lecture content and guest lecture topics.

8.5.1 Part I: Introduction to the Drug Discovery Process

The objective of the first part of the course was to provide students with an understanding of drug discovery and development, and to specify the role of the organic chemist in these processes.[16] To begin, a brief history of drug discovery was described, showcasing key landmarks in the field. This included discussions of impactful drugs such as ephedrine, morphine, and penicillin. Important terms and drug categorizations (e.g., small molecules vs. biologics) were defined to clarify the scope of the course and relevant terminology. During the remainder of the first week, the students were presented with a blueprint of drug discovery in the modern era. This included a detailed overview of medicinal chemistry and techniques for target selection (e.g.,

identifying a particular protein to inhibit), lead discovery, and lead optimization. This was followed by an introduction to process chemistry, which included guiding principles in route design, optimization, and scale-up, as well as brief industrial examples. Clear contrasts were drawn between the objectives and route design strategies pursued by medicinal chemists (e.g., design of diversifiable routes) in comparison to process chemists (e.g., design of a convergent route). In week two, in-depth case studies in drug discovery served to apply concepts from the first week by conveying the stories behind the discovery of particularly impactful drugs, from concept to market. As delineated in Figure 8.2, this included the discovery and development of therapeutics such as atorvastatin (Lipitor), norethindrone (the Pill), and antiviral drugs developed to treat global health crises such as HIV, influenza, and COVID-19. These case studies were typically structured in the form of a story, first capturing background on the ailment and key biological mechanisms of action before describing strategic features of target selection, lead discovery, hit-to-lead optimization, route optimization, scale-up, and lastly broader impacts of the therapeutic developed. Overall, the objective of these case studies was to solidify and contextualize key concepts in hit-to-lead optimization and the development of process routes. More broadly, we hoped to highlight the strategic aspects of drug discovery and development, as well as the long-term impact of therapeutics developed in part by organic chemists.

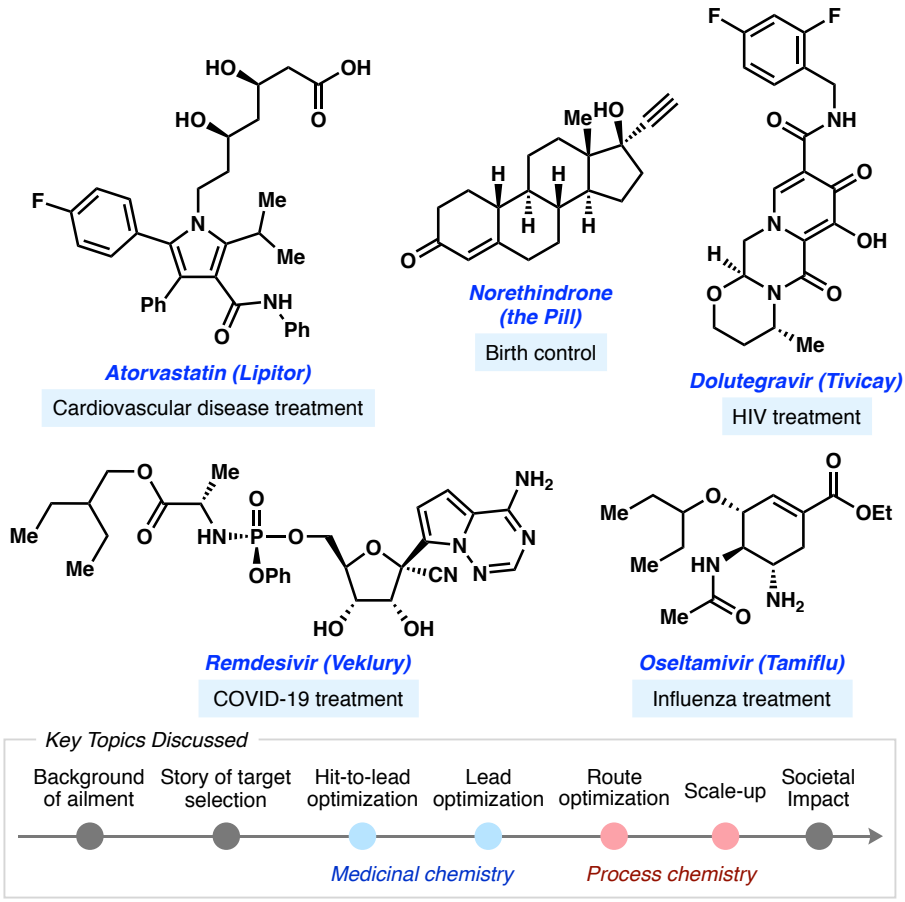

Figure 8.2. Exemplary drug scaffolds discussed in Part I of the course, and generalized flow of lecture content.

8.5.2 Part II: Transition-Metal Chemistry

In Part II of Catalysis in Modern Drug Discovery, the focus of the course shifted from drug discovery into transition-metal catalysis. To introduce this new topic, basic principles of catalysis and transition-metal chemistry (e.g., definition of a catalyst, kinetics versus thermodynamics, and electron counting of metal complexes) were described in the first lecture of this section.[17] Following this introduction, a series of lectures dedicated to important bond-forming methodologies was presented. This included the Suzuki–Miyaura cross-coupling reaction, the Mizoroki–Heck reaction, olefin metathesis, and enantioselective processes such as the Sharpless

asymmetric epoxidation. As illustrated in Figure 8.3, the organization of each topic featured an introduction of the reaction, its mechanism, guiding principles, and scope studies and insights. Overall, this structure allowed students to develop a conceptual understanding of key C–C, C–O, and C–N bond-forming processes in organic chemistry that rely upon transition-metal catalysis. In addition, the focus on the scope and limitations of a particular reaction served to highlight the challenges that organic chemists still face in the synthesis of small molecule therapeutics.

8.5.3 Part III: Catalysis in Modern Drug Discovery

Following Parts I and II, the final section of the course was focused on highlighting the use of transition-metal catalysis in the syntheses of notable pharmaceuticals.[8,18] This section served to link together all aspects of the course up to this point by incorporating transition-metal catalysis into the students' retrosynthetic toolbox. Each case study first introduced a small molecule therapeutic and described the disease or condition that it treats. Following this introduction, the development of the drug was described and a key aspect of the drug discovery process was highlighted in each case study. Examples included the rational design of lead structures, SAR studies, and process scale optimization. The compound was then analyzed from a synthetic chemistry perspective, with a focus on identifying particular bonds that were formed using the methodologies identified in Part II. By identifying these key disconnections, the students were exposed to strategy level retrosynthetic analysis. The final lecture provided a future outlook within the field of catalysis, underscoring the importance of developing new synthetic methods to accelerate the process of drug development.

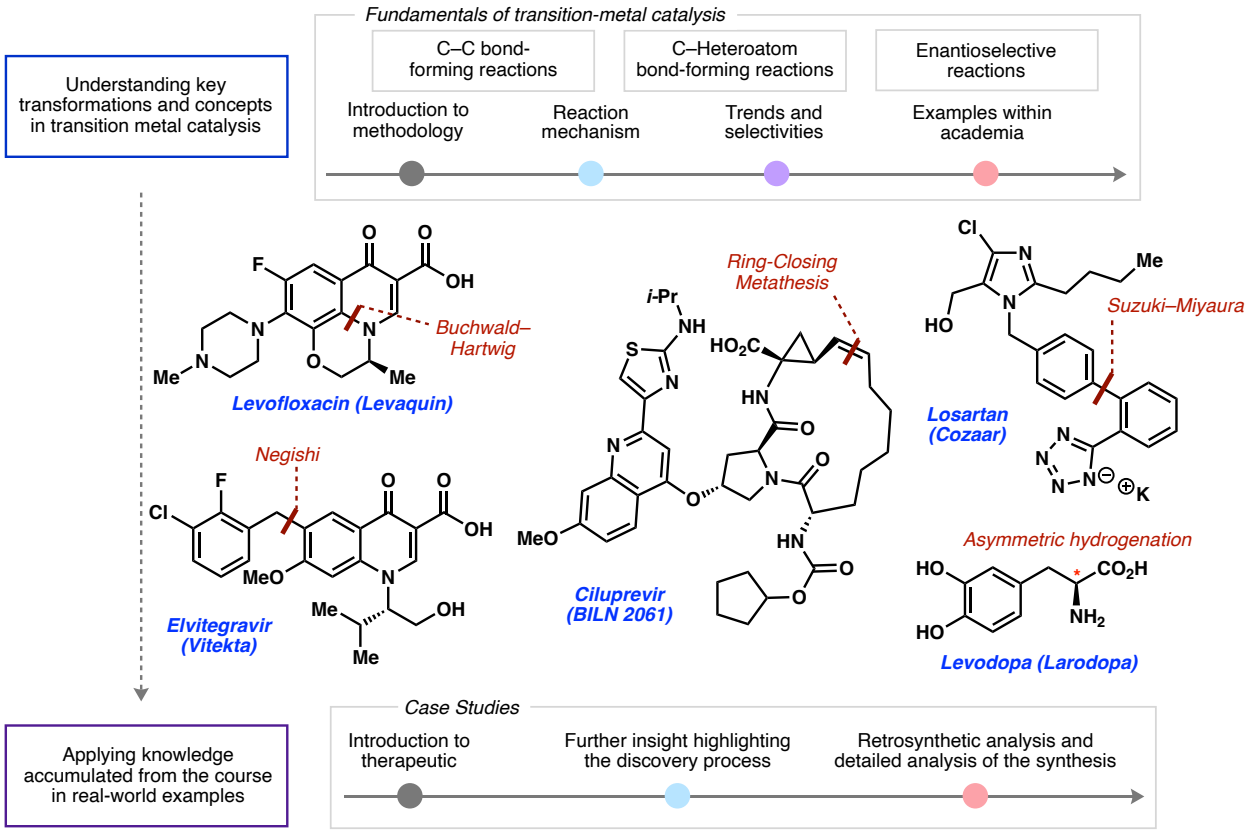

Figure 8.3. Fundamentals of transition-metal catalysis (Part II of the course) and case studies presented (Part III of the course).

8.6 Course Grading

Students were assessed through a combination of exams, quizzes, problem sets, and participation, weighted as follows: weekly problem sets 30%, weekly quizzes 20%, midterm exam 20%, final exam 30%, and up to 5% extra credit. The extra credit, which served to incentivize participation and engagement from the students, was offered on the basis of attendance at the discussion sections and guest lectures, as well as posing questions for the guest speakers live (via Zoom) or via the course's online forum. The problem sets and quizzes, which were based on the previous week's course material, were comprised of multiple-choice questions that assessed students' understanding of the content and evaluated critical thinking skills toward solving applied

problems. Following week three of the course, a midterm exam was administered and consisted of multiple choice and short answer questions based on course content from weeks 1–3. At the end of the course, a cumulative final exam was administered that consisted of multiple choice questions.

8.7 Student Reflections

At the end of the course, the students completed an anonymous feedback report through UCLA's course evaluation form. The responses were collected from students who attended the course in summer 2020 (number of responses, n = 19) and summer 2021 (n = 39).[19] Across the two terms, the "overall rating" average for the course was 8.43 out of 9.00 (94%), demonstrating a strongly positive overall response. Additionally, it was found that student interest in the subject grew substantially upon completion of the course, increasing from a score of 2.22 to 2.71 (where 1 = low, 2 = medium, and 3 = high interest). At the end of the course evaluation, open-form comments provided by students reflected highly on two major aspects of the course: the structure/design of the course and its impact on students' perspectives of career paths post-graduation.

Regarding the course structure, students' comments displayed an appreciation for the three sections and how they were ultimately unified to highlight real-world applications:

> *"I really enjoyed the structure of the course, as well as the guest lectures that have been integrated throughout the 6 weeks. It was such an eye opening and amazing experience to be able to hear from both medicinal and process chemists, and learn more about their work experience."*

"Before, I didn't really have much interest in the subject, but after seeing so many examples of how these reactions were used, I saw the importance and applicability of catalysis in drug synthesis. I feel like the class was structured very very well, and the schedule was very logical."

"I liked the real-world applications included throughout the lectures and how practical the material was."

"In [the third] part of the course we are taking what we learned about transition metal catalysis and applying it to some case studies of real drugs that use these methods. It was very interesting to see how what we are learning is applied to drugs that are being used in the market."

Additionally, the students described the impact the course had on them in showcasing career paths post-graduation:

"This is perhaps the first organic chemistry-based course that I've taken that I have thoroughly enjoyed! Learning about actual applications of organic chemistry and hearing from experts in the field of drug discovery has been very rewarding and has helped me narrow down potential career choices."

"Ultimately, this course was fairly interesting and showed me that the pharmaceutical industry may be a route for me to think about going into later on in my career."

"The first two weeks of this course piqued my interest in the pharmaceutical industry, especially in the synthesis of various drug molecules, which I haven't thought much about prior to the course, giving me something to think about as I continue to decide on what to do with my education in chemistry."

"I appreciated hearing his unique backstory in terms of what led to him becoming a grad student."

Overall, the feedback from students highlighted the impact of connecting chemistry concepts to real world applications and career avenues.

8.8 Personal Reflections

This course was created to serve as a bridge between fundamental organic chemistry curricula and real-world applications. Toward this end, the course focused on the centrality of organic chemistry in the discovery of new medicines and the importance of transition-metal catalysis in the modern synthetic chemists' toolbox. Despite the broad impact of transition-metal catalysis, which has been reflected in the awarding of multiple Nobel Prizes over the past two decades,[6] it can often be overlooked or considered a minor focus in introductory coursework. Furthermore, the unique reaction mechanisms of these transformations require a deeper analysis of reaction mechanism and selectivity principles, as well as compel students to consider new disconnections in the synthesis of small molecule drugs.

Due to the diverse range of skillsets required in drug development, a number of career opportunities are achievable for students majoring in fields such as chemistry or biochemistry. However, when these career avenues are not made clear to students, they may be unaware of these potential opportunities. In our multi-pronged approach, we sought to incorporate discussions of career opportunities into the video lectures, guest lectures, and discussion sections. The guest lectures provided a glimpse into what the careers of successful scientists might look like, from chemists at small biotechnology companies to large pharmaceutical companies, as well as those in

academia. We sought to showcase diverse roles in our selection of guest lecturers, which included process chemists, medicinal chemists, and scientists in management-type roles. We also placed an important emphasis on selecting guest lecturers from diverse backgrounds, including women, scientists of color, and individuals with non-linear career paths. We hope to have inspired students to follow their interests and pursue careers in drug discovery that they may not have considered previously.

As described, the course was led by graduate student instructors, who in turn received guidance from a faculty member, representing a fairly uncommon feature in undergraduate curricula. This provided an environment in which the students enrolled in the course could relate more to the instructors and lowered the barrier for communication about the course or related topics. Moreover, creating this direct interface allowed the undergraduate students to gain insight into the day-to-day lifestyle of graduate students in chemistry. This additionally sparked meaningful conversations about how to get involved in research, reasons for pursuing a Ph.D. program, and perspective on the instructors' own personal career plans. We would encourage the design of other STEM elective courses that are organized and led by senior graduate students.

Given the COVID-19 pandemic, instructors globally have been required to transition into online learning. We remained highly focused on maintaining an interactive environment, despite the challenges of the virtual setting, and explored several avenues to achieve this. An illustrative example from the course was the incorporation of QR codes (powered by QRChem.net[20]) into the lecture content that link to the 3D structure of a particular chemical compound, which the students can interact with on their smartphones. This not only sought to make the lectures feel more immersive to the students, but also aided in conveying key chemical concepts that require 3D visualization. We also incorporated exciting video content into the lectures that served to make the

course content more vibrant. The small group setting of the discussion sections also provided students an opportunity to ask questions. Finally, we utilized an online forum which allowed students to pose questions about course content or guest lecture material.

8.9 Conclusion

In conclusion, we have described the rationale, design, and structure of a new graduate student-led course on drug discovery with a focus on transition-metal catalysis. Addition of this course to UCLA's curriculum exposed students to the importance of organic synthesis in the development of novel medicines. Through this exposure, undergraduate students were introduced to potential avenues for careers within chemistry and engaged in direct interactions with leaders in the field. We hope this course encourages the development of new courses in STEM that sharpen the connection between fundamental concepts and their applications, while also highlighting career avenues. Moreover, we look forward to the development of new graduate student-led courses that serve to reduce barriers to higher education in STEM and curate an environment where students can explore potential avenues for their careers post-graduation.

8.10 Notes and References

(1) Rotella, D. P. The Critical Role of Organic Chemistry in Drug Discovery. *ACS Chem. Neurosci.* **2016**, *7*, 1315–1316.

(2) Hardy, M. A.; Wright, B. A.; Bachman, J. L.; Boit, T. B.; Haley, H. M. S.; Knapp, R. R.; Lusi, R. F.; Okada, T.; Tona, V.; Garg, N. K.; Sarpong, R. Treating a Global Health Crisis with a Dose of Synthetic Chemistry. *ACS Cent. Sci.* **2020**, *6*, 1017−1030.

(3) Mullard, A. 2020 FDA Drug Approvals. *Nature Rev. Drug Discov.* **2021**, *20*, 85–90.

(4) (a) Dorn, S. K.; Newman, J. D.; van Kessel, J. C.; Brown, L. C. Synthesis and Biological Assay of Small-Molecule Quorum Sensing Inhibitors: A Three-Week Course-Based Undergraduate Research Experience. *J. Chem. Educ.* **2021**, *98*, 3533–3541. (b) Bailie, A. E.; Nortcliffe, A. Synthesis of Quinolone Antibiotic Analogues: A Multistep Synthetic Chemistry Experiment for Undergraduates. *J. Chem. Educ.* **2021**, *98*, 3333–3340. (c) Funicello, M.; Cerminera, I.; Chiummiento, L.; Lupattelli, P.; Felluga, F.; Berti, F. Biginelli Reaction and β-Secretase Inhibition: A Multicomponent Reaction as a Friendly Educational Approach to Bioactive Compounds. *J. Chem. Educ.* **2021**, *98*, 1756–1761. (d) Yang, J.; Yuan, Y.; Gu, J.; Li, A.; Wei, Z.; Ouyang, Q. Drug Synthesis and Analysis of an Acetylcholinesterase Inhibitor: A Comprehensive Medicinal Chemistry Experience for Undergraduates. *J. Chem. Educ.* **2021**, *98*, 991–995.

(5) For recent examples and reviews of computer-aided drug design courses, see: (a) Sydow, D.; Wichmann, M.; Rodríguez-Guerra, J.; Goldmann, D.; Landrum, G.; Volkamer, A. TeachOpenCADD-KNIME: A Teaching Platform for Computer-Aided Drug Design Using KNIME Workflows. *J. Chem. Inf. Model.* **2019**, *59*, 4083–4086. (b) Romero, R. M.; Bolger, M. B.; Morningstar-Kywi, N.; Haworth, I. S. Teaching of Biopharmaceutics in a Drug Design Course: Use of GastroPlus as Educational Software. *J. Chem. Educ.* **2020**, *97*, 2212–2220. (c) Ragno, R.; Esposito, V.; Di Mario, M.; Masiello, S.; Viscovo, M.; Cramer, R. D.

Teaching and Learning Computational Drug Design: Student Investigations of 3D Quantitative Structure–Activity Relationships through Web Applications. *J. Chem. Educ.* **2020**, *97*, 1922–1930. (d) Shi, X.-X.; Li, J.-Y.; Chen, Q.; Zhu, X.-L.; Hao, G.-F.; Yang, G.-F. Development of a Web-Based Laboratory Class to Reduce the Challenges in Teaching Fragment-Based Drug Design. *J. Chem. Educ.* **2020**, *97*, 427–436. (e) Tuvi-Arad, I. Computational Chemistry in the Undergraduate Classroom – Pedagogical Considerations and Teaching Challenges. *Isr. J. Chem.* **2021**, *61*, 1–10. (f) Clent, B.; Wang, Y.; Britton, H. C.; Otto, F.; Swain, C. J.; Todd, M. H.; Wilden, J. D.; Tabor, A. B. Molecular Docking with Open Access Software: Development of an Online Laboratory Handbook and Remote Workflow for Chemistry and Pharmacy Master's Students to Undertake Computer-Aided Drug Design. *J. Chem. Educ.* **2021**, *98*, 2899–2905. (g) Tantillo, D. J.; Siegel, J. B.; Saunders, C. M.; Palazzo, T. A.; Painter, P. P.; O'Brien, T. E.; Nuñez, N. N.; Nouri, D. H.; Lodewyk, M. W.; Hudson, B. M.; Hare, S. R.; Davis, R. L. Computer-Aided Drug Design for Undergraduates. *J. Chem. Educ.* **2019**, *96*, 920–925.

(6) Nobelprize.org: The Official Web Site of the Nobel Prize. All Nobel Prizes in Chemistry. https://www.nobelprize.org/prizes/lists/all-nobel-prizes-in-chemistry (accessed Nov 2021).

(7) Buskes, M. J.; Blanco, M.-J. Impact of Cross-Coupling Reactions in Drug Discovery and Development. *Molecules* **2020**, *25*, 3493–3514.

(8) Brown, D. G.; Boström, J. Analysis of Past and Present Synthetic Methodologies on Medicinal Chemistry: Where Have All the New Reactions Gone? *J. Med. Chem.* **2016**, *59*, 4443−4458.

(9) For notable examples of successful laboratory-based undergraduate courses in transition-metal catalysis, see: (a) Hie, L.; Chang, J. J.; Garg, N. K. Nickel-Catalyzed Suzuki−Miyaura Cross-Coupling in a Green Alcohol Solvent for an Undergraduate Organic Chemistry Laboratory. *J. Chem. Educ.* **2015**, *92*, 571–574. (b) Costa, N. E.; Pelotte, A. L.; Simard, J. M.; Syvinski, C. A.; Deveau, A. M. Discovering Green, Aqueous Suzuki Coupling Reactions: Synthesis of Ethyl (4-Phenylphenyl)acetate, a Biaryl with Anti-Arthritic Potential. *J. Chem. Educ.* **2012**, *89*, 1064−1067. (c) Aktoudianakis, E.; Chan, E.; Edward, A. R.; Jarosz, I.; Lee, V.; Mui, L.; Thatipamala, S. S.; Dicks, A. P. "Greening Up" the Suzuki Reaction. *J. Chem. Educ.* **2008**, *85*, 555−557. (d) Hamilton, A. E.; Buxton, A. M.; Peeples, C. J.; Chalker, J. M. An Operationally Simple Aqueous Suzuki−Miyaura Cross-Coupling Reaction for an Undergraduate Organic Chemistry Laboratory. *J. Chem. Educ.* **2013**, *90*, 1509−1513. (e) Horikoshi, R. Illustrating Catalysis with Interlocking Building Blocks: A BINAP−Ruthenium Complex Catalyzed Asymmetric Hydrogenation. *J. Chem. Educ.* **2015**, *92*, 332–335. (f) Dander, J. D.; Morrill, L. A.; Nguyen, M. M.; Chen, S.; Garg, N. K. Breaking Amide C–N Bonds in an Undergraduate Organic Chemistry Laboratory. *J. Chem. Educ.* **2019**, *96*, 776–780. (g) Wathen, B.; Lanehart, E.; Woodis, L. A.; Rojas, A. J. Buchwald−Hartwig Amination, High-Throughput Experimentation, and Process Chemistry: An Introduction via Undergraduate Laboratory Experimentation. *J. Chem. Educ.* **2021**, *98*, 996–1000.

(10) Bettinger, E. P.; Long, B. T.; Taylor, E. S. When Inputs Are Outputs: The Case of Graduate Student Instructors. *Econ. Educ. Rev.* **2016**, *52*, 63–76.

(11) Wang, L.; Arnaud, C. H. Grad School, in Students' Own Words. *C&E News* https://cen.acs.org/education/graduate-education/Grad-school-in-students-own-words/96/i36# (accessed 2022-01-06).

(12) Of note, guest lectures serving to highlight the expertise of academic and industrial professionals have been implemented previously in undergraduate coursework; for an example, see Ref 5g.

(13) Reisman, S. E.; Sarpong, R.; Sigman, M. S.; Yoon, T. P. Organic Chemistry: A Call to Action for Diversity and Inclusion. *J. Org. Chem.* **2020**, *85*, 10287–10292.

(14) For a comment on the importance of storytelling in chemical education to help address equity in chemistry, see: Collins, S. N. The Importance of Storytelling in Chemical Education. *Nat. Chem.* **2021**, *13*, 1–2.

(15) Since the beginning of the COVID-19 pandemic, several successful virtual courses have been reported. For pertinent examples, see: (a) Giordano, A. N.; Gardner, D.; Kennerly, W. W.; Bruce, C. D. Conversations Among Physical Chemists: Strategies and Resources for Remote Teaching and Learning Catalyzed by a Global Pandemic. *J. Chem. Educ.* **2021**, *98*, 2228–2235. (b) Accettone, S. L. W. Student Perceptions of Remote Chemistry Lecture Delivery Methods. *J. Chem. Educ.* **2021**, *98*, 3667–3679. (c) Silverberg, L. J. Three-Part Approach to Remote/Residential Organic Chemistry Lab During the COVID-19 Pandemic. *J. Chem. Educ*. **2021**, *98*, 3898–3903. (d) Kimble-Hill, A. C.; Rivera-Figueroa, A.; Chan, B. C.; Lawal, W. A.; Gonzalez, S.; Adams, M. R.; Heard, G. L.; Gazley, J. L.; Fiore-Walker, B. Insights Gained into Marginalized Students Access Challenges During the COVID-19 Academic Response. *J. Chem. Educ.* **2020**, *97*, 3391–3395. (e) Alright, H.; Stephenson, C. R. J.;

Schindler, C. S. Converting a Two-Week Chemistry Course for High School Students to a Virtual Format During COVID. *J. Chem. Educ.* **2021**, *98*, 2457–2464. (f) Anzovino, M. E.; Mallia, V. A.; Morton, M. S.; Barker Paredes, J. E.; Pennington, R.; Pursell, D. P.; Rudd, G. E. A.; Shepler, B.; Villanueva, O.; Lee, S. Insights and Initiatives While Teaching Organic Chemistry I and II with Laboratory Courses in the Time of COVID-19. *J. Chem. Educ.* **2020**, *97*, 3240–3245. (g) Ramachandran, R.; Rodriguez, M. C. Student Perspectives on Remote Learning in a Large Organic Chemistry Lecture Course. *J. Chem. Educ.* **2020**, *97*, 2565–2572. (h) For an editorial summarizing ideas and approaches for virtual instruction arising from the response of chemistry educators to the COVID-19 pandemic, see: Holme, T. A. Introduction to the *Journal of Chemical Education* Special Issue on Insights Gained While Teaching Chemistry in the Time of COVID-19. *J. Chem. Educ.* **2020**, *97*, 2375–2377.

(16) For an excellent introductory textbook describing the modern drug discovery process, see: Stevens, E. *Medicinal Chemistry: The Modern Drug Discovery Process, 1st ed.*; Pearson Education, 2013.

(17) (a) Hegedus, L. S.; Söderberg, B. C. G. *Transition Metals in the Synthesis of Complex Organic Molecules, 3rd ed.*; University Science Books, 2009. (b) *White Lab; Lecture Notes.* http://faculty.scs.illinois.edu/white/index.php?p=lectures (accessed 2022-01-06).

(18) Crawley, M. L.; Trost, B. M. *Applications of Transition Metal Catalysis in Drug Discovery and Development: An Industrial Perspective, 1st ed.*; John Wiley & Sons, Inc., 2012.

(19) The increase in student response rate from 2020 to 2021 is likely due to the offering of a small extra credit incentive.

(20) Dang, J.; Lin, B.; Yuan, J.; Schwartz, S. T.; Shah, R. M.; Garg, N. K. Smart Access to 3D Structures. *Nat. Rev. Chem.* **2018**, *2*, 95–96.

CHAPTER NINE

Advancing Global Chemical Education Through Interactive Teaching Tools

Francesca M. Ippoliti,† Jason V. Chari,† and Neil K. Garg.

Chem. Sci. **2022**, *13*, 5790–5796.

9.1 Abstract

This chapter highlights our recent efforts to develop interactive resources in chemical education for worldwide usage. First, we highlight online tutorials that connect organic chemistry to medicine and popular culture, along with game-like resources for active learning. Next, we describe efforts to aid students in learning to visualize chemical structures in three dimensions. Finally, we present recent approaches toward engaging children and the general population through organic chemistry coloring and activity books. Collectively, these tools have benefited hundreds of thousands of users worldwide. We hope to promote a spirit of innovation in chemical education and spurs the development of additional free, interactive, and widely accessible chemical education resources.

9.2 Introduction

As researchers, we devote the majority of our professional efforts, and often even free time, to thinking about and addressing challenges we face in the laboratory. Simultaneously, we have come to realize the impact we researchers are poised to make—and have an obligation to make—when it comes to science education and scientific literacy. Scientific literacy, as described by the *National Academy of Sciences*, "means that a person can ask, find, or determine answers to

questions derived from curiosity about everyday experiences. It means that a person has the ability to describe, explain, and predict natural phenomena."[1] In other words, scientific literacy pertains to more than simply the ability to recite scientific facts; it extends to an individual's own judgment and decisions when it comes to science and therefore represents a complex, but critical issue. Heightening the value and importance of scientific literacy, scientific misinformation represents a growing problem in the age of social media.[2]

The key to addressing *global* scientific literacy lies in how we educate and, importantly, ensuring the accessibility of educational resources. As we consider chemical education, an all-too-common historical approach involves memorization and recitation of facts. This approach can be counterproductive in many ways and lead to negative perceptions by students. With regard to accessibility, resources for chemical education vary widely throughout the world, with many students not having access to costly textbooks, molecular model kits, or sometimes instructors.

Toward addressing these challenges, we have taken a keen interest in developing non-traditional educational platforms[3] that focus on growing students' critical thinking and problem-solving skills. In particular, these tools serve to put students "in the driver's seat" by compelling them to actively engage and connect with the material. Furthermore, many of our resources seek to make chemistry relatable and engaging to the students by incorporating real-world applications and examples. Engagement is known to correlate well with learning outcomes.[4] In addition, we have sought to create educational tools that are available online for worldwide use given that 4.95+ billion people have internet access already (and this figure is expected to grow).[5] Moreover, the COVID-19 era of virtual education has created an even greater need for readily accessible online teaching materials. Indeed, studies have demonstrated a marked decline in student engagement in

virtual settings during the pandemic.[6] The creation of effective online teaching materials not only benefits students studying chemistry, but also engages the broader population in our field.

Herein, we highlight our efforts to develop interactive and widely accessible resources that are available to all students. These resources were each created by teams comprised of individuals with diverse sets of experiences and backgrounds. This included undergraduate and graduate students, postdoctoral researchers, high school students, and even children. This allowed us to target a variety of audiences by better understanding challenges that exist in different stages of learning scientific topics. Critical to all of these projects was our collaboration with Dr. Daniel Caspi of Element26, Inc. who is a computing expert and master of creating user interfaces across various platforms.

9.3 Development and Application of Interactive Online Learning Tools

An important means of engaging students in chemistry is in relating course content to students' everyday lives. As an example, connecting organic chemistry to biology and popular culture helps to demonstrate that the course material is highly relevant to the students' lives, even if they do not intend to pursue further studies in that field. In particular, we hoped to engage students whose studies are not primarily focused in the area of chemistry.

With this in mind, we sought to create an online platform that connects chemistry concepts to medicine and popular culture. This ultimately led us to create BACON (Biology And Chemistry Online Notes, learnbacon.com), an online set of tutorials that serve as a vehicle for students to make extensive connections between organic chemistry, human health, and popular culture (Figure 9.1).[7] BACON consists of sixteen learning modules that cover organic chemistry topics such as 'Stereochemistry and Chirality,' 'Diels–Alder and Pericyclic Reactions,' and 'Polymers.' Each

module highlights several examples of the topic in both medicine and popular culture to deepen students' understanding of both the concepts and their importance. We also strive to keep these modules relevant to current topics, such as highlighting CRISPR gene editing technologies—which were the subject of the 2020 Nobel Prize in Chemistry[8]—as well as updated popular culture references that mention these scientific breakthroughs. Importantly, the tutorials also highlight members of the scientific community from underrepresented backgrounds in chemistry.

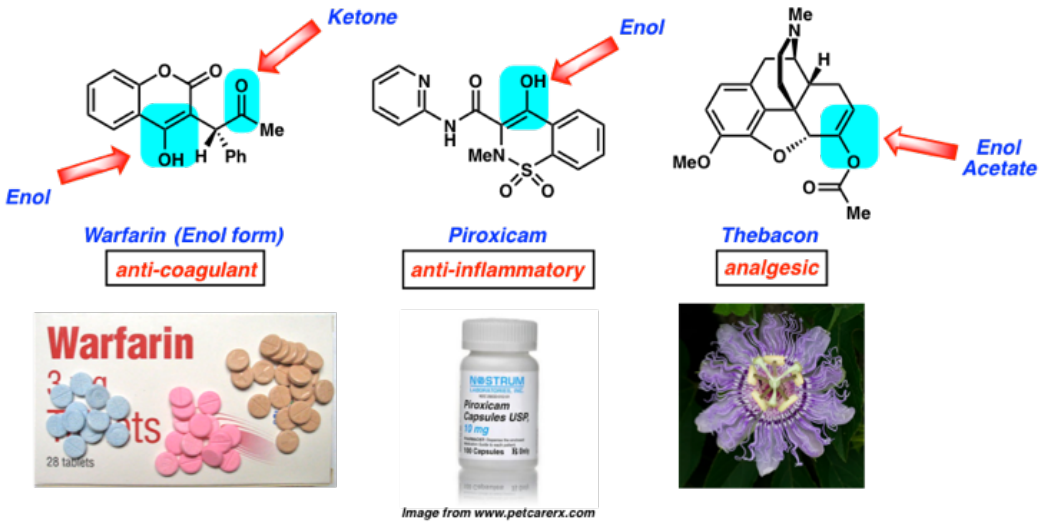

Figure 9.1. A selected example from BACON (Biology and Chemistry Online Notes), an online set of tutorials that connect organic chemistry to human health and popular culture.

As mentioned earlier, we have prioritized the creation of online teaching tools for chemical education in order to not only impact our local community, but also countries around the world. With respect to its global impact, BACON has been used by over 228,000 people in 169 different countries,[9] and over 165 universities have integrated BACON into some of their chemistry curricula.[10]

In addition to online learning modules, we have also sought to develop game-based learning tools that create fun and interactive learning environments for students. For example, the smartphone app Backside Attack (Figure 9.2) was launched to help students interact directly with a fundamental chemical reaction, the S_N2 reaction. This topic was specifically chosen as it involves several critical concepts that appear throughout undergraduate organic chemistry curricula. These concepts include nucleophilicity, electrophilicity, and the effect of sterics and solvents on reaction outcomes. This free smartphone app was conceived of and developed by undergraduate students who had used BACON in their organic chemistry coursework. These students appreciated the connections between biology, popular culture, and chemistry, but also envisioned a game-like resource that could help students learn the nuances of a new concept through an entertaining and interactive format. Backside Attack involves an enticing user interface, where participants launch a nucleophile from a syringe into a "solution" containing an electrophile with which it can react. The user is then prompted to draw an arrow-pushing mechanism for the reaction. Next, the user must physically tap repeatedly on the screen to simulate the energy required to overcome the activation barrier for the S_N2 reaction. Finally, the user is tasked with answering a textbook-style problem about the material covered in the level. This free application allows students to explore each aspect of the S_N2 reaction, which is anticipated to provide greater engagement with and absorption of the material. The "Chem Yourself" feature provides an opportunity for users to share their progress with their friends by creating a fun and personalized, chemistry-themed image. Other innovative games have also been created to help students connect with chemistry concepts, such as those developed by Alchemie.[11] Overall, these tools provide exciting opportunities for students to learn challenging concepts in an interactive and fun environment.

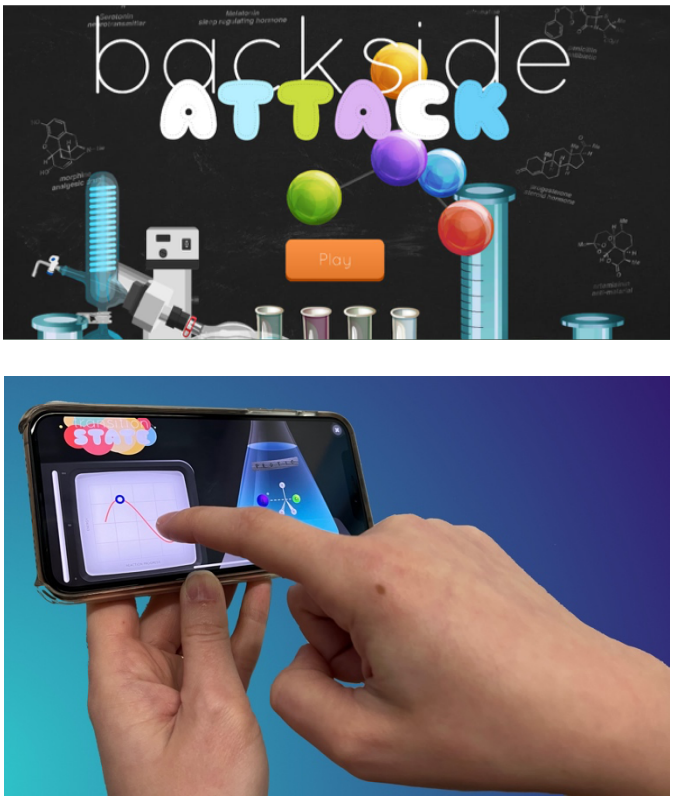

Figure 9.2. Backside Attack, a smartphone game that challenges students to master the S_N2 reaction, an important reaction in undergraduate organic chemistry coursework.

9.4 Teaching in Three Dimensions

A crucial skill for any chemistry student is the ability to visualize chemical structures. In particular, understanding chemical structures in two dimensions and carrying this knowledge into three dimensions is central to introductory coursework in chemistry. This involves concepts such as Valence Shell Electron Pair Repulsion (VSEPR) theory, chirality, and stereochemistry. Although these concepts make up a critical foundation of chemistry education, they consistently represent major obstacles for students, with reports of these challenges dating back to the 1940s.[12] Common teaching tools such as physical model kits, while powerful in many cases, can sometimes be inconvenient or costly. Alternatively, one might consider leveraging modern technology to

address this challenge. This offers an immense opportunity for chemistry educators to innovate by developing new interactive tools that facilitate the visualization of chemical structures. Such tools offer the potential to not only aid in students' understanding of three-dimensional structures, but also in generating excitement about these fundamental concepts.

Given the need for alternative approaches to teach students how to visualize chemical structures, we sought to develop a resource that takes advantage of smartphone technology. Our vision was to create a resource that would allow students to visualize any chemical structure instantly and without the need for a physical model kit. Toward achieving this, we opted to leverage the wide utility of quick-response (QR) code technology and in 2018, launched QR Chem (QRChem.net).[13] This project was initially led by a team of undergraduate students, who were later joined by graduate students for further development of the content. This site allows educators and researchers to create QR codes, as well as bit.ly URLs, that link directly to a three-dimensional structure of interest (Figure 9.3). As an example, an instructor may create and present a QR code to a class of students, each of whom can then scan the QR code using their smartphone's built-in camera to open the interactive structure directly on their device. The student is then able to rotate, as well as zoom-in and zoom-out on, the chemical structure in order to compare it to a two-dimensional representation that is also displayed on the screen (an example of this is shown in Figure 9.3).

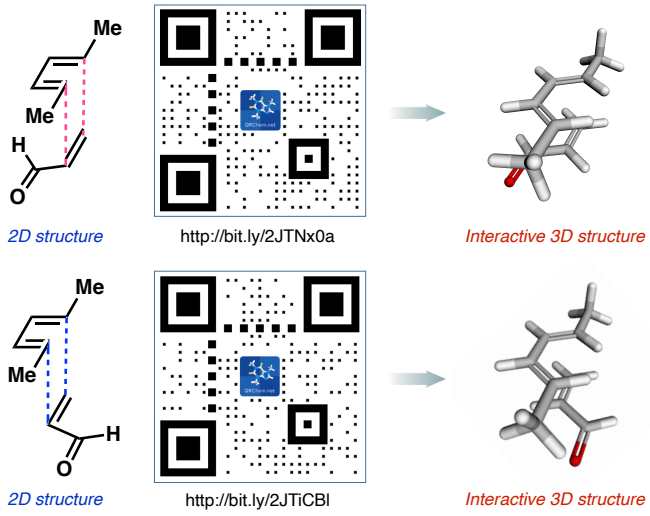

Figure 9.3. QR Chem, a site that allows students, instructors, and researchers to create QR codes that link to interactive 3D structures. In this example, two potential scenarios for the classic Diels–Alder reaction are depicted, each leading to different isomeric outcomes.

Since the initial launch of QR Chem, we have created a Molecule of the Day page for the site that showcases over fifty different molecules with important societal impact. This module takes the form of slide-based presentations with embedded QR codes that link to three-dimensional structures, as well as provide interesting information about each molecule. Additionally, the Lesson Plans page on the site contains useful slide-based presentations with embedded QR codes that cover a variety of topics that rely on the visualization of chemical structures (e.g., the Diels–Alder reaction, as depicted in Figure 9.3). It should also be noted that any user can generate a sharable QR code by simply uploading a 2D and 3D structure file, or submitting a valid PubChem CID number for virtually any molecule of interest. In our own experience, QR Chem helped to facilitate interactive learning in courses taught remotely.[14] QR codes generated from QR Chem can also be found in Wikipedia entries, as well as in some textbooks.[15] Excitingly, QR Chem has been used by over 62,000 people in over 150 countries.

In addition to being able to visualize chemical structures, assigning a stereocenter on a molecule is a critical skill for organic chemistry students. We sought to create a learning tool to help teach this skill while also being more interactive and engaging than textbook-based approaches. We envisioned that a game-like interface could serve to achieve this, as such a platform would provide the ability for students to receive direct feedback as they learn how to assign stereocenters and put their knowledge to the test. R/S Chemistry (RSChemistry.com), launched in 2019, represents our interactive solution to this challenge of learning how to assign stereocenters (Figure 9.4). As with QR Chem, the idea for this resource was originally devised by undergraduate students, with graduate students joining the team later to develop the content. It features multiple levels of gameplay with both a guided 'Learn' mode and a timed 'Expert' mode for all levels of student mastery. R/S Chemistry leverages the visualization technology used in QR Chem to include interactive three-dimensional structures that assist in the stereochemical assignments. In selecting example molecules for the game, we sought to highlight compounds with broad societal impact, such as medicines and fragrances, to help students connect with the content. Of note, such connections are often missing in traditional teaching tools, further underscoring the need for alternative educational approaches that showcase them. Since its launch, R/S Chemistry has been used by more than 21,000 people in over 100 countries.[16]

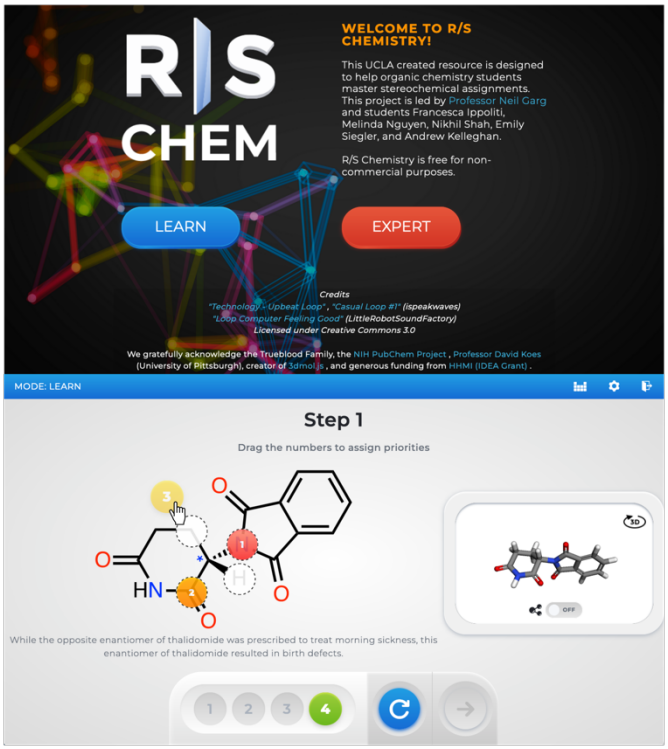

Figure 9.4. R/S Chemistry, a resource for students to practice assigning stereocenters in a game-like environment.

Advances in modern technology continue to provide new opportunities for chemical visualization, and, in turn, new areas for innovation. Virtual Reality (VR) and Augmented Reality (AR) technology enable the creation of immersive environments for teaching in three dimensions. Excitingly, these technologies offer the ability to teach abstract concepts that may be very challenging to describe in detail using traditional teaching tools. Several examples of immersive VR[17,18] and AR[19] technology in chemical education have been reported, many of which provide compelling evidence that implementation of virtual reality tools improve student performance. For example, Kurushkin and co-workers have demonstrated that the implementation of a virtual reality program called MEL Chemistry VR in coursework at ITMO University in Russia has improved undergraduate students' ability to grasp challenging concepts pertaining to atomic structure.[17a]

Additionally, Diaconescu and co-workers developed a VR laboratory session to teach advanced inorganic chemistry students about metal coordination and molecular orbitals, which resulted in higher exam scores by the students who participated in the VR session compared to those who did not.[17b] Compelling smartphone-based applications that employ AR technology have also been developed, including Isomers AR by Alchemie,[20] a game that allows users to build and discover new molecules in 3D without the need for a specialized headset. We have also begun to adapt content from QR Chem into a virtual reality interface (VRChem.net) to create an immersive environment where students can view and interact with three-dimensional structures, as well as learn about important molecules that connect to their everyday lives.

9.5 Reaching New Audiences

A crucial aspect of addressing scientific literacy lies in connecting with audiences outside of higher education. As a personal anecdote, one of us (N.K.G.) noticed that his daughter was particularly afraid of chemicals from an early age. Before trying a new food, she would often ask, "does it have chemicals in it?" and express wariness about the food. However, once it was explained to her that chemicals make up everything around her, including her favorite things, she became more curious about which chemicals were part of her daily life. We saw this as an opportunity to expand our impact as scientists and educators to a younger generation. In particular, we envisioned that introducing chemistry to children through fun and engaging activities could serve to reduce the negative association they have with the word "chemical." In considering interactive activities that children are familiar with, we opted to develop a coloring book about organic molecules. The final product, *The Organic Coloring Book*, features molecules such as sucrose, cellulose, and chlorophyll (Figure 9.5). Exposing children to the connection between

science and everyday life serves to increase children's curiosity about the world around them and hopefully spark lifelong interest in science. We have also received positive feedback from parents, who note that the book also helped them learn about chemistry in the world around them. *The Organic Coloring Book* is accessible for purchase online,[21] although we regularly distribute free copies throughout the world. To make this resource accessible to a broader global population, we have also published a Spanish edition of *The Organic Coloring Book*, entitled *El Libro Para Colorear Orgánico*.[22]

Figure 9.5. *The Organic Coloring Book* series and *The O-Chem (Re)Activity Book* are designed to connect organic chemistry to the everyday lives of both children and adults.

The success of *The Organic Coloring Book*, as well as its medicine-themed sequel (*Cheesy Goes to the Doctor*),[23] led us to wonder whether we could develop similar resources to reach adults

as well. Indeed, we felt that our motivations for creating the organic coloring book for children could also be extended to adults. As an example, "chemical-free" products are often marketed as desirable despite the impossibility of a product that does not contain chemicals. We ultimately created *The Adult Organic Coloring Book*,[24] highlighting molecules that have relevance to adult life, such as ethanol and creatine, an amino acid used for muscle growth.

Another interactive resource that we felt would be exciting to children is an activity book, which we envisioned would consist of chemistry-themed exercises. Similar to *The Organic Coloring Book*, each of these activities would serve to expose children to chemistry and its connection to daily life. We ultimately developed *The O-Chem (Re)Activity Book*, which is comprised of fun exercises including connect-the-dots, word searches, mazes, and 'spot the difference,' each of which highlight chemistry in the world around us. The book is available free of charge online as a downloadable PDF,[25] allowing parents around the world to download the book and enjoy it with their children.

Additionally, we recently launched ChemMatch (ChemMatch.net), an online matching game that includes several chemistry-oriented subjects designed to reach various audiences (Figure 9.6). This includes topics relevant to all audiences such as "Chemistry in Your Life" and "Kids Movies," as well as topics for high school chemistry students and college general chemistry students including "Elements" and "Polyatomic Ion Charges." Organic Chemistry specific categories are also included.

Figure 9.6. ChemMatch, an online matching game that serves as an educational resource for children, students, and adults.

In addition to the books and online resources created by our lab, there have been a multitude of chemistry books and activities that connect children with the science found around them.[26] Introducing chemistry to children at a young age can have a lasting impact on the importance of science in their worldview. More broadly, developing resources that reach a wide audience can also help to promote a positive public perception of chemistry among non-scientist adults. We look forward to seeing future efforts in this area.

9.6 Global Impact and Innovation in Education

A crucial objective of our efforts in education is reaching audiences across the globe. Accordingly, we have evaluated the usage of our web-based resources in countries worldwide and have been gratified to observe that our online resources have been used all around the world. To illustrate this, Figure 9.7 depicts global usage of QR Chem, R/S Chemistry, and ChemMatch,

which have a combined total of over 90,000 users in 157 countries. These widely accessible resources not only engage chemistry students, but also present a step toward educating the more general population. We hope to continue expanding the reach of these resources around the world.

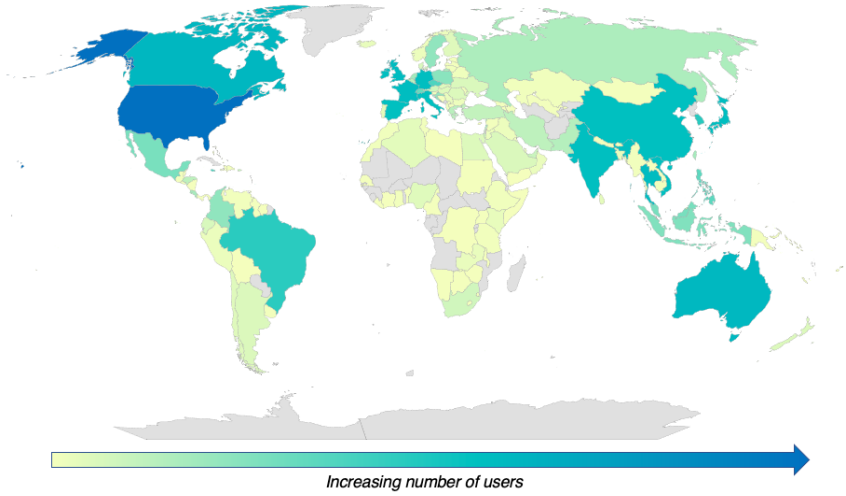

Figure 9.7. Map of combined users of QR Chem, R/S Chemistry, and ChemMatch worldwide (data from Google Analytics).

9.7 Conclusion

We have developed a multitude of non-traditional chemical education resources, including a smartphone application, several websites, and children's books. These tools transcend classic teaching methods, such as those primarily focused on textbooks and memorization. Instead, we largely rely on internet-based technologies that enable critical thinking and engagement in order to help students learn about and appreciate chemistry. In addition, our educational resources for children and the general population contribute to the widespread societal challenge of improving scientific literacy. Collectively, the resources we have developed so far have positively benefitted hundreds of thousands of people all over the world.

Our goal in writing this chapter is not to simply advertise our educational materials. Instead, we offer our view as active researchers of the potential impact we, as a community of scientists, can make as we think about science education on a global scale. It is incumbent upon *all of us* to contribute to science education worldwide. Such efforts not only benefit our own fields by engaging individuals in chemistry, but more importantly, have the capacity to benefit society in the long-term. We should also prioritize the development of resources that are fun, engaging, promote critical thinking skills, and are accessible to everyone.

Lastly, we offer sentiments regarding "innovation," a term frequently employed in academia. Although there exists a strong spirit of innovation in scientific research, a comparable sentiment is notably lacking in many research-intensive colleges and universities when discussing chemical education. By choosing to prioritize innovation in chemical education, we stand to improve the student experience, educate the scientific leaders of the future, enhance global education and scientific literacy, and even strengthen the public perception of our fields.

9.8 Related Links

BACON: https://learnbacon.com/

Backside Attack: https://apps.apple.com/us/app/backside-attack/id1278956096/

QR Chem: https://qrchem.net/

R/S Chemistry: https://rschemistry.com/

ChemMatch: https://chemmatch.net/

Organic Coloring Book Series: https://www.amazon.com/dp/B08NXL4SWP/

The O-Chem (Re)Activity Book: https://garg.chem.ucla.edu/ochem-re-activity/

Element26: https://www.element26.net/

9.9 Notes and References

(1) National Research Council. *National Science Education Standards*; The National Academies Press: Washington, D.C., 1996. DOI: 10.17226/4962.

(2) Scheufele, D. A.; Krause, N. M. Science Audiences, Misinformation, and Fake News. *Proc. Natl. Acad. Sci.* **2019**, *116*, 7662–7669.

(3) Garg, N. K. Empowering Students to Innovate: Engagement in Organic Chemistry Teaching. *Angew. Chem., Int. Ed.* **2018**, *57*, 15612–15613.

(4) (a) Handelsman, M. M.; Briggs, W. L.; Sullivan, N.; Towler, A. A Measure of College Student Course Engagement. *J. Educ. Res.* **2005**, *98*, 184–192. (b) Martin, F.; Bolliger, D. U. Engagement Matters: Student Perceptions on the Importance of Engagement Strategies in the Online Learning Environment. *Online Learn. J.* **2018**, *22*, 205–222.

(5) *Digital 2022: Global Overview Report.* https://datareportal.com/reports/digital-2022-global-overview-report/ (accessed March 2022).

(6) (a) Wester, E. R.; Walsh, L. L.; Arango-Caro, S.; Callis-Duehl, K. L. Student Engagement Declines in STEM Undergraduates during COVID-19–Driven Remote Learning. *J. Microbiol. Biol. Educ.* **2021**, *22*, ev22i1.2385. (b) Wu, F.; Teets, T. S. Effects of the COVID-19 Pandemic on Student Engagement in a General Chemistry Course. *J. Chem. Educ.* **2021**, *98*, 3633–3642.

(7) Shah, T. K.; Garg, N. K. Organic Chemistry Can Sizzle. *Nat. Rev. Chem.* **2017**, *1*, 0020.

(8) Nobelprize.org: The Official Web Site of the Nobel Prize. All Nobel Prizes in Chemistry. https://www.nobelprize.org/prizes/lists/all-nobel-prizes-in-chemistry (accessed February 2022).

(9) Data obtained from Google Analytics.

(10) BACON tutorials are available for less than 1 USD each, although full cost waivers are commonly granted.

(11) *Alchemie*. https://www.alchem.ie/ (accessed February 2022).

(12) (a) Fromm, F. On Teaching Stereochemistry. *J. Chem. Educ.* **1945**, *22*, 43. (b) Shine, H. J. Aids in Teaching Stereochemistry: Plastic Sheets for Plane Projection Diagrams. *J. Chem. Educ.* **1957**, *34*, 355. (c) Evans, G. G. Stereochemistry in the Terminal Course. *J. Chem. Educ.* **1963**, *40*, 438−440. (d) Beauchamp, P. S. "Absolutely" Simple Stereochemistry. *J. Chem. Educ.* **1984**, *61*, 666−667. (e) Lyon, G. L. Ph.D. Dissertation, Louisiana State University and Agricultural & Mechanical College, Baton Rouge, LA, USA, 1999; https://digitalcommons.lsu.edu/gradschool_disstheses/7105/ (accessed February 2022). (f) Raupp, D.; Del Pino, J. C.; Prochnow, T. R. Teaching of Stereochemistry in High School: An Approach Based on Vergnaud's Conceptual Theory. *ESERA Conference*; Dublin City University: Dublin, Ireland, 2017.

(13) Dang, J.; Lin, B.; Yuan, J.; Schwartz, S. T.; Shah, R. M.; Garg, N. K. Smart Access to 3D Structures. *Nat. Rev. Chem.* **2018**, *2*, 95–96.

(14) Chari, J. V.; Knapp, R. R.; Boit, T. B.; Garg, N. K. Catalysis in Modern Drug Discovery: Insights from a Graduate Student-Taught Undergraduate Course. *J. Chem. Educ.* **2022**, *99*, 1296–1303.

(15) QR Chem is currently used in several *Top Hat* online textbooks for General Chemistry and Organic Chemistry.

(16) Ippoliti, F. M.; Nguyen, M. M.; Reilly, A. J.; Garg, N. K. Gaming Stereochemistry. *Nat. Rev. Chem.* **2022**, Accepted Article. DOI: 10.1038/s41570-022-00395-5

(17) (a) Maksimenko, N.; Okolzina, A.; Vlasova, A.; Tracey, C.; Kurushkin, M. Introducing Atomic Structure to First-Year Undergraduate Chemistry Students with an Immersive Virtual Reality Experience. *J. Chem. Educ.* **2021**, *98*, 2104–2108. (b) Dai, R.; Laureanti, J. A.; Kopelevich, M.; Diaconescu, P. L. Developing a Virtual Reality Approach Toward a Better Understanding of Coordination Chemistry and Molecular Orbitals. *J. Chem. Educ.* **2020**, *97*, 3647−3651. (c) Edwards, B. I.; Bielawski, K. S.; Prada, R.; Cheok, A. D. Haptic Virtual Reality and Immersive Learning for Enhanced Organic Chemistry Instruction. *Virtual Reality* **2019**, *23*, 363−373. (d) O'Connor, M.; Deeks, H. M.; Dawn, E.; Metatla, O.; Roudaut, A.; Sutton, M.; Thomas, L. M.; Glowacki, B. R.; Sage, R.; Tew, P.; Wonnacott, M.; Bates, P.; Mulholland, A. J.; Glowacki, D. R. Sampling Molecular Conformations and Dynamics in a Multiuser Virtual Reality Framework. *Sci. Adv.* **2018**, *4*, eaat2731. (e) O'Connor, M. B.; Bennie, S. J.; Deeks, H. M.; Jamieson-Binnie, A.; Jones, A. J.; Shannon, R. J.; Walters, R.; Mitchell, T. J.; Mulholland, A. J.; Glowacki, D. R. Interactive Molecular Dynamics in Virtual Reality from Quantum Chemistry to Drug Binding: An Open-Source Multi-Person Framework. *J. Chem. Phys.* **2019**, *150*, 220901. (f) Merchant, Z.; Goetz, E. T.; Keeney-Kennicutt, W.; Kwok, O. M.; Cifuentes, L.; Davis, T. J. The Learner Characteristics, Features of Desktop 3D Virtual Reality Environments, and College Chemistry Instruction: A Structural Equation Modeling Analysis. *Comput. Educ.* **2012**, *59*, 551−568. (g) Ferrell, J. B.; Campbell, J. P.; McCarthy, D. R.; McKay, K. T.; Hensinger, M.; Srinivasan, R.; Zhao, X.; Wurthmann, A.; Li, J.; Schneebeli, S. T.

Chemical Exploration with Virtual Reality in Organic Teaching Laboratories. *J. Chem. Educ.* **2019**, *96*, 1961−1966. (h) Fung, F. M.; Choo, W. Y.; Ardisara, A.; Zimmermann, C. D.; Watts, S.; Koscielniak, T.; Blanc, E.; Coumoul, X.; Dumke, R. Applying a Virtual Reality Platform in Environmental Chemistry Education to Conduct a Field Trip to an Overseas Site. *J. Chem. Educ.* **2019**, *96*, 382−386. (i) Bennie, S. J.; Ranaghan, K. E.; Deeks, H.; Goldsmith, H. E.; O'Connor, M. B.; Mulholland, A. J.; Glowacki, D. R. Teaching Enzyme Catalysis Using Interactive Molecular Dynamics in Virtual Reality. *J. Chem. Educ.* **2019**, *96*, 2488−2496. (j) Goddard, T. D.; Brilliant, A. A.; Skillman, T. L.; Vergenz, S.; Tyrwhitt-Drake, J.; Meng, E. C.; Ferrin, T. E. Molecular Visualization on the Holodeck. *J. Mol. Biol.* **2018**, *430*, 3982−3996.

(18) For a review of VR tools developed for chemical education, see: Fombona-Pascual, A.; Fombona, J.; Vásquez-Cano, E. VR in Chemistry, a Review of Scientific Research on Advanced Atomic/Molecular Visualization. *Chem. Educ. Res. Pract.* **2022**, *23*, 300–312.

(19) (a) Clemons, T. D.; Fouché, L.; Rummey, C.; Lopez, R. E.; Spagnoli, D. Introducing the First Year Laboratory to Undergraduate Chemistry Students with an Interactive 360° Experience. *J. Chem. Educ.* **2019**, *96*, 1491−1496. (b) Sanii, B. Creating Augmented Reality USDZ Files to Visualize 3D Objects on Student Phones in the Classroom. *J. Chem. Educ.* **2020**, *97*, 253−257. (c) Yang, S.; Mei, B.; Yue, X. Mobile Augmented Reality Assisted Chemical Education: Insights from Elements 4D. *J. Chem. Educ.* **2018**, *95*, 1060−1062.

(20) *Isomers AR*. https://www.alchem.ie/isomers-ar/ (accessed February 2022).

(21) Garg, N. K.; Garg, E.; Garg, K. *The Organic Coloring Book*; 2017. https://www.amazon.com/gp/product/0692860541.

(22) Garg, N. K.; Garg, E.; Garg, K. *El Libro Para Colorear Orgánico*; 2021. https://www.amazon.com/gp/product/B0991DVNTC.

(23) Garg, N. K.; Garg, E.; Garg, K. *Cheesy Goes to the Doctor*; 2020. https://www.amazon.com/gp/product/B08CWJ8FN7.

(24) Garg, N. K.; Dander, J. E.; Darzi, E. R. *The Adult Organic Coloring Book*; 2020. https://www.amazon.com/gp/product/B08NWQZVWK.

(25) *The O-Chem (Re)-Activity Book.* https://garg.chem.ucla.edu/ochem-re-activity/ (accessed February 2022).

(26) For examples of children's books that connect children with chemistry in the world around them, see: (a) Sperber, C. *The Organic Chemistry Alphabet Book*; Nanoscale Scientists Publishing LLC, 2019. https://www.amazon.com/Organic-Chemistry-Alphabet-Book/dp/1732926514. (b) Barfield, M. *The Element in the Room: Investigating the Atomic Ingredients that Make Up Your Home*; Laurence King Publishing, 2018. https://www.amazon.com/Element-Room-Investigating-Atomic-Ingredients/dp/1786271788. (c) Huggins-Cooper, L. *Chemistry for Curious Kids: An Illustrated Introduction to Atoms, Elements, Chemical Reactions, and More!*; Arcturus, 2021. https://www.amazon.com/Chemistry-Curious-Kids-Illustrated-Introduction/dp/1398802670. (d) Wynne P. J.; Silver, D. M. *My First Book About Chemistry*; Dover Publications, 2020. https://www.amazon.com/First-About-Chemistry-Childrens-Science/dp/0486837580.